THE CATHOLIC UNIVERSITY OF AMERICA

Effects of Principal Stress Direction and the Intermediate Principal Stress on The Stress-Strain-Strength Behavior of a Cross-Anisotropic Fine Sand Deposit

A DISSERTATION

Submitted to the Faculty of the

Department of Civil Engineering

School of Engineering

Of The Catholic University of America

In Partial Fulfillment of the Requirements

For the Degree

Doctor of Philosophy

By

Eugene J. Van Dyck, V

Washington, D.C.

2012

Effects of Principal Stress Direction and the Intermediate Principal Stress on the Stress-Strain-Strength Behavior of a Cross-Anisotropic Fine Sand Deposit

Eugene J. Van Dyck, V, Ph.D.

Director: Poul V. Lade, Ph.D.

Variations in the principal stress inclination and the intermediate principal stress ratio can significantly affect the behavior of cross-anisotropic soils. The main focus of this investigation is to explore the stress-strain-strength behavior of a cross-anisotropic granular soil by performing a series of drained tests on air pluviated specimens of fine Nevada Sand.

A newly developed Hollow Torsional Shear Apparatus was used to shear specimens to failure following a predetermined stress path that maintained constant values of principal stress inclination, principal stress ratio, and mean normal effective stress.

Tests showed that soil stiffness decreased with increasing principal stress inclinations up to 67.5 degrees after which a moderate increase in stiffness was observed to 90 degrees. Peak shear strength values followed a similar trend for mid range b-values. However, the trough occurring at 67.5 degrees was not observed near the end conditions of b = 0 or 1.

Increasing b-values from 0 to 0.5 resulted in significantly increased stiffnesses. A more subtle increase in stiffness occurred from 0.5 to 1. Peak shear strength increased from b = 0 to 0.5 and decreased from 0.5 to 1. However, the strength at b = 1 was somewhat higher than b = 0.

During the elastic portion of the test, the strain increment directions were several degrees higher than the stress directions for tests with principal stress inclinations of 22.5 degrees and 45 degrees while at 67.5 degrees the strain increments were several degrees lower than the stress directions. All strain increment directions approached the stress directions at failure.

Shear bands propagating parallel to the specimen wall intersected the rigid end platens and were generally thin and ubiquitous. At both high and low b-values shear bands propagated perpendicular to the specimen wall. These shear bands, which intersected flexible membranes rather than rigid end platens, were typically thick and well defined.

The inclination of shear bands propagating parallel to the specimen wall agreed well with Coulomb's theoretical prediction. It was not possible to measure the inclination of shear bands propagating perpendicular to the specimen wall.

This dissertation by Eugene J. Van Dyck, V fulfills the dissertation requirement for the doctoral degree in Civil Engineering approved by Poul V. Lade, Ph.D., as director, and Lu Sun, Ph.D., and George P. Mavroeidis, Ph.D., as readers.

_____

Poul V. Lade, Ph.D., Director

_____

Lu Sun, Ph.D., Reader

_____

George P. Mavroeidis, Ph.D., Reader

TABLE OF CONTENTS

TABLE OF FIGURES

TABLE OF TABLES

ACKNOWLEDGMENT

I would like to express my sincere thanks to Professor Poul V. Lade, whose encouragement, guidance and expertise were greatly appreciated during my studies at Catholic University of America.

I would also like to thank my wife and family for their understanding and support throughout this process.

1 INTRODUCTION

Many natural and some manmade soil deposits have cross-anisotropic fabrics. Variations in the principal stress inclination (α) and the intermediate principal stress ratio (b-value) can significantly affect the strength, stiffness and volume change behavior of such deposits.

This investigation's main focus is to explore the failure surface of a cross-anisotropic granular soil, by performing a series of drained tests on fine Nevada Sand using a newly developed Hollow Torsional Shear Apparatus (HTSA).

1.1 Background

The principal stress inclination and the intermediate principal stress ratio play an important role in many geotechnical engineering problems. The principal stress inclination, typically denoted by the Greek letter α, is defined as the angle that the major principal stress makes with a vector normal to the bedding plane. It can vary from α = 0° when the major principal stress is perpendicular to the bedding plane to α = 90°when the major principal stress is parallel to the bedding plane.

The intermediate principal stress ratio (b), as shown in Equation (1.1), provides a convenient means for describing the relative magnitude of the intermediate principal stress as compared to the major and minor principal stresses. The b-value varies from 1 when the major and intermediate principal stresses are equal to 0 when the minor and intermediate principal stresses are equal.

$$b = \frac{\sigma_2 - \sigma_3}{\sigma_1 - \sigma_3} \quad (1.1)$$

Where:

b = intermediate principal stress ratio

σ_1 = major principal stress

σ_2 = intermediate principal stress

σ_3 = minor principal stress

Both of these factors can vary for a given geotechnical problem. For instance, foundation and slope stability evaluations are commonly affected by these factors. Load tests involving strip footings on granular subgrades have shown that inclined static loads result in bearing capacity variations that can be attributed to loading direction (Oda et al. 1978). As shown in Figure 1-1, even perpendicular loading of a shallow spread footing can produce variations in the intermediate principal stress ratio and principal stress inclination.

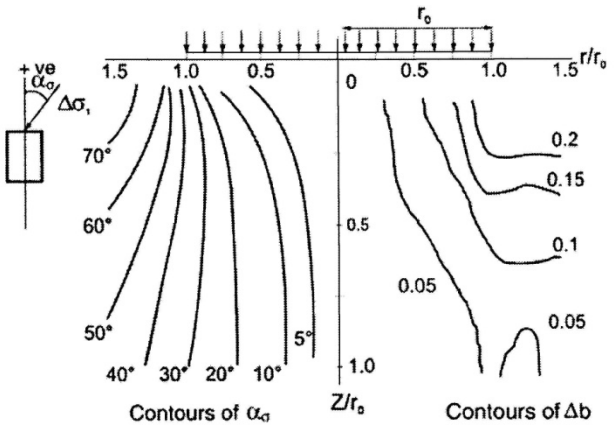

Figure 1-1: Contours of α and b Beneath Footing
After (Leroueil and Hight 2002)

Slope stability analysis must consider a potential failure surface that forms many intermediate angles with a soil's bedding plane as it traverses from the top to the toe of a slope (Murthy et al. 1980). Figure 1-2 illustrates how the principal stress directions change within a slope.

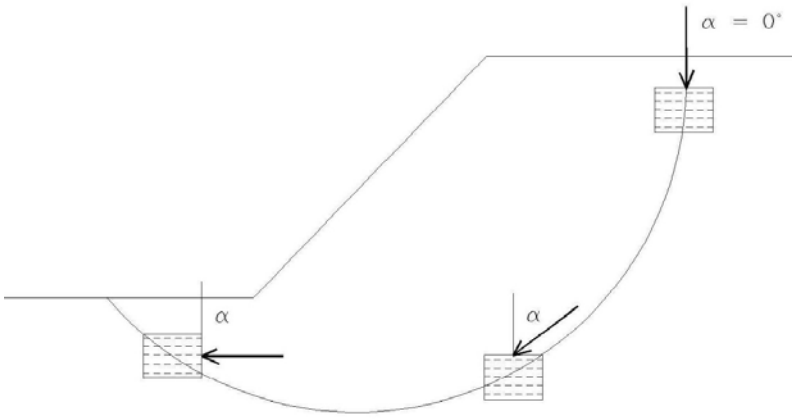

Figure 1-2: Variation in α for Slope Stability Problem
After (Pradhan et al. 1988)

For a constitutive model to accurately represent both of the problems discussed above, it must have a 3-dimensional component to account for the intermediate principal stress and a cross-anisotropic component to account for the principal stress direction.

Due to the effects of anisotropy, these two variables do not act independently of each other. Therefore, the soil behavior cannot be explained without exploration of the entire failure surface ($\alpha = 0°$ to $90°$, $b = 0$ to 1).

1.2 Purpose

The purpose of this research investigation is to explore the failure surface of a cross-anisotropic granular soil. This will be accomplished by maintaining constant values of α and b during testing in a hollow torsional shear apparatus. The resulting test data will be appropriate for correlation of existing cross-anisotropic models, or creation of new ones.

1.3 Originality

This is the first study to explore the failure surface of a granular material over a wide range of stress conditions with constant values of α, b, and σ_{avg}. Previous studies have been confined to limited areas of exploration. These studies have been completed using either: a true triaxial test apparatus, a plane strain device, or a hollow torsional shear apparatus with equal inner and outer pressures.

A true triaxial device allows a full range of b-values. However, as shown by the shaded regions in Figure 1-3, the principal stress inclination is limited to either 0° or 90° to the bedding planes.

Testing at intermediate values of α using this device has been attempted by forming or extracting specimens with inclined bedding planes. However by contrasting *free-end platen* with *fixed-end platen* tests (see Figure 1-4), it has been shown that interaction with rigid platens creates moments and shear forces that invalidate tests results for this method (Saada 1988).

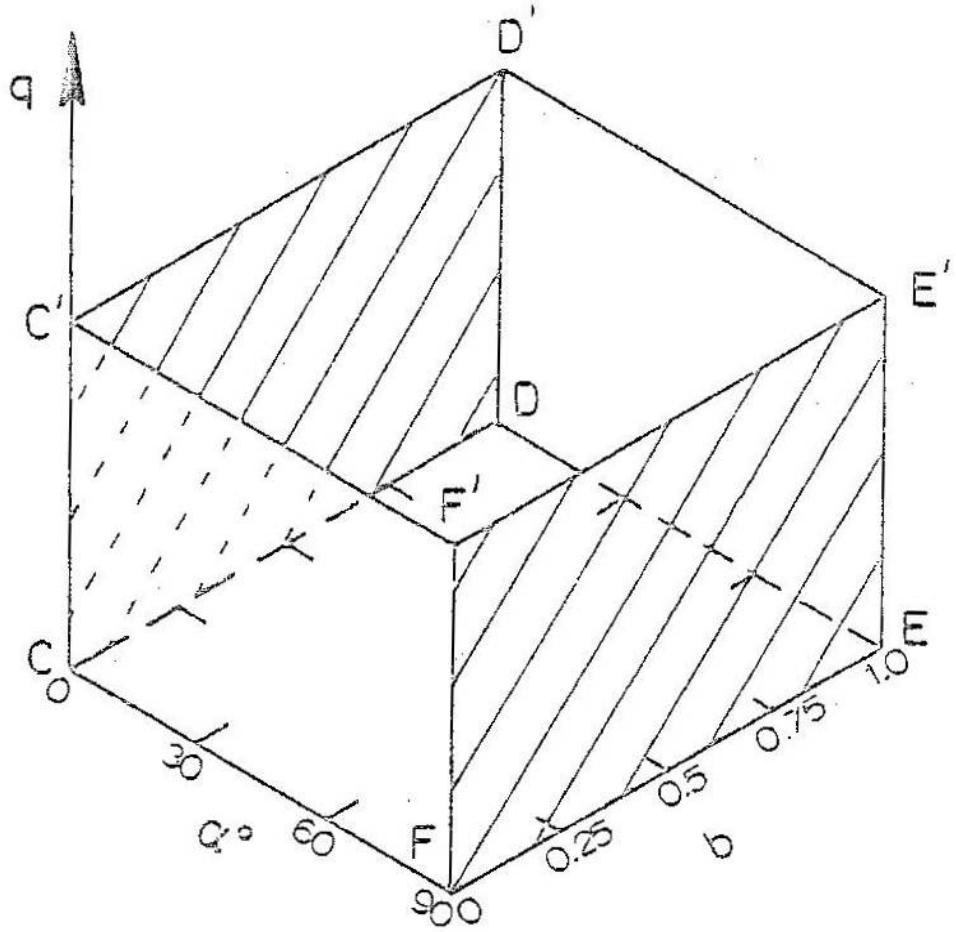

Figure 1-3: True Triaxial Test Apparatus Test Space
After (Symes et al. 1982)

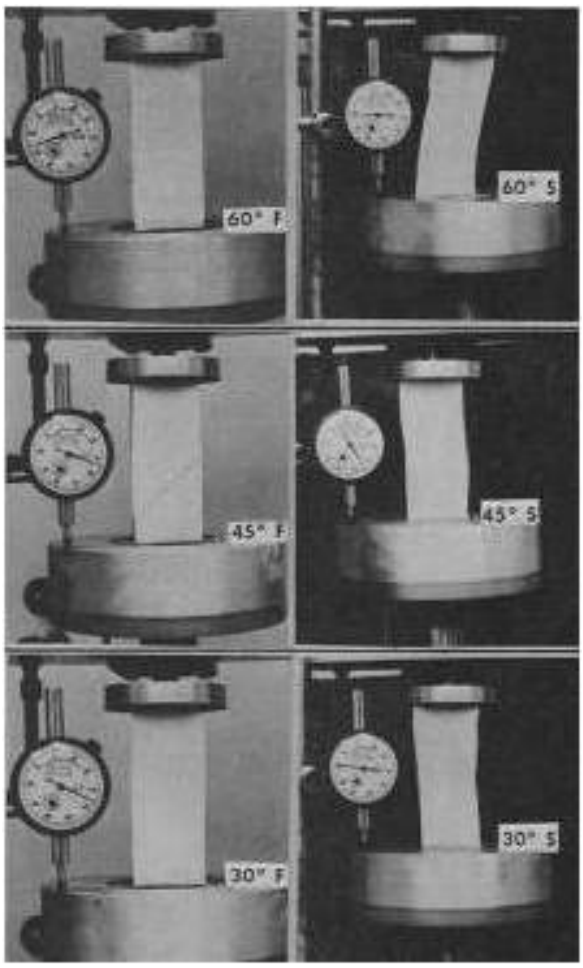

Figure 1-4: True Triaxial Inclined Specimens (Fixed Versus Free Platens) After (Saada 1988)

Plane strain devices have been constructed that allow the application of shear stress to soft membrane type boundaries, resulting in the ability to rotate the principal stress directions (Arthur 1977a). However, only a single b-value, usually between 0.2 and 0.3, can be achieved, greatly limiting the stress space (see Figure 1-5) that can be explored using this method.

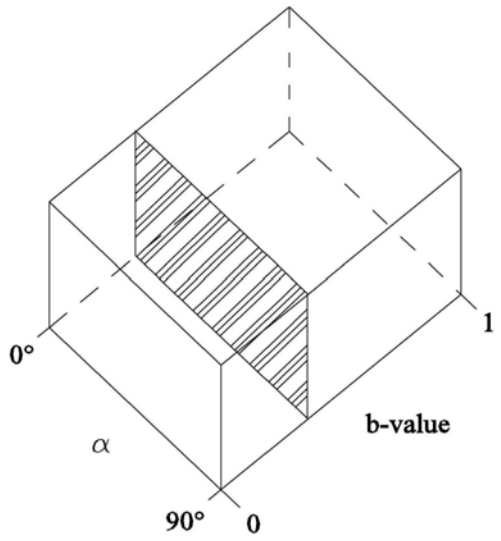

Figure 1-5: Plane strain Device Test Space

Previous investigations of granular soils using the HTSA have been conducted with the same inner and outer cell pressures. This condition minimizes the effects of stress concentrations. However, as shown in Figure 1-6, it greatly reduces the stress area that can be explored.

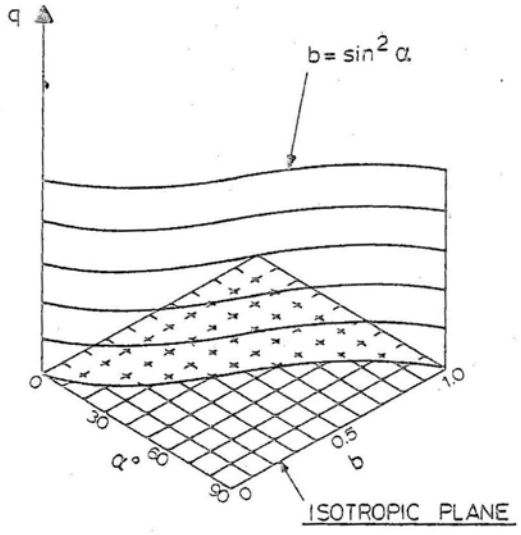

Figure 1-6: HTSA Test Space with $P_i = P_o$
After (Symes et al. 1982)

An in depth review of these devices is contained in Section 1.

1.4 Contribution

This investigation will contribute to geotechnical engineering in the following ways:

- The production of a detailed failure surface for a granular soil will provide a blueprint for fine tuning and verification of anisotropic constitutive models. This will lead to improved constitutive models resulting in increased accuracy for geotechnical and geostructural designs, more confident factor-of-safety(s), and more efficient designs.
- A fully-automated HTSA capable of independently controlling the inner and outer cell pressures was developed as part of this investigation.
- The HTSA was used to explore many different stress conditions, including those that theoretically result in stress concentrations.
- The effects of the intermediate principal stress and the HTSA boundary conditions on shear band orientation will be investigated. This effort will concentrate on especially low and high b-values.

1.5 Methodology

The stress-strain-strength behavior of a fully drained Nevada Sand was investigated through a series of 14 HTSA tests. The basic soil properties was determined by performing specific gravity, gradation, and relative density testing. The specimens was constructed at a constant void ratio using the dry pluviation method, which consists of free-falling sand grains into place from a predetermined and constant height. Each test specimen was fully saturated with de-aired water using the carbon dioxide method. The

specimens were sheared to failure following a predetermined stress path that maintains constant values of the mean normal effective stress (σ_{avg}), the intermediate principal stress ratio, and the principal stress direction.

1.6 Organization

This dissertation has been organized into the following eight chapters:

Chapter 1) Introduction – This chapter defines the purpose, originality, contribution, and methodology of this investigation.

Chapter 2) Literature Review – This chapter presents a discussion of soil anisotropy, previous studies into the effects of the intermediate principal stress and principal stress rotation, and the devices that have been created to investigate these parameters.

Chapter 3) Description of HTSA – A full description of the new HTSA is presented including: the physical dimensions, loading capability, stress control, and measurement capabilities.

Chapter 4) HTSA Theory – The general theory behind HTSA operation is presented. This chapter includes the derivation of calculations that were used to maintain constant α and b-values during shear testing.

Chapter 5) Test Program – The test plan is presented in this chapter, including the number of tests, target stress path, and target void ratio. A detailed test methodology and test corrections are also presented.

Chapter 6) Test Results from Series A – Results from testing that did not include the proper piston uplift correction factor are presented. The discussion of this testing is limited to stress-strain and strength behavior.

Chapter 7) Test Results from Series B – These tests were completed as planned. The test results are discussed in terms of stress-strain and volume change behavior, the failure surface, stress direction versus strain increment, and shear band formation.

Chapter 8) The conclusion.

2 LITERATURE REVIEW

2.1 Soil Anisotropy

2.1.1 History

The study of anisotropy, as it relates to particle mechanics, did not begin with soils. The earliest work utilized idealized particles, such as glass beads for three-dimensional studies, or steel rods to simulate two-dimensional plane strain conditions.

In their study titled, "Systematic Packing of Spheres with Particular Relation to Porosity and Permeability" Graton and Fraser (1935) investigated the packing and characteristic fabric of two-dimensional and three-dimensional particles, paving the way for Casagrande and Carillo (1944) to observe a correlation between anisotropy and soil strength.

Following this pioneering work, many studies were undertaken in the late 1960s and early 1970s aimed at characterizing the initial fabric of granular soils and studying the evolution of the internal fabric during shearing (Weindieck 1963, Parkin et al. 1968, Arthur and Menzies 1972, Oda 1972a, Oda 1972b, El-Sohby and Andrawes 1973).

2.1.2 Soil Fabric

To fully understand soil anisotropy, it is first necessary to quantify the internal soil fabric. The fabric of any cohesionless particle assembly has been defined as, "the spatial arrangement of solid particles and the associated voids" (Brewer 1964). This definition was later adopted by Oda (1972a) to describe the internal soil fabric.

Soil possesses either a homogeneous or heterogeneous fabric. A heterogeneous soil fabric is comprised of submasses of homogenous fabric having different kinds and degrees of configurations (Oda 1972a).

2.1.3 Fabric Tensor

Granular soils are comprised of an arrangement of generally non-spherical particles. Although the particle placement is seemingly random, it still has a characteristic statistical arrangement. The "fabric tensor" is used to quantify this statistical arrangement (Oda and Iwashita 1999).

The anisotropic fabric of a soil can be described by orientation and packing structure. Orientation is defined by the means length and inclination of a soil particle's major axis.

Assuming a cross-anisotropic soil, in which the horizontal contacts can be defined in a single plane, the soil's packing tensor is defined by the relationship between an individual soil particle and the contacts it forms with neighboring particles. This relationship is quantified by unit vectors introduced at each contact point to indicate the contact direction.

2.1.4 Types of Anisotropy (Inherent or Induced)

Casagrande and Carrillo (1944) identified two distinct types of anisotropy, defined as “inherent” or “induced”.

2.1.4.1 INHERENT ANISOTROPY

Inherent anisotropy refers to the anisotropic condition of the soil fabric prior to shearing; it is mainly attributable to the grain shape and orientation. Soils particles tend to align their long axis perpendicular to the application of force. Typically, the dominate force is gravity, and soil grains will be oriented with the long axis parallel to horizontal.

Gravity can even be the dominating force for some methods of mechanical compaction. For example, a cross-anisotropic soil structure is generally observed in sands compacted beneath a vibratory plate.

Inherent anisotropy is heavily dependent upon the shape and initial void ratio of the soil particles. Elongated particles show the greatest effect of inherent anisotropy. However, even spherical particles show the effects of inherent anisotropy.

Utilizing spherical glass beads instead of sand particles Haruyama (1981) demonstrated the effects of an initially anisotropic fabric. These tests were terminated at relatively low strains (i.e. 0.5 to 1.0 percent) and were not carried to failure.

Oda (1972) showed that for spherical particles with high relative densities, the inherent anisotropy has little effect upon the peak mobilized shear strength. However, for loose sands with low to medium levels of shear stress, researchers have reported that the soil fabric’s inherent anisotropic structure has a strong influence on deformation properties (Yamada and Ishihara 1979).

2.1.4.2 INDUCED ANISOTROPY

Induced anisotropy results from the evolution of a soils microstructure during shearing, regardless of the initial particle and contact arrangement. Researchers suggested that the soil fabric continuously changes during the shearing process, causing contacts to be created in the direction of applied stress and destroyed in the direction perpendicular to the applied stress. This can be partially attributed to sliding, which causes a change in the packing structure of the soil. However, much of the change must come from particle rotation and redistribution (e.g. dilatancy).

In general terms, contact points with normals that coincide with the major principal strain axis are created, while those with normals perpendicular to the major axis are lost (Oda and Iwashita 1999).

Oda (1972b) suggested that because the soil fabric is constantly changing and reorienting itself, it is unlikely that induced anisotropy has a significant effect on the internal friction angle of the soil, presumably due to the evolution that accompanies the relatively large strain the soil is subjected to during shearing.

Subsequent torsional shear testing on medium-loose Ham River Sand has shown that for a given loading direction, the friction angle is relatively unaffected by previous stress rotation (Symes et al. 1984), providing confirmation of Oda's theory with respect to peak shear strength. However, the induced anisotropy does have a significant effect on the *strain* required to achieve a given stress ratio (Arthur et al. 1977a).

2.2 Triaxial and Plane Strain Device Anisotropy Investigations

2.2.1.1 THREE DIMENSIONAL EFFECTS

As early as 1963 it had been shown that some foundation failures occur under plane strain conditions (Leussnik and Wittke 1963). Because of this, many researchers (Bjerrum et al. 1961, Cornforth 1964, Tong 1970, Lee 1970) investigated the differences between plane strain and triaxial tests of granular materials and they began to notice differences in soil behavior. In general when comparing the results of triaxial tests with plane strain tests the authors made the following conclusions (Oda et al. 1978):

- For a dense sand at low confining pressure, the plane strain friction angle is usually 10 to 20 percent greater than that measured by the triaxial compression test. However, no significant difference between the two friction angles is observed in loose sands, or when dense sands are tested at sufficiently high confining pressures.
- For a given void ratio, the strain to failure is less in a plane strain condition than it is in a triaxial condition.
- Sand dilates more extensively in triaxial compression than it does in a plane strain test.

2.2.1.2 PRINCIPAL STRESS INCLINATION

Arthur and Menzies (1972) performed drained triaxial testing of specimens constructed at various bedding plane angles by using a tilt box, and found that peak strengths decreased as the major principal stress became coincident with the bedding plane.

At about the same time, Ode (1972a) performed drained triaxial tests on soil particles of differing shapes and initial void ratios at principal stress inclinations of 0°, 30°, 60° and 90°. The two different soil types were denoted as Type "D", which had very spherical grains and no statistical preferential orientation of the long axis, and Type "B", which was composed of long flat grains which were highly aligned with each other.

The early to mid stage deformation characteristics were evaluated by calculating the secant modulus at 50 percent of the soil's ultimate shear strength. The relationship between the secant modulus and the void ratio is shown in Figure 2-1 and Figure 2-2.

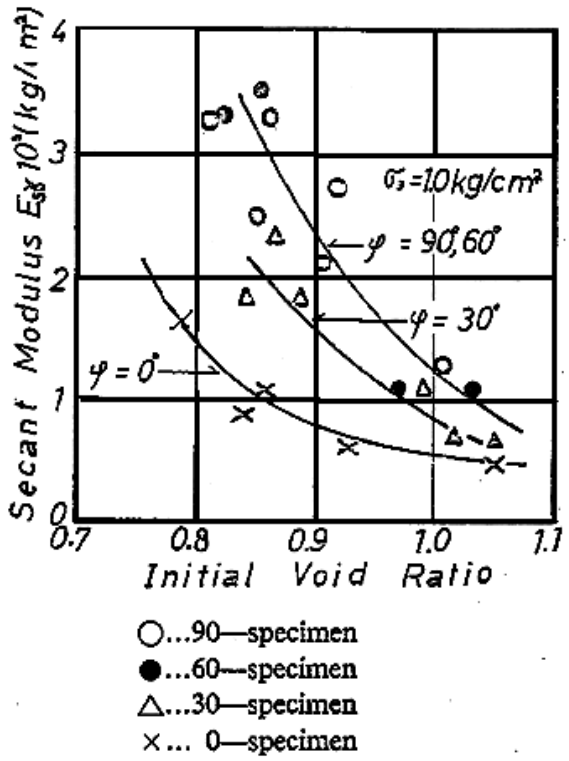

Figure 2-1: Secant Modulus versus Void Ratio Soil "D"
After (Oda 1972a)

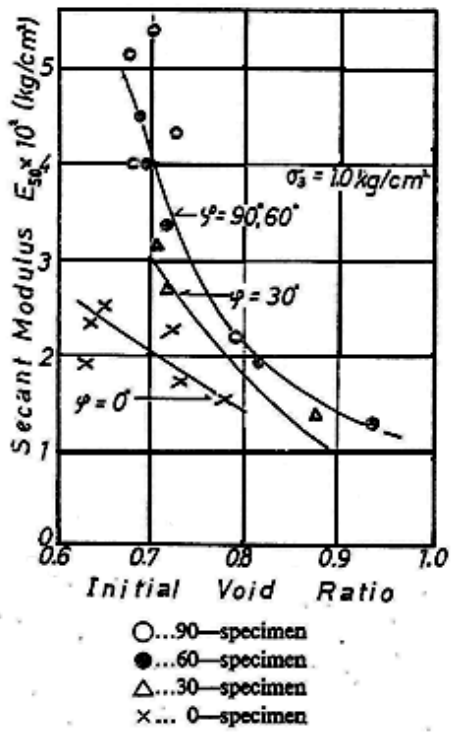

Figure 2-2: Secant Modulus versus Void Ratio Soil "B"
After (Oda 1972a)

At each void ratio, a unique relationship was noticed between the secant modulus and the tilt angle[1] (90° - α). As the principal stress direction begins to align with long axis of the soil grains, the secant deformation modulus decreases by a factor of about 3. This was initially thought to be caused by the soil particles orientation. However, the same general trend was observed for both spherical and elongated particles, making it reasonable to surmise that the packing of the particles, not the shape determines the deformation behavior at early stages of shearing (Oda 1972a).

[1] Note that the angle (δ) represents the angle made between the long axis of the grain and the principal stress. Therefore, principal stress perpendicular to the long axis will have an angle (δ) equal to 90° which is the same as an α = 0° condition.

The effects of principal stress inclination were also investigated using plane strain devices. In comparison to the triaxial tests, the plane strain tests indicate a more pronounced decrease in the mobilized stress ratio (σ_1 / σ_3) as the principal stress rotates from perpendicular to parallel to the long axis of the granular particles. Of special note is the fact the lowest stress ratio tends to occur when the bedding plane is nearly coincident with direction of shear bands. This is illustrated in Figure 2-3 at a tilt angle of around 30 degrees.

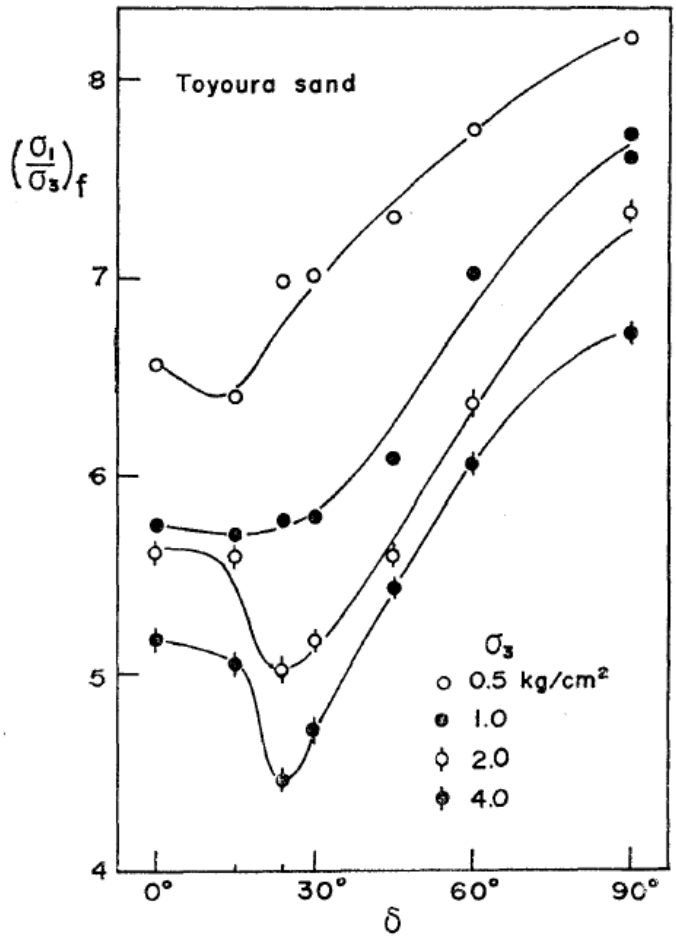

Figure 2-3: Effect of Tilting Angle on Stress Ratio at Failure in Plane Strain After (Oda et al. 1978)

The early triaxial investigations showed only a slight reduction in mobilized stress ratio as the principal stress direction approaches horizontal. Figure 2-4 shows test results from a series of triaxial compression tests performed on specimens having inclined bedding planes in triaxial compression tests. In comparison to plane strain testing, the effects of anisotropy appear to be less pronounced in triaxial tests. However, it is evident that the stress-strain-strength behavior of granular soils is affected by anisotropy at a b = 0 condition.

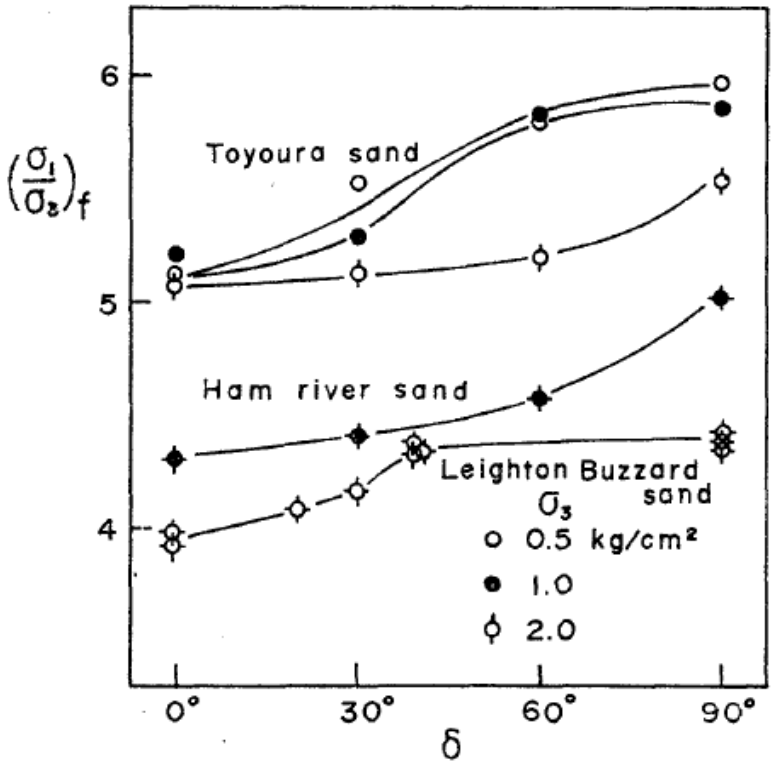

Figure 2-4: Effect of Tilting Angle on SR at Failure in Triaxial Compression After (Oda et al. 1978)

The test results show a trend of steadily decreasing strength as the major principal stress comes into alignment with the bedding plane. However, no drop in strength was observed at the condition in which the plane of shear banding was aligned with the

bedding plane (i.e. $\delta \approx 30°$), and the pattern of strength reduction was somewhat erratic. The erratic behavior may be a product of stress non-uniformity and bending moments that are inherent in the testing of inclined specimens.

Ochiai and Lade (1983) investigated the effects of fabric anisotropy by performing triaxial compression tests on specimens of sand with bedding planes parallel and perpendicular to the major principal stress. For the test results shown in Figure 2-5, the difference in peak shear strength was 0.5 degrees for high confining pressure (4 kg/cm^2) and 2 degrees for low confining pressure (0.5 kg/cm^2).

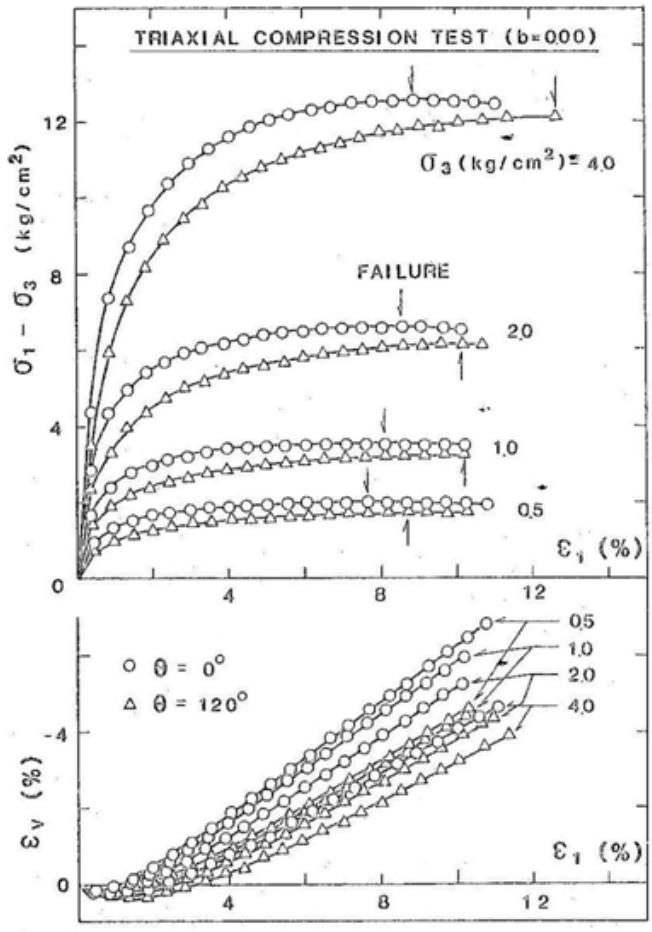

Figure 2-5: Stress Strain and Volume Change in Triaxial Compression After (Ochiai and Lade 1983)

The observed difference in behavior between the triaxial compression and plane strain conditions was attributed to the fabric reconstruction process. It was suggested that for soils subjected to triaxial conditions ($\sigma_2 = \sigma_3$) the grains may be relatively easily reoriented, while for plane strain conditions, it becomes difficult for grains to orient themselves and the effects of inherent anisotropy are more pronounced (Oda 1972b).

2.3 Development of New Testing Devices

Three-dimensional and anisotropic effects were partially evident when comparing triaxial compression, triaxial extension, and plane strain test results. However, these devices were not specifically designed to investigate these topics.

As the importance of the three-dimensional and anisotropic effects was realized, it became apparent that a new generation testing devices would be beneficial. Many researchers developed cubical devices capable of independent principal stress control to study three-dimensional effects on drained specimens of sand (Ko and Scott 1967, Sutherland and Mesdary 1969, Green and Bishop 1969, Hambly 1969, Procter and Barden 1969, Lade and Duncan 1973, Ramamurthy and Rawat 1973, Matsuoka and Nakai 1974, Arthur et al. 1977b, Yamada and Ishihara 1979, Ochiai and Lade 1983, Ergun 1981, Wang and Lade 2001).

At about the same time, Hollow Torsional Shear Apparatus (HTSA) devices were being developed to evaluate the effects of anisotropy through the study of principal stress inclination and rotation.

The new devices greatly expanded the area of stress space that could be studied. Symes et al. (1982) illustrated the stress space that could be investigated with a conventional or true triaxial test apparatus in Figure 2-6. Conventional triaxial testing is limited to two axes (C-C' for compression and E-E' for extension), but by using a cubical specimen and a true triaxial device the planes C-C'/D-D' and F-F'/E-E' can also be covered.

With an HTSA the entire stress space can be covered. It should be noted that stress rotation is restricted to one plane, and if the inner and outer pressures are equal, HTSA testing is confined to the ribbon ($b = \sin^2 \alpha$) shown in Figure 2-7.

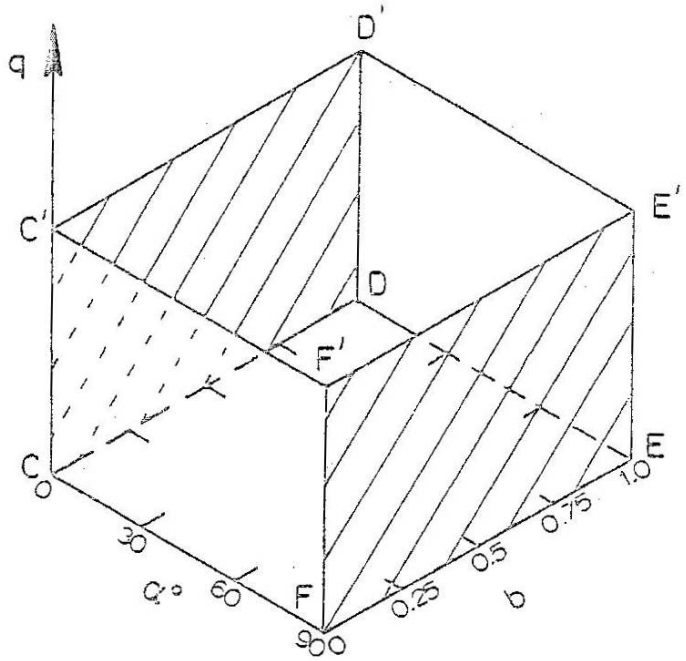

Figure 2-6: True Triaxial Test Apparatus Test Space
After (Symes et al. 1982)

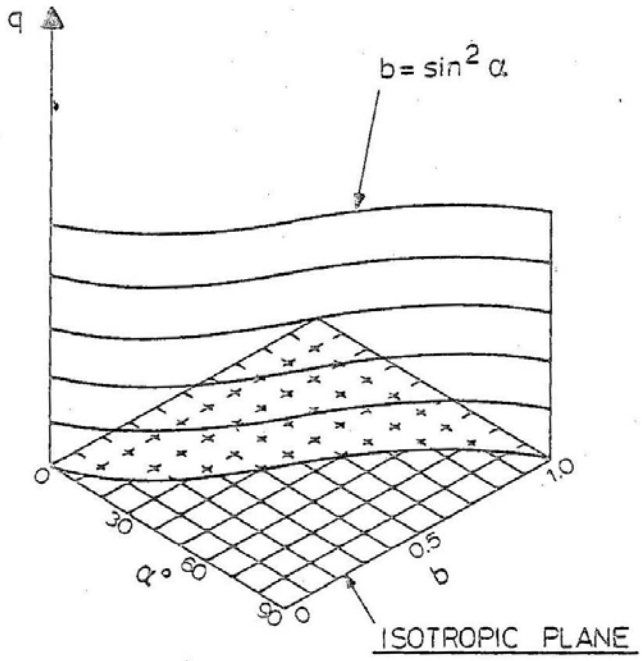

Figure 2-7: HTSA Test Space with $P_i = P_o$
After (Symes et al. 1982)

2.3.1 Cubical Apparatus

Cubical apparatuses were created to observe soil behavior under generalized stress conditions. In any study of generalized stress conditions, it must be possible to accurately vary the magnitudes of the principal stresses. The cubical shape allows for application of uniform shear and normal stresses at the specimen boundaries (Arthur 1986).

There are several types of cubical devices, such as the directional shear apparatus and the true-triaxial device. Due to the importance of plane strain analyses, plane strain devices have been developed as well.

For the proper design of any cubical apparatus, the device must be capable of accommodating large enough strains to produce failure while minimizing the development of non-uniform stresses. It is equally important that the device not impart any unintended shear forces to the specimen (Lade 1978).

It is also beneficial to keep the specimen preparation method relatively simple, avoid interference between the devices that apply principal stresses, and maintain an overall low level of friction so that correction factors are kept to a minimum.

Boundary conditions for cubical devices can be flexible, rigid, or a combination of both types. Although several different types of cubical devices exist, incremental design improvements have generally focused on minimizing or quantifying the effects of boundary / specimen interaction.

2.3.1.1 APPARATUS BOUNDARY TYPE

2.3.1.1.1 Rigid Boundary

Rigid boundary devices that apply uniform stresses on all sides of a cubical specimen using rigid platens have been designed by Goldscheider and Gudehus (1973), Matsuoka and Ishizaki (1981), and Hambly (1969).

When designed correctly, rigid boundary devices have the advantage of applying uniform stresses to the cubical specimen. It is also relatively easy to measure principal strains and normal stresses. Side friction, which can impart undesired shear stresses can be alleviated by applying a layer of grease and an additional latex membrane to the loading platens.

Constructing a rigid boundary cubical device can be challenging and expensive. The design must be interlocking, and capable of performing complex movements, such as Hambly's design (1969), or as is often the case, a gap must be left around the edge of the plates to allow movement. Any such gap will result in areas of non-uniform stresses and strains.

Additionally, the presence of stiff platens on all six sides of the specimen prevents the natural development of shear bands, which initiates failure in the hardening regime of specimens subjected to intermediate stress ratios between 0.18 and 0.85 (Lade and Wang 2001).

Matsuoka and Ishizaki (1981) designed a true triaxial device, shown in Figure 2-16, that is capable of independently controlling all three principal normal stresses. Spacing between the rigid plates was selected based on a pre-test analysis of the expected deformations.

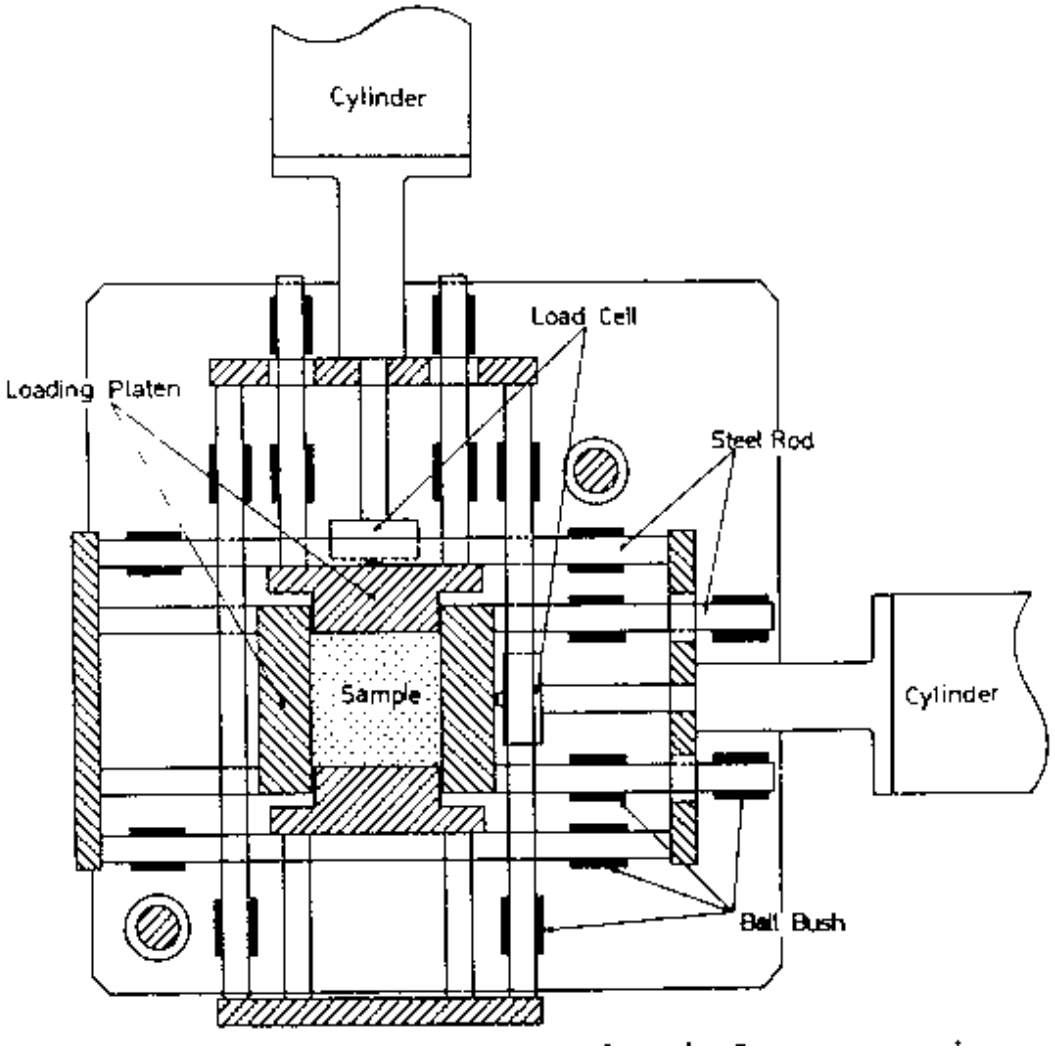

Figure 2-8: Rigid Boundary Device
After (Matsuoka and Ishizaki 1981)

2.3.1.1.2 Flexible Boundary

Cubical devices utilizing either three flexible boundaries, or two flexible boundaries and cell pressure were originally developed to investigate the effects of the intermediate principal stress (Ko and Scott 1967, Lomize, et al. 1969, Arthur and Menzies 1972).

Ko and Scott (1967) introduced the first true triaxial device which consisted of a cubical specimen surrounded by six flexible membranes. They compared the results of their testing to conventional triaxial testing, but did not find good agreement.

This was probably due to interference between the membranes at the edges of the specimen; the authors constructed a thin aluminum frame to help alleviate this problem. As it turned out, the rigid frame ended up carrying a significant portion of the load leading to the development of non-uniform stress distribution within the specimen (Green 1967, Arthur and Menzies 1972).

Although the design of their test apparatus was somewhat flawed, Ko and Scott (1967) devised an ingenious solution to the problem of automated stress control. Prior to the widespread use of computer control systems, maintaining desired stress paths was difficult. Ko and Scott constructed a mechanical hydraulic analogue of an octahedral plane, so that the mean normal stress stayed constant during testing.

The device consisted of a triangular plate with 3 hydraulic cylinders supporting each corner. A load was applied to the top of the plate, and as that load was moved around the plate, the magnitudes of stress in each hydraulic cylinder line changed. However, the sum of all three pressures remained constant. In this way, pressures could be changed in a simultaneous and smooth manner.

Subsequent to the efforts of Ko and Scott, Arthur and Menzies (1972) introduced a new apparatus, that applied stress to a cubical soil specimen by using a system of water filled pressurized rubber bags. Like their predecessors, they also used metallic vanes to keep the pressurized bags separated. However, through an iterative process, they made

several improvements on their vane system which greatly reduced errors associated with this portion of the test apparatus.

Their testing program consisted of performing drained triaxial compression tests on Leighton Buzzard Sand. The specimens were prepared using a combination of air pluviation and a specially designed tilt box, so that the principal stress direction with respect to the bedding plane could be changed for each test.

2.3.1.1.3 Combined Boundary

A third type of cubical device was designed, using a combination of rigid platens, fluid filled pressure bladders, and cell pressure to apply stresses to the specimen (Green 1967, Procter and Barden 1969, Sutherland and Mesdary 1969, Lade and Duncan 1973, Ramamurthy and Rawat 1973, Arthur et al. 1977a).

Ramamurthy and Rawat (1973) developed a device to study effects of the intermediate principal stress. The new apparatus applied vertical stress via rigid platens to a 7.6 cm^3 specimen. Flexible rubber membranes were used for horizontal stress application. Sponge prismatic lateral reinforcing elements were used to minimize interference between the horizontal membranes.

The first cubical device capable of applying smooth and continuous stress rotation was designed and constructed by Arthur et al. (1977). This apparatus applied normal and shear stress to four of the six cubical sides. The other two sides were comprised of fixed plates, making this device a type of plane strain apparatus.

The normal force was applied to the specimen via laterally reinforced pressure membranes. Multiple rubber bands glued to the sides of the specimen membrane were used to apply shear stress to the specimen. The shear stress was transmitted from the membrane to the specimen by gluing grains of sand to the membrane prior to forming the specimen.

This new apparatus was used to investigate the effects of induced anisotropy. Cross-anisotropic specimens were formed by air pluviation parallel to the direction of intermediate principal stress. This created a specimen that was isotropic in the major and minor principal stress plane.

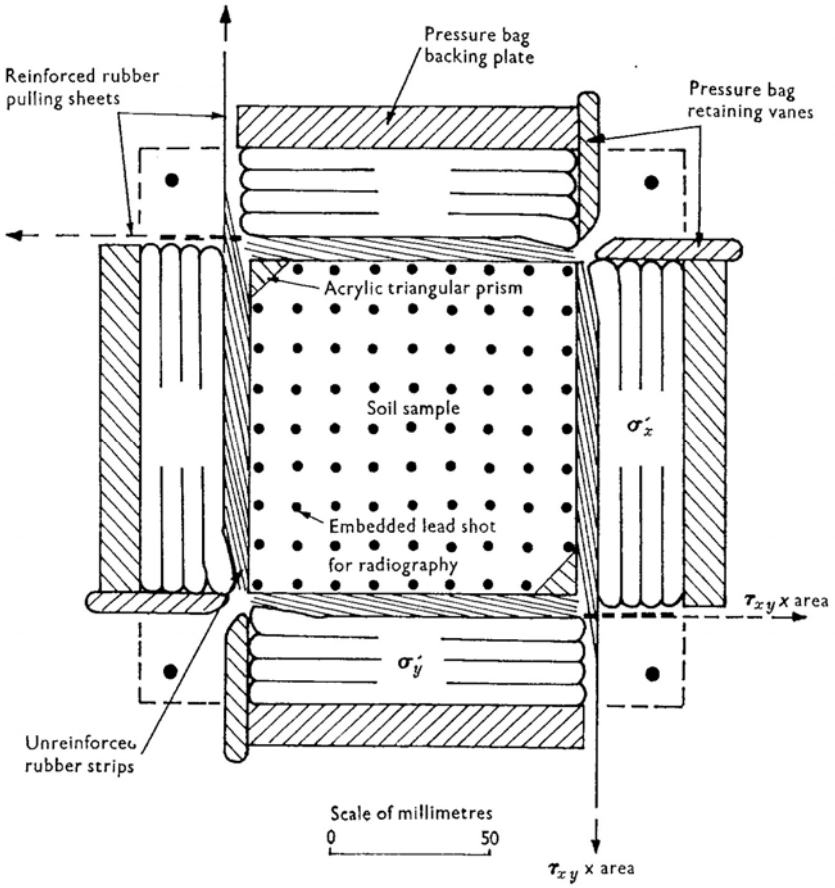

Figure 2-9: Combined Boundary Device
After (Arthur et al. 1977a)

Green and Bishop (1969) introduced their Independent Stress Control (ISC) apparatus. This device reduced some of the stress concentrations and non-uniformities of its predecessors by maintaining a small gap between the axial and lateral plates during shearing.

Test results from the ISC apparatus and traditional triaxial testing were in good agreement for compression testing. However, in extension the ISC showed an increase of 4.9 degrees, while the traditional testing showed an increase of only 2 degrees. The direct comparison of these two extension tests is somewhat in error. The ISC test was performed at b = 1 in Sector I, while the triaxial test was performed at b = 1 in Sector III. Due to the effects of anisotropy test results from Sector III are expected to be somewhat lower than those observed in Sector I.

In an effort to reduce frictional effects, lubricated rubber membranes were attached to the rigid platens of the ISC device. The effectiveness of this technique was evaluated by comparing the gain in peak friction angle from triaxial compression to ISC extension with the gain in peak friction angle from triaxial compression to true cubical extension.

The authors found that the both the ISC and true cubical extension tests had the same 4.9° increase over triaxial compression tests. They concluded that this was proof that the rigid boundary condition and associated friction from the platens had little effect on test results.

However, the true cubical device extension tests were performed in Sector III, while the ISC extension tests were performed in Sector I. Due to the effects of anisotropy, the difference in strength between the triaxial compression and the ISC extension tests should have been greater than the difference in strength between the triaxial compression and true cubical device extension tests.

2.3.2 Hollow Torsional Cylinder Apparatus

As shown in Figure 2-10, a hollow torsional shear apparatus (HTSA) is capable of applying independently controlled axial force (W), torque (T), and inside and outside fluid pressures (P_i and P_o) to a hollow cylinder of soil. These forces combine to apply vertical (σ_z) and shear ($\tau_{z\theta}$) stresses to the top and bottom of the specimen through stiff frictional end platens and radial (σ_r) and tangential (σ_θ) stresses to the vertical sides of the specimen through flexible membranes. Control of these stresses allows any combination of principal stresses and principal stress rotation to be applied to the specimen.

The vertical deformation and rotation of the specimen, as well as the inner cell and specimen volume changes, are used to calculate the volumetric, vertical, radial, and tangential strains.

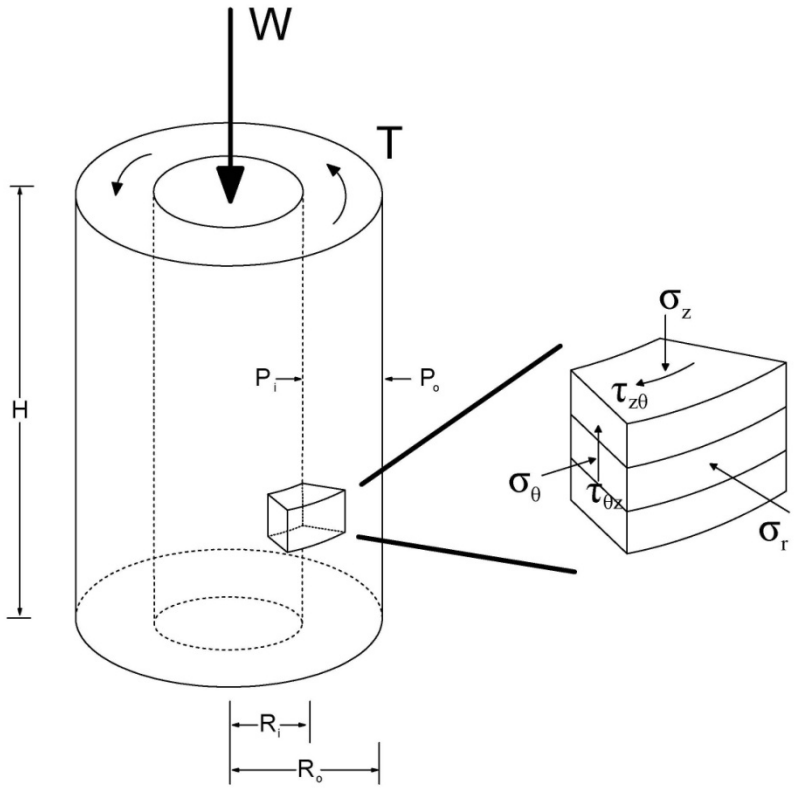

Figure 2-10: HTSA Forces and Stresses

2.3.2.1 DEVELOPMENTS OF THE HOLLOW TORSIONAL CYLINDER APPARATUS

The Hollow Torsional Cylinder Apparatus (HTSA), as we know it today, is the culmination of incremental improvements over a lengthy period of time. Some of the earliest precursors to the modern device were not even devised for soil testing.

Hollow cylinders, subjected to both axial force and torque were used by Taylor and Quinney (1931) and Goode and Helmy (1967), to investigate the relationship between distortion and stress distribution in metals and concrete respectively. Taylor and Quinney also presented a methodology for analyzing the stress and strains in a thin walled cylinder subjected to combined loading.

One of the earliest investigations utilizing a hollow cylinder of soil was performed by Cooling and Smith (1936). After realizing direct shear specimens are subjected to non-uniform stress distribution along the shearing plane, they developed a hollow torsional shear apparatus for testing a puck like hollow cylinder of clay. Their test methods did not utilize confining pressure or vertical pressure, and the specimens were not constrained by membranes.

Haythornthwaite (1960) developed an HTSA capable of applying rotational, inner, outer, and axial stresses to a hollow cylindrical specimen. He plotted his HTSA test results in an octahedral plane, shown in Figure 2-11, a method that would be used in many subsequent investigations.

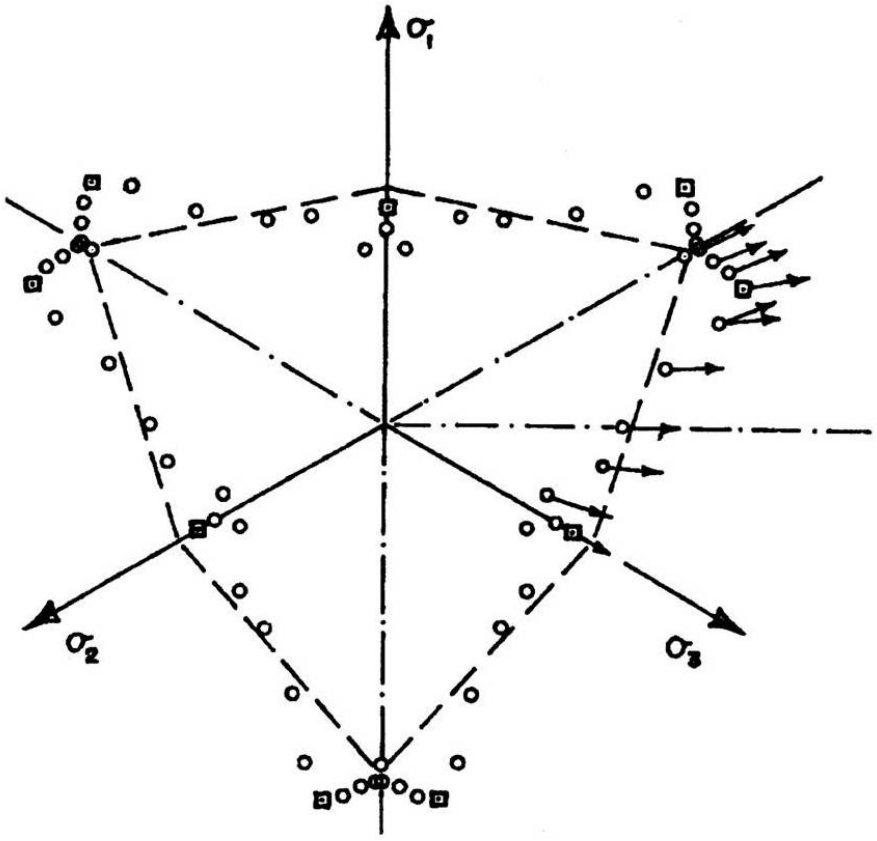

Figure 2-11: Test Results Plotted in an Octahedral Plane

After (Haythornthwaite 1960)

Broms and Casbarian (1965) were among the first to develop an HTSA capable of applying independently controlled inner and outer pressure to the specimen's vertical boundaries[2]. This attribute made possible their investigation into the effects of principal stress axes rotation and the influence of the intermediate principal stress. Their investigation included three series of tests on remolded specimens of Kaolinite Clay.

Saada and Baah's investigation of clay anisotropy (1967) was the first published study that used torsion as a principal means of creating stress. The data from their investigation was used by Saada and Zamani (1969) to validate one of the first anisotropic models for clay.

Height et al. (1983) presented a thorough discussion of design and operational principles for a new HTSA. Methods for determining the average stresses and strains within the specimen were presented, as well as calculated stress non-uniformities due to both curvature and end restraint.

Although the equations proposed by Height et al. (1983) are frequently used, many other methods have been developed for calculating radial and tangential stresses in an HTSA:

Frydman *et al.* (1973) assumed:

- A linear variation of radial stress across the wall
- Equilibrium between the radial and tangential stresses at any radius
- Stresses are defined at the mean radius

[2] It is unclear if Haythornthwaite's device was capable of independent control of the inner and outer cell pressure.

Hight *et al.* (1983) assumed:

- Linear elasticity
- Equilibrium between the radial and tangential stresses at any radius
- Stresses are averaged without weighting for the radius

Miura *et al.* (1986) assumed:

- Linear elasticity
- Equilibrium between the radial and tangential stresses at any radius
- Stresses are averaged with weighting for the radius

Symes et al. (1982) isolated the effects of b and α in three-dimensional space by using an HTSA to conduct drained testing on specimens of Ham River Sand. Only limited regions of stress space were explored, but those test results indicated that an HTSA is capable of testing with generalized stresses and directions.

In 1990 Vaid et al. introduced a new hollow torsional shear apparatus and a new method for calculating average stresses based on averaging over the entire volume of the specimen, rather than across the wall of the specimen. He also assuming a plastic constitutive law for evaluating the shear stress rather than assuming linear elasticity, which led to a revised domain of stress space that can be explored with the HTSA

Several investigations have compared the results of traditional test methods with HTSA tests. For similar stress states, HTSA test results have shown good agreement with plane strain testing (Fukushima and Tatsuoka 1982, Tatsuoka et al. 1986).

In the 1970s, researchers discovered that hollow cylindrical specimens could present unique opportunities for advancement in the area of soil dynamics. The later addition of a resonant column testing capability made the HTSA a preferred device for dynamic properties testing. By adding resonant column capability to an HTSA, testing could be performed over the full range of shear strain amplitude required for a dynamic analysis.

This constituted a major improvement over the previous method of performing tests on two specimens, which is not ideal because each specimen may have slightly different properties. With the combined device researchers were able to perform small strain high frequency and high strain low frequency testing on a single specimen (Allen and Stokoe 1982, Alarcon, et al. 1986, d'Onofrio et al. 1999).

Dynamic testing accuracy was improved by the ability to measure very small strains using an HTSA outfitted with a layered series of proximity transducers (Ampadu and Tatsuoka 1993).

The HTSA has been used to investigate the cyclic response of sands by Ishibashi and Sherif (1974), Yang et al. (2007) and many others. Cyclic testing using an HTSA rather than a triaxial cell has the advantage of allowing testing between principal stress angles of 45 and -45 degrees. In this way the effects of soil anisotropy are accounted for, which is not the case when comparing the results of compression and extension testing (Georgiannou and Tsomokos 2008).

The continued development of closed loop feedback computer controlled systems for HTSA testing has enabled complex stress paths to be followed with reliability (Shibuya 1988, Yoshimine, et al. 1999, Serra and Hooker 2003, and O'Kelly and Naughton 2009).

In recent years, many HTSAs have been developed with or retrofitted with hardware based controllers to regulate instrumentation and transducers. This advance allowed transducer control to be performed externally, freeing computational power for data collection and stress path calculation (Serra and Hooker 2003).

Many researchers have evaluated the drained and undrained effects of the initial stress state and the stress path on the stress-strain-strength response of sands during monotonic or cyclic loading.

2.3.2.2 STRESS CONCENTRATIONS

Several researchers have raised concerns regarding the development of non-uniform stresses and strains in HTSA specimens. Stress concentrations due to end effects, curvature, and differential cell pressures have been investigated experimentally, theoretically and by numerical simulation.

The effects of curvature and differential cell pressures have resulted in the recommendation of "No Test" areas for the HTSA that are typically located in two corners $b = 1$, $\alpha = 0°$ and $b = 0$, $\alpha = 90°$ (Hight et al. 1983, Sayao and Vaid 1991, Vaid et al. 1990). Due in part to concerns regarding non-uniform stress concentrations and in part to the inherent difficulty in conducting such a test, many of the early HTSA investigations maintained the same inner and outer cell pressures.

Although, the HTSA used in the current test program was designed to minimize the effects of non-uniformity by accommodating a slender thin-walled specimen with a large outer radius, Non-uniformities can still develop due to the application of torque, differences in inner and outer cell pressure, or axial strain with no associated volume change (Sayao and Vaid 1991, Gens and Potts 1984).

Lade (1975) asserted that considerable non-uniformity may be encountered for sands that dilate, and therefore, the results of HTSA testing alone are not useful for determining fundamental soil properties.

In a State of the Art paper, Saada (1988) recommended against using different inner and outer pressures due to the development of non-uniform normal stresses across the specimen. Saada stated that investigation into the effects of the intermediate principal stress should be performed with a cubical apparatus rather than an HTSA due to these undesired stress concentrations.

2.3.2.2.1 Stress Non-uniformity Due to End Restraint

Radial frictional forces develop at the end platens any time there is an axial strain at a constant volume. These forces can cause circumferential normal forces, bending moments, and rotation of the principal stress directions out of the plane of the cylinder wall. However, it is generally believed that these effects reduce rapidly with distance from the end platens.

During drained torsion shear testing of cohesionless soils, Lade (1975) noted that the distribution of the tangential stress was very likely non-uniform due to the restraint provided by the end platens, as evidenced by increases in the vertical or radial

deformations due to changes in tangential stress. However, the apparatus used for these tests had a height to diameter (H:D) ratio of only 0.25.

Lade theorized that stresses and strains within an HTSA specimen could be evaluated near the middle of the specimen with greater H:D values. In this way, the bottom and top of the specimen will serve as pseudo-boundaries allowing the middle of the specimen to maintain uniform strains without the addition of unintended stresses.

Parametric analyses evaluating the effects of end restraint on the average tangential stress have indicated that specimens with H:D ratios of about 2 were not significantly affected (Lade 1981, Fukushima and Tatsuoka 1982). However, end restraints significantly affected test results for specimens with H:D ratios less than 1.0.

Finite element modeling (FEM) has been employed to evaluate non-uniformities using both elastic and plastic analyses[3]. A minimum H:D ratio of 1.0 was recommended based on FEM studies (Hight et al. 1983). Saada and Townsend (1981) suggested a theoretical minimum specimen height, as shown in Equation (2.1), based on the assumption of linear elasticity. While Vaid et al. (1990) recommended a ratio of specimen length to outer diameter in the range of 1.8 to 2.2.

[3] Strain-hardening Modified Cam-Clay model

$$h \geq 5.44\sqrt{r_o^2 - r_i^2}\ for\ \frac{r_i}{r_o} \geq 0.65 \quad (2.1)$$

Where:

h = specimen height

r_o = outer radius

r_i = outer radius

2.3.2.2.2 Stress Non-Uniformity Due to Curvature

Either torque application or differential inner and outer cell pressures can cause stress non-uniformities in hollow cylindrical specimens.

Hight et al. (1983) based the vertical ($\bar{\sigma}_z$) and tangential ($\bar{\sigma}_\theta$) stress formulations on equilibrium. However, linear elasticity was assumed for the radial ($\bar{\sigma}_r$) and shear ($\bar{\tau}_{\theta z}$) stresses.

Two parameters were proposed to quantify the magnitude of stress non-uniformity. β_1, as shown in Equation (2.2), quantifies the difference between the calculated and real average stress.

$$\beta_1 = \frac{|\bar{\sigma}^* - \bar{\sigma}|}{\sigma_L} \quad (2.2)$$

Where:

$\bar{\sigma}^*$ = real average stress

σ_L = measure of stress level

$\bar{\sigma}$ = calculated average stress

The level of stress non-uniformity is quantified by Equation (2.3). The parameter β_3 describes the absolute value of the difference between the stress distribution and the real average, as shown in Figure 2-12.

$$\beta_3 = \frac{\int_a^b |\sigma(r) - \bar{\sigma}^*| dr}{(b-a)\sigma_L} \quad (2.3)$$

Where:

$\sigma(r)$ = real average stress

a = inner radius

b = outer radius

The parameters are normalized by the stress level σ_L. For pressure differences across the specimen wall, σ_L is described by Equation (2.4).

$$\sigma_L = \frac{\bar{\sigma}_\theta + \bar{\sigma}_r}{2} \quad (2.4)$$

Where:

$\bar{\sigma}_\theta$ = average tangential stress

$\bar{\sigma}_r$ = average radial stress

For calculating shear stress non-uniformity parameters, the stress level is equal to the average shear stress ($\bar{\tau}_{\theta z}$).

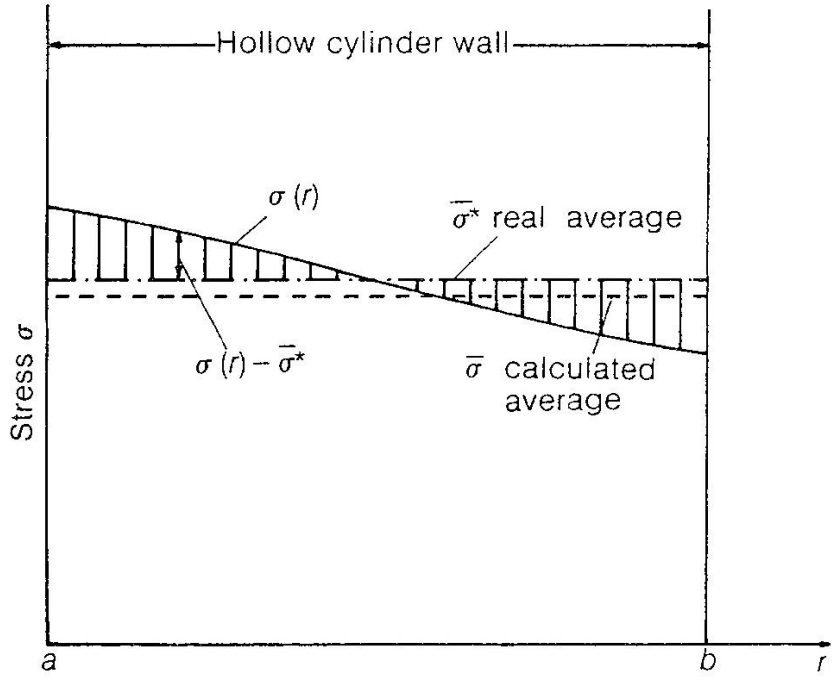

Figure 2-12: Stress Distribution Across HTSA Specimen After (Hight et al. 1983)

Assuming the average radial stress is determined using linear elasticity and the average tangential stress is calculated assuming equilibrium, β_1 is equal to 0. The parameter β_3 is dependent on the specimen geometry. Figure 2-13 shows the value of β_3 that is calculated for different ratios of inner to outer specimen radius, and for different stress conditions as described by the ratio between the radial and tangential stresses.

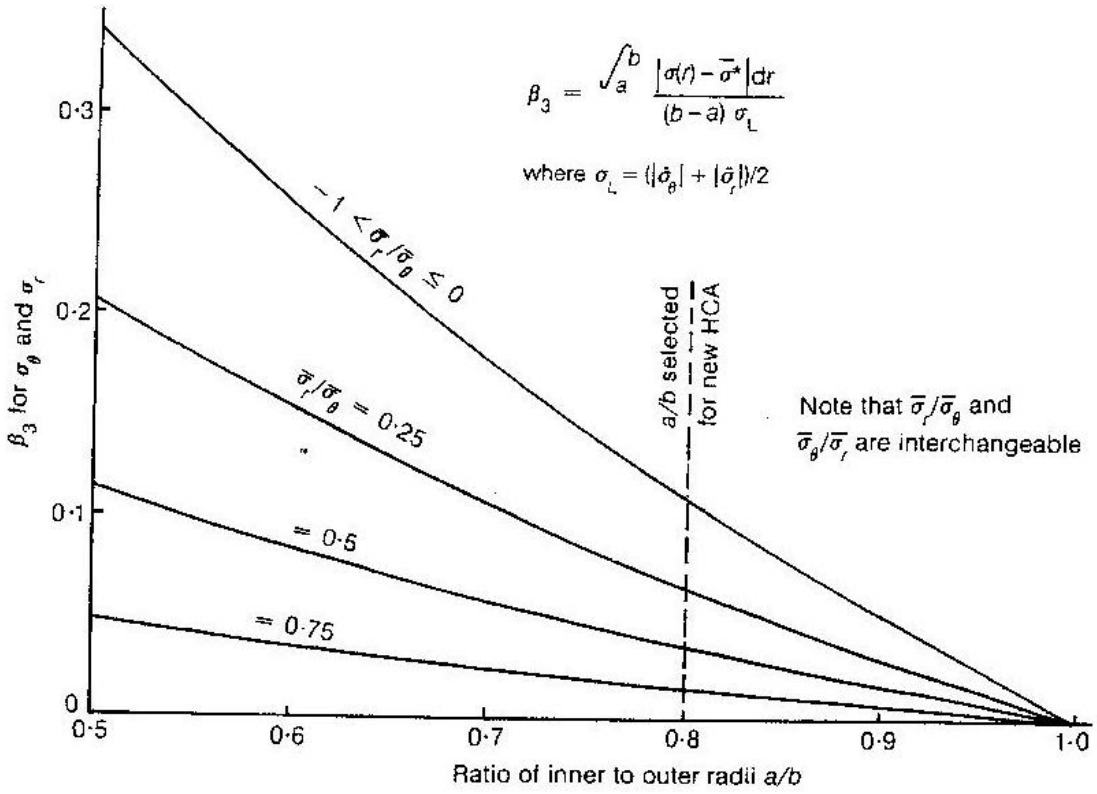

Figure 2-13: Variation in Stress Non-Uniformity with Geometry and Stress Path After (Hight et al. 1983)

Figure 2-14 shows the variation in both shear stress accuracy β_1, and non-uniformity β_3 with respect to the specimen geometry.

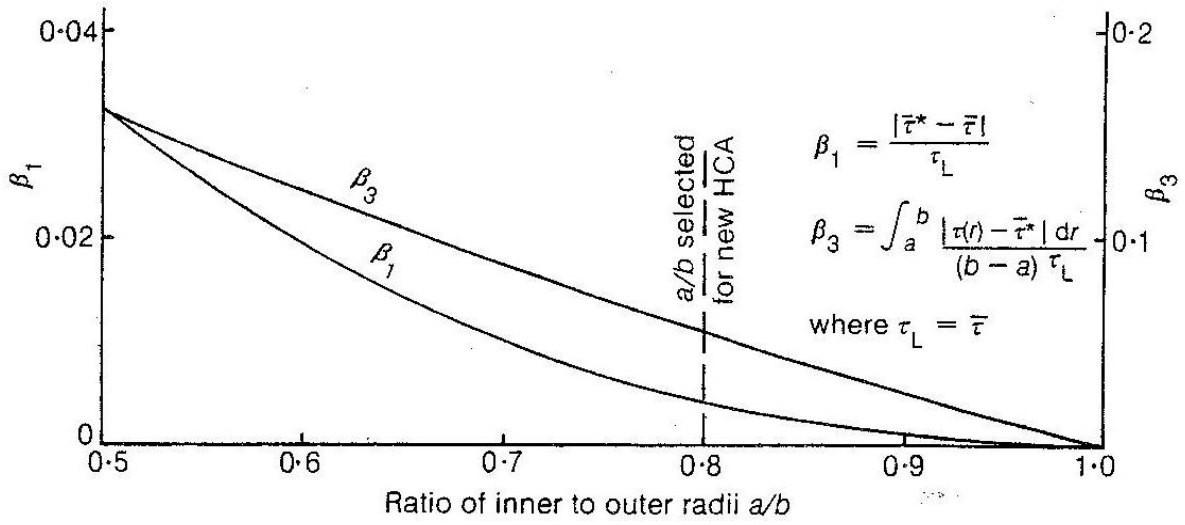

Figure 2-14: Variation in Shear Stress Non-Uniformity and Accuracy With Geometry After (Hight et al. 1983)

Vaid et al. (1990) proposed an alternate index for evaluating stress non-uniformity that is based on the stress ratio (R). The non-uniformity coefficient is expressed in Equation (2.5), and is considered acceptable if $\beta_r < 0.2$, which corresponds to a 10% difference across the specimen wall.

$$\beta_r = \frac{R_{max} - R_{min}}{R_{avg}} \tag{2.5}$$

Where:

β_r = Non-uniformity coefficient

R_{max} = Maximum stress ratio

R_{min} = Minimum stress ratio

R_{avg} = Average stress ratio

Vaid et al. (1990) noted that Hight et al. (1983) assumed linear elasticity for radial and tangential stress distribution, but then assumed a uniform stress distribution for shear stress. In an effort to stay consistent, Vaid assumed a linearly elastic distribution of shear stress as well. This assumption resulted in the formation of a high concentration of stress non-uniformity along the $\alpha = 45°$ ridge, as shown in Figure 2-15.

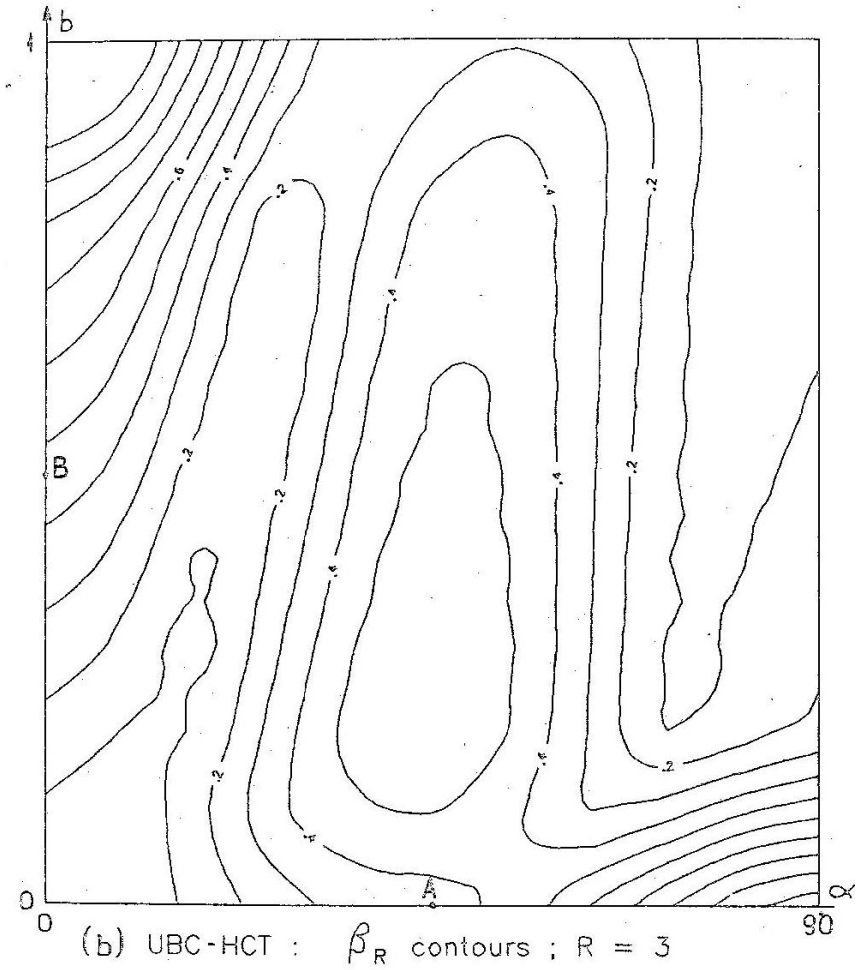

Figure 2-15: Non-uniformity Coefficient (β_R) at Stress Ratio of 3 After (Vaid et al. 1990)

This ridge was not present in Hight's method, shown in Figure 2-16.

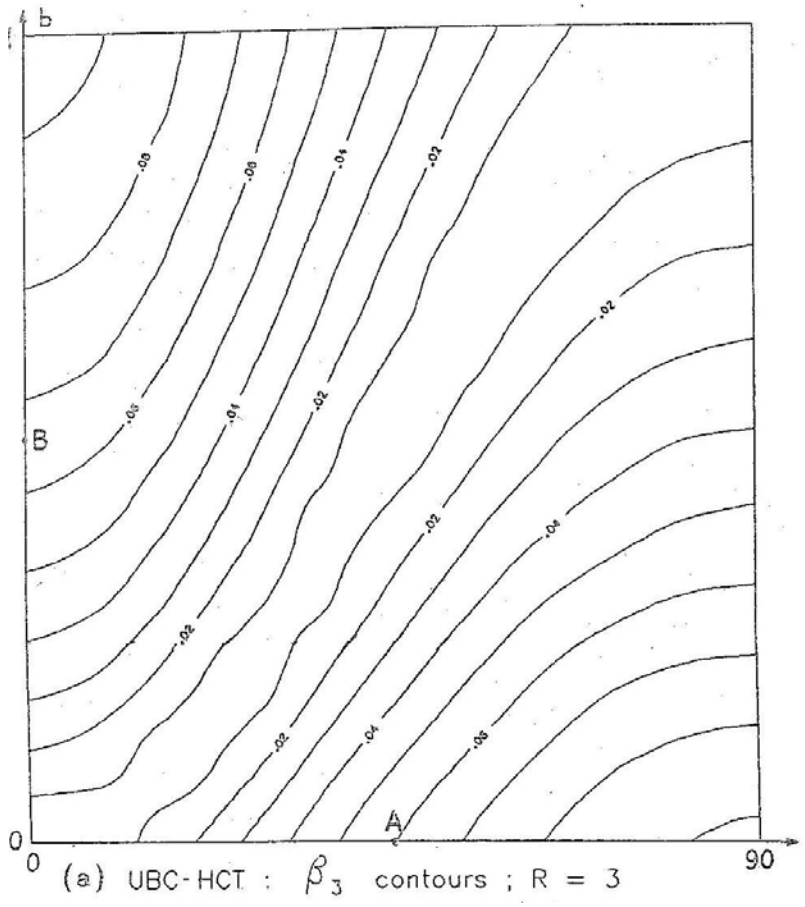

Figure 2-16: Height et. al (1983) Non-uniformity Coefficient (β_R) at Stress Ratio of 3 After Figure by (Vaid et al. 1990)

This ridge of high non-uniformity suggests that $P_o = P_i$ may not always minimize stress non-uniformities. However, the authors realized that the degree of non-uniformity calculated by assuming a liner elastic soil model is more severe than that actually present in a non-linear soil.

2.3.2.2.3 Recommendations for Selection of Specimen Geometry

Stress non-uniformity due to the effects of geometry, differing cell pressures, and end restraint can be minimized by selecting the proper specimen radius, height, and wall thickness.

Many HTSA devices are designed by first selecting a wall thickness. The specimen wall thickness should be selected to optimize the following factors (Hight et al. 1983):

- Sufficiently large in comparison to the grain size so that the predominate failure mechanism will not be constrained.
- Specimen volume should be large enough so that volumetric changes will not be greatly affected by the effects of membrane penetration.
- Should have a uniform density across the wall.

These requirements are more readily satisfied by large wall thicknesses. However, large wall thicknesses require large outer diameters to reduce the β_1 and β_3 parameters. Hight et al. recommended a minimum 25.4 mm wall thickness to satisfy the above requirements.

For a known wall thickness stress non-uniformity due to curvature can be considered. Height et al. demonstrated that for a 25.4 mm specimen wall thickness little improvement in stress non-uniformity is achieved for outer diameters greater than 125 mm.

With the wall thickness and specimen diameter selected the height can be determined to minimize the effect of end restrains. Lade (1981) recommended maintaining a height : diameter ratio of 2.

All of these recommendations can be satisfied by following recommendations for optimal HTSA made by Sayao and Vaid (1991):

- Wall thickness: $R_o - R_i = 20$ to 26 mm
- Inner radius: $0.65 \leq R_o/R_i \leq 0.82$
- Height: $1.8 \leq H/2R_o \leq 2.2$

Sayao and Vaid also compiled dimension from numerous HTSA devices, which are represented by black dots on Figure 2-17. Their recommended dimensions are represented by a black box. An annotation and arrow indicate the location of the dimensions for the HTSA used in the present investigation. The current HTSA meets all recommended dimensions, thereby minimizing the effects of stress non-uniformity.

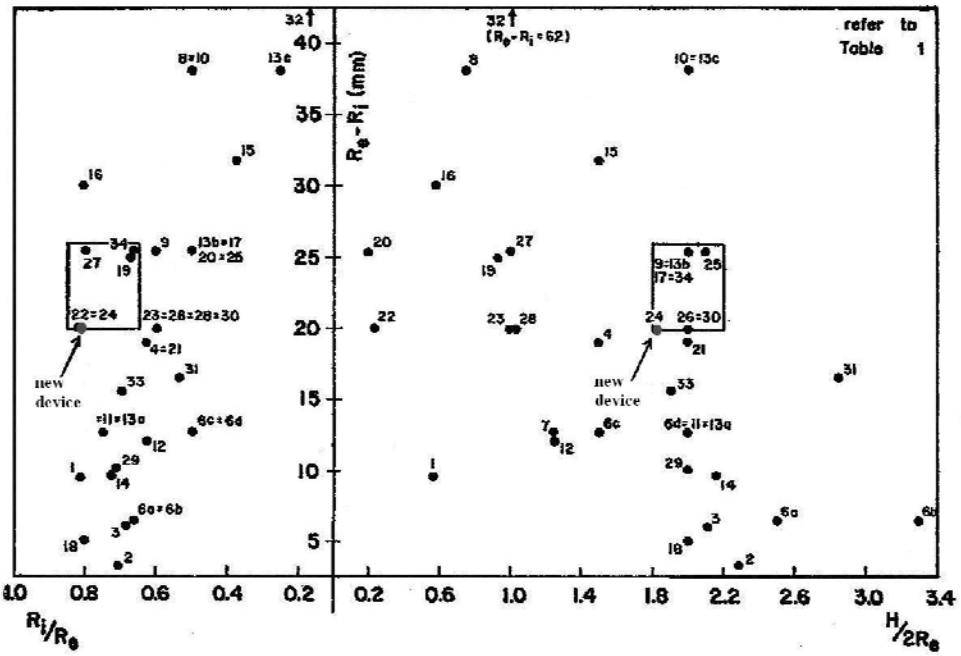

Figure 2-17: Recommended HTSA Specimen Geometry After (Sayao and Vaid 1991)

2.3.2.2.4 Conservatism in Stress Concentration Predictions

The HTSA devices used in the current investigation has acceptable dimensions. However, even with optimized dimension, a number of studies have investigated stress non-uniformities and suggested stress areas to avoid for HTSA testing (Hight et al. 1983, Gens and Potts 1984, Vaid et al. 1990, Wijewickreme and Vaid 1991). These areas are located in the b=0 α=90° and b=1 α=0° corners of a b vs. α plot, as previously shown in Figure 2-16.

Hight et al. (1983) and Sayao and Viad (1991) have stated that the stress concentrations in these areas become more severe with increases in the stress ratio and their investigations have greatly influenced the stress conditions that have been investigated using the HTSA.

However, the stress concentrations predicted in these investigations may be overly conservative due the use of linear elasticity for the soil model. During their elasto-plastic finite element analysis using the Modified Cam-Clay model to examine stress non-uniformities in hollow cylindrical specimens Potts and Gens (1984) found that stress non-uniformity decreased after the onset of yield.

Wijewickreme and Vaid (1991) utilized a three-dimensional numerical model of an HTSA specimen to compare and contrast stress non-uniformities with both linear elastic and hyperbolic constitutive models. They found that due to stress redistribution that occurred in plasticity models stress non-uniformities were probably acceptable even in the extreme cases near the corners (i.e. b=0 α=90° and b=1 α=0°).

Three-dimensional finite element calculations using the Modified Cam Clay model (Menkiti 1995) shows that stress small stress non-uniformities are generated before yield, but that they become negligible as failure is approached, and the average stress and strain equations proposed by Hight et al. (1983) are sufficient for accurately interpreting hollow cylinder tests (Menkiti 1995).

Linear elasticity overestimates the magnitude of stress non-uniformity (Wijewickreme and Vaid 1991). Elasto-plastic analyses of specimens free from the effects of end restraint (i.e. H:D ≈ 2) has shown that during the elastic portion of testing, stress concentrations increase with the stress ratio. However, once plastic strains become significant the stress concentrations decrease (Wijewickreme and Vaid 1991).

2.4 Previous Investigations

To maintain relevance with testing completed during this investigation, the review of previous investigations presented herein has been generally limited to investigations of granular soils or those of prominent historical significance. The investigations that have the most direct applicability to the present testing program consist of drained tests performed on reconstituted cohesionless soils (Lade 1975, Lade 1976, Lade 1981, Fukushima and Tatsuoka 1982, Hight et al. 1983, Ishihara and Towhata 1983, Tatsuoka et al. 1986, Pradhan et al. 1988, Saada, et al. 1999, Chaudhary and Kuwano 2003, Lade et al. 2008).

However, since research has shown equivalency between the point of phase transformation[4] (Georgiannou, et al. 2008) in drained and undrained testing, observations from selected undrained investigations have also been included in this literature review.

This review of previous investigations has been organized into five sections:

1. Test parameters
2. Interpretation of three-dimensional test results
3. Failure criteria
4. Stress, stress increments, and strain increments
5. Shear band formation

2.4.1 Test Parameters

This section contains a review of the four test parameters used in this investigation, the two that are intentionally varied for each test, principal stress inclination (α) and the intermediate principal stress ratio (b), and the two that are held constant for each test, the mean normal confining stress (σm) and the density.

2.4.1.1 PRINCIPAL STRESS ROTATION AND INCLINATION

The effect of principal stress rotation on fully saturated drained sand specimens has been the subject of much research (Lade 1975, Lade 1976, Symes et al. 1982, Hight et al. 1983, Symes et al. 1984, Miura et al. 1986, Tatsuoka et al. 1986, Symes et al. 1988, Vaid et al. 1990, Wijewickreme and Vaid 1993, Zdravkovic and Jardine 2001, Wijewickreme and Vaid 2008).

[4] The point at which the soil behavior transforms from contractive to dilative.

They have found that most naturally deposited sands possess a cross-anisotropic fabric that exhibits a reduction in the peak stress ratio and the soil stiffness as the principal stress is rotated from $\alpha = 0°$ to 90° (Wijewickreme and Vaid 2008). However, the lowest values are found near 67.5°, the point at which the plane of maximum stress obliquity is aligned with the bedding plane (Tatsuoka et al. 1990, Zdravkovic and Jardine 2001).

HTSA testing of anisotropic sand specimens clearly indicates that principal stress rotation alone can cause shear deformation and volume change (Miura et al. 1986). It may even cause plastic deformation under conditions of constant deviator stress (Yang et al. 2007, Wijewickreme and Vaid, 1993).

For undrained testing, principal stress rotation can generate excess pore pressure (Ishihara and Towhata 1983, Sivathayalan and Vaid 2002, Broms and Casbarian 1965). For principal stress rotation at a constant deviator stress, pore water pressures are affected by the magnitude of the initial deviator stress. Greater stresses produce a faster rate of pore pressure generation (Yang et al. 2007).

Height et al. (1983) performed a series of tests on drained sand specimens. Alternative stress paths were followed to reach the same values of stress ratio (3.5) and stress rotation (45°), after which a common stress path was followed to failure. The test results indicated:

- Strains are dependent on stress path. However, Wijewickreme and Vaid (1993) later found that strains are independent of stress path at low stress ratios and are only stress path dependant at higher stress ratios.

- Volumetric strains can occur due to isolated stress rotation at constant stress ratios.
- The peak strength is not significantly affected by the previous stress path, only the stress conditions at the time of failure affects the peak strength. Additionally, O'Kelly and Naughton (2009) found that the peak stress ratio is relatively unaffected by principal stress reorientation during the consolidation phase.

Symes et al. (1984) performed a series of monotonic and cyclic undrained HTSA tests on medium loose Ham River Sand. By first shearing several specimens at different constant principal stress directions ($\alpha = 0°$, 22.5°, and 45°) and then conducting a series of tests involving principal stress rotations at a constant stress ratio, the effects of stress rotation were isolated from the initial anisotropy.

It was observed that differences in soil behavior due to initial anisotropy can be quite different than those due to stress rotation. This was especially evident when the direction of stress rotation was reversed. The authors proposed a State Boundary Surface (SBS) to help qualitatively describe this behavior. Their SBS for Ham River sand is shown in Figure 2-18.

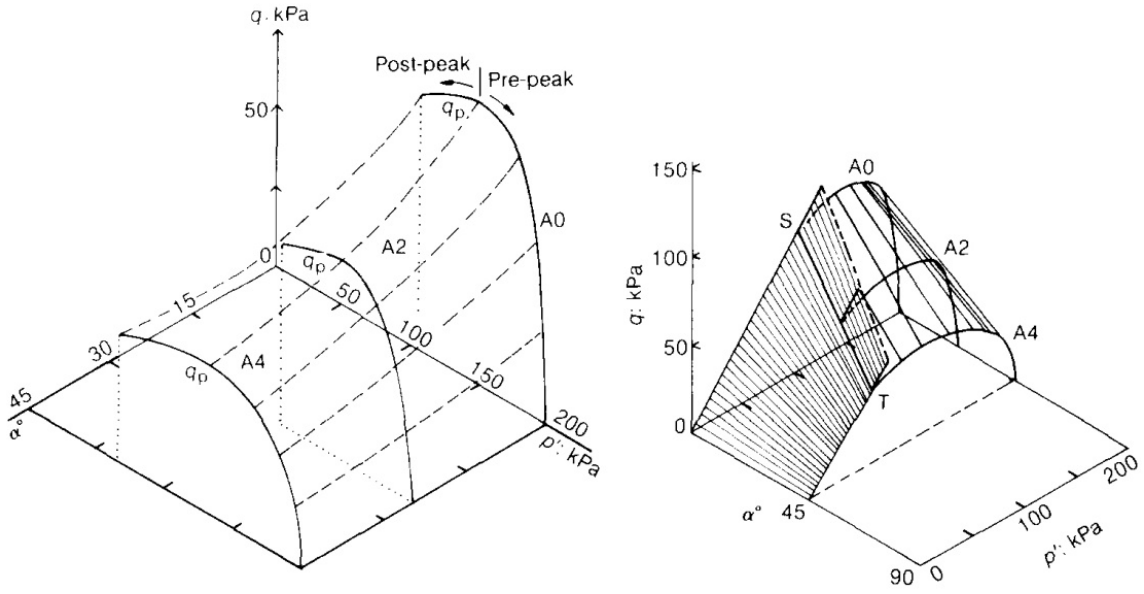

Figure 2-18: State Boundary Surface
After (Symes et al. 1984)

Using the SBS as a model, stress rotation is considered loading if it causes the state of stress to stay on the SBS, or unloading if it causes the state of stress to go beneath the SBS. The development of large pore pressures was observed when the state of stress was on the SBS.

In addition to proposing a SBS model for qualitatively predicting soil behavior, the authors found that for any loading direction, neither the principal strain increment nor the ratio of deviator stress to mean confining stress was affected by previous stress rotations. This can be taken as confirmation that the initial anisotropy is the predominant factor affecting the sand behavior.

Symes et al. (1988) investigated the possibility of using a boundary surface defined in terms of q, p, and α, similar to the one used for undrained testing (Symes et al. 1984), for drained tests in which changes in void ratio are possible.

In a manner similar to his previous investigation of 1984, Symes conducted three initial tests with constant principal stress inclinations of $\alpha = 0°$, 22.5° and 45°, and no stress rotation. The stress paths for these three tests (designated L0, L2, and L4) are shown in Figure 2-19 (a). Two tests (LR1 and LR3) were then conducted that had principal stress rotation from $\alpha = 0°$ to $\alpha = 45°$ while holding the deviator stress constant, as shown in Figure 2-19 (b), and finally two tests (LR2 and LR4) were conducted with principal stress rotation from $\alpha = 45°$ to $\alpha = 0°$ while holding the deviator stress constant, as shown in Figure 2-19 (c).

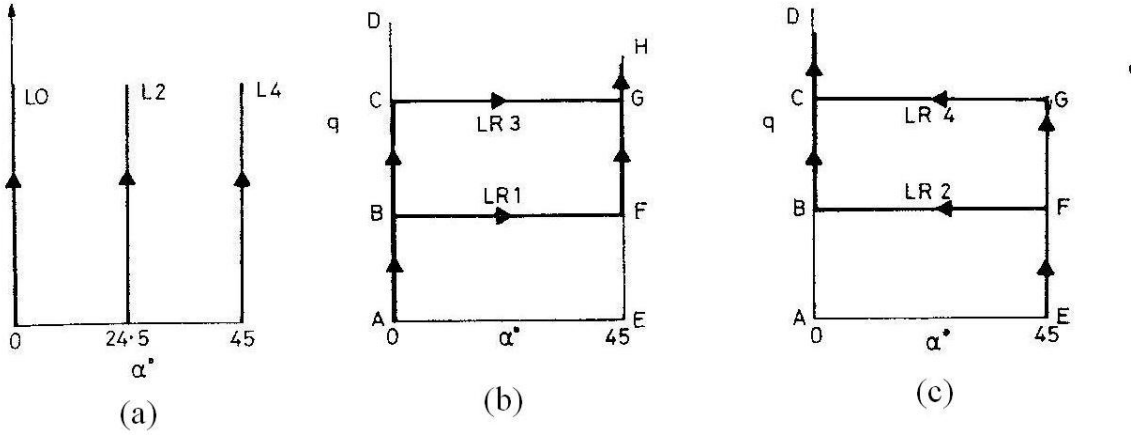

Figure 2-19: Stress Paths (a) No Rotation,
(b) Rotation from 0° to 45°, (c) Rotation from 45° to 0°
After (Symes et al. 1988)

Results from the first three tests that did not include stress rotation showed that the specimens had an inherent anisotropic fabric which affected both strength and modulus. Results from the next four tests, which included principal stress rotation, showed that stress rotation at a constant deviator stress produces contraction. However, the magnitude of the contraction is dependent upon the direction of rotation.

Tests which rotated from $\alpha = 0°$ to $\alpha = 45°$ experienced a greater degree of contraction and ultimately the strains agreed well with the test at $\alpha = 45°$ that did not undergo principal stress rotation. Conversely, the tests with principal stress rotation from $\alpha = 45°$ to $\alpha = 0°$ had a smaller magnitude of compression and ultimately had different strains than those observed in the test performed at $\alpha = 0°$ with no stress rotation.

A final test was performed which subjected a specimen to stress rotation while steadily increasing the deviatoric stress. This combination of loading and stress rotation was increased almost to failure. The test results indicated that the specimen followed closely along the boundary surface during the entire test, confirming that the concept of the boundary surface can be used to qualitatively predict the response of sand even when stress is being rotated close to the failure surface in a drained specimen.

Vaid et al. (1990) studied the drained behavior of both loose and dense specimens of Ottawa Sand and confirmed that water pluviated sand is inherently anisotropic in nature, as evidenced by principal stress rotation alone causing volumetric strains, and isotropic changes in mean confining stress alone producing shear strains.

Wijewickreme and Vaid (1993) investigated the stress-strain behavior of loose sands subjected to stress rotation. By using a variety of stress paths to reach the same stress state, the authors found that for low stress levels, and low principal stress inclinations (i.e. $< 45°$) the material behavior was stress path independent. However, for stress ratios greater than 2 and large principal stress rotations the observed behavior was stress path dependent.

Figure 2-20 shows strains as a function of principal stress direction for stress rotation at a constant stress ratio (A3002), and stress rotation with a simultaneous increase in stress ratio (remaining tests). For stress ratios equal to or less than 2.0, there is no stress path dependency for stress rotations less than 60°. This is indicated by the merging of strain paths at common values of α. However, a distinct difference is observed for large stress rotation associated with Test A3901.

During subsequent research, the authors found that the magnitude of b does not appear to influence shear deformations at tests with R < 2 and α < 45°. They also developed a hyperbolic relationship between shear stress and shear strain as shown in Equation (2.6) for states of stress with R < 2 and α < 45° (Wijewickreme and Vaid 2008).

$$\gamma_{z\tau}/\tau_{z\tau} = \gamma_{z\tau}\left(1/\tau\right) + \left(1/G\right) \tag{2.6}$$

Where:

γ_{zt} = shear strain in the vertical plane

τ_{zt} = horizontal shear stress in the vertical plane

τ = Large strain shear resistance from hyperbolic model curve fitting

G = initial stiffness from hyperbolic model curve fitting

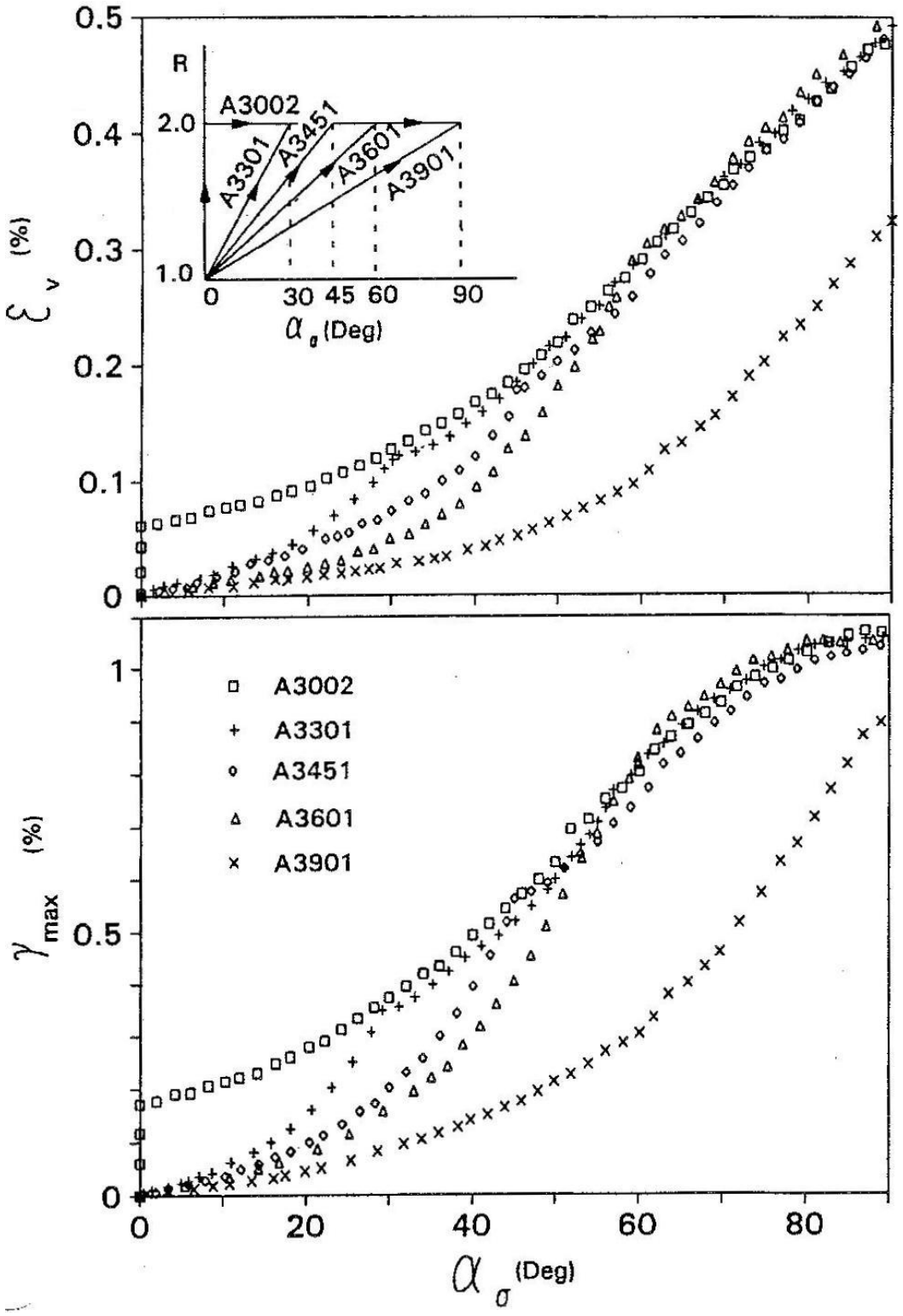

Figure 2-20: Volumetric and Shear Strain versus Principal Stress Inclination (α) After (Wijewickreme and Vaid 1993)

2.4.1.2 INTERMEDIATE PRINCIPAL STRESS

The intermediate principal stress (b-value), as previously defined in Equation (1.1), has been shown to have a significant effect on soil behavior. Early researchers have studied this parameter by comparing the results of triaxial compression (b=0), triaxial extension (b=1), and plane strain tests ($0.2 < b < 0.3$). As the importance of this parameter was realized, cubical test devices were developed that were capable of independently controlling all three principal stresses, and hence the b-value.

Researchers found that the peak stress ratio is significantly affected by the b-value. For drained tests, increased b-values lead to increases in peak stress ratio, up to values of about 0.8 after which there is some reduction in peak strength (O'Kelly and Naughton 2009). This reduction may be due to the inherent difficulty of running extension tests (Lade 2006). Zdravkovic and Jardine (2001) theorized that b=1 might have the highest friction values, if it were not for the fact the test is inherently unstable and often fails due to necking.

For undrained tests, increasing the b-value at a constant stress ratio have been shown to produce excess pore water pressure (Yoshimine et al. 1998), consistent with volumetric contraction and the development of shear strains (Sayao and Vaid 1996). However, the magnitude of b does not appear to influence shear deformations or pore water pressures for stress ratios less than 2 and principal stress directions less than 45°.

2.4.1.3 MEAN NORMAL CONFINING STRESS

Increases in the mean normal confining stress result in a slightly decreased peak friction angle. This occurs slightly faster in HTSA testing than it does in plane strain

testing or triaxial testing. The stress-dilatancy relationship does not appear to be affected by the confining stress. For stress ratios less than six, the rate of shear strain is not affected by the confining stress. The degree of post peak strain softening increases with an increase in confining stress. For HTSA testing, increases in confining stress result in the development of shear bands at lesser shear strains (Tatsuoka et al. 1986).

Tatsuoka et al. (1986) investigated the effects of the confining stress by performing two series of drained HTSA tests on specimens of different densities. The first series of tests was conducted with a constant b-value of 0.5 and α of 45°. For the second series of tests $\sigma_\theta = \sigma_r$ but the principal stress and intermediate principal stress ratio were allowed to vary during the test. Increasing the confining stress in a hollow torsional shear apparatus had the following effects on the stress-strain relationship:

- With increasing confining stress, the peak friction angle decreases slightly. This occurred slightly faster in HTSA testing than in plane strain or triaxial testing.
- The stress-dilatancy relationship does not appear to be affected by the confining stress.
- For stress ratios greater than 6, the rate of shear strain is not affected by the confining stress.
- The degree of post peak strain softening increases with an increase in confining stress.
- For HTSA testing, increases in confining stress result in shear banding at lower levels of shear strain.

A comparison of HTSA and plane strain test results showed that for similar general stress conditions and principal stress directions, the friction angle and stress-strain behavior obtained in the two test devices were in good agreement.

The effects of b and α were not uncoupled in Tatsuoka's investigation, creating some uncertainty regarding the effect of these parameters on the peak shear strength. Additionally, the test apparatus was not capable of measuring the inner volume change, making it impossible to evaluate the inner and outer radius change, creating additional uncertainty regarding calculated stresses.

2.4.1.4 Relative Density

Increases in relative density lead to higher peak stress ratios (Fukushima and Tatsuoka 1982). In undrained testing, looser soil specimens tend to develop pore water pressures at a faster rate during stress rotation (Yang et al. 2007).

2.4.2 Interpretation of Three-Dimensional Test Results

It is reasonable to assume that variations in the intermediate principal stress ratio should exhibit a characteristic pattern for both fine and coarse grained soils. Therefore, the failure surface for all sands should have a common shape that could be used to create a single three-dimensional constitutive model.

Many investigations of the intermediate principal stress have neglected the effects of soil anisotropy and shear banding, resulting in improper plotting and interpretation of test results. This can be illustrated by reviewing the results from drained tests on air pluviated Ottawa Sand specimens tested by Ramamurthy and Rawat (1973).

The test results from this investigation, Figure 2-21, clearly show that the peak friction angles are affected by the intermediate principal stress. However, if these tests had been plotted in the octahedral plane, all of them would have been contained in the first sector, with the exception of the final series of extension tests.

The extension tests have a principal stress direction that is orthogonal to the other tests (i.e. parallel to the bedding plane), resulting in much lower peak friction angles. Therefore, at the b = 1 condition (extension tests) the effects of the intermediate principal stress are not isolated from the effects of principal stress rotation, preventing the proper evaluation of the effects of the intermediate principal stress.

Additionally, the cubical specimens used in this investigation did not have a height to base ratio of 2:1, preventing these specimens from naturally developing shear bands, which likely led to inappropriately high shear strength from b = 0.2 to 0.8.

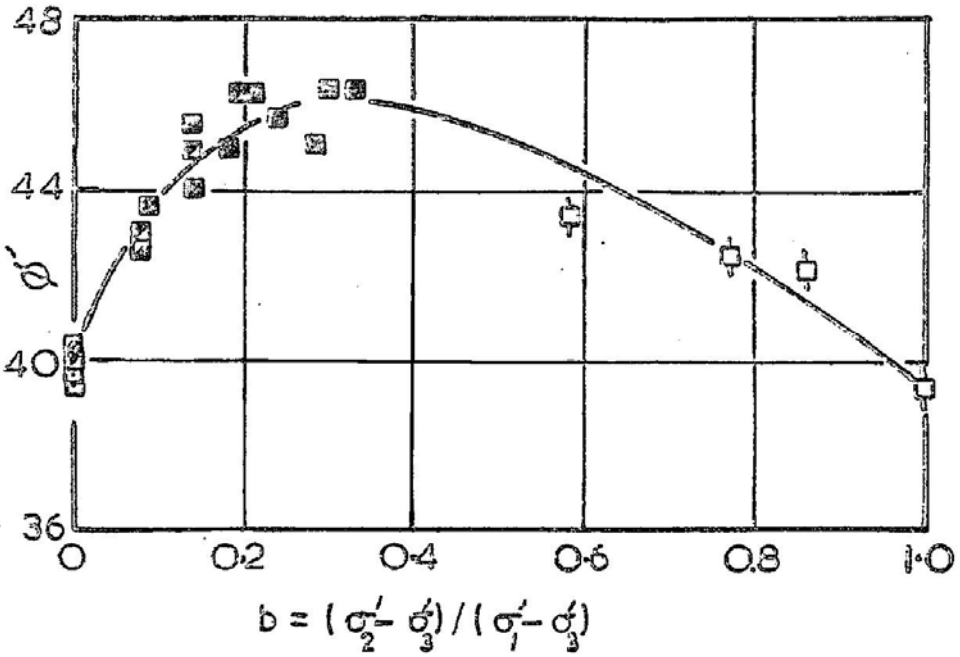

Figure 2-21: Friction Angle versus Intermediate Principal Stress Ratio After (Ramamurthy and Rawat 1973)

Similar difficulties in the interpretation of test results occurred in many studies. This resulted in a considerable amount of apparent disarray when plotting test results from many investigations together. However, Lade (2006) pointed out that this disarray can generally attributed to one or more of several factors that can affect test results:

1. Effects of shear banding
2. Boundary conditions and/or slenderness ratio
3. Cross-anisotropy
4. Experimental technique stability

Lade (2006) showed that there were similarities between many investigations, by sorting the test results from each investigation into categories of common shapes, as shown in Figure 2-22.

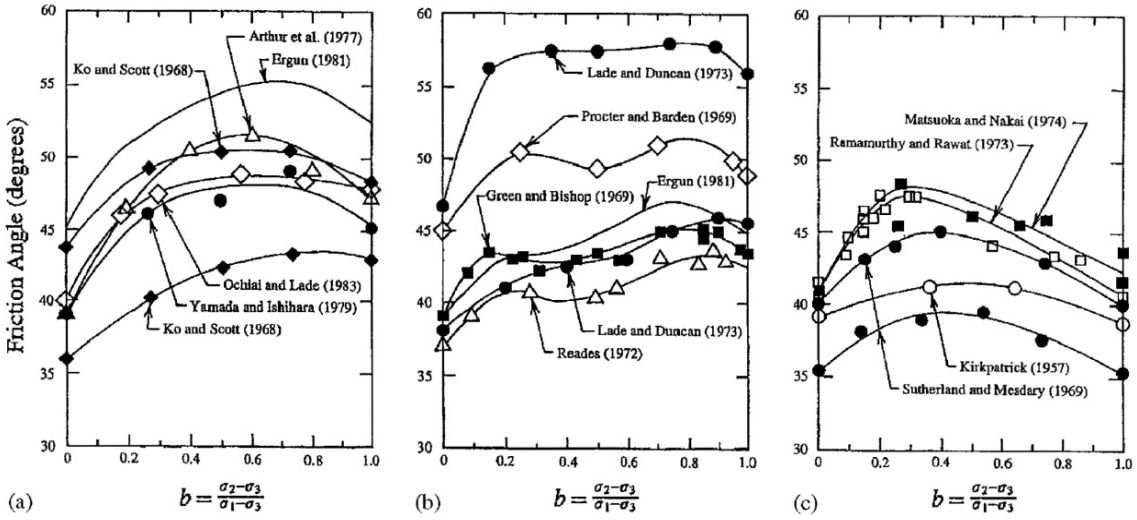

Figure 2-22: Groups of φ – b Relationships from True-Triaxial Testing After (Lade 2006)

In general, the investigations presented in Figure 2-22(a) match well with constitutive models. However, most of these investigations were performed using short specimens with stiff end platens that tend to produce uniform strains.

Unnatural strain uniformity inhibits the formation of shear bands, which can result in erroneously high peak stress ratios for b-values between 0.18 and 0.85.

The failure surfaces presented in Figure 2-22 (c) generally underestimate the friction angle for b-values greater than 0.5. These investigations have either ignored the effects of cross-anisotropic soil fabric and combined Sector I and Sector III testing into a single $\varphi - b$ relationship, or populated Sector III with test results obtained from conventional triaxial extension tests which are inherently unstable.

During extension testing in a conventional triaxial apparatus, it is inevitable that stresses will concentrate in a portion of the specimen having a geometric or material abnormality. A slightly smaller cross section will result in higher stresses. The higher stresses will result in higher strains and cause this portion of the specimen to deform much more quickly than the rest of the specimen, leading to a necking failure.

2.4.3 Failure Criteria for Non-Cohesive Sands

To validate a constitutive soil model, the predicted stress-strain and strength response for a number of differing three-dimensional stress states should be compared with actual laboratory test results. Many laboratory investigations have included a comparison of test results with three-dimensional failure criteria.

Investigations in the mid to late 1960s generally compared test results to one of the classic failure criteria: 1) Mohr-Coulomb, 2) Extended Tresca, 3) Extended von Mises. However, as shown in Figure 2-23, the Extended Tresca and Extended von Mises reach into regions of stress space where one of the principal stresses is negative, which is clearly not possible for a cohesionless soil. The Mohr-Coulomb failure envelope remains in compressive stress space for reasonable friction angles. However, the Mohr-Coulomb failure criterion does not include the effects of the intermediate principal stress, and therefore does not constitute a three-dimensional failure criterion.

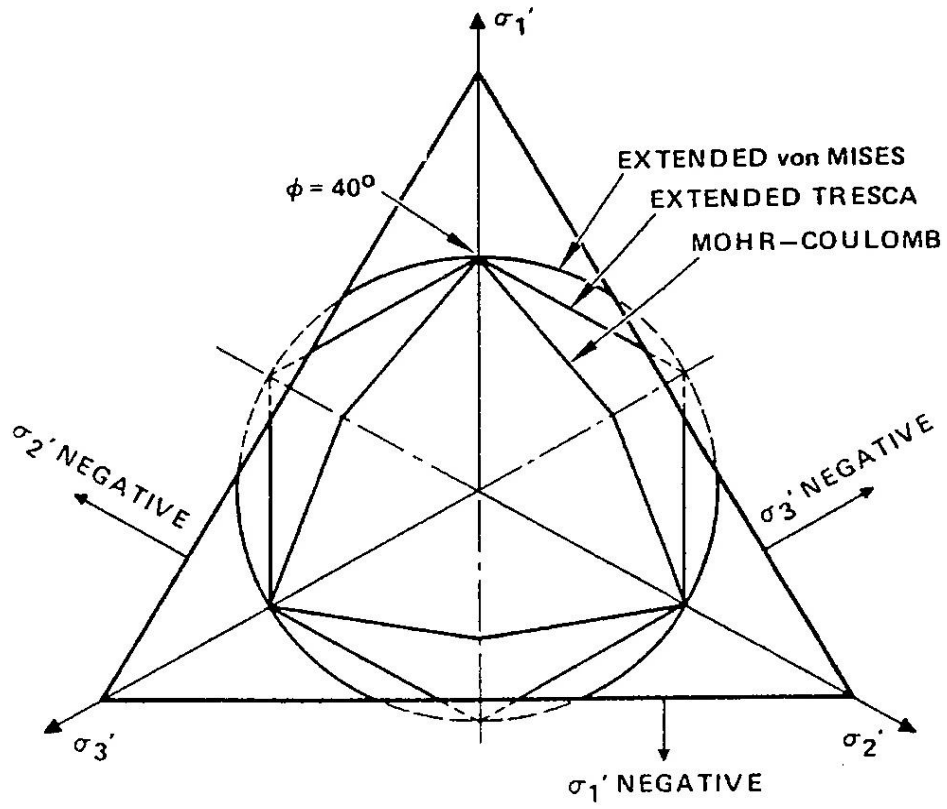

Figure 2-23: Various Failure Criterion in Octahedral Stress Space After (Lade 1984)

As early as 1969, Saada and Zamani used the results of torsion shear tests to validate one of the first anisotropic constitutive models for clay (Saada 1988).

Matsuoka and Nakai (1974) proposed a three-dimensional failure criteria based on the angle between the bedding plane and the mobilized plane. This formulation was theoretically derived, but it was compared to the results of true triaxial tests performed by Sutherland and Mesdary (1969) and by Ramamurthy and Rawat (1973). Test results from Sutherland and Mesdary are shown with respect to the proposed failure criterion in Figure 2-24.

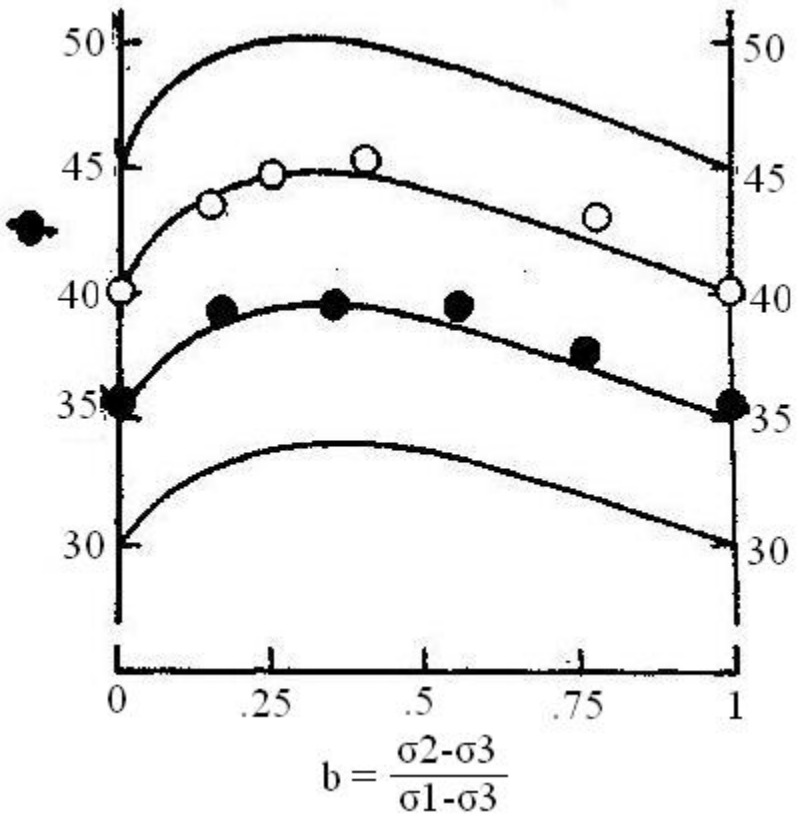

Figure 2-24: Friction Angle versus Intermediate Principal Stress Ratio After (Matsuoka and Nakai 1974)

Matsuoka and Nakai reported that their failure criterion was in "good agreement" with the test results, as well as results of plane strain tests and triaxial tests in compression and extension.

However, for the reasons discussed in Section 2.4.2, the data used to formulate the failure criterion was flawed. The authors did not realize the importance of anisotropy, and therefore produced a failure criterion, that predicts lower than expected shear strength for b-values over 0.5. This is due to ignoring the effects of shear banding in the mid range of b-values and performing the b=1 test using a conventional triaxial apparatus, causing that test to be located in Sector III rather than Sector I, as was intended (Lade 2006).

Lade (1977) proposed an isotropic three-dimensional failure criterion expressed in terms of the first and third stress invariants. Other investigations have used this model as a comparative basis for experimental results (Yamada and Ishihara 1979).

This model was later used as a basis to develop a cross-anisotropic model (Abelev and Lade 2004). Drained true triaxial tests on dense Santa Monica beach sand were used to verify the accuracy of the model in the octahedral stress space.

Figure 2-25 shows a plot of the test results in octahedral stress space compared to the 1977 isotropic model and the 2004 cross-anisotropic model. Similar plots were prepared for test results from San Francisco Bay mud and Toyoura Sand.

It is evident that the cross-anisotropic model has an improved ability to capture the soil strength in the third sector. However, neither model is able to accurately capture the affects of hardening regime shear banding that occurs in the mid range of b-values where an indentation occurs in the middle of each sector for the actual test data due to shear banding.

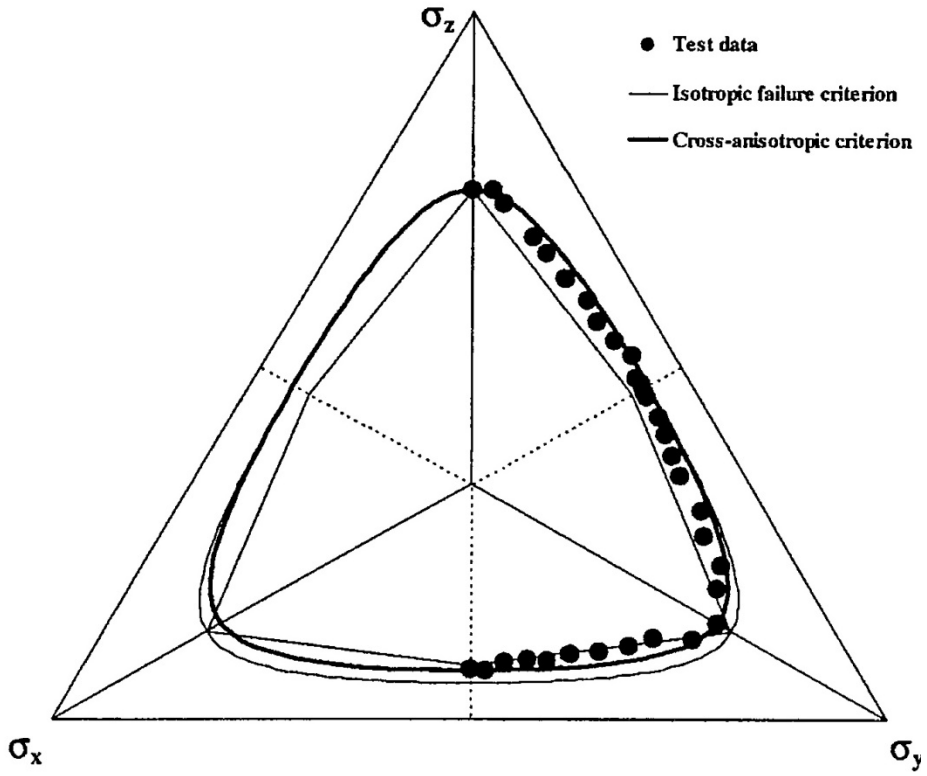

Figure 2-25: Test Data Compared to Model in Octahedral Space After (Abelev and Lade 2004)

2.4.4 Direction of Stress, Stress Increment, and Strain Increment in the HTSA

Lade (1975) performed drained torsion shear tests on K_o and isotropically consolidated specimens of Monterey No. 0 sand. The test results showed that the stress directions and strain increment directions were reasonably similar at failure, meaning that plasticity theory can be used at high stress levels and that cohesionless soils may be considered as elasto-plastic materials.

Miura et al. (1986) investigated the effects of principal stress rotation by conducted drained testing on specimens of dense cross-anisotropic sand.

Cross-anisotropy was verified by observing that the principal strain increments did not coincide with the principal stress directions, except at $\alpha = 0°$ and $\alpha = 90°$. The difference was most striking at $\alpha = 45°$ where the two directions diverged by almost 7°.

The HTSA is well suited for studying the stress (ψ), stress increment (χ), and strain increment (ξ) directions, which can be calculated using Equations (2.7) through (2.9), reported by Lade (2009).

The HTSA can easily control and monitor α, which can be held constant or be smoothly rotated. Other devices, such as the Cambridge Simple Shear Apparatus are capable of monitoring principal stress rotation (Roscoe 1970). However, the drawback of the simple shear apparatus is that control of the principal stress directions is not possible.

The principal stress, principal stress increment, and principal strain increment directions have been reported in many HTSA investigations (Lade 1975, Symes et al. 1984, Miura et al. 1986, Symes et al. 1988, Hong and Lade 1989, Wijewickreme and Vaid 1993, Lade and Kirkgard 2000, Wijewickreme and Vaid 2008, Lade et al. 2009).

The relative directions of each parameter have been used to evaluate the applicability of elasticity and plasticity theories, and associated versus non-associated flow.

$$tan(2\Psi) = \frac{2\tau_{z\theta}}{\vartheta_z - \vartheta_\theta} \tag{2.7}$$

$$tan(2X) = \frac{2\dot{\tau_{z\theta}}}{\dot{\vartheta_z} - \dot{\vartheta_\theta}} \tag{2.8}$$

$$tan(2\xi) = \frac{2\dot{\varepsilon}_{z\theta}}{\dot{\varepsilon}_z - \dot{\varepsilon}_\theta} \tag{2.9}$$

Where:

Ψ = Stress direction

X = Stress increment direction

ξ = Strain increment direction

$\tau_{z\theta}$ = Shear stress

$\dot{\tau}_{z\theta}$ = Shear stress increment

$\dot{\varepsilon}_{z\theta}$ = Shear strain increment

ϑ_z = Vertical stress

ϑ_θ = Tangential stress

$\dot{\vartheta}_z$ = Vertical stress increment

$\dot{\vartheta}_\theta$ = Tangential stress increment

$\dot{\varepsilon}_z$ = Vertical Strain Increment

$\dot{\varepsilon}_\theta$ = Tangential Strain Increment

2.4.4.1 ELASTO-PLASTIC BEHAVIOR

For cohesionless soils to behave as elasto-plastic materials, the stress increment and strain increment must be coincident in the soil's elastic range (i.e. low stress levels). At high stress levels most of the strain will be plastic in nature and the strain increment will be coincident with the overall stress direction (Lade 1975).

Wijewickreme and Vaid (1993) performed HTSA tests on drained sand specimens with constant stress ratios of either: 1.35, 1.65, 2.0, or 2.5. They found that during continuous stress rotation from $\alpha = 0°$ to 90° the strain increment is coincident with the stress increment for low stress levels, while at higher stress levels, the strain increment aligns more closely with the stress direction.

Their test results confirmed earlier findings by Symes et al. (1988) who found the recoverable strain increments were more closely aligned with the stress increments, while the direction of irrecoverable strain increments were more closely aligned with the stress directions.

During a more recent investigation, Wijewickreme and Vaid (2008) found that the direction of major principal strain increment is almost coincident with the direction of major principal stress increment when the direction of stress increment is in the direction of deposition (i.e. $< 45°$). However, for $\alpha > 45°$ the major strain increment tends to leave the major stress increment and begins to align with the major principal stress directions, as shown in Figure 2-26.

This data was obtained from tests which did not exceed stress ratios of 2.0. For this state of stress it is reasonable to assume that all tests with $\alpha < 45°$ are well within the yield surface. However, for tests with principal stress directions closer to the bedding plane, it is not unreasonable to think that the yield surface has been approached and a portion of the strain increment is plastic in nature.

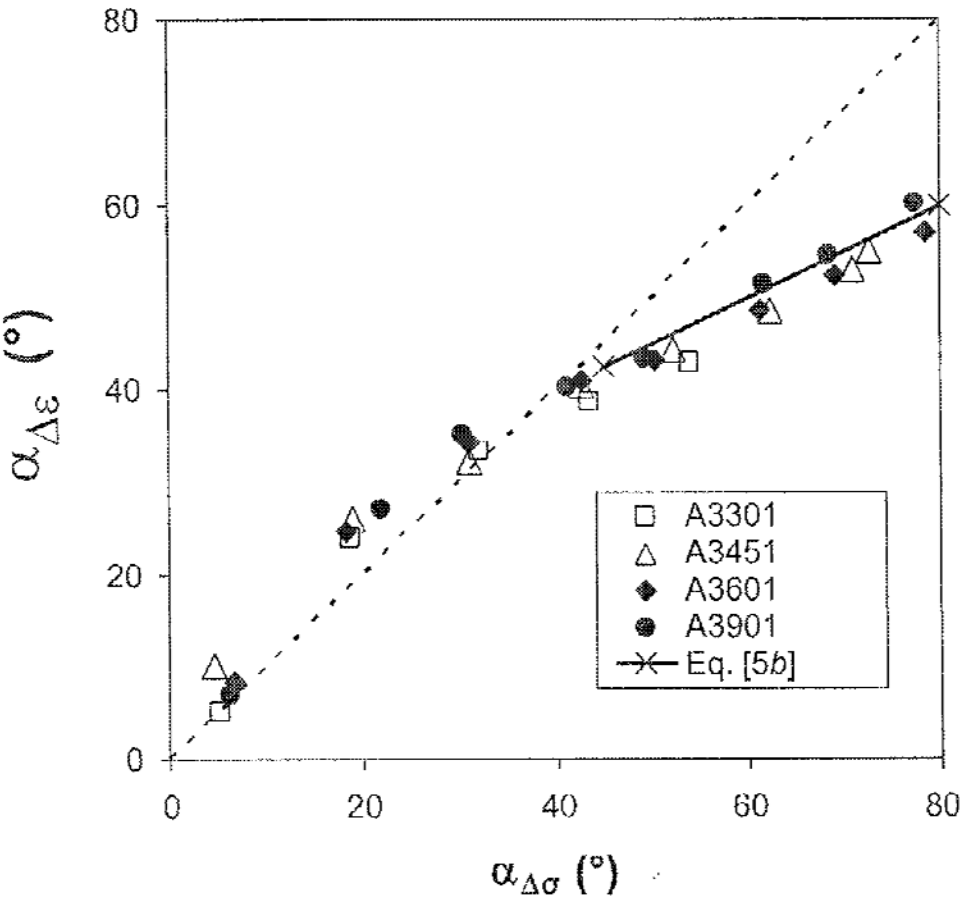

Figure 2-26: Stress Increment versus Strain Increment
After (Wijewickreme and Vaid 2008)

Hong and Lade (1989) performed similar testing on K_o consolidated clay specimens of Edgar Plastic Kalonite. Their test results showed coincidence of the strain increment and stress direction at failure, meaning that any anisotropy due to the K_o consolidation was eliminated at failure.

However, at stress levels well inside the yield surface, the major strain increment coincided with the stress increment, as predicted for elastic behavior. Based on analysis of the test data, the authors conclude that stress rotation in a K_o consolidated clay can be modeled using elasto-plastic theory.

2.4.4.2 ASSOCIATED VERSUS NON-ASSOCIATED FLOW

For a material to behave in an "associated" manner, the plastic strain increment direction (i.e. strain increment at failure) should be normal to the failure surface when superimposed on the stress space in which the yield surface is depicted (Lade et al. 2009). Materials are said to behave in a "non-associated" manner if vectors normal to a separate plastic potential function are necessary to define the plastic flow.

Lade et al. (2009) evaluated "associated" versus "non-associated" flow rules for predicting the strain increment direction near failure, by testing 34 undrained specimens of anisotropic Santa Monica Beach Sand in a torsion shear device.

The strain increments at failure were not normal to the failure surface, indicating that the material behaves in a non-associated manner. Comparison of the strain increment direction with normals to the plastic potential function showed relatively good agreement, indicating that an isotropic non-associated flow rule can adequately characterize a granular material.

2.4.4.3 ANISOTROPY

A comparison of the major principal stress direction and major plastic strain increment direction can also be used to confirm soil anisotropy. According to isotropic plasticity theory, the principal plastic strain increment axis should coincide with the principal stress axis (Lade 1975).

Since elastic strains are small near failure, it is reasonable to assume that the inclination of the total strain increment at failure coincides with the inclination of the plastic strain increment. Therefore, if the total strain increment direction at failure is coincident with the stress direction, the soil is isotropic. However, the anisotropic nature of a soil may be destroyed by the shearing process.

Ochiai and Lade (1983) compared the strain increment direction with the stress direction during their investigation into the drained behavior of cross-anisotropic Cambria Sand using a true triaxial apparatus. Their report contained plots of the plastic strain increment in relation the Lade failure criterion in triaxial and octahedral stress space. The directions plotted in the triaxial stress space were the same regardless of what sector the testing was performed. In octahedral stress space plots, the direction of strain increment was roughly perpendicular to the failure surface.

These test results support the theory that the fabric of a cross-anisotropic cohesionless soil subjected to relatively large strains may be destroyed at failure, leading to coincidence of the principal stress and plastic strain increment directions (Lade et al. 2009).

In contrast to a cohesionless soil, the anisotropic fabric of a clay subjected to relatively large strains may remain intact. Investigations using a HTSA performed on anisotropic specimens of K_o consolidated clay performed by Lade and Kirkgard (2000) showed the strain increment at failure to be non-coincident with the stress direction as depicted in Figure 2-27. These tests suggest that cohesive soils may preserve their cross-anisotropic fabric at large strains.

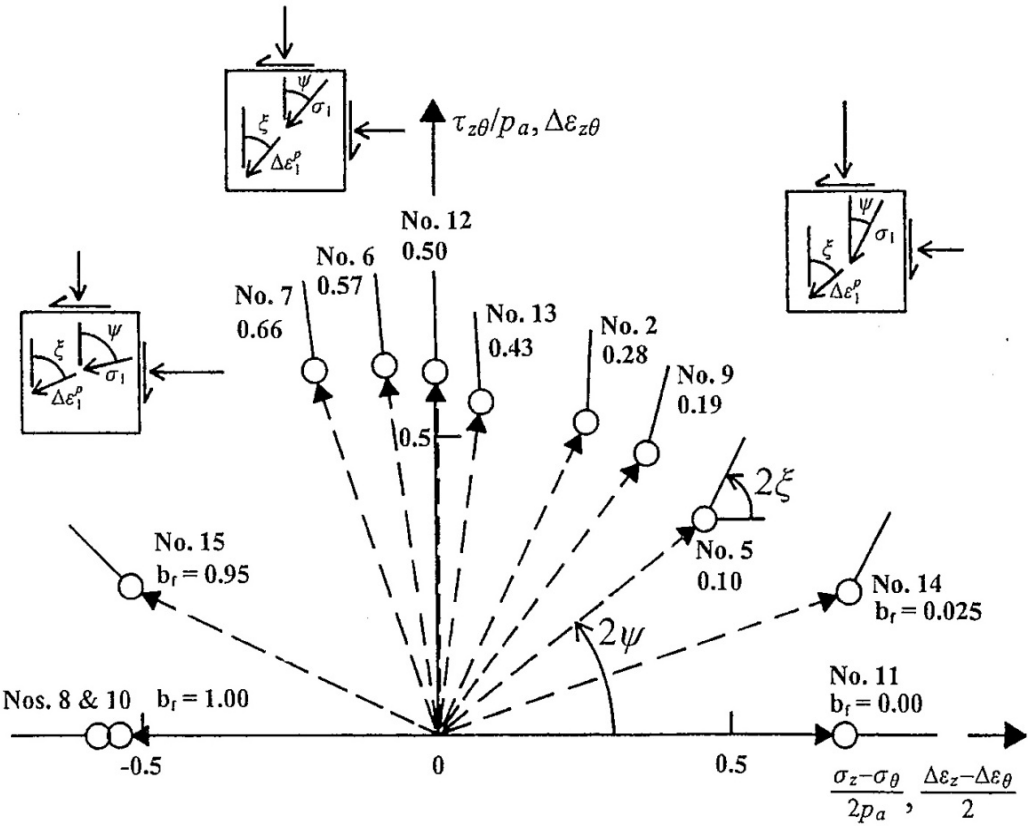

Figure 2-27: Stress Direction versus Strain Increment at Failure After (Lade and Kirkgard 2000)

2.4.5 Shear Banding

The inclination and development of shear bands within granular soils has been the subject of several investigations (Oda et al. 1978, Tatsuoka et al. 1986, Tatsuoka et al. 1990, Saada et al. 1999, Lade and Wang 2001, Wang and Lade 2001, Lade and Wang 2002, Lade 2008, Lade et al. 2008).

A "shear band" is the term used to describe a zone of strain concentration that usually develops near the peak shear stress. The relative movement of particles within a shear band eventually dominates the strain profile.

The occurrence of shear banding can be detected through diligent visual observation, or by analysis of experimental test results. Shear banding that occurs in the hardening regime can be characterized by a steeply peaked stress-strain curve and a large drop in shear strength following failure (Lade 2006). All shear banding is associated with an abrupt change in the slope of a ε_1 versus ε_2 plot.

2.4.5.1 EFFECTS OF SHEAR BANDING ON STRESS-STRAIN BEHAVIOR

Wang and Lade (2001) performed drained true triaxial testing on slender specimens of loose, medium, and dense Santa Monica beach sand over a range of b-values. Their test results, shown in Figure 2-28, depict a failure surface that is characterized by an increase in shear strength from b = 0 to b = 0.18, then a very slight decrease to b = 0.40 followed by a gradual increase to b = 0.8 and finally a drop in strength as b approaches 1.

For intermediate principal stress ratios between 0.18 and 0.8, the formation of shear bands in the hardening regime causes the plot of the peak shear strength versus b-value to become flat, when compared to predictions from an isotropic failure model. This concept is illustrated in Figure 2-28, in which the results of true triaxial testing are compared to predicted friction angles obtained from Lade's model and the Mohr-Coulomb failure criteria (Lade and Wang 2001).

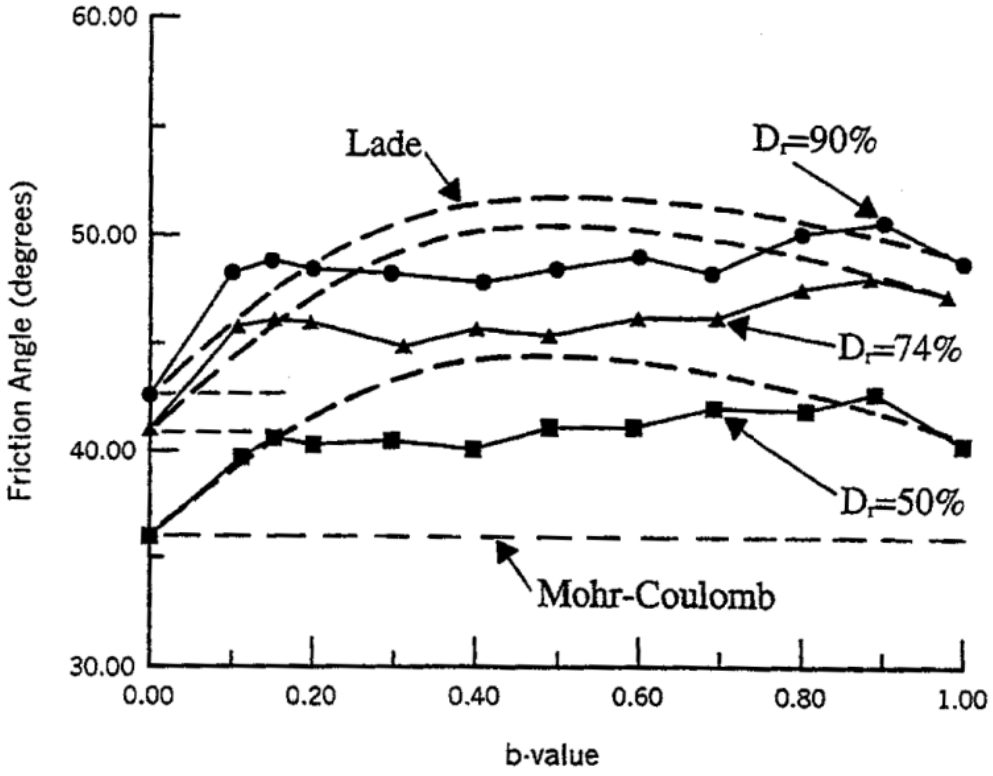

Figure 2-28: Experimental True Triaxial Test Results With m-Coulomb and Lade Failure Criteria After (Lade and Wang 2001)

It should be noted that shear banding observations that have been made during HTSA testing have indicated that shear band formation, even in the hardening regime, does not appear to affect the peak shear strength in HTSA testing (Lade et al. 2008). This is presumably because all shear bands in an HTSA test will eventually intersect the cap.

For intermediate principal stress values between 0.18 and 0.85, shear banding occurs in the hardening regime and acts as the primary failure mechanism. The b = 0.5 portion of Figure 2-29 illustrates a typical hardening regime failure. The stress-strain relationship is sharply peaked and an abrupt change in the ε_1 versus ε_2 plot is concurrent with shear band formation. There is little to no change in the volumetric strain increment, until the specimen has reached its residual state.

Shear banding in the hardening regime, is characterized by two stages of failure (Lade and Wang 2001):

1. Shear banding is characterized by an abrupt decrease in shear strength and strain localization.
2. Shear band development is complete and the specimen is in a residual state, characterized by no additional change in volume, strength, or the intermediate principal strain.

For b-values less than 0.18 or greater than 0.85, shear banding occurs in the softening regime after the peak stress has been achieved. The b = 0.0 portion of Figure 2-29 shows a typical softening regime failure. If shear banding occurs in the softening regime, there are three stages of failure:

1. Material softening – The strength decreases slowly from the peak.
2. Shear banding – strain becomes localized in the shear band and strength decreases abruptly.
3. Residual – the shear band is fully developed and there is no further volume change, strength reduction, or change in intermediate principal strain.

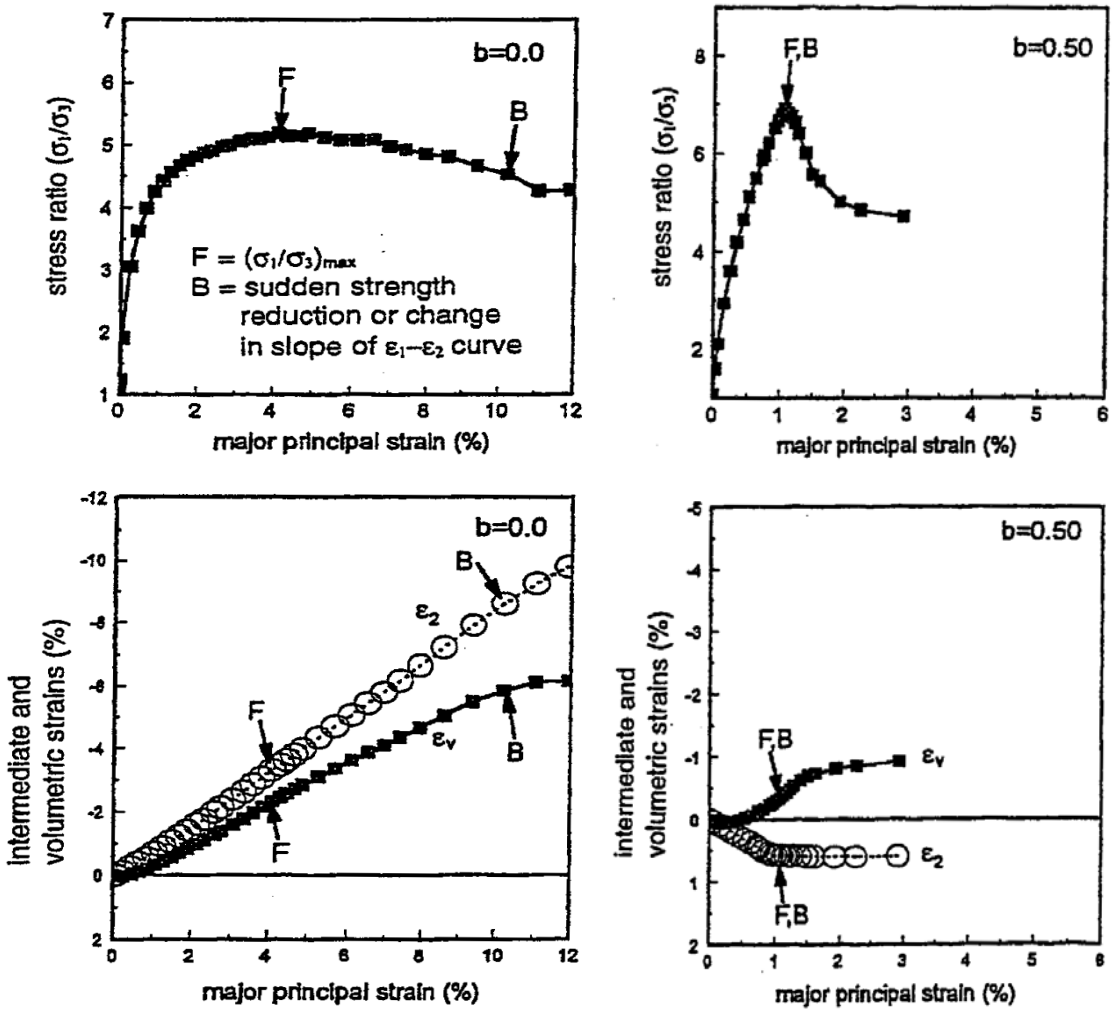

Figure 2-29: Stress Ratio, Intermediate, Volumetric Strain Versus Major Principal Strain After (Wang and Lade 2001)

2.4.5.2 INCLINATION

Shear band inclination can be theoretically predicted using closed form solutions. Coulomb's theory, shown in Equation (2.10), states that shear bands will form on the plane having the highest ratio of shear to normal stress (Lade et al. 2008).

$$\theta = 45° + \frac{\phi}{2} \tag{2.10}$$

Where:

θ = inclination between shear band and direction of minor principal stress

ϕ = friction angle

Roscoe (1970) countered this theory based on his review of simple shear radiographs. Equation (2.11) is based on his observations that shear bands develop along the zero extension lines.

$$\theta = 45° + \frac{\psi}{2} \tag{2.11}$$

Where:

ψ = angle of dilation

Subsequent research performed by Arthur et al. (1977b) concludes that the shear band inclination lies between the Coulomb and Roscoe predictions, as predicted by Equation (2.12).

$$\theta = 45° + \left[\frac{\phi+\psi}{4}\right] \tag{2.12}$$

Figure 2-30 shows shear band directions obtained from testing dense specimens of Santa Monica beach sand. The shear band directions align well with the Coulomb predictions and are not particularly sensitive to the intermediate principal stress ratio.

Although predictions from dense specimens agree well with the Coulomb criteria, experimental shear band inclinations can be expected to decreases slightly for medium and loose specimens.

Analysis of the shear band directions shown in Figure 2-30 suggests that with a higher intermediate principal stress ratio, slight increases in inclination can be expected. This deviates slightly from Figure 2-31, which shows a decrease in inclination as the intermediate principal stress ratio increases.

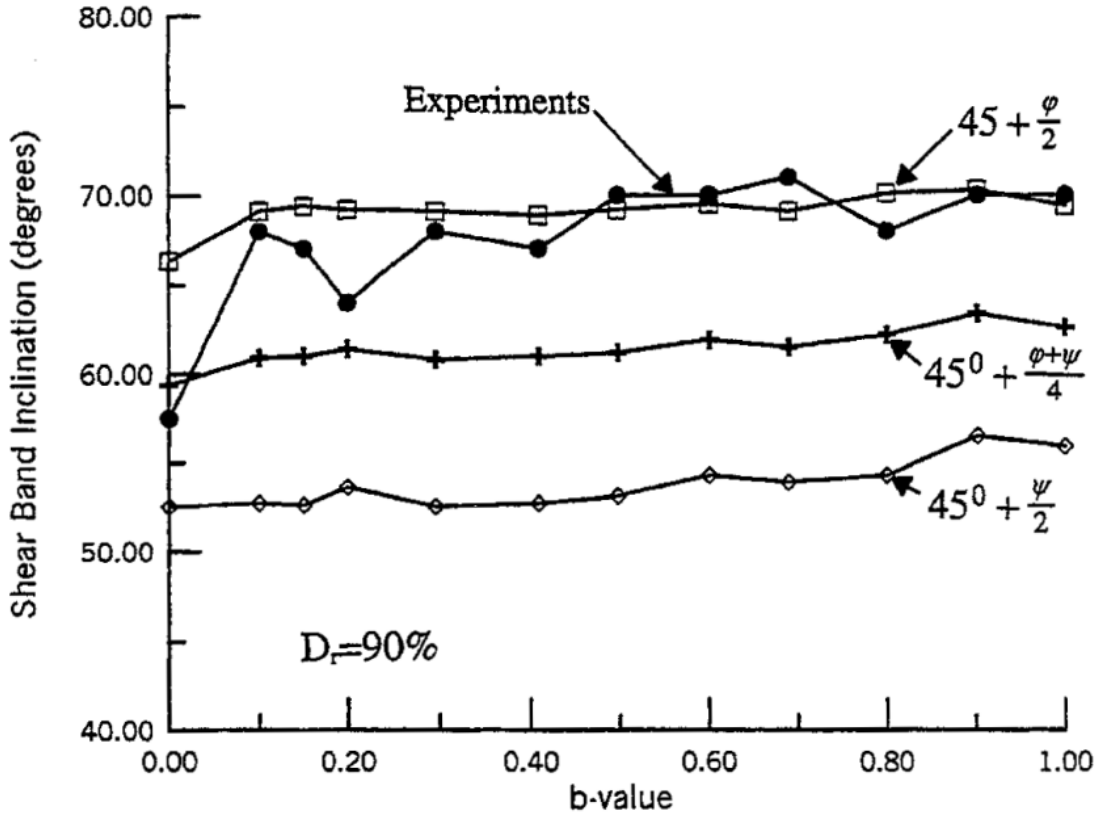

Figure 2-30: Shear Band Inclination versus Intermediate Principal Stress Ratio After (Lade and Wang 2001)

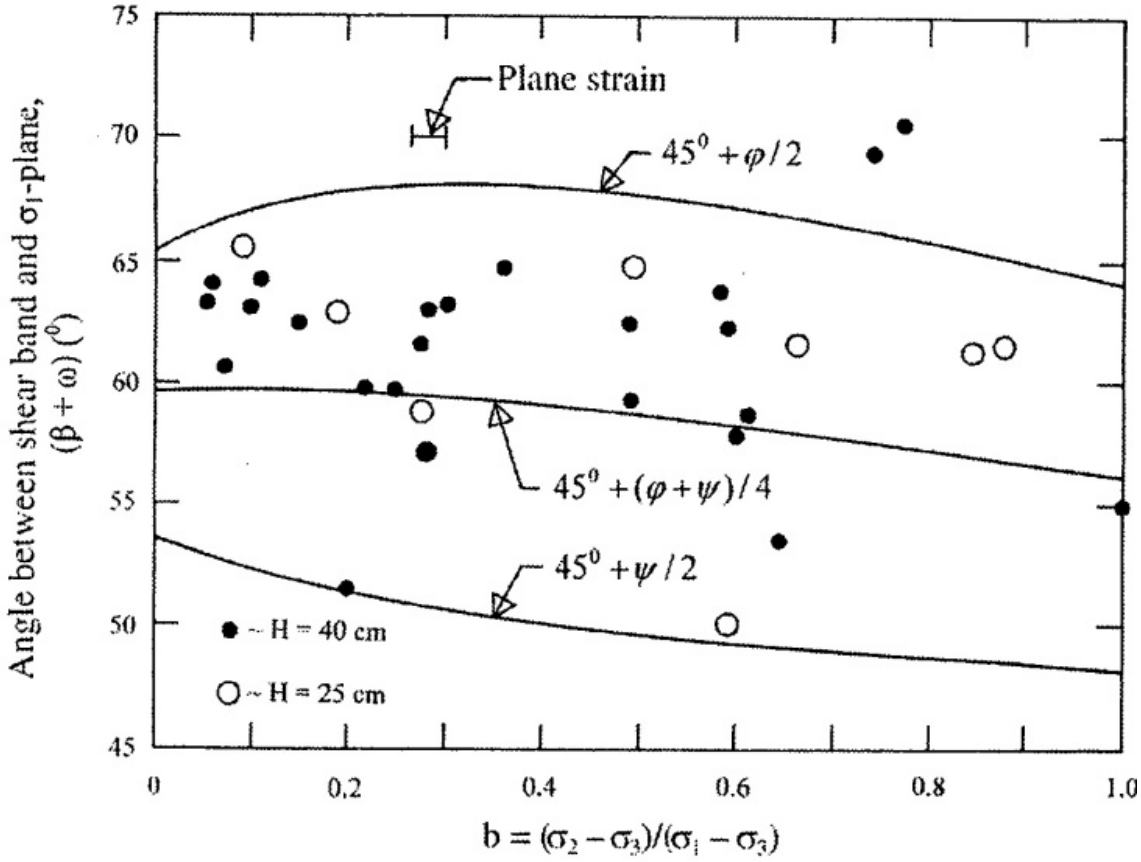

Figure 2-31: Experimental and Predicted Shear Band Inclinations from Medium Dense Torsion Shear Testing
After (Lade et al. 2008)

The discrepancy between the two sets of test results is attributed to two factors:

- The results presented in Figure 2-30 are from testing in a true triaxial apparatus and all tests are constrained to the 1st sector, which is relatively free from the effects of cross-anisotropy. By contrast, Figure 2-31 contains test results from a torsion shear apparatus that did not isolate the intermediate principal stress ratio from the direction of principal stress. Therefore, the major principal stress begins to rotate as the b-value increases. This causes the plane having the highest ratio of shear to normal stress to move in the direction of the bedding plane. The bedding

plane is an attractant for shear banding, which acts to pull the shear band in a more horizontal direction resulting in an overall lower angle (Lade et al. 2008).

- The data contained in Figure 2-31 was obtained from testing of a medium density sand. As previously mentioned, this will lead to slightly lower inclinations, usually somewhere between the Coulomb and Arthur predictions.

2.4.5.3 FACTORS AFFECTING THE DEVELOPMENT OF SHEAR BANDS

Lade and Wang (2002) conducted drained testing on loose, medium, and dense air pluviated specimens of Santa Monica beach sand in a cubical true triaxial apparatus. The purpose of the study was to compare the effects of specimen slenderness on the stress-strain and shear strength behavior of specimens subjected to different intermediate principal stress ratios.

Two sets of specimens were tested for this investigation. The first set was comprised of short specimens with a height to diameter ratio of 1.0. The second set consisted of tall specimens that had a height to diameter ratio of 2.47.

The short specimens exhibited the following characteristics:

- Shear bands always intersect the lubricated cap and base
- Stress-strain behavior was prone to have a smooth peak around failure
- Stress-strain behavior exhibited some degree of strain softening after failure prior but to development of a shear band

In contrast, the taller specimens showed the following characteristics:

- The shear bands intersect the confining membrane
- The stress-strain behavior exhibited a greater degree of strength reduction after formation of the shear band
- The tests resulted in slightly lower peak stress ratios
- The peak mobilized friction angle was usually 1 to 2 degrees lower, with the greatest variance occurring in the mid range b-values

This investigation proves that a minimum slenderness ratio is necessary to allow the natural development of shear bands, which are the primary failure mechanism for the mid range b-values. Many early investigations into the effects of the intermediate principal stress ratio utilized cubical specimens that did not have appropriate slenderness ratios. This prevented the natural development of shear banding, and produced flawed failure surfaces that were closer to smooth curves over the full range of b-values.

3 HTSA THEORY

3.1 Stress Application

Independent control of the inner pressure, outer pressure, axial load, and torque are possible with the HTSA. By controlling these four parameters, any generalized state of stress can be achieved. A schematic drawing of the four independently controlled stresses acting on a specimen is shown in Figure 3-1.

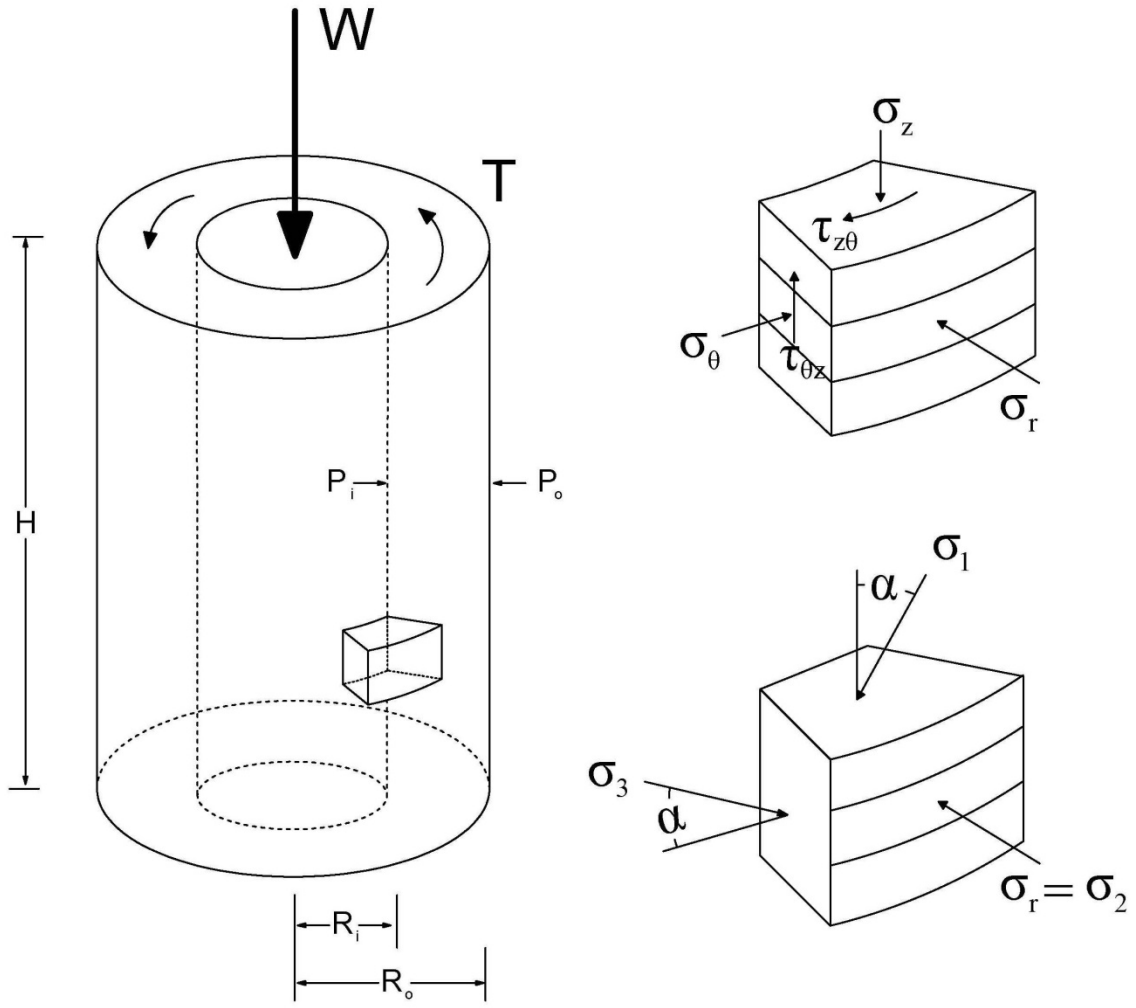

Figure 3-1: HTSA Applied Stresses

The symbols used in Figure 3-1 are defined in Table 3-1. These definitions will remain consistent throughout this document and will not be explained elsewhere.

Table 3-1: Definition of Symbols

Symbol	Definition	
W	vertical load	
T	torque	
P_i	inner cell pressure	
P_o	outer cell pressure	
H	specimen height	
R_i	specimen inner radius	
R_o	specimen outer radius	
σ_z	vertical stress	torsion shear stress space
σ_θ	circumferential stress	
σ_r	radial stress	
$\tau_{z\theta}$	shear stress in horizontal plane	
α	inclination of major principal stress with vertical	
σ_1	major principal stress	principal stress space
σ_2	intermediate principal stress	
σ_3	minor principal stress	
$\tau_{\theta z}$	shear stress in vertical-radial plane	
$\bar{\varepsilon}_z$	average axial strain	
$\bar{\varepsilon}_\theta$	average circumferential strain	
$\bar{\varepsilon}_r$	average radial strain	
$\bar{\tau}_{z\theta}$	average shear strain	

Vertical stress is applied to the specimen by a combination of vertical load and net cell pressure acting on the top cap. Torque applied through the frictional bottom ring produces shear stress ($\tau_{z\theta}$) in the horizontal plane. A complimentary shear stress ($\tau_{\theta z}$) automatically develops on a plane that lies perpendicular to the tangential normal stress (see Figure 3-1).

The inner and outer cell pressures are used to apply radial and circumferential confining stress to the specimen. The flexible vertical boundaries prevent the application of shear stress to the specimen's vertical surfaces, although some unintended shear stresses are introduced due to the effects of end restraint and specimen geometry.

Principal stress rotation in the z-θ plane is created by varying the magnitudes of deviator and shear stresses. Neglecting the effects of stress non-uniformity, the plane of stress rotation is always perpendicular to the radial direction.

The relative magnitude of the intermediate principal stress can be controlled by adjusting the inner and outer cell pressures. If the cell pressures are equal, the radial and circumferential stresses are equal. This condition creates a relatively uniform stress distribution across the wall of the cylinder, but limits the stress states that may be explored by creating a unique relationship between α and b, as shown in Equation (3.1).

$$b = sin^2 \alpha \tag{3.1}$$

Independent control of the inner and outer pressure allows the decoupling of b and α, so that the entire stress space can be explored. However, differences in the inner and outer cell pressure result in non-uniform stress across the specimen's wall.

Torsion shear space, shown in Figure 3-2, is often used to plot HTSA tests since it can capture rotation, which cannot be plotted in general stress space.

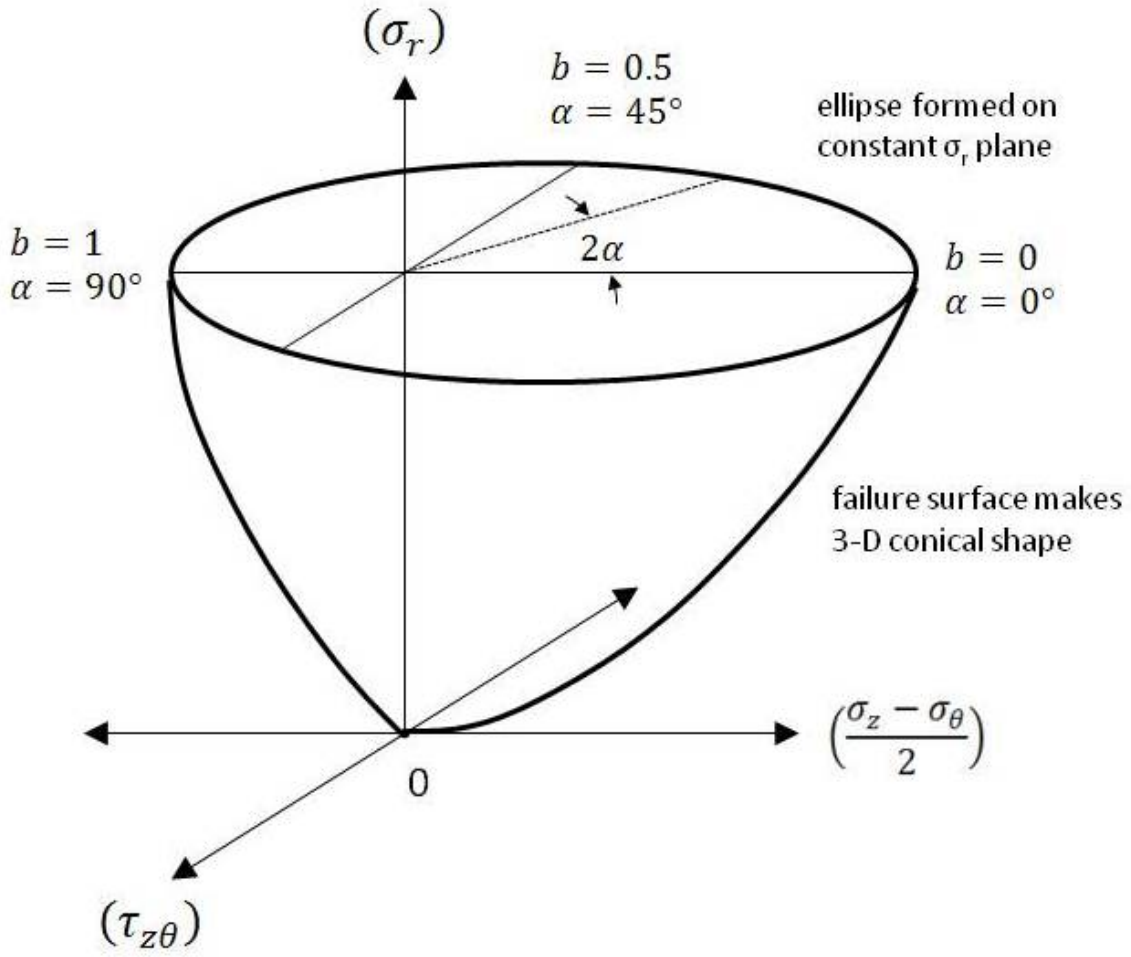

Figure 3-2: Torsion Shear Stress Space
After (Lade and Kirkgard 2000)

The Mohr's circle shown in Figure 3-3 can be used to visualize the relationship between torsion shear and principal stress spaces.

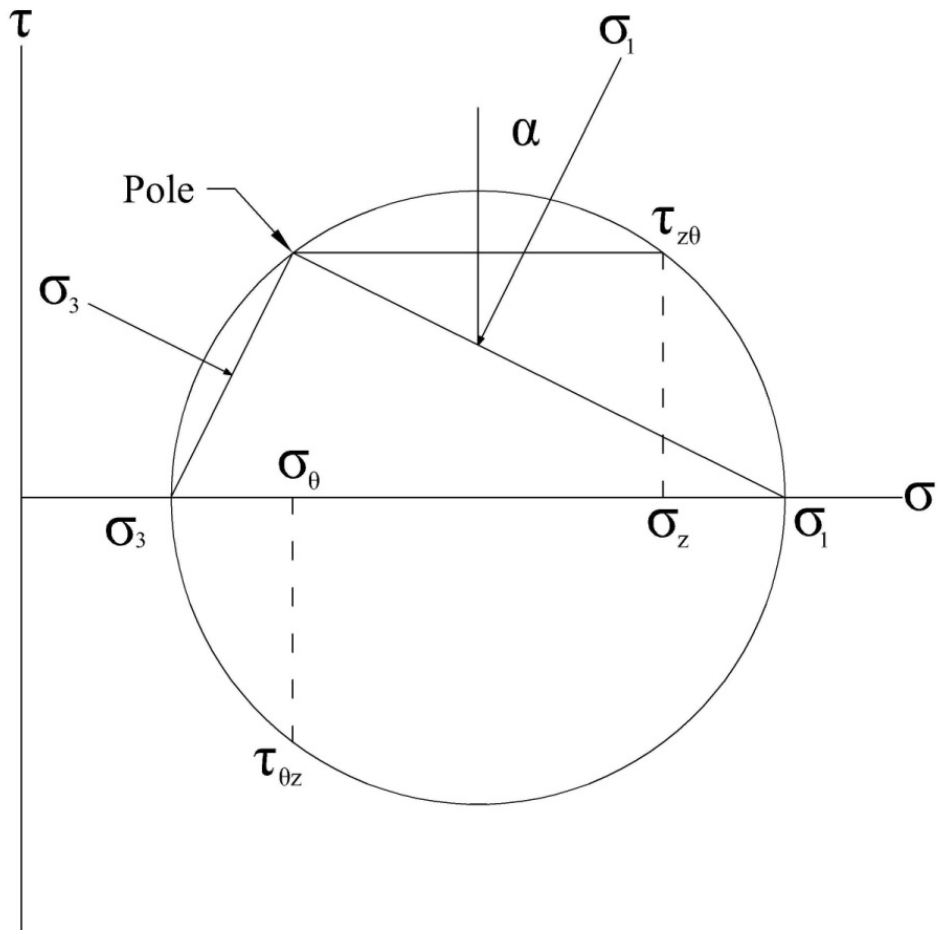

Figure 3-3: Mohr Circle Diagram

3.2 Stress and Strain Equations

Analyses of the stresses and strains acting on the hollow cylinder specimen are performed assuming the specimen is a single element that deforms as a right cylinder. As is the case with many types of test apparatus, stresses and strains within the specimen are not completely uniform. For instance, the shear stress at any point within the specimen is a function of the radius, which varies across the wall of the specimen.

Due to the inherent non-uniformities, the stresses and strains are analyzed in terms of their average values across the cylinder wall, as proposed by Hight et al. (1983). Equilibrium methods, which are independent of constitutive law, were used to derive equations for the vertical and circumferential stress. A linear elastic law was assumed for the radial stress, and a uniform distribution was assumed for the shear stress.

Alternate methods have been proposed that utilize: 1) a single constitutive law, 2) average stresses with weighting for the radius, or 3) compute average stresses over the cylinder volume rather than wall (Vaid et al. 1990, Miura et al. 1986). However, these different methods have been shown to produce similar results (Sayao 1989).

Equation (3.2) is used to calculate the average vertical stress. The original equation has been modified to calculate the stress at the mid height of the specimen by adding a term accounting for half of the specimen's weight.

$$\sigma_z = \frac{[W-(P_o A_r)]}{\pi(r_o^2-r_i^2)} + \frac{P_o r_o - P_i r_i}{r_o^2-r_i^2} + \frac{\gamma' H}{2} \tag{3.2}$$

Where:

A_r = load piston area

γ' = buoyant unit weight of sand

The average radial stress is calculated using Equation (3.3).

$$\sigma_r = \frac{P_o R_o + P_i R_i}{R_o + R_i} \tag{3.3}$$

The average circumferential stress is calculated using Equation (3.4).

$$\sigma_\theta = \frac{P_o R_o - P_i R_i}{R_o - R_i} \tag{3.4}$$

The average shear stress is calculated using Equation (3.5).

$$\tau_{z\theta} = \frac{3T}{2\pi(r_o^3 - r_i^3)} \tag{3.5}$$

Horizontal strains and changes in specimen thickness can be calculated directly using measurements obtained from clip gauges or position sensing instrumentation. However, calculating average horizontal strains based on changes in the inner and outer specimen diameter are a much better alternative (Lade et al. 2009). Specimen diameter changes are calculated using the inner cell volume change, the specimen volume change, and the vertical deformations.

The following equations for specimen diameter change have been altered slightly from those presented by Lade et al. (2009). Lade used a correction factor applied to the inner cell volume to account for volume taken up by the loading piston. No such correction is necessary for this investigation, as the HTSA loading piston is located in the outer cell. Additionally, in order to maintain consistency with the average strain equations presented by Height et al. (1983), the following equations have been presented in terms of changes to the specimen radius rather than the specimen diameter. Equation (3.6) was used to calculate the inner radius change. Terms that have already been defined elsewhere are not defined below the equation.

$$\Delta R_i = \frac{1}{2}\sqrt{R_i^2 + \frac{R_i^2 * \Delta H - \frac{4}{\pi}(V_i)}{H_o - \Delta H}} - R_i \tag{3.6}$$

Where:

ΔR_i = specimen inner radius change

H_o = specimen initial height

ΔH = change in specimen height

V_i = inner cell volume

The specimen outer radius change was calculated using Equation (3.7).

$$\Delta R_o = \frac{1}{2}\sqrt{R_o^2 + \frac{R_o^2 * \Delta H - \frac{4}{\pi}(V_i + V_s)}{H_o - \Delta H}} - R_o \tag{3.7}$$

Where:

ΔR_o = specimen outer radius change

V_s = specimen volume change

Average vertical and shear strains are calculated based on strain compatibility only. Therefore, Equations (3.8) and (3.9) are not a function of the specimen's constitutive law. The radial and circumferential strain calculations are based on the assumption of a linear variation of radial stress across the wall (Hight et al. 1983).

Shear strains have a relatively uniform distribution across the cross-section of a specimen for its entire height, as evidenced by the commonality of numerous simultaneous developing shear bands at failure (Alarcon et al. 1986).

The average vertical strain is calculated using Equation (3.8).

$$\bar{\varepsilon}_z = \frac{H - H_o}{H_o} \tag{3.8}$$

The average shear strain is calculated using Equation (3.9).

$$\bar{\gamma}_{\theta z} = \frac{2\theta\left(R_o^3 - R_i^3\right)}{3H\left(R_o^2 - R_i^2\right)} \tag{3.9}$$

The average radial strain is shown in Equation (3.10).

$$\bar{\varepsilon}_r = \frac{\Delta R_o - \Delta R_i}{R_o - R_i} \tag{3.10}$$

The average circumferential strain is shown in Equation (3.11).

$$\bar{\varepsilon}_\theta = \frac{\Delta R_o + \Delta R_i}{R_o + R_i} \tag{3.11}$$

3.3 Stress Path Calculations

All tests performed as part of this investigation had the following constant test parameters: 1) intermediate principal stress ratio (b), 2) principal stress inclination (α), and 3) mean normal stress (σ_m). Both b and σ_m are typically defined in terms of general stress parameters (σ_1, σ_2, and σ_3), as shown in Equations (3.12) and (3.13). The principal stress inclination cannot be plotted in general stress space, as it must include a shear stress parameter. Therefore, Equation (3.14) is defined in torsion stress space.

$$b = \frac{\sigma_2 - \sigma_3}{\sigma_1 - \sigma_3} \tag{3.12}$$

$$\sigma_m = \frac{\sigma_1 + \sigma_2 + \sigma_3}{3} \tag{3.13}$$

$$\alpha = \frac{1}{2} tan^{-1}\left(\frac{2\tau_{z\theta}}{\sigma_z - \sigma_\theta}\right) \tag{3.14}$$

For tests involving principal stress rotation, the stress path is maintained by controlling the dependant variables (P_i, P_o, and W). Equations for these variables have been developed in terms of the independent variables (T, R_i, and R_o) and the test constants (b, α, σ_m).

To develop a working relationship between these parameters it is first necessary to define the general stress parameters in terms of torsion shear parameters (σ_z, σ_θ, σ_r, and $\tau_{z\theta}$) using Equations (3.15), (3.16), and (3.17) for $\alpha \leq 45°$. For $\alpha > 45°$ the tangential stress (σ_θ) becomes larger than the vertical stress (σ_z). Therefore, these parameters exchange places in equations (3.15) and (3.17).

$$\sigma_1 = \frac{\sigma_z+\sigma_\theta}{2} + \sqrt{\left(\frac{\sigma_z-\sigma_\theta}{2}\right)^2 + \tau_{z\theta}^2} \tag{3.15}$$

$$\sigma_2 = \sigma_r \tag{3.16}$$

$$\sigma_3 = \frac{\sigma_z+\sigma_\theta}{2} - \sqrt{\left(\frac{\sigma_z-\sigma_\theta}{2}\right)^2 + \tau_{z\theta}^2} \tag{3.17}$$

By substituting Equations (3.15) through (3.17) into (3.12) through (3.14), and replacing the torsion shear parameters (σ_z, σ_θ, σ_r, and $\tau_{z\theta}$) with the test variables (P_i, P_o, W, T, R_i, and R_o), the test parameters (b, α, and σ_m) can be defined in terms of the test variables.

$$\sigma_m = \frac{1}{3\left(R_o^2 - R_i^2\right)}\left(\frac{W}{\pi} + 3\left(P_o R_o^2 - P_i R_i^2\right)\right) \tag{3.18}$$

$$b = \frac{\frac{W}{\pi}(1-cos[2\alpha])+(R_o R_i)(P_i-P_o)(1+3\,cos[2\alpha])}{2\left(\frac{W}{\pi}+(R_o R_i)(P_i-P_o)\right)} \tag{3.19}$$

$$\alpha = \frac{1}{2} tan^{-1}\left[3T\frac{\left(R_o^2-R_i^2\right)}{\left(R_o^3-R_i^3\right)}\frac{1}{W+\pi R_i R_o(P_i-P_o)}\right] \tag{3.20}$$

The result of this set of substitutions is a matrix of three Equations (3.18) through (3.20) and three unknowns (P_i, P_o, and W). The remaining parameters are constants (b, α, and σ_m) or independent variables (T, R_i, and R_o). Solving for the unknowns results in set of three Equations (3.21) through (3.23) that can be used in conjunction with the automated control system to maintain the stress path.

$$W = \frac{3T(R_i+R_0)(1-2b+3\,cos[2\alpha]\,csc[2\alpha])}{4\left(R_i^2+R_i R_o+R_o^2\right)} \tag{3.21}$$

$$P_i = \frac{1}{4\pi R_i\left(R_i^3 - R_o^3\right)} csc[2\alpha] \cdot \left(-(-1+2b)T(R_i+3R_o) + 3T(R_i - R_o)\,cos[2\alpha] + 4\pi R_i(R_i^3 - R_o^3)\sigma_m\, sin[2\alpha]\right) \tag{3.22}$$

$$P_o = \frac{1}{4\pi R_o\left(-R_i^3+R_o^3\right)} csc[2\alpha] \cdot \left((-1+2b)T(3R_i+R_o) + 3T(R_i - R_o)\,cos[2\alpha] + 4\pi R_o(-R_i^3 + R_o^3)\sigma_m\, sin[2\alpha]\right) \tag{3.23}$$

The equations shown above are used to control tests with α values from $0° < \alpha \leq 45°$. For the condition $45° \leq \alpha < 90°$, the major and minor principal stresses are reversed and Equations (3.24) through (3.26) are used to control the stress path. The derivation for these equations is contained in Appendix D.

$$W = \frac{3T(R_i+R_0)(-1+2b+3\,cos[2\alpha]\,csc[2\alpha])}{4\left(R_i^2+R_iR_o+R_o^2\right)} \tag{3.24}$$

$$P_i = \frac{1}{4\pi R_i(R_i^3 - R_o^3)} csc[2\alpha] \cdot \left((-1+2b)T(R_i+3R_o) + 3T(R_i-R_o)\,cos[2\alpha] + 4\pi R_i(R_i^3 - R_o^3)\sigma_m\, sin[2\alpha]\right) \tag{3.25}$$

$$P_o = \frac{1}{4\pi R_o\left(-R_i^3+R_o^3\right)} csc[2\alpha] \cdot (-(-1+2b)T(3R_i+R_o) + 3T(R_i-R_o)\,cos[2\alpha] + 4\pi R_o(-R_i^3 + R_o^3)\sigma_m\, sin[2\alpha]) \tag{3.26}$$

At α = 0° and α = 90°, the tests are function of vertical load (W) rather than torque (T). Derivation of these equations is also contained in Appendix D. Equations (3.27) and (3.28) are used for α = 90° conditions, while Equations (3.29) and (3.30) are used for α = 0° conditions.

$$P_i = \frac{W\left((1+b)R_i+3(-1+b)R_o\right)+3(1+b)\pi R_i\left(R_i^2-R_o^2\right)\sigma_m}{3(1+b)\pi R_i\left(R_i^2-R_o^2\right)} \tag{3.27}$$

$$P_o = \frac{-W(3(-1+b)R_i+(1+b)R_o)+3(1+b)\pi R_o\left(-R_i^2+R_o^2\right)\sigma_m}{3(1+b)\pi R_o\left(-R_i^2+R_o^2\right)} \tag{3.28}$$

(3.29)

$$P_i = \frac{(2b-1)\left(W(R_i+3R_o) + 3\pi R_i\sigma_m(R_i^2 - R_o^2)\right) - 3(R_i - R_0)\cos(2\alpha)\left(W + 3\pi R_i\sigma_m(R_i+R_o)\right)}{3\pi R_i(\mathrm{R_i^2} - \mathrm{R_o^2})(-2\mathrm{b} + 3\cos(2\alpha) + 1)}$$

(3.30)

$$P_o = \frac{(2b-1)\left(W(3R_i+R_o) + 3\pi R_o\sigma_m(R_i^2 - R_o^2)\right) - 3(R_i - R_0)\cos(2\alpha)\left(W - 3\pi R_o\sigma_m(R_i+R_o)\right)}{3\pi R_o(\mathrm{R_o^2} - \mathrm{R_i^2})(-2\mathrm{b} + 3\cos(2\alpha) + 1)}$$

4 DESCRIPTION OF THE HTSA

A new Hollow Torsional Shear Apparatus (HTSA) has been constructed for this investigation. This device is fully automated and capable of accurately following a wide range of stress paths during loading or unloading of a specimen. The torque, inner pressure, outer pressure, and vertical load are all independently controlled. The device has relatively large dimensions to minimize stress non-uniformities due to curvature or end restraint.

Two design modifications make this device unique from most previous iterations:

- A comprehensive control board has been constructed that allows the user to select either a manual or computer automated test mode.
- A precision rotary table is used to apply torque to the bottom of the specimen. However, the torque is measured at the top of the specimen.

To minimize corrections, the apparatus has been designed using a very stiff reaction frame and strain measurements have been made in a relative manner between the frame and the specimen.

Tests involving principal stress rotation are conducted in a strain controlled manner by applying a constant shear strain rate to the specimen through a precision rotary table. Tests that do not involve stress rotation are performed in a stress controlled manner, by changing the vertical load at a constant rate.

4.1 The Physical Apparatus

This section describes the design and construction of the HTSA load frame, test cell, and control board.

4.1.1 Loading Frame

A schematic drawing of the load frame and test cell is shown in Figure 4-1. The top and sides of the load frame are constructed from ⅜ inch thick steel. The ⅞ inch thick torque reaction bar is slightly more robust, and the base of the frame is constructed from a single piece of ½ inch steel.

The sides, top, and torque reaction bar have been welded together so that they form one cohesive unit. This unit is bolted to the bottom of the load frame during testing. However, the upper portion of the loading frame is permanently founded on a wheel and rail system so that it can slide out of the way during specimen construction. Figure 4-2 shows the load frame, specimen forming jacket, and pluviation funnel during specimen construction.

A precision rotary table powered by a DC brushed motor is integrated into the base of the load frame.

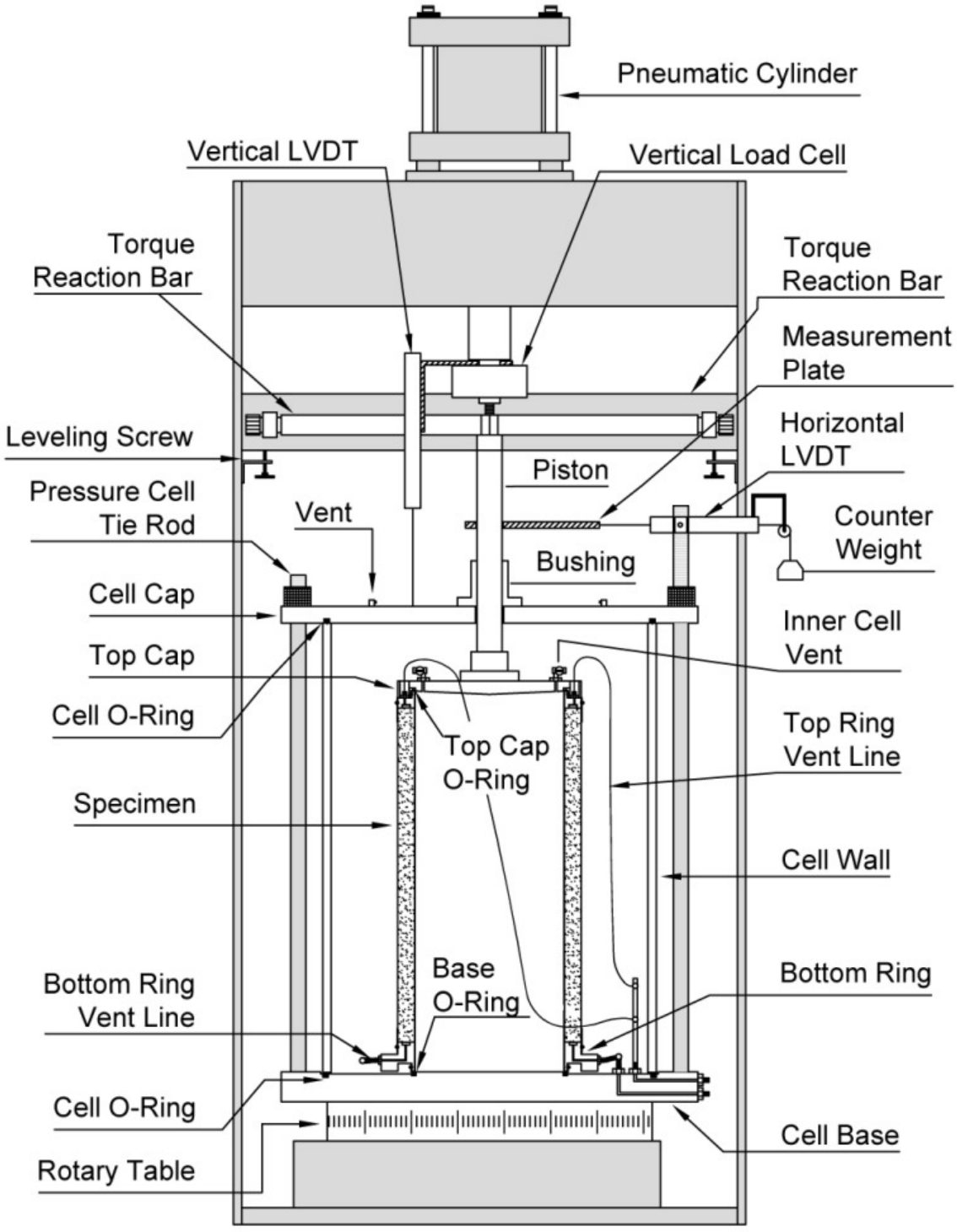

Figure 4-1: Loading Frame and Test Cell

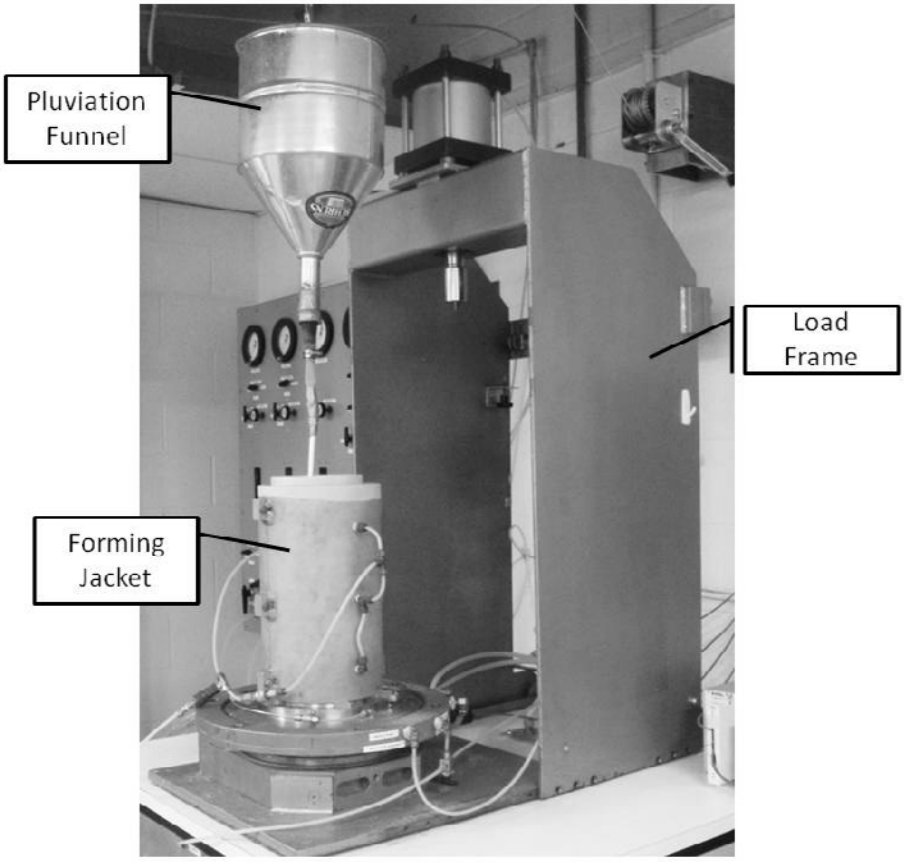

Figure 4-2: Load Frame, Specimen Form, and Pluviation Funnel

4.1.2 Test Cell

The test cell is comprised of a $^{3}/_{8}$ inch thick acrylic plastic cylinder reinforced with stainless steel bands. The test cell cap and cell base are also constructed from stainless steel. Both have grooves for perimeter O-Rings that create a watertight seal with the cylinder. The entire assembly is rigidly bolted to the rotary table and is held together by six tie rods.

The cell cap has two atmospheric vents that can be opened and closed during filling or draining operations. The loading piston penetrates the cell cap through a bushing that contains four nylon-lined plain linear bearings that keep the piston aligned while allowing vertical movement and rotation. Vacuum grease is applied to the linear bearings and shaft to create a watertight seal and reduce friction to negligible levels.

The piston is rigidly connected to the top cap, which is rigidly connected to the top ring by four socket cap screws. The underside of the top cap is tapered to high points located along the outer edge of the top cap. Four vents are located at the high points so that no gases are trapped inside the inner cell during the saturation process.

The top cap clamps down on the top ring to create an airtight barrier between the inner and outer cells at the top of the specimen, as shown in Figure 4-3.

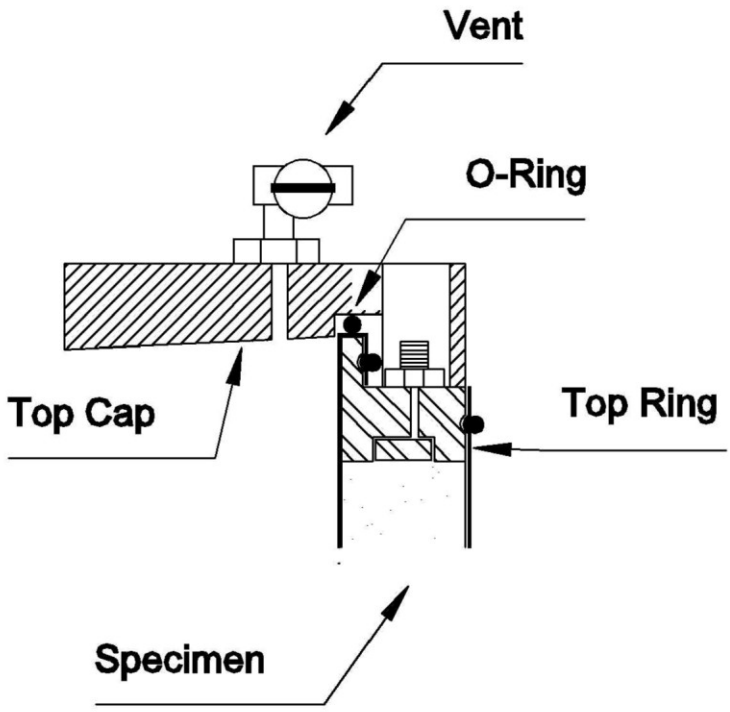

Figure 4-3: Inner and Outer Cell Separation Seal (Top Cap)

At the bottom of the specimen, the airtight barrier between the inner and outer cells is maintained by using four socket cap screws to compress an O-Ring between the cell base and the bottom ring, as shown in Figure 4-4.

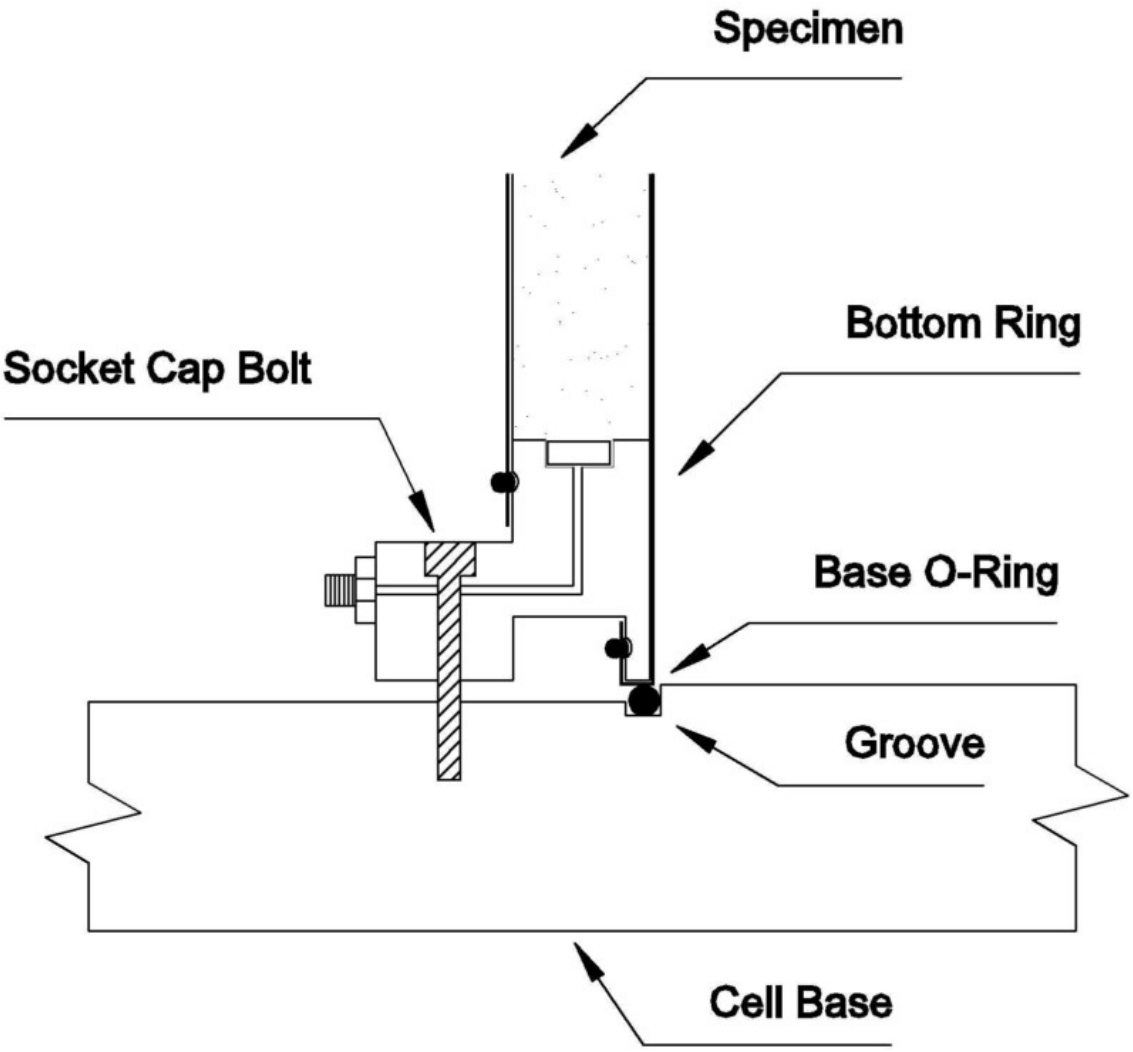

Figure 4-4: Inner and Outer Cell Separation Seal (Bottom Ring)

The cell base has internal conduit for filling and draining the inner and outer cells, as well as the top and bottom rings. These conduits are connected to exterior supply/drain lines by Swagelok NPT-tube fittings. A schematic plan view drawing of the cell base is shown in Figure 4-5.

Three-way valves located at the cell base allow the inner cell and outer cell conduit to be used for either filling or draining purposes. The inner cell drain line also doubles as a carbon dioxide fill line during the inner cell saturation process. A three-way valve attached to the top cap conduit can be set to vent during the saturation process, or it can be directed to a pressure transducer that monitors the specimen pressure.

The net pressure applied by the inner and outer cells is measured at the cell base by two differential pressure transducers. These transducers monitor the pressure difference between the inner and outer cells and the specimen back pressure.

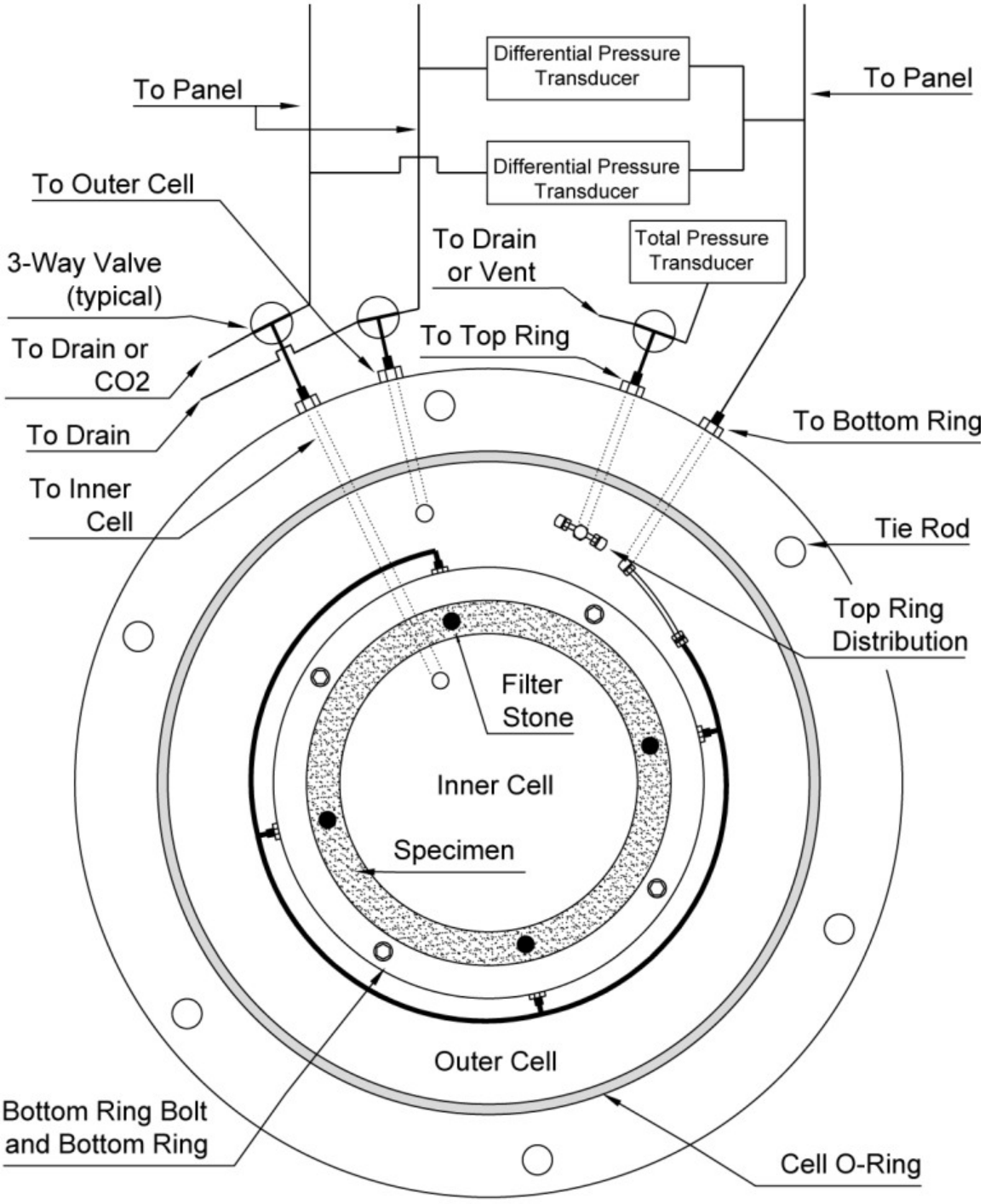

Figure 4-5: Plan View of Cell Base with Fill/Drain Lines

4.1.3 Specimen Top and Bottom Rings

The specimen's horizontal boundaries consist of rigid stainless steel rings. These rings, shown in Figure 4-6, were designed to meet the following criteria:

- Transmit vertical and torque loading to the specimen, while preventing slippage
- Allow free drainage
- Create a watertight seal with the inner and outer membranes

Fully frictional boundaries are created by gluing sand grains, of the same type being tested, to both rings. The sand grains are glued to the rings using Devcon 2-ton clear epoxy. Prior to installation, epoxy is applied to the bottom ring, which is then pressed into a layer of sand. During the pluviation process, sand grains fall onto the bottom ring and become interlocked with the epoxied sand grains. A frictional surface on the top ring is created by applying a thin layer of epoxy to the top ring and then gently pressing it into the specimen.

Four filter stones are located in both the top and bottom rings to maintain free drainage. Each porous plastic filter stone has a cross sectional area of 78.5 mm^2 for a total drainage area of 628 mm^2. It is important to keep epoxy from touching the filters during application of the frictional surfaces to the rings.

Separate inner and outer membranes are used to create an airtight barrier around the specimen. Each membrane is attached to the top and bottom rings using a standard ⅛ inch Buna-n O-ring. Attachment of the outer membrane is straight forward. However, the inner membrane must wrap over the top and bottom ring in order for the O-ring to

work properly. This necessitates attaching the inner membrane to the bottom ring prior to attaching this ring to the cell base.

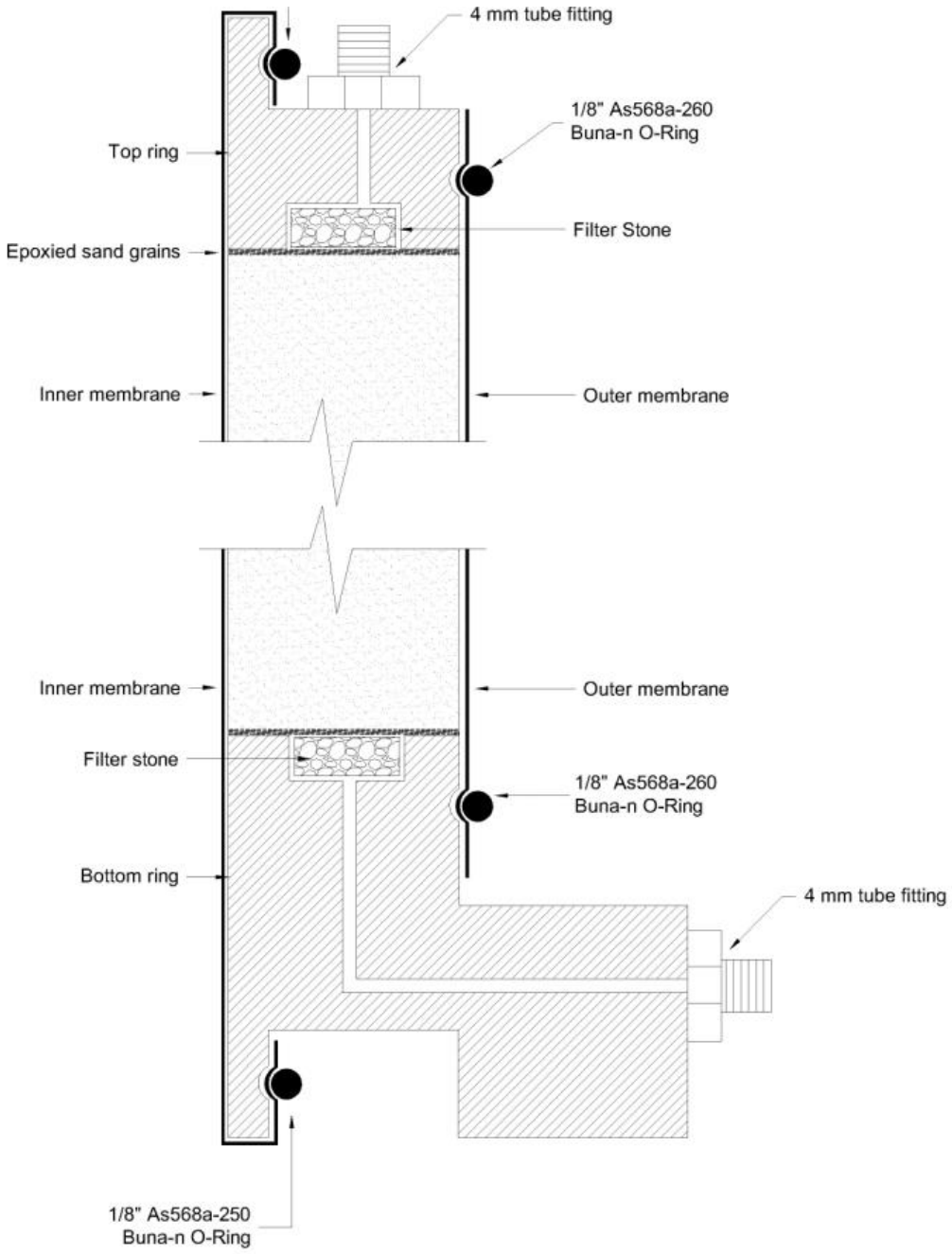

Figure 4-6: Top and Bottom Ring Connection Detail

4.1.4 Specimen Form

Specimens are formed by air pluviation of sand between an inner and outer form. Both forms are rigidly constructed to prevent deformation or movement during pluviation. The cylindrical halves are bolted together during specimen formation, but the halves can be unbolted and detached for easy removal after confining vacuum has been applied to the specimen.

The outer form, shown in Figure 4-7 is made up of a ¼ inch aluminum cylinder split into two semi-circular halves. The inside of the form is completely lined with porous plastic, which evenly distributes the vacuum that is applied through four connection ports embedded in the aluminum form. It requires 40 kPa of vacuum to hold the outer membrane against the form during pluviation.

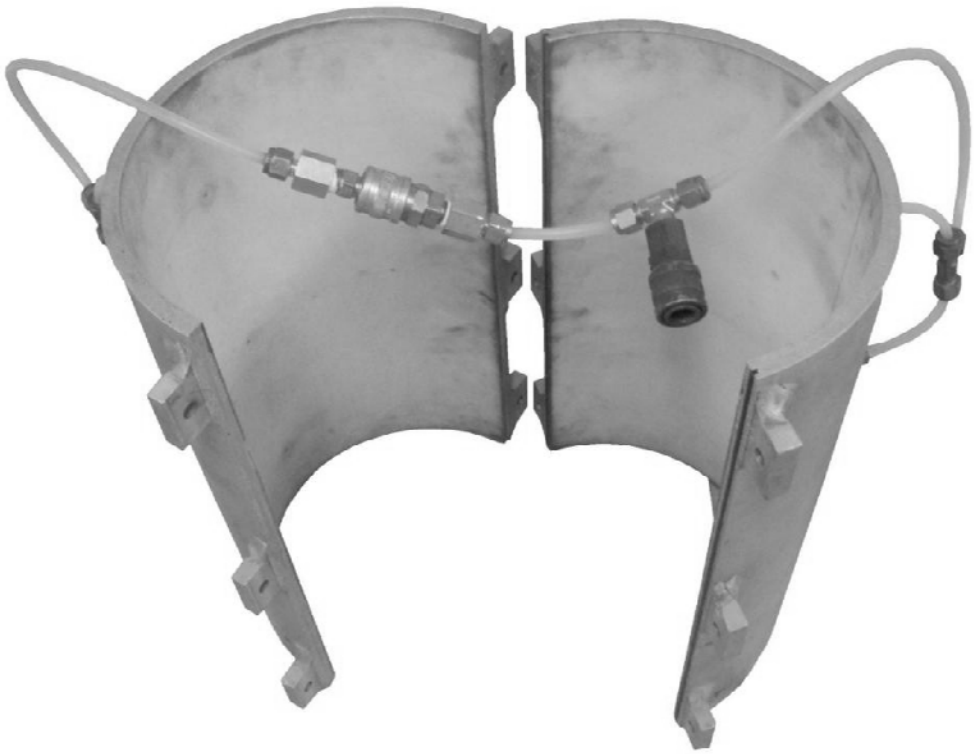

Figure 4-7: Outer Form

The inner form, shown in Figure 4-8, is comprised of a single ⅛ inch thick aluminum cylinder. A vertical slit runs the entire length of the cylinder so that it functions as a spring form. Two adjustment screws have been installed on the inside of the cylinder. When extended, these screws prevent the cylinder from compressing. After the confining vacuum has been applied to the specimen, the adjustment screws are loosened and the cylinder is compressed so that it can be easily removed.

The outside of the inner membrane is liberally sprinkled with baby talcum powder and it is stretched over the inner form. Poisson's effects keep this membrane securely in-place during specimen pluviation.

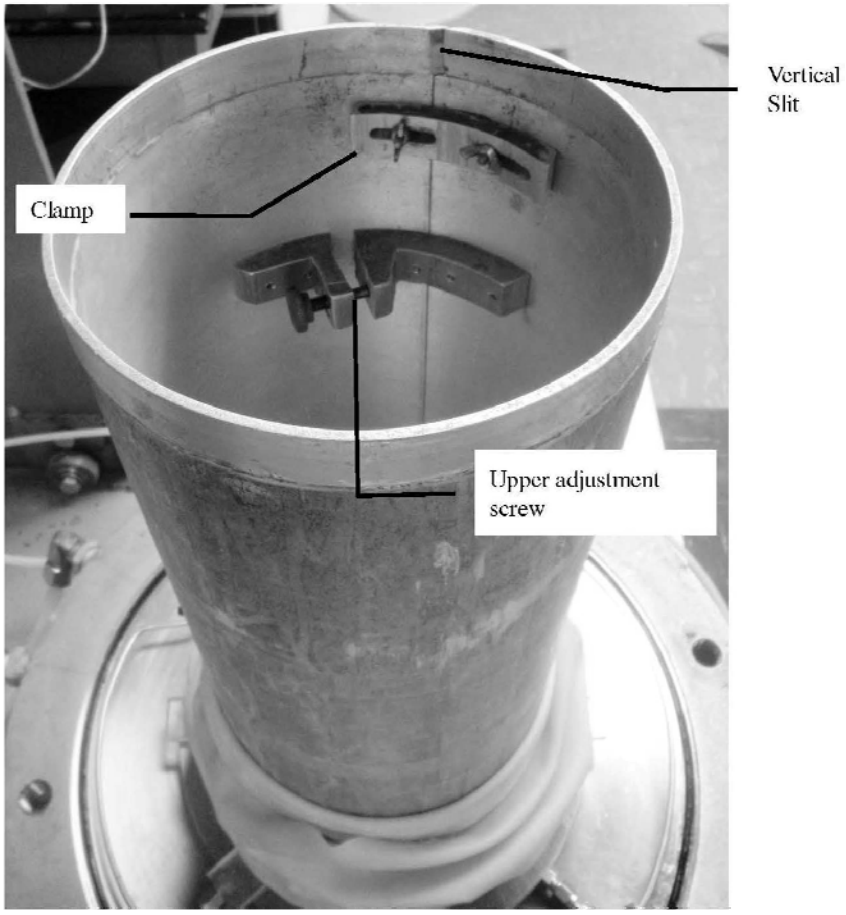

Figure 4-8: Inner Form

4.1.5 Tubing, Valves, and Connections

The de-aired water supply tubing for the inner and outer cells consist of ½ inch O.D. polyethylene tubing. The tubing (Seal Plastics #88P) has a wall thickness of 0.062 inches and is pressure rated to 1,034 kPa at 24° C. All other tubing used in the control panel consists of ¼ inch O.D. polyethylene. The ¼ inch tubing (Seal Plastics #44P) has a wall thickness of 0.040 inches and is pressure rated to 1,310 kPa at 24° C.

The control panel contains 20 valves. All valves are one-piece brass Swagelok 40-Series ball valves that have been pressure tested to 17.24 MPa at 20° C.

All tube-to-tube connections within the control panel are made using brass Swagelok tube fittings. The fittings are pressure rated to exceed the recommended working pressure of the polyethylene tubing. Tube-to-sensors or tube-to-control connections within the control panel are made using Swagelok NPT-tube fittings, which have maximum recommended working pressures of 16.55 MPa at 20° C.

4.2 Load Application

4.2.1 Vertical Normal Load

Vertical loading is provided by a double acting 16 cm diameter pneumatic load cell that is bolted to the top of the loading frame. The harness holding the load cell is adjustable so that the center of the load cell can be perfectly aligned with the center of the specimen, preventing load eccentricity.

The load produced by the cylinder is transmitted to the specimen by the top ring / top cap assembly. A rigid piston connects the cap assembly to a vertical load cell located on the underside of the pneumatic cylinder.

The entire system is completely rigid so that both compression and tension forces can be imparted to the specimen.

Prior to testing, a minimum pressure of (34.5) kPa is simultaneously applied to the cylinder's upper and lower chambers, resulting in zero net load. The pressure in the bottom chamber is then fixed and a downward vertical load is applied by increasing the pressure in the upper chamber or an upward load is applied by decreasing the pressure in the upper chamber.

The maximum available air pressure is (414) kPa, resulting in an available load of (8,314) N. Not accounting for vertical stress due to differences in inner cell and outer cell pressures, the maximum available vertical soil stress is (662) kPa.

4.2.2 Shear

Shear stress is applied to the specimen by the relative rotation of the end rings that is created by rotating the bottom ring while preventing movement of the top ring. The top ring and cap are rigidly connected to the load frame by the torque reaction system, as shown in Figure 4-9.

The bottom ring is bolted to the cell base and a Bison-Bial 9060-320 rotary table. The rotary table has a gear ratio of 90:1, and is driven by a high precision DC brushed motor with low backlash planetary gearhead. The motor, Maxon RE25 # 118746, has a maximum continuous torque of 28.8 mNm, and a stall torque of 2.9 mNm. The planetary gearhead, GP32A #166201, has a ratio of 4060:1. The theoretical maximum torque available for this system is equal to (10,524) N·m.

The combined efficiency of the planetary gearhead and rotary table worm gear is in the 40 to 60 percent range. In the worst case, this leaves a working torque of about (4,200) N·m available for testing. Thus the confining pressure must be chosen so that higher levels of torque are not required to fail the cylindrical sand specimen.

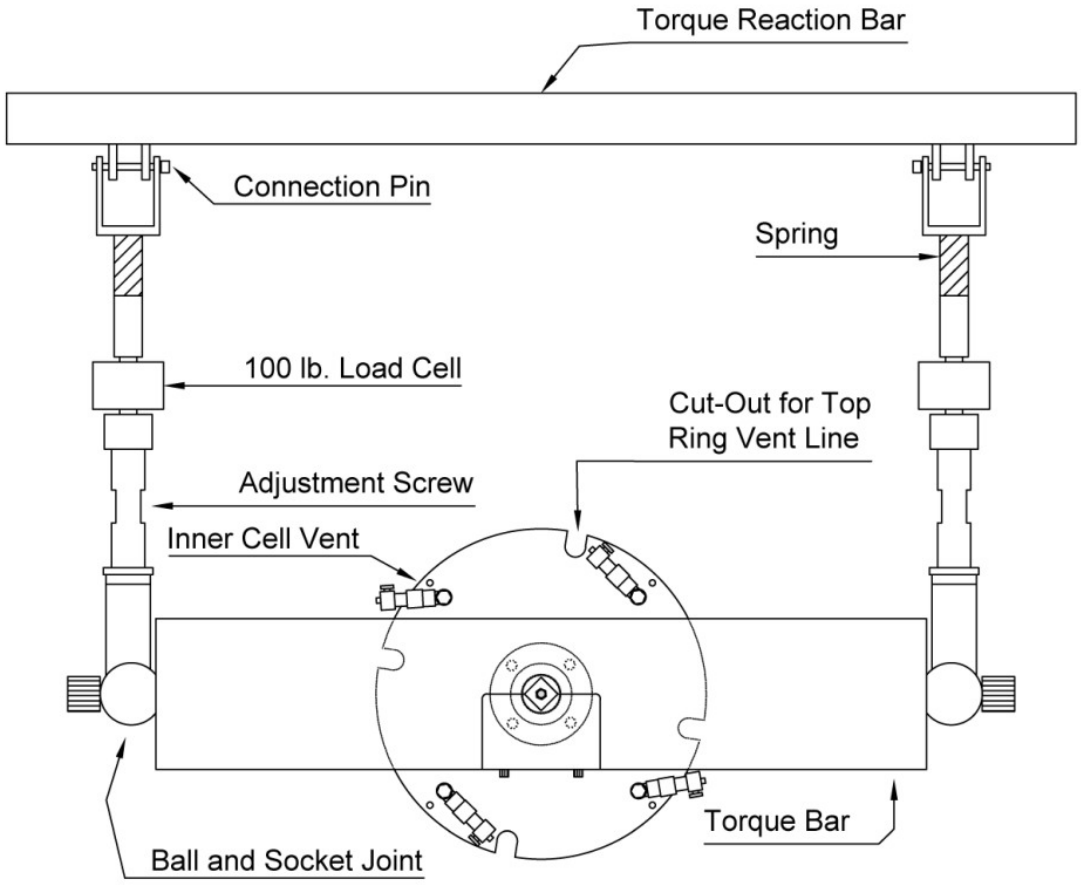

Figure 4-9: Torque Reaction System

4.2.2.1 TORQUE BALANCING

As shown in Figure 4-9, the torque applied at the bottom of the specimen by the rotary table is resisted at the top of the specimen by two stiff reaction arms, each having a torque arm distance of 261 mm from the center.

The forces in each reaction arm should be kept equal so that no normal forces are applied to the linear bearings in the bushing. Additionally, the reaction arms must be capable of extending slightly as vertical deformation occurs.

These requirements were met by integrating precision compression springs in the torque reaction arms. The compression spring properties are listed in Table 4-1. The spring was designed by considering the test conditions that require maximum torque (i.e. b=1.0 and α=45°). At this condition, a mean normal stress of 101.3 kPa and an estimated peak friction angle of 45.5° will produce a load of 233.1 N in each torque reaction arm. This is slightly less than 235.8 N, the maximum working load of the spring.

Table 4-1: Compression Spring Data

Supplier	Century Spring
Part Number	72297
Free Length (mm)	25.40
Compressed Length (mm)	12.19
Maximum Deflection	10.92
Maximum Load (N)	235.8
Outer Diameter (mm)	21.59
Inner Diameter (mm)	16.51

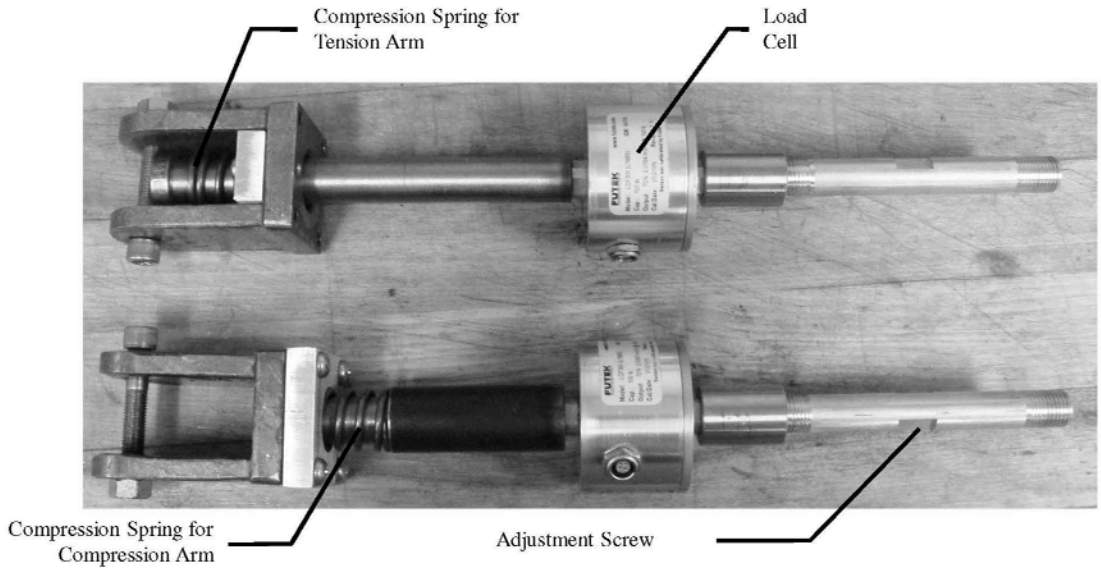

Figure 4-10: Torque Arms

4.2.3 Horizontal Normal Pressure

Horizontal loading is applied to the specimen's vertical boundaries by pressurized water acting over a flexible membrane. Both the inner and outer membranes are sealed at the top and bottom rings to isolate the inner and outer cells from the water within the specimen.

A control panel (described in Section 4.3) is used to convert pneumatic pressure to water pressure, which is applied to the specimen. The pneumatic pressure is applied by calibrated electo-pneumatic pressure regulators. However, because rising or falling water columns within the volume change device result in unaccounted for pressure changes of up to 1.5 kPa, the pressure regulators cannot maintain highly accurate cell pressures by themselves. Two differential pressure transducers located near the base of the test cell account for any rise or fall in the water columns in the volume change device.

The pressure transducers continuously monitor the net pressure difference between the back pressure and the inner and outer cell pressures. This information

provides a source of continuous feedback to the control computer which makes incremental adjustments to the pressure regulators to achieve the target pressures. Using this close looped system, the radial and tangential stresses, which are a function of the inner and outer cell pressures can be accurately controlled.

For HTSA testing, differential pressure between the inner and outer cells must be known with accuracy. A maximum discrepancy between the inner and outer cell transducers of 0.276 kPa (0.04 psi) was measured during sensor calibration. This corresponds to 0.09 percent error over the full scale. The calibration was performed by using a single pressure regulator to simultaneously supply both pressure transducers with exactly the same pneumatic pressure.

4.3 Control Panel

The control panel, shown in Figure 4-11 and Figure 4-12, contains the tubing, valves, transducers, gauges, and volume change devices used to supply the HTSA with de-aired water, compressed air, carbon dioxide, and vacuum. This panel has the ability to operate in either manual or fully automated mode.

The control board contains several different types of sensors and controls. Table 4-2 presents a listing of their manufacturer, model number, range, and accuracy.

Table 4-2: Sensors and Controls

Type	Supplier	Model (#)	Range (kPa)	Accuracy (kPa)
Electo-Pneumatic Pressure Transducer	Fairchild	T7800	0 – 400	1.034
Differential Pressure Transducer	Validyne	P300D	-3.5 - 3.5	0.008618
Analogue Pressure Gauge	Omega	PGT	0 – 400	1.034
Manual Pressure Regulator	Fairchild	30	0 – 400	n/a
Analogue Vacuum Gauge	Omega	16	0 - 101.3	0.517

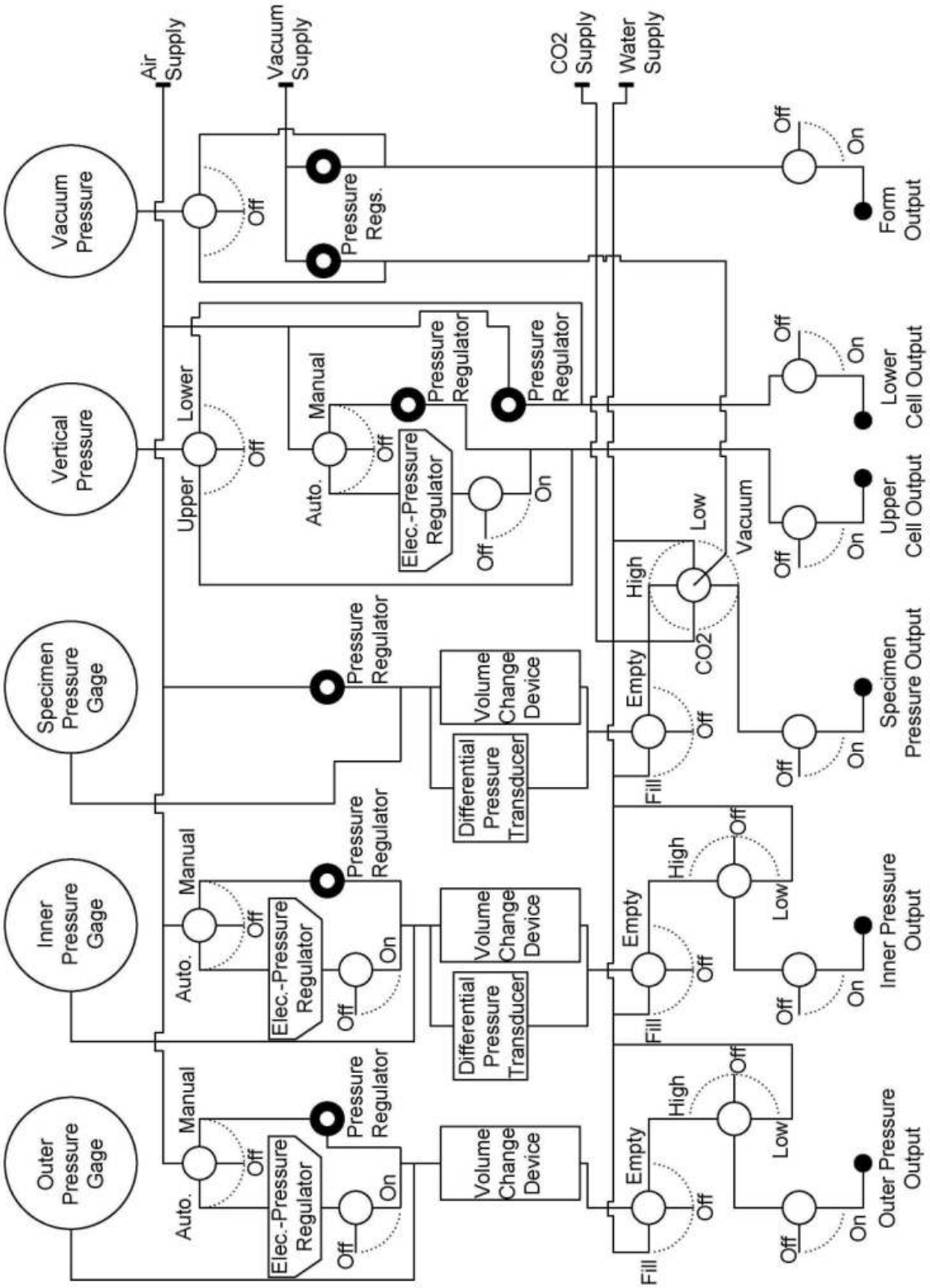

Figure 4-11: Control Panel

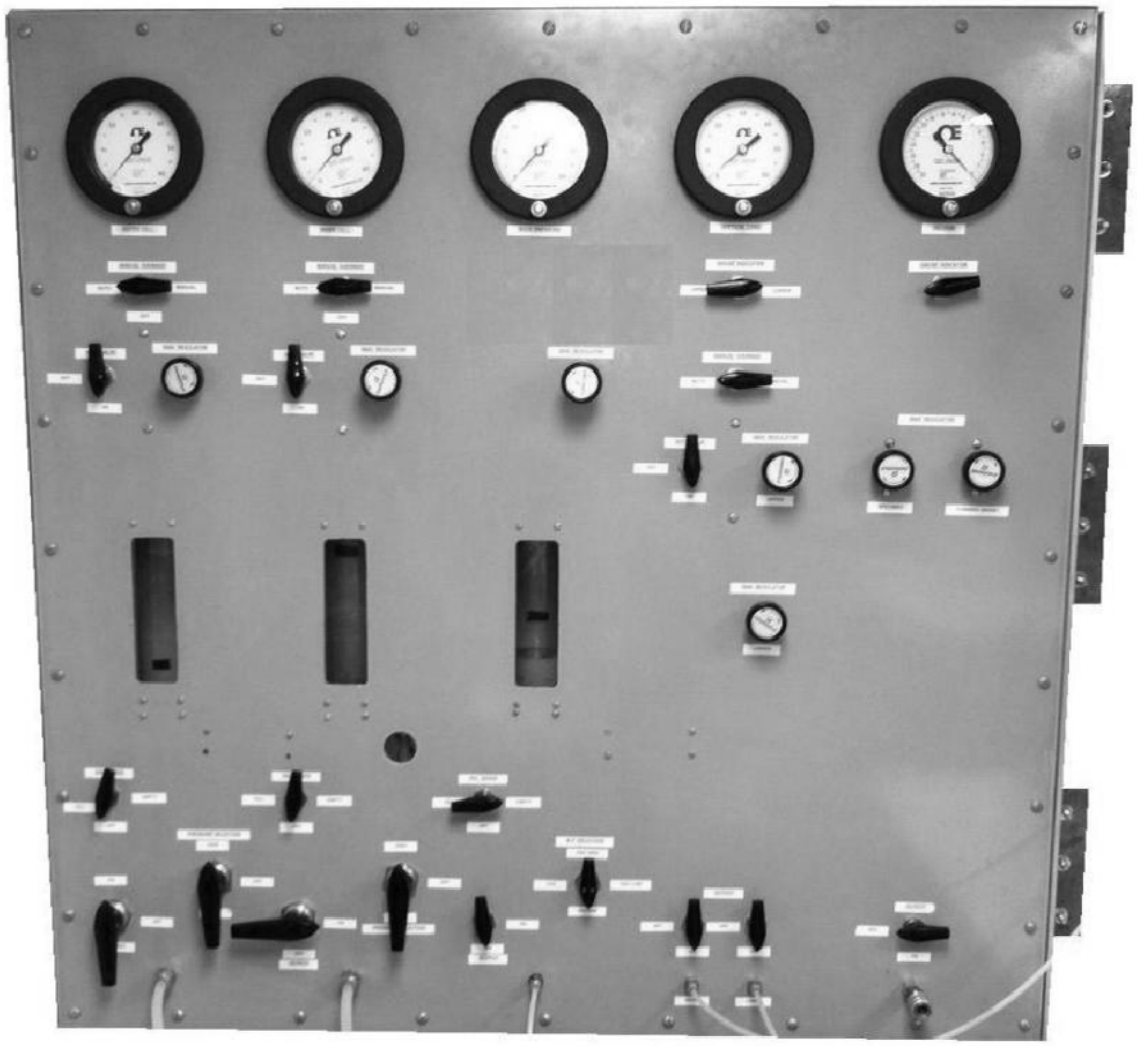

Figure 4-12: Control Board

The aluminum panel is 48 inches wide, 48 inches tall, and 6 inches thick. The outer panel is constructed from a powder coated ⅛ inch thick aluminum plate bolted to a rigid frame made of perforated zinc coated 1¼ inch angle steel. The entire assembly is attached to the laboratory wall with heavy duty hinges so that it can swing open to provide access for maintenance and transducer calibration.

The panel controls are organized into 5 columns. The first three columns are used to control the water flow and pressure of the inner cell, outer cell, and specimen. These

three columns have similar configurations. The fourth column is used to supply pressure to the vertical load cell. The fifth column supplies vacuum that is only used during test preparation.

4.3.1 Columns for Outer Cell, Inner Cell, and Specimen Control

At the top of each column is a mechanical pressure gauge that monitors the air pressure at the top of the volume change device. The gauge indicates the air pressure applied by the regulator, but it does not take into account the pressure created by the water column within the volume change device. Therefore, although these gauges are an excellent source of qualitative information, data obtained from the gauges can't be used for analysis without correcting it for the water column height.

A three-way valve connecting the pressurized air supply to the pressure regulator is located directly beneath the pressure gauges. This valve allows the user to select either the "automatic" or the "manual" control mode. In the automatic mode the air pressure is directed to an electro-pneumatic pressure regulator. If the "manual" mode is selected, the air pressure is directed to a mechanical pneumatic pressure regulator. No automatic mode is necessary for the specimen column, because the back pressure does not change during testing.

Each volume change device has a maximum capacity of (650) ml and is located directly beneath the pressure regulators. They are constructed from 207 mm long polycarbonate cylinders with inner diameters of 63.28 mm. The volume change devices have been leak tested to a pressure of (414) kPa.

Volume changes within the inner cell and specimen can be calculated from the water column height within each cylinder. A Validyne model P300D-26 differential pressure transducer connected to the top and bottom of each volume change device, continuously monitors the height of water within the volume change device.

A "Fill/Empty" three-way valve is located beneath each volume change device. The valve can be set to: 1) fill the volume change device with de-aired water from the supply tanks, 2) connect the volume change device with the cells/specimen, or 3) prevent water from entering or leaving the volume change device.

The next valve in the column allows the user to select:

- High pressure de-aired water from the volume change device
- Low pressure water, directly from the de-aired tanks

Two additional options are available for the specimen column:

- Carbon dioxide (for saturation)
- Vacuum (for confining stress during specimen construction)

The final two fittings in each column consist of on/off valves and bulkhead tube connections, which bring the output to the front of the control panel.

4.3.2 Column for Vertical Pressure Control

The fittings located in this column control the air pressure in the upper and lower chambers of the vertical load cylinder. A single mechanical pressure gauge connected to a three-way valve is used to monitor either the upper or lower chamber pressure.

The lower chamber pressure is held at a constant value during the test. Therefore, its control is maintained by a manual pressure regulator. The upper chamber pressure is either increased or reduced to apply vertical load during a test. A three-way valve allows the upper chamber to be controlled by either an electo-pneumatic pressure regulator, or a manual pressure regulator.

Two on/off valves and bulkhead tube fittings are located at the bottom of the panel. These fittings provide connection ports for the vertical load cell.

4.3.3 Column for Vacuum

The last control column is used to apply vacuum to the specimen and forming jacket. A single mechanical gauge connected to a three-way valve is used to monitor either the specimen or forming jacket vacuum. Two manual vacuum regulators are located below the three-way valve.

The regulator on the left hand side is used to control the vacuum applied to the specimen prior to filling and pressurizing the inner and outer cells with de-aired water. The vacuum line from this regulator is connected to a four-way valve in the specimen control column that allows the user to apply either: 1) low pressure de-aired water, 2) high pressure de-aired water, 3) carbon dioxide, or 4) vacuum to the specimen.

The vacuum regulator on the right hand side is used to control the vacuum applied to the outer specimen form. This regulator is connected to an on/off valve and bulkhead Foster fitting, which provides a connection port for the forming jacket vacuum line.

4.4 Deformation Measurement

Average vertical and shear deformations are measured using linear variable differential transformers (LVDTs) located outside the test cell. In both cases, measurements are made between the test cell cap and the load piston, which is rigidly attached to the specimen. Using these two reference points isolates the measurements from both the loading frame and load cell stiffnesses.

4.4.1 Shear Deformation

Shear deformation is measured by monitoring the relative movement between the load piston and the cell cap. The measurement configuration is shown in Figure 4-13. A pie-shaped measurement arm is rigidly attached to the load piston. An LVDT is rigidly mounted to one of the load cell tie rods. An inelastic radio cord is used to connect the LVDT to a tangential point on the measurement plate, converting the relative radial motion to a liner motion. A 400 gram counter weight is attached to the back side of the LVDT core, keeping the radio cord taught and allowing the LVDT to move in both directions.

The LVDT used in this system is a Schaevitz 2000 DC-EC with a range of ± 50 mm and an accuracy of 0.17 mm. The accuracy, in terms of average shear strain, is 0.03 percent. LVDT accuracy calculations and the measurement arm dimensions are contained in Appendix C.

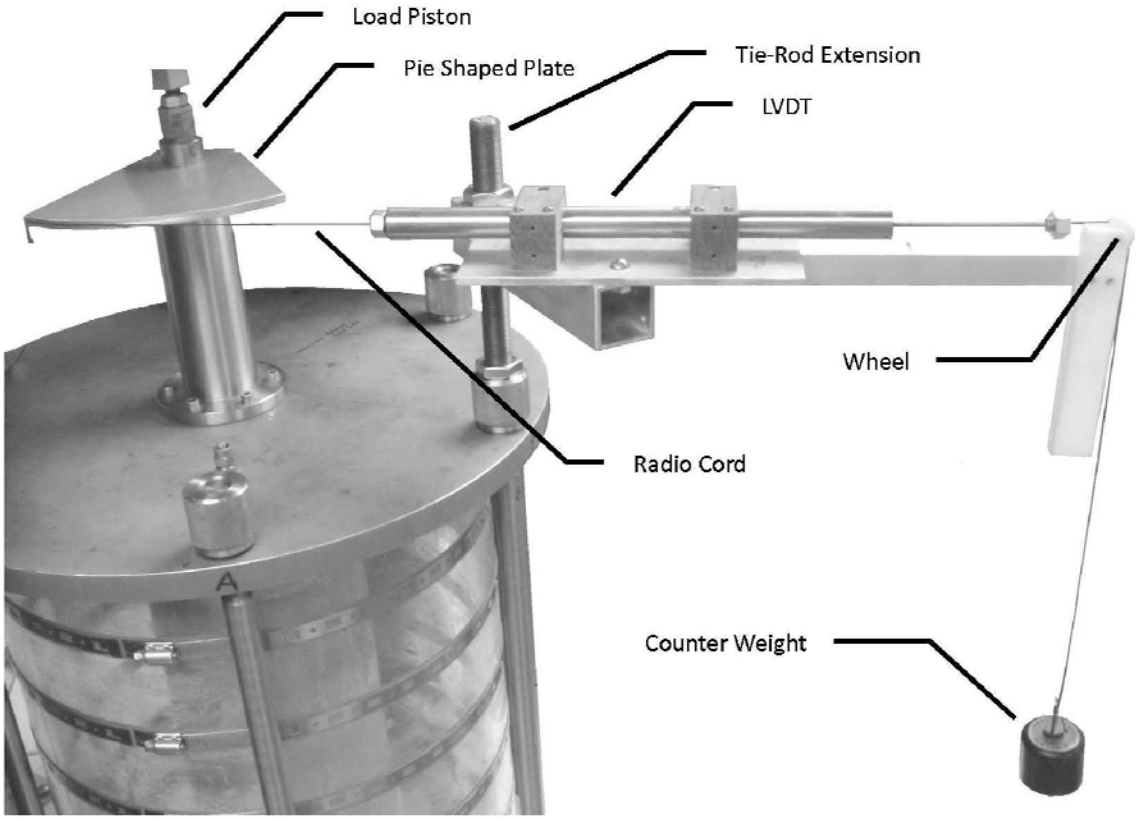

Figure 4-13: Shear Deformation Measurement System

4.4.2 Vertical Deformation

Vertical deformation is measured by monitoring the relative movement between the loading piston and the cell cap. The measurement configuration is shown in Figure 4-14. An LVDT is rigidly mounted to a bracket that is attached to the top of the load piston, and held into place between the load piston and the vertical load cell. A threaded brass extension rod is connected to the LVDT core. It rests on top of the cell cap and moves up or down with the differential movement between the loading piston and the cell cap.

The LVDT used in this system is a Schaevitz 1000 DC-EC with a range of ± 25 mm and an accuracy of 0.035 mm. The accuracy, in terms of average vertical strain, is 0.008 percent. The LVDT accuracy calculations are contained in Appendix C.

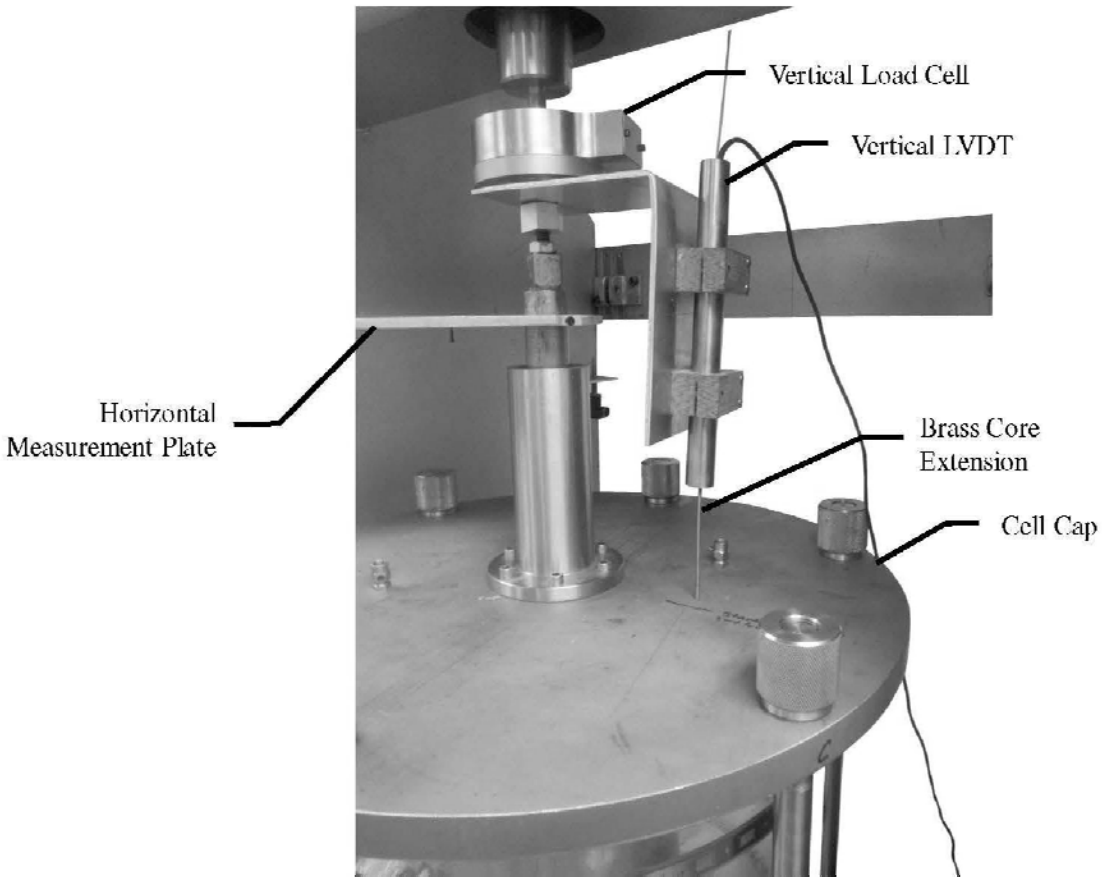

Figure 4-14: Vertical Deformation

4.4.3 Volume Change

Inner cell and specimen volume changes cause increases or decreases in the water column heights of the volume change devices. Figure 4-15 shows a volume change device and differential pressure transducer located on the back side of the control panel.

The four-way tube connection located at the top of the figure distributes high pressure air to the mechanical pressure gage, the top of the water column, and the negative side of a Validyne model P300D-26 differential pressure transducer. The air pressure at all three locations is always equal.

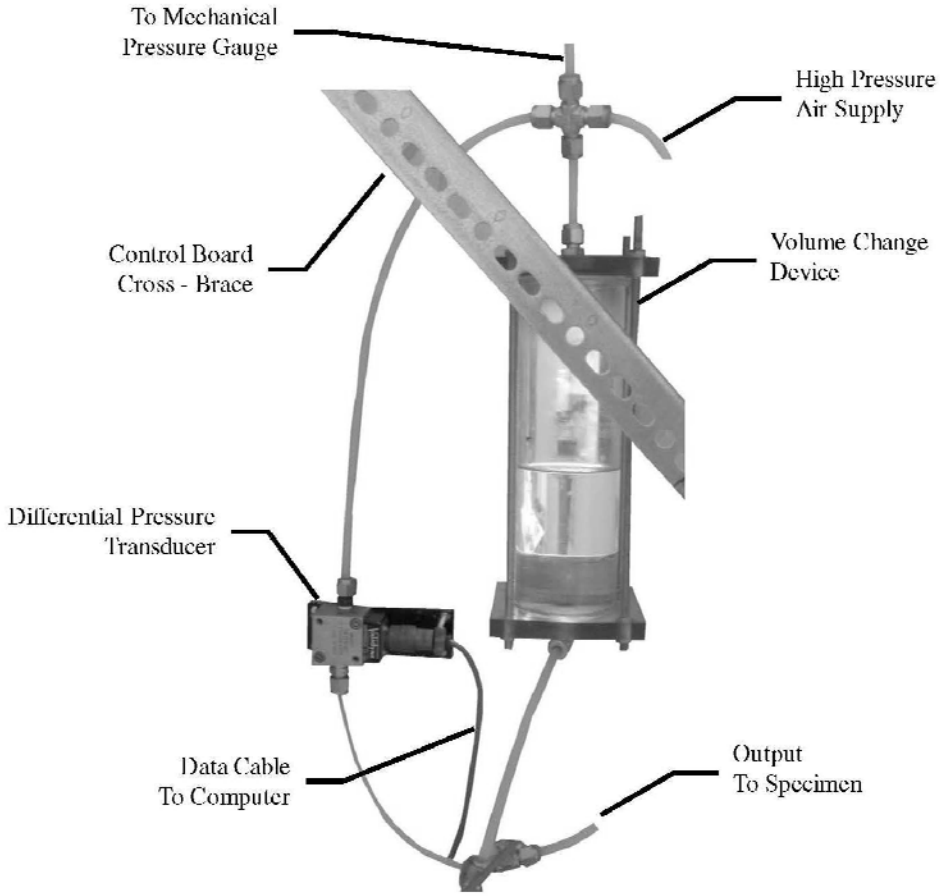

Figure 4-15: Volume Change Device and Differential Pressure Transducer

The three-way connection at the bottom of the volume change device distributes high pressure de-aired water to the specimen and the positive side of the differential pressure transducer.

Changes in pneumatic pressure are simultaneously measured by both sides of the differential pressure transducer and produce a canceling effect. Therefore, the net change in stress across the pressure transducer is equal to the change in the water column height. The volume change within the inner cell and specimen can be calculated from the water column height within each cylinder.

The volume change device and associated tubing expand and contract in response to pressure changes, producing a slight change in the water column height. A calibration performed to correct for this effect is contained in Appendix B. A straight line method produces the best fit for this calibration data. The maximum non-linearity associated with this calibration is 0.1038 ml.

4.5 Test Control and Data Acquisition

A close-looped system with error sensing feedback is used to provide the new HTSA with fully automated stress path control and data acquisition. A conceptual layout of this system is shown in Figure 4-16, and its logic is explained in Section 4.5.1.

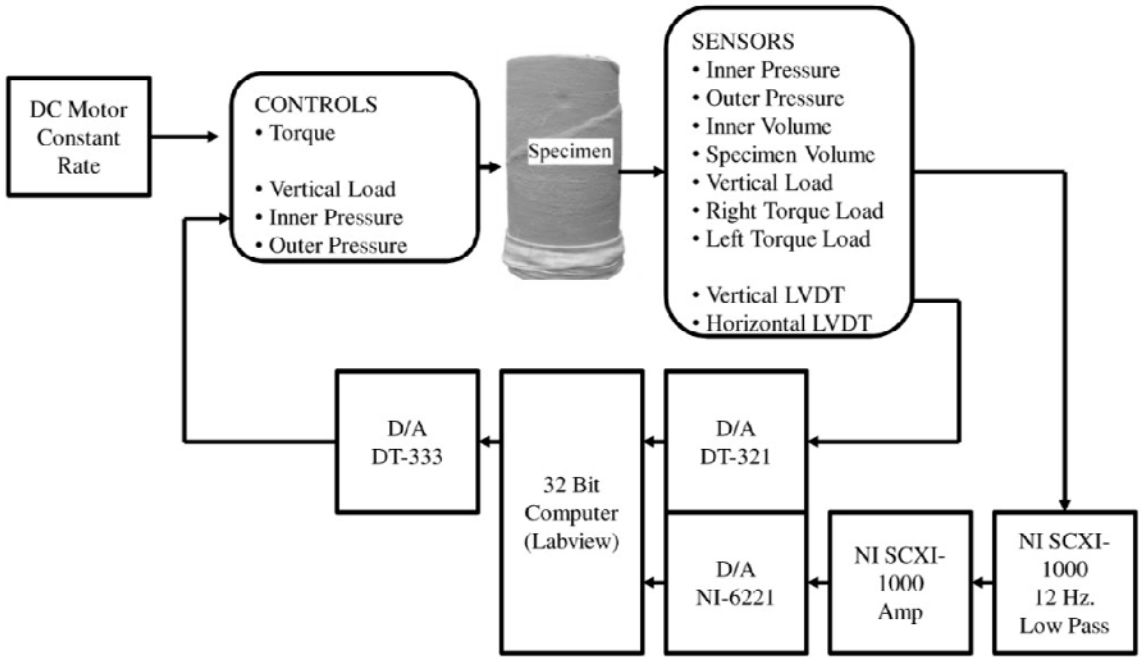

Figure 4-16: Conceptual Diagram of Test Control and Acquisition System

4.5.1 Test Logic

This section describes the logical flow for tests with inclined principal stress directions. Words emphasized in bold refer directly to the icons which make up Figure 4-16.

Each test starts by using a brushless **DC Motor** to apply a constant rate of rotation to a rotary turn-table. The rotation creates torque which **Controls** the test by applying shear stress to the S**pecimen,** where it affects a physical change that is measured by the **Sensors.**

There are two groups of sensors. The upper group of sensors returns an unfiltered signal in the millivolt range, while the lower group of sensors has integral signal conditioning and returns a filtered and amplified signal.

Readings from the upper **Sensors** are transferred to **NI SCXI Low Pass** for noise filtering and then **NI SCXI Amp** for amplification. The filtered and amplified signal is then transferred to **NI-6221,** a digital-to-analogue conversion card that converts the analogue voltage to a digital signal.

The lower **Sensors** signals do not need filtering and amplification, so they are transferred directly to the **DT-321** D/A card where they are converted from an analogue voltage to a digital signal.

The digital signals from each D/A card, **NI-6221 and DT-321**, are transferred to the C**omputer**. A custom Labview based program reads the signals and converts them to equivalent movements, loads, and pressures which describe the stress and strain states of the specimen. The current stress state is compared to the desired stress path and revised loads and pressures are calculated to maintain the intended stress path.

Voltages equal to the desired pressures and loads are calculated and digitally transferred from the **Computer** to the **DT-333** D/A card where they are converted to analogue signals.

The analogue signals are transferred from the **DT-333** to each **Control** transducer, where the analogue signal is converted to air pressure. The air pressure is used to apply inner and outer cell pressures and vertical loads to the specimen. The entire process is repeated in a loop until the test is finished.

For stress path conditions that do not involve torque application (i.e. $\alpha = 0°$ and $\alpha = 90°$), the independent variable becomes the vertical load. These types of tests are run in a stress controlled manner by applying a constant rate of pneumatic pressure increase to the vertical load cylinder.

4.5.2 Specifications

Specifications for the data collection system are as follows:

- Computer – 32-bit PC based desktop computer with 1 GHz processor.
- Analogue Output – The Data Translation DT-333 is a PCI based 16-bit digital-to-analogue (D/A) conversion card programmed for 0 to 10 volts analogue output on up to 4 isolated channels. PCI is one of the most widely adopted internal buses for PCs. A PCI D/A conversion card is shown in Figure 4-17. While a typical PCI bus located within a desktop computer is shown in Figure 4-18.

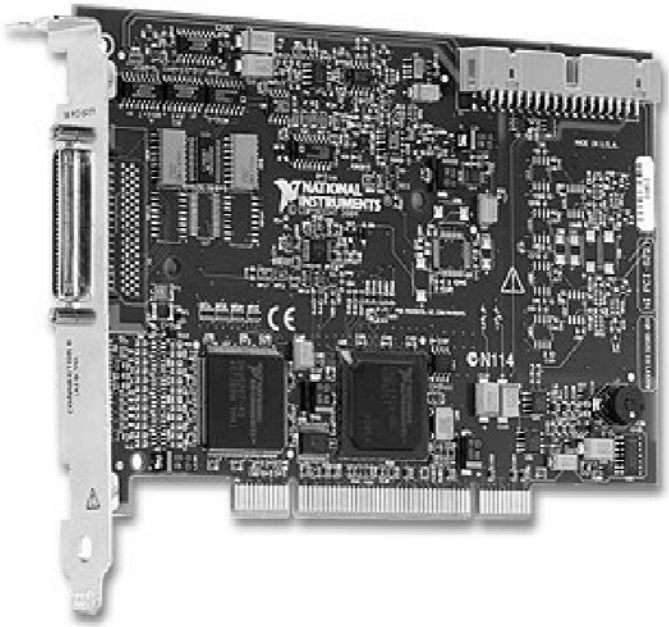

Figure 4-17: PCI-6221 D/A Card

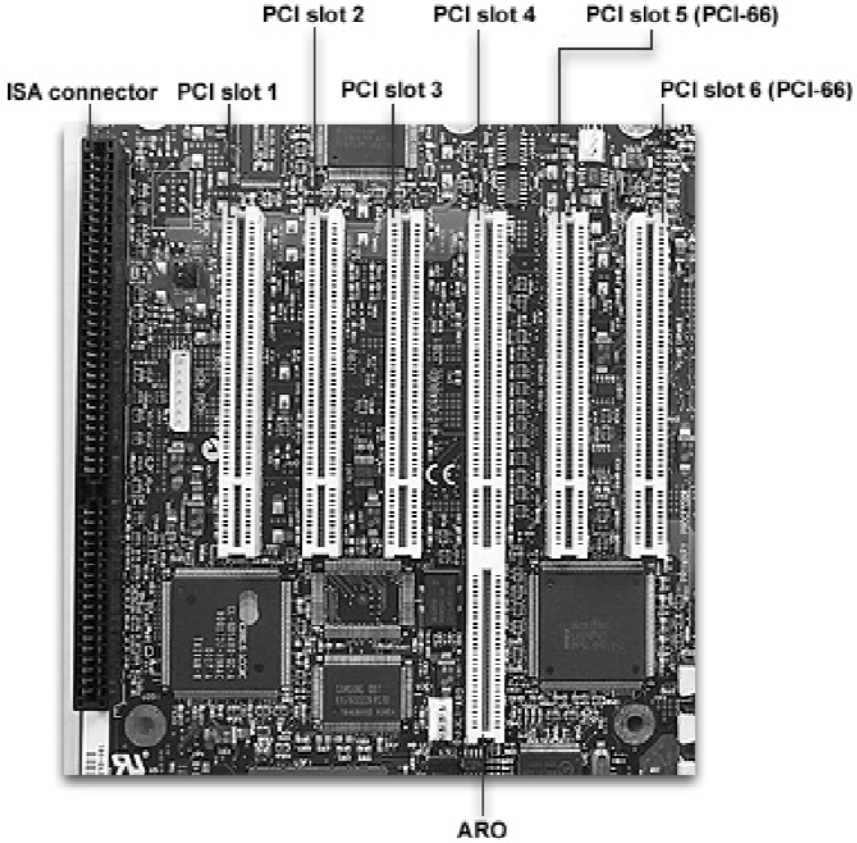

Figure 4-18: Typical PCI bus

- Analogue Input – The Data Translation DT-321 and National Instruments PCI-6221 are each 16-bit PCI based D/A conversion card with 8 differential input channels. Each card is programmed to take readings at a rate of 0.5 kHz. The DT-321 is programmed for ± 10 volt input and the PCI-6221 input range is set at ± 5 V.
- Data Cable Shielding – Voltage signals to/from the transducers are transmitted through four wire data cables, which consist of two sets of twisted pairs encased by a shield that shares the same ground as the computer.
- Transducer Isolation – All transducers are grounded to the data collection system and electrically isolated from the control panel to prevent development of a ground loop[5]. LVDTs are isolated by using non-conductive reinforced phenolic mounting blocks, nylon standoffs are used for all other transducers.
- Load cells – All load cells behave as full Wheatstone Bridge circuits. They are supplied with a nominal 10 volts excitation and return between 3 and 5 mV/V at full span.
- LVDTs – Schaevitz DC-EC series LVDTs have an integrated oscillators that converts the DC input to AC current. Excitation is provided by an independent 15 volt DC power supply. The return signal is ± 10 volts. The LVDT cores consist of non-magnetic threaded brass-rods.

[5] A circular path created between the data lines and the ground wires of electronic devices that are grounded though different power sources or have different earth grounds.

- Signal Conditioning – National Instruments SCXI-1121 modules are used for signal conditioning. Each signal conditioning module has four isolated channels capable of differential voltage measurements in the ± 250 mV range. The modules have been set for 10 Hz low pass noise filtering and signal amplification to reach a ± 5 V range. The SCXI-1121 modules are contained within a National Instruments SCXI-1000DC Chassis. This 4-slot shielded enclosure provides a fan-cooled low-noise environment that is grounded to the computer. A National Instruments SCXI-1321 terminal block is connected to each signal conditioning module. The terminal block provides strain relief to isolate the electronics from cable movement and offset nulling so that the input voltage can be easily zeroed during calibration.
- Accuracy – The National Instruments (NI) data acquisition system has a total system accuracy of ±0.3971 percent (National Instruments 2011). The Data Translation data acquisition system has a total system accuracy of 0.012 percent. The total error associated with the NI data acquisition system is more than an order of magnitude greater the Data Translation system, due to the presence of an SCXI signal condition device which is necessary for milli-voltage returns.

4.6 Stress Path Control

Stress path control and data collection are fully automated during the shearing process. During the consolidation phase, data collection is automated and cell pressures are maintained using computer control, however, the user manually keys in the desired pressures.

All automation and control programming utilizes the Labview version 8.5 graphical programming environment. A finished Labview program includes a "front panel" that has controls and indicators which serve as interactive input and output terminals for the program. The logic behind the front panel is contained in a "block diagram" that is generally hidden from view. This diagram contains graphical representations of functions that are wired to front panel objects and/or subroutines in a logical order to create a program.

The main program that controls the new HTSA is called, "Sequence". The main program uses a stacked sequence structure contained in a loop to maintain control of the test. Approximately, fifty unique subroutines are called with each iteration through the loop.

The subroutines can be operated as stand-alone programs. They each accomplish a specific task, such as monitoring sensors, calculating stress path targets, or recording data points. The most important and complex subroutine is named, "Untitled 4". This subroutine controls the manner in which the cell pressures and vertical loads are adjusted to meet target values.

A narrative description of the programming logic used in the main program (Sequence) and the most important subroutine (Untitled 4) is contained in the following sections. The block diagrams for both of these programs are contained in Appendix A.

4.6.1 Front Panel – Main Program

The front panel for *Sequence* is shown in Figure 4-19.

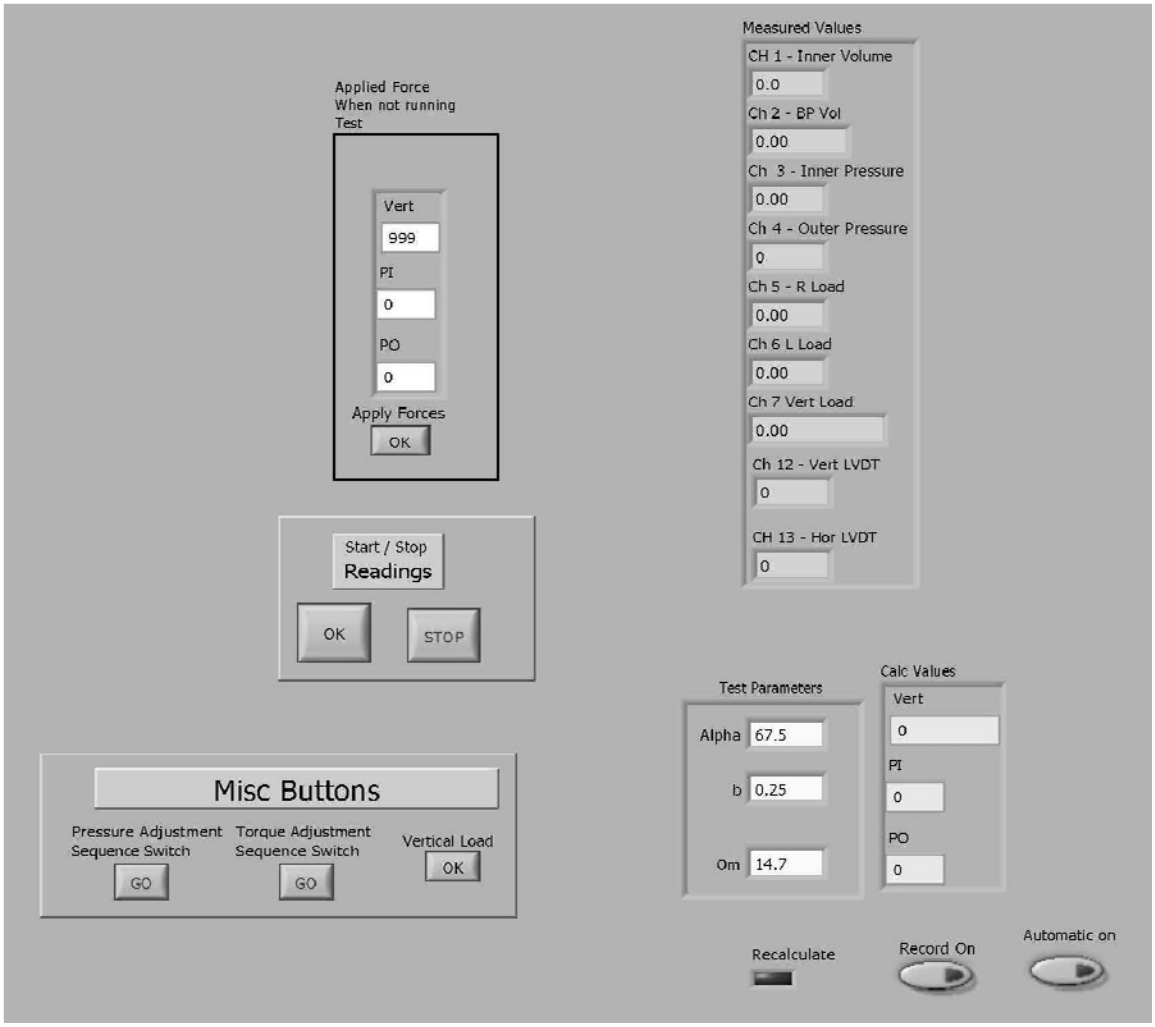

Figure 4-19: Labview Front Control Panel

The following items briefly describe the function of each control or indicator contained on the panel.

- The buttons **Vert, PI,** and **PO** contained in the top left box are used to enter input values for vertical load, inner cell pressure, and outer cell pressure during the consolidation phase. After entering the desired values the **Apply Forces** button must be pushed to execute the application of the new forces.
- Input pressures and loads are continously maintained by the computer. Due to volume change and the inter-related nature of these parameters, the computer automatically makes adjustments to each control to maintain the desired value. If a value of **999** is entered for any parameter, the automatic contol function is disabled for that particluar parameter.
- The **OK** and **STOP** buttons are used to start the computer readings and to shut down the test. Computer readings start a half an hour prior to testing, so that the sensors have sufficient time to warm up, and final adjustments can be made to zero offsets, or calibrations.
- The **Pressure Adjustment Sequence Switch** is used to launch a subroutine that reads only the inner and outer pressures. This subroutine is used if the inner and outer pressure transducers require a manual adjustment of the zero offset after saturation, but prior to the consolidation phase.

- The pressures are displayed on the front panel at one second intervals. The front panel objects are magnified so that they can be read from across the room.
- The **Torque Adjustment Sequence Switch** is used to launch a subroutine that reads only the right and left torqe arm loads. This subroutine is used prior to shearing to make sure that both torque arms are load free. The loads are displayed on the front panel at one second intervals and magnified sufficiently so that they can be read from across the room.
- The **Vertical Load** button sets the vertical load electro-pneumatic cylinder to 0 volts. This button is typically used after completion of the test to remove pressure from the control board and vertical load cylinder.
- The **Test Parameters** bundle is used to input the target test values for the principal stress inclination angle, intermediate principal stress ratio, and mean normal stress.
- The **Calc Values** bundle displays the targeted pressures and vertical load that must be followed to maintain the desired stress path.
- The target pressures and vertical load are only recalculated if the average load in the torque arms changes by greater than 0.1 lbs. The **Recalculate** button bypasses this logical statement and manually forces a recalculation of the target pressures and vertical load.
- After the **Record On** button is depressed the computer will start logging data.

- The **Automatic On** button causes the computer program to begin to follow the desired stress path automatically. This button is generally used after completion of the consolidation phase.
- The **Measured Values** bundle displays all sensor values. It is updated after completion of each loop.

4.6.2 Block Diagram – Main Program

The primary purpose of the main program is to define the logical sequence for monitoring, recording, and controlling a torsional shear test. A diagram describing the logical progression of the program is contained in Figure 4-20. The program also contains many secondary functions (i.e. pressure cell calibration, torque arm calibration, setting consolidation pressures, etc.) which are included in the Appendix A block diagrams.

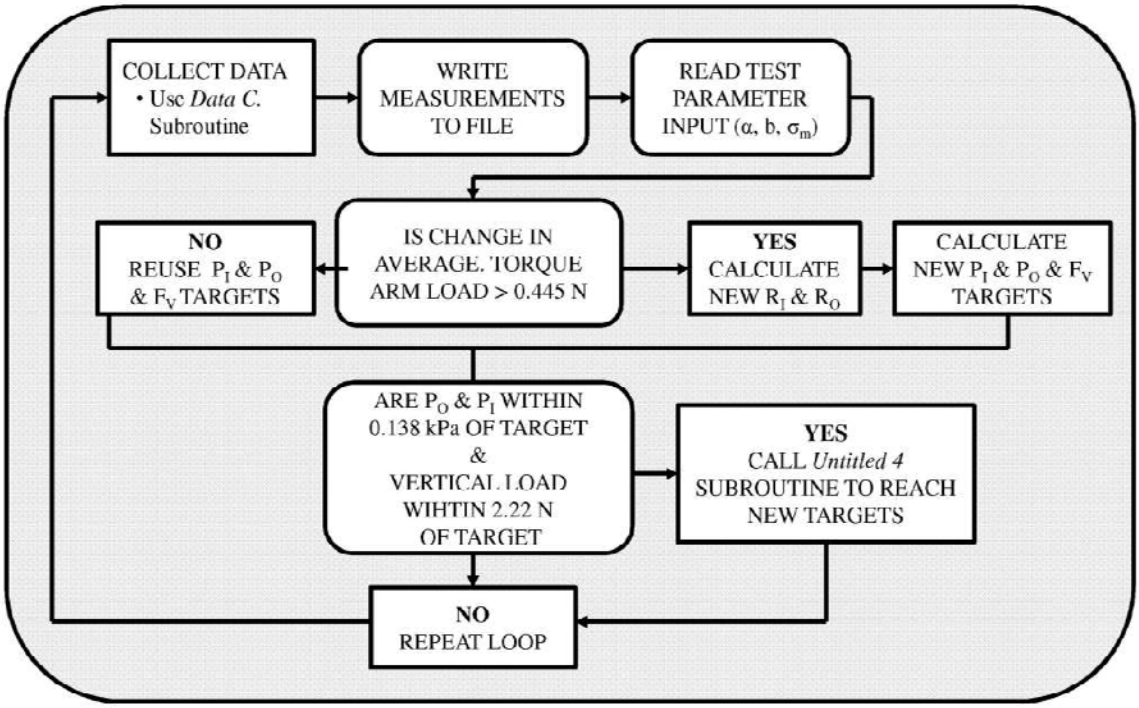

Figure 4-20: Sequence Program Logic

After the front panel **Automatic On** button has been selected, the *Sequence* program enters a loop structure. The first step in the loop consists of calling the *Data C.* subroutine to collect the real time sensor values. The data is then written to a file stored on the computer's hard drive.

The controlling test parameters: 1) the inclination of major principal stress; 2) the intermediate principal stress ratio, and 3) the mean normal stress, can be changed at any time during the test. Therefore, after writing the data to file, the program reads these test parameters.

The average of the most recent torque arm loads is compared to the average of the loads used to calculate the current state of stress. If the average torque arm load has not changed by greater than 0.445 N, the target pressures and vertical load remains unchanged. If the average load has changed by more than 0.445 N a new state of stress must be calculated.

To make this calculation, it is necessary to calculate new values of inner and outer specimen radius. These values are used to adjust the cross-sectional area of the specimen. The new area, torque, and controlling stress parameters are fed into a subroutine to calculate new target pressures and vertical load.

In the next step, the most recent cell pressures and vertical load are compared to the target cell pressures and vertical load. If either of the cell pressures is more than 0.0138 kPa out of tolerance or the vertical load is more than 2.22 N out of tolerance the *Untitled 4* subroutine is called. This subroutine described in Section 4.6.3 adjusts the cell pressures and vertical load to meet the target values.

Once the all parameters are within tolerance of the target values, the loop is repeated. This loop continues until it is manually stopped at the end of the test.

4.6.3 Pressure and Loading Subroutine

The subroutine named, "Untitled 4" (Appendix A) prescribes the manner in which the vertical load, inner pressure, and outer pressure are applied to the specimen to reach a desired target value.

As shown in Figure 4-21, the target values are passed to the subroutine and act as constant values each time the subroutine is called. The constants enter a loop, where they are compared to the real-time sensor values (i.e. actual values) that are read by the data collection subroutine.

If the actual cell pressures and vertical load is within 0.0138 kPa and 2.22 N of the target values respectively, the subroutine ends. If any value is outside of these tolerances, all three controls are reset to move ½ of the remaining distance to the target value.

The inner and outer pressures are adjusted simultaneously followed the vertical load. A two second pause is built in to the loop to allow the specimen and sensors to come into equilibrium prior to taking the next set of readings.

The loop is limited to ten iterations. However, during shear testing three to five iterations is usually sufficient to meet tolerances.

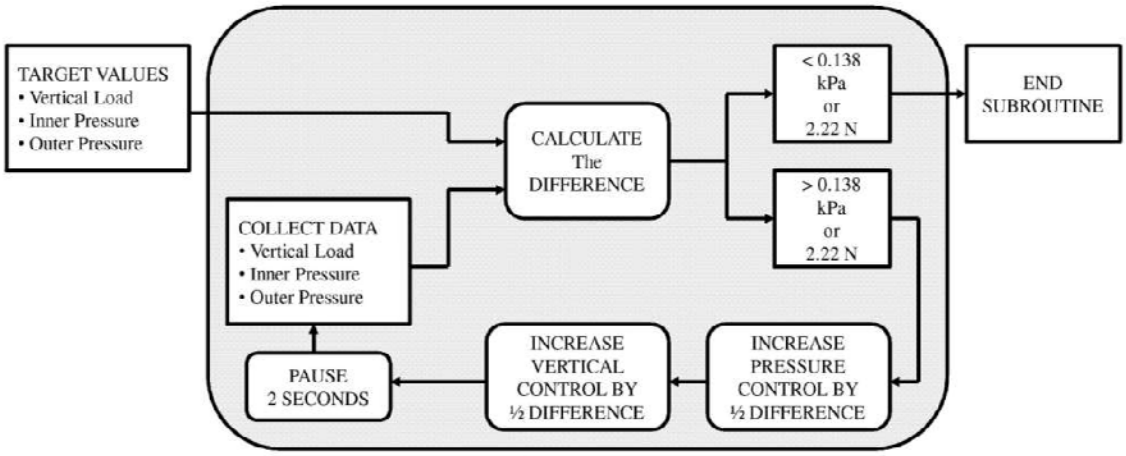

Figure 4-21: Logic for Subroutine "Untitled 4"

5 TEST PROGRAM

The test program described in this chapter has been developed to evaluate the effects of principal stress inclination and the intermediate principal stress on the failure surface of a granular soil.

To achieve this goal, drained shear testing has been conducted on isotropically consolidated specimens of Fine Nevada Sand at uniformly spaced intervals, of b and α. By maintaining the stress paths outlined in Section 5.1, the effects of b and α can be isolated from each other.

Fine Nevada sand was selected as the test material. This well-sorted sand is fine enough to minimize membrane penetration effects, but clean enough (≈ 1% passing the No. 200 sieve) to allow a reasonable strain rate without increasing pore pressures during shearing. The chemical and mechanical properties of this sand are listed in Section 5.2.

A detailed methodology for performing each test is described in Section 0, which includes directions for procurement and preparation of tests: consumables, fluids, and equipment. Furthermore, it explains specimen construction, saturation, and consolidation, and finally moves on to a discussion of specimen shearing and dismantling.

Section 5.4 concludes this chapter with a discussion of test corrections.

5.1 Stress Path

The test program initially consisted of a single series of 11 torsion shear tests, designated as the "A-Series" tests. However, in actuality, two tests were performed at α = 22.5° and b = 0.25, resulting in 12 A-Series tests.

The A-Series specimens were to be isotropically consolidated to 101.3 kPa, and sheared following stress paths that maintained constant values of σ_m, b, and α. The A-Series planned stress paths in (σ_m, b, α)-space are shown in Figure 5-1.

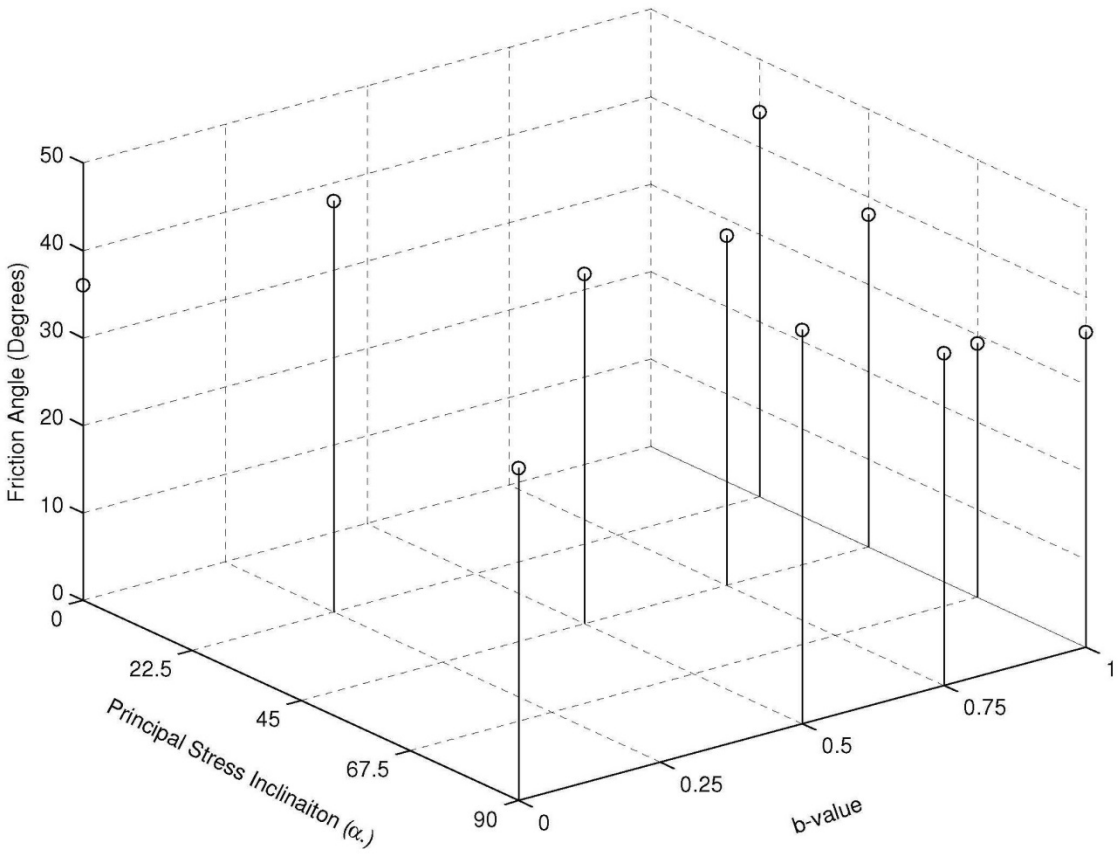

Figure 5-1: A-Series Planned Stress Paths

Conditions for each test were selected with wide b and α intervals so that the effects of changing these parameters would be more easily discernible. A greater number of tests with high b and α values were planned, although the test series was to be "anchored" to a triaxial compression and extension test.

After completion of the A-Series tests, it was determined that tests involving inclined principal stresses did not adequately adhere to the planned stress paths. Therefore, a second set of 10 torsion shear tests was planned, designated the B-Series tests. Stress paths for the B-Series tests are shown in Figure 5-2.

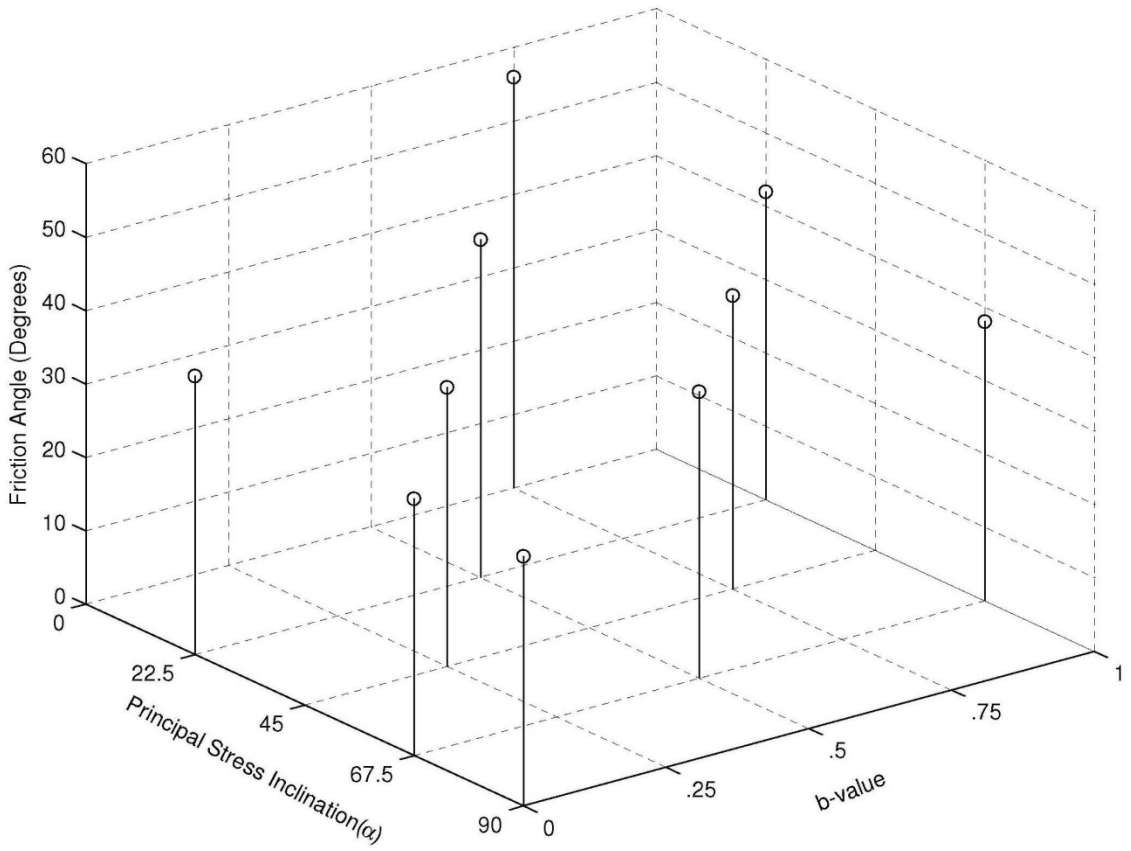

Figure 5-2: B-Series Planned Tests

Since the A-Series tests at α = 0° and 90° were considered adequate for use in defining the failure surface, most B-Series tests were conducted with inclined principal stress directions. The exceptions being at (α = 90°, b = 0), which repeated an earlier A-Series test, and at (α = 0°, b = 0.75) which was added since there were too few tests in this vicinity.

As is discussed in Section 7.1, all B-Series tests adhered well to their intended stress paths. Combining these tests with the A-Series testing that did not involve inclined principal stresses resulted in a total of 15 torsion shear tests at 14 locations[6] comprising the failure surface.

5.2 Soil Properties

The soil used for this test program consisted of No. 70 Fine Nevada Sand from Overton, Nevada. This commercially available sand has been washed and sieved so that it has a minimal fines content (≈ 1%).

It is comprised of predominantly angular particles and classifies as a UCS poorly graded sand. It was selected because it produces a cross-anisotropic fabric when deposited by the air pluviation method and it is fine enough to make membrane penetration effects negligible.

Additionally, Nevada Sand has a long history of use in geotechnical testing. Kutter et al. (1994) and Chen (1995) used it for HTSA testing, Kammerrer, et al. (2000) used it for cyclic shear testing, Yamamuro and Lade (Yamamuro and Lade 1997, Lade and Yamamuro 1997) studied the static liquefaction of fines sands with it, and most notably the Verification of Liquefaction Analysis using Centrifuge Studies program (VELACS) used it for centrifuge testing (Arulanandan and Scott 1993) including several test programs utilizing the HTSA (Kutter et al. 1994, Chen 1995).

[6] Both A and B-Series had tests at the same condition ($\alpha = 90°$, b=0)

5.2.1 Chemical Composition

This sand is predominantly comprised of quartz. The chemical make-up is shown in Table 5-1.

Table 5-1: Chemical Properties of Nevada Sand

Silicon Dioxide (SiO_2)	99.04
Iron Oxide (Fe_2O_3)	0.05
Aluminum Oxide(Al_2O_3)	0.43
Titanium Oxide (TiO_2)	0.03
Calcium Oxide (CaO)	0.04
Magnesium Oxide (MgO)	0.01
Sodium Oxide (Na_2O)	0.10
Other Constituents	0.30

5.2.2 Mechanical Properties

The sand's pertinent mechanical properties are listed in Table 5-2.

Table 5-2: Nevada Sand Mechanical Properties

Minimum Void Ratio, E_{min}	0.507
Maximum Void Ratio, E_{max}	0.771
Specific Gravity, G_s	2.65
D10 (mm)	0.122
D30 (mm)	0.157
D50 (mm)	0.200
D60(mm)	0.224
Coefficient of Uniformity, C_u	1.836
Coefficient of Curvature[7], C_c	1.265

[7] Calculations for the granular soil parameters C_c and C_u are contained in Appendix C.

The maximum void ratio was determined by the "dry tipping" method as described by Yamamuro and Lade (1997). The minimum void ratio was determined by using a small spoon to deposit sand from a height of greater than 80 cm into a 250 ml graduated cylinder, over a period of two hours. These methods for determining E_{min} and E_{max} produce a wider range of values than the methods described by ASTM.

The specific gravity was determined by the technique described in ASTM D854 (2010). The sieve analysis, as shown in Figure 5-3, was conducted per ASTM D6913 (2009).

Sieve Number	Percent Finer
No. 30	100.00
No. 40	94.95
No. 60	68.48
No. 90	39.03
No. 100	27.00
No. 120	11.42
No. 140	5.35
No. 170	2.08
No. 200	1.04
Pan	0.00

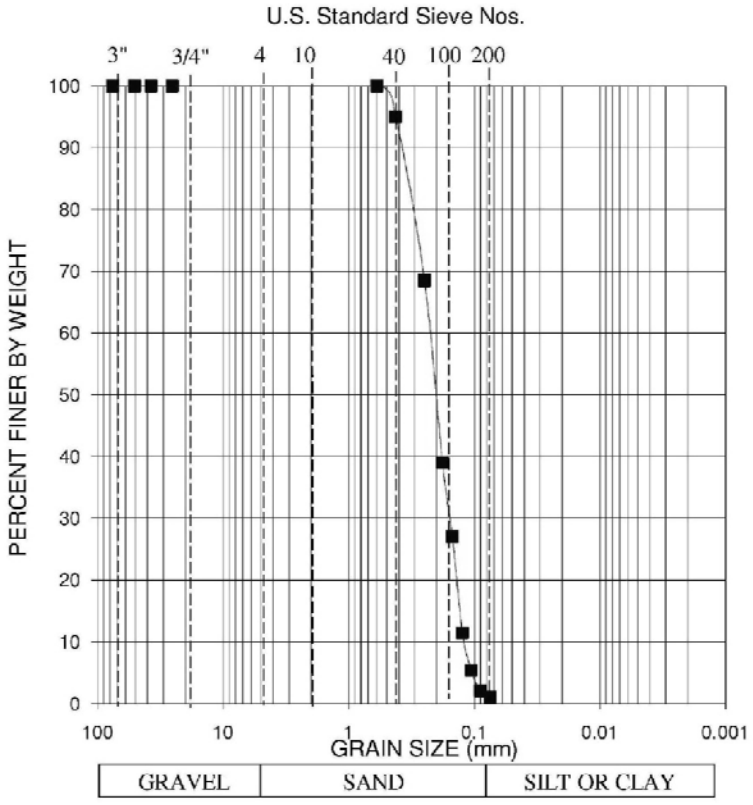

Figure 5-3: No. 70 Nevada Sand Sieve Analysis

5.3 Test methodology

A typical HTSA test takes three days from preparation to dismantling and clean up. During this time, about 330 sequential steps must be completed without making an error. This section presents the test methodology that was followed during this investigation. Including a detailed discussion of the following topics:

- Consumables used for each test
- Fluids used for each test
- Preparation of test equipment
- Specimen construction
- The saturation process
- Consolidation and shearing
- Specimen dismantling

A detailed step by step procedure is contained in Appendix E.

5.3.1 Test Consumables

Prior to beginning an HTSA test, it is advisable to verify that there is a sufficient supply of test consumables:

5.3.1.1 VACUUM GREASE

The vacuum grease used in this study is Dow Corning High Vacuum Grease available from McMaster Carr.

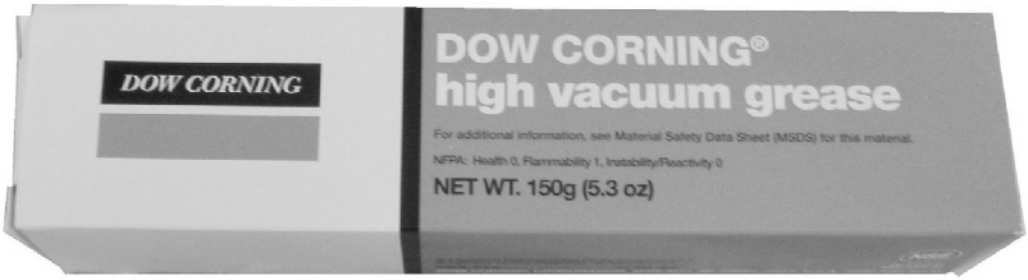

Figure 5-4: Vacuum Grease

5.3.1.2 TEST MEMBRANES

The specimen requires separate inner and outer membranes. The inner and outer membranes are fabricated from a single doughnut shaped aluminum mandrel using a latex dipping technique. The latex dipping technique requires the molds to be withdrawn from a latex bath at about 1 in/sec. Since, the thickness of the membrane is a function of the duration the form is submerged in the bath, this technique results in membranes that are thicker at the bottom than the top. On average, the membranes used for this testing have a bottom thickness of 0.635 mm and a top thickness of 0.318 mm.

Membrane fabrication was originally performed in-house using the materials, equipment, and procedures that are detailed in Appendix F. The methods described in the Appendix worked quite well for medium and small sized membranes. However, inconsistent membrane quality was the norm for large sized membranes. Therefore, the

membranes were procured at a cost of about $20 per set[8] from North American Latex located in Sullivan, Indiana.

North American Latex
Attn: Barb
049 East Industrial Park Drive
Sullivan, Indiana 47822
(812) 268-6608

5.3.1.3 EPOXY

Devcon 14260 Two-ton Clear Epoxy was used to adhere sand grains to the top and bottom rings. The epoxy is available for about $12 from McMaster Carr – Product No. 66215A24. This particular epoxy is has excellent strength and is water resistant. It begins to harden within 8 to 12 minutes and reaches full strength within 16 hours.

Figure 5-5: Two Part Epoxy

5.3.1.4 SAND

Fine Nevada Sand can be purchased from Scott Sales Company – www.scottsalesco.com phone (323) 277-9033. The quarry that mines this sand is Simplot Silica Products in Overton, Nevada. The Simplot representative is Chris Harrington (314) 616 5525.

[8] A set includes an inner and outer membrane

5.3.2 Fluids

In addition to consumables, adequate pressure and quantities of the following fluids should be confirmed prior to testing.

5.3.2.1 VACUUM

The vacuum supply system reservoir tank should be at nearly full vacuum prior to testing. A nearly full vacuum can be pulled on the 60 liter tank shown in Figure 5-6 using a ¾ horse power 150 l/min. Precision Scientific D150 Belt Drive Rotary Vane Vacuum Pump.

The oil filled rotary vane pump is capable of continuous operation for an extended period of time (e.g. greater than 1 week). However, the oil reservoir must be refilled periodically (after about 2 weeks of continuous use) with vacuum supply fluid, available from capitol vacuum www.capvac.com.

The use of the 150 l/min. pump is generally limited to operations that involve maintaining vacuum on the forming jacket. This particular operation necessitates a large vacuum due to all of the vacuum losses associated with the outer form.

When the forming jacket vacuum is no longer necessary, the 150 l/m vacuum is switched with a ¼ horsepower HyVac 2 rotary vane belt drive pump that is very similar to the Precision Scientific model, but operates at maximum of only 25.5 l/min. This small pump requires less oil and produces a much smaller oil mist[9] that must be filtered.

[9] Usually mistaken for a smoke cloud.

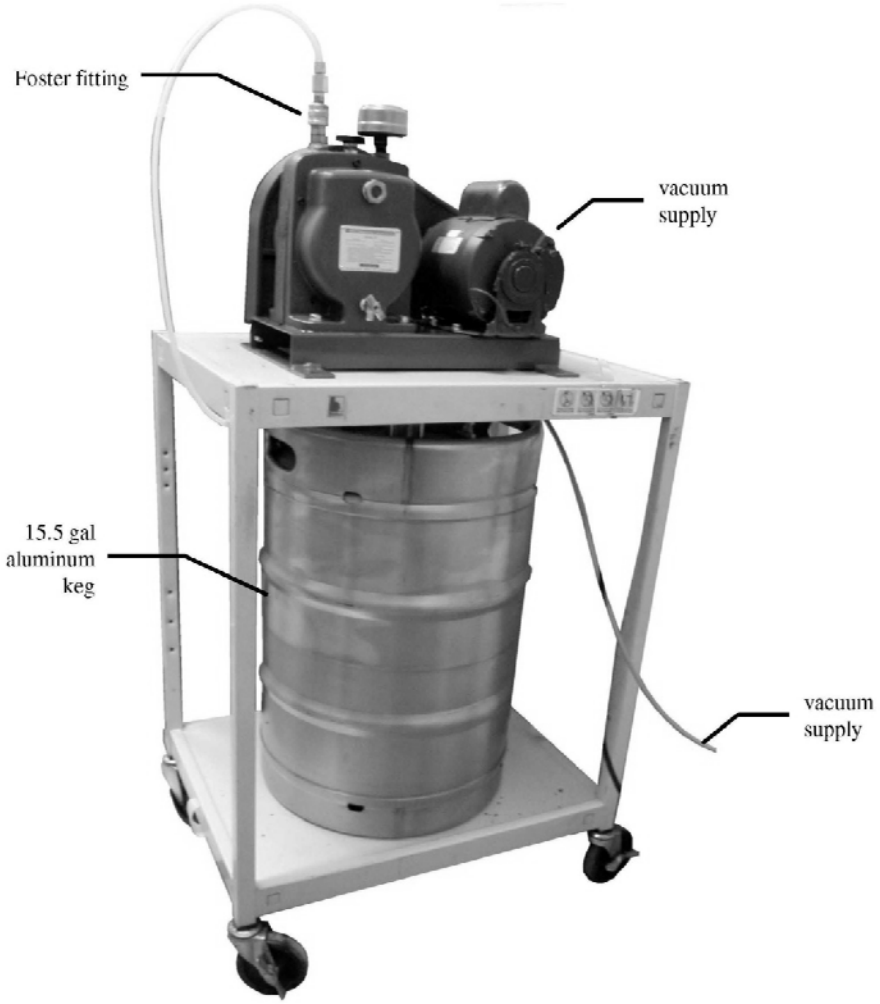

Figure 5-6: Vacuum Supply System

5.3.2.2 COMPRESSED AIR

Compressed air is provided throughout the laboratory space by a 2-stage positive displacement reciprocating air compressor with a 300 liter reservoir tank. The air supply has an in line drier and is pressure regulated at 827 kPa.

5.3.2.3 DE-AIRED WATER

Approximately 75 gallons of de-aired water are required to conduct a single HTSA test. This requires a volume larger than that typically available in geotechnical testing laboratories, necessitating the design and construction of a large custom de-aired water producing system.

De-aired water is produced by spraying tap water through a vacuum of at least 88 kPa. A flat spray nozzle was selected for this application. It has a maximum throughput of 1 gpm at 140 kPa and a spray angle of 120°. The nozzle, shown in Figure 5-7, is available from McMaster Carr part number 3404K145.

Figure 5-7: Flat Spray Nozzle

It is important to note that the de-aired water tanks should only be filled to a ¾ level. Filling past this level decreases the time and distance that the water spray has to fall through vacuum to unacceptable levels.

The de-aired water reservoir tanks are rigidly attached to the laboratory wall, and are located sufficiently high off the ground to allow the entire system to function under gravity feed. An annotated photograph of the reservoir tanks and supply lines is shown in Figure 5-8.

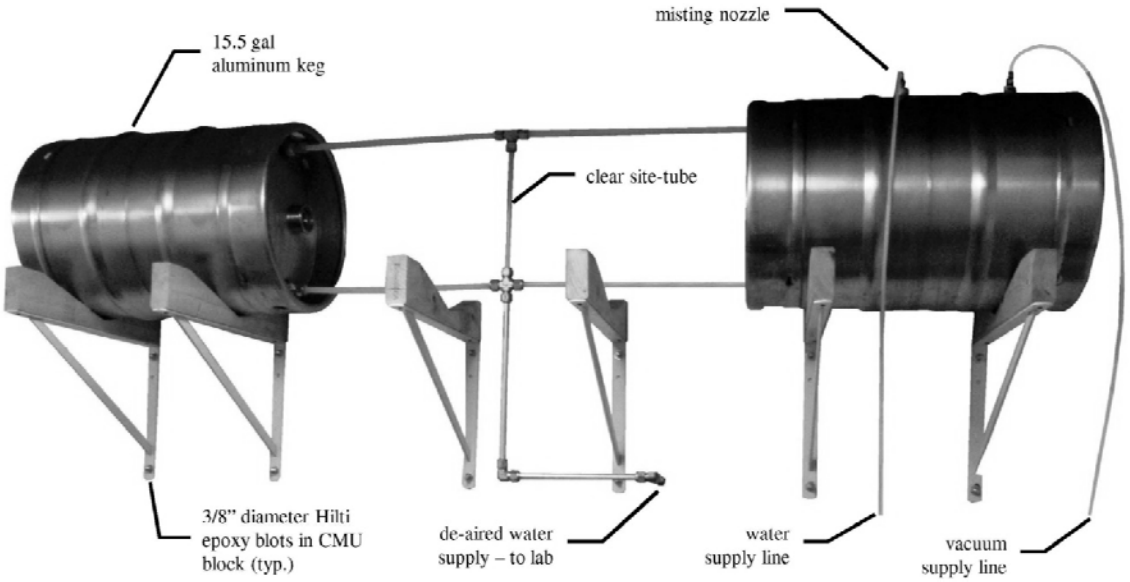

Figure 5-8: De-aired Water Supply System

The de-aired water tanks are manually controlled using a system of valves attached to a control panel. The system flow diagram is shown in Figure 5-9. A step by step procedure for creating de-aired water is contained in Appendix G.

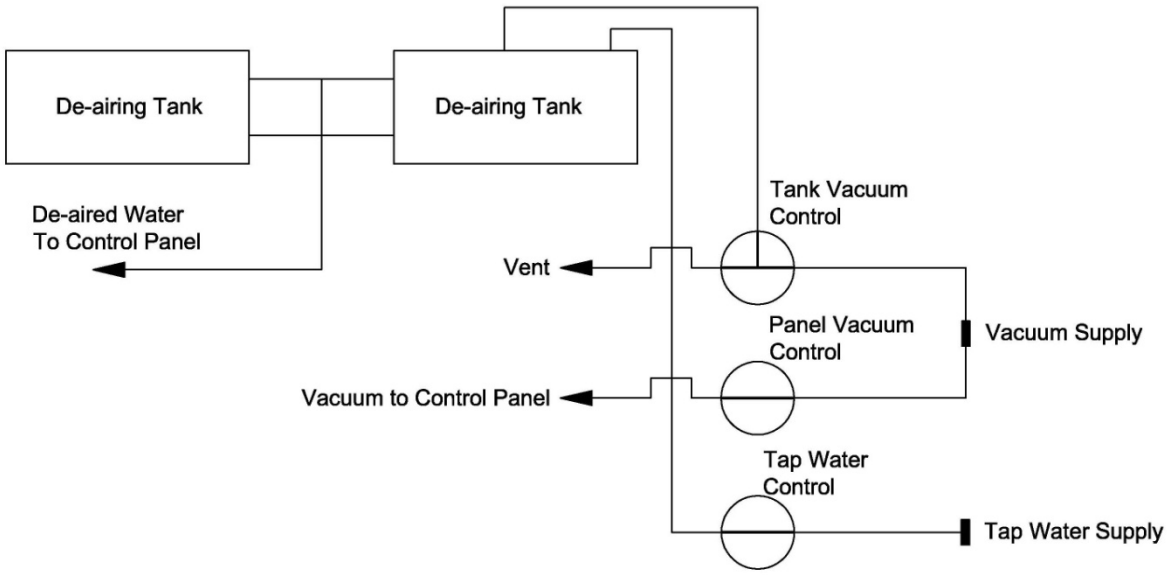

Figure 5-9: De-Aired Water Supply Flow Diagram

5.3.3 Equipment Preparation

Certain portions of both the mechanical and electronic equipment must be prepared prior to specimen construction. First, the data collection system and transducer excitation voltage should be turned on. The electronic system must be allowed to warm up for at least 30 minutes prior to testing to reduce inaccuracy associated with temperature drift.

The turn-table should be counter rotated so that the same initial starting location is maintained for each test. The cell base should be carefully cleaned of all sand and vacuum grease, compressed air can be used to blow sand from all of the screw holes.

The back pressure and inner cell supply lines must be cleared of water so that the CO_2 saturation method can be used. All de-aired water lines within the control panel should be carefully inspected to ensure that no trapped air bubbles are present.

Sand grains should be epoxied to the bottom ring. This is accomplished by evenly spreading a layer of epoxy over the surface of the bottom ring. A thin layer of fine sand is spread over a flat surface, and the epoxied surface is gently pressed into the layer of sand.

5.3.4 Specimen Construction

Inner and outer membranes should be trimmed to 52 cm in length. The membranes should also be inspected for holes. If holes are found, they should be circled with a waterproof marker so that they will be easy to locate in the future and painted with latex sealant.

The inner membrane should be slid over the adjustable inner form. The inner form and membrane should be attached to the bottom ring, with the thick side of the membrane down. This assembly will then be placed on the cell base. An O-Ring compressed between the cell base and the bottom ring will prevent the movement of water between the inner and outer cell by way of seepage beneath the bottom ring.

The outer membrane should then be pulled over the inner form and bottom ring. The bottom of the membrane is about twice as thick as the top. Therefore, to keep the average membrane thickness on the specimen the same, the thin side of the outer membrane should be down.

After an O-Ring is used to seal the outer membrane to the bottom ring, the outer form is placed on top of the bottom ring, and around the outer membrane. The vacuum lines are connected to the forming jacket, and at 28 kPa vacuum is used to adhere the outer membrane to the inside of the outer form.

8,840.0 grams of dry sand are placed into a funnel that is suspended on a block - swivel rigidly attached to the laboratory ceiling, as shown in Figure 5-10.

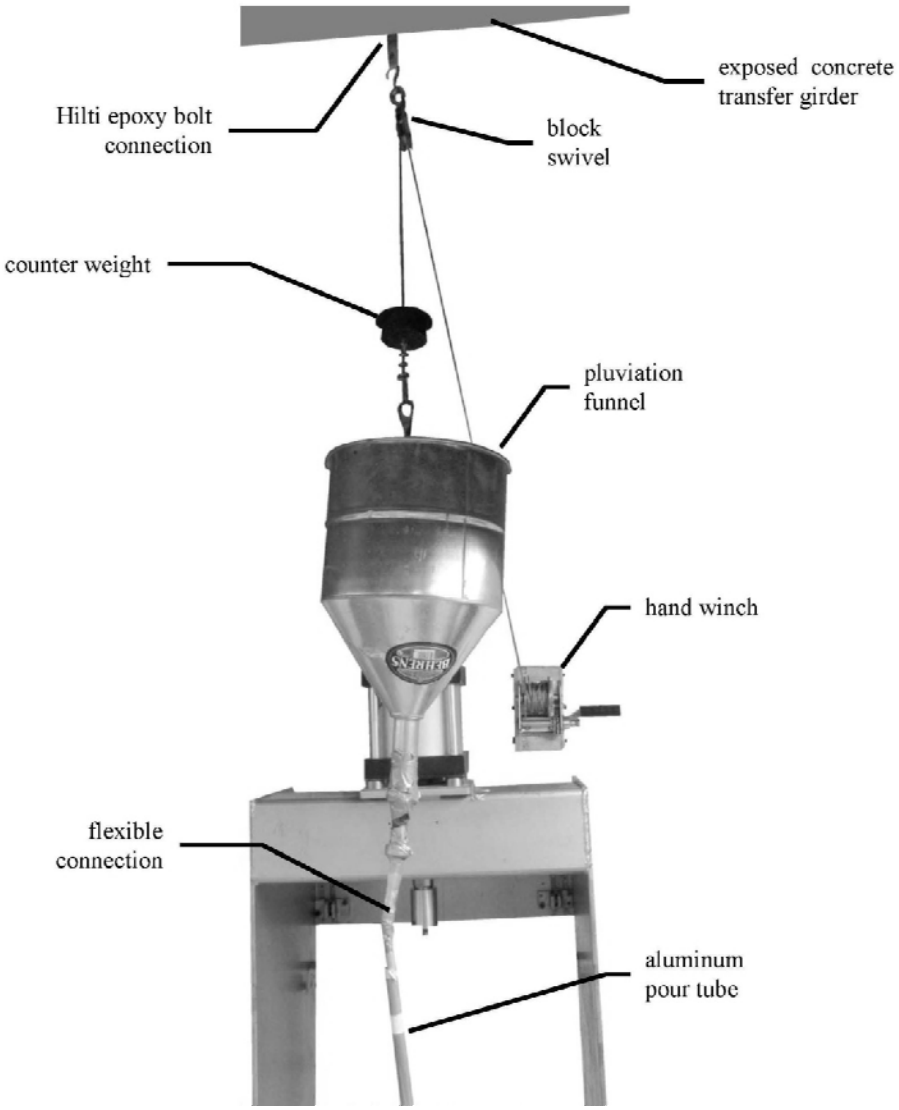

Figure 5-10: Pluviation Funnel

The sand is then deposited into the specimen mold using the air pluviation technique, which mimics a natural aeolian deposition process (Kuerbis and Vaid 1988). When used with well-sorted sands, this method has been shown to produce relatively uniform specimens (Miura and Toki 1982) with significant anisotropy (Ko and Scott

1967). The density of the specimen can be varied by making adjustments to the drop height or duration of deposition.

However, for all testing performed as part of this investigation the sand was pluviated through a 460 mm long tube, with a diameter of 13 mm. The flow at the top of the tube was restricted by maintaining a 4.36 mm diameter entry orifice. The tip of the deposition tube was maintained 35 cm above the surface during deposition. The typical time required for deposition was 60 minutes.

After pluviation, the sand is leveled using a small straight edge. The sand should be held 1 mm above the top of the outer form. It is sometimes necessary to redistribute sand by vacuuming high areas and redepositing in low areas. Small amounts of additional sand are occasionally required to achieve the proper height. The mass of any sand added to the specimen must be recorded and added to the initial 8,840 g.

After the specimen has been prepared, all excess sand or sand that has been spilled on the cell base should be carefully swept and vacuumed into a beaker with a known tare weight. The mass of this spilled sand should be subtracted from the initial starting weight of 8,840 g.

The top ring is epoxied to the top of the leveled sand surface. An even layer of epoxy is spread over the bottom of the top ring surface, taking care to avoid the filter stones. The top ring is then placed on top of the specimen. A level is used to ensure that the top cap is perfectly level in every direction. After allowing 15 minutes for the epoxy to set, the inner and outer membranes are attached to the top ring using O-Rings.

A bubble chamber is connected to the back pressure saturation line, and this line is used to apply a 48.3 kPa (7 psi) vacuum to the specimen. Once the vacuum appears stable, the outer and inner temporary forms can be removed.

The specimen diameters are measured at the top and bottom of the specimen using a PI tape with an uncertainty of 0.008 mm. The specimen height is measured to within 0.05 mm at three locations using a steel ruler.

The inner and outer membranes are painted with liquid latex to clog the inevitable leaking. The painting continues until there are no more bubbles visible in the bubble chamber.

Using a thin ball point pen, a grid is drawn on the outer membrane so that the relative movement of the specimen and formation of shear bands is more easily observed. These lines are drawing at 2.5 cm on center in both the vertical and horizontal direction and cover the entire height and about 1/3 of the outer circumference of the specimen. After completing the lines, a test label is fixed to the cell base and the "initial conditions" photograph is taken.

5.3.5 Saturate Specimen and Test Cell

The top cap is bolted to the top ring, compressing an O-Ring to create a watertight seal between the inner and outer cells. Vents in the top cap are opened and the inner cell is saturated with CO_2 for a period of 10 minutes.

Using the same supply line, the inner cell is filled with de-aired water from the bottom up. When water is observed trickling out of the top cap vents, the supply is shut off and the top cap vents are closed creating an incompressible fluid filled inner cell.

The outer cell wall, cell cap, tie-rods, and piston are put into place. The nuts are threaded on to the tie rods compressing O-rings above and beneath the cell wall and creating a watertight seal. The cell cap vent is opened and the outer cell is saturated with de-aired water. The outer cell volume is not monitored or used for calculating changes in the inner or outer specimen diameter. Therefore, although it is important for the outer cell to maintain a desired pressure, the fluid does not have to be completely compressible and the CO_2 saturation method is not necessary.

A confining pressure of 24.1 kPa is simultaneously applied to both the inner and outer cells. The vacuum is then decreased from 48.3 kPa to 27.6 kPa. The inner and outer pressure is increased to 48.3 kPa in 6.9 kPa increments. Each time fluid pressure is added to the inner and outer cells an equivalent amount of vacuum pressure is removed.

After the confining stress has been applied, the specimen is saturated using the CO_2 method described by Lade and Duncan (1973). A 48.3 kPa back pressure is applied to the specimen in 6.9 kPa increments. By using 6.9 kPa increments, the net confining stress is never less than 41.4 kPa. The specimen is then allowed to sit for a minimum of 2 hours to ensure that all CO_2 bubbles are dissolved.

- After this rest period, the specimen back pressure line is closed and the inner and outer cell pressures are simultaneously increased to 82.7 kPa. The resulting increase in the specimen pore water pressure is measured and recorded and the saturation is determined by calculating the pore pressure coefficient (B) as described by Skempton (1954) and shown in Equation 4. Skempton's B values for each test are shown in Appendix K.

$$B = \frac{\Delta u}{\Delta \sigma_3} \tag{5.1}$$

Where:

Δu = change in pore pressure

$\Delta \sigma_3$ = change in isotropic cell pressure

5.3.6 Connect Instrumentation

After confirming that the specimen has been fully saturated, the instrumentation can be connected. First the specimen back pressure line is closed to prevent volume change from taking place during the instrumentation phase. The sensor readings are recorded by hand at this point.

The vertical LVDT and vertical load cell are connected to the piston. The vertical pneumatic cylinder is lowered onto the assembly and connected to the vertical load cell creating a rigid connection between the load specimen and the loading cylinder. The horizontal LVDT and torque reaction bar are assembled and connected to the top of the piston.

The buoyant weight of the top cap, piston, load cell, LVDT, and torque reaction system is 16.87 kg (36.81 lbs) (the calculations are contained in Appendix C). After all instrumentation has been connected, this weight is removed from the specimen by applying an upward force to the vertical load cylinder. After this weight has been removed the specimen is subjected to an isotropic stress only, and the back pressure line is reopened so that volume change may occur. The sensor readings are recorded and compared to the readings taken before the instrumentation was connected to confirm that minimal disturbance took place as a result of the installation of monitoring equipment.

5.3.7 Isotropic Consolidation

Prior to the start of isotropic consolidation, the back pressure is increased from 48.3 kPa to 101.3 kPa. The data logging automatic recording function is turned on, and isotropic pressure is applied to the specimen in 6.9 kPa increments up to an effective pressure of 101.3 kPa.

The water level within each volume change device is adjusted to ensure adequate capacity for the current test conditions, and the torque arms are connected to the torque reaction bar and set to zero load.

5.3.8 Shearing

The test parameters (σ_{avg}, b, and α) are input into the computer program. The turn-table rotation is initiated and the computer program is set to "automatic mode". In this mode the computer will read the applied torque and automatically calculate and apply cell pressures and vertical load to maintain the desired stress path.

Tests that involve torque (all tests other than $\alpha=0°$ or $\alpha=90°$) are driven by the turn-table rotation. The rotation produced by an electric motor turning at a constant rate of speed creates a strain controlled test condition. Tests that do not involve the application of torque are driven by the application of vertical stress. These tests ($\alpha=0°$ and $\alpha=90°$) are stress controlled.

The water columns in the volume change devices are continuously monitored during testing to ensure that they do not completely empty or overfill. The specimen is visually monitored so that the shear band development time can be correctly documented.

5.3.9 Dismantling and Documentation

After the specimen has failed and clear shear bands have developed, the inner cell, outer cell, and specimen supply lines should all be closed so that no further deformation can take place. The turn-table rotation is stopped, and the vertical load is removed.

The shear band inclinations are measured and photographed though the test cell. A vacuum is applied to the specimen and the inner and outer cells are drained. The instrumentation is disconnected and the load frame, cell cap, tie-rods, and cell wall are removed.

At this point the specimen is free standing under vacuum. The membranes are dried and each shear band is labeled, remeasured, and photographed. The top cap is removed and the inner wall of the specimen is inspected for additional shear bands or to verify the continuity of those observed on the exterior of the specimen.

After all documentation has been completed, the vacuum is removed and the specimen is taken down.

5.4 Test Corrections

5.4.1 Membrane Strength

Stresses were corrected for the effects of membrane strength by using Equations (5.2) through (5.5) taken from Tatsuoka et al. (1986). Strains occurring during consolidation were included in the calculation.

The specimen formation method described in Section 5.3.4, requires minimal membrane stretching, so it was not necessary to include initial strains due to the membrane prestressing

Figure 5-11 shows corrected versus uncorrected stress-strain curves from a typical test. In this particular case, the uncorrected peak stress ratio is 6.10 versus a corrected peak stress ratio of 5.75. This equates to a difference in peak mobilized friction angle of 1.18°. A sample membrane strength correction calculation for Test B03 has been included in Appendix C.

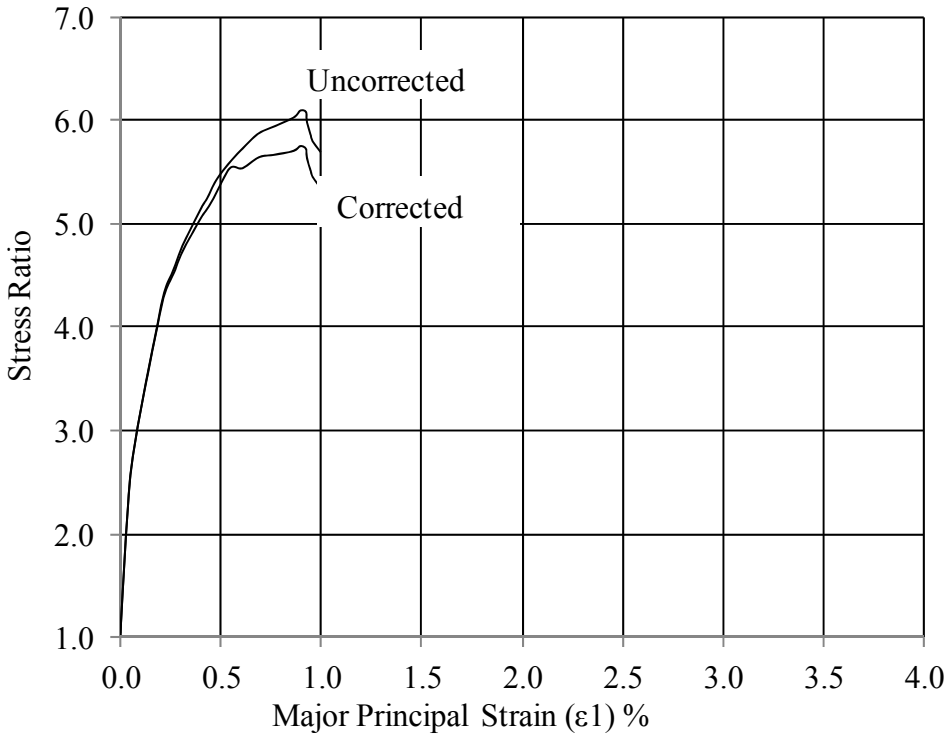

Figure 5-11: Test B03 Corrected Vs. Uncorrected Stress Strain Plot

All corrections resulted in reduced stress ratios. The maximum correction resulted in a 2.12° reduction in peak shear strength, while the minimum correction resulted in a reduction of 0.09°. This range of values is similar to those presented by Tatsuoka et al. (1986).

Deviations to the planned stress path due to membrane strength were insignificant, typically less than: 0.01 for b-value, 0.1 for α, and 1 kPa for σ_m.

$$\Delta\sigma_z = -\frac{4}{3}\frac{E_m * t_m}{R_o^2 - R_i^2}[R_o\{2(\varepsilon_{zm})_o + (\varepsilon_{\theta m})_o\} + R_i\{2(\varepsilon_{zm})_i + (\varepsilon_{\theta m})_i\}] \tag{5.2}$$

$$\Delta\sigma_\theta = -\frac{2}{3}\frac{E_m \cdot t_m}{r_o - r_i}[\{(\varepsilon_{zm})_o + 2(\varepsilon_{\theta m})_o\} + \{(\varepsilon_{zm})_i + 2(\varepsilon_{\theta m})_i\}] \tag{5.3}$$

$$\Delta\sigma_r = -\frac{2}{3}\frac{E_m \cdot t_m}{r_o + r_i}[\{(\varepsilon_{zm})_o + 2(\varepsilon_{\theta m})_o\} - \{(\varepsilon_{zm})_i + 2(\varepsilon_{\theta m})_i\}] \tag{5.4}$$

$$\Delta\tau_{z\theta} = -2E_m \cdot t_m \cdot \frac{r_o^3 + r_i^3}{(r_o^3 - r_i^3)(r_o + r_i)} \tag{5.5}$$

Where:

$\Delta\sigma_z$ = correction to z stress

E_m = modulus of elasticity for membrane

t_m = average thickness of membrane

$(\varepsilon_{zm})_o$ = axial strain of outer membrane

$(\varepsilon_{\theta m})_o$ = circumferential strain of outer membrane

$(\varepsilon_{zm})_i$ = axial strain of inner membrane

$(\varepsilon_{\theta m})_i$ = circumferential strain of inner membrane

5.4.2 Piston Area Correction

The outer cell pressure, P_o, is not applied over the area of the top cap that is occupied by the piston. The pressure that would be acting over this area must be compensated by application of additional vertical force. Equation (5.6) is used to calculate the magnitude of corrective force that is needed to satisfy the stress equations.

$$P_f = A_p\left(B_p + P_o\right) \tag{5.6}$$

Where:

P_f = piston force

A_p = piston area

B_p = back pressure

This correction has been derived in the following manner:

$$(P_o + B_o)\left(A_o - A_p\right) + P_f = (A_o - A_i)\left(B_p + \sigma_z\right) + A_i\left(B_p + P_i\right)$$

$$P_f = -P_oA_o - \cancel{B_pA_o} + B_pA_p + P_oA_p + \cancel{B_pA_o} - \cancel{B_pA_i} + \sigma_zA_o - \sigma_zA_i + \cancel{B_pA_i} + P_iA_i$$

$$P_f = -P_oA_o + B_pA_p + P_oA_p + \sigma_zA_o - \sigma_zA_i + P_iA_i$$

Solving for the case where inner and outer pressures are equal.

$$P = P_o = P_i = \sigma_z$$

$$P_f = -\cancel{PA_o} + B_pA_p + P_oA_p + \cancel{PA_o} - \cancel{PA_i} + \cancel{PA_i}$$

$$P_f = A_p\left(B_p + P_o\right)$$

5.4.3 Membrane Penetration

Volume change due to the effects of membrane penetration have been evaluated. These effects are primarily a function of the grain size, effective confining pressure, and the membrane's rigidity and thickness. All of these parameters are captured in Baldi and Nova's (1984) method for evaluating the effects of membrane penetration during triaxial

testing which has been tailored for the HTSA as shown in Equation (5.7). This method has been experimentally shown to produce reasonable results for clean Ham River Sand (Kuwano 1999) with an average grain size similar to the Nevada Sand used in this study.

$$v_m = \frac{D_{50}}{8}\left(\frac{\sigma_h' D_{50}}{E_m t_m}\right)^{1/3} \tag{5.7}$$

Where:

v_m = unit area volume change (mm^3/mm^2)

D_{50} = mean particle size (mm)

D = specimen diameter (mm)

σ_h' = inner or outer confining pressure (kPa)

E_m = Young's modulus of membrane (kPa)

t_m = average membrane thickness (mm)

The total membrane penetration can be calculated by multiplying the v_m by either the inner our outer membrane area. For the case of triaxial compression, the inner and outer pressure changes are the same, so the equation can be multiplied by the total membrane area.

The effects of membrane penetration during shearing are most pronounced for the condition $\alpha = 0°$ and $b = 0$. Since the mean normal stress is held constant, the horizontal confining stress varied by 56.54 kPa from the start of shearing to failure. Using Equation (5.7), the change in volumetric strain associated with the membrane penetration is -0.01%. The observed volumetric strain for this test condition was -0.54 %, much greater than the membrane penetration, serving as confirmation that Nevada sand has an average grain size sufficiently small so that membrane penetration effects can be neglected in HTSA tests (Chen 1995).

5.4.4 Bushing Friction

The top cap bushing and piston are comprised of greased linear bearings and a precision ground rod. If the piston is centered and co-linear with the bearings the grease forms a nearly frictionless watertight seal around the piston. However, if the piston is off center or out of alignment with the bushing an initial friction effect is observed.

5.4.4.1 CENTERED AND CO-LINEAR FRICTION

The magnitude of rotational piston friction was determined by direct testing. The test set-up consisted of installing the entire torque resisting and horizontal LVDT assembly. However, no specimen was constructed. Instead, the top cap was suspended freely inside the pressure cell. The top cap was connected to the piston which extended though the bushing, where it was connected to the load cell and vertical loading cylinder as usual. The torque resisting springs were set so that both reaction arms were just touching the springs, ensuring a balanced load.

1.5 volts was applied to the precision turn-table motor. This voltage produced a rate of rotation similar to that employed during testing. The computer program "sequence" was called and an output file named "PistonFric" was created to record data. Because the top cap is freely suspended and no specimen is in place, the only transfer of load between the turn-table and torque reaction system occurs through the friction between the bushing and piston. Figure 5-12 shows the torque measured by the system as the turn-table was advanced in both directions. The steady state torque observed during this test was equal to 102 N-cm. This resistance was accounted for during processing of test data.

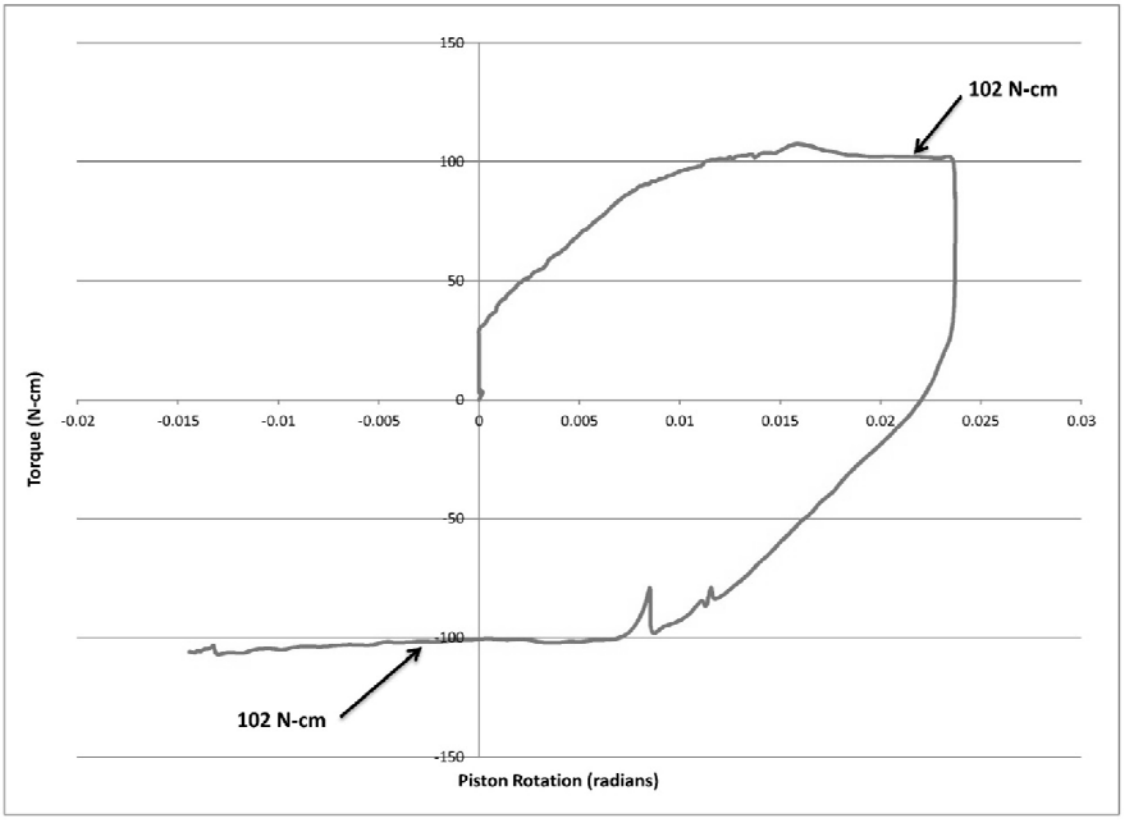

Figure 5-12: Piston Friction Testing (Piston Rotation Vs. Torque)

5.4.4.1 NON-CENTERED AND NON-LINEAR FRICTION

The piston and bushing must be perfectly aligned at the start of a test. If they are out of alignment or not centered the bushing will bind or cam the piston until a critical level of torque is reached, usually around 2,000 N-cm. Any one of the following factors can create this condition:

- Specimen is not perfectly centered on turntable
- Top cap not perfectly centered on specimen
- Specimen slightly out of plumb
- Top of specimen slightly out of level

If one of these conditions is present, placement of the cell cap and tightening of the tie rods cams the piston against the bushing and creates a slight separation between a portion of the cap and the specimen, as shown in the middle graphic of Figure 5-13.

This camming results in additional friction that is temporary in nature. A small amount of specimen deformation, allows the piston to self-align dissipating the temporary camming friction, as shown in the right graphic of Figure 5-13.

However, translation of the piston during realignment combined with a slight rotational slipping of the top cap against the specimen caused by the slight separation creates rotational movement that is not attributable to shear strain. This initial "seating movement" results in less than 2 mm of horizontal LVDT travel.

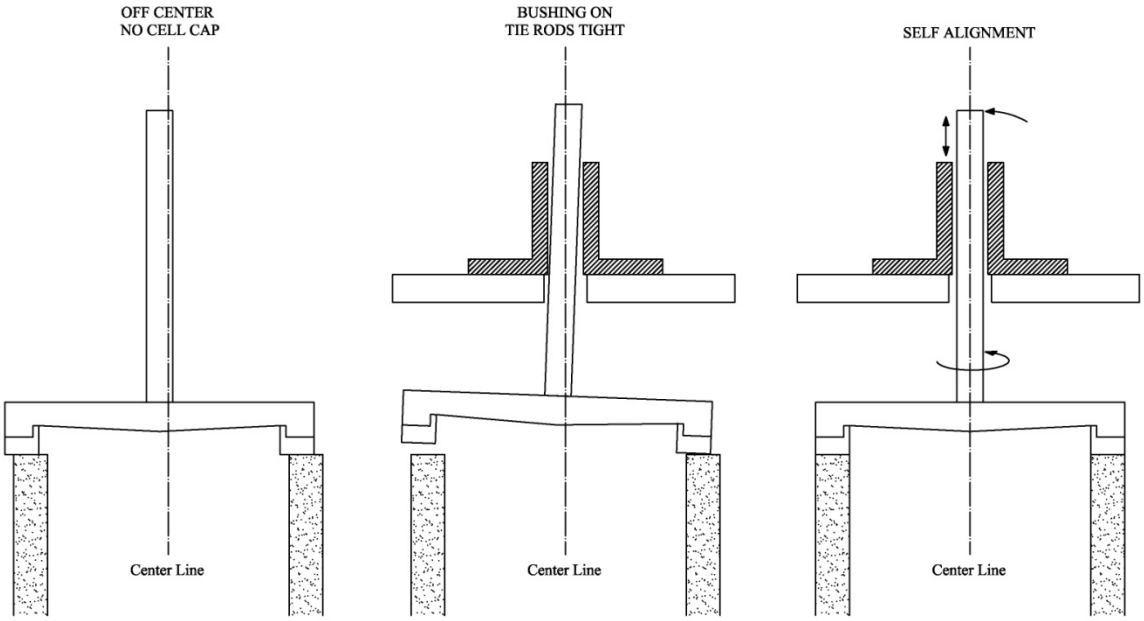

Figure 5-13: Exaggeration of Non-Centered Cap Sequence

Since the initial camming friction is temporary, it is only necessary to correct the Horizontal LVDT data for slippage. The horizontal LVDT measurements are corrected for the seating movement by extending a polynomial curve fit to the early time test data.

Figure 5-14 shows the typical behavior observed for tests with rotation. No corrections involving forces (i.e. torque, vertical load, or pressures) are necessary.

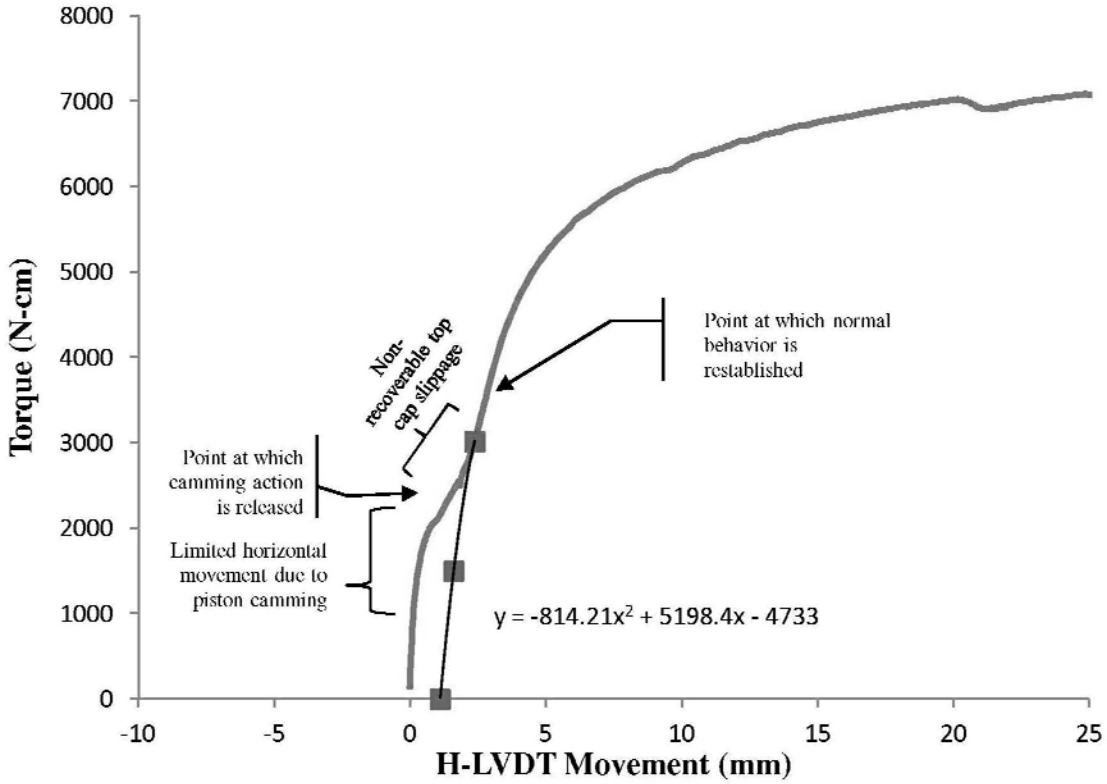

Figure 5-14: HLVDT Correction

5.4.5 Constant Mean Normal Stress

All shear testing was to be conducted at a constant mean normal stress of 101.3 kPa. However, the A-Series testing did not take into account the piston area correction as described in Section 5.4.2, until after the test. This created test conditions with mean normal stresses somewhat less than 101.3 kPa.

The lowest mean normal pressure observed during failure for the A-Series tests was 96.7 kPa, while the highest mean normal pressure at failure for the A-Series tests was 98.0 kPa.

Principal stress corrections based on a straight line approximation between the origin and an orthogonal plane containing an mean normal stress point at 101.3 kPa is possible. However, the correction does not affect the friction angle mobilized at failure, only the stress-strain and volume change plots. The data comprising these plots was not corrected for differences in mean normal pressure because unique behavior due to differences in void ratio would still be present, and differences caused by variations in void ratio can only be accounted for at failure.

6 A-SERIES TEST RESULTS

A-Series testing was performed from April 22, 2010 to December 03, 2010. As previously discussed, the intent of this testing was to evaluate the effects of principal stress inclination and the intermediate stress ratio on drained soil strength. However, for this series of tests, the piston area correction (Section 5.4.2) was made after test completion, rather than interactively during testing. Solving the stress path equations without the unaccounted for uplift force resulted in:

- A reduction in mean normal stress, as described in Section 5.4.5
- Principal stress rotation for all tests with principal stress inclinations other than 0° and 90°
- An intermediate principal stress ratio that always starts at b = 1 and then smoothly transitions to the desired value, rather than starting at the desired value

The principal purpose of this investigation was to isolate the effects of inclination, confining stress, and the intermediate principal stress by holding each of these factors constant during shearing. Due to the variable nature of each of these factors during A-Series testing, it is not possible to directly compare the stress-strain and volume change behavior between A-Series tests. Therefore, the test data and plots from these tests has been presented for informational purposes only.

6.1 Testing with Principal Stress Inclinations of 0° and 90°

6.1.1 Conformance with Planned Stress State (b, σ_m, α)

Neglecting the piston correction factor resulted in an additional uplift force acting in a purely vertical direction. Therefore, no unintended stress rotation was imposed on specimens that were sheared at principal stress inclinations of 0° or 90°.

However, the mean normal stress was between 3 and 4 percent lower than the planned value of σ_m = 101.3 kPa. The average mean normal stress with respect to the major principal strain is shown in

Figure 6-1. In general, the values have good consistency for the duration of the test, with the exception of Test No. A09. This test had a slight drop in confining stress associated with a pause in shear application that was associated with adjustment of the inner cell volume change device.

The intermediate principal stress ratio for A-Series testing starts at a value of 1 and quickly approaches the test target value in an asymptotic fashion. As shown in Figure 6-2, the majority of variation in this parameter occurs during the elastic portion of the test.

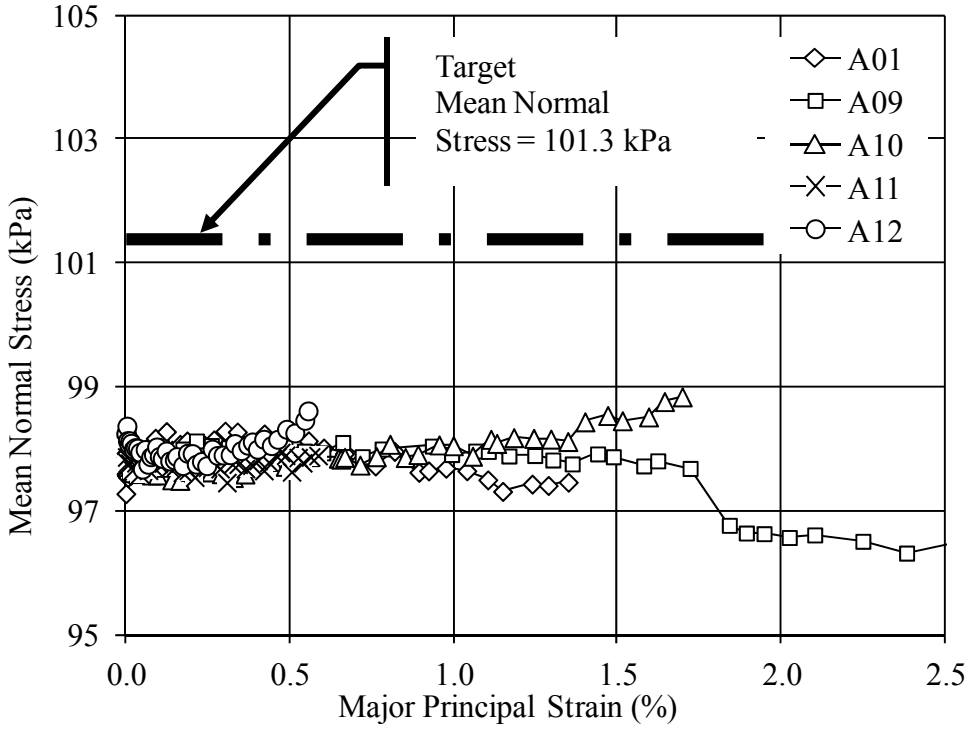

Figure 6-1: Mean Normal Stress (kPa)

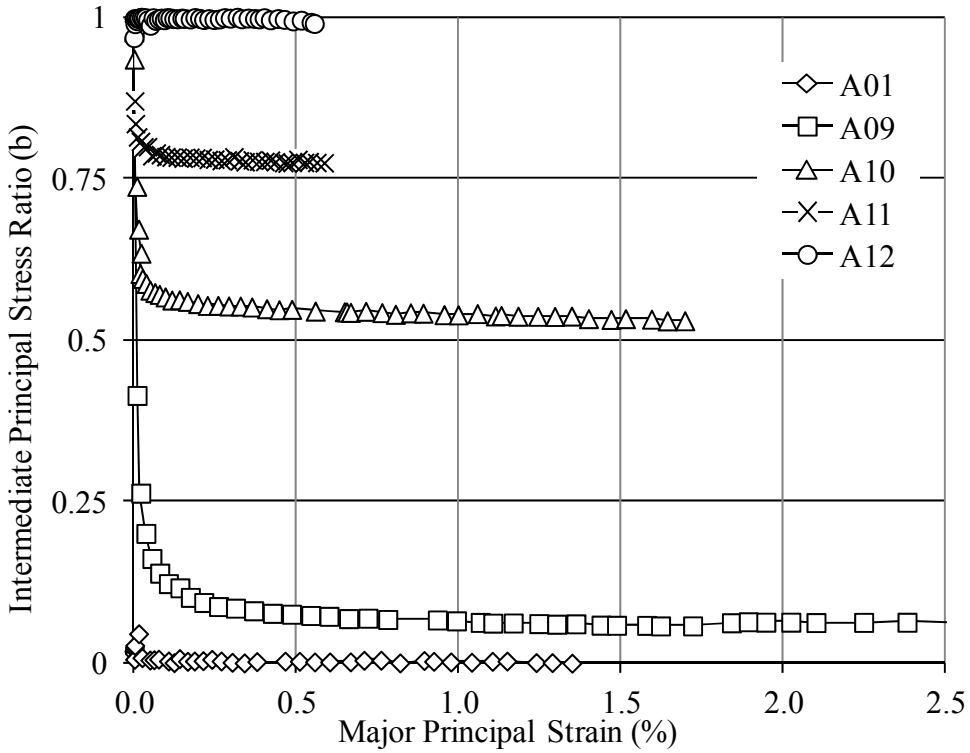

Figure 6-2: Intermediate Principal Stress Ratio (b)

6.1.2 Stress – Strain and Volume Change Behavior

The target stress conditions for Test A01 were the same as a typical triaxial compression test ($\alpha = 0°$, $\sigma_m = 101.3$ kPa, and $b = 0$). The stress-strain relationship for this test is shown on Figure 6-3. A peak stress ratio of 4.19 was reached at a major principal strain of 1.24%. There was no sharp post peak stress reduction observed for this b=0 condition.

The volume change behavior is shown in Figure 6-4. This specimen compressed very little during shearing, which can be partly attributed to this specimen's initial void ratio of 0.505 giving it a relative density of 100% compared to the target value of 91.3%. Dilation started after a major principal strain of 0.27% and progressed until a volumetric strain of 0.36 % had been reached at failure.

As shown in Figure 6-2, this test's b-value adhered well to the desired value of 0. However, the mean normal stress of 98.0 kPa, was somewhat less than the desired value of 101.3 kPa.

Tests A09 through A12 had target stress conditions of $\alpha = 90°$, $\sigma_m = 101.3$ kPa, and $b = 0$, 0.5, 0.75, and 1, respectively. Test A12 had the same target stress conditions as a typical triaxial extension test.

As shown in Figure 6-5, specimen A09, with a b-value of 0.06, exhibited a much softer response than the specimens with higher b-values. The maximum stress ratio for this test was 4.13 occurring at a major principal strain of 2.25%.

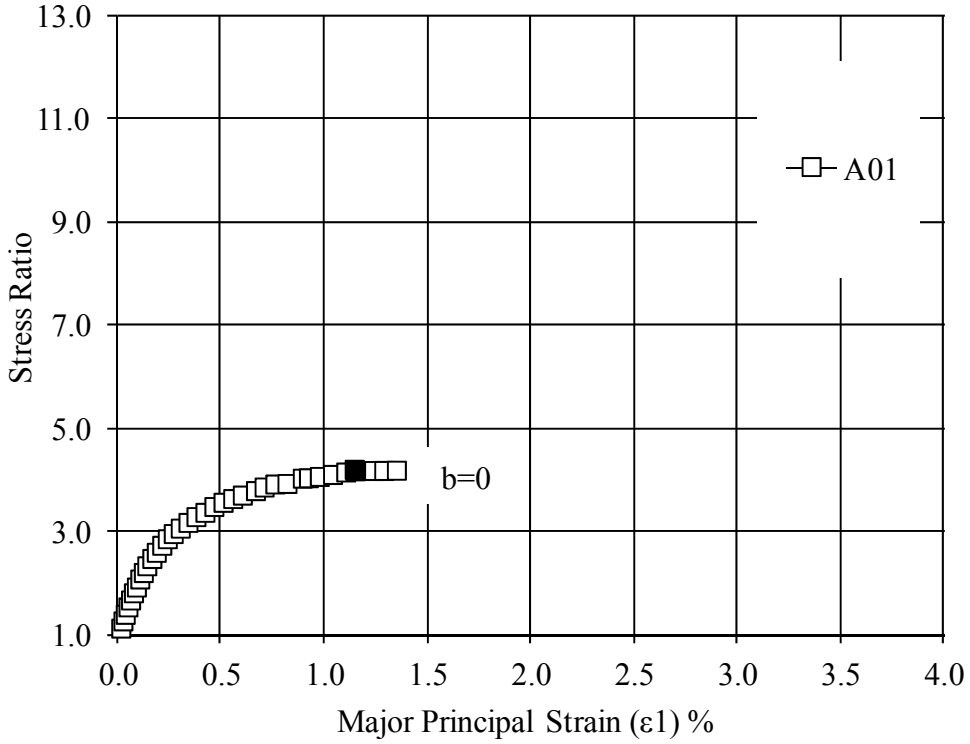

Figure 6-3: Stress – Strain Relationship for α = 0°

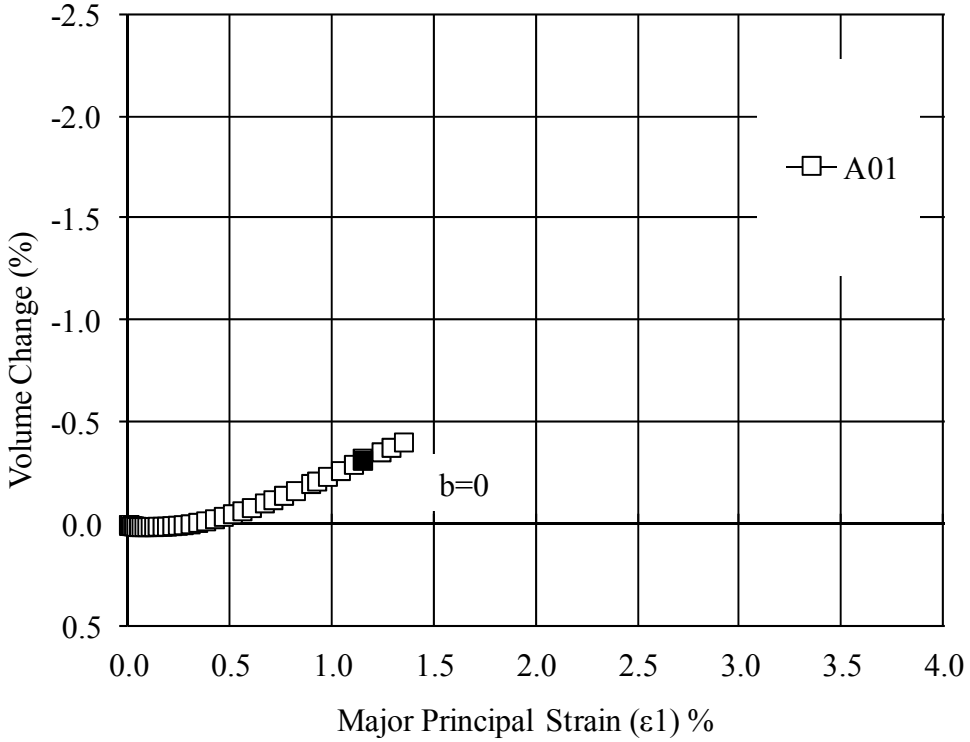

Figure 6-4: Volume Change Relationship for α = 0°

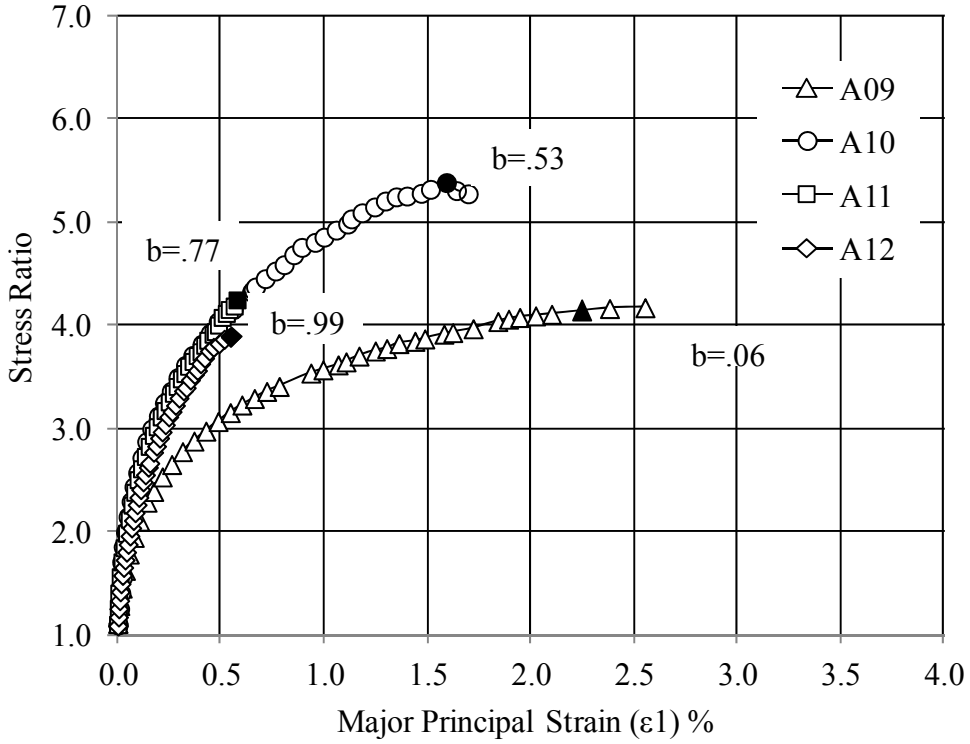

Figure 6-5: Stress – Strain Relationship for α = 90°

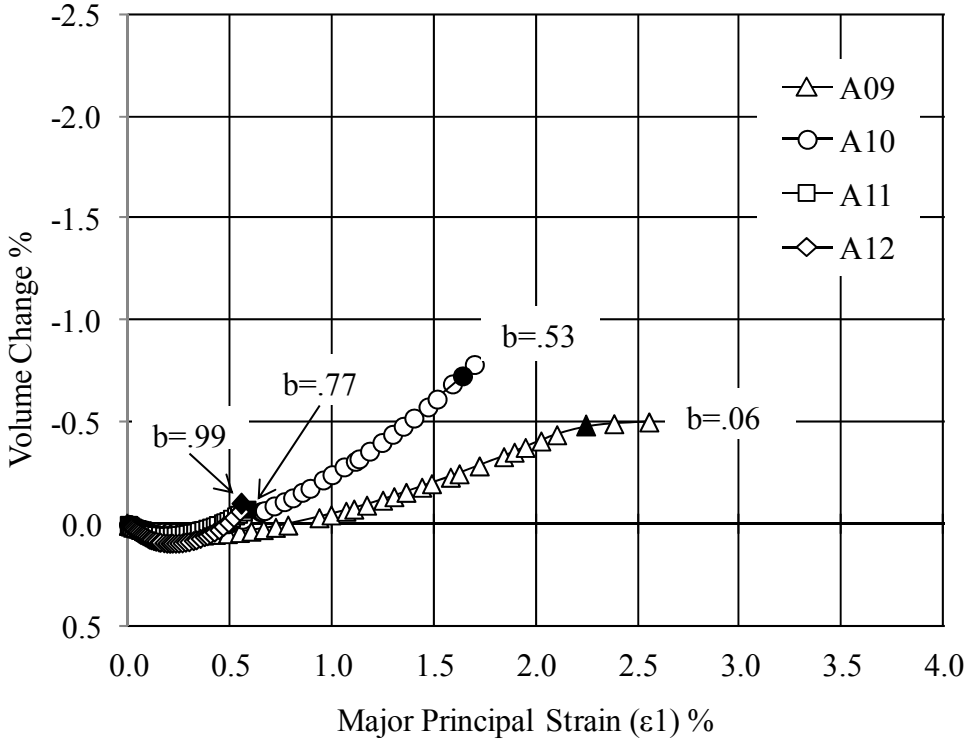

Figure 6-6: Volume Change Relationship for α = 90°

The post failure behavior for this test appears to show an increasing stress ratio. However, this increase in stress ratio is due to a calculated reduction in specimen area rather than an increase in shearing forces. The area reduction was caused by a sharp decrease in the inner volume resulting from an irregular specimen failure shape, violating the assumption that the specimen deforms as a right cylinder. Figure 6-6 shows an abrupt change in the volumetric strain rate of Specimen A09 at failure.

Tests A10, A11, and A12 all have very similar stiffnesses. Although the initial b-value for each of these tests starts out at 1, the target values are approached relatively quickly and it is unlikely that this is the cause of the similarity between tests.

It is possible that a more discernible difference in stiffnesses would have been evident if Tests A11 and A12 had achieved higher stress ratios. Extension tests with b-values approaching 1 are inherently unstable due to a reduction in specimen area during failure.

The volume change for Specimens A10, A11, and A12 is shown Figure 6-6. Test A12, represented by the diamond markers, exhibits the greatest degree of compression. The compression magnitude has a decreasing trend with the reduction in b.

6.1.3 Strength

Table 6-1 presents the calculated stress parameters for the A-Series tests. The following stress parameters: 1) inclination (α), 2) intermediate principal stress ratio (b), and 3) mean normal stress (σ_m), have been reported at failure. The table also lists the initial void ratio (e_i) for each specimen.

Kerisel's formula shown in Equation (6.1) was used to derive Equation (6.2).

$$LLL \qquad e \cdot tan\,\phi = k \tag{6.1}$$

Where:

e = void ratio

ϕ = friction angle (degrees)

k = constant

Derivation

$$k_1 = k_2$$

$$e_1 \tan(\phi_1) = e_2 \tan(\phi_2)$$

$$\phi_1 = \tan^{-1}\left(\frac{e_2 \tan(\phi_2)}{e_1}\right)$$

Equation (6.2), was used to correct the peak friction angle for each test to a planned initial void ratio or 0.530. The corresponding magnitude of the major principal strain at failure is shown adjacent the corrected friction angle. No void ratio correction has been made to the strain data.

$$\phi_1 = tan^{-1}\left(\frac{e_2\, tan\,\phi_2}{e_1}\right) \tag{6.2}$$

Where:

ϕ_1 = corrected friction angle

ϕ_2 = friction angle from test

e_1 = target void ratio (0.530)

e_2 = initial void ratio from test

Table 6-1: Test Results Summary for α = 0° and 90°

Test	Actual				Uncorrected	Corrected	ε_1
	α	b	σ_m	e_i	Fric Angle	Fric Angle	failure
A01	0.00	0.00	97.44	0.5047	37.90	36.55	1.24
A09	90.00	0.06	96.51	0.5329	37.62	37.77	2.25
A10	90.00	0.53	98.52	0.5277	43.31	43.19	1.59
A11	90.00	0.77	97.90	0.5242	38.14	37.84	0.59
A12	90.00	0.99	98.62	0.5172	36.24	35.58	0.56

6.2 Testing with Inclined Principal Stress Directions

In addition to the compression and extension testing presented in Section 6.1, a number of tests, designated A02 through A08, were performed with inclined principal stress directions. This section presents the results obtained for these tests.

6.2.1 Conformance with Planned Stress State (b, σ_m, α)

As discussed in Section 6.1.1, all A-Series stress paths neglected the piston correction (defined in Section 5.4.2) resulting in additional uplift force acting in a purely vertical direction. This additional uplift force resulted in unintended stress rotation and an offset from the planned stress inclination direction at failure.

Figure 6-7, Figure 6-8, and Figure 6-9 show the rotating principal stress direction with respect to the major principal stress. Due to the excess uplift force, all tests start with σ_z less than σ_θ. This results in tests A02 through A08 all starting at an α = 90° condition, since there are no other initial shear stresses that are applied to the specimen.

As shearing progresses, all tests trend asymptotically in the direction of the planned α value, although as shown in Table 6-2, the values of α at failure are still higher than intended.

Unlike the variation in b-value, stress rotation occurs during the majority of the shearing phase and is not confined to the elastic portion of the test. Rotation occurring during each test has a unique effect on measured strains, making comparisons of strain related data between tests difficult.

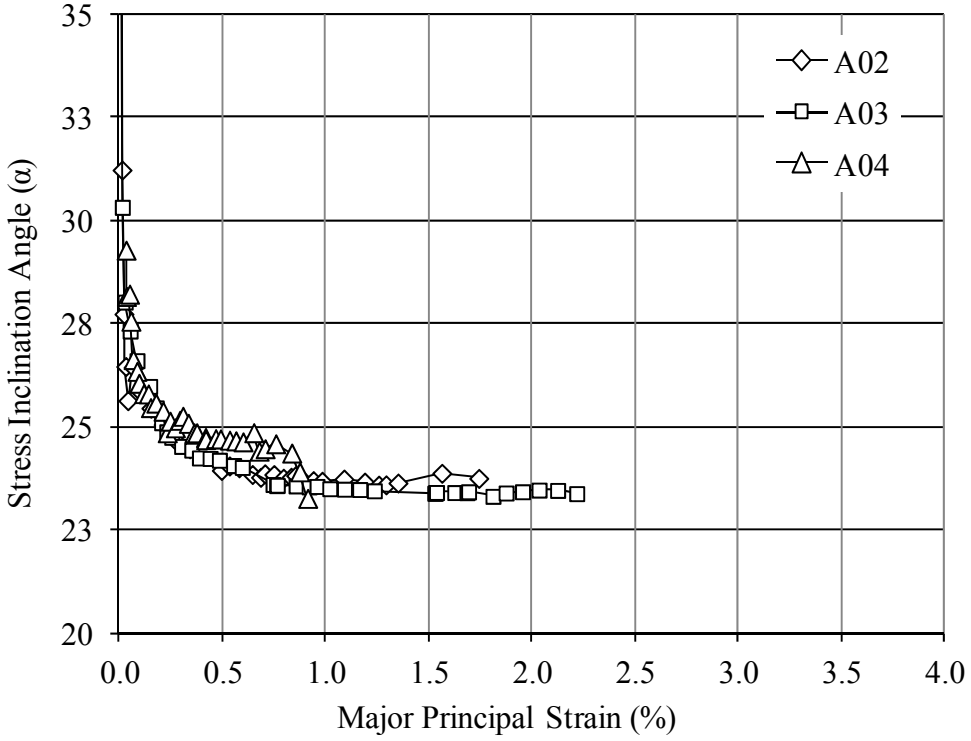

Figure 6-7: Stress Inclination Angle (α) for Tests Planned at 22.5°

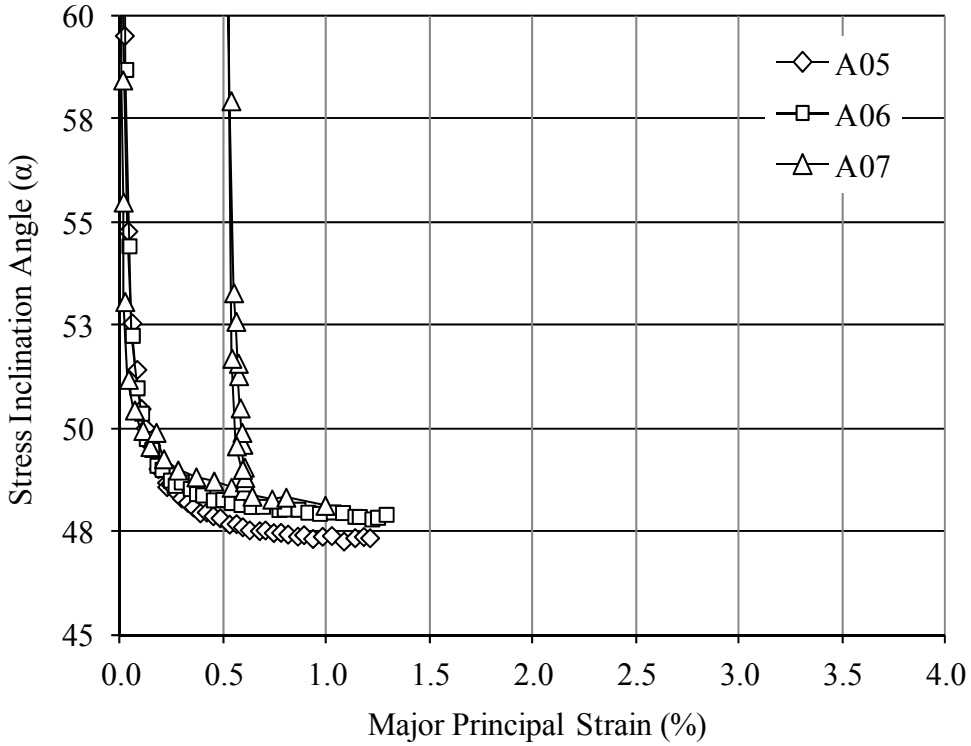

Figure 6-8: Stress Inclination Angle (α) for Tests Planned at 45°

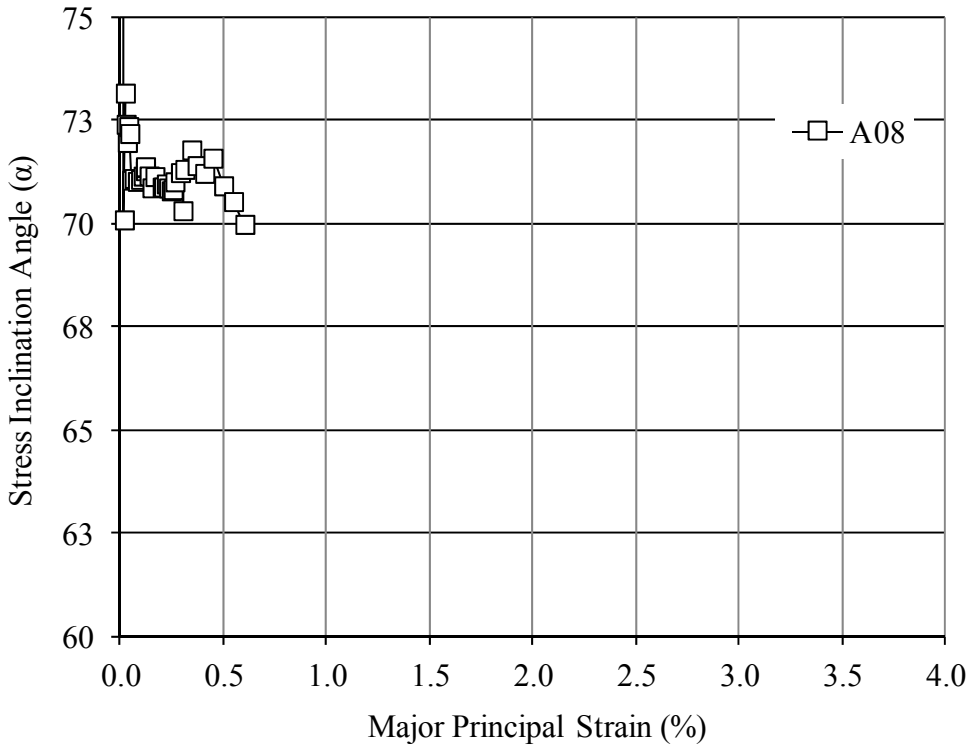

Figure 6-9: Stress Inclination Angle (α) for Tests Planned at 67.5°

Figure 6-10 shows the variation in mean normal stress with respect to the major principal strain. For these tests, the mean normal stress was between 3 and 4 percent lower than the planned value of σ_m = 101.3 kPa. This trend is similar to observations made for tests at $\alpha = 0°$ and $\alpha = 90°$, that can be seen in

Figure 6-1. The last 3 points for Test A04 show a sharp drop in σ_m associated with rapid volume change taking place near failure.

The intermediate principal stress ratio with respect to the major principal strain is shown in Figure 6-11. Similar to the trend observed in Figure 6-2, the b-values quickly trend in an asymptotic fashion from a starting value of 1 to the test target value.

Test A04 does not follow this trend. An initial torque was applied to this specimen before the vertical load and cell pressures started following the prescribed test path. Although this problem was corrected after a very short duration, it resulted in a transitional b-value that started at 0.791 and then increased in the target direction. Test A06 had an unload-reload portion that caused the b-value to decrease and increase in step with the load.

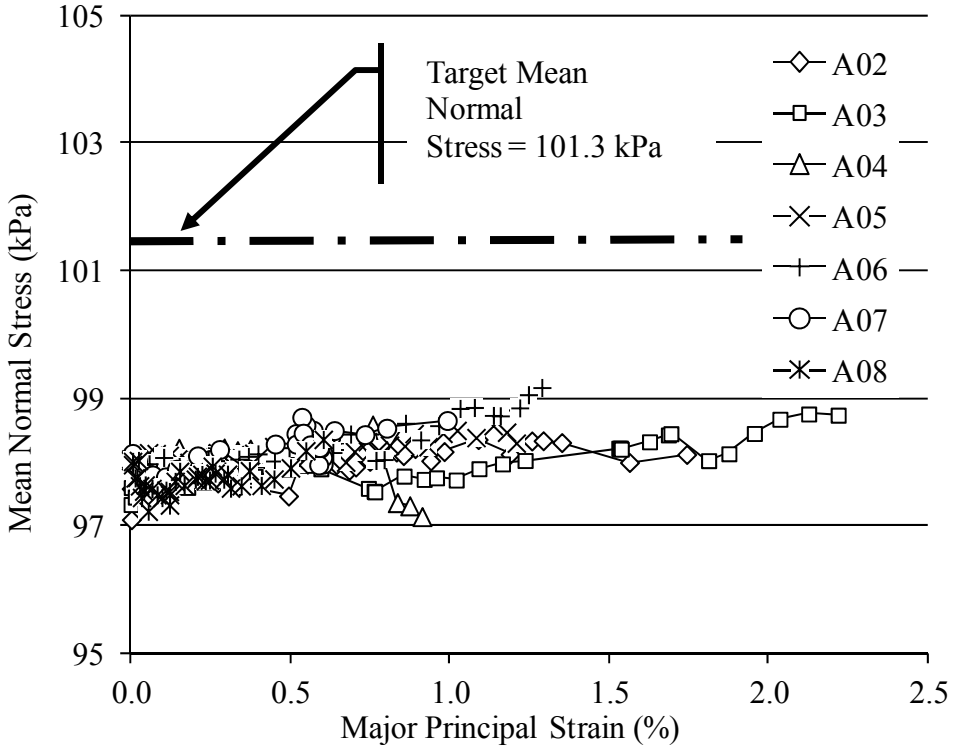

Figure 6-10: Mean Normal Stress (kPa)

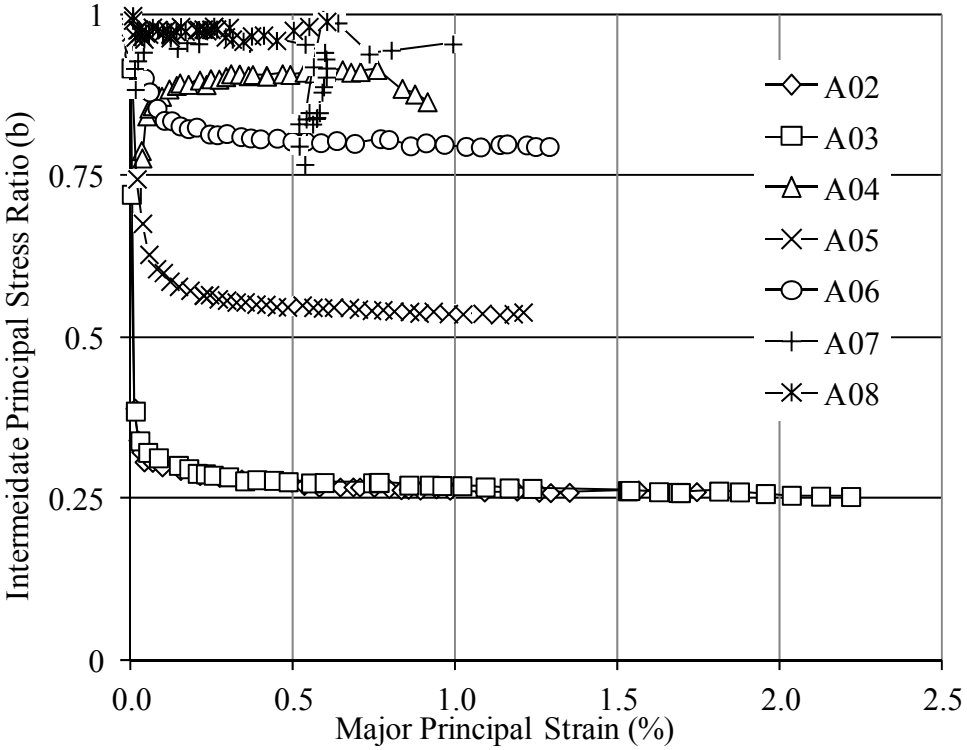

Figure 6-11: Intermediate Principal Stress Ratio (b)

6.2.2 Stress – Strain and Volume Change Behavior

Figure 6-12 shows the stress ratio versus the major principal strain for tests performed with a target α of 22.5°. Test A03 is shown for informational purposes only. The absolute value of the right side torque load cell measurements for this test lags behind the absolute value of the left side load cell. This is inconsistent with the pattern observed during other tests. The cause of this inconsistency was not discovered, however, it does cast doubt on the calculated stress ratio for this test.

As explained in greater detail (Section 6.2.2.1), the major principal stress and strain for Test A04 occurred in the radial direction. Figure 6-13 shows the volume change relationship for tests conducted with α near 22.5°. Based on the strain data presented in this figure Tests A02 and A03 had similar responses, as expected.

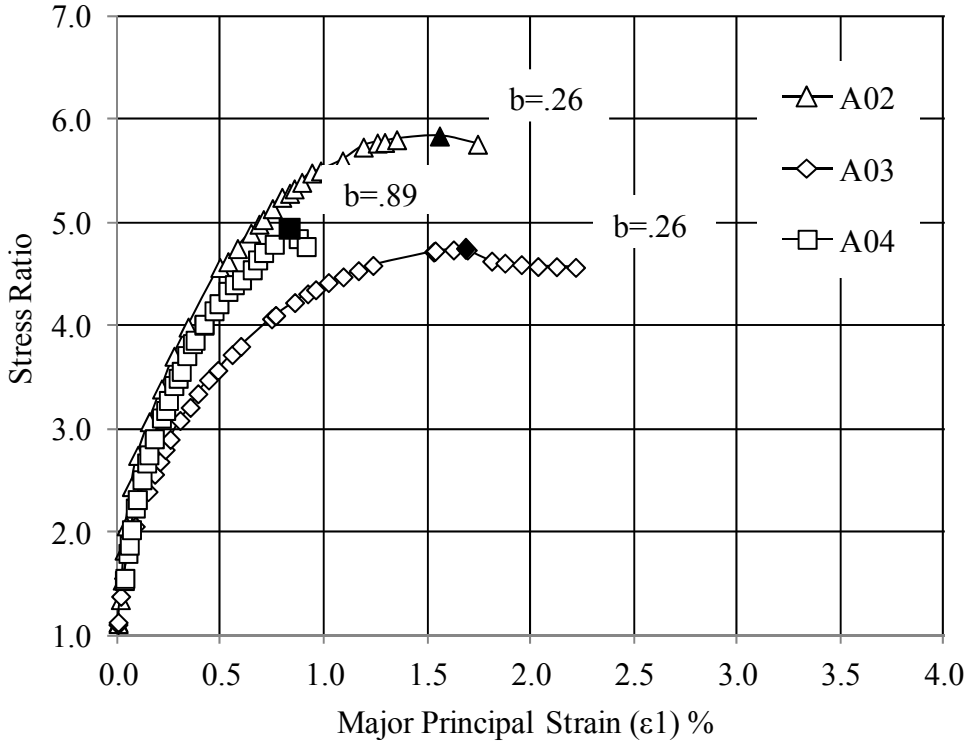

Figure 6-12: Stress – Strain Relationship for α ≈ 22.5°

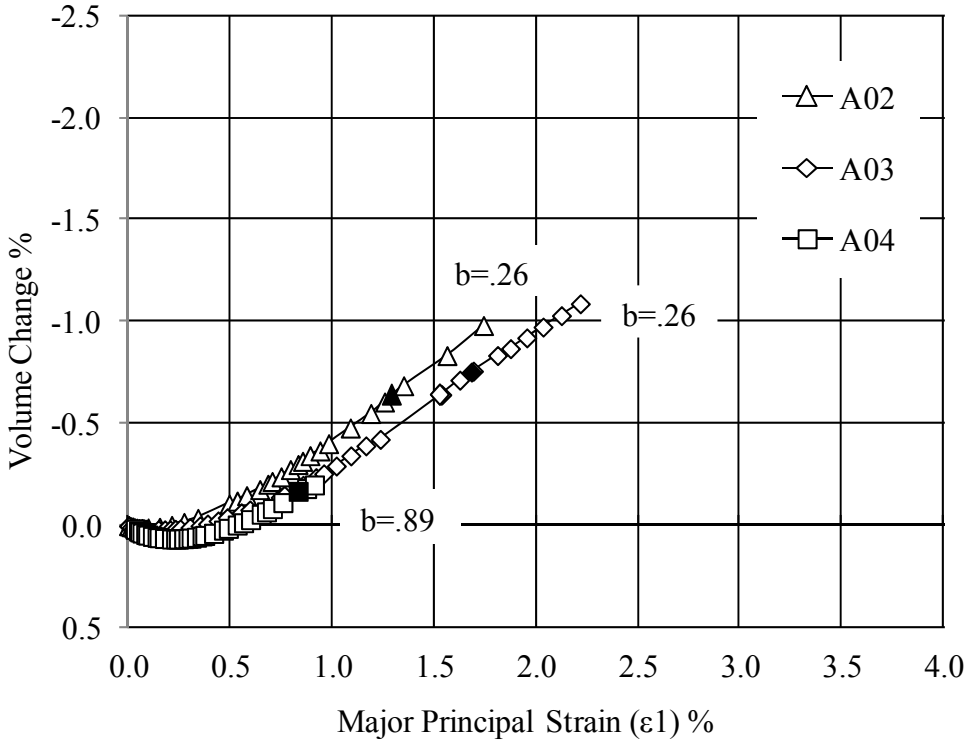

Figure 6-13: Volume Change Relationship for α ≈ 22.5°

Test A04 did not exhibit a rapid increase in volumetric strain after the onset of dilation as is typically observed during tests with high b-values. This may be due to the effects of anisotropy. The major principal strain (ε1) occurred in the radial direction aligning it more closely with the bedding plane, resulting in a greater magnitude and softer curve.

However, when the volumetric strain is plotted against the intermediate principal strain (ε2), as shown in Figure 6-14, a much steeper ascent is observed. A steepening of the curve is produced by the smaller intermediate principal strains.

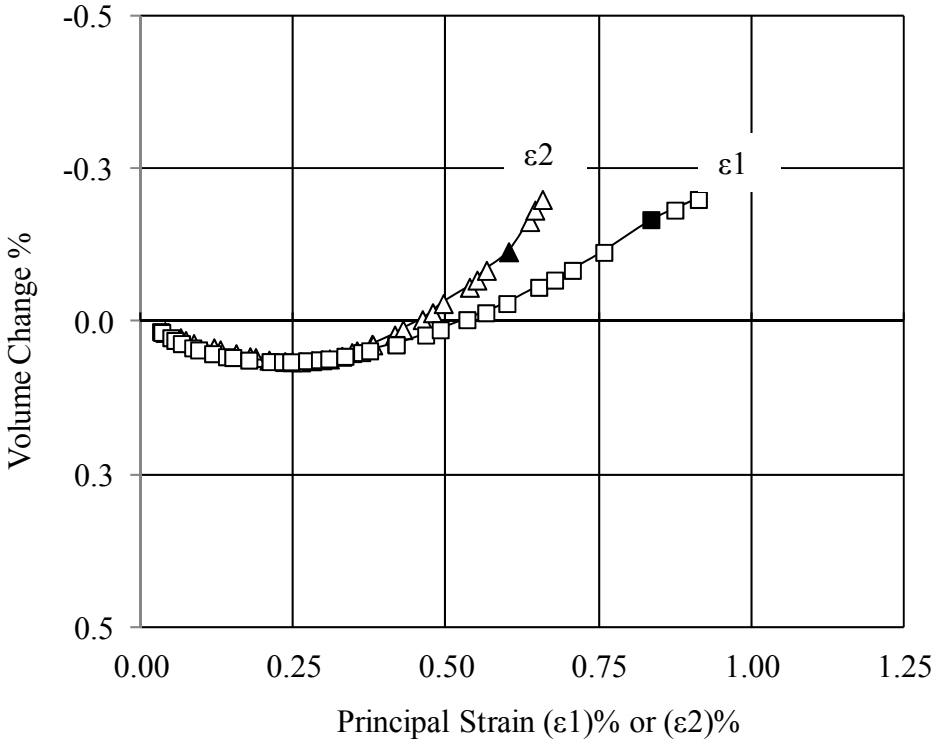

Figure 6-14: Test A04 Volumetric Strain Versus Major and Intermediate Principal Strians

The stress ratio versus major principal strain for tests ending near 45°, is shown in Figure 6-15. These tests show that an increasing b-value is accompanied by a slight increase in stiffness.

The response of Test A07 (b = 0.95) may be slightly softer than expected. As shown in Figure 6-8, the principal stress inclination for this test was slightly larger than the others. This fact, coupled with the unload cycle may have softened the response of Test A07.

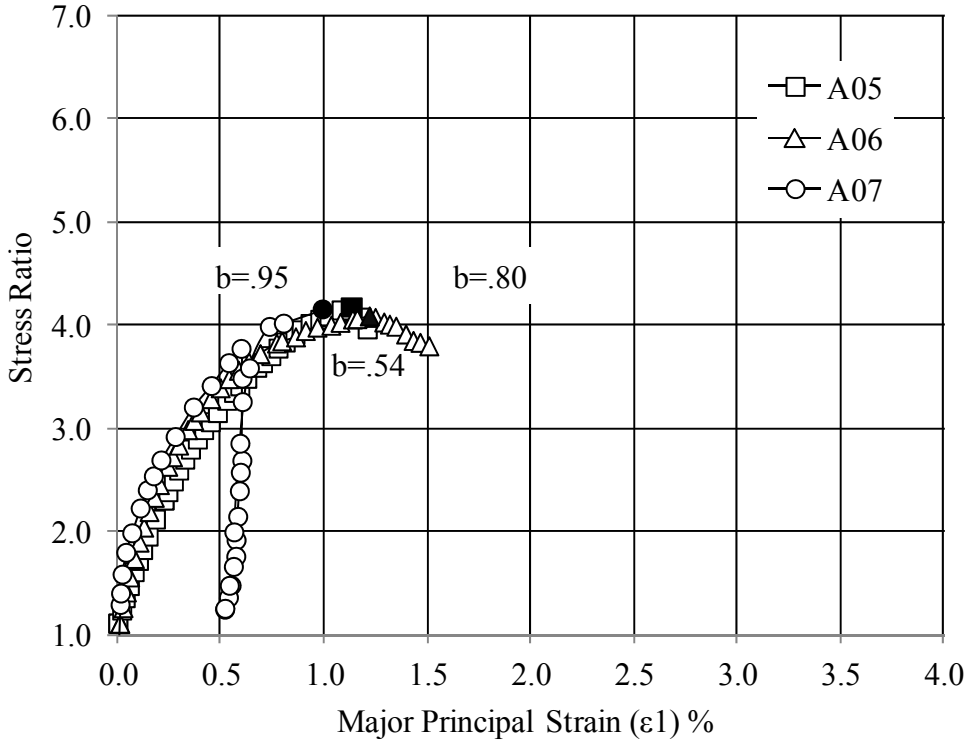

Figure 6-15: Stress–Strain Relationship for α ≈ 45°

The volume change with respect to the major principal strain is shown in Figure 6-16, for tests with α near 45°. As expected, Test A07, with the highest b-value exhibits the most rapid rate of dilation. However, the curve softens after the load/reload cycle.

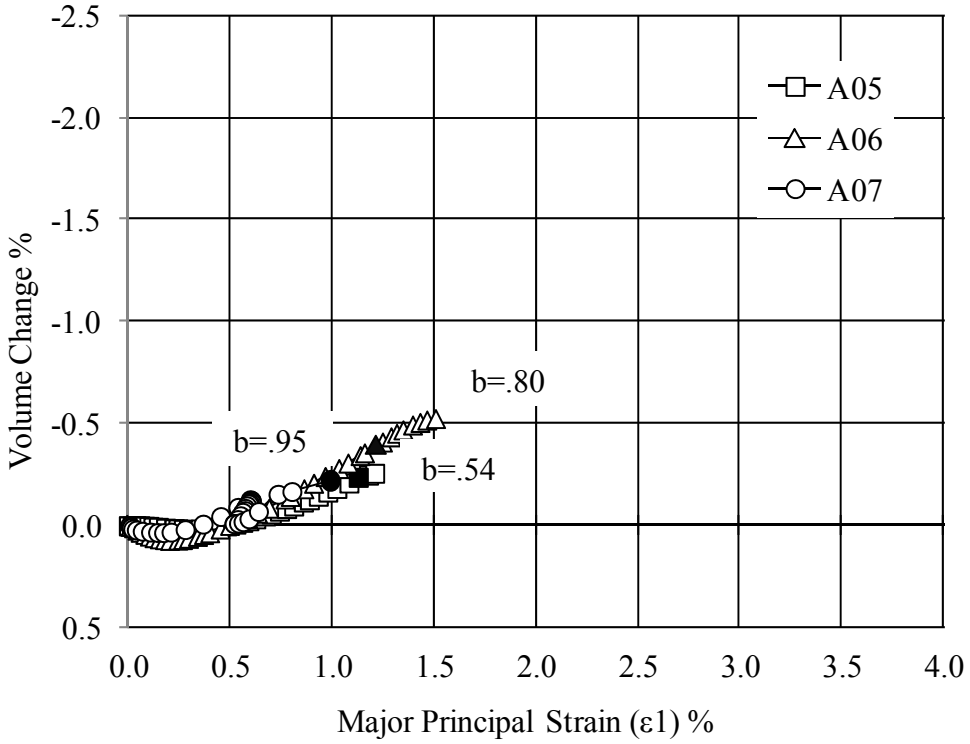

Figure 6-16: Volume Change Relationship for α ≈ 45°

Figure 6-17 and Figure 6-18 respectively, show the change in stress ratio and volumetric strain with respect to the major principal strain for tests with α near 67.5°.

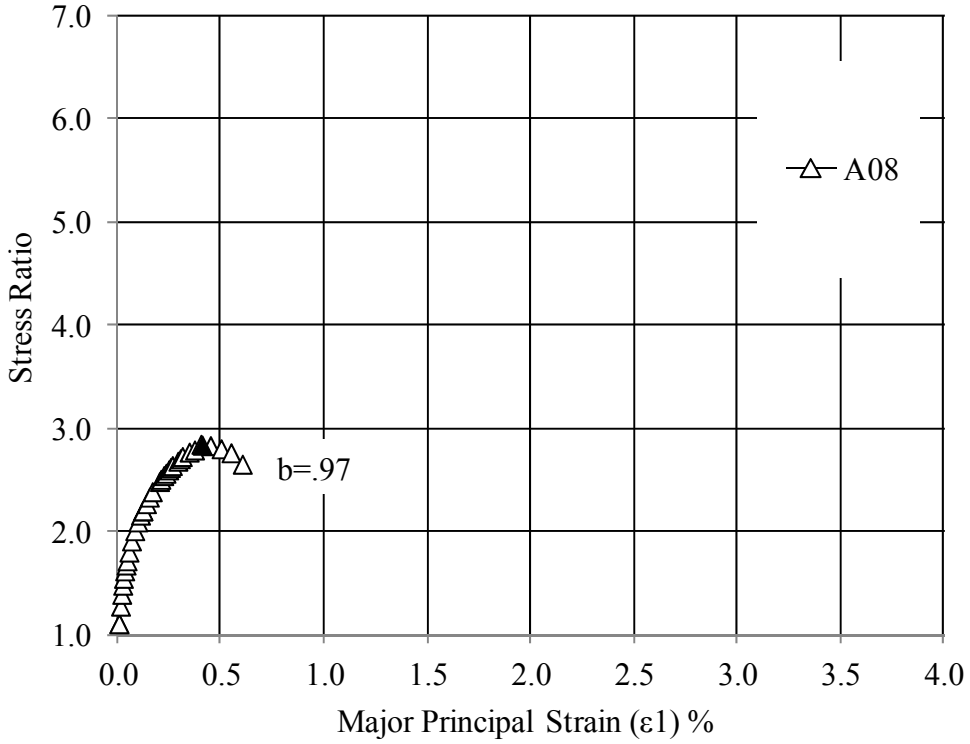

Figure 6-17: Stress–Strain Relationship for α ≈ 67.5°

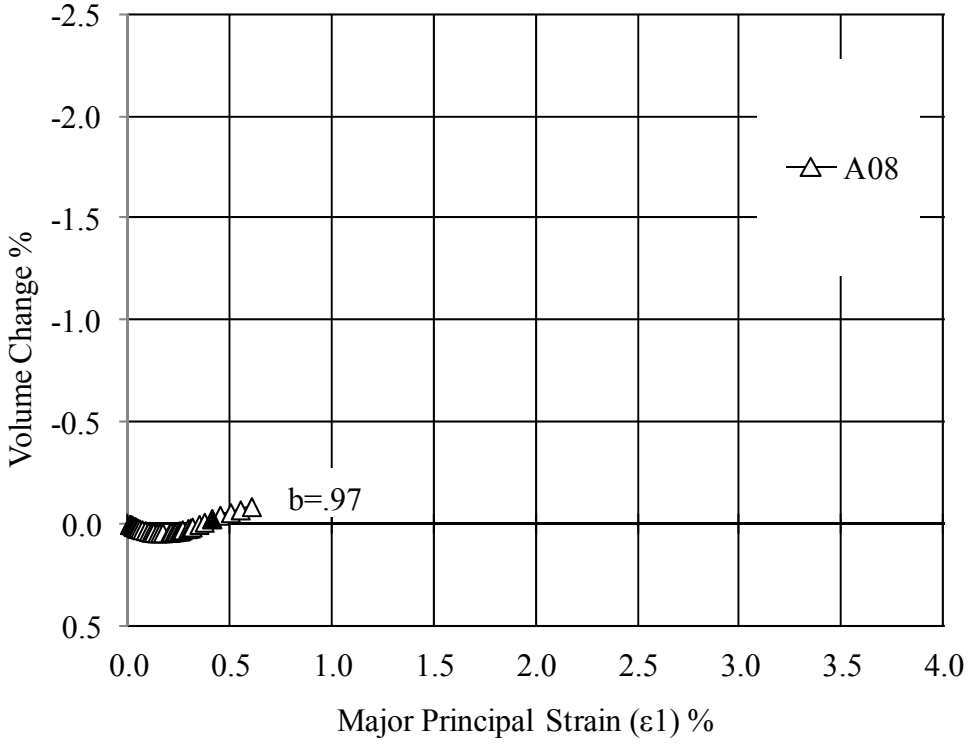

Figure 6-18: Volume Change Relationship for α ≈ 67.5°

6.2.2.1 OUT OF PLANE MAJOR PRINCIPAL STRESS

The test data obtained during the shearing of specimen A04 has been included in this document. However, for that particular stress state, neglecting the piston correction resulted in a vertical stress reduction of sufficient magnitude to cause the major and intermediate principal stresses to interchange.

This creates a condition where the critical shear (σ_1-σ_3) occurs in the r-θ plane. To account for this, the traditional major and intermediate principal stress and strain equations have been interchanged for analysis of this test, as shown in Figure 6-19.

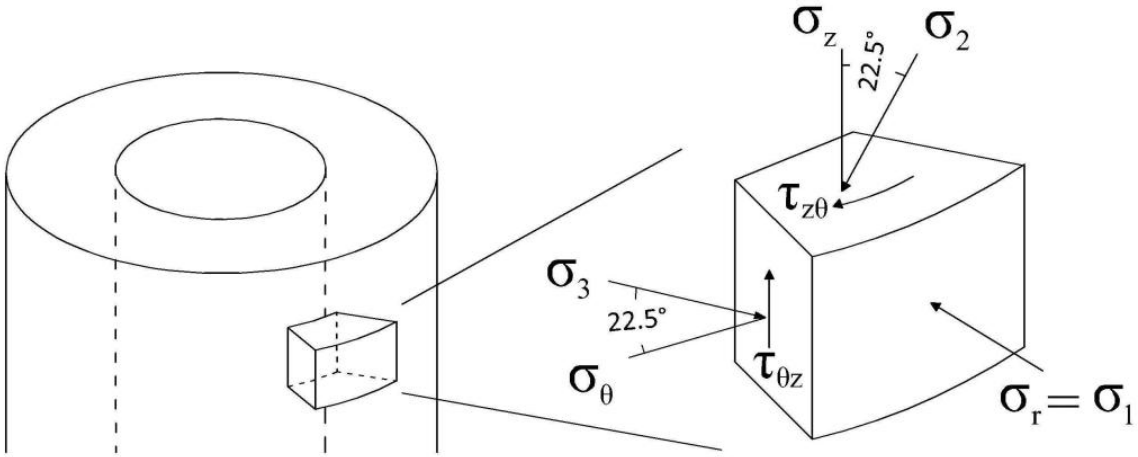

Figure 6-19: Stress Direction Schematic
For Interchanged Principal Stress Directions

The b-value calculated for this test describes the relative magnitude of the larger of the two principal stresses in the z-θ plane. For this test condition of α = 22.5°, the intermediate principal stress is the more vertical of the two stresses.

Stress rotation (α) is caused by movement of the turn table and is confined to the z-θ plane (i.e. within the specimen wall). The stress rotation (α) is calculated within the z-θ plane. No rotation is possible within either the r-z or r-θ planes, because shear stresses can't be applied to the flexible membrane that makes the cylinder's vertical walls.

To the best of this author's knowledge, no research has been conducted relating the effects of strength and stiffness to rotation occurring in the z-θ plane which is also the σ_2-σ_3 plane. Nor have torsional shear test results been encountered in which the major principal stress was applied in the radial direction.

However, as discussed, it is possible to apply the major principal stress in the radial direction. This is accomplished by a reduction in vertical stress resulting from an upward force. Equation (6.3) can be used to calculate the force that is needed to interchange the major and intermediate principal stresses. The full derivation of this equation is contained in Appendix J.

This relationship was developed for the test conditions in A04. This relationship will not work for any test with α > 45°, because the more vertical of the two stresses in the z-θ plane would actually be the minor principal stress. However, a similar derivation could be developed for testing under those conditions.

$$F_v < \pi R_o R_i (P_o - P_i) \frac{[3cos(2\alpha)-1]}{[cos(2\alpha)+1]} \tag{6.3}$$

Test A04's most prominent shear band can be seen in Figure 6-20. This shear band has a characteristically wide trough and the specimen has obviously "bellied out" in the mid section. Both of these observations indicate a rupture in the r-θ plane.

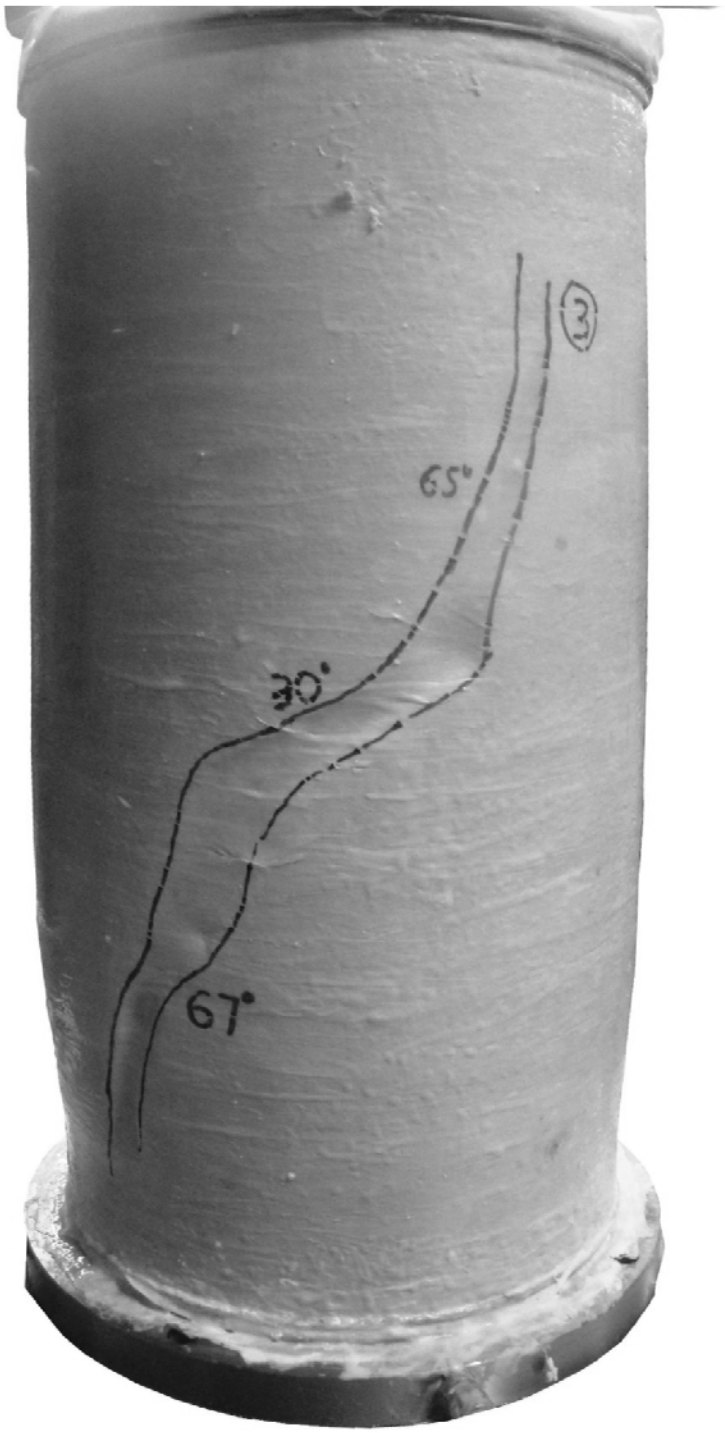

Figure 6-20: A04 Specimen Failure Shear Band

6.2.3 Strength

Using the same format described in Section 6.1.3, Table 6-2 presents the strength and stress parameters calculated at failure for the A-Series tests with inclined principal stress directions. The peak friction angle values have been corrected for variations in initial void ratio using Equation (6.2).

Table 6-2: Test Summary for Tests with Inclined Principal Stress Directions

Test	Actual				Uncorrected	Corrected	ε_1
	α	b	σ_m	e_i	Fric Angle	Fric Angle	failure
A02	23.88	0.26	98.00	0.5476	45.01	45.95	1.56
A03	23.43	0.26	98.45	0.5237	40.64	40.30	1.69
A04	24.37	0.89	97.37	0.5523	41.54	42.72	0.84
A05	47.36	0.54	98.58	0.5551	37.79	39.08	1.14
A06	47.81	0.80	98.85	0.5591	37.37	38.85	1.22
A07	48.14	0.95	98.66	0.5326	37.69	37.83	0.99
A08	71.23	0.97	97.64	0.5364	28.62	28.91	0.41

A relative comparison of strain to failure or stiffness is not reliable for this series of test, due to strains associated with unintended stress rotation. However, the general trend for these tests shows a decrease in peak friction angle with increase in α.

As expected, Test A08 had the lowest friction angle. However, the corrected value of 28.91° is considerably lower than the other tests and may not be a reliable value. As will be explained in the following paragraphs, the combined effects of specimen geometry and shear band formation may have lead to this lower than expected friction angle.

The specimen preparation procedure detailed in Appendix E, steps E.9 and E.10 calls for leveling the sand that comprises the top of the specimen 1 mm above the exterior forming jacket. The epoxy coated top ring is then pressed down into this 1 mm sand

layer. Since there is a small gap between the bottom of the cap and the exterior forming jacket, the sand grains beneath the outside edge of the cap slough off slightly leaving a very small indentation in the outer wall of the specimen directly beneath the top cap. A schematic exaggeration of this condition is shown in Figure 6-21.

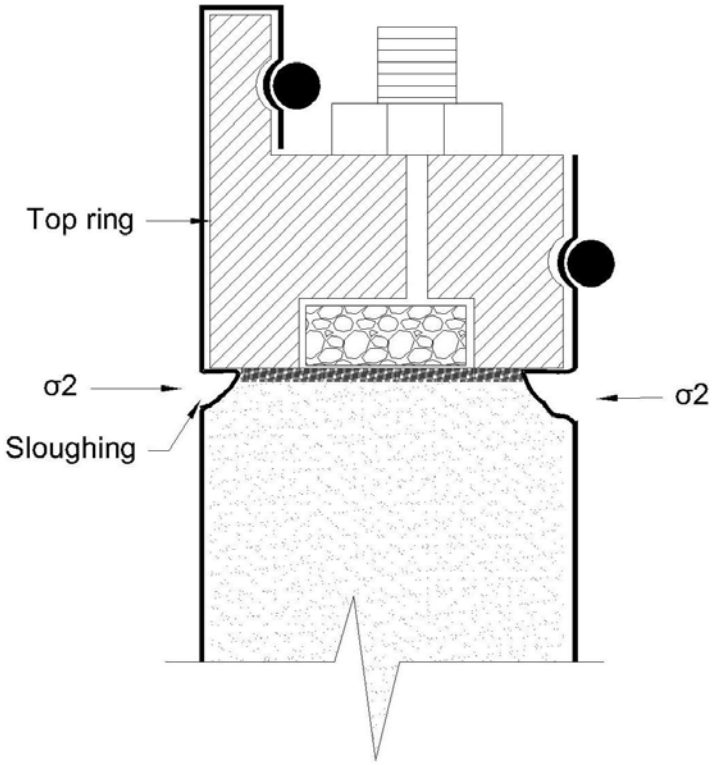

Figure 6-21: Sloughing of Sand Grains Beneath Top Ring

The sloughing sand grains cause a slight reduction in the cross sectional area of the specimen directly beneath the cap. This effect is not problematic for most test conditions. However, for tests with $\alpha = 67.5°$, Coulomb's equation for shear band inclination, as defined in Equation (2.10), results in a nearly horizontal shear band direction.

For Test A08, it appears that horizontal shear banding was attracted to the reduced area zone located direction beneath the cap, possibly exaggerating the indentation that was already present due to the specimen formation technique.

For high b-value tests (i.e. > 0.7), application of the radial stress (σ_2) to this reduced zone produce an additional area reduction resulting in higher stress ratios. This condition is inherently unstable and will ultimately result in premature failure or top cap slippage.

Figure 6-22 presents a photograph of the area directly beneath the top cap at failure for Test A08. The indentation and relative rotation of the top cap in relation to the specimen supports the previously described failure mechanism.

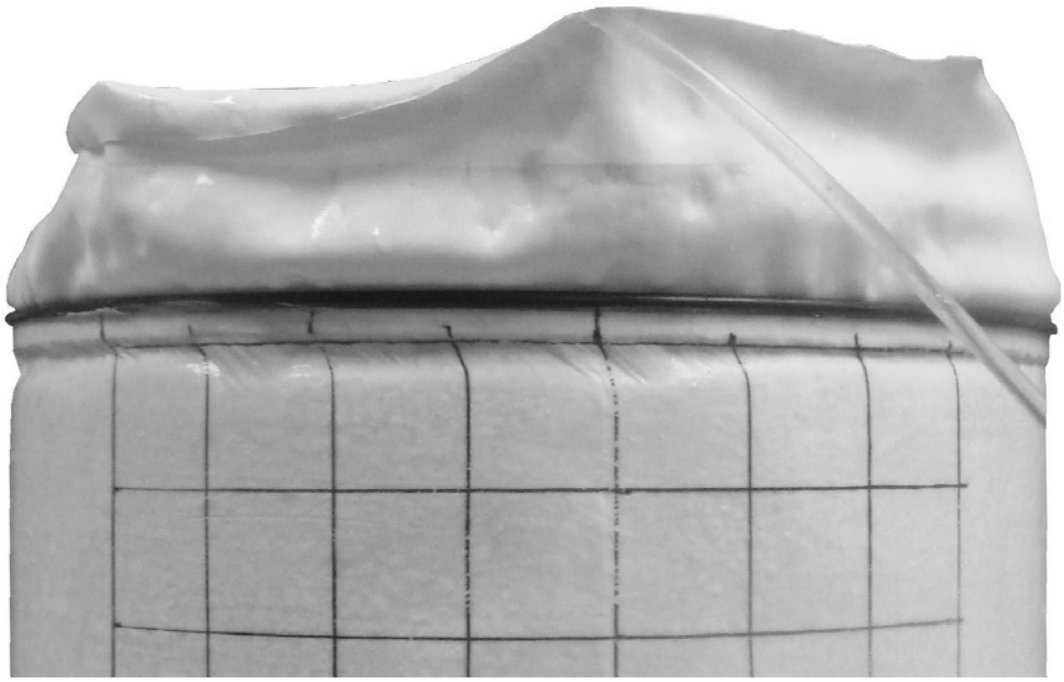

Figure 6-22: Top Cap and Specimen for Test A08

7 SERIES B TEST RESULTS

Neglecting the piston area uplift correction during A-Series testing caused a deviation from the intended stress path. Therefore, it became necessary to conduct a second series of tests that correctly accounted for the piston uplift correction. This second, B-Series, of tests was performed from July 29, 2011to October 13, 2011.

7.1 Adherence to Test Program

To evaluate the effects of the principal stress inclination and the intermediate principal stress ratio on drained soil behavior, certain stress parameters must be held constant: Principal stress inclination, mean normal stress, and the intermediate principal stress ratio.

7.1.1 Mean Normal Stress

The mean normal stress for all ten B-Series tests is presented in this section. Due to the large number of tests, the data has been split between two figures. Figure 7-1 presents the results of Tests B01 through B05 and Figure 7-2 presents the results of Tests B06 through B10.

The data indicate good conformance with the planned mean normal stress of 101.3 kPa (1 Atm.). With the exception of Test B10, most of the values are within the 1 kPa bounds indicated by the darkened lines on each chart. This is slightly less than 1 percent of the target value.

The vertical load applied to Test 10 was offset by 82.78 N due to a calibration error that was discovered immediately after the test was completed. This factor resulted in a slightly reduced mean normal stress that was within 3 kPa of the target value.

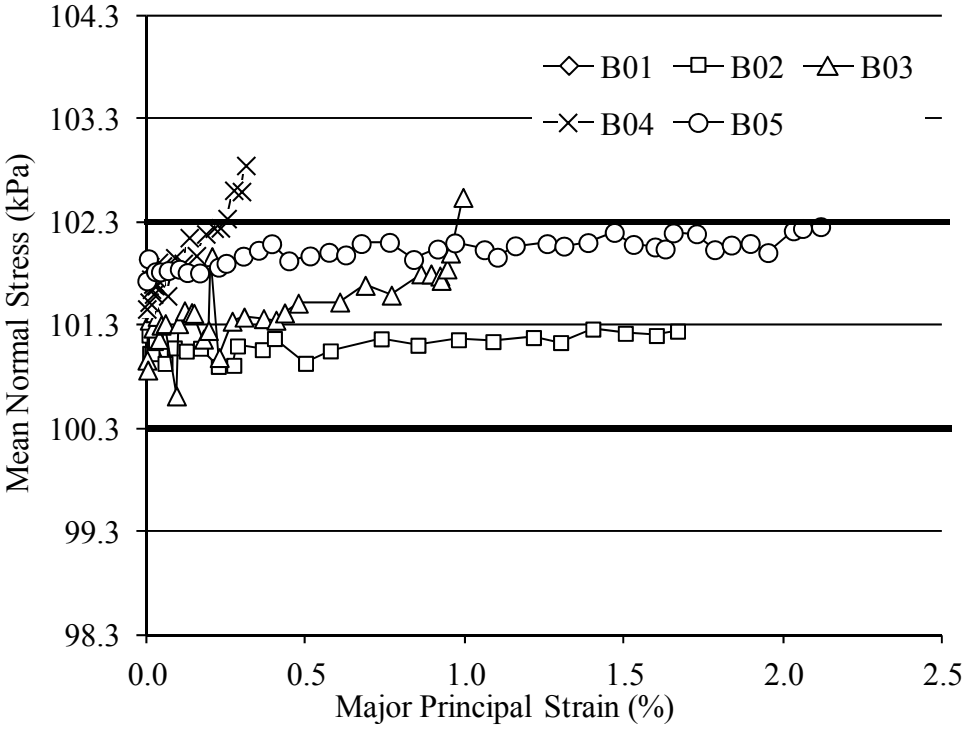

Figure 7-1: Variation of Mean Normal Stress

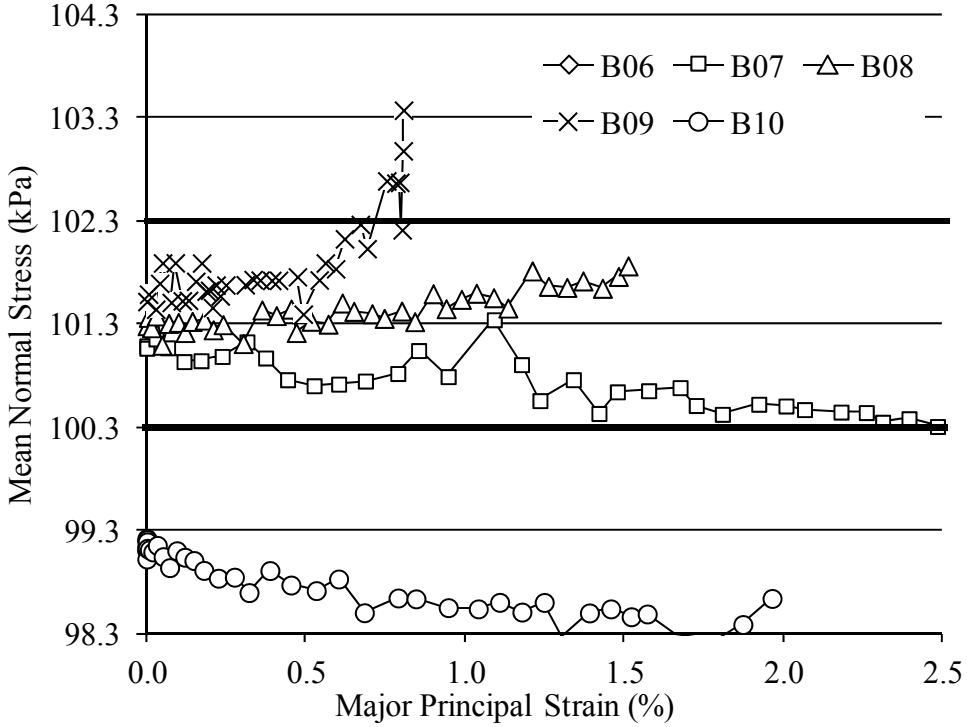

Figure 7-2: Variation of Mean Normal Stress

7.1.2 Intermediate Principal Stress Ratio

The variation in b-value during the shearing of all ten B-Series tests are presented in this section. Similar to the previous section, the data has been split between two figures. Figure 7-3 presents the results of Tests B01 through B05 and Figure 7-4 presents the results of Tests B06 through B10. With the exception of Test B10, all b-values conform closely with the target values.

Because shearing is initiated from a specimen that has been isotropically consolidated ($\sigma_1 = \sigma_2 = \sigma_3$) the deviator stress during the first few loading intervals is very small, leading to slight deviations in b-value for the very early data. Although the variation in the intermediate principal stress ratio is easily seen, the actual magnitude that σ_2 deviates from its intended target is small. These variations also occur within the elastic phase, making this initial deviation insignificant.

As previously discussed in Section 7.1.1, test B10 was conducted with an additional vertical force of -82.78 N. Test B10 was performed with $\alpha = 90°$. Therefore, the additional vertical force caused a decrease in σ_3 while σ_1 and σ_2 remained constant. This resulted in an intermediate principal stress that was relatively closer to the major principal stress than intended. This effect was observed throughout shearing. The final value of b was for Test B10 was 0.05.

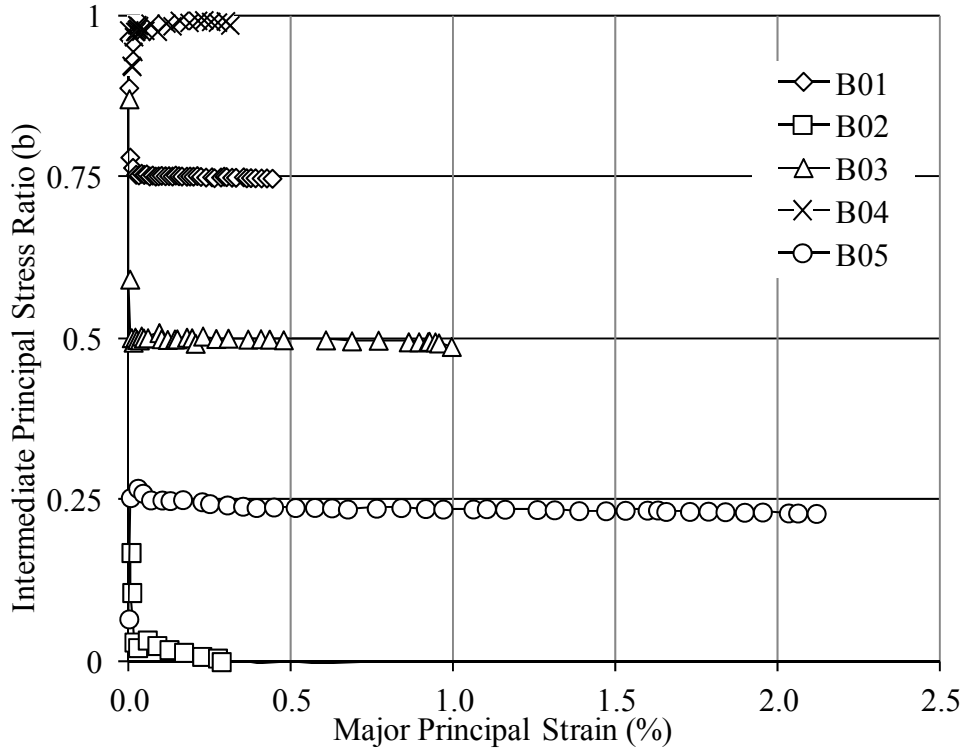

Figure 7-3: Variation of the Intermediate Principal Stress Ratio (b)

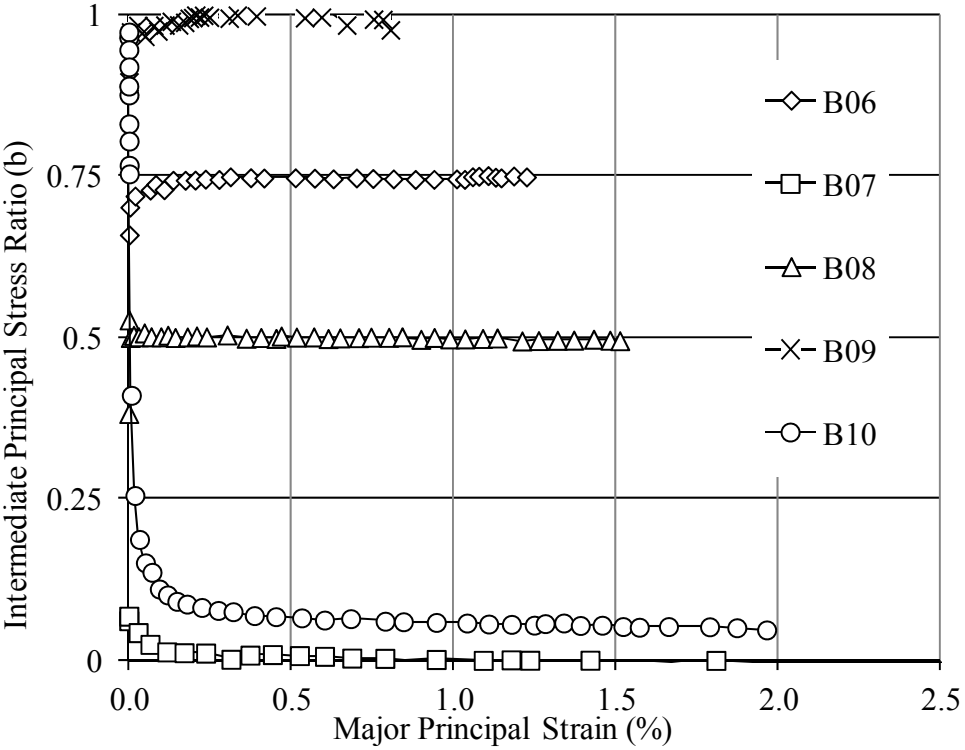

Figure 7-4: Variation of the Intermediate Principal Stress Ratio (b)

7.1.3 Principal Stress Inclination (α)

The variation of α during the shearing for all ten B-Series tests is presented in this section. The data has been split into four figures. By using two separate scales for the vertical axis, Figure 7-5 presents the results of α at both 0° and 90°.

Since no torque is applied to the specimen during either of these stress conditions, $\tau_{z\theta} = 0$ and α is always equal to either 0° or 90°. Equation (7.1) is used for compression tests and Equation (7.2) is used for extension testing.

$$\alpha = \frac{1}{2} tan^{-1}\left(\frac{2\tau_{z\theta}}{\sigma_z - \sigma_\theta}\right) \tag{7.1}$$

$$\alpha = 90 - \left[\frac{1}{2} tan^{-1}\left(\frac{2\tau_{z\theta}}{\sigma_z - \sigma_\theta}\right)\right] \tag{7.2}$$

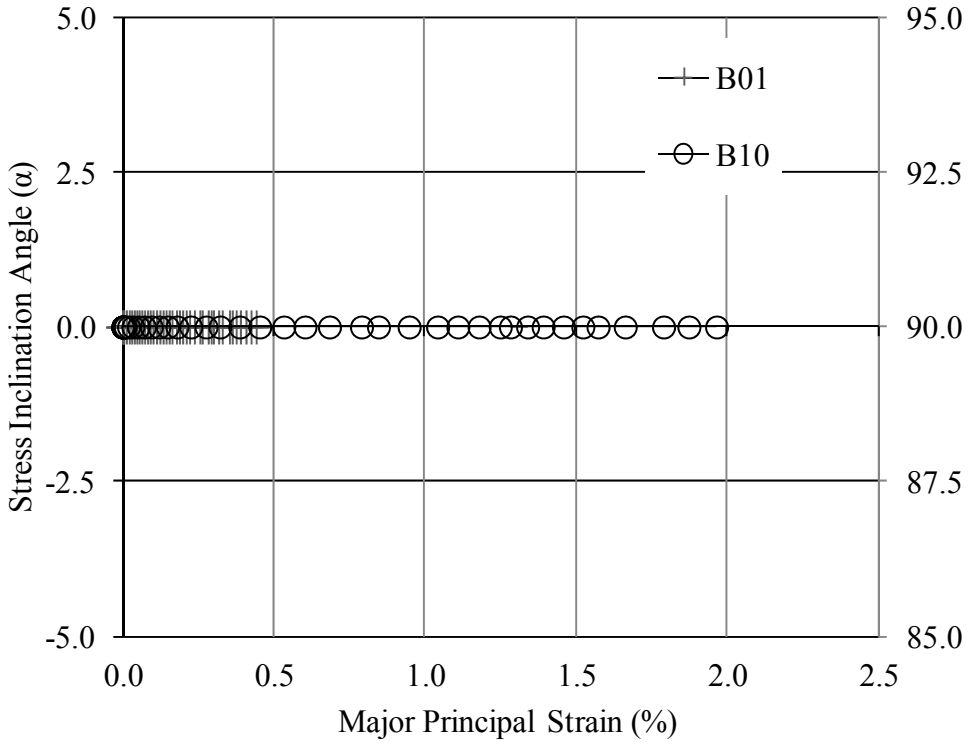

Figure 7-5: Variation of the Principal Stress Inclination (α)

Figure 7-6, Figure 7-7, and Figure 7-8 show the variation in α for tests with inclined principal stress directions. Much like the b-value, α is also defined by a ratio of stresses. This leads to some variability during the first few loading intervals when the deviator stress is small. The initial α values are usually slightly biased towards 45°. However, after the initial few increments, all tests except B09 quickly approach their target values. The oscillation observed in Test B09 is explained in Section 7.1.3.2

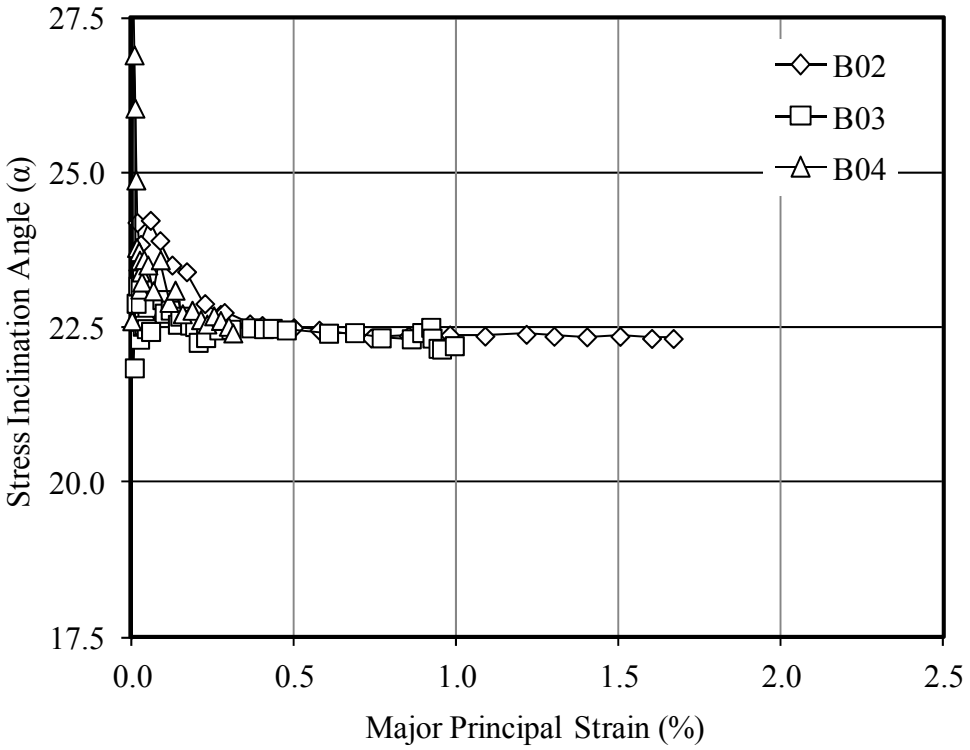

Figure 7-6: Variation of the Principal Stress Inclination (α)

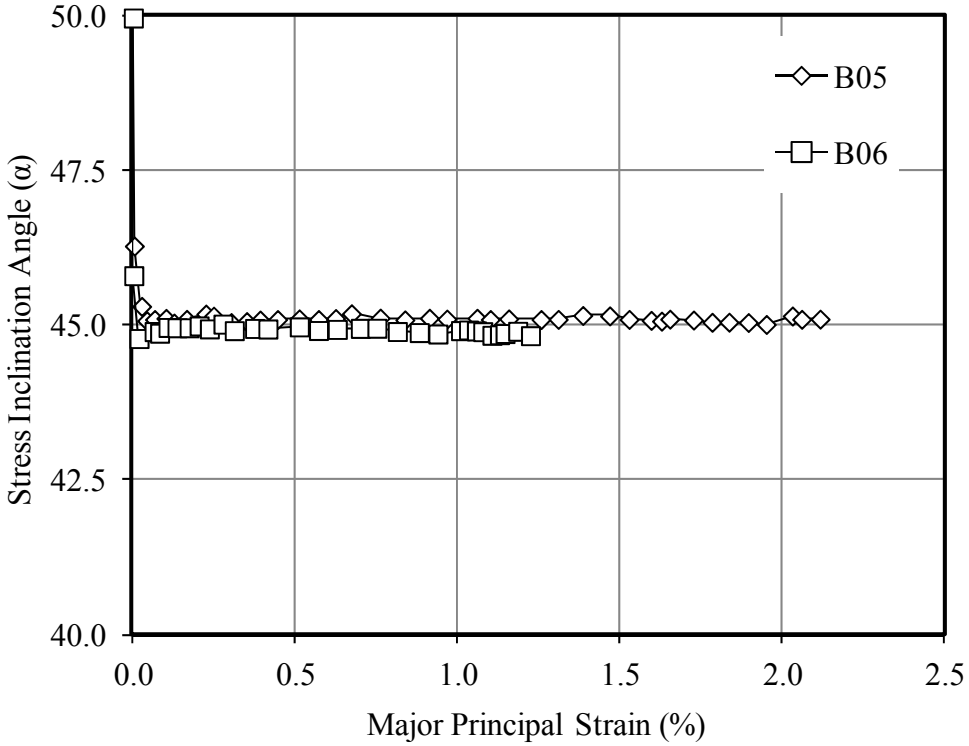

Figure 7-7: Variation of the Principal Stress Inclination (α)

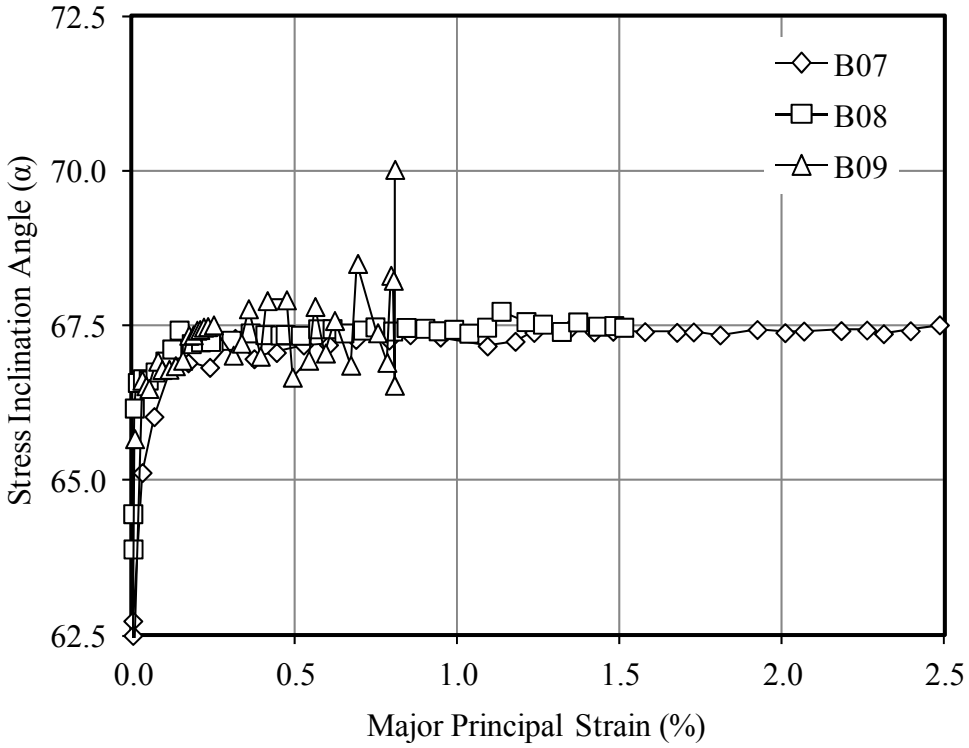

Figure 7-8: Variation of the Principal Stress Inclination (α)

7.1.3.1 Initial Bias of the Stress Inclination Angle

As explained in Section 0, for all tests with inclined principal stress directions, applied torque is the independent variable that controls the test. Torque measurements are used to calculate the desired vertical load and cell pressures. Since the cell pressures and vertical load are applied in response to the measured torque, all tests start with an α value biased to 45° inclination. This is because applying torque to the initial stress condition with the same inner and outer cell pressures and no vertical load follows the stress path for $\alpha = 45°$ and $b = 0.5$.

7.1.3.2 The Variation in the Stress Inclination Angle for Test B09

As shown in Figure 7-8, the values of α near failure for B09 begin to fluctuate somewhat. During isotropic consolidation, a leak was noticed between the inner cell and the specimen. Although the volume change data was corrected after testing, the volume change was not corrected during testing. The uncorrected volume change resulted in the stress path control system calculating changes in specimen radius that were not real.

The specimen area is calculated in real time based on the specimen radius. This value is then used to calculate applied forces and pressures. Therefore, a slight deviation from the planned stress condition resulted from the leak, ultimately producing a deviation in α of slightly less than 2.5°.

7.2 Stress-Strain and Volume Change Behavior

Plots of the stress-strain and volume change behavior for all B-Series tests are presented in Figure 7-9 through Figure 7-30. Tabular data associated with each test is contained in Appendix I, and post-failure specimen photographs are contained in Appendix L.

Tests with common principal stress inclinations are grouped together. The actual b-value at failure is contained in a text box located near the end of each curve. Data points are represented by unfilled data markers, with the failure point for each test emphasized by a single solid filled marker.

The maximum stress ratios shown by each solid filled marker provide an indication of the relative strength of each specimen. However, the plotted data has not been corrected for void ratio. A summary of corrected peak friction angles is presented in Table 7-1. The mean normal stress for each test was well controlled. Therefore, it was not necessary to correct for the effects of confining stress.

Both the stress ratio and the volumetric strain are plotted with respect to the major principal strain. The major principal strain is defined as the strain that is roughly coincident with the principal stress direction.

This strain usually, but not always, has the largest magnitude. For compression tests with high b-values, the intermediate principal strain often has a greater magnitude than the major principal strain, due to the effects of anisotropy.

7.2.1 Tests at α = 0°

B01 was the only B-Series test performed with the major principal stress direction perpendicular to the bedding plane. The b-value for the test was 0.75. This combination of high b-value and low α resulted in the highest initial modulus for all B-Series tests. Only Test B04 (α=22.5°, b=0.99) had a shorter strain (ε_1) to failure than the 0.44 percent observed for this test, and that is slightly misleading since the largest strain during Test B04 was in the intermediate (ε_2) direction. The magnitude of the intermediate strain (ε_2) at failure for Test B01 was 0.26%, a little more than ½ of ε_1.

The volume change behavior is shown in Figure 7-10. In general, all tests performed during this study have relatively small compression phases due to: low confining pressure, high relative density, and fine grain size.

As expected, the curve B01 shows a small amount of compression (ε_v = 0.027%) occurring at 0.046 % strain, at which point dilation begins. A comparison of B01 with other tests indicates that the strain to this transition point tends to decrease for high b-values and low values of α.

The maximum stress ratio achieved for Test B01 was 10.53 corresponding to a friction angle of 55.75°. This failure point coincided with shear band development. This specimen failed in a brittle manner, and the post failure response has not been presented as it was not accurately captured.

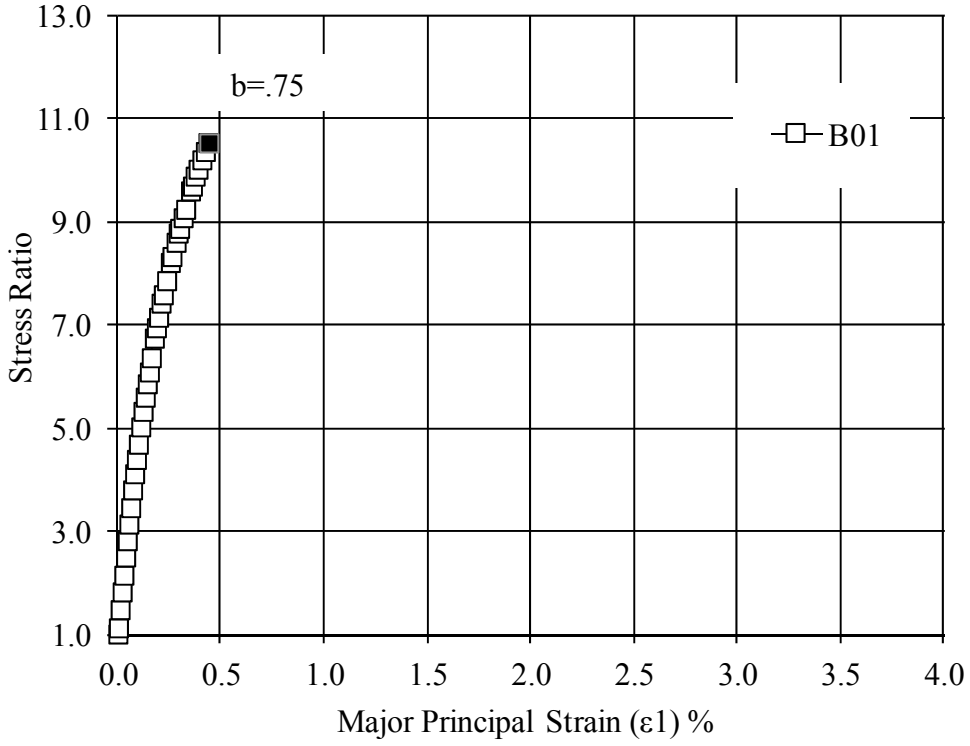

Figure 7-9: Stress – Strain Relationship for α = 0°

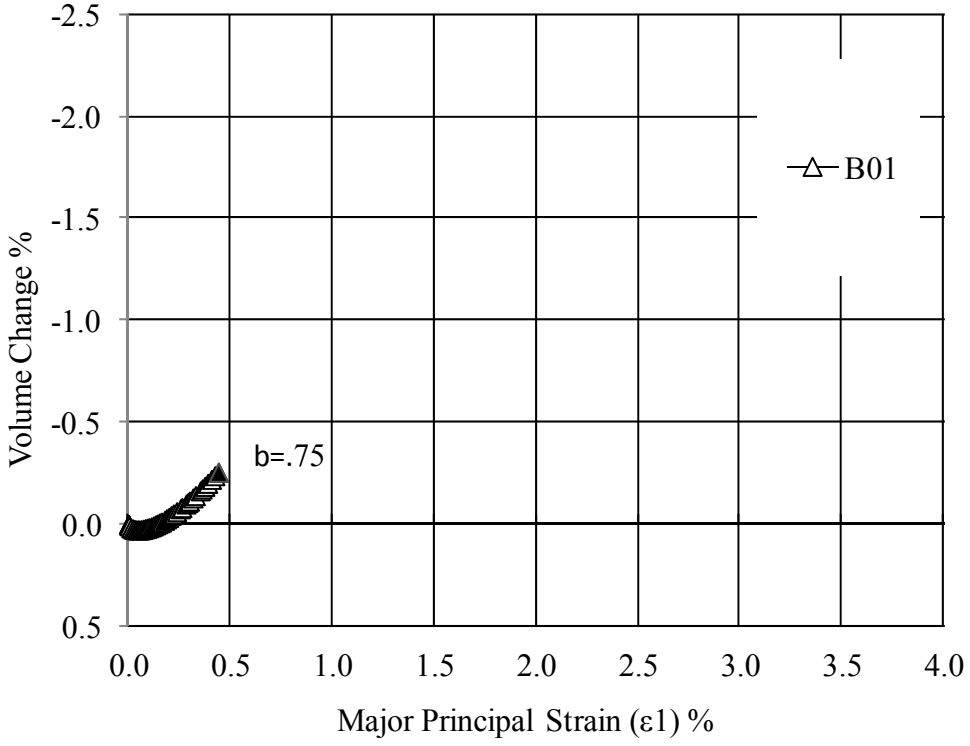

Figure 7-10: Volume Change Relationship for α = 0°

7.2.2 Tests at α = 22.5°

Three tests, designated B02 through B04, were performed with principal stress inclinations of 22.5°. The intermediate principal stress ratios at failure were -.01 for B02, 0.50 for B03, and 0.99 for B04. Curves for each test depicting the stress ratio with respect to the major principal strain are shown in Figure 7-11.

The stress-strain response becomes stiffer with increasing b-value. However, this trend is much more pronounced between b-values of -0.01 and 0.50 than it is between 0.50 and 0.99. With increasing b-value, the rate of volumetric change with respect to major principal strain increases while the total magnitude of volumetric strain at failure decreases, as shown in Figure 7-12. All specimens start with a small amount of compression followed by a dilation phase.

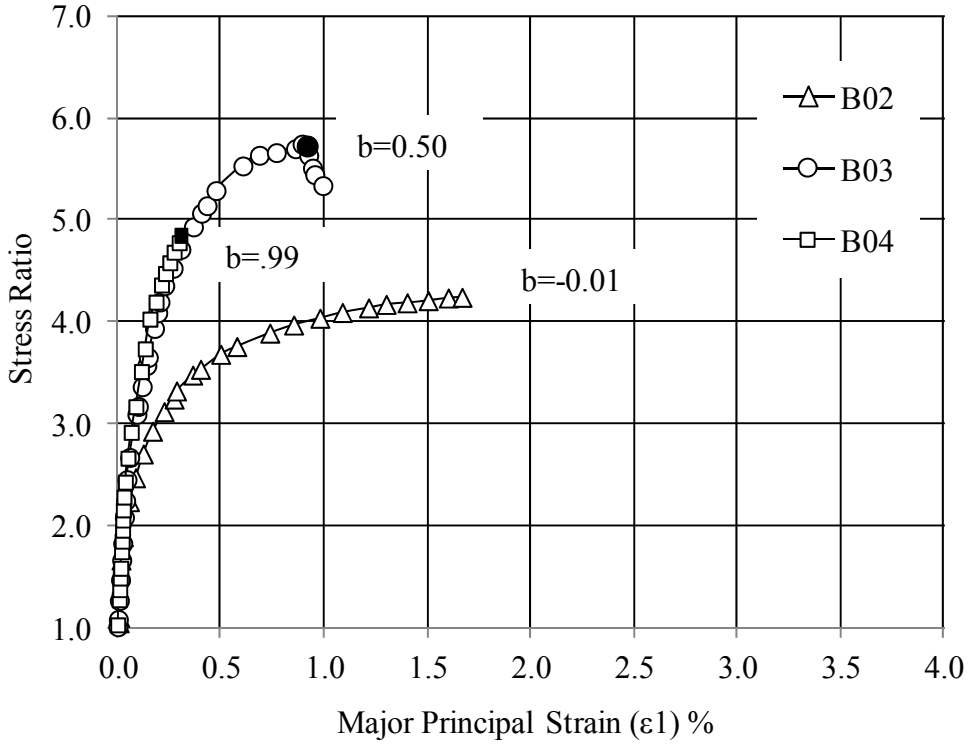

Figure 7-11: Stress – Strain Relationship for α = 22.5°

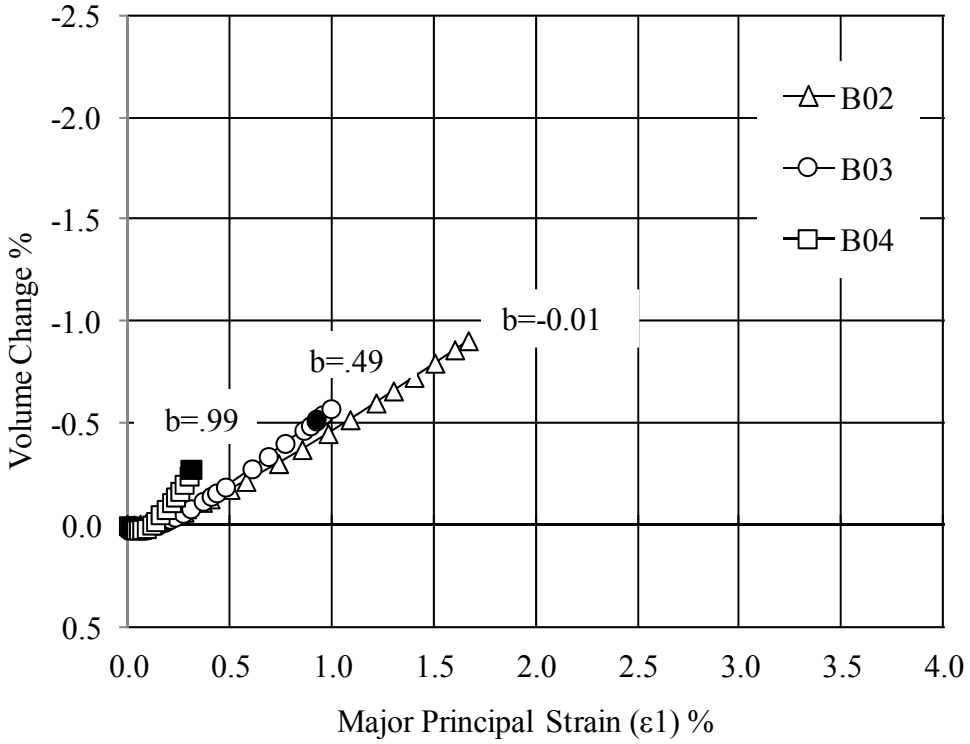

Figure 7-12: Volume Change Relationship for α = 22.5°

Test B02 had a peak stress ratio of 4.24 at a major principal strain of 1.67%. A post test photograph of the specimen with a grid overlay stenciled on the membrane is presented in Appendix L, Figure L-2. The spacing between grid lines is 25 mm in each direction.

The failure point was selected as the point directly before the development of the shear band and the sharp stress reduction that accompanied that event. A slight increase in stress ratio occurred after shear band development, but was not considered reliable.

Test B02 had a slight leak between the inner cell and outer cell. This breach was so slight that both the inner and outer pressures were easily maintained during testing. However the inner volume change values have been corrected to account for this leak. The correction had a negligible effect on the friction angle.

After test completion, the test membrane was successfully removed without damaging the specimen. Photographs of the front and rear of the specimen without the membrane are shown in Figure 7-14. The single well defined shear band indicates a simultaneous failure in the σ_z-σ_θ and σ_z-σ_r planes. A schematic of this condition is shown in Figure 7-13.

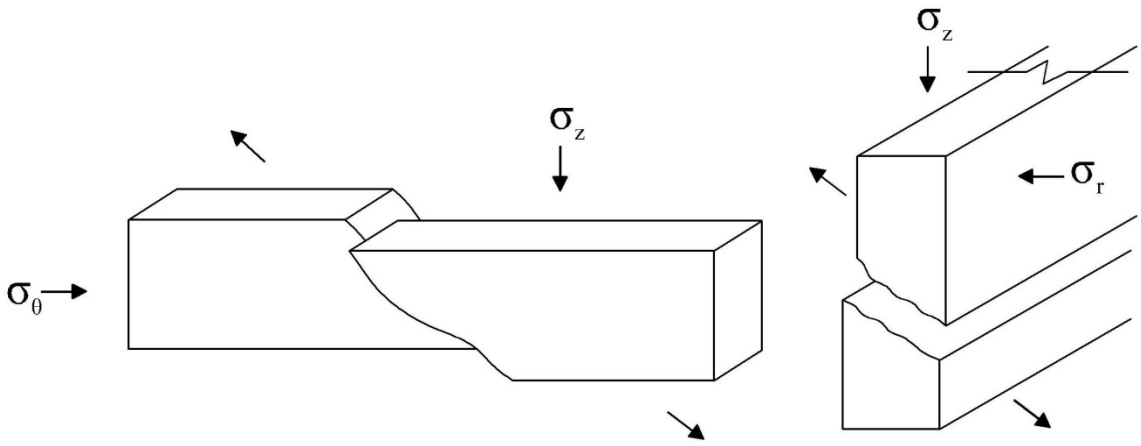

Figure 7-13: Specimen B02 Failure Schematic

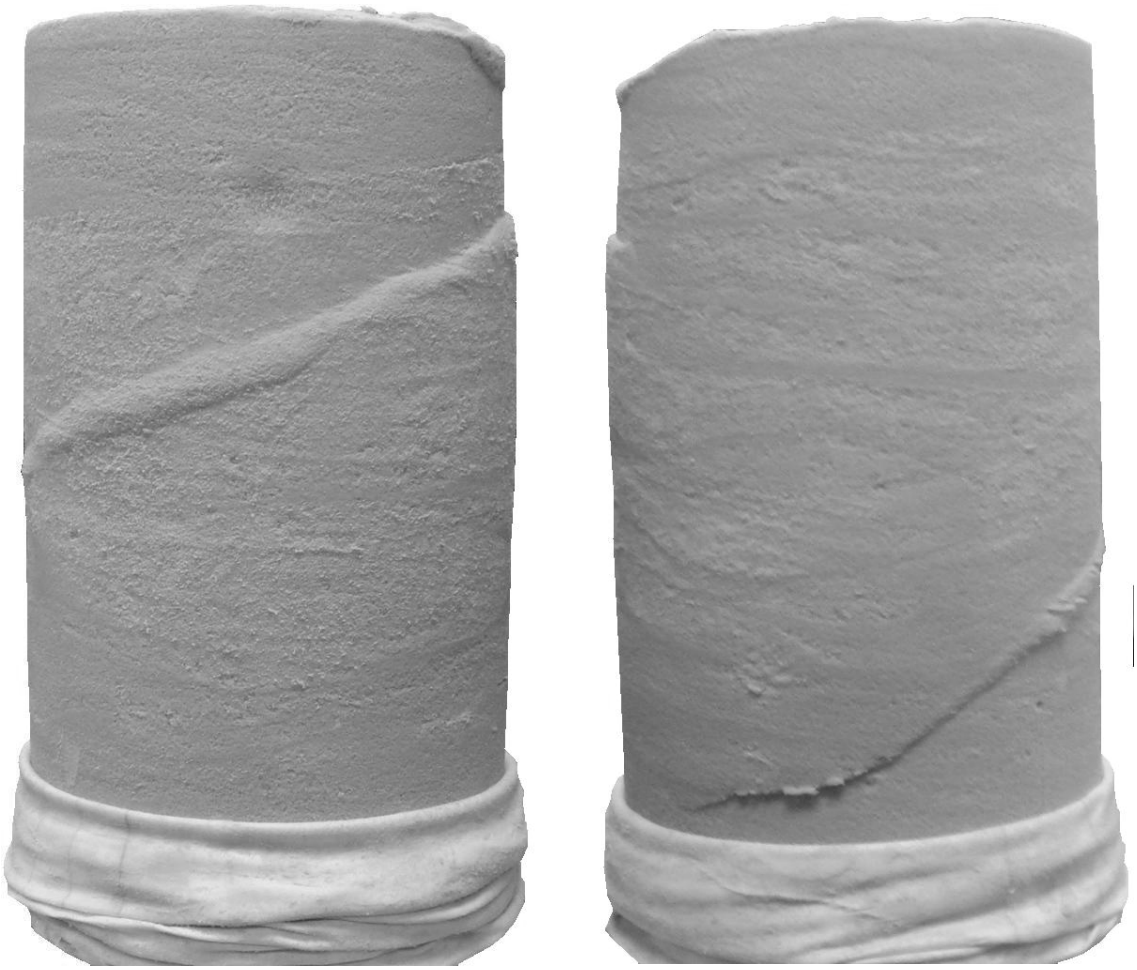

Figure 7-14: Front and Rear Photograph of Specimen B02

Test B03 achieved a peak stress ratio of 5.75 at a major principal strain of 0.89%. The post peak behavior showed a sharp reduction in stress ratio. The specimen contracted to a maximum $\varepsilon_v = 0.0086\%$ at $\varepsilon_1 = 0.0425\%$, prior to moving into a dilation phase. A post failure photograph of this specimen is shown in Figure L-3.

Test B04 achieved a peak stress ratio of 4.84 at a major principal strain of 0.31%. The specimen contracted to a maximum $\varepsilon_v = 0.0211\%$ at $\varepsilon_1 = 0.0531\%$, prior to moving into a dilation phase. Observations of the stress strain curve shown in Figure 7-11 indicate that this specimen failed in a brittle manner prior to the onset of large plastic strains that accompanied failure in Tests B02 and B03.

At a b-value of 0.99 the major-minor stress ratio and the intermediate-minor stress ratios are essentially equal. Each of these stress ratios were plotted with respect to their corresponding principal strain in Figure 7-15. Due to the effects of anisotropy the largest strains were observed in the intermediate direction. Although the ε_2 shows some increase in plastic strain prior to failure, the failure is still somewhat brittle in nature.

The shear band associated with failure of specimen B04 is pictured in Figure L-4 and Figure 7-55. As discussed in Section 7.5.3.2, this specimen failed in the (r-θ) plane as evidence by the canyon type shear band that was observed. This type of failure, propagates in the direction of flexible boundaries, and may be inherently unstable. For this reason, the failure is premature, brittle, and no post-peak residual behavior is possible.

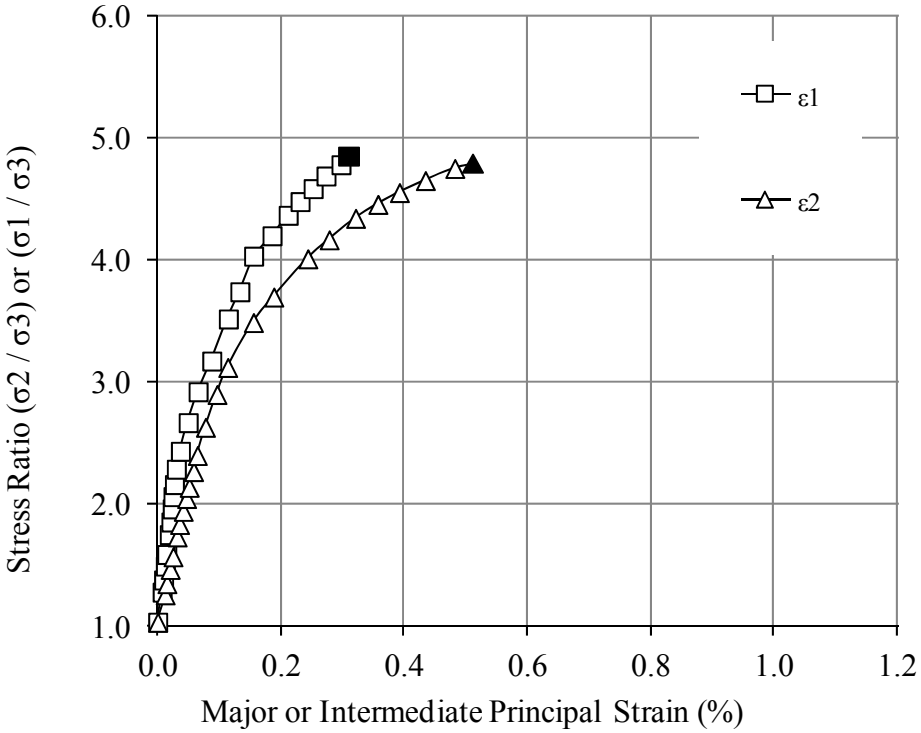

Figure 7-15: Test B04 Stress – Strain Plot

7.2.3 Tests at α = 45°

Two tests, designated B05 and B06, were performed with principal stress inclinations of 45°. The intermediate principal stress ratios at failure were 0.23 for B05 and 0.74 for B06. Curves depicting the stress ratio with respect to the major principal strain for each test are shown in Figure 7-16. The volumetric strain curves are plotted in Figure 7-17.

Test B05 achieved a peak stress ratio of 4.34 at a major principal strain of 1.63%. The post peak behavior showed a slight reduction in stress ratio. The specimen contracted to a maximum ε_v = 0.019% at ε_1 = 0.25%, prior to moving into a dilation phase. A post failure photograph of this specimen is shown in Figure L-5.

Test B06 achieved a peak stress ratio of 4.10 at a major principal strain of 1.63%. The post peak behavior showed a sharp reduction in stress ratio. The specimen contracted to a maximum ε_v = 0.049% at ε_1 = 0.28%, prior to moving into a dilation phase. A post failure photograph of this specimen is shown in Figure L-7.

Similar to the trend observed at α = 22.5°, the stress-strain responses become stiffer with increasing b-value. The stiffer response is also characterized by a higher peak stress ratio and a more brittle post-peak stress reduction.

The b-value's influence on volumetric strain at α=45° is similar to that observed at α=22.5°. Increasing b-values result in greater initial compression and volumetric dilation rate, although the cumulative volumetric strain at failure tends to decrease.

A full range of post-peak behavior could not be captured for either test due to limitations of the volume change device. However, the data that was captured shows a sharp decrease in the post-peak volumetric strain rate at failure. The curves for B05 and B06, shown in Figure 7-17, both appear to be trending to a critical state of zero volumetric strain.

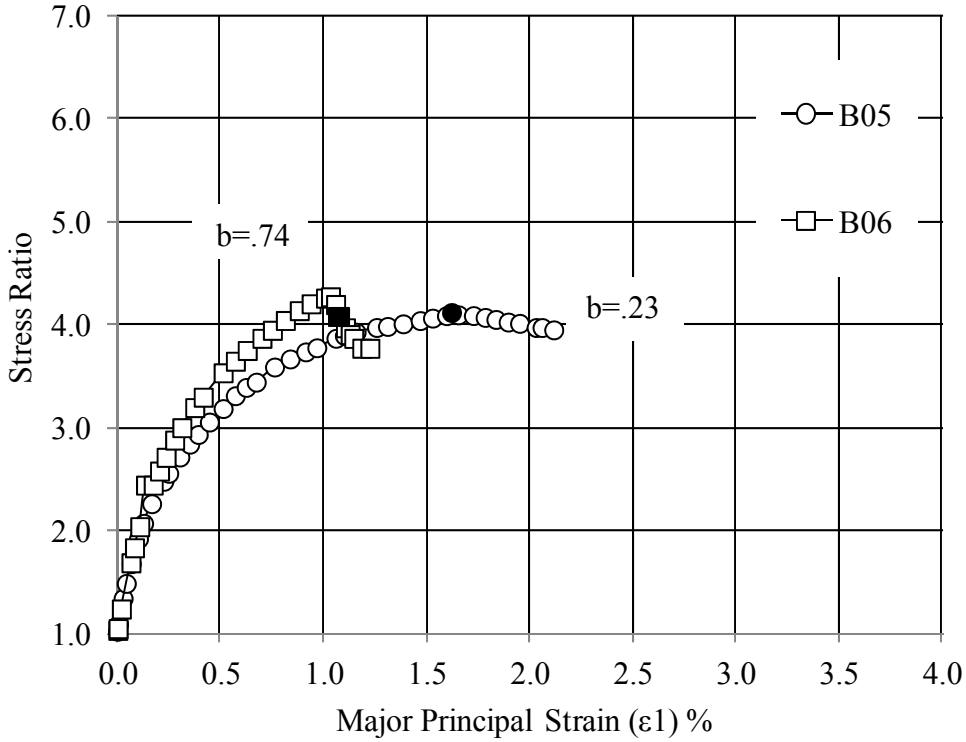

Figure 7-16: Stress – Strain Relationship for α = 45°

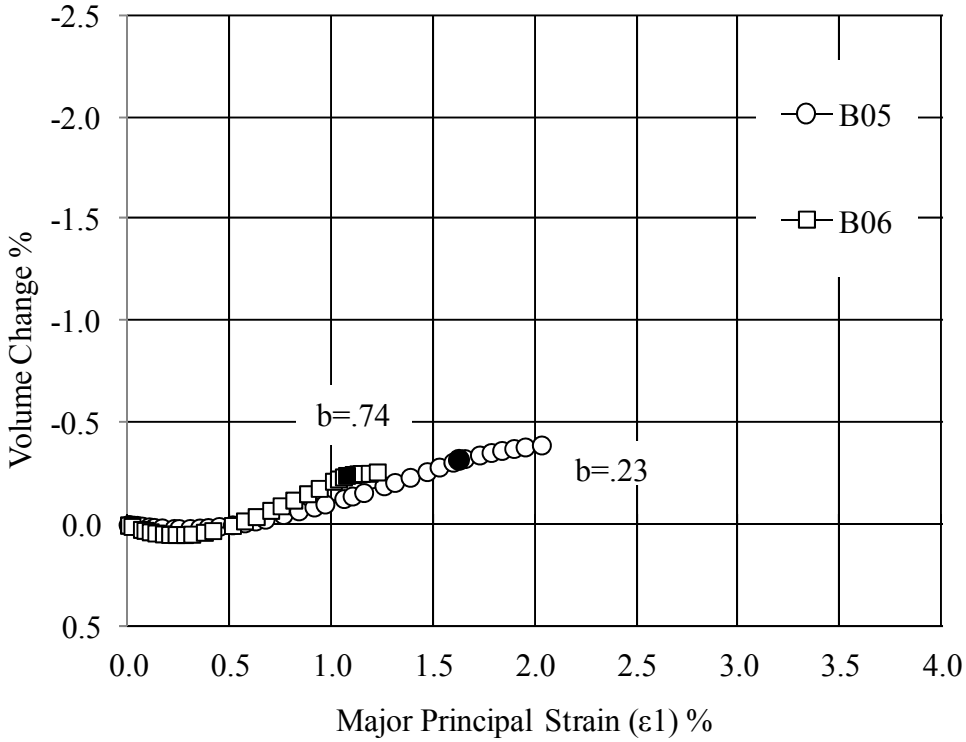

Figure 7-17: Volume Change Relationship for α = 45°

The failure of specimens B05 and B06 produced many thin shear bands, but no single large “canyon” type shear band was observed. The absence of canyon type shear bands indicates that the shear failure occurred in the (z-θ) plane.

Typical shear bands for Specimens B05 and B06 are shown in the magnified photographs of Figure 7-18 and Figure 7-19. The shear band in Figure 7-19 runs from the bottom left to top right. There is a fold in the membrane that looks similar to a shear band running from the top left to bottom right. This fold is thought to have little effect on the response of the specimen.

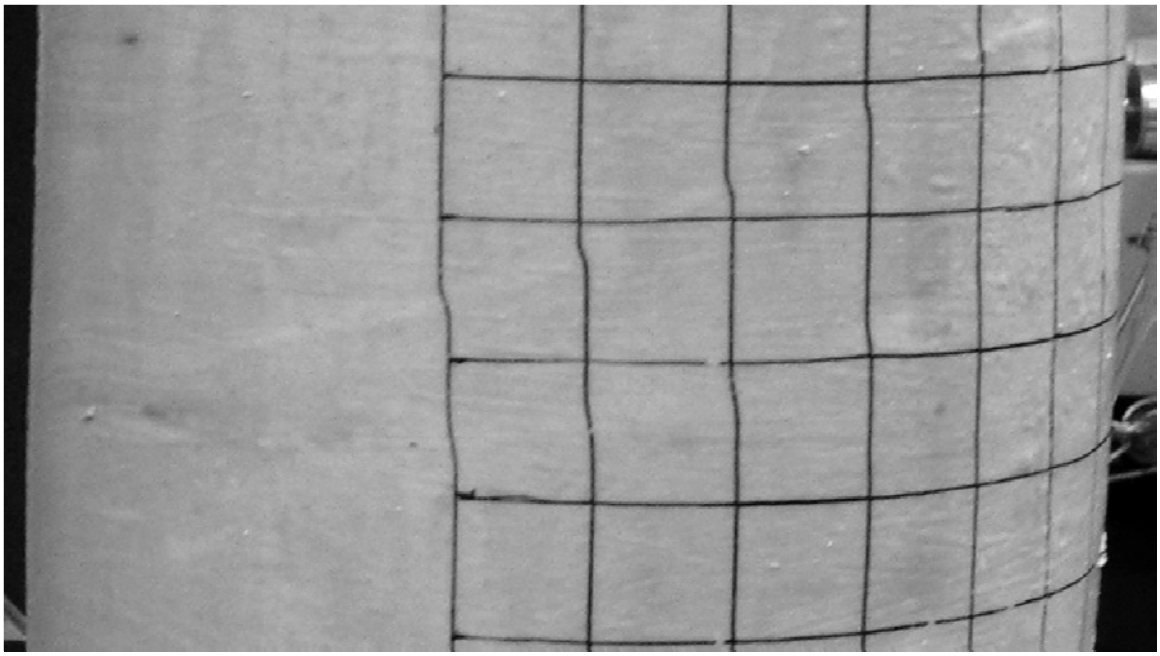

Figure 7-18: Test B05 Typical Shear Band

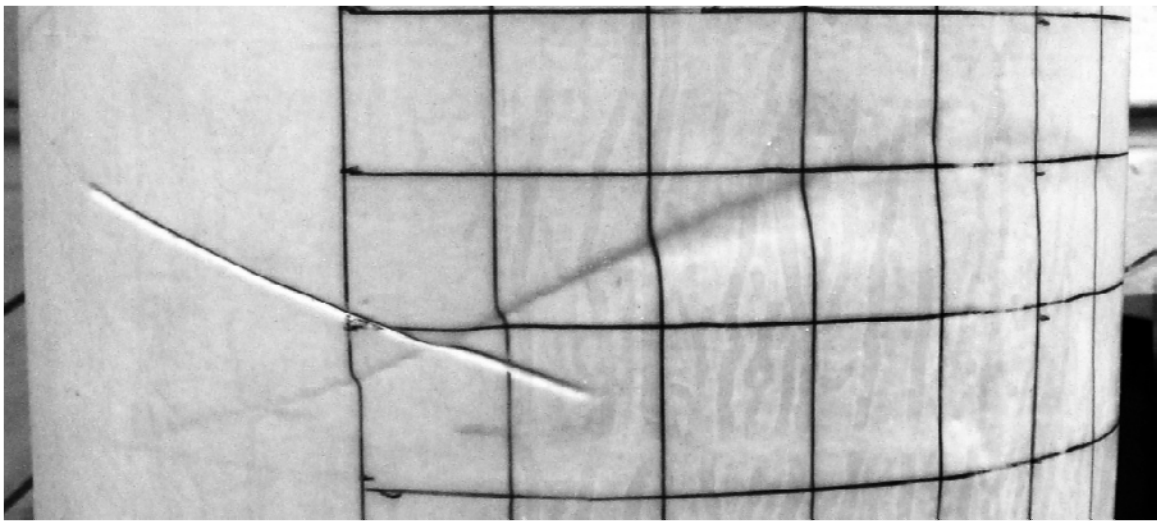

Figure 7-19: Test B06 Typical Shear Band

7.2.4 Tests at α = 67.5°

Three tests, designated B07, B08, and B09 were performed with principal stress inclinations of 67.5°. The b-values at failure were 0.00 for B07, 0.50 for B08, and 1.01 for B09. Curves depicting the stress ratio with respect to the major principal strain for each test are shown in Figure 7-20. The volumetric strain curves are plotted in Figure 7-21.

As observed previously, the stress-strain responses become stiffer with increasing b-value. The trend is still more pronounced between b-values of 0.00 and 0.50 than it is between 0.50 and 1.00. However, the difference is not as great as that observed with α = 22.5° shown in Figure 7-11.

The post peak behavior exhibits larger and sharper stress reductions for tests with high b-values. Note that post peak behavior was not captured for Test B08.

Volumetric strains exhibit similar trends to those observed for tests with lower principal stress inclinations. With increasing b-value, the volumetric strain rate increases, while the total magnitude of volumetric strain at failure decreases, as shown in Figure 7-21. All specimens start with a small amount of compression followed by a dilation phase.

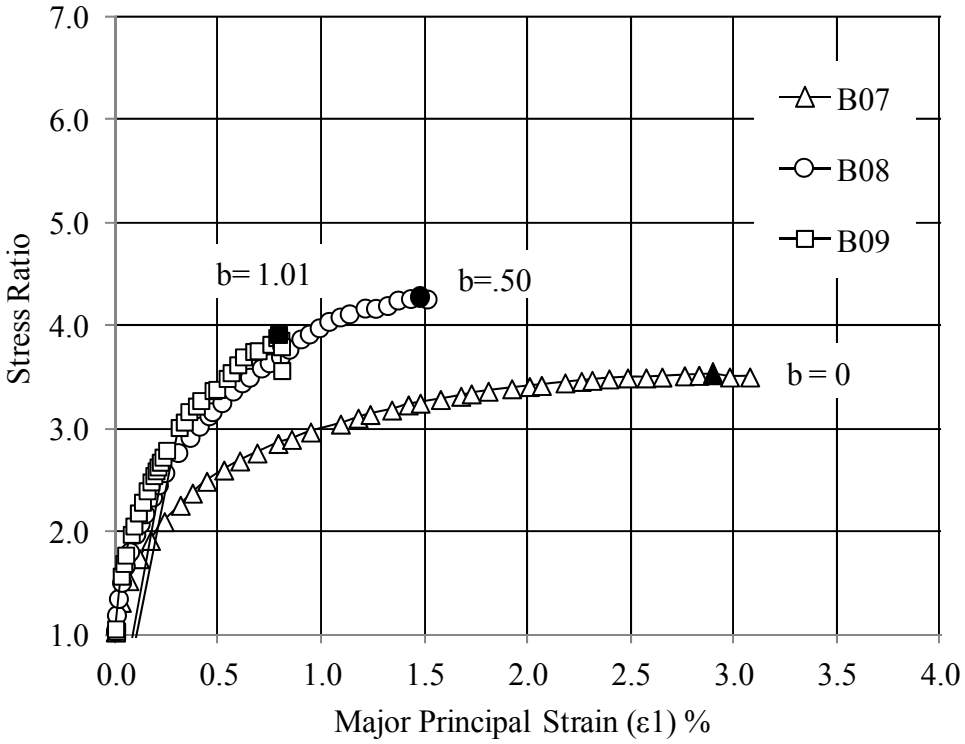

Figure 7-20: Stress – Strain Relationship for α = 67.5°

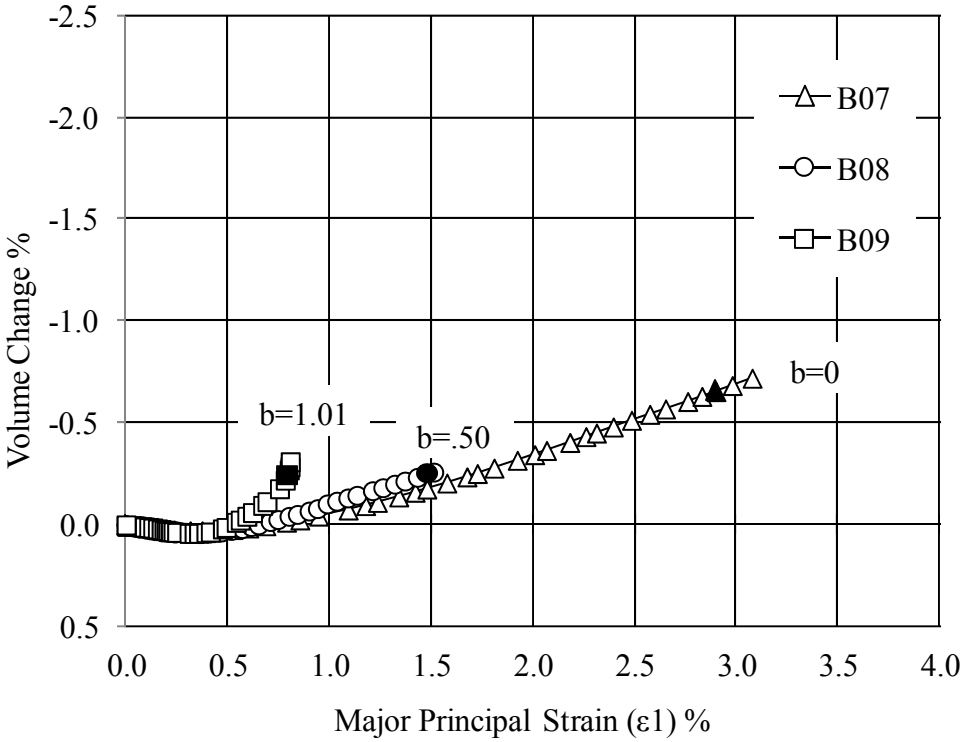

Figure 7-21: Volume Change Relationship for α = 67.5°

Test B07 achieved a peak stress ratio of 3.53 at a major principal strain of 2.90%. The post peak behavior showed no appreciable reduction in stress ratio. The specimen contracted to a maximum ε_v = 0.029% at ε_1 = 0.35%, prior to moving into a dilation phase.

As shown in Figure L-7, the outer layer of latex bubbled during testing. This bubbling occurred because the latex was mixed with too much water prior to application. The resultant bubbling occurred between the permanent membrane and the latex layer that was applied as a base for drawing gridlines. Its only effect on testing is that it makes shear band observation more difficult.

Specimen B07 developed a single horizontal shear band located directly beneath the top ring, as shown in Figure 7-22. This photograph was taken on the back side of the

specimen. The grid lines in this picture are remnants of previous testing, and therefore are not aligned with the bottom of the top ring.

At first glance, this shear band might be mistaken for top cap slippage. However, this shear band has significant thickness, encompassing many sand grains. It also weaves up and down as it transverses the specimen. Top cap slippage is evidenced by a thin perfectly horizontal line directly beneath the top cap.

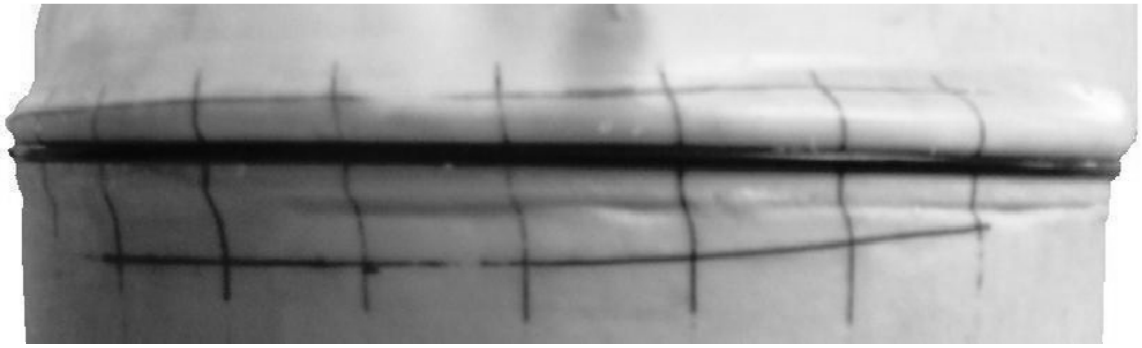

Figure 7-22: B07 Shear Band

Test B08 achieved a peak stress ratio of 4.28 at a major principal strain of 1.48%. Due to limitations of the volume change device, no post peak behavior was captured for this specimen. The specimen contracted to a maximum $\varepsilon_v = 0.043\%$ at $\varepsilon_1 = 0.35\%$, prior to moving into a dilation phase.

A photograph of the post failure specimen is contained in Figure L-8. A final watery layer of latex was applied to the sides of this specimen. This layer successfully mitigated a small leak in the permanent membrane, however, it bubbled in a similar manner to the latex applied to specimen B07. This bubbling has no adverse affect on the test other than making it more difficult to observe shear band development.

Horizontal shear bands developed beneath the top ring and above the bottom ring during failure of specimen B08. As shown in Figure 7-23, the shear band that developed above the bottom ring weaves up and down and is often several millimeters above the bottom ring.

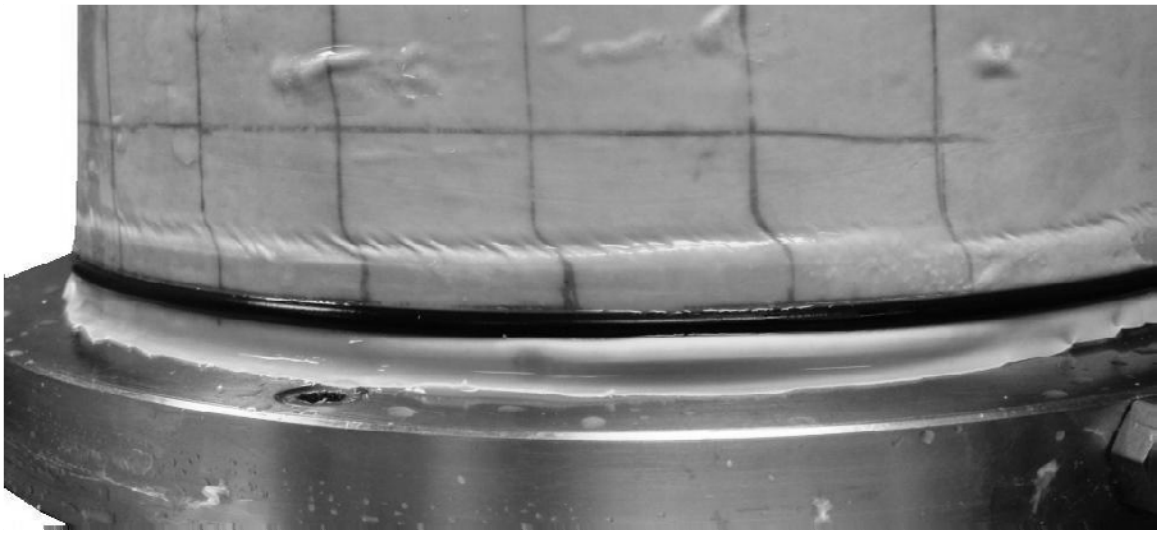

Figure 7-23: Shear Band at Bottom Ring

Test B09 achieved a peak stress ratio of 3.92 at a major principal strain of 0.79%. The post peak behavior showed a sharp reduction in stress ratio. The specimen contracted to a maximum ε_v = 0.042% at ε_1 = 0.33%, prior to moving into a dilation phase.

A photograph of the post failure specimen is contained in Figure L-9. Similar to the other specimens, this specimen developed horizontal shear bands during failure. However, unlike the other specimens, these shear bands were of the "canyon" variety. The combination of horizontal shear band angle and width indicates a simultaneous failure in both the (θ-z) and (r-z) planes. An illustration of this type of failure is shown in Figure 7-24, and a typical shear band from Specimen B09 is shown in Figure 7-25.

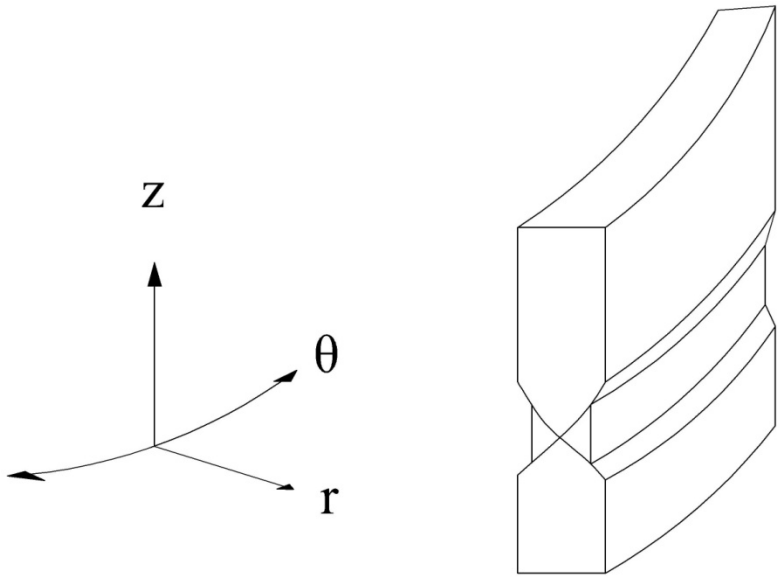

Figure 7-24: Simultaneous Failure in (σ_θ-σ_z) and (σ_r-σ_z) Planes

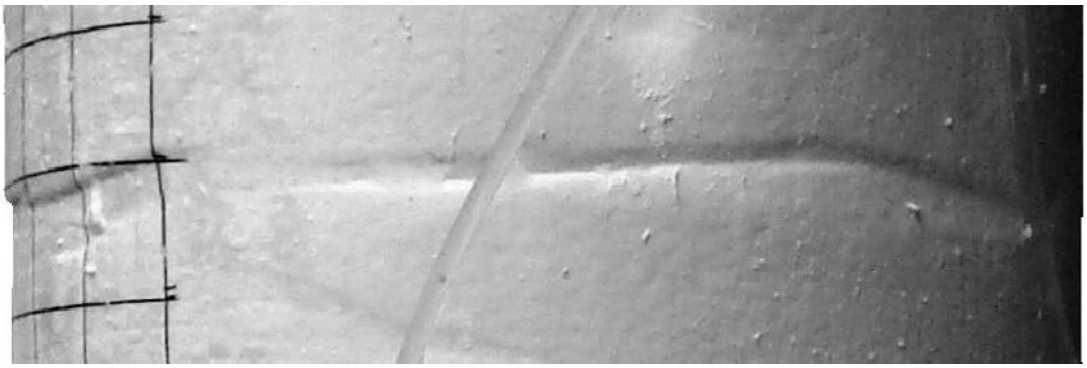

Figure 7-25: Typical B09 Shear Band

In addition to these thick primary shear bands, a second set of thinner shear bands was observed. Although most of the thinner shear bands are horizontal, a few have developed at an angle of 12° degrees. Since they are difficult to see in photographs, the shear bands have been highlighted and are shown in Figure 7-26 and Figure 7-27.

The shear band labeled No. 3 shows the intersection of a horizontal and angled shear band. Only shear bands No. 3 and No. 4 had inclinations that were not essentially horizontal.

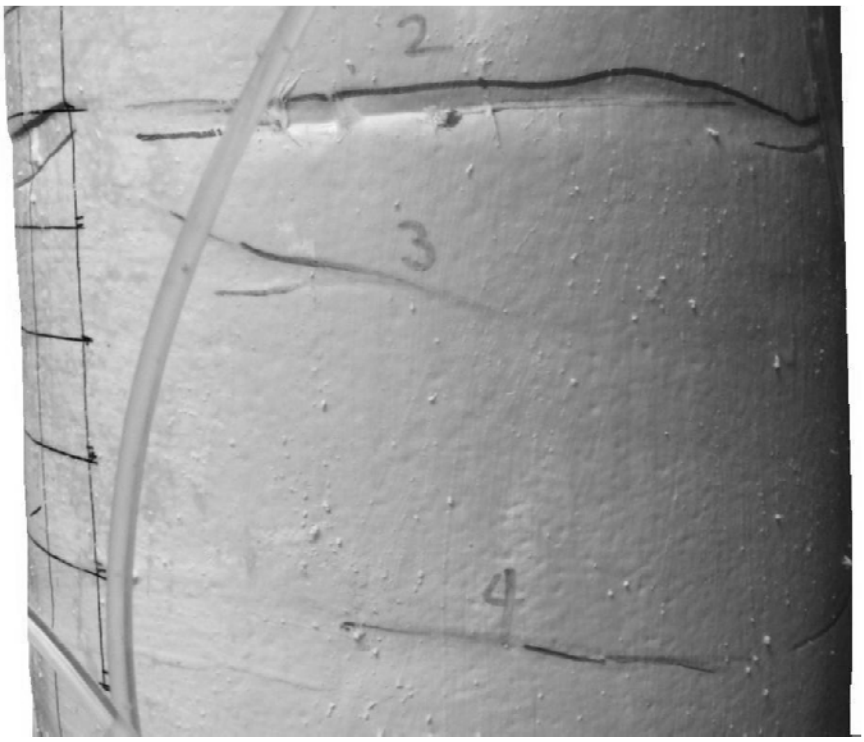

Figure 7-26: Specimen B09 Right Side Middle

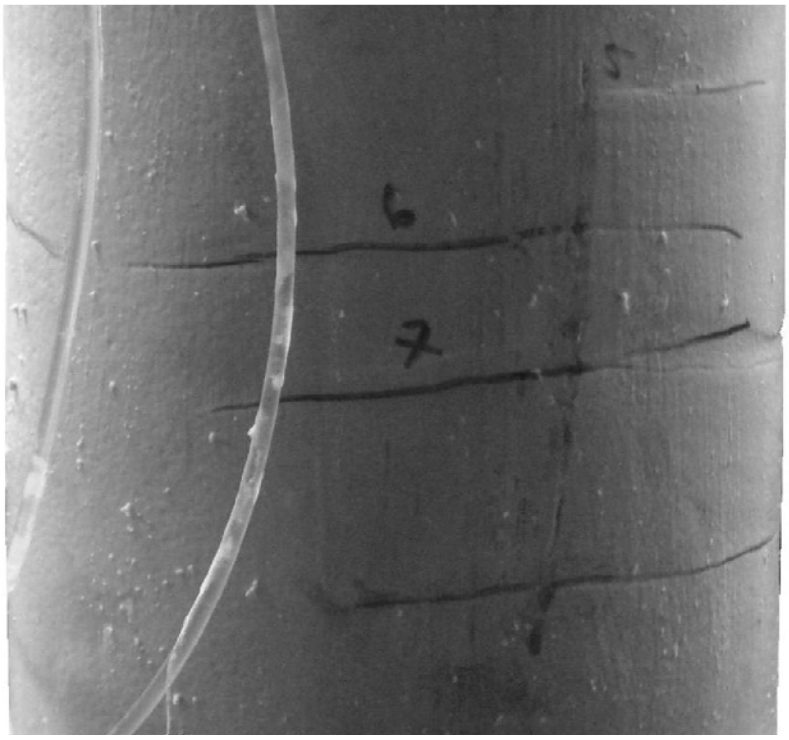

Figure 7-27: Specimen B09 Rear Middle

7.2.5 Tests at α = 90°

B10 was the only B-Series test performed with the major principal stress direction parallel to the bedding plane. The b-value for the test was 0.05, which is slightly greater than the target of 0.00. As previously discussed in Section 7.1.1, the vertical load cell calibration was slightly offset resulting in an additional 82.78 N of upward force. The calibration and resulting data were corrected after testing. However, the offset calibration resulted in a slight deviation from the intended stress path.

The stress-strain plot for Test B10 is shown in Figure 7-29. A maximum stress ratio of 3.47 was achieved after a relatively large principal strain of $\varepsilon_1 = 1.96\%$. The volume change behavior is shown in Figure 7-30. Except for a small amount of initial dilation caused by the unintended uplift, this test followed the same pattern as all other specimens with a small amount of initial compression followed by dilation.

The specimen became unstable at failure rendering the post peak strains meaningless. However, "X" shaped shear bands developed in the (θ-z) plane, indicating that failure occurred as intended.

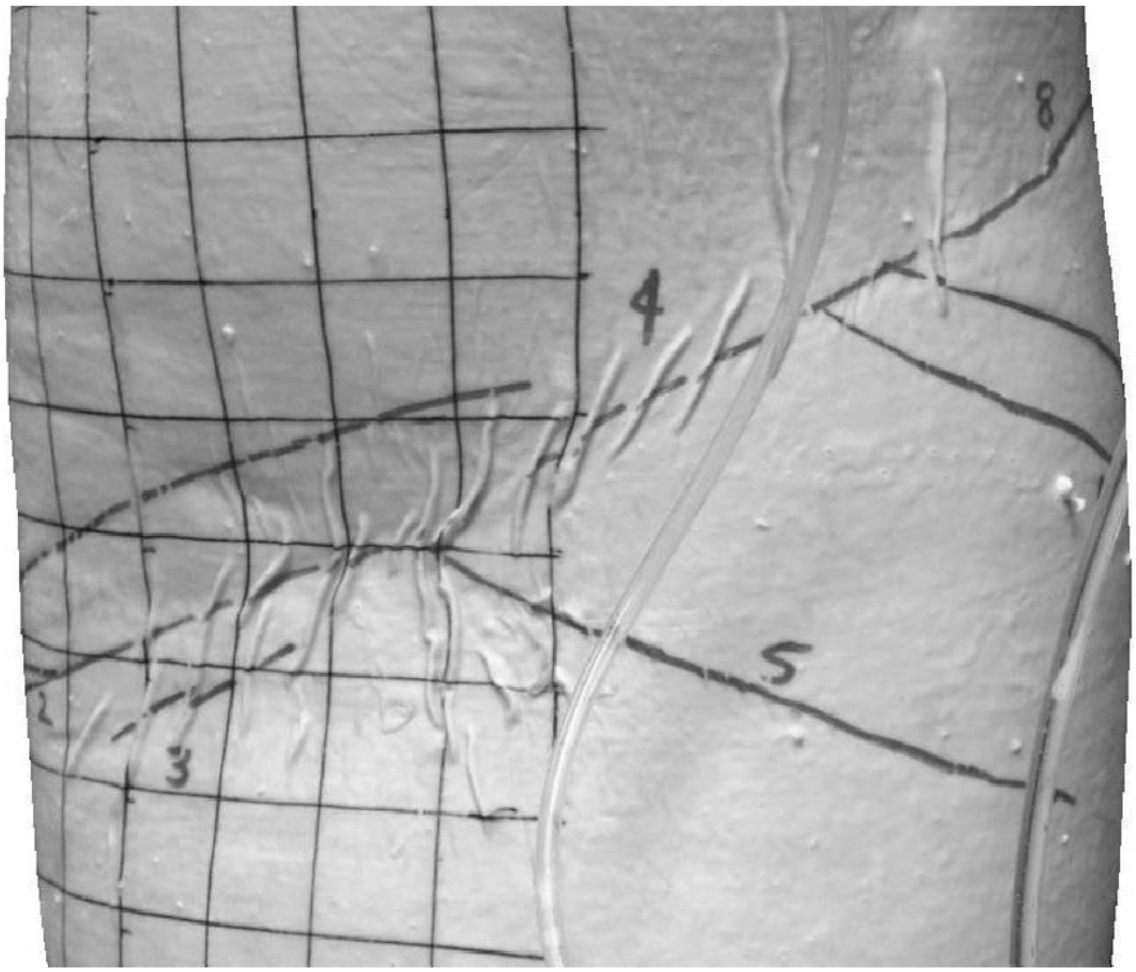

Figure 7-28: Test B10 Shear Bands

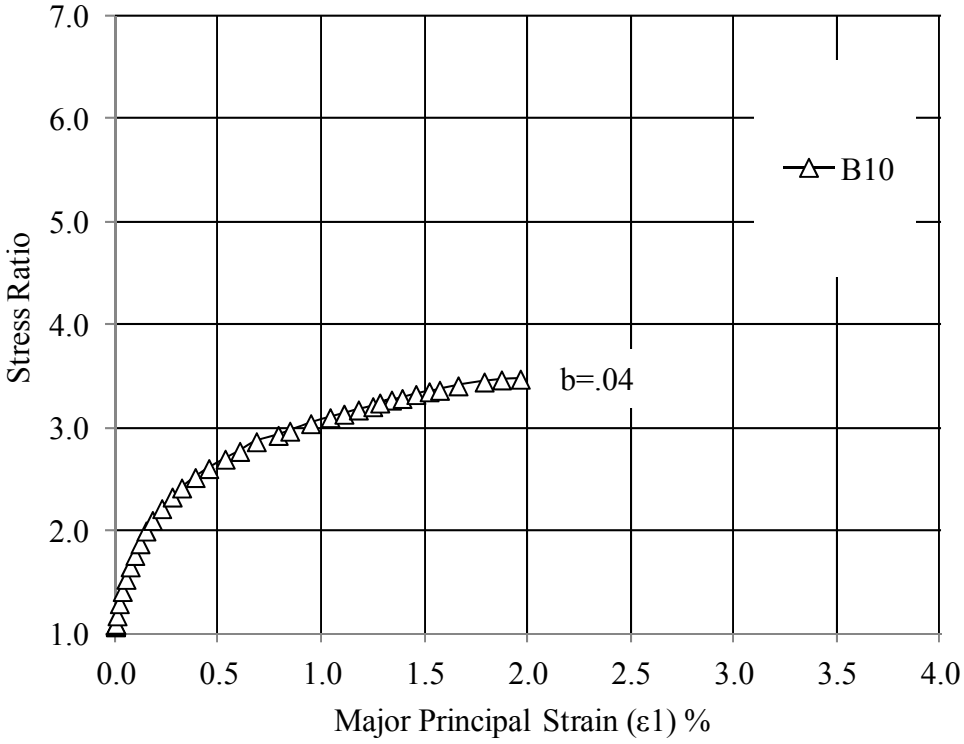

Figure 7-29: Stress – Strain Relationship for α = 90°

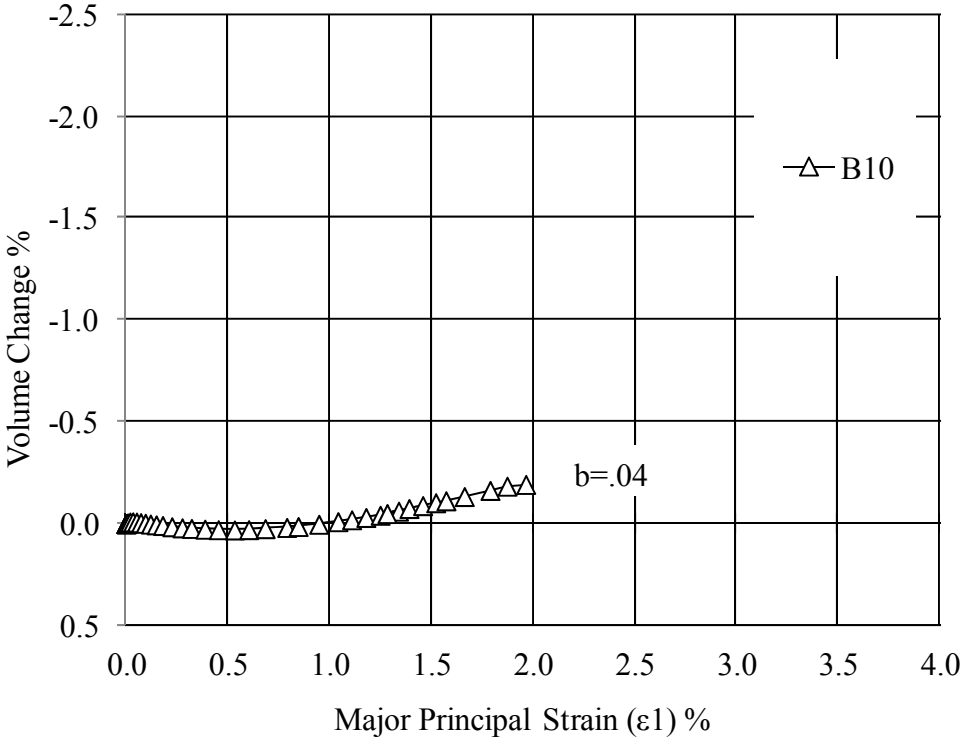

Figure 7-30: Volume Change Relationship for α = 90°

7.2.6 The Effects of Principal Stress Inclination (α)

The effect of α on stress-strain response is best illustrated by comparing specimens sheared at different principal stress inclinations, but with the same intermediate principal stress ratios.

Stress strain plots of tests with similar b-values are shown in Figure 7-31, which compares α = 0° with α = 45° and Figure 7-32, Figure 7-33, and Figure 7-34, which compare α = 0°, 67.5°, and 90° for different b-values. From these plots it is evident that increasing the principal stress inclination while holding all other factors equal results in:

- A softer stress-strain response
- A greater strain to failure
- Lower peak shear strength

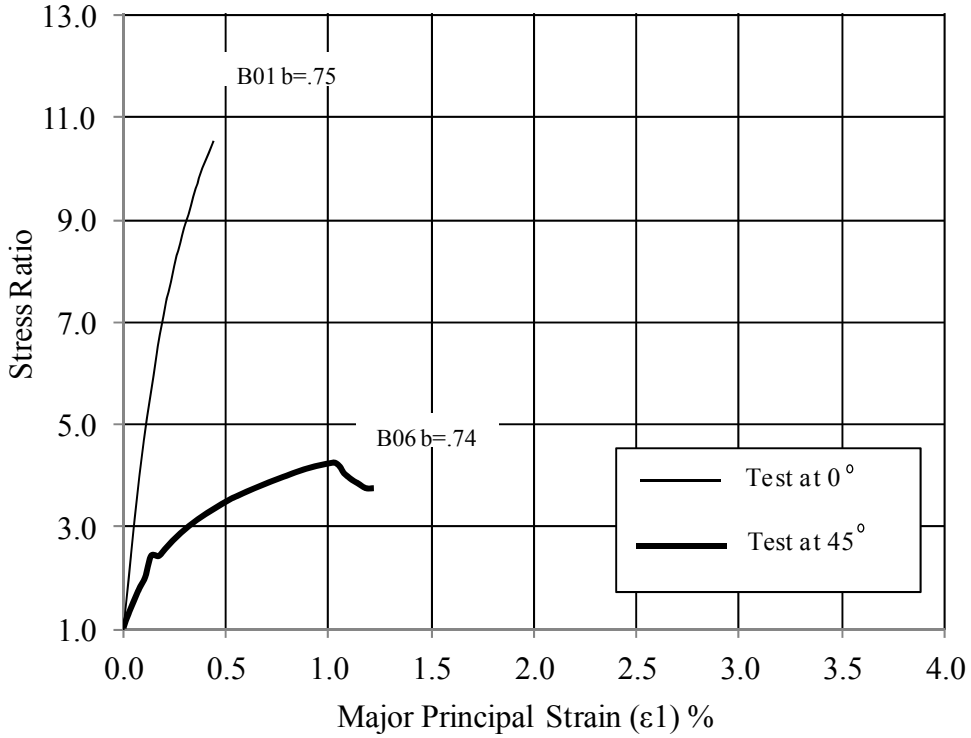

Figure 7-31: Stress-Strain Relationship for α = 0° vs. α = 45°

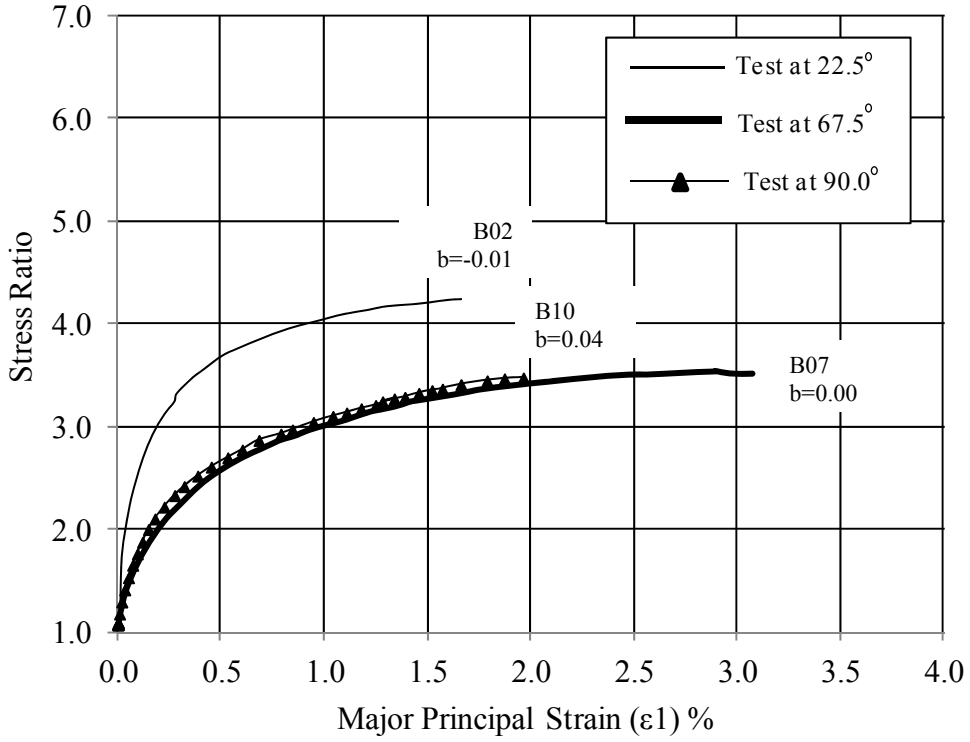

Figure 7-32: Stress-Strain Relationship at b ≈ 0.0

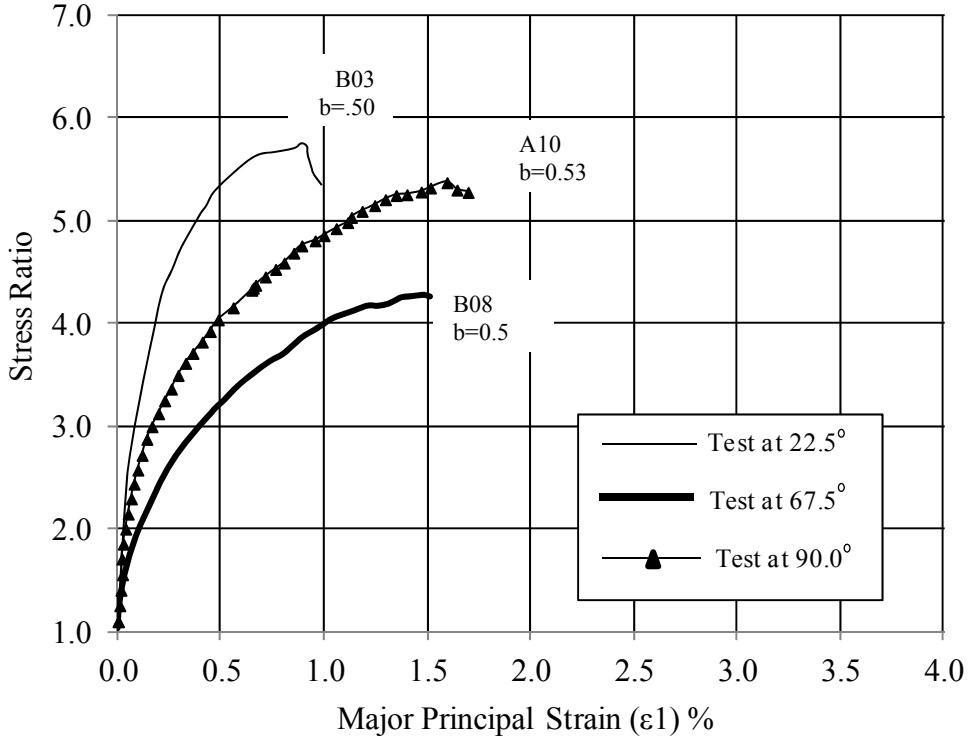

Figure 7-33: Stress-Strain Relationship at b ≈ 0.5

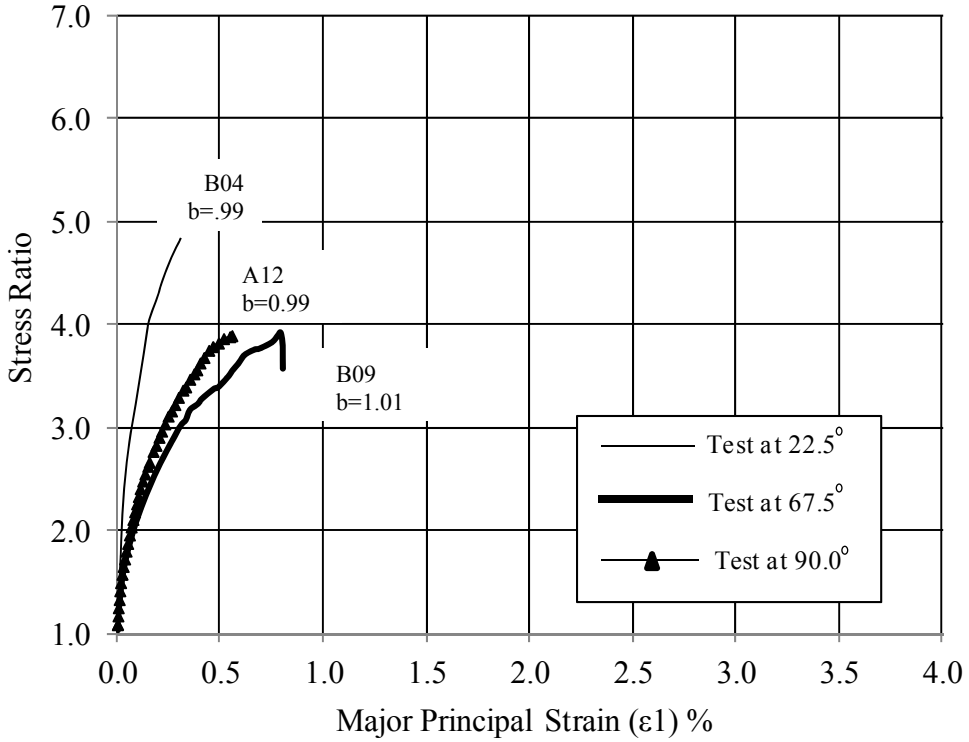

Figure 7-34: Stress-Strain Relationship at b ≈ 1

The volumetric strain effects are shown in Figure 7-35, which compares α = 0° with α = 45° and Figure 7-37, which compares α = 22.5° with α = 67.5°. The compressive portion of each chart has been magnified and is shown in Figure 7-36 and Figure 7-38. Note that the compressive phase for test B02 was so small that it is still barely visible on the magnified figure. It has not been labeled, although it is just visible in the top left corner of the chart.

Increasing the principal stress inclination while holding all other factors equal results in:

- Decreasing volumetric strain rate
- Increasing magnitude of compression
- Decreasing total volumetric strain at failure for mid and low range b-values
- Insignificant effects at high b-values
- Increasing major principal strain prior to the onset of dilation

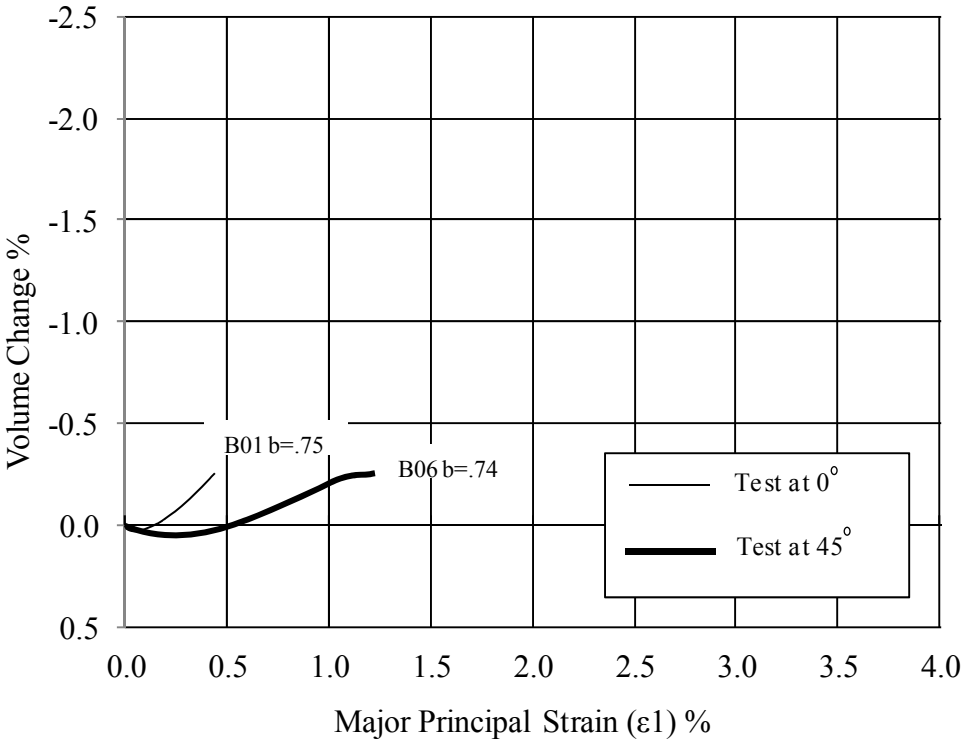

Figure 7-35: Volume Change Relationship for α = 0° vs. α = 45°

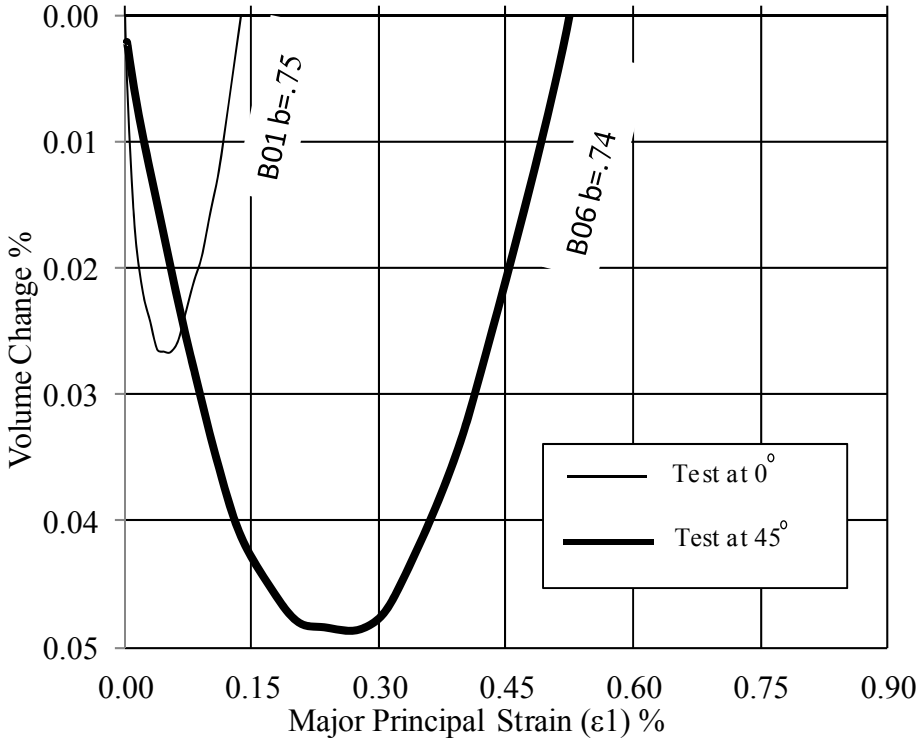

Figure 7-36: Volume Change Relationship for α = 0° vs. α = 45° In Compression Region Only

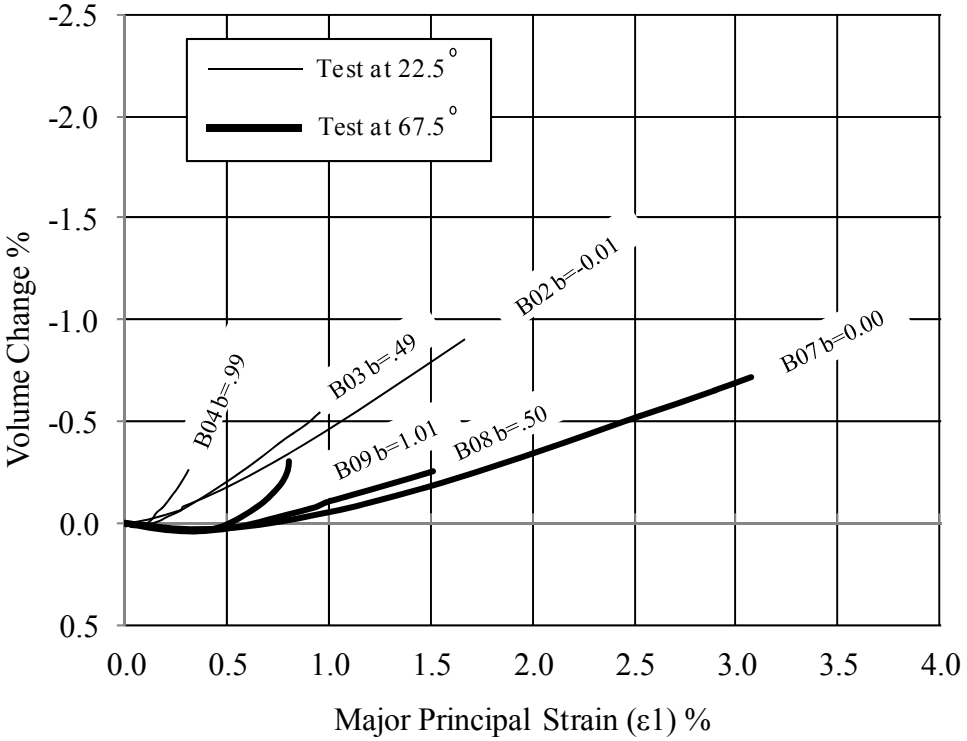

Figure 7-37: Volume Change Relationship for α = 22.5° vs. α = 67.5°

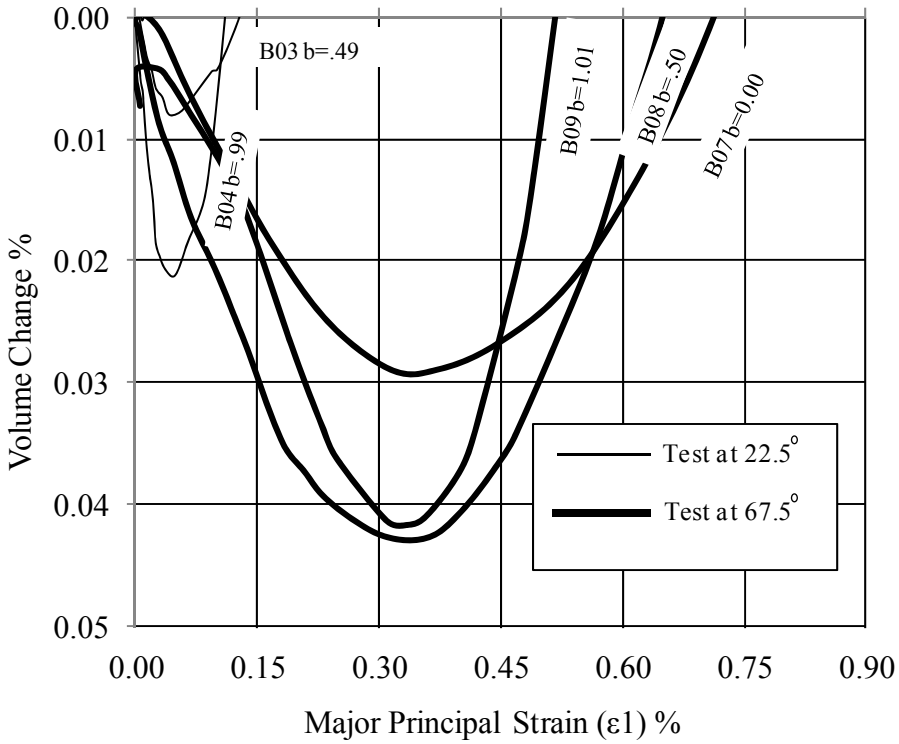

Figure 7-38: Volume Change Relationship for α = 22.5° vs. α = 67.5° In Compression Region Only

7.2.6.1 EFFECT OF α ON THE INFLUENCE OF THE INTERMEDIATE PRINCIPAL STRESS

The stress ratios σ_1/σ_3 and σ_2/σ_3 are prescribed by the b-value. For high b-values these ratios approach each other, and for b = 1 they are equal. However, because the soil fabric is anisotropic, the shearing resistance is a function of α.

For low values of α, shear bands forming in the (z-θ) plane must cross many bedding planes, resulting in a high shear resistance. However, the intermediate principal stress is always applied parallel to the bedding plane, where the shearing resistance in the (r-θ) plane is comparatively lower. The lower shear resistance in the (r-θ) plane creates a condition in which the intermediate principal stress can initiate failure, even for b-values as low as 0.75.

As α increases, the shear band direction begins to align more closely with the bedding plane direction and the shearing resistance in the (z-θ) plane begins to decrease. At α = 45°, shear banding theoretically occurs at 20°. This is much closer to the bedding plane than 65° , the theoretical angle of shear banding for tests at α = 0°.

The relative influence of the intermediate principal stress decreases as the shear resistance in the (z-θ) plane decreases. Near α = 67.5°, the intermediate principal stress may no longer be able to initiate failure, even at a b-value of 1.

This point is illustrated by comparing Tests B01 (α = 0°) and B06 (α = 45°). Both tests had b-values of 0.75, however as shown in Figure 7-39, a large canyon type failure occurred in Test B01 indicating shear band development in the (r-θ) plane. On the other hand, the thin shear bands observed in Test B06, shown in Figure 7-40 indicates a failure mechanism confined to the (z-θ) plane.

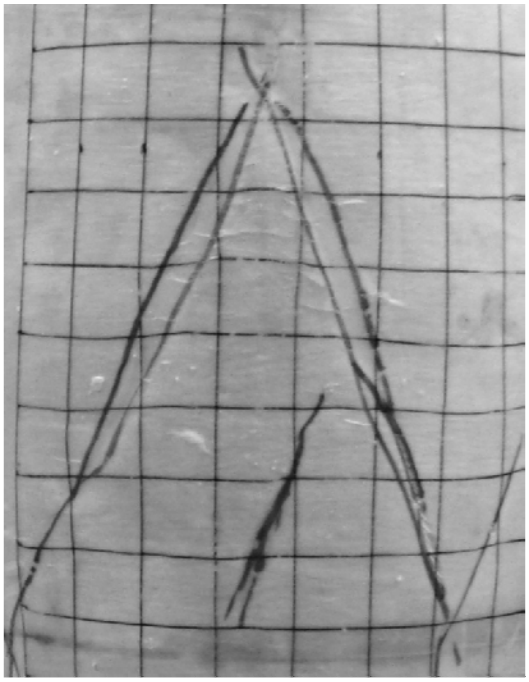

Figure 7-39: Test B01 Canyon Shear Band

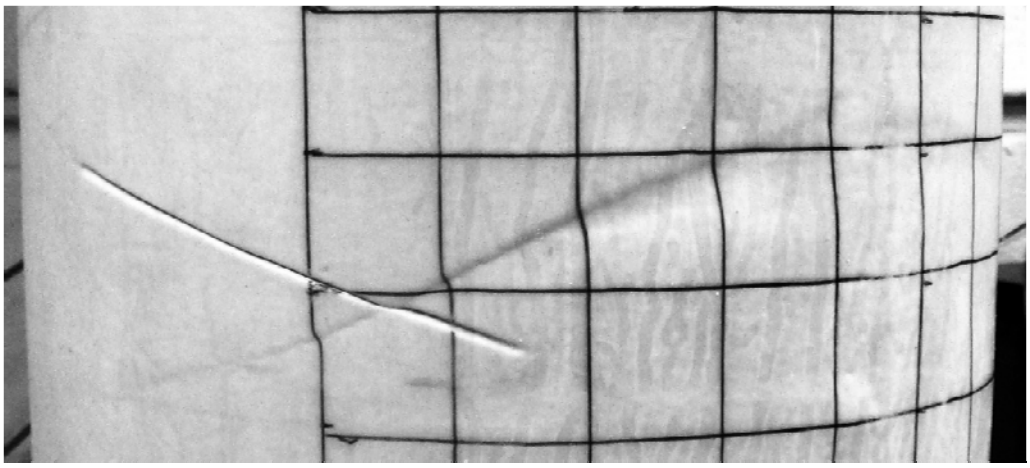

Figure 7-40: Test B06 Shear Band Confined to (z-θ) Plane

7.3 Failure Surface

Table 7-1 presents the B-Series test results using the same format described in Section 6.1.3. The stress parameters (α, b, and σ_m) are reported at failure, and the initial void ratio is reported prior to consolidation. The peak friction values have been corrected for initial void ratio variations by using Equation (6.2) considering a target void ratio of 0.530. No strain data has been corrected for variations in void ratio.

Table 7-1: B Series Test Results

Test	Actual				Uncorrected	Corrected	ε1
	α	b	σ_m	e_i	Fric Angle	Fric Angle	failure
B01	0.00	0.75	101.90	0.5291	55.75	55.70	0.44
B02	22.33	-0.01	101.25	0.5241	38.21	37.90	1.67
B03	22.42	0.50	101.80	0.5478	44.71	45.65	0.89
B04	22.42	0.99	102.85	0.5410	41.11	41.69	0.31
B05	45.07	0.23	102.04	0.5296	37.45	37.44	1.63
B06	44.92	0.74	102.16	0.5402	38.36	38.89	1.03
B07	67.33	0.00	100.16	0.5384	33.94	34.36	2.90
B08	67.51	0.50	101.76	0.5248	38.38	38.11	1.48
B09	68.32	1.01	102.68	0.5325	36.38	36.51	0.79
B10	90.00	0.05	98.64	0.5376	33.56	33.94	1.96

A three-dimensional plot of the stress path and failure surface for fine Nevada sand is shown in Figure 7-41. The bold lines represent the stress paths from the end of consolidation to failure for the B-Series tests, while the thin vertical lines represent the A-Series tests that were performed without inclined principal stress directions.

A-Series test results with inclined major principal stress directions have not been included in this failure surface plot due to the unintended principal stress rotation that occurred during shearing of each specimen.

A-Series tests at $\alpha = 0°$ and $\alpha = 90°$ have been included, but as the thin line indicates, with less emphasis than the Series B tests. All A-Series tests started with b-values equal to 1 and quickly transitioned to the target value during the elastic phase of shearing. This transition is thought to have little effect on the final friction angle. However, it constitutes a deviation from the test plan, hence the de-emphasis in this data.

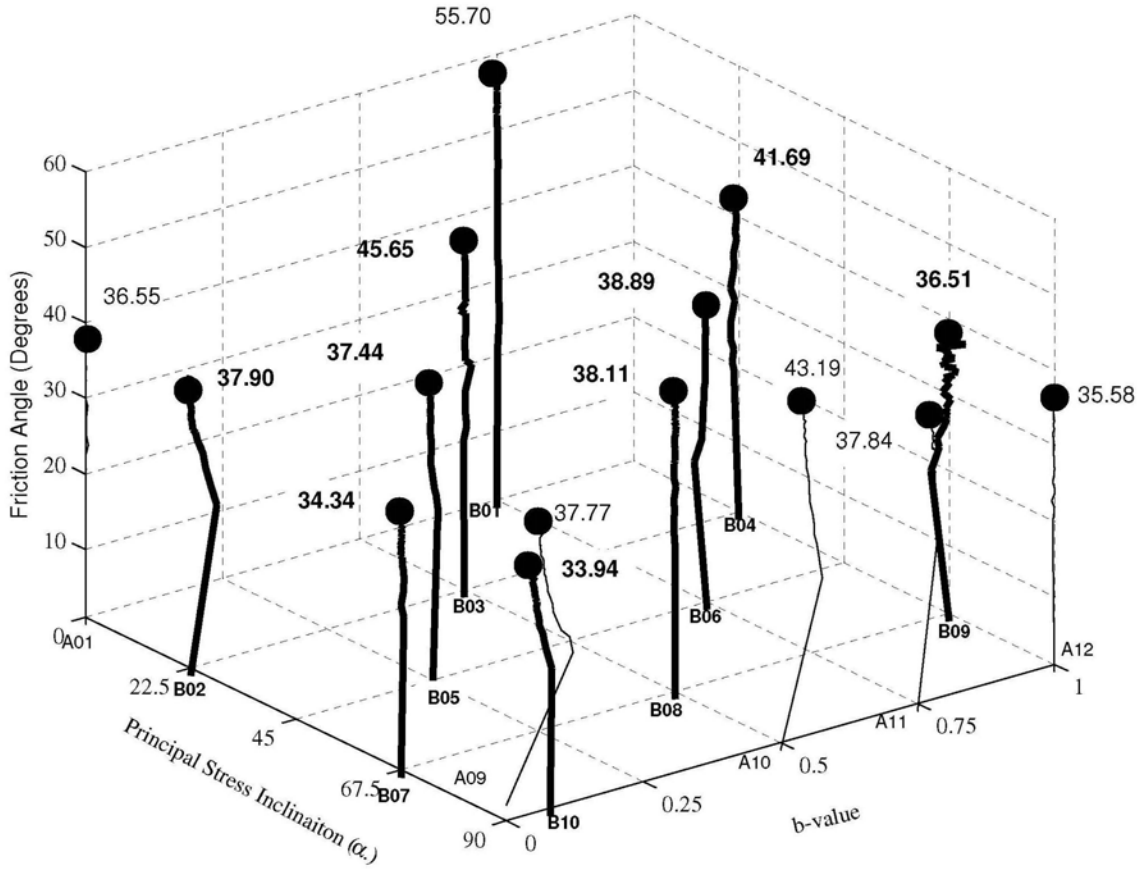

Figure 7-41: Stress Path and Failure Surface[10]

7.3.1 The Effects of α and b on the Peak Mobilized Friction Angle

Figure 7-42 shows the variation in peak friction angle as the intermediate principal stress changes. Tests with the same principal stress inclinations are grouped together by marker type. Closed markers denote B-Series testing, while open markers denote A-Series testing. A-Series tests with inclined principal stresses have not been included.

[10] Since shearing of all specimens starts after isotropic consolidation, initially $\sigma_1 = \sigma_2 = \sigma_3$. This causes the b-value during the first few steps to be highly variable. Due to this factor, the stress paths in Figure 7-41 all begin at the intended stress state and no additional data points are plotted until a stress ratio of 2 is achieved.

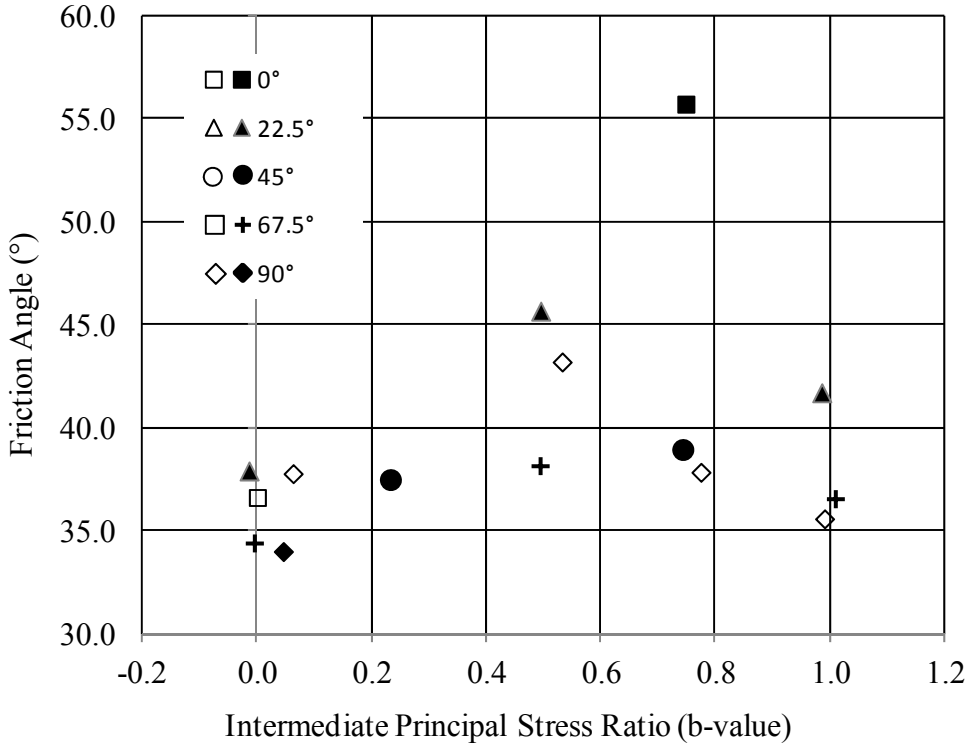

Figure 7-42: Variation of Friction Angle with b-value

7.3.1.1 THE EFFECT OF α ON THE PEAK FRICTION ANGLE

The data shown in Figure 7-42 indicates that for a given value of b, the peak friction angle reduces with increasing α. This trend was observed for all tests except A01. The strength of Test A01 (α=0°, b=0) was lower than B02 (α=22.5°, b=0).

For midrange values of b, there is a low point trough at α = 67.5°, which is the angle at which the shear band can be expected to coincide with the bedding plane. However, for b = 0 and b = 1 no trough has been detected and the friction values at α = 67.5° and α = 90° are similar.

Due to the neglected piston correction factor, shearing for specimen A01 started at a stress ratio less than 1 (i.e. horizontal stress > vertical stress) This caused the major principal stress to occur in the radial direction until the piston correction force had been

countered by the applied vertical force. The effects of the major principal stress initially occurring in the radial direction are unknown and may have attributed to the lower than expected shear strength.

7.3.1.2 THE EFFECT OF b-VALUE ON THE PEAK FRICTION ANGLE

As the b-value transitions from 0 to 0.5, there is a large gain in strength followed by a reduction as b continues to 1.0. At $\alpha = 90°$ the strength reduces from 0.5 to 0.75, but there are not enough data points to confirm this trend for other values of α.

Test results indicate that peak friction angles at b = 1 are greater than for b = 0. However, actual strengths at b=1 are probably much greater than test results indicate. As previously discussed, instability due to "necking" or "canyoning" is difficult to avoid at b = 1. The typical "necking" failure shown in Figure 7-43 took place during test A12 ($\alpha = 90°$, b=1). This instability results in brittle failure behavior and premature termination of the test.

The failure of specimen B04 ($\alpha=22.5°$, b=1) and B09 ($\alpha=67.5°$, b=1) were also brittle in nature. The failure of these specimens were discussed in Sections 7.2.2 and 7.2.4 respectively, and as shown in Figure 7-55 and Figure 7-25 both specimens developed large "canyon" type shear bands that are associated with instability in the radial direction.

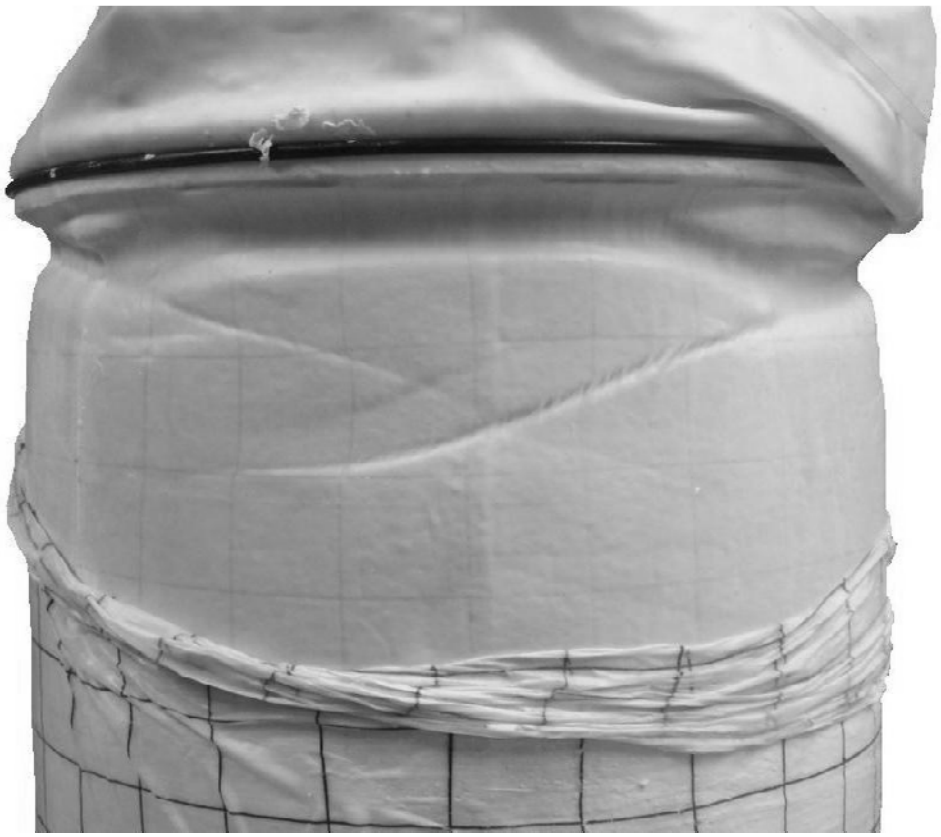

Figure 7-43: Test A12 Necking Failure

7.4 Stress Direction and Strain Increments

The major principal stress direction (ψ) and the major principal strain increment direction (ξ) have been calculated for tests performed with inclined principal stress directions using Equations (2.7) and (2.9). These tests have been performed with constant α values, and as such, have an average stress increment direction (χ) that is the same as the stress direction.

Figure 7-44 through Figure 7-48, are grouped by b-value and show plots of the stress and strain increment directions with respect to torsion shear strain. These plots stop at failure and the directions are calculated assuming vertical = 0° and horizontal = 90°.

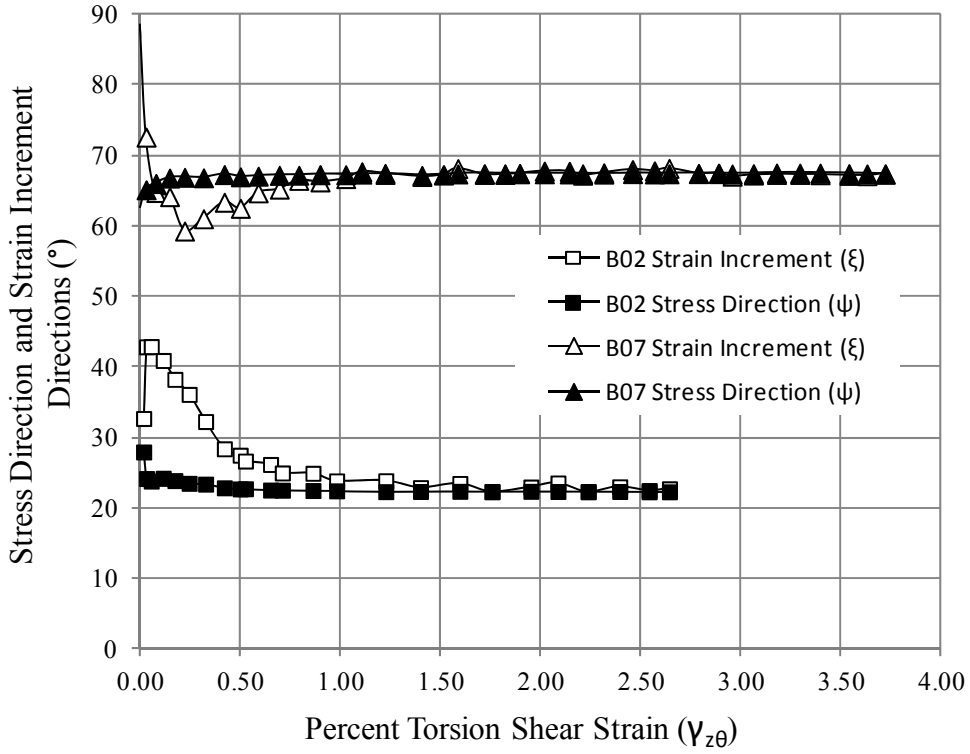

Figure 7-44: Contrast between Stress and Strian Increment Directions for b = 0

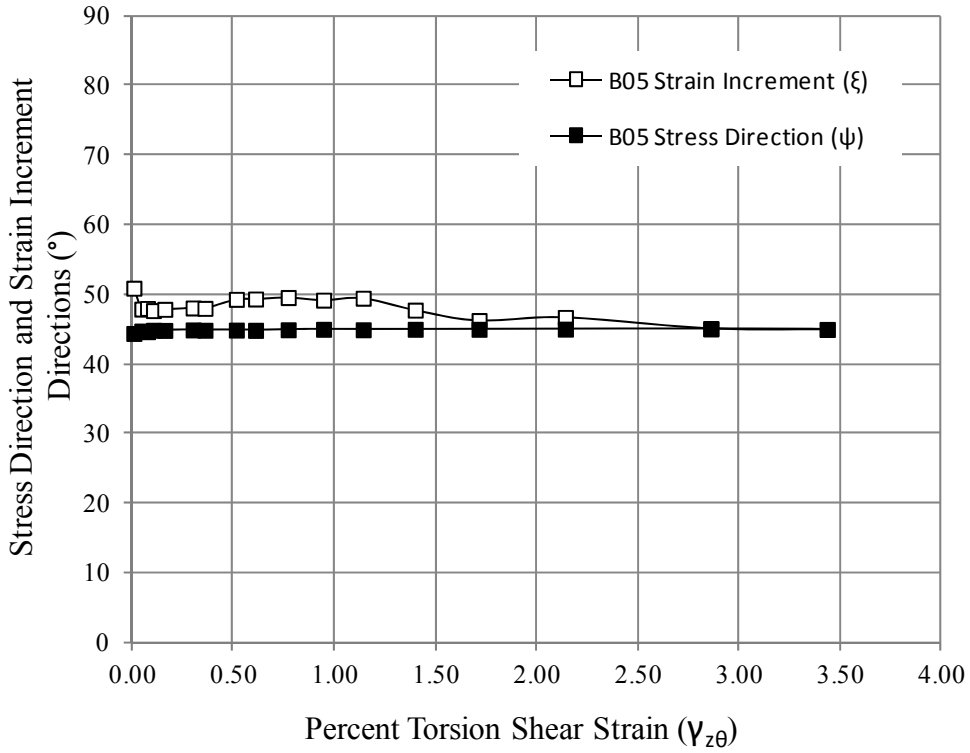

Figure 7-45: Contrast between Stress and Strian Increment Directions for b = 0.25

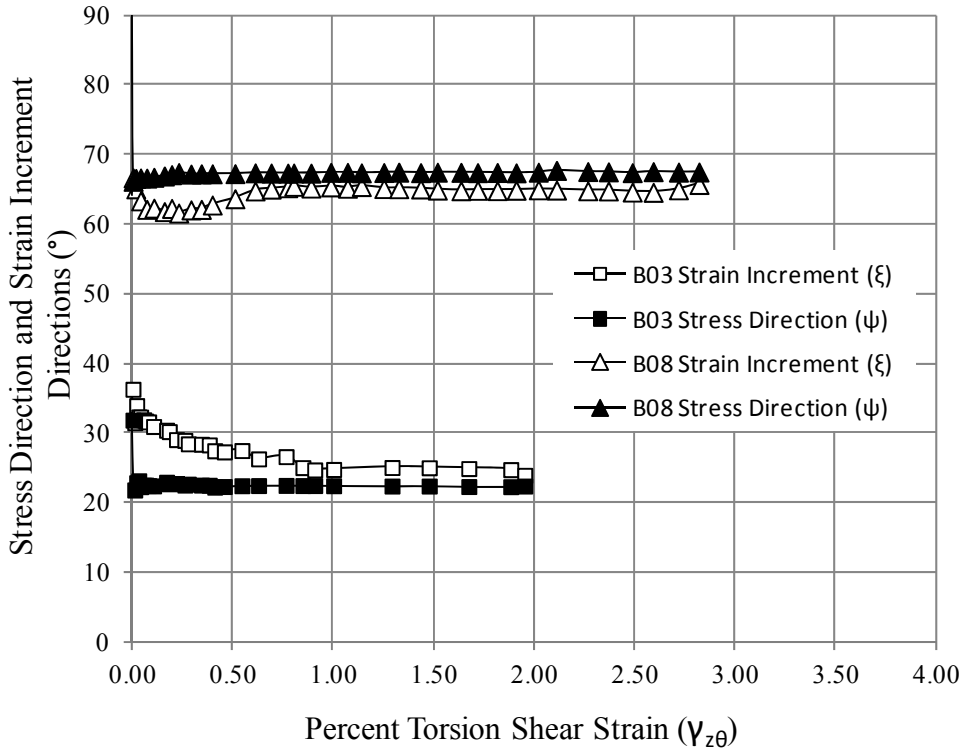

Figure 7-46: Contrast between Stress and Strian Increment Directions for b = 0.5

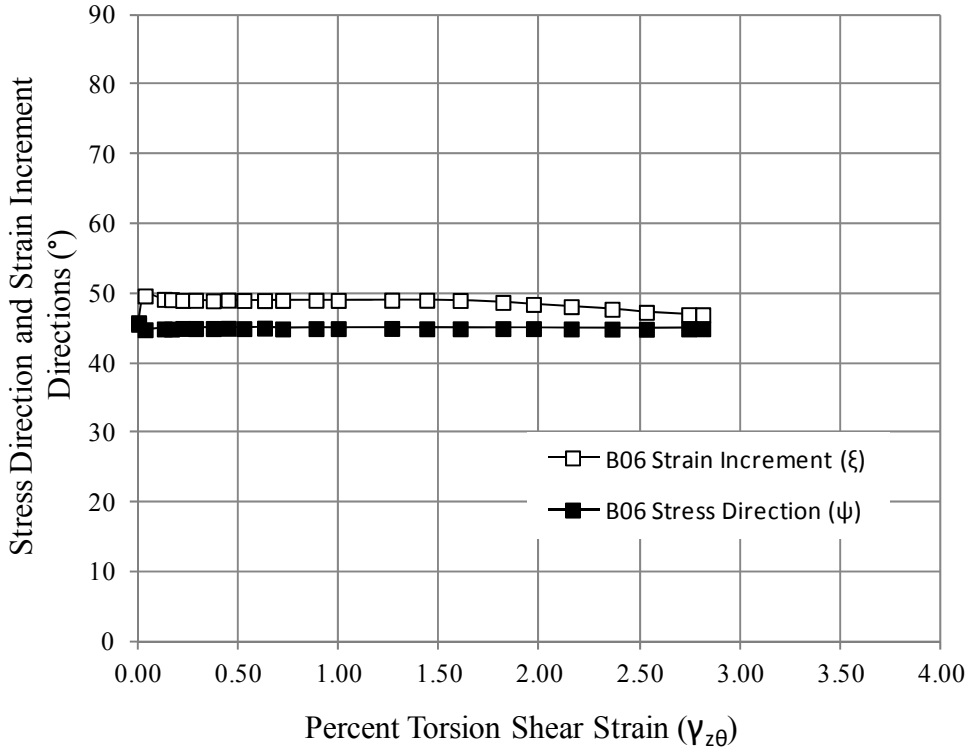

Figure 7-47: Contrast between Stress and Strian Increment Directions for b = 0.75

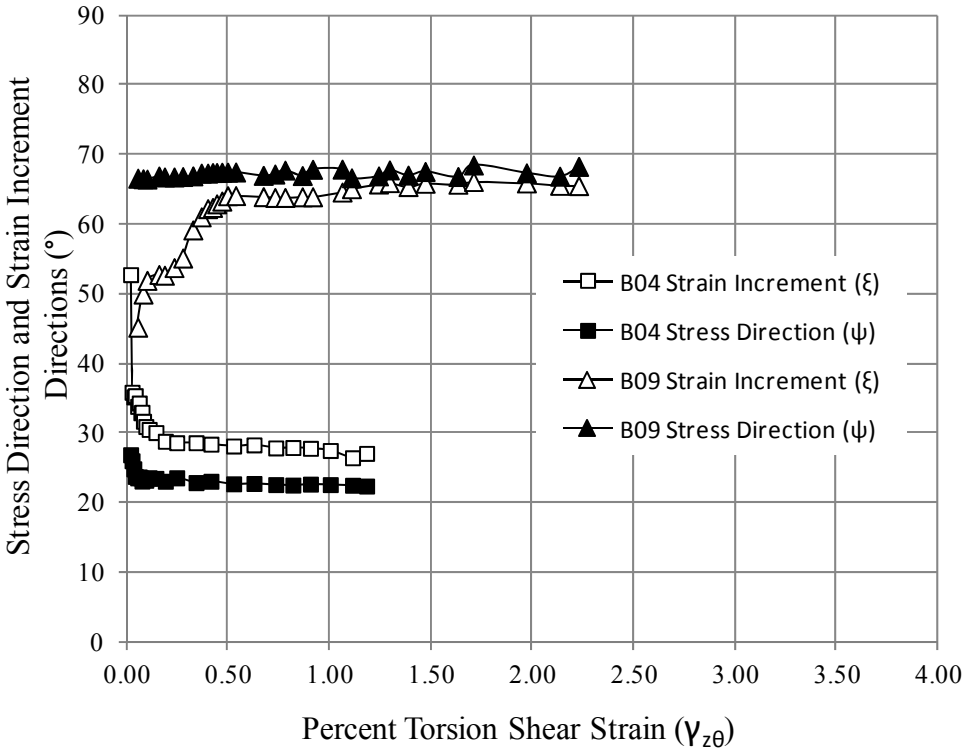

Figure 7-48: Contrast between Stress and Strian Increment Directions for b = 1

7.4.1 Major Principal Stress Direction (ψ)

The stress directions follow their intended paths well. However, they usually begin with a bias in the $\alpha = 45°$ direction. This is not totally unexpected, since these tests are controlled by torque, which is the initial stress applied to the specimen. See Figure 4-16 in Section 0 for a more detailed explanation regarding the sequence of applied loads.

7.4.2 Major Principal Strain Increment Direction (ξ)

The test results show deviations between the stress directions and the strain increment directions that are most pronounced during the elastic portion of shearing. As shearing progresses into the plastic zone, the strain increment directions gradually begin to approach the stress directions.

The differences between the stress directions and the strain increment directions at failure are shown in Table 7-2. The values of these differences with respect to b-value are shown in Figure 7-49.

Table 7-2: Difference Between Stress Direction and Strain Increment Direction at Failure

Test	b-value	ψ °	ξ °	Δ °
B02	0.00	22.33	22.75	-0.42
B03	0.50	22.42	23.96	-1.53
B04	0.99	22.42	27.10	-4.69
B05	0.23	44.98	44.97	0.01
B06	0.74	44.92	46.95	-2.02
B07	0.00	67.35	67.42	-0.07
B08	0.50	67.51	65.72	1.78
B09	1.00	68.32	65.56	2.76

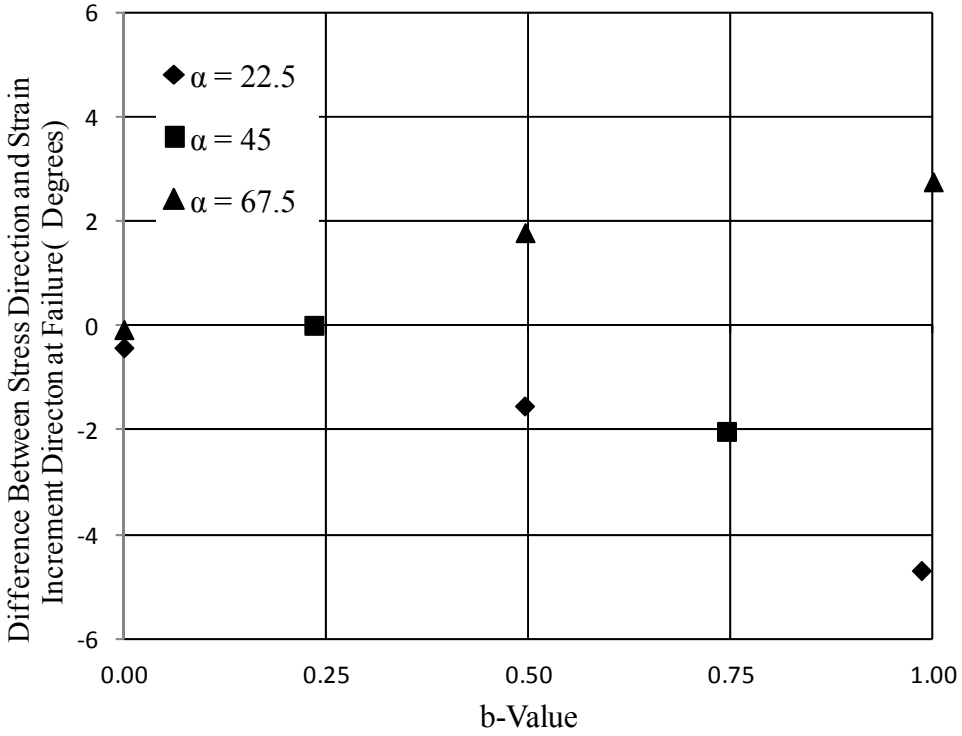

Figure 7-49: Difference between Stress Direction and Strain Increment with Respect to b-value

The strain increment directions trend toward the stress directions with increasing shear strain for all b-values. At low b-values the strain increment directions coincide with the stress directions at failure. However, at higher b-values the strain increment directions approach, but does not coincide with the stress directions, indicating that the soil fabric is still anisotropic, or at least that it partly remains that way in the (z-θ) plane. The variation in behavior observed at different b-values can be explained by the relative magnitude of the out-of-plane particle movement, as illustrated in Figure 7-50.

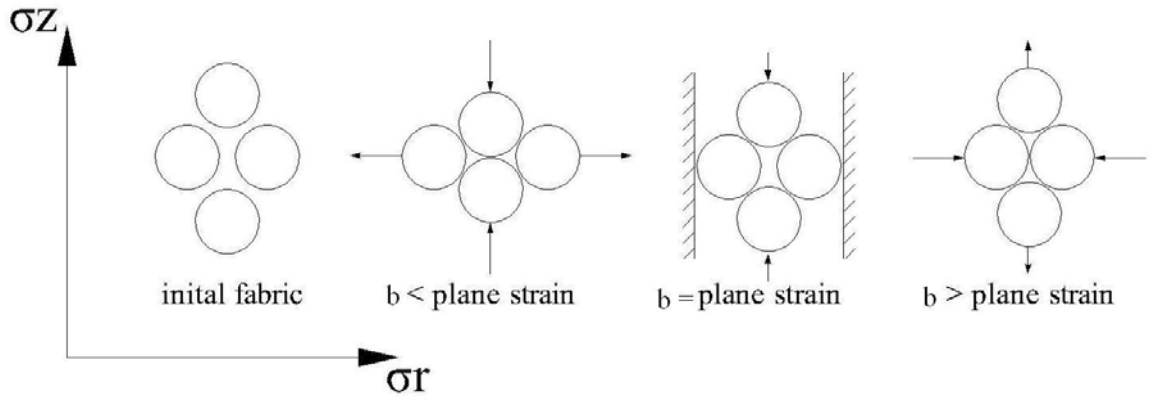

Figure 7-50: Degradation of Soil Fabric

In concept, for b-values less than plane strain, soil particles can move relatively freely in the radial direction. They are able to slide against each other and rearrange themselves to destroy the anisotropic fabric. Sliding as the primary method of realignment is evidenced by the soft stress strain curves and small amount of post peak softening for tests at low b-values.

For conditions at plane strain, soil particles in the radial direction lock the soil fabric together and increasingly force particle movement to occur via dilation rather than sliding. The soil fabric retains the majority of its anisotropic nature, until dilation causes well defined shear bands to form in the (z-θ) plane.

For conditions where b is greater than b at plane strain, the largest strain increments may actually be in the (r - θ) or (r-z) plane. In this case, the anisotropic fabric in the (z-θ) plane may still be intact when the intermediate principal stress or some combination of the intermediate and major principal stresses cause the specimen to fail. This type of failure has been evidenced by the large "canyon" type shear bands that occur due to failure in the (r-z) or (r-θ) planes.

7.5 Shear Band Formation

In this section, a coordinate system is defined and shear band types are specified based on their direction of propagation. The HTSA boundary effects for each type of shear band are discussed and the average shear band inclinations and narrative comments for each specimen are presented. A set of comprehensive shear band sketches and measurements is contained in Appendix M.

7.5.1 Coordinate System

Shear band designation and discussion will take place in the z-r-θ space. The schematic figures contained in this section have generally been drawn using 3-dimensional isometric views of the actual cylinder. However, in some cases the simplified Cartesian coordinate system shown in Figure 7-51 is used. In this system, the hollow cylinder has been "rolled out" into a flat bar to make the creation of figures less cumbersome.

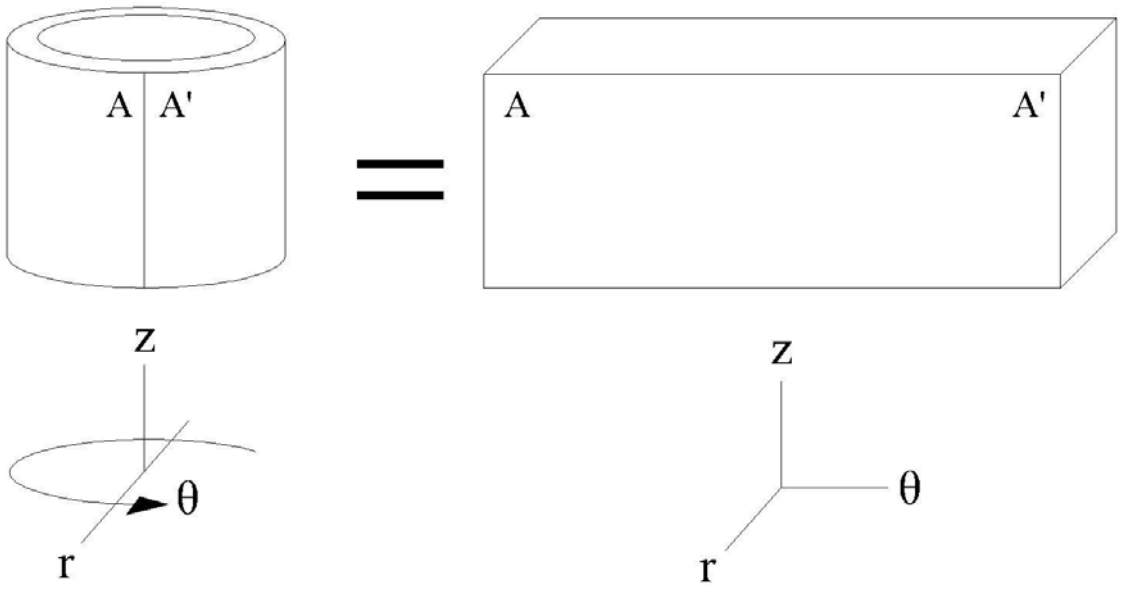

Figure 7-51: Cartisien Coordinate System for Shear Band Discussion

7.5.2 Shear Band Types

Shear bands are denoted according to the plane that they propagate in, with the larger of the two stresses listed first. A typical (z-θ) or (θ-z) plane shear band is shown in Figure 7-52, i.e. the normal to the shear band is located in the (z-θ) plane.

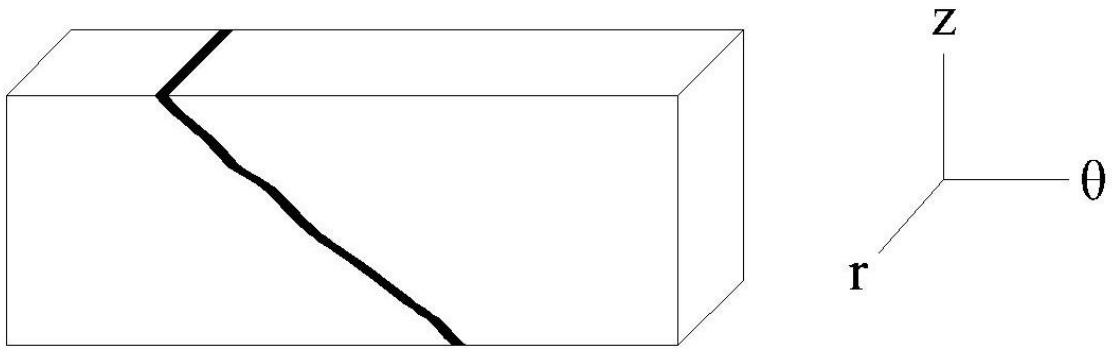

Figure 7-52: (z-θ) Plane Shear Band

Typical (r-θ) or (θ-r) plane shear band are shown in Figure 7-53, and Figure 7-54 depicts typical (r-z) or (z-r) shear bands.

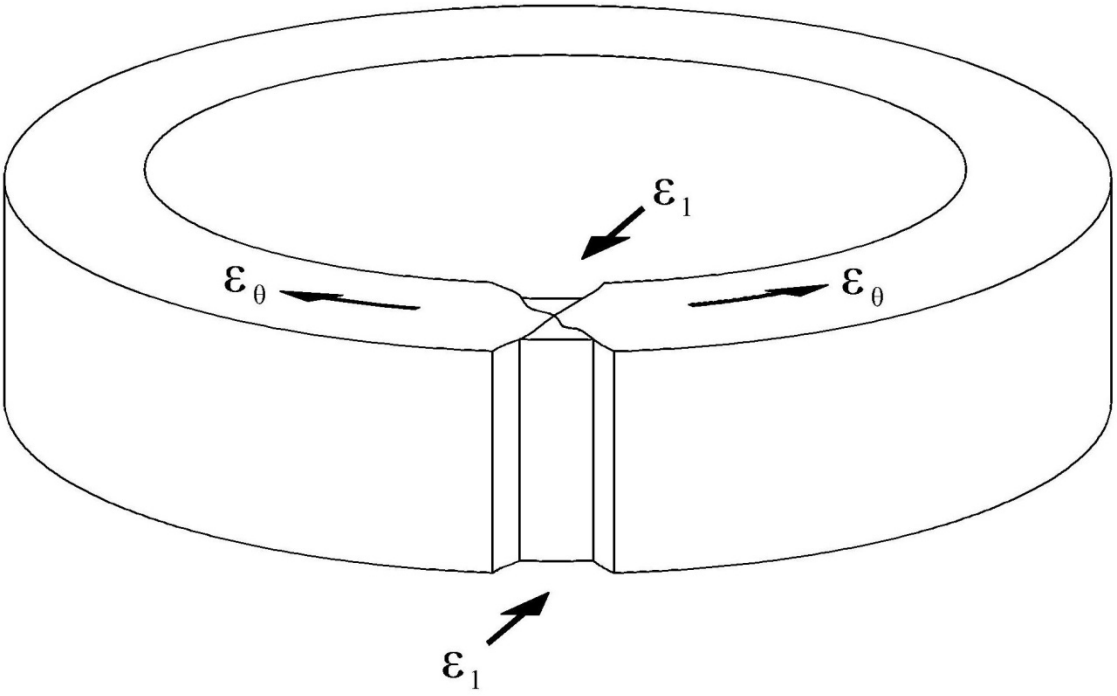

Figure 7-53: (r-θ) Plane Shear Band

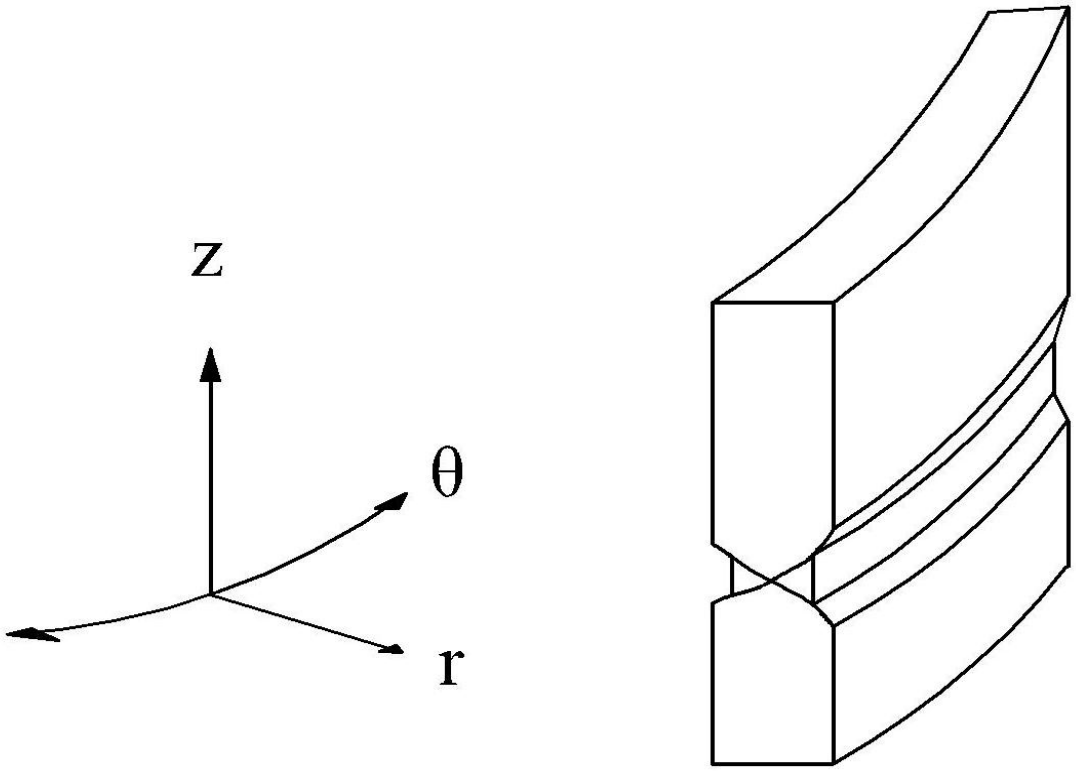

Figure 7-54: (r-z) Plane Shear Band

7.5.3 Boundary Effects

As previously discussed, shear bands may develop in one or more of three principal stress planes. The boundary conditions, which are not the same for each plane, may have a significant effect on shear band development.

7.5.3.1 RIGID BOUNDARIES

Shear bands propagating in the (z-θ) plane usually intersect hard boundaries; the notable exception being at α=67.5°, which produces nearly horizontal shear bands.

At the rigid boundaries, no relative movement between opposing sides of the shear band is possible. This may impede shear band development allowing a continued increase in stress ratio and the development of additional shear bands after formation of the initial shear band.

Test results have shown that when (z-θ) shear bands develop, they develop in the middle of the specimen and they are often thin and ubiquitous in nature and do not intersect the top or bottom rings.

7.5.3.2 FLEXIBLE BOUNDARIES

Shear bands propagating in the (r-θ) or (r-z) planes intersect the flexible membranes that make up the specimen's inner and outer cell walls. These shear bands propagate all the way to the specimen's surface allowing relative displacement between opposing sides to occur freely. The result of this free movement is that shear bands occurring in either of these planes may be likely to initiate failure.

Shear bands with flexible boundaries have been observed to develop into large "canyons" on both the inner and outer sides of the specimen, as shown in Figure 7-55.

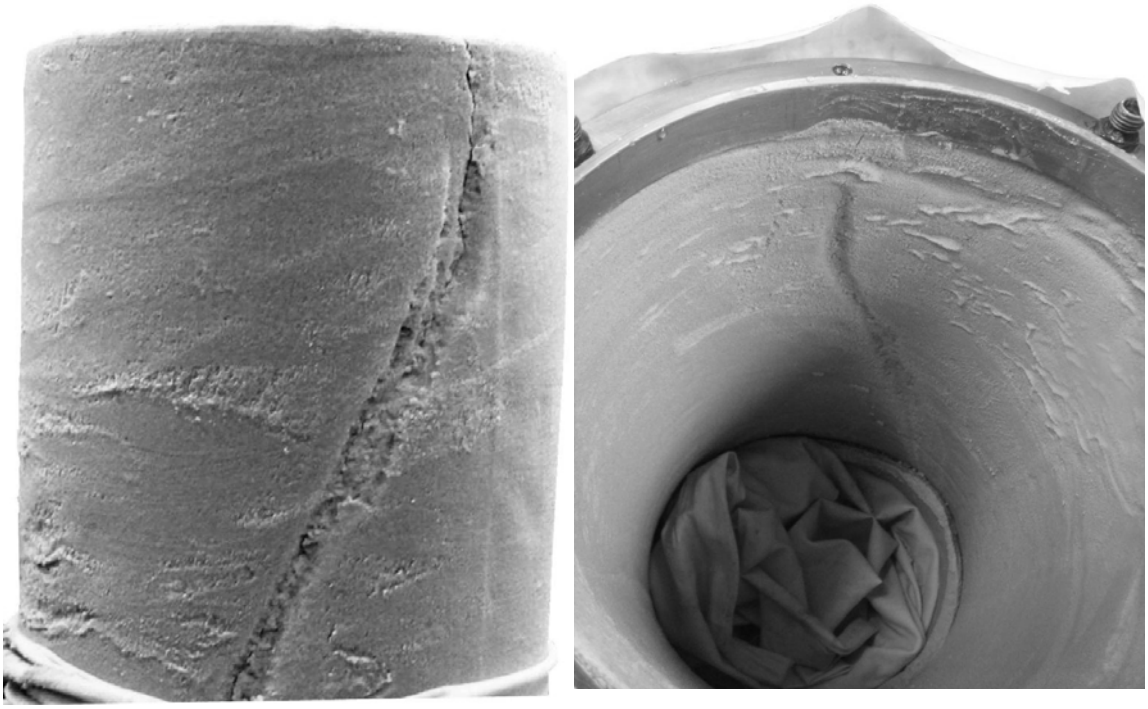

Figure 7-55: Test B04 r-θ Shear Band (Outer and Inner Surface)

This canyon style shear band locally reduces the specimen area. Since the inner and outer cell pressures are applied over flexible boundaries, the stress applied to this reduced area increases, creating an increasingly deeper shear band and higher local stresses.

This "canyon" condition is similar to "necking" which causes instability in extension tests. As the inner cell pressure begins to push the specimen outward, a separation occurs at the canyon. The soil grains within the shear band begin to pull away from each other rather than sliding against each other, resulting in a very brittle failure with no residual strength.

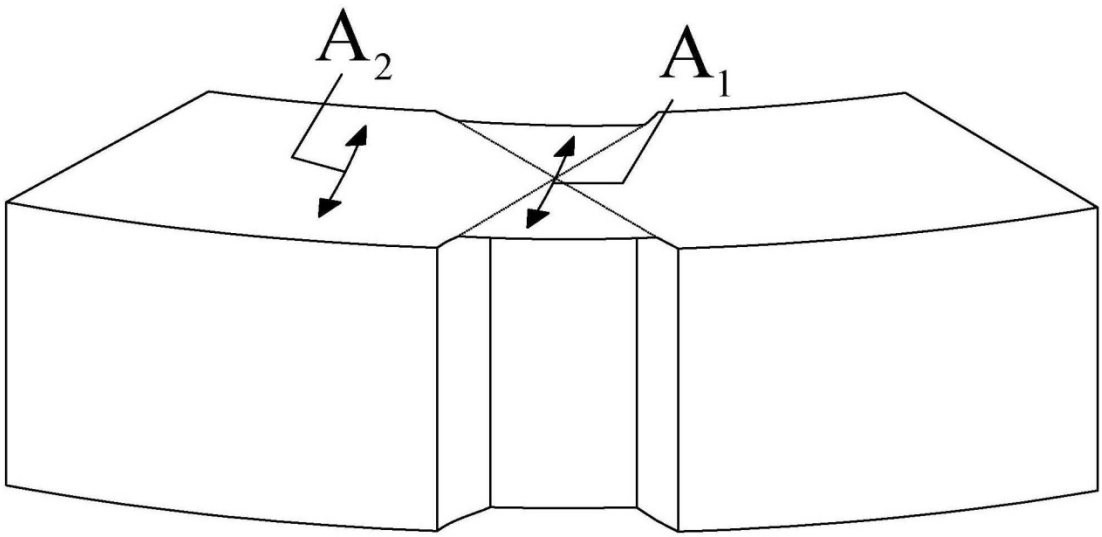

Figure 7-56: Specimen Area Reduction due to Canyon Shear Band

7.5.4 Observations

After completing each test, the specimen was left standing under vacuum so that shear band angles could be measured and sketches of their locations could be created. These sketches and the angle of each individual shear band are contained in Appendix M.

Common shear band angles have been averaged together and the results are presented in Table 7-3. For combined failures, the first plane listed in the "mode" column is thought to be the primary failure plane.

Although shear bands may occur in 3 planes, all measurements were made in the (z-θ) plane, as it was not possible to measure angles in the other planes. The angles were measured using a protractor placed directly on the specimen and are accurate to 0.5°. In some cases a distinct secondary set of shear bands was observed. When appropriate, the average angle for the secondary set of shear bands has also been presented.

Table 7-3: Shear Band Angles and Predictions

Test	*Primary Shear Band*				*Secondary Shear Band*	
	Inclination σ1 (°)	Theoretical Band (°)	Observed Avg. (°)	Mode	Inclination (°)	Mode
B01	0.00	72.9	65.7	**(z-θ)** & (r-θ)	90.0	(r-θ)
B02	22.33	41.6	20.7	(z-r) & (z-θ)	na	
B03	22.42	45.4	47.6	**(z-θ)**	na	
B04	22.42	43.4	67.0	(r-θ)	na	
B05	45.07	18.7	19.3	**(z-θ)**	na	
B06	44.92	19.5	22.5	**(z-θ)**	3.5	(z-θ)
B07	67.33	5.2	0.0	**(θ-z)**	na	
B08	67.51	3.5	0.0	**(θ-z)**	na	
B09	68.32	5.1	5.8	**(θ-z)** & (r-z)	12.0	(θ-z)
B10	90.00	28.0	22.4	**(θ-z)**	na	

Comments regarding the development of shear bands for each specimen are summarized in the following bullitized paragraphs.

- B01(α = 0.00°, b = 0.75) – This specimen developed numerous shear bands in the (z-θ) and (r-θ) planes. The shear bands were observed at 65.7° which is reasonably close to the prediction of 73.4°. It seems likely that the (r-θ) component of the shear band developed after the (z-θ). This is based on the large number of shear bands that developed and the relatively good agreement between the observed and predicted angles.
- B02 (α = 22.33°, b = -0.01) – The shear band for this specimen appears to be a true combination of the (z-r) and (z-θ) planes. The shear band angle of 20.7° measured in the (z-θ) plane is not close to the theoretically predicted angle of 42°. However, it is not possible to measure the inclination in the (z-r) plane, and for this condition of b=0 it may be the critical failure plane.

It is also noteworthy that the observed inclination is about 45° from the major and minor principal stress directions.

- B03 ($\alpha = 22.42°$, $b = 0.50$) – Most shear banding occurs only in the (z-θ) plane. There is one portion of the shear band that opens into a wide canyon. The shear band at 28° was not included in the average shear band direction as its inclination appeared to be substantially affected by its proximity to the bottom ring.
- B04 ($\alpha = 22.42°$, $b = 0.99$) – This specimen developed a single large (r-θ) plane canyon type shear band. This canyon has an inclination of 67°, which is much steeper and seems unrelated to the inclination of 43.9° predicted for a (z-θ) plane shear band. It is noteworthy that the observed inclination is the same as the major principal stress direction (α).
- B05 ($\alpha = 45.07°$, $b = 0.23$) – Many thin shear bands developed in the (z-θ) plane. The observed inclination of 19.3° matched well with the theoretical prediction of 19.4°.
- B06 ($\alpha = 44.92°$, $b = 0.74$) – Two independent sets of shear bands developed in the (z-θ) plane. The primary set had an observed inclination of 22.5°, very close to the predicted value of 20.1°. A second set of nearly horizontal shear bands was also observed with an inclination of 3.5°.

A single shear band at 10° was not included in the average shear band directions as it seemed to be connecting the two prominent shear band groupings.

- B07 ($\alpha = 67.33°$, $b = 0.00$) – A single (θ-z) horizontal shear band developed beneath the top ring. For this case of α=67.5°, the shear band is collinear with the bedding plane and does not have to intersect the top cap, ensuring that the preferential shear band propagation plane is (θ-z) rather (θ-r).
- B08 ($\alpha = 67.51°$, $b = 0.50$) – As expected, horizontal shear bands developed in the (θ-z) plane. One was located directly beneath the top ring while the other was located directly above the bottom ring.
- B09 ($\alpha = 68.32°$, $b = 1.01$) – This specimen developed a primary set of nearly horizontal shear bands at 5.8°compared to a prediction of 4.2°. Some of these shear bands also showed combined development in the (r-z) plane. Based on the large number of shear bands and the fact that they developed at nearly the same angle as the prediction, it seems likely that the (θ-z) plane developed prior to the (r-z) plane. A secondary set of shear bands was observed at 12°.
- B10 ($\alpha = 90.00°$, $b = 0.05$) – This specimen developed many thin shear bands in the (θ-z) plane. The average observed shear band inclination was 22.4°, which is lower than the predicted value of 27.9°. However, the shear band scatter was relatively uniformly distributed from 20° to 30°.

8 SUMMARY AND CONCLUSIONS

A fully-automated Hollow Torsional Shear Apparatus (HTSA) has been developed to investigate the failure surface of a dense cross-anisotropic sand. This new device utilizes a precision turn-table rotating at a constant rate to apply shear strain to the hollow cylinder specimen. The device and servo-control system have demonstrated the ability to accurately maintain preprogrammed stress paths.

A series of drained tests have been performed on air pluviated specimens of fine Nevada Sand with a target relative density of 91.3 percent (e_i = 0.530). The air pluviation method resulted in the creation of a cross-anisotropic fabric.

To study the effects of principal stress inclination and the intermediate principal stress, the specimens were sheared at stress conditions that maintained constant values of principal stress inclination, α, intermediate principal stress ratio, b, and mean normal stress, σ_m. Appropriate stress path equations were developed as part of this investigation.

For tests with inclined principal stress directions, the stress path was maintained by measuring the applied shear stress and calculating and applying the desired vertical load, and inner and outer cell pressures. For tests at α = 0° or α = 90°, the stress path was maintained by measuring the applied vertical load and calculating the inner and outer cell pressures.

8.1 Test Plan

Two series of tests were completed as part of this investigation. All twelve A-Series tests deviated from the intended stress paths because the piston uplift correction was not accounted for during shearing.

This lead to unintended stress rotation for some tests and an initial b-value that always started at 1.0.

For the five A-Series tests with $\alpha = 0°$ or $\alpha = 90°$, no stress rotation occurred and the b-values quickly approached the intended targets. Therefore, these tests were included on the failure surface. For the seven tests with inclined principal stress directions, actual stress paths varied significantly from the plan. These test results have not been included in plotting of the failure surface.

A second set of ten tests was completed that did consider the piston uplift correction during shearing. These tests, designated as the B-Series, followed their intended stress paths well. Two tests were performed with $\alpha = 0°$ or $\alpha = 90°$ to supplement the five A-Series tests that had already been performed and eight tests with inclined principal stress directions were performed to replace the inclined A-Series tests.

8.2 Test Results

8.2.1 Stress-Strain-Strength Behavior

Effects of the principal stress inclination and the intermediate principal stress have been studied by comparing test results from specimens sheared at constant α and b-values.

8.2.1.1 EFFECTS OF α

A decrease in stiffness was observed from α = 0° to α = 67.5° followed by a moderate increase in stiffness from 67.5° to 90°. Peak shear strength values followed a similar trend for mid range b-values.

However, the trough occurring at α = 67.5° was not observed near the end conditions of b = 0 or 1. At b = 0 the peak friction angles at 67.5° and 90° were nearly the same. At b = 1 the peak shear strength at α = 90° was actually slightly less than for α = 67.5°. This may be because failure for this stress condition (α=90°, b=1) is caused by "sidewall instability". The actual strength at this location may be somewhat higher than reported.

8.2.1.2 EFFECTS OF B-VALUE

Increases in b-value from 0 to 0.5 result in significantly increased stiffness. A more subtle increase in stiffness is observed as the b-values increase from 0.5 to 1. The peak shear strength increases from b = 0 to 0.5 and then decreases from 0.5 to 1. However, the strength at b = 1 is somewhat higher than b = 0.

8.2.2 Volume Change Behavior

Increasing the principal stress inclination from $\alpha = 0°$ to $\alpha = 67.5°$ results in a decreased volumetric strain rate and in increase in the magnitude of compression. It also increases the amount of major principal strain that occurs prior to the onset of dilation. Due to the instability of testing at $\alpha = 90°$ and b=1, it was not possible to establish a trend from $\alpha = 67.5°$ to $\alpha = 90°$.

8.2.3 Intermediate Principal Stress

A soil's shearing resistance parallel to the bedding plane is less than it is perpendicular to the bedding plane, making the influence of the intermediate principal stress a function of stress inclination.

The intermediate principal stress is applied in the radial direction parallel to the bedding plane. However, the major principal stress is applied perpendicular to the bedding plane for low values of α and parallel to the bedding plane for high values of α.

For a condition of ($\alpha=0°$, b=1) the major and intermediate stresses are equal, but the shear resistance is greater in the major stress direction, creating a condition in which the intermediate principal stress causes failure. For low α values, the intermediate principal stress may be the primary cause of failure for b-values as low as 0.75.

As the inclination (α) increases, resistance to the major principal stress decreases and the influence of the intermediate principal stress becomes less pronounced. At $\alpha = 90°$ both the intermediate and major principal stresses are applied parallel to the bedding plane and each should contribute equally to failure.

8.2.4 Stress Direction and Strain Increment Directions

The stress directions and strain increment directions for all B-Series test involving inclined principal stress directions have been calculated using Equations (2.7) and (2.9). For $\alpha = 22.5°$ and $\alpha = 45°$ the strain increment directions were several degrees higher than the stress directions through the elastic portion of the tests. As failure is approached, the strain increment directions aligned with the stress directions for b-values near 0, but it only trends to the stress directions for higher b-values.

At $\alpha = 67.5°$, the strain increment directions are several degrees lower than the stress direction during the elastic portion of the test. At large shear strains associated with b = 0 the strain increment directions aligned with the stress directions and at shorter shear strains associated with higher b values, the strain increment directions trend toward, but do not reach the stress directions.

8.2.5 Shear Bands

8.2.5.1 SHEAR BAND DIRECTIONS

Shear band propagation was observed occurring in one or a combination of the (z-θ), (z-r), and (θ-r) planes. However, it was only possible to take measurements of shear bands occurring in the (z-θ) plane. For failures confined to the (z-θ) plane, the measured shear band inclinations agreed well with the Coulomb's theoretical prediction of $(45+\varphi/2)$ degrees from the minor principal stress direction.

For specimens simultaneously developing shear bands in two planes, inclinations did not agree with the Coulomb prediction. Test B02 ($\alpha=22.33°$, b=-0.01) failed simultaneously in the (z-r) and (z-θ) planes. It is noteworthy that the measured

inclination in the (z-θ) plane was about midway between the major and minor principal stress directions. Test B04 (α=22.42°, b=0.99) had a b-value of 1 and developed a single large (r-θ) plane canyon type shear band. The canyon had an inclination indicating that the (z-θ) may also have played a significant role in its development. It is noteworthy that the inclination measured in the (z-θ) plane is the same as the major principal stress direction (α).

8.2.5.2 SHEAR BAND FORMATION

Shear band formation may be partially influenced by the HTSA boundary conditions. All non-horizontal shear bands forming in the (z-θ) plane will eventually intersect the top and bottom rings. These rings stunt shear band development, resulting in the creation of many thin shear bands rather than one or two well defined shear bands.

Shear bands propagating in the (r-θ) or (r-z) planes intersect the flexible membranes that allow relative displacement between opposite sides to occur freely. As a result, these shear bands are likely to initiate failure and only one or two well defined shear bands will develop.

Shear bands intersecting flexible boundaries often develop into canyon type bands due to sidewall instability that is similar in nature to the "necking" condition often observed in extension tests.

Appendix A **Computer Program**

Untitled4.vi
C:\Program Files\National Instruments\LabVIEW 8.5\Testing Machine\Untitled4.vi
Last modified on 10/16/2010 at 1:33 PM
Printed on 4/15/2011 at 4:27 PM

Untitled4.vi

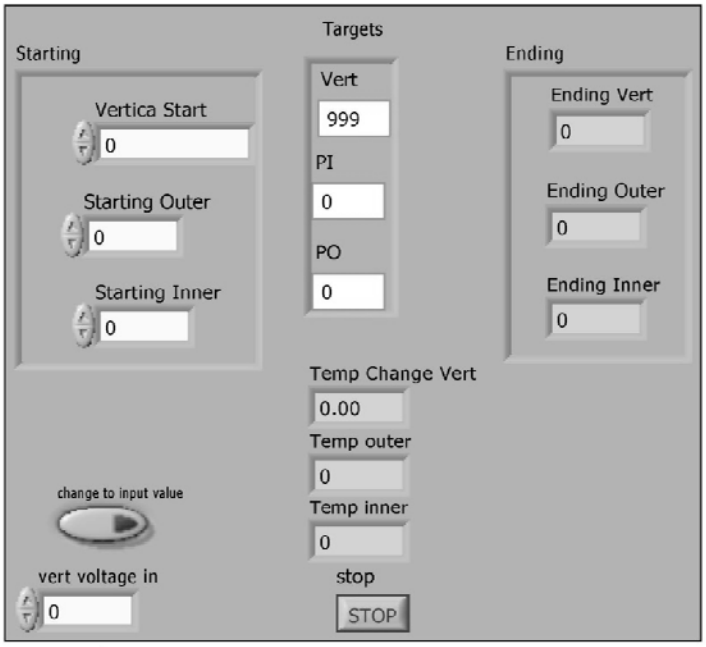

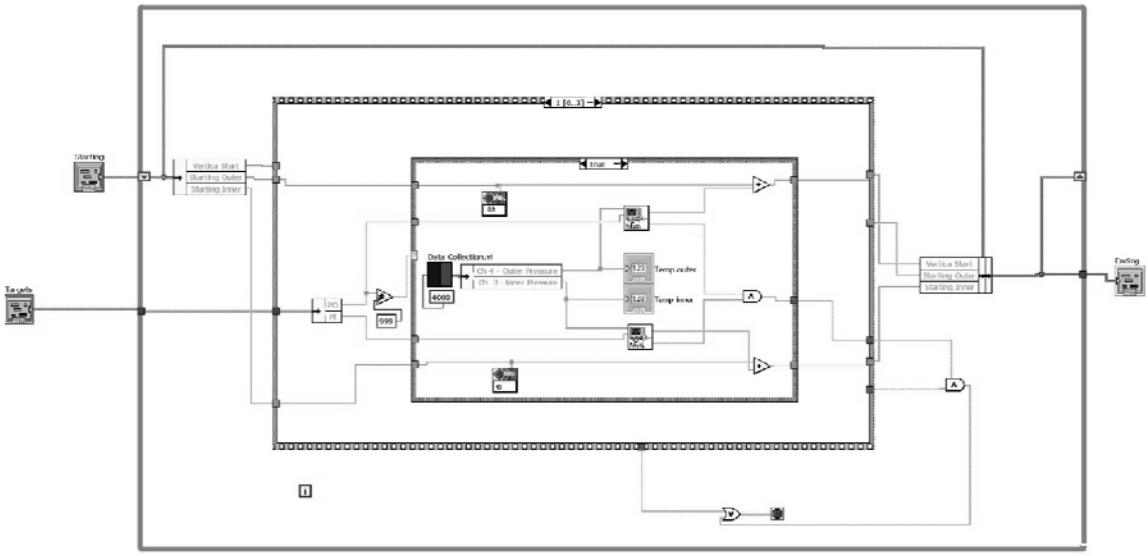

Untitled4.vi
C:\Program Files\National Instruments\LabVIEW 8.5\Testing Machine\Untitled4.vi
Last modified on 10/16/2010 at 1:33 PM
Printed on 4/15/2011 at 4:27 PM

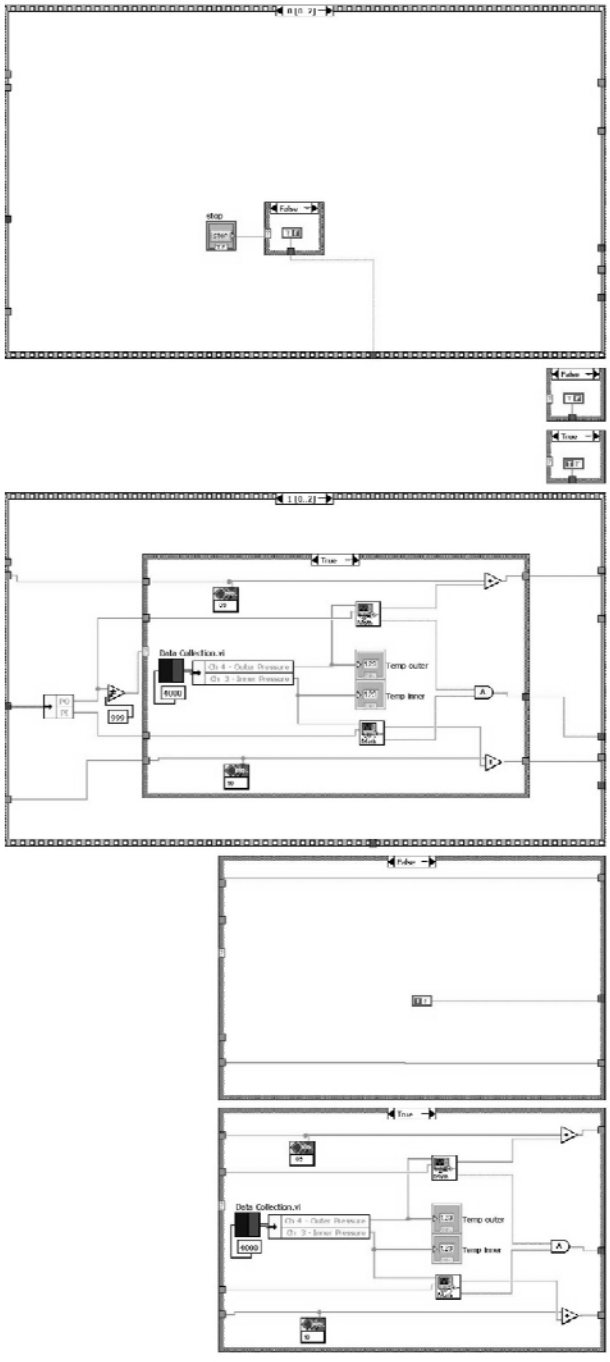

Untitled4.vi
C:\Program Files\National Instruments\LabVIEW 8.5\Testing Machine\Untitled4.vi
Last modified on 10/16/2010 at 1:33 PM
Printed on 4/15/2011 at 4:27 PM

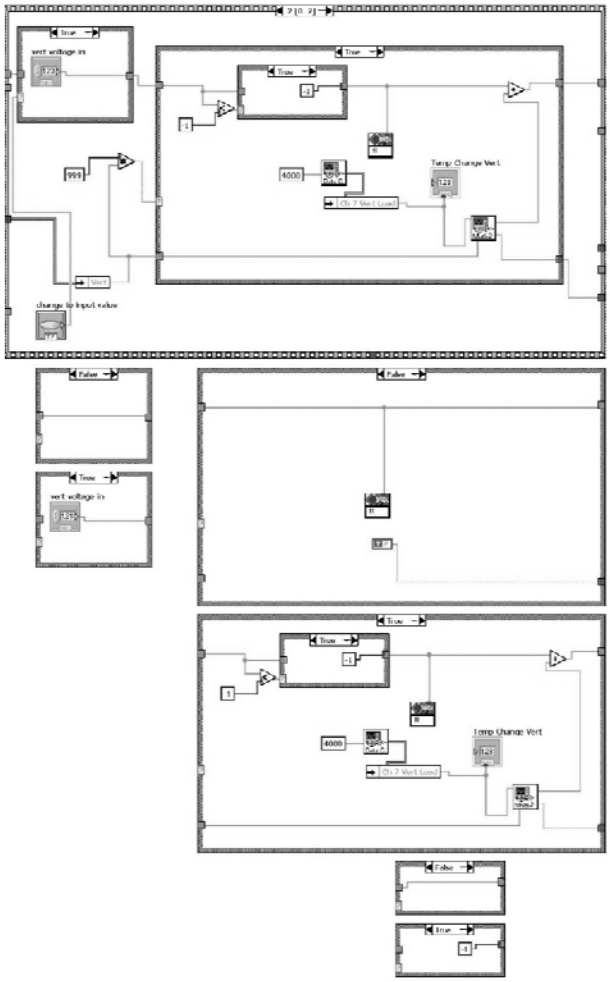

sequence.vi
C:\Program Files\National Instruments\LabVIEW 8.5\Testing Machine\sequence.vi
Last modified on 11/26/2010 at 10:42 AM
Printed on 4/15/2011 at 4:25 PM

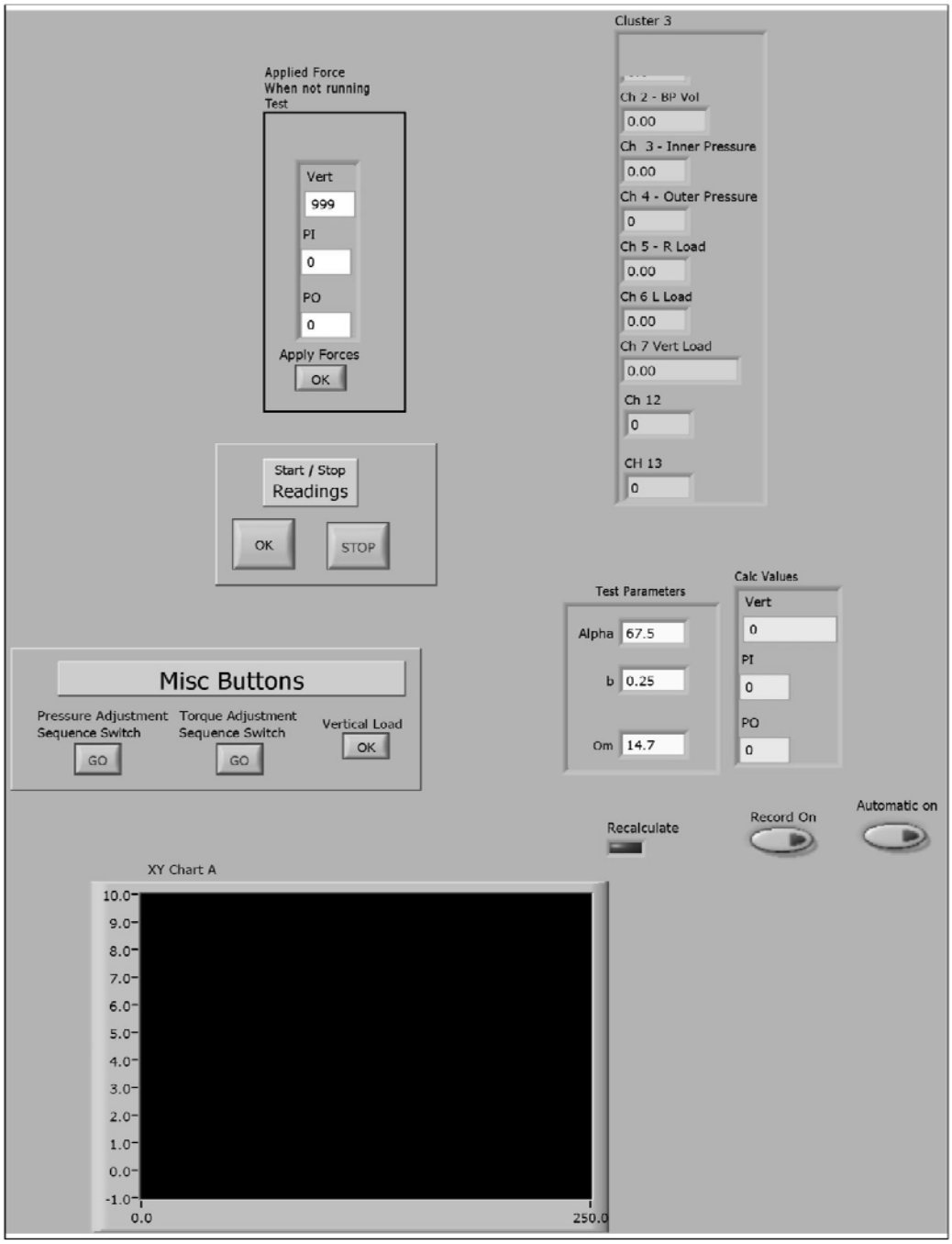

sequence.vi
C:\Program Files\National Instruments\LabVIEW 8.5\Testing Machine\sequence.vi
Last modified on 11/26/2010 at 10:42 AM
Printed on 4/15/2011 at 4:25 PM

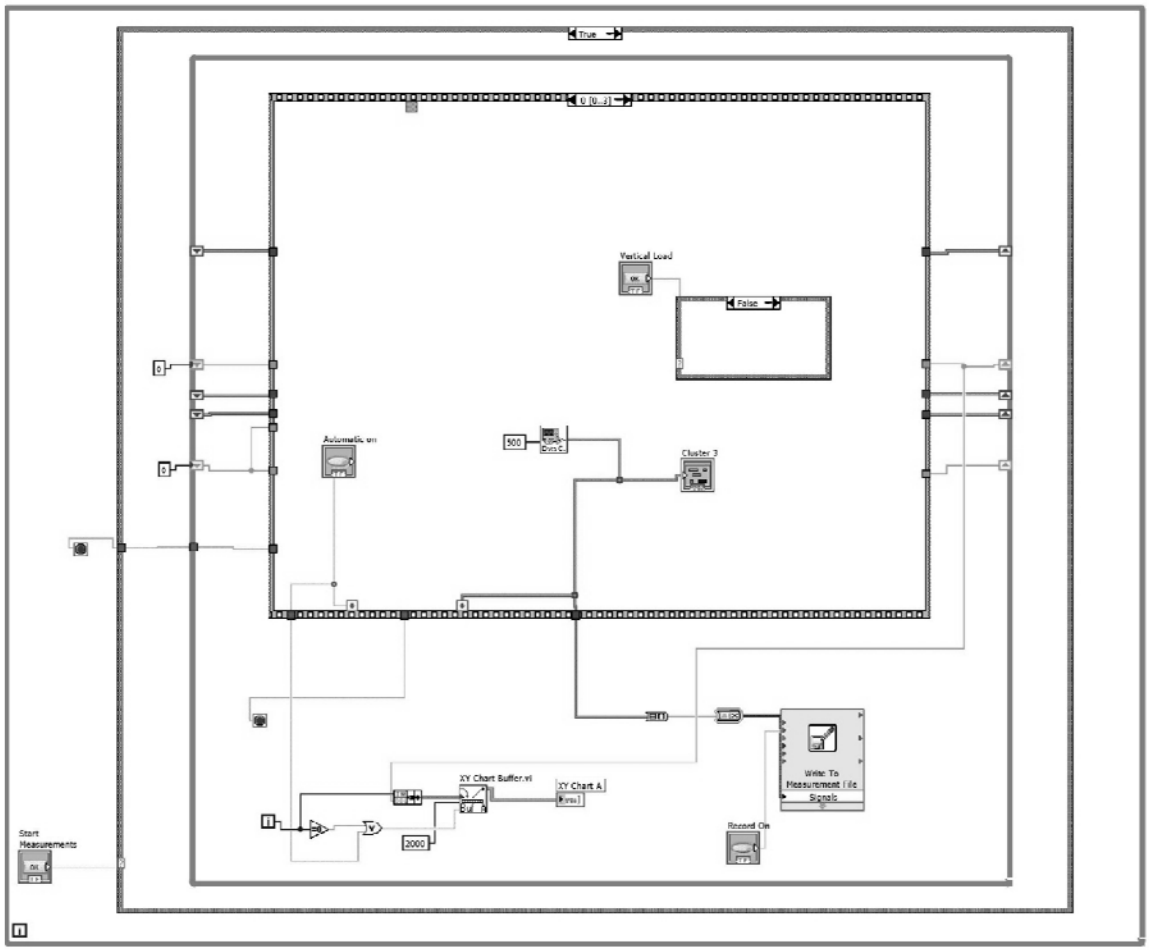

sequence.vi
C:\Program Files\National Instruments\LabVIEW 8.5\Testing Machine\sequence.vi
Last modified on 11/26/2010 at 10:42 AM
Printed on 4/15/2011 at 4:25 PM

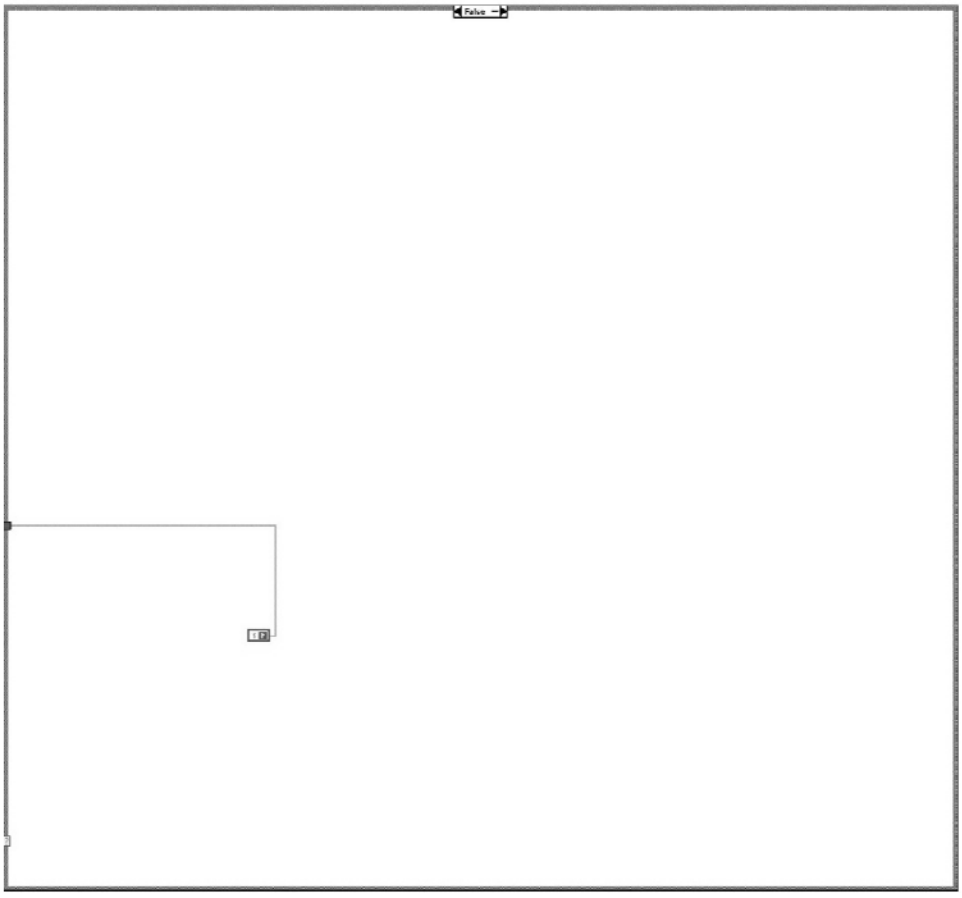

sequence.vi
C:\Program Files\National Instruments\LabVIEW 8.5\Testing Machine\sequence.vi
Last modified on 11/26/2010 at 10:42 AM
Printed on 4/15/2011 at 4:25 PM

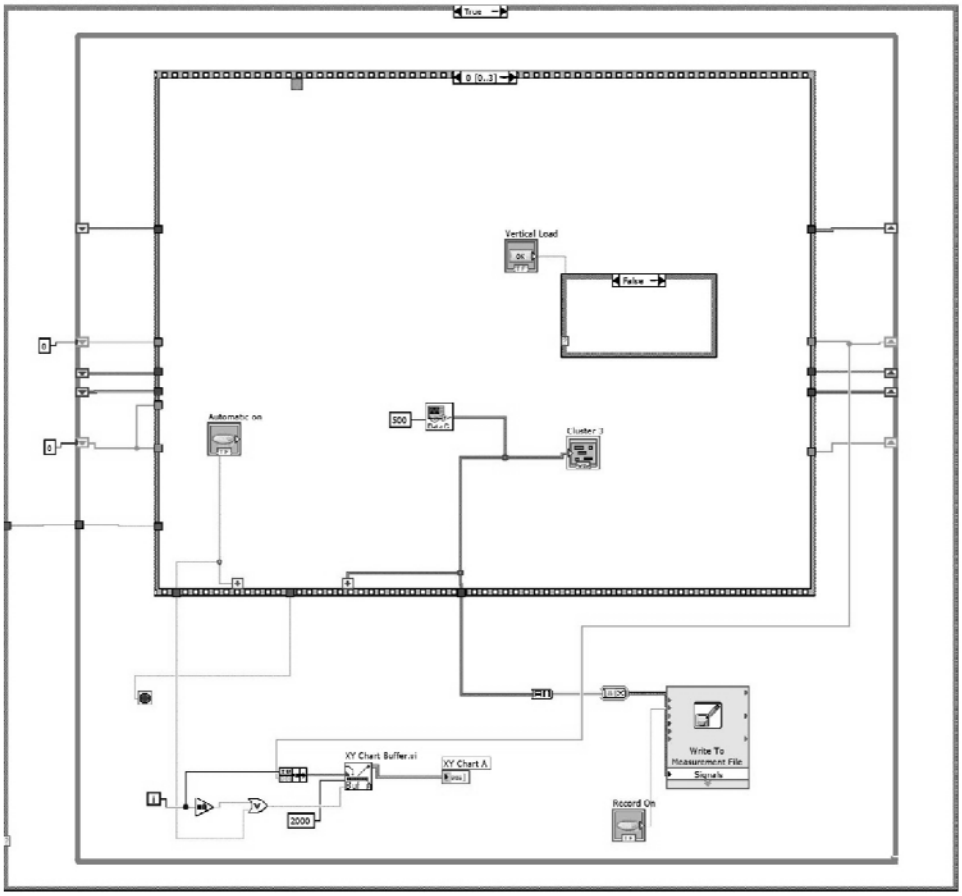

sequence.vi
C:\Program Files\National Instruments\LabVIEW 8.5\Testing Machine\sequence.vi
Last modified on 11/26/2010 at 10:42 AM
Printed on 4/15/2011 at 4:25 PM

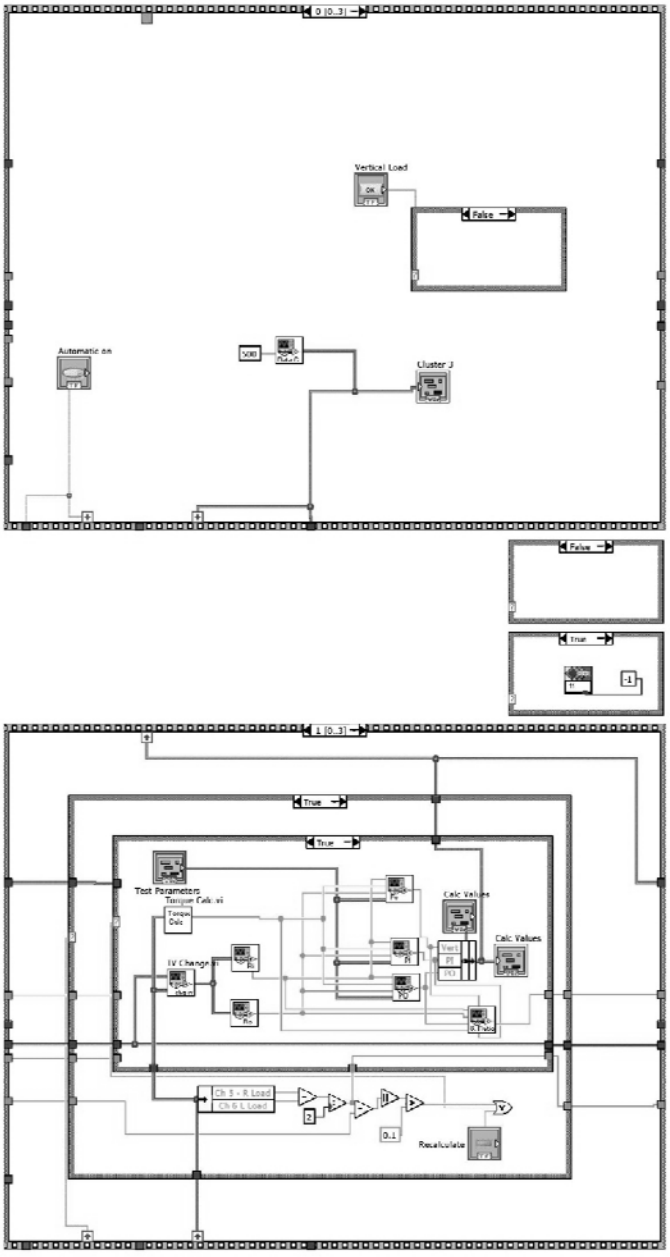

sequence.vi
C:\Program Files\National Instruments\LabVIEW 8.5\Testing Machine\sequence.vi
Last modified on 11/26/2010 at 10:42 AM
Printed on 4/15/2011 at 4:25 PM

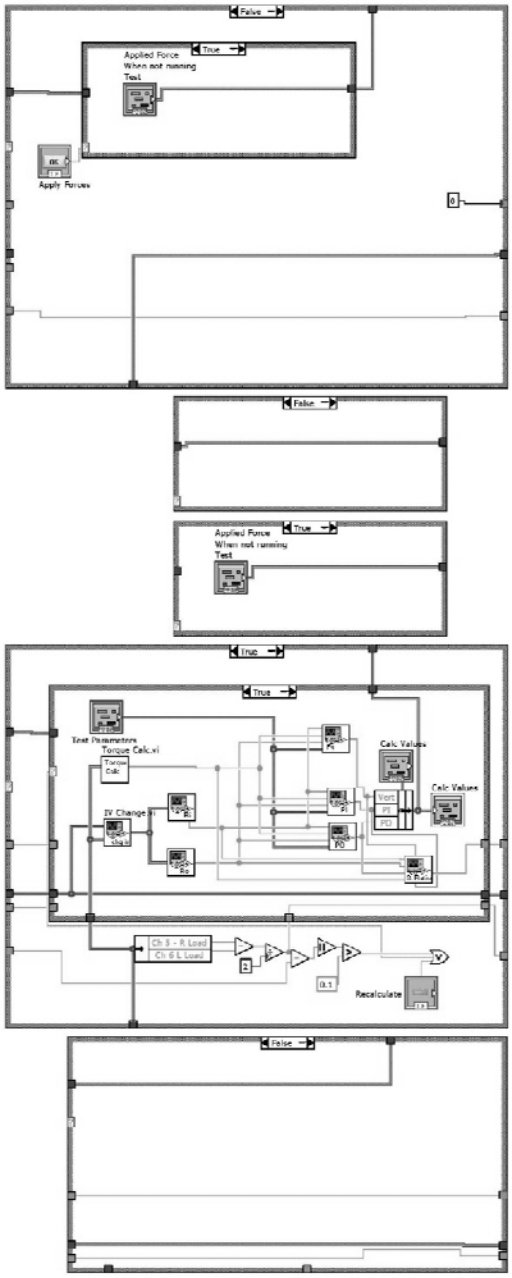

sequence.vi
C:\Program Files\National Instruments\LabVIEW 8.5\Testing Machine\sequence.vi
Last modified on 11/26/2010 at 10:42 AM
Printed on 4/15/2011 at 4:25 PM

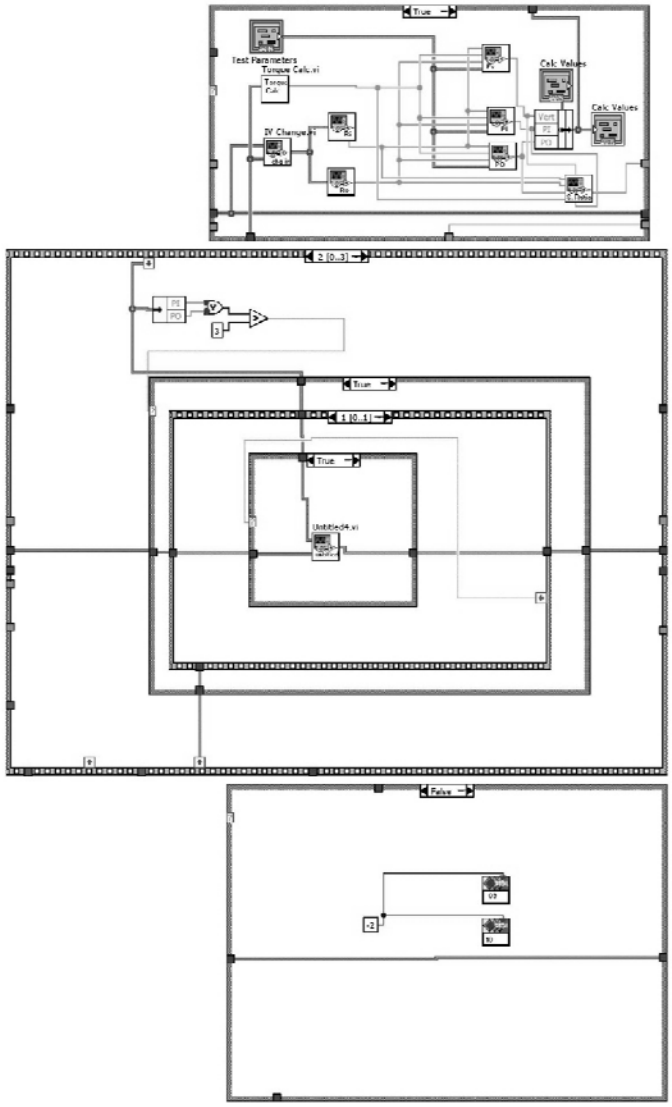

sequence.vi
C:\Program Files\National Instruments\LabVIEW 8.5\Testing Machine\sequence.vi
Last modified on 11/26/2010 at 10:42 AM
Printed on 4/15/2011 at 4:25 PM

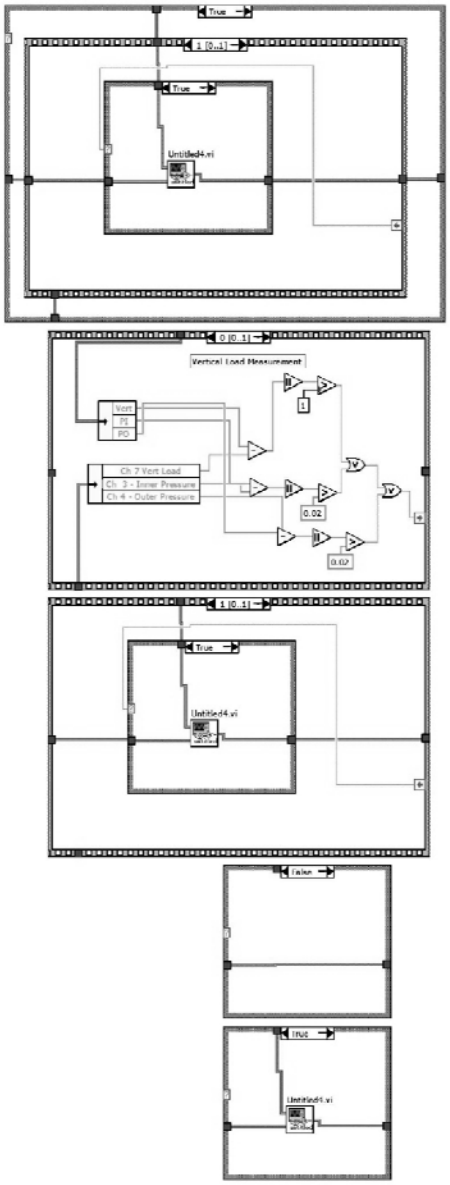

sequence.vi
C:\Program Files\National Instruments\LabVIEW 8.5\Testing Machine\sequence.vi
Last modified on 11/26/2010 at 10:42 AM
Printed on 4/15/2011 at 4:25 PM

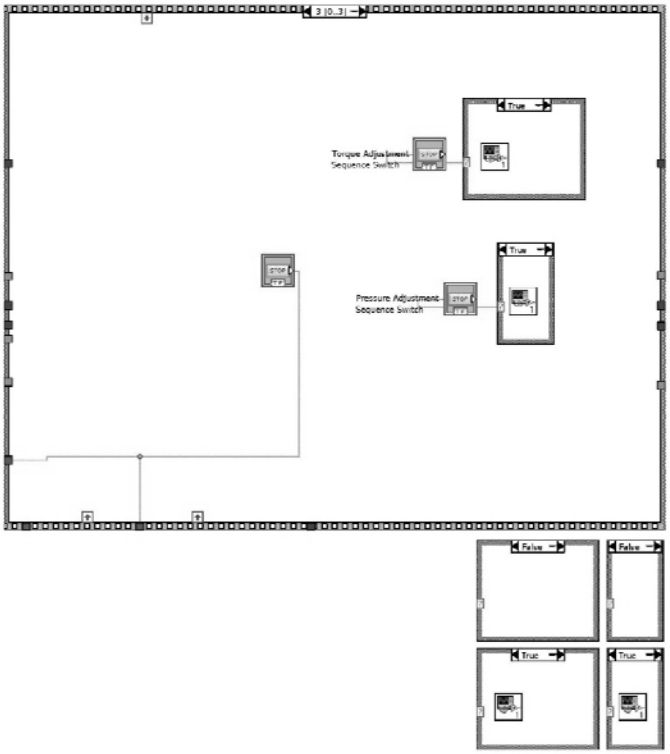

Appendix B **Inner Cell Volume Change Device and Supply Line Calibrations**

Inner Cell Volume Change Device & Supply Lines					
Calibration for Pressure Changes					
Inner Pressure	**Volume**	**Best Fit**	**Non-linearity**	**B. P. Pressure**	**Volume**
(psi)	**(ml)**	**(ml)**	**(psi)**	**(psi)**	**(ml)**
5	-1.1502	-1.1892	0.0390	5	219.06
6	-1.3902	-1.4288	0.0386	5	219.05
7	-1.6502	-1.6684	0.0182	5	219.08
8	-1.9102	-1.9080	-0.0022	5	219.05
9	-2.1902	-2.1476	-0.0426	5	219.05
10	-2.3802	-2.3872	0.0070	5	219.08
11	-2.6402	-2.6268	-0.0134	5	219.06
12	-2.9702	-2.8664	-0.1038	5	219.06
13	-3.1702	-3.1060	-0.0642	5	219.05
14	-3.4202	-3.3456	-0.0746	5	219.05
15	-3.6702	-3.5852	-0.0850	5	219.05
16	-3.8502	-3.8248	-0.0254	5	219.08
17	-4.1002	-4.0644	-0.0358	5	219.06
18	-4.3602	-4.3040	-0.0562	5	219.05
19	-4.6202	-4.5436	-0.0766	5	219.01
20	-4.8402	-4.7832	-0.0570	5	219.04
21	-5.0402	-5.0228	-0.0174	5	219.01
22	-5.2702	-5.2624	-0.0078	5	219.02
23	-5.4402	-5.5020	0.0618	5	219.05
24	-5.6702	-5.7416	0.0714	5	219.05
25	-5.9678	-5.9812	0.0134	5	219.04
26	-6.2340	-6.2208	-0.0132	5	219.05
27	-6.4801	-6.4604	-0.0197	5	219.03
28	-6.7130	-6.7000	-0.0130	5	219.06
29	-6.9501	-6.9396	-0.0105	5	219.05
30	-7.1933	-7.1792	-0.0141	5	219.05
31	-7.4492	-7.4188	-0.0304	5	219.01
32	-7.6730	-7.6584	-0.0146	5	219.02
33	-7.9342	-7.8980	-0.0362	5	219.04
34	-8.1675	-8.1376	-0.0299	5	219.04
35	-8.3230	-8.3772	0.0542	5	219.05
36	-8.6311	-8.6168	-0.0143	5	219.03
37	-8.8326	-8.8564	0.0238	5	219.05
38	-9.1524	-9.0960	-0.0564	5	219.05
39	-9.3322	-9.3356	0.0034	5	219.06
40	-9.5788	-9.5752	-0.0036	5	219.04
41	-9.8167	-9.8148	-0.0019	5	219.03
42	-10.1198	-10.0544	-0.0654	5	219.04
43	-10.3014	-10.2940	-0.0074	5	219.05
44	-10.5167	-10.5336	0.0169	5	219.06
45	-10.7789	-10.7732	-0.0057	5	219.02
46	-11.0683	-11.0128	-0.0555	5	219.01
47	-11.2700	-11.2524	-0.0176	5	219.04
48	-11.5789	-11.4920	-0.0869	5	219.06
49	-11.7298	-11.7316	0.0018	5	219.04
50	-12.0109	-11.9712	-0.0397	5	219.05

Appendix C **Calculations**

Calculation for Horizontal LVDT Accuracy in Terms of Shear Strain

Equation (C.1) was used to calculate the distance from the center of the loading piston to the mid-point of the radio cord. The groove in the measurement arm is exactly ½ of the radio cord diameter. Therefore, the midpoint of the radio cord is located at the edge of the measurement plate.

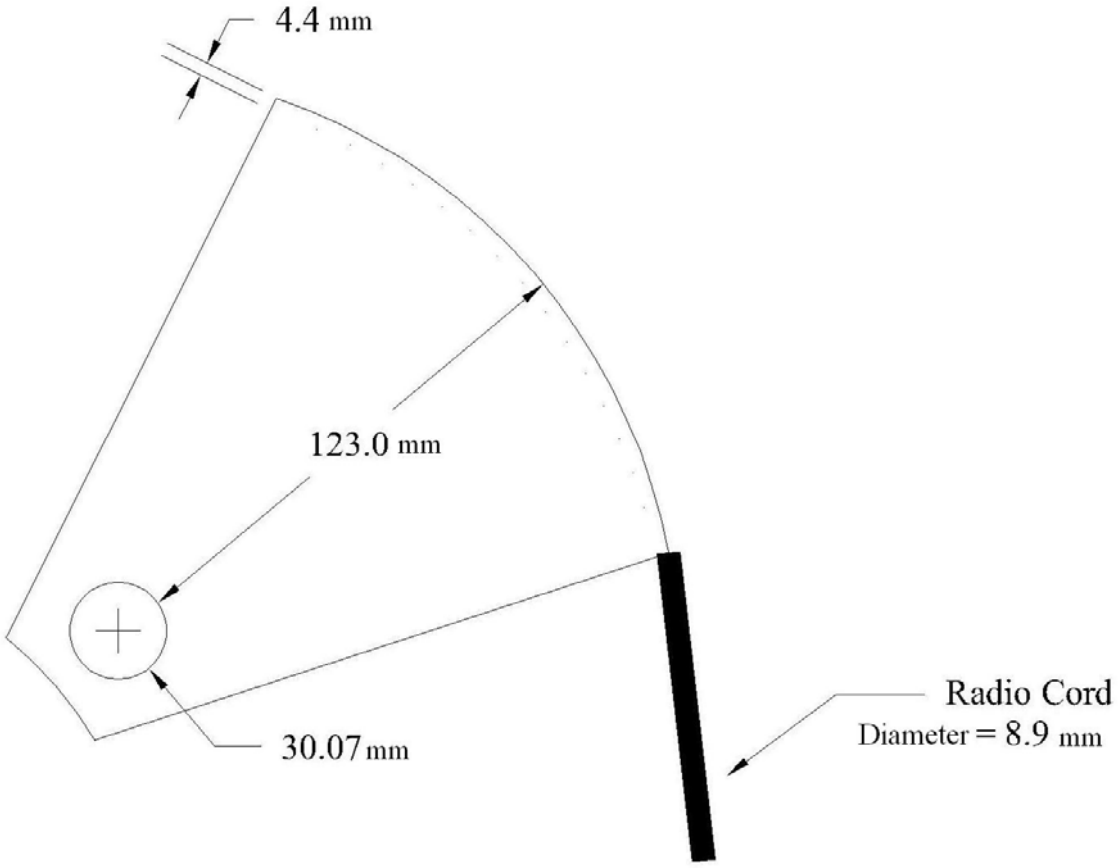

Figure C-1: Radio Cord and Pie Plate

$$d = \frac{R_h}{2} + x \quad \text{(C.1)}$$

Where:

d = distance from center of loading piston to center of radio cord (mm)

R_h = radius of loading piston hole in pie plate (mm)

x = distance from edge of hole to outside of pie plate

The horizontal movement of the measurement plate is converted to radians of rotation using Equation (C.2)

$$\Delta\theta = \frac{\Delta X}{R_p} \quad \text{(C.2)}$$

Where:

$\Delta\theta$ = change in specimen rotation (radian)

ΔX = change in horizontal LVDT measurement (mm)

R_p = radius of measurement plate (mm)

The change in rotation is converted to change in shear strain using Equation (C.3).

$$\Delta\gamma_{\theta z} = \frac{2\Delta\theta\left(R_o^3 - R_i^3\right)}{\left[3H\left(R_o^2 - R_i^2\right)100\right]} \quad \text{(C.3)}$$

Where:

$\Delta\gamma_{\theta z}$ = change in average shear strain (%)

R_o = specimen outer radius (mm)

R_i = specimen inner radius (mm)

H = specimen height (mm)

Equation (C.4) is used to calculate the average vertical strain.

$$\Delta\epsilon_z = \frac{\Delta H}{H(100)} \tag{C.4}$$

Where:

$\Delta\epsilon_z$ = change in average vertical strain (%)

H = specimen height (mm)

ΔH = change in specimen height (mm)

Calculation for LVDT Accuracy

The accuracy calculations are made using the method suggested by National Instruments.

$$e = \frac{[(a)(d) + b + c]}{d} \tag{C.5}$$

Where:

a = percent of max reading

b = offset error

c = system noise

d = input voltage (assume full scale)

e = absolute accuracy relative to input voltage

Granular Soil Parameter Calculations

The *Uniformity Coefficient* is expressed in Equation (C.6) :

$$C_u = \frac{D_{60}}{D_{10}} \tag{C.6}$$

Where:

C_u = uniformity Coefficient

D_{60} = diameter of particle corresponding to 60% finer

D_{10} = diameter of particle corresponding to 10% finer

The *Coefficient of Gradation* is expressed in Equation (C.7).

$$C_c = \frac{D_{30}^2}{(D_{60})(D_{10})} \tag{C.7}$$

Where:

C_c = coefficient of gradation

D_{30} = diameter of particle corresponding to 30% finer

Buoyant Weight of Cap Assembly, Torque Bar, ½ Torque Arm Assembly

Measured Weight

Weight of Piston, Connector, Upper Ring, and Top Cap 18.32 lbs
Weight of Piston 3.02 lbs
Weight of Inner Threaded Rod 0.51 lbs
Weight of Blue Bar 18.08 lbs
Weight of Arm Extensions, connectors, load cells, and cylinders 4.761 lbs

Length of Piston/Threaded Rod

Total Length Piston 12.0 in
Total Length Threaded Rod 14.5 in
Dry Length of Piston 8.5 in
Dry Length of Threaded Rod 11 in

Total Dry Weight Calculation

Piston

$$PW_d = \frac{P_{dl}}{P_{tl}}\left(PW_t\right) = \frac{8.5in}{12in}\left(3.02lbs\right) = 2.14lbs$$

Where:

PW_d = Dry Piston Weight
P_{dl} = Dry Piston Length
P_{tl} = Total Piston Length
PW_t = Total Piston Weight

Threaded Rod

$$PR_d = \frac{R_{dl}}{R_{tl}}\left(RW_t\right) = \frac{11.0in}{14.5in}\left(lbs\right) = 0.387lbs$$

Where:

RW_d = Dry Rod Weight
R_{dl} = Dry Rod Length
R_{tl} = Total Rod Length
RW_t = Total Rod Weight

Total Dry Weight

$$W_d = PW_d + RW_d = 2.14lbs + 0.387lbs = 2.527lbs$$

Where:

W_d = Total Dry Weight

Total Submerged Weight

$$W_s = W_t - W_d = 18.32lbs - 2.527lbs = 15.79lbs$$

Where:

W_s = Total Submerged Weight
W_t = Weight of Piston, Connector, Upper Ring, and Top Cap

<u>Buoyant Force</u>

$$F_b = \frac{W_s}{\rho_s}\rho_w = \frac{15.79lbs}{499.8pcf}\left(62.4\,pcf\right) = 1.97lbs$$

Where:

F_b = Buoyant Force
ρ_s = density of steel (499.8 pcf)
ρ_w = density of water (62.4 pcf)

Total Weight of Cap Assembly

$$WC_b = W_t - F_b = 18.32lbs - 1.97lbs = 16.35lbs$$

Where:

WC_b = Buoyant Weight of Cap Assembly

½ Weight of Torque Arms, Load Cells, Cylinders, and Assembly

$$PTA = \frac{1}{2}(TA) = \frac{1}{2}(4.761lbs) = 2.381lbs$$

Where:

PTA = Proportionate weight of Torque Arms, Load Cells, Cylinder, and Assembly
TA = Total Weight of Torque Arms, Load Cells, Cylinders, and Assembly

Buoyant Weight of Cap Assembly, Torque Bar, ½ Torque Arm Assembly

$$W_b = W_{cb} + W_{tb} + PTA = 16.35lbs + 18.08lbs + 2.38lbs = 36.81lbs$$

The adjustment value is **36.81 lbs**

$H_o = Height\ Initial = 15.9554\ in$

$H = Current\ Height = 15.8850\ in$

$(R_o)_o = Outer\ Radius\ Initial = 4.3433\ in$

$(R_i)_o = Inner\ Radius\ Initial = 3.5425\ in$

$R_o = Outer\ Radius\ Current = 4.3862\ in$

$R_i = Inner\ Radius\ Current = 3.5870\ in$

$\gamma_{z\theta} = Engineering\ Shear\ Strain = 0.01954$

$t_m = Average\ Membrane\ Thickness = 0.01875\ in$

$E_m = Membrane\ Tensile\ Modulus = 350\ psi$

$$(\varepsilon_{zm})_o = (\varepsilon_{zm})_i = \frac{H_o - H}{H_o} = \frac{15.9554 - 15.8850}{15.9554} = 0.004412$$

$$(\varepsilon_{\theta m})_o = \frac{(R_o)_o - R_o}{(R_o)_o} = \frac{4.3433 - 4.3862}{4.3433} = -0.009877$$

$$(\varepsilon_{\theta m})_i = \frac{(R_i)_o - R_i}{(R_i)_o} = \frac{3.5425 - 3.5870}{3.5425} = -0.01256$$

$$\Delta\sigma_z = -\frac{4}{3}\frac{E_m * t_m}{R_o^2 - R_i^2}[R_o\{2(\varepsilon_{zm})_o + (\varepsilon_{\theta m})_o\} + R_i\{2(\varepsilon_{zm})_i + (\varepsilon_{\theta m})_i\}]$$

$$\Delta\sigma_z = -\frac{4}{3}\frac{350 * 0.01875}{4.3862^2 - 3.5870^2}[4.3862\{2(0.004412) + (-0.009877)\} + 3.5870\{2(0.004412) + (-0.01256)\}]$$

$$= \boxed{0.02474}$$

$$\Delta\sigma_\theta = -\frac{2}{3}\frac{E_m * t_m}{R_o - R_i}[\{(\varepsilon_{zm})_o + 2(\varepsilon_{\theta m})_o\} + \{(\varepsilon_{zm})_i + 2(\varepsilon_{\theta m})_i\}]$$

$$\Delta\sigma_\theta = -\frac{2}{3}\frac{350 * 0.01875}{4.3862 - 3.5870}[\{(0.004412) + 2(-0.009877)\} + \{(0.004412) + 2(-0.01256)\}] = \boxed{0.1973}$$

$$\Delta\sigma_r = -\frac{2}{3}\frac{E_m * t_m}{R_o + R_i}[\{(\varepsilon_{zm})_o + 2(\varepsilon_{\theta m})_o\} - \{(\varepsilon_{zm})_i + 2(\varepsilon_{\theta m})_i\}]$$

$$\Delta\sigma_r = -\frac{2}{3}\frac{350 * 0.01875}{4.3862 + 3.5870}[\{(0.004412) + 2(-0.009877)\} - \{(0.004412) + 2(-0.01256)\}] = \boxed{-0.002944}$$

$$\Delta\tau_{z\theta} = -2E_m * t_m * \frac{R_o^3 + R_i^3}{(R_o^3 - R_i^3)(R_o + R_i)}$$

$$\Delta\tau_{z\theta} = -2(350) * 0.01875\frac{4.3862^3 + 3.5870^3}{(4.3862^3 - 3.5870^3)(4.3862 + 3.5870)}(0.01954) \boxed{= -0.1098}$$

Uncorrected Stress

$(\sigma_z)_o = 22.16$

$(\sigma_\theta)_o = 7.23$

$(\Delta\sigma_r)_o = 14.70$

$(\tau_{z\theta})_o = 7.45$

$$\sigma_1 = \frac{\sigma_z + \sigma_\theta}{2} + \sqrt{\left(\frac{\sigma_z - \sigma_\theta}{2}\right)^2 + \tau_{z\theta}^2} = \frac{22.16 + 7.23}{2} + \sqrt{\left(\frac{22.16 - 7.23}{2}\right)^2 + 7.45^2} = \boxed{25.24}$$

$$\sigma_3 = \frac{\sigma_z + \sigma_\theta}{2} - \sqrt{\left(\frac{\sigma_z - \sigma_\theta}{2}\right)^2 + \tau_{z\theta}^2} = \frac{22.16 + 7.23}{2} - \sqrt{\left(\frac{22.16 - 7.23}{2}\right)^2 + 7.45^2} = \boxed{4.15}$$

$$\phi = \sin^{-1}\left(\frac{\sigma_1 - \sigma_3}{\sigma_1 + \sigma_3}\right) = \sin^{-1}\left(\frac{25.24 - 4.15}{25.24 + 4.15}\right) = 45.86°$$

Membrane Corrected Stress

$$\sigma_z = (\sigma_z)_o + \Delta\sigma_z = 22.16 + 0.02474 = 22.1847$$

$$\sigma_\theta = (\sigma_\theta)_o + \Delta\sigma_\theta = 7.23 + 0.1973 = 7.4273$$

$$\tau_{z\theta} = (\tau_{z\theta})_o + \Delta\tau_{z\theta} = 7.45 + (-0.1098) = 7.3402$$

$$\sigma_1 = \frac{22.1847 + 7.4273}{2} + \sqrt{\left(\frac{22.1847 - 7.4273}{2}\right)^2 + 7.3402^2} = \boxed{25.2139}$$

$$\sigma_3 = \frac{22.1847 + 7.4273}{2} - \sqrt{\left(\frac{22.1847 - 7.4273}{2}\right)^2 + 7.3402^2} = \boxed{4.3981}$$

$$\phi = \sin^{-1}\left(\frac{\sigma_1 - \sigma_3}{\sigma_1 + \sigma_3}\right) = \sin^{-1}\left(\frac{25.2139 - 4.3981}{25.2139 + 4.3981}\right) = 44.66°$$

$$\Delta\phi° = 45.86° - 44.66° = 1.20°$$

Note: The revised friction angle for this sample calculation of 44.66° is slightly different than the 44.71° reported in the body of the text due to rounding errors. The deviation is small compared to the overall correction.

Appendix D **Stress Equations**

Equations for $\alpha = 0$ °

Definitions

Independent variable = W

Dependent variables = po, pi, ro, ri

Torsion stress space = $\sigma\theta$, σz, $\sigma\tau$

General stress space = $\sigma 1$, $\sigma 2$, $\sigma 3$

Test constants = b, σm

Derive torsion stress space in terms of variables

$$\sigma\theta = \frac{(po * ro) - (pi * ri)}{(ro - ri)}$$

$$\sigma z = \frac{W}{\Pi\left(ro^2 - ri^2\right)} + \frac{po\, ro^2 - pi\, ri^2}{ro^2 - ri^2}$$

$$\sigma\tau = \frac{(po * ro) + (pi * ri)}{(ro + ri)}$$

Derive general stress space in terms of torsion stress space

$$\sigma 1 = \frac{\sigma z + \sigma\theta}{2} + \sqrt{\left(\frac{\sigma z - \sigma\theta}{2}\right)^2}$$

$$\sigma 2 = \sigma\tau$$

$$\sigma 3 = \frac{\sigma z + \sigma\theta}{2} - \sqrt{\left(\frac{\sigma z - \sigma\theta}{2}\right)^2}$$

Define constants in terms of variables

$$\sigma m = \frac{\sigma 1 + \sigma 2 + \sigma 3}{3} = \frac{\frac{W}{\pi} + 3\left(po\, ro^2 - pi\, ri^2\right)}{3\left(ro^2 - ri^2\right)}$$

$$b = \frac{\sigma 2 - \sigma 3}{\sigma 1 - \sigma 3} = \frac{2\, ri\, ro\, (pi - po)}{\frac{W}{\pi} + ri\, ro\, (pi - po)}$$

Solve for dependent variables in terms of constants and independent variables

$$pi \to -\frac{(2b - 1)\left(W\,(ri + 3\,ro) + 3\pi\, ri\, \sigma m\left(ri^2 - ro^2\right)\right) - 3\,(ri - ro)\cos(2\alpha)\,(W + 3\pi\, ri\, \sigma m\,(ri + ro))}{3\pi\, ri\left(ri^2 - ro^2\right)(-2b + 3\cos(2\alpha) + 1)}$$

$$po \to \frac{(2b - 1)\left(W\,(3\,ri + ro) + 3\pi\, ro\, \sigma m\left(ri^2 - ro^2\right)\right) + 3\,(ri - ro)\cos(2\alpha)\,(W - 3\pi\, ro\, \sigma m\,(ri + ro))}{3\pi\, ro\left(ro^2 - ri^2\right)(-2b + 3\cos(2\alpha) + 1)}$$

Equations for $\alpha = 1\,°$ to $45\,°$

Definitions

Independent variable = T

Dependent variables = po, pi, ro, ri, W

Torsion stress space = $\sigma\theta, \sigma z, \sigma\tau$

General stress space = $\sigma 1, \sigma 2, \sigma 3$

Test constants = b, σm, α

Derive torsion stress space in terms of variables

$$\sigma\theta = \frac{(po * ro) - (pi * ri)}{(ro - ri)}$$

$$\sigma z = \frac{W}{\Pi\left(ro^2 - ri^2\right)} + \frac{po\, ro^2 - pi\, ri^2}{ro^2 - ri^2}$$

$$\sigma\tau = \frac{(po * ro) + (pi * ri)}{(ro + ri)}$$

$$\tau z\theta = \frac{3\,T}{2\,\pi\left(ro^3 - ri^3\right)}$$

Derive general stress space in terms of torsion stress space

$$\sigma 1 = \frac{\sigma\theta + \sigma z}{2} + \sqrt{\left(\frac{\sigma z - \sigma\theta}{2}\right)^2 + \tau z\theta^2}$$

$$\sigma 2 = \sigma\tau$$

$$\sigma 3 = \frac{\sigma\theta + \sigma z}{2} - \sqrt{\left(\frac{\sigma z - \sigma\theta}{2}\right)^2 + \tau z\theta^2}$$

Define constants in terms of variables

$$\sigma m = \frac{\sigma 1 + \sigma 2 + \sigma 3}{3} = -\frac{W - 3\,pi\,\pi\,ri^2 + 3\,\pi\,po\,ro^2}{3\,\pi\,ri^2 - 3\,\pi\,ro^2}$$

$$b = \frac{\sigma 2 - \sigma 3}{\sigma 1 - \sigma 3} = \frac{W + \pi\,(-pi + po)\,ri\,ro}{W + \pi\,(pi - po)\,ri\,ro}$$

$$\alpha = 1/2\,\text{ArcTan}\left[\frac{\tau z\theta}{\frac{\sigma z - \sigma\theta}{2}}\right] = \frac{1}{2}\,\text{ArcTan}\left[3\,T\,\frac{\left(ro^2 - ri^2\right)}{\left(ro^3 - ri^3\right)}\,\frac{1}{W + \pi * ri * ro(pi - po)}\right]$$

Solve for dependent variables in terms of constants and independent variables

$$W \to \frac{3\,T\,(ri + ro)\,(1 - 2\,b + 3\,\text{Cos}[2\,\alpha]\,)\,\text{Csc}[2\,\alpha]}{4\left(ri^2 + ri\,ro + ro^2\right)}$$

$$pi \to \frac{1}{4\,\pi\,ri\left(ri^3 - ro^3\right)}\,\text{Csc}[2\,\alpha]\left(-(-1 + 2\,b)\,T\,(ri + 3\,ro) + 3\,T\,(ri - ro)\,\text{Cos}[2\,\alpha] + 4\,\pi\,ri\left(ri^3 - ro^3\right)\sigma m\,\text{Sin}[2\,\alpha]\right)$$

$$po \to \frac{1}{4\,\pi\,ro\left(-ri^3 + ro^3\right)}\,\text{Csc}[2\,\alpha]\left((-1 + 2\,b)\,T\,(3\,ri + ro) + 3\,T\,(ri - ro)\,\text{Cos}[2\,\alpha] + 4\,\pi\,ro\left(-ri^3 + ro^3\right)\sigma m\,\text{Sin}[2\,\alpha]\right)$$

Equations for $\alpha = 46\,°$ to $89\,°$

Definitions

Independent variable = T

Dependent variables = po, pi, ro, ri, W

Torsion stress space = $\sigma\theta, \sigma z, \sigma\tau$

General stress space = $\sigma 1, \sigma 2, \sigma 3$

Test constants = b, σm, α

Derive torsion stress space in terms of variables

$$\sigma\theta = \frac{(po * ro) - (pi * ri)}{(ro - ri)}$$

$$\sigma z = \frac{W}{\Pi\left(ro^2 - ri^2\right)} + \frac{po\,ro^2 - pi\,ri^2}{ro^2 - ri^2}$$

$$\sigma\tau = \frac{(po * ro) + (pi * ri)}{(ro + ri)}$$

$$\tau z\theta = \frac{3\,T}{2\,\pi\left(ro^3 - ri^3\right)}$$

Derive general stress space in terms of torsion stress space

$$\sigma 1 = \frac{\sigma\theta + \sigma z}{2} + \sqrt{\left(\frac{\sigma\theta - \sigma z}{2}\right)^2 + \tau z\theta^2}$$

$$\sigma 2 = \sigma\tau$$

$$\sigma 3 = \frac{\sigma\theta + \sigma z}{2} - \sqrt{\left(\frac{\sigma\theta - \sigma z}{2}\right)^2 + \tau z\theta^2}$$

Define constants in terms of variables

$$\sigma m = \frac{\sigma 1 + \sigma 2 + \sigma 3}{3} = -\frac{W - 3\,pi\,\pi\,ri^2 + 3\,\pi\,po\,ro^2}{3\,\pi\,ri^2 - 3\,\pi\,ro^2}$$

$$b = \frac{\sigma 2 - \sigma 3}{\sigma 1 - \sigma 3} = \frac{\frac{po\,ro + pi\,ri}{ro + ri} - \left(\frac{\frac{W}{Pi} + 2\left(po\,ro^2 - pi\,ri^2\right) + ro\,ri\,(po - pi)}{2\left(ro^2 - ri^2\right)} - \left(\frac{\frac{-W}{Pi} + (po - pi)\,ri\,ro}{2\,Cos[2\,\alpha]\left(ro^2 - ri^2\right)}\right)\right)}{\frac{\frac{-W}{Pi} + ri\,ro\,(po - pi)}{Cos[2\,\alpha]\left(ro^2 - ri^2\right)}}$$

$$\alpha = 1/2\,\text{ArcTan}\left[\frac{\tau z\theta}{\frac{\sigma\theta-\sigma z}{2}}\right] = \frac{1}{2}\,\text{ArcTan}\left[\frac{3\,T\,(\text{ri}+\text{ro})}{(W+\pi\,(\text{pi}-\text{po})\,\text{ri}\,\text{ro})\left(\text{ri}^2+\text{ri}\,\text{ro}+\text{ro}^2\right)}\right]$$

Solve for dependent variables in terms of constants and independent variables

$$W \to \frac{3\,T\,(\text{ri}+\text{ro})\,(-1+2\,b+3\,\text{Cos}[2\,\alpha])\,\text{Csc}[2\,\alpha]}{4\left(\text{ri}^2+\text{ri}\,\text{ro}+\text{ro}^2\right)}$$

$$\text{pi} \to \frac{1}{4\,\pi\,\text{ri}\left(\text{ri}^3-\text{ro}^3\right)}\,\text{Csc}[2\,\alpha]\left((-1+2\,b)\,T\,(\text{ri}+3\,\text{ro})+3\,T\,(\text{ri}-\text{ro})\,\text{Cos}[2\,\alpha]+4\,\pi\,\text{ri}\left(\text{ri}^3-\text{ro}^3\right)\sigma\text{m}\,\text{Sin}[2\,\alpha]\right)$$

$$\text{po} \to \frac{1}{4\,\pi\,\text{ro}\left(-\text{ri}^3+\text{ro}^3\right)}\,\text{Csc}[2\,\alpha]\left(-(-1+2\,b)\,T\,(3\,\text{ri}+\text{ro})+3\,T\,(\text{ri}-\text{ro})\,\text{Cos}[2\,\alpha]+4\,\pi\,\text{ro}\left(-\text{ri}^3+\text{ro}^3\right)\sigma\text{m}\,\text{Sin}[2\,\alpha]\right)$$

Equations for $\alpha = 90°$

Definitions

Independent variable = W

Dependent variables = po, pi, ro, ri

Torsion stress space = $\sigma\theta, \sigma z, \sigma\tau$

General stress space = $\sigma 1, \sigma 2, \sigma 3$

Test constants = $b, \sigma m$

Derive torsion stress space in terms of variables

$$\sigma\theta = \frac{(po * ro) - (pi * ri)}{(ro - ri)}$$

$$\sigma z = \frac{W}{\Pi\left(ro^2 - ri^2\right)} + \frac{po\, ro^2 - pi\, ri^2}{ro^2 - ri^2}$$

$$\sigma\tau = \frac{(po * ro) + (pi * ri)}{(ro + ri)}$$

Derive general stress space in terms of torsion stress space

$$\sigma 1 = \frac{\sigma\theta + \sigma z}{2} + \sqrt{\left(\frac{\sigma\theta - \sigma z}{2}\right)^2}$$

$$\sigma 2 = \sigma\tau$$

$$\sigma 3 = \frac{\sigma\theta + \sigma z}{2} - \sqrt{\left(\frac{\sigma\theta - \sigma z}{2}\right)^2}$$

Define constants in terms of variables

$$\sigma m = \frac{\sigma 1 + \sigma 2 + \sigma 3}{3} = -\frac{W - 3\, pi\, \pi\, ri^2 + 3\, \pi\, po\, ro^2}{3\, \pi\, ri^2 - 3\, \pi\, ro^2}$$

$$b = \frac{\sigma 2 - \sigma 3}{\sigma 1 - \sigma 3} = \frac{W + \pi\,(-pi + po)\, ri\, ro}{W + \pi\,(pi - po)\, ri\, ro}$$

Solve for dependent variables in terms of constants and independent variables

$$pi \to \frac{W\,((1 + b)\, ri + 3\,(-1 + b)\, ro) + 3\,(1 + b)\,\pi\, ri\left(ri^2 - ro^2\right)\sigma m}{3\,(1 + b)\,\pi\, ri\left(ri^2 - ro^2\right)}$$

$$po \to \frac{-W\,(3\,(-1 + b)\, ri + (1 + b)\, ro) + 3\,(1 + b)\,\pi\, ro\left(-ri^2 + ro^2\right)\sigma m}{3\,(1 + b)\,\pi\, ro\left(-ri^2 + ro^2\right)}$$

Appendix E **Test Procedure**

E.1 PREPARE MEMBRANE

The inner and outer membranes are fabricated from a single form, and as such are connected.

- Cut outer membrane to 52 mm in length
- Cut inner membrane to 52 mm in length
- Inspect the inner and outer membranes for visible defects. If visible defects are located, paint them with latex at this time.

E.2 PREPARE DATA COLLECTION SYSTEM

- Turn on computer and data collection system. Let system warm up for ½ hour.
- Make sure that the transducer supply voltage is about 9.95 Volts. Check this on the computer program and by hand using a multi-meter if necessary.

E.3 LOCATE THE TURN TABLE BASE

- Rotate the turn table until the "A" on the bottom plate and the "A" on the turn table are aligned.
    - Hint: Rotate the table slightly past A in the negative direction and then approach A in the positive direction. This ensures zero "backlash" when the test is started.
- Turn the power supply off. Then reconnect the torque motor wires to the power supply so that red is on the + terminal and black is on the – terminal. Adjust the power supply so that black is 0 volts and red is 2 volts (the voltage will be subject to change).

E.4 CLEAR AND/OR RE-SATURATE SUPPLY LINES

- MAKE SURE THAT THE BUBBLE CHAMBER IS NOT CONNECTED
- Confirm that the outer cell O-Ring has not yet been installed.
- Clear the Inner Pressure Line from the valve on the turn table to the turn table itself of all water.
    - Set the Inner Pressure Valve on the table to drain. Using a hose with two male Foster fittings, connect the master air supply to the drain line of the Inner Pressure Valve.
    - Cover the inner cell output on the turn table with a bucket and reverse blow water through the system.

- Confirm that the inner cell supply line is saturated from the control panel to the turn table valve.

- Confirm that there are no air bubbles in behind the control panel and that no water has seeped into the dry side of the volume change device sensors.

- Using the data collection system, confirm that the inner and outer pressure sensors are both calibrated and indicate the same reading (Hint: if the water in the volume change devices is at different levels the readings will not be identical).

- **AGAIN - MAKE SURE THAT THE BUBBLE CHAMBER IS NOT HOOKED UP**

- Clear the back pressure line from the turn table to the control panel of all water.

    - Hint: Connect the master supply air line directly to the CO2 supply on the control board.

    - Turn the B. P. Output Selection valve to CO2 and then blow air all of the way through the B. P. line.

    - A second B. P. line running directly from the B. P. volume change device to the pressure sensors will stay fully saturated.

- Confirm that the de-aired water tanks are at least ¾ full.

E.5 PREPARE THE TORSION SHEAR BASE

- If necessary, use high air pressure air to clean sand out of all the bolt holes on the turn table base.

- Clean all of the sand and grease out of the O-Ring grooves. At this time, the groove under the bottom cap must be perfectly clean. However, don't worry outer cell groove too much as it will be cleaned in a later step.

- Clean off the base O-Ring, making sure that no sand grits that adheres to the ring. Check the ring for continuity to confirm that there are no breaks or cracks.

- Grease the base O-Ring with a generous amount of vacuum grease and place it in the inner bottom ring groove. Do not install the large outer cell O-Ring at this time.

E.6 INNER MEMBRANE BOTTOM RING

- Create a line two inches from the bottom edge (thick side) of the membrane. Create a second line, 1 $^{1}/_{8}$" from the first line in shorter direction, which is the bottom of the specimen. The marks should be placed on what will be the Inner Cell side of the membrane, not the side that will go against the inner form (**mandrel**).

- Be sure to liberally apply baby powder the mandrel side of the membrane (the opposite side that the marks were made on.

- Place a small piece of duct tape over the gap in the top of the mandrel at the 1" wide permanently attached strip (it should already be there).

- Pull inside membrane over the mandrel and leave 2" free on the bottom (smooth side of membrane facing out). The bottom is the end of the mandrel that does not have a 1"thick attachment. It should also be ¾" over the top of the mandrel.

- Pull the membrane from the top of the mandrel to the bottom of the mandrel. This means gripping the thick end of the membrane.

- Fold the thin side of the membrane down over the mandrel so that when it is turned upside down the edge of the membrane is not cut by the mandrel. Obviously this will have to be pulled up at a later time.

- Clean the non-mandrel side of the membrane using a wet sponge to remove any baby powder than may have migrated to that side of the form.

- If not already done, loosen the bottom inner set screw inside the mandrel.

- With the bottom ring placed right side up on the table squeeze the mandrel and membrane together and set it into the bottom ring, until the 2" marks are even with the top of the bottom ring.

- Make sure the mandrel is as plumb as possible and tighten the set screw inside the mandrel and turn the assembly upside down

- Place the bottom-ring inner O-ring into its groove.

- Pull the 2" portion of the inside membrane over the fastening lip and clip into place using about 4 small binder clips for temporary fastening. Just pull the membrane so that the bottom of the membrane is about 1/8" longer than touching the surface of the ring. Make sure to put a piece of paper underneath the clips so that the membrane is not pinched.

- Work the membrane underneath the O-Ring by extending the O-ring with a

tool which will not pinch the membrane (a dull edge screwdriver can work).

- Pull the membrane by hand through the gap made by slightly extending the O-Ring
- Release the O-Ring so that it returns to the groove and replace the binder clip.
- Keep performing this pattern until the O-ring is completely securing the liner in by using the groove
- Insert the free 1" wide mandrel extension into the membrane sitting adjacent the bottom of the large mandrel.
- Insert the greased O-Ring on the turn table if it hasn't been done already.
- Place the mandrel / membrane / bottom ring assembly in its correct place on top of the turn table. Be careful during placement to get the bolts line up with the holes.
- Double check O-ring continuity where visible and screw down the ring with bolts using a 5mm Allen wrench.
- Loosen the bottom mandrel set screw, so that the mandrel is free to move.
- Looking at the inside of the mandrel, squeeze the top together so that it is perfectly flush, then batten down the top mandrel latch so that the mandrel does not change size at the top.
- Temporarily set the outer form in place.
- Pull the inner membrane down slightly from the top of the mandrel and put the upper ring around the inner mandrel and make sure that if fits inside the outer form ensuring perfect alignment.
- Confirm that the inner mandrel is perfectly parallel to the out mandrel and extend the bottom inner mandrel screws to keep the mandrel in the perfect position.
- Remove the outer form.
- Fold the membrane up over the top of the mandrel.
- Measure the top and bottom of the inner form using a 50-300 mm PI tape and record the measurements on the test datasheet.
- Using a 12 mm wrench connect the bottom fill/drain line to the bottom ring.

E.7 OUTER MEMBRANE BOTTOM RING

- Pull the outer membrane down over the mandrel and base ring. Make sure the thin side of the membrane is down and the smooth side of the membrane is facing to the inside of the specimen.

- Place the O-Ring over the bottom ring outer O-Ring groove.

- Clip the outer membrane to the top of the mandrel so that the membrane touches the surface of the metal ring, but no further (excess membrane can cause problems at later times).

- Work the membrane underneath the O-Ring. It is best to have two people for this so that one can pin the O-Ring to keep it from popping off. However, it is really not all that difficult with only one person.

- Disconnect the vacuum lines that join the outer forming jacket, so that the two halves of the forming jacket are not together.

- Position four short spacing blocks on top of the outer ring. Keep the blocks on one half of the base, because they will support half of the outer forming jacket.

- Pull the outer membrane upward until it is taught and reclip it to the inner mandrel using the small binder clips.

- Put two small daps of grease on the bottom corners of the forming jacket to keep the membrane from being pinched when putting together the forming jacket. Place one half of the forming jacket on top of the spacing blocks and around the bottom ring. Be very careful not to pinch the membrane between the forming jacket and the ring. This can shear the membrane.

- Put two small daps of grease on the bottom of the other half of the form. Place the remaining 3 spacer blocks on the outer ring, and slide the second half of the forming jacket together.

- Bolt the two halves together. Tighten the bolts tightly so that no air can move between the two halves of the form, but do not lift the form as you tighten the bolts.

- Reconnect the vacuum lines, to the control board forming jacket output.

- If possible remove the binder clips and pull the outer membrane over the forming jacket. With two people, each pull both sides of the membrane over the top part of the membrane. When doing so, make sure there are no big folds when pulling it over.

- Visually inspect the outer membrane at the O-ring seal to ensure that an air tight seal has been formed.

- Set the deaired water tank control board to the directions for "Dispensing Air".

- Turn vacuum on, control board should read:

    - Vacuum = on
    - Water = off
    - Tank = hold/tank vac

- Keep the control panel output for the forming jacket on off. Wait for the vacuum to pull 20 inches of mercury and then set the control panel valve on.

- Using a flashlight inspect the outer forming jacket within the mold to make sure that there are no flaps or extra membrane folds. If they are observed, work them out by pulling the membrane up gradually without letting all of the air out.

E.8 PLUVIATE SAND SPECIMEN

- Dispense **8,840** grams of sand into two stainless steel vessels.

    - The best way to do this is to start with three bowls. Place one empty bowl on the scale and hit the tare button. Fill the other two bowls with sand that has been run through a No. 20 sieve. Transfer the sand into the bowl on the scale until you have about 4400 grams total in the bowl.

    - Calculate the amount needed in the second bowl. Place the second empty bowl on the scale and press tare. Pour the sand from the third bowl into the second so that you have a total of **8,840** grams between the two bowls.

- Place the temporary inner cardboard *spill protection form* inside the inner mandrel. Lightly secure the form to the inner membrane with tape. This will prevent sand from falling into the inner cell during pluviation.

- Place the short temporary outer form on top of the outer membrane/forming jacket.

- Pull the funnel and drop tube out of its hiding place in the ceiling.

- Bind the soft portion of the fill tube so that sand cannot freely flow through the tube when the funnel is filled. Usually use a piece of duck tape to put a

kink in the tube. The duct tape should be easily removable when the time comes for filling.

- Check opening of tube to ensure nothing is stuck on behind the wires. Also check the tube to funnel connections (duct tape) to make sure it does not break during pluviation.

- Fill the funnel hopper with both stainless steel containers of sand.

- A 35 cm fall height should be maintained by using the attached stick as a sort of "story board".

- The filling operator should hold the filling tube in one hand and the small pen flashlight in the other hand so that they can see the soil at the bottom of the form.

- As the funnel rises to an elevation higher than the temporary forms, use the paper guard tube on the aluminum pouring tube to prevent sand from falling onto the turn table or inner cell.

- When the funnel hopper is empty about the right amount of sand will have been placed in the form. **NOTE: It is best to raise the funnel in TWO click increments using the winch on the wall.**

E.9 DETERMINE WEIGHT OF SAND IN SPECIMEN

- Clean a stainless steel pan and take the tare weight.

- Carefully tap the filling tube and funnel while holding over the stainless steel pan to remove and stray grains of sand left behind in the filling tube.

- If necessary, take the funnel down from the ceiling and turn it upside down over the stainless steel bowl to catch any remaining grains that did not come down in the funnel. Set the bowl off to the side in a safe place.

- Attach the small glass vacuum chamber that has been constructed from a chemistry beaker to the non-oil based vacuum located under the desk in the center of the room.

- While the extension forms are still in place, vacuum out soil in the high areas so that sand doesn't spill onto the base when the extension forms are removed.

- Remove the extension forms.

- Fill in the low areas with sand that has been collected in the vacuum beaker.

- Level the sand using a small piece of cardboard, so that it is evenly distributed

about 1/2mm above the top of the outer jacket. Keeping it ½ mm high is **very** important.

- Vacuum all remaining sand on the base or in the middle of the base into a beaker. Pour the beaker sand contents into the steel pan that was used when cleaning out the funnel. Weigh and record the volume of sand and subtract from the initial volume to arrive at the total amount of sand used for the experiment.

E.10 GLUE TOP RING

- Inspect the top ring to make sure that no old sand grains were sticking to the face. Especially the inner and outer edge, because sand grains in this location will make it very difficult to place the ring over the form.

- Mix the two part epoxy (Devcon 2-Ton Clear) on a piece of cardboard and spread the epoxy liberally over the base of the upper ring. Be careful not to let the epoxy cover or touch the drain stones. Also try not to put on so much epoxy that it squeezes out the sides when place on the sand. This will lead to gluing the membrane to the top ring making it difficult to take apart after the test.

- Spread a thin line of vacuum grease around the inner bottom edge of the ring so that it slides easily over the inner mandrel during installation and does not pinch the inner membrane.

- Position the top ring so that a single bolt hole lines up with the front of the specimen. This will help when positioning the piston.

- Slide the top ring over the inner mandrel, moving it very slightly back and forth to spread the grease and make sure it isn't bunching or pinching the inner membrane.

- Put a level on top of the ring to make sure it is perfectly level, push it down in areas that it may be high and vacuum the excess sand that squeezes out on top of the form.

E.11 ATTACH THE INNER AND OUTER MEMBRANE

- While maintaining the outer forming jacket vacuum, stretch an O-ring over top ring inner groove. Incrementally, work the membrane underneath the O-Ring. This can be accomplished by using clips to hold the O-Ring in place and then stretching the O-Ring using a dull screwdriver so that space is created for working the membrane in place (Hint: it is best to start at the brass connection and work your way out).

- While keeping the outer forming jacket vacuum on, pull the outer membrane

over the outer lip and stretch the top ring outer O-Ring over the outer groove.

E.12 PULL BACK PRESSURE VACUUM ON SPECIMEN

- Set the control panel B. P. Output to “off”.
- Verify that there is about 2-inches of water in the bubble chamber.
- Connect the bubble chamber. Connect the higher of the two lines in the bottle to the B. P. output and connect the lower of the two lines in the bottle to the B. P. supply line.
- Connect the B. P. line to the specimen cap and ensure that all lines, including the lines to the cap are connected and tight (the tree and lines should be connected at this time.
- Make sure the top cap drain line valve is closed.
- Turn the vacuum gage indicator from forming jacket to specimen.
- Adjust the pressure regulator for the specimen to 7 psi.
- Set the control panel B. P. selection valve to read “vacuum”.
- Set the control panel B. P. output valve to “on”.
- Make sure the vacuum pressure appears stable.
- Gradually decrease the forming jacket vacuum and use the gauge indicator to verify that the specimen has 7 psi of vacuum and all vacuum has been removed from the forming jacket.
- Turn the forming jacket output to off.
- Disassemble and remove the outer form
- Remove the inner form. This step will require loosening the set screws inside the form. It is also noteworthy that the inner form should be at it’s smallest circumference during removal. This is most easily accomplished by pinching the form together by using a regular pliers to apply pressure to the set screw flanges.
- Measure specimen the top and bottom diameters with a PI Tape and record in the test booklet.
- If there are bubbles in the bubble chamber apply latex paint to the specimen until the bubbling stops.

E.13 DRAW LINES

- **Note:** Do not use the flat side of the ruler to draw lines, it will stick to the membrane and pull the membrane slightly off of the specimen when the ruler is removed.

- Make sure the top ring is clear of any latex epoxy.

- Using a ball point pen, create a horizontal line about 1/3 of the way around the circumference at bottom of the specimen (should be right at the specimen bottom ring interface). Make vertical "tick" marks at 2.5 cm on center over the length of the line.

- Extend the first, last, and middle tick marks vertically to the top ring using a level.

- Place horizontal "tick" marks over the length of each vertical line at 2.5 cm on center.

- Using a strip of heavy duty construction paper, extend horizontal lines from tick to tick. Be very careful not to let the construction paper bulge in the middle, take your time.

- Draw a horizontal line at the interface between the specimen and the top cap. Create ticks at 2.5 cm on center. The fist, middle, and last ticks will coincide with the vertical lines that have already been drawn.

- Connect the tick lines from the bottom and top horizontal lines.

- Take a picture of the specimen

- Measure the height of the specimen in at least three different locations. Record these heights in the test booklet.

- Fold down the inner and outer cell excess membranes to prepare for when putting on the top cap.

E.14 SATURATE THE INNER CELL

- Grease the O-Ring and place it in the top of the torque cap. **Make absolutely sure that no grease gets into the vent holes on the top cap.**

- Inspect the upper side of the top ring to make sure that there are no obstructions or latex that will prevent a tight seal between the top cap and top ring.

- Place the top cap on the top ring.

- Insert the top cap screws (4x) using a 5 mm Allen wrench.
- Visually inspect the seal to verify that the top cap is perfectly clamped down.
- Fold the outer membrane over the top cap so that the entire specimen is visible. If needed, use tape to hold the outer membrane in place. Finish drawing any extensions to lines that have not been drawn.
- Make sure the "Inner Cell" valve located on the table is set to "hold".
- Make sure the de-aired water panel board in the back room is set to tank bleed.
- Set the de-aired water supply valve to "on". This will connect the water supply to the panel board.
- Make sure that the inner volume change device on the main panel is set to "off" and that the pressure selection on the main panel is set to "low" (for the inner cell).
- Turn the master supply on the CO2 bottle on while keeping the 3-way Swagelok valve closed.
- Make sure the 4 green toggle valves on the top cap are open.
- Place the CO2 bottle supply "pig tail" in a shallow bowl of water and slowly open the 3 way valve until a small amount of CO2 bubbles are seen.
- Remove the pig tail from the bowl of water and connect it to the "Inner Cell" drain line on the turn table.
- Set the Inner Cell valve on the table to "drain/CO2" and listen to the upper green valves to make sure that you can hear a CO2 hissing sound.
- Wait 10 minutes for the air in the inner cell to become completely replaced by CO2. While waiting the 10 minutes:
    - Clean out the bottom groove on the turn table. Make sure that there are no sand grains in the groove at all. Grease the bottom O-Ring and install in the groove.
    - Clean sand off of the bottom of the cylinder.
    - Insert the long threaded rods into the holes on the turn-table. Be sure to leave the long thread portion facing upward. Use an 11/16" wrench to tighten the bottom of the rods snugly into the turn-table.

- Place the large diameter cylinder around the specimen taking care to make sure the up end is pointing up and the "A" arrow lines up with the "A" on the turntable.

- Clean sand off of the top of the cylinder.

- Clean the groove out of the top cap groove. Grease the O-Ring and install in the top lid groove.

- Set the control panel Inner Cell Output to "On".

- Switch the Inner Cell valve on the table from drain/CO2 to Fill. Keep it all the way open for about 3:15 minutes and then move the valve on the table to the mark. If this valve is too open the pressure that it puts on the main specimen will deform the specimen, so be very careful. The water should start to come out at about 3:45 minutes.

- When water begins to come out of the green toggles close the pressure selection valve on the panel immediately. Open the valve very slowly until water just barely drips out of the green toggles.

- Close three toggles, starting with the one that drips the most water.

- Set the Inner Cell Pressure Selection valve on the control panel to "Off" close the 4th toggle and Set the Inner Cell Volume to full "Fill" on the table.

- Fold the outer membrane back up.

E.15 SATURATE THE OUTER CELL

- De-aired water should have been made prior to the start of this set of procedures, but go to the back room to verify an adequate supply at this time. The level should be at least ¾ full.

- Ensure that the piston sheath has been disconnected from the threaded rod that runs up the center of the piston sheath. Carefully place the cell cap over the glass cylinder. Set the cap on top of the cylinder taking care to line up the "A" markings. Do not disturb the threaded rod attached to the top of the top cap.

- Visually inspect the underside of the top lid to ensure that it has been set properly. The O-ring should not be easily visible and should not be possible to touch the bottom O-ring. An improperly placed cell cap will result in an outer cell leak.

- Thread the nuts on the ends of the pressure cell tie rods. Tighten them by hand in a star shaped pattern, so that the lid comes down with even pressure

on top of the O-Ring. Do not use a wrench to tighten these nuts, hand pressure is more than sufficient.

- Open the pressure relief valves on top of the lid using a needle-nose pliers.
- Set the Control Board Outer Cell Pressure Selection valve to "Low".
- Ensure that the de-aired water production has stopped and set the Outer Cell Output Selection on the Control Board to "On". Set the Outer Cell 3-Way valve on the table panel to about 1/4 "Fill". Adjust the flow so that it's fast, but no so fast that air gets drawn into the fill lines from the de-aired water tank. It should take about 15 minutes to fill. During this time complete the following activities:
    - Watch the De-aired Water Supply in the back room carefully to make sure that it does not run out of de-aired water during outer cell filling. If the water level reaches the top of the 4-way brass connector shut off the flow to the specimen at the table, and then the main water supply on the wall and make more de-aired water.
    - Lightly grease the piston sheath (use vacuum grease) and insert it through the top cover. By hand, thread a nut on the end of threaded rod. The extruding part of the threaded rod should be almost exactly between ⅜" and ½" inches in length. If it is shorter the piston has not been set correctly in the top of the cap.
    - While holding the top of the piston sheath from rotating with a crescent wrench, use a 17 MM wrench to tighten the nut attached to the threaded rod.
    - Raise the vertical load cylinder by applying pressure to the lower pressure regulator.
    - Connect the blue frame to the base using the 5 mm long socket Allen wrench and ratchet. The following connection sequence is recommended.
        - **MANDATORY** Loosen the bottom back horizontal stability rod using two 11/16" wrenches before starting this procedure.
        - Grease the sides of the frame so that it slides easily and check to make sure the piston is out of the way.
        - Put a single bolt in the back left middle hole. Sink the bolt flush but do not tighten the bolt completely.

- Put a single bolt in the front left middle hole. **Do not screw in the bolt until the frame has been fixed. Right now it's cross threaded. For now, bolt in the left front and sink it but to not tighten completely.**
- While pressing the right side wall forward, put a single bolt in the front right middle hole. Sink the bolt but do not tighten the bolt completely.
- While pressing the right side wall forward, put a single bolt in the back right middle hole. Sink the bolt but do not tighten completely.
- Put all the remaining bolts in the holes.
- Tighten all bolts.
- Tighten the bottom back horizontal stability bar with two 11/16" wrenches if they were loosened in the first procedure.

- When water flows from the top cap vents, shut off the pressure selection for the outer cell on the control panel.
- Close the valves on the top cap with needle nose pliers.
- Turn the outer cell on the table to "full fill".

E.16 APPLY INNER AND OUTER PRESSURE TO THE SPECIMEN

- Confirm that the Inner and Outer 3-way valves read "Fill" on the turn table.
- Set the bubble chamber bottle on its side, so that no water goes in or out. Be very careful with the top of the bottle so that the top doesn't come off.
- Set the volume change device on the control panel for the inner and outer to empty.
- Set the pressure selection for the inner and outer to high.
- Set the output selection on the control panel for the inner and outer to on.
- Make sure that the air is hooked up to the control panel.
- Set the Inner and Outer Cell 3-Way valves on the table control to "Hold"
- For the inner and outer cell set the Manual Override to "Auto" and the Auto

Valve to “On”. Start the computer program making sure that no pressure is being applied to the system.

  - To start the computer program, open the sequence.vi file and press the start/stop readings ok button.

- Make sure that the inner and outer pressures are each at 0 psi.

- Set the inner and outer pressure to 3.5 psi each using the computer, remember to set the vertical load to 999. After confirming that the pressure is 3.5 psi on each, simultaneously open the table panel 3-way valves to read “Fill”.

- Adjust the vacuum downward to read 4 psi on the control panel board.

- In 1 psi increments, move the pressure to 7 psi using the computer. Each time you raise the psi on the inner and outer cells you decrease the vacuum on the specimen.

- Shut down the vacuum in the back room.

- Adjust Inner and Outer volume devices

  - Lock off inner and outer on the control panel output and table, simultaneously.

  - Set Inner and Outer output to off on Control Board

  - Flip Inner and Outer override to Manual

  - Adjust water level

  - Set inner and outer to empty

  - Flip Inner and Outer back to Auto

  - Set Output Inner and Outer to Open

  - Confirm 7 psi on the computer for both the Inner and Outer

  - Set Control table for the Inner and Outer to Fill simultaneously

E.17 SATURATE THE SPECIMEN

- Disconnect B.P. line running to the specimen at the control board. Remove the bubble chamber. Reconnect the B. P. line to the control board.

- Set the control panel B. P. Output to “off”.

- Connect the CO_2 bottle to the bottom of the control panel at the Foster Fitting.
- Set the control panel B.P. Selection valve to "CO_2".
- Connect a small pig-tail line to the output of the CO_2 on the turn table and run the pig-tail through a glass of water. **Open the upper drain valve** connected to the pigtail.
- Set the control panel B. P. Output to "on" and slowly open the CO_2 Swagelok valve until the bubbles run through the water very slowly.
- Let the CO_2 saturate the specimen for 15 minutes.
- Turn the control panel B.P. Output valve to "off".
- Turn the control panel B.P. Selection valve to "H20 Low"
- Open the control panel valve marked B.P. output. The pig-tail bubble chamber on the table should bubble slowly. Wait about 15 minutes
- Close the Swagelok valve and the main valve on the CO_2 canister and disconnect the CO_2 supply line.
- When water begins to come out of the pigtail, turn the B. P. Output on the control panel to "Off", then turn the pigtail valve to the pressure sensor.
- Turn the B. P. selection to "High Pressure."

E.18 APPLYING INITIAL BACK PRESSURE TEST SATURATION OF SPECIMEN

- Turn B. P. Selection valve from Low to High and put 7 psi back pressure on the specimen. This must be done very slowly so that the computer can catch up (at 1 psi increments with the B. P. manual regulator). Wait for the CO2 bubbles to disappear.
- Open and watch the temporary pressure subroutine (untitled 4.vi). Make sure to change the B. P. only while the program is within this subroutine.
- Let specimen sit overnight, or for a minimum of 2 hour.

E.19 TEST SATURATION OF SPECIMEN

- Set the control panel B. P. output to "off"
- Record the Inner and Outer Pressure on the computer and zero the B. P. on the stand alone transducer.
- Set the Inner and Outer Pressure to 12 psi and click OK

- Record Inner and Outer Pressure and B. P.
- Set Inner and Outer Pressure to 7 psi and click OK.
- Set the control panel B. P. Output to “on”.
- Close the valve going to the pressure transducer.

E.20 RESUME CONNECT INSTRUMENTATION

- After confirming everything is in equilibrium close the control panel B. P. Output valve.
- Place the blue angle measurement collar over the piston on the left side with the silver face up on the left front hand side. A 3/32” Allen wrench should be used to tighten the blue angle.
- Using a 6mm Allen wrench, loosen the diamond shaped insert contained in the torque bar that keeps the piston from rotating. A reasonable amount of “play” must be maintained in this joint.
- Lift the torque arm bar and short portion of the torque arms over the piston assembly with the open side facing out. Tighten the diamond shaped insert using a 6 mm Allen wrench.
- If necessary, rotate the base until the torque bar is equal distance from the back plate on both sides. Measurement from the back plate to the front of the torque bar should be 47.4 cm. (Try not to rotate by using the double threaded bolts. Different lengths are available).
- Step up onto the table and walk around to the back of the specimen. Make sure you have the two torque measurement arms and the cap screws that attach the arms to the back slide plate.
- Carefully attach the left and right torque arms to the torque bar using the two way threads. Use a long connector for the right side and a short connector for the left side. Extend or contract the threads until the vertical holes in the back plate line up perfectly with the torque arms. Adjust the direction so that it is perfectly in-line. Place the bolts though the holes and tighten them. A 1/2” wrench and 6mm Allen wrench can be used to attach the bolts. Make them very tight so that the pivot will not move.
- The vertical pressure cylinder should be fully retracted
- Place the piston adaptor on the piston threaded rod
- Slide the vertical LVDT over the piston adaptor, rotate the assembly until the

Vertical LVDT rod lines up the start mark which is drawn on the lid of the cell

- With the text facing up, rotate the load cell on the piston adaptor
- Connect the load cell cable
- If the vertical piston is not perfectly lined up with the load cell use this procedure:
    - Make sure the collar adaptor is turned all the way to the right
    - Release all the pressure off of the lower and upper vertical load regulators
    - Unscrew the top bolds of the pneumatic cylinder with a crescent wrench.
    - Take the top off the pneumatic cylinder
    - The piston should drop into place. If not, move the cylinder up and down to get it to the right location.
    - Once the load cell is lined up with the piston, connect the load cell to the piston by turning the collar adapter.
    - Place the top back on the pneumatic cylinder and with the crescent wrench, tighten the bolts.
- If the vertical load piston is perfectly lined up with the load cell use this procedure:
    - Make sure the collar adaptor is turned all the way to the right
    - Release all the pressure off of the lower and upper vertical load regulators
    - Disconnect both the upper and lower vertical load lines at the control board
    - The piston should drop into place
    - Once the load cell is lined up with the piston, connect the load cell to the piston by turning the collar adapter.
    - Reconnect both the upper and lower vertical load lines.
- Connect the tall threaded rod to where the A is located (to the front right hand

side). The horizontal tubular bar should extend to the left and the bottom edge of the bar should be about 125 mm above the top surface of the top cap plate.

- Move the pie shaped plate about the piston until it lines up vertically with the horizontal LVDT. Make sure the LVDT is tangent with the far side of the pie shaped plate, the side that should have the small screw. This should be about 185mm from the top surface of the top plate.

- Make sure all of the LVDT bolts and screws are tight. The angle adjustment bolt and nut are tightened with a large regular drive screwdriver and a 7/16" box end wrench.

- Make sure the valves on the top of the plate do not hit the vertical LVDT.

- Insert the horizontal LVDT core and connect the string/weight set up to the end of the rod.

- Connect the other string end to the other end of the core and pass the free end of the string through the hole on the triangular blue plate.

- Set the horizontal LVDT so that it reads about -1.75.

- Insert the vertical LVDT rod.

- Set the vertical LVDT to 0.75 (for compression) or -0.75 (for extension)

- For 45 degree tests set it to about 0 in

TAKE READING SET NO 1. Record all readings.

- Set the vertical load indicator to lower.

- Apply 1.5 psi lower pressure until the computer vertical load is at +40 lbs.

- Then turn manual override for the vertical load to auto

- Set the Auto valve to on.

- On the computer program, change the vertical load from 999 to +40lbs (click the OK button). Then slowly adjust the lower regulator until you get to 4psi (for different tests, the load will have to be calculated, around 30 psi for extension tests has been used) while letting the computer try to keep the load at 20 pounds. Make sure that the load never goes to negative and is always inside the vertical load subroutine. If the temp load gets close to 20, do not keep increasing the pressure.

- Set the vertical pressure to 20 lbs, click OK, and wait until it stabilizes on the

computer. Then set the load to 10 lbs, let it stabilize, then 5 lbs let it stabilize, then set the vertical load to 2 lbs and wait until it stabilizes.

TAKE READING SET NO 2..

- Open the B. P. output and let B. P. volume stabilize. Turn the B. P. volume device to empty.

TAKE READING SET NO 3.

E.21 ISOTROPIC CONSOLIDATION:

- Make sure that 14.7 psi back pressure is on the specimen. To do this, the subroutine must be outside of the vertical load subroutine. Once the program is not in the vertical load subroutine, manually change the back pressure on the control board by one psi. When it's at about 6.8 on the inner and outer pressures, increment. Do this up to 14.7 psi while watching untitled 4.

- Click Record On. Wait to input test name.

E.22 TAKE READING SET NO. 4 – INITIAL READING

- Increase Inner and Outer Pressure by one increment. Click Ok. Wait for Untitled 4 subroutine to stabilize. Record values.

- Repeat increments until 14.7 psi pressure is reached for inner and outer pressures.

- Check the inner and outer volume cylinders on the control panel to make sure that they are not too high/low.

- If too high/low:

    - For Inner and Outer:

        - Turn output to off.

        - Turn Manual override to Manual

        - Turn Vol device to Fill/Empty until desired amount is reached

        - Make sure Vol Device is on Fill

        - Set manual override to Auto

        - Turn output back to On.

- For B. P.:
    - Turn B. P. output to off
    - Volume device to Empty/Fill to desired level
    - Set back to Empty
    - Open B. P. Output

E.23 CONNECTING TORQUE LOAD CELLS.

- Depress the torque sequence adjustment button on the *Sequence* program's front panel.
- Go to the block diagram of the sequence.vi program and find the torque sequence adjustment vi. Open the program.
- Adjust the torque readings so that the right reads +1 and the left reads -1. This can be done manually or using a 10mm wrench.
- Once set, make sure to stop the program. Close the program and return to the front panel.
- Set the vertical load to zero.

TAKE READING SET NO 5.

E.24 RUNNING THE TEST

- Set load increment, alpha and b to desired value
- Click Start Test button
- Click start on the stop watch to have a second method to confirm test time.
- Find the rotational bench-top power supply. With the output off, plug in the cables, red to red, black to black, and turn the voltage on. Start at 0.6 V. Monitor the torque arms to make sure that they are level as well as the water levels of the volume change devices.
- Take intermittent recordings by hand.
- During the test, monitor the current readings displayed on the bench-top power supply. Ensure that it is fluctuating and not displaying a static value. A static value is an indication that the turn table has stopped turning. If this happens, a slight increase in voltage may be necessary to restart the table. Record any changes made to the voltage.

- Check volume device cylinders to ensure they are not too high/low. If so, fill/empty according to process described in isotropic consolidation.

- As specimen is approaching failure, note the time of any shear bands or changes to the specimen.

- At failure, quickly lock off both inner and outer valves at the table.

- Shut down the torsion power supply.

- Lock off the control panel B. P. output and vertical cylinder upper and lower pressure outputs at the control panel.

- On the *Sequence* front panel, change the Automatic Off button to "off" and the Record button to "off".

- Set the *Sequence* program, outer and vertical load to 0, 0, and 999, and click ok.

- Click the vertical load release button on the front panel of the *Sequence* program.

- Click "stop" on the "start/stop readings" button on the front panel of the *Sequence* program.

- Close all computer programs.

- Remove the manual applied lower vertical load and switch both of the vertical load output valves back to on.

E.25 TAKING SPECIMEN APART

- Hook up the bubble chamber.

    - Disconnect the B. P. line.

    - Connect the short end of the bubble chamber to the specimen and the long end to the control panel.

- Start the vacuum pump in the back room.

- Remove the back pressure from the specimen with the manual regulator.

- Apply 7 psi vacuum pressure to the specimen with the manual regulator. The vacuum gauge indicator should be set to specimen.

- Set the control panel B. P. selection valve to Vacuum.

- Set the control panel B. P. output valve to “on”.
- Set the outer and inner output volume devices to off on the control panel.
- Place a bucket under the outer cell drain tube.
- Remove the foster fitting located under the table.
- Set the outer cell to drain on the table.
- Open the top cap vents.
- While water is draining, disconnect the instrumentation.
- Disassemble the blue frame by taking apart the bolts. Before removing the bolts, loosen the horizontal stabilizing bar in the back of the blue frame. Once all the bolts have been removed, push back the blue frame.
- **DO NOT** remove the tie rod nuts holding the cell cap until all of the outer cell water has drained.
- Remove the piston.
- Remove the cell cap.
- Set the inner cell to drain and open the green toggles on the top cap.
- While the water drains from the inner cell, remove the 6 vertical rods.
- Watch the bubble chamber and make sure it does not get full. If it does, close the B. P. valve, empty and reconnect. Then open the B. P. valve.
- Measure any shear bands, the height of the specimen and take any pictures that may be needed. Make sure to document the test number in the pictures as well as any other information from the test.
- Drain the pore water from the specimen by opening the pig tail a small amount.
- Disconnect the bottom screws, the B. P. line, and the tree. Hold down the ends of the B. P. line and tree to maintain the vacuum on the specimen as best possible.
- Place the specimen on the sand pan.
- Bring down the inner membrane and outer member to measure thickness and document any findings.

Appendix F **Membrane Fabrication Notes**

F.1 PRODUCTS

- Ethyl Alcohol (this is the same as ethanol)
- Calcium Nitrate
    - Use "refined grade" anything else is too expensive
    - The best product is "75 % Calcium Nitrate Trihydrate" from Golden Eagle Products - http://www.goldeneagleproducts.com/ a 50 lb bag is about $20
- Latex
    - Natural Latex Compound – Product ID 001438 from Heveatex Corporation Fall River, MA 508 675 0181 – This product is for Catheter balloon dipping and is pre-vulcanized. Air drying will achieve 80% of ultimate strength which is fine for most soil testing. 5 gallons is about $ 150. Phone 18009220078 – Ray Minardi is very knowledgeable.
    - Latex Accelerator – Product ID 00D710 from Heveatex – This makes the process quick, but is not necessary, time will do the same thing.
- Calcium Carbonate – Did not use, but 10% "refined grade" in the solution will aid in stripping the membranes.
- Dipping Tank – Heavy Duty PVC Etching Tank (4"x18"x24") with lid. US Plastics Cost about $300. The tank must be fitted with some type of slow agitation device. Usually a slow moving paddle, this keeps the latex from skimming on the top.
- Aluminum – form was constructed from aluminum because it was easy to polish and fabricate, however ceramic molds are also common.

F.2 FORM

- Create a form out of aluminum. The form does not have to be circular in shape. Since the membrane is made from latex a flat piece of metal is sufficient, however the edges should be rounded to prevent thin areas which form at any sharp edges during dipping. Latex will shrink as it cures. The shrinkage is dependant upon the type of latex used. We have observed about 4 % shrinkage, so the form was constructed with a 4% larger radius than that desired for the final product.
- The form should have two eyelet holes on the top to affix a cord or rope for

dipping. The best way to do this is by tapping two threads in the top of the form and screwing two threaded eyelets into the holes. Make sure the holes are centered across the width of the form so that it hangs in a relatively plumb condition.

- The form should be sanded using a progressively finer sand paper. Starting with 100 grit and working to 400 grit wet sand paper. Emory cloth did not work as well as the wet/dry sand paper. After the form is completely smooth use metal polish to finish smoothing the surface.

F.3 TANKS

- One PVC tank should be filled with ethanol and then thoroughly mixed with 30% Calcium Nitrate and 10% Calcium Carbonate (optional Calcium Carbonate). Note: It is a actually just 30% of the weight of the ethanol it isn't really 30% of the entire mixture. It is possible to get the vast majority of the Calcium products into solution, very little if any powder residue should be left on the bottom of the tank and the solution should be relatively clear when mixing is complete.

- The other tank should be filled with Liquid Latex; a rotating paddle should keep the latex in a state of gentle agitation.

- Both tanks should have tight fitting lids to keep the latex from forming a skim coat and curing. Even with a tight fitting lid, the latex is only good for about 3 months.

F.4 PREPARATION

- The entire form should be cleaned using soap and then acetone to make sure all oils and other impurities are removed from the form. The form should only be touch using sterile gloves from this point forward.

- The form should be preheated by placing it in an oven at about 200 degrees Fahrenheit overnight. It is possible that the time required to bring the form up to 200 degrees is less, but this seems to make the most sense.

F.5 DIPPING PROCESS

- Make sure you are working in a well ventilated area as the Ammonium that comprises much of the liquid latex compound is highly volatile and will form quite a lot of vapors during the dipping and drying process.

- Also, a hook sufficient to hang the form during drying should be present. It is wise to place a mat, beneath the hook as a little latex will likely drip during the cure.

- Remove the form from the oven and dip direction in the ethanol mixture.

Hang on the hook and observe the form. The ethanol should "flash" off of the form leaving a uniform powder coating of Calcium Nitrate and Calcium Carbonate. If the form has been sufficiently heated, this should take less than 5 minutes.

- Depending upon how well the latex dipping tank is agitated, you can dip directly or wait for the form to cool (about 15 minutes). If you dip directly, the heat present in the form will make the latex cure very quickly. This will stop the formation of drip lines on the outside of the membrane. However, if the form is too hot a skim of partially cured latex can form on the tank surface. This skim will be picked up by the form during removal and ruin the membrane. The size of each form in relation to the dipping tank volume and the agitation of the tank governs the wait time, but generally it is between 0 and 15 minutes.

- Dip the form smoothly and evenly. Try to enter the latex as quickly as possible without drawing air bubbles down into the latex with the form.

- Let the form sit in the mixture for 20 seconds for a membrane thickness of between 12 and 25 thousands (12 at the top 25 at the bottom).

- Pull the form out of the mixture at a rate of about 1 cm/ sec

- Hang the form and newly formed membrane on the hook for at least an hour. The cure time will vary based on the temperature of the form, the ambient temperature, and the ventilation.

- Make sure to dust the outside of the membrane with baby powder prior to stripping as the new membrane will tend to stick to itself otherwise.

- After stripping dust the rest of the membrane. The vulcanization process can be completed by placing the membrane back in the oven at 200 degrees for about 45 minutes. Alternatively the membrane may be hung in the laboratory and allowed to air dry. This will not achieve 100% vulcanization, but there is no risk in "over-cooking" the membrane.

F.6 POST PRODUCTION

- Inspect the membrane for any areas of the membrane that are habitually weak. Sometimes this area is located at the edge of the form. This means that your radius of curvature is insufficient.

- Any area in the middle of the former plate that produces poor quality on a consistent basis must be resanded and thoroughly cleaned. It is likely the Calcium Nitrate solution is not being spread evenly in this are due to surface irregularities.

Appendix G **De-aired Water Production Procedure**

G.1 CREATE DE-AIRED WATER

- Do not make water without closing the 3-way valve in the soils testing laboratory
- The valves should have the following starting configurations:
    - Tap water supply set to "off"
    - Tank vacuum control set to "de-airing tank"
    - Panel vacuum control can be set to either
- Confirm that the vacuum pressure it the de-airing tanks is at least 26 inches of mercury.
- Set the tap water control valve to "on"
- After water in site tube reaches ¾ of the tank height, set the tap water control to "off" and the tank vacuum control to "hold"

G.2 DISPENSE DE-AIRED WATER

- If not already done, set the tap water control to "off"
- Set the tank vacuum control to "vent"
- The panel control valve can be set to either
- Open the 3-way de-aired water supply valve in the soils testing laboratory.

G.3 DISPENSE VACUUM TO THE CONTROL PANEL

- The tap water supply control can have either setting
- The tank vacuum control can have either setting
- The panel vacuum control must be set to "on" and the vacuum pump must be operating.

Appendix H **Series A Test Data**

Torsion Shear Test on Fine Nevada Sand at a Target Void Ratio = 0.530 (D_r = 91.28 %) Test No. A01

Test Date: 05/10/2010

Test Data

Specimen Height = 39.85 cm

Initial Void Ratio = 0.505

Final Average Confining Pressure (σavg) = 97.4 kPa

Maximum Friction Angle = 37.90°

Intermediate Principal Stress Ratio (b) at Failure = 0.00

Principal Stress Rotation Angle (α) = 0.0°

Shear Band Description

Average Inclination: 65°

Failure Method: (z-θ) mode

Point (No.)	εz (%)	εr (%)	εθ (%)	εv (%)	γθz (%)	σz (kPa)	σr (kPa)	σt (kPa)	τθz (kPa)	b	α (°)	φ (°)
1	0.000	0.000	0.000	0.000	0.000	89.1	101.2	101.5	0.0	0.019	90.0	-3.71
2	0.001	0.002	0.000	0.003	0.000	90.8	101.0	101.0	0.0	-0.005	90.0	-3.05
3	0.002	0.002	0.000	0.003	0.000	91.1	100.8	100.9	0.0	0.015	90.0	-2.94
4	0.002	0.001	0.000	0.003	0.000	91.4	100.7	100.9	0.0	0.021	90.0	-2.84
5	0.002	0.001	0.000	0.003	0.000	91.7	100.6	100.9	0.0	0.025	90.0	-2.74
6	0.002	0.001	-0.001	0.002	0.000	92.0	100.3	100.4	0.0	0.006	90.0	-2.48
7	0.003	0.000	0.000	0.003	0.000	92.8	100.0	100.2	0.0	0.028	90.0	-2.20
8	0.006	-0.001	-0.001	0.004	0.000	96.7	98.0	97.9	0.0	-0.107	90.0	-0.36
9	0.015	-0.005	-0.005	0.005	0.000	105.6	93.8	93.3	0.0	0.046	0.0	3.56
10	0.025	-0.012	-0.006	0.007	0.000	113.9	89.7	89.5	0.0	0.009	0.0	6.88
11	0.037	-0.018	-0.009	0.009	0.000	121.0	86.3	86.4	0.0	-0.002	0.0	9.60
12	0.050	-0.026	-0.013	0.010	0.000	127.9	83.1	82.9	0.0	0.005	0.0	12.34
13	0.062	-0.035	-0.017	0.010	0.000	134.0	80.2	79.9	0.0	0.005	0.0	14.65
14	0.076	-0.046	-0.020	0.010	0.000	139.5	77.2	76.8	0.0	0.006	0.0	16.84
15	0.090	-0.056	-0.023	0.011	0.000	144.7	74.7	75.1	0.0	-0.006	0.0	18.47
16	0.107	-0.069	-0.029	0.009	0.000	149.9	72.2	71.9	0.0	0.003	0.0	20.57
17	0.124	-0.081	-0.033	0.010	0.000	154.7	70.1	70.0	0.0	0.001	0.0	22.13
18	0.141	-0.094	-0.038	0.009	0.000	158.1	68.2	67.6	0.0	0.007	0.0	23.65
19	0.165	-0.112	-0.045	0.009	0.000	162.8	65.9	65.6	0.0	0.003	0.0	25.18
20	0.187	-0.128	-0.050	0.008	0.000	166.2	64.3	63.9	0.0	0.003	0.0	26.40
21	0.213	-0.149	-0.059	0.006	0.000	169.8	62.5	62.0	0.0	0.004	0.0	27.69
22	0.240	-0.170	-0.066	0.004	0.000	172.8	61.0	60.3	0.0	0.006	0.0	28.84
23	0.269	-0.191	-0.077	0.001	0.000	175.6	59.6	59.2	0.0	0.003	0.0	29.70
24	0.303	-0.218	-0.088	-0.003	0.000	178.4	58.3	58.1	0.0	0.001	0.0	30.56
25	0.340	-0.248	-0.103	-0.010	0.000	181.0	57.0	56.9	0.0	0.000	0.0	31.44
26	0.379	-0.279	-0.118	-0.018	0.000	182.8	55.9	55.5	0.0	0.003	0.0	32.28
27	0.422	-0.315	-0.135	-0.028	0.000	185.1	54.8	54.8	0.0	0.000	0.0	32.88
28	0.466	-0.351	-0.155	-0.040	0.000	186.8	54.0	53.5	0.0	0.003	0.0	33.67
29	0.510	-0.389	-0.174	-0.053	0.000	188.4	53.2	52.8	0.0	0.003	0.0	34.22
30	0.557	-0.430	-0.195	-0.067	0.000	189.9	52.4	52.1	0.0	0.002	0.0	34.69
31	0.603	-0.470	-0.216	-0.083	0.000	190.9	51.7	51.5	0.0	0.002	0.0	35.12
32	0.667	-0.525	-0.248	-0.106	0.000	192.2	50.9	50.6	0.0	0.002	0.0	35.66
33	0.709	-0.562	-0.269	-0.122	0.000	192.9	50.5	49.9	0.0	0.005	0.0	36.09
34	0.761	-0.608	-0.296	-0.143	0.000	193.8	50.0	49.4	0.0	0.005	0.0	36.43
35	0.820	-0.661	-0.325	-0.166	0.000	194.8	49.6	49.5	0.0	0.001	0.0	36.49
36	0.894	-0.726	-0.368	-0.201	0.000	195.4	49.0	48.4	0.0	0.004	0.0	37.08
37	0.924	-0.753	-0.383	-0.213	0.000	195.7	48.8	48.4	0.0	0.003	0.0	37.13
38	0.976	-0.802	-0.411	-0.236	0.000	196.3	48.5	48.2	0.0	0.002	0.0	37.27
39	1.040	-0.860	-0.445	-0.264	0.000	196.9	48.1	47.9	0.0	0.002	0.0	37.49
40	1.104	-0.917	-0.482	-0.295	0.000	197.2	47.9	47.4	0.0	0.003	0.0	37.75
41	1.149	-0.959	-0.505	-0.315	0.000	197.1	47.7	47.2	0.0	0.003	0.0	37.88
42	**1.239**	**-1.042**	**-0.553**	**-0.356**	**0.000**	**197.7**	**47.4**	**47.2**	**0.0**	**0.001**	**0.0**	**37.90**
43	1.289	-1.089	-0.577	-0.378	0.000	197.7	47.3	47.2	0.0	0.001	0.0	37.91
44	1.350	-1.146	-0.608	-0.404	0.000	197.9	47.2	47.2	0.0	0.000	0.0	37.93

Torsion Shear Test on Fine Nevada Sand at a Target Void Ratio = 0.530 (D_r = 91.28 %)

Test No. A02
Test Date: 08/01/2010

Test Data

Specimen Height = 40. cm
Initial Void Ratio = 0.548
Final Average Confining Pressure (savg) = 98.0 kPa
Maximum Friction Angle = 45.01°
Intermediate Principal Stress Ratio (b) at Failure = 0.26
Principal Stress Rotation Angle (a) = 23.9°

Shear Band Description

Average Inclination: 41.7°
Failure Method: (z-θ) mode

Point (No.)	εz (%)	εr (%)	εθ (%)	εv (%)	γθz (%)	σz (kPa)	σr (kPa)	σt (kPa)	τθz (kPa)	b	α (°)	φ (°)
1	0.000	0.000	0.000	0.000	-0.003	89.9	101.4	101.4	0.8	0.991	86.1	3.48
2	0.001	-0.001	-0.001	-0.001	-0.003	90.8	100.6	100.0	2.4	1.003	76.0	3.13
3	0.013	-0.003	-0.004	0.005	-0.001	105.5	95.6	92.0	12.9	0.390	31.2	8.50
4	0.022	-0.008	-0.008	0.006	0.006	111.7	93.0	87.8	17.4	0.341	27.7	12.22
5	0.026	-0.006	-0.010	0.011	0.026	118.6	90.4	83.1	23.5	0.323	26.5	17.00
6	0.028	-0.003	-0.012	0.012	0.053	124.1	88.3	79.9	27.6	0.307	25.6	20.29
7	0.030	0.005	-0.021	0.013	0.113	129.4	86.5	77.2	34.5	0.307	26.4	24.77
8	0.037	0.008	-0.034	0.011	0.176	134.2	84.7	74.1	38.1	0.300	25.9	27.77
9	0.048	0.015	-0.055	0.008	0.295	138.7	83.0	71.3	41.5	0.294	25.5	30.58
10	0.062	0.021	-0.085	-0.001	0.422	143.0	81.3	69.0	44.3	0.286	25.1	32.97
11	0.078	0.028	-0.122	-0.016	0.554	146.4	80.0	66.6	46.5	0.283	24.7	35.09
12	0.103	0.032	-0.171	-0.036	0.697	149.1	78.9	64.9	48.3	0.281	24.5	36.80
13	0.161	0.037	-0.304	-0.106	1.031	154.1	76.9	61.5	51.2	0.276	23.9	39.84
14	0.183	0.033	-0.336	-0.120	1.104	155.4	76.6	61.9	52.1	0.271	24.1	40.11
15	0.198	0.034	-0.379	-0.147	1.210	156.7	76.1	61.5	52.9	0.268	24.0	40.70
16	0.245	0.021	-0.443	-0.177	1.318	157.6	75.7	60.6	53.3	0.268	23.8	41.37
17	0.259	0.022	-0.485	-0.203	1.410	158.1	75.5	60.1	53.6	0.269	23.8	41.74
18	0.266	0.022	-0.505	-0.217	1.457	158.3	75.4	60.1	54.0	0.268	23.9	41.93
19	0.293	0.015	-0.547	-0.239	1.537	159.1	75.2	59.8	54.6	0.268	23.8	42.38
20	0.309	0.016	-0.601	-0.275	1.646	160.1	74.8	59.4	55.0	0.266	23.8	42.82
21	0.326	0.016	-0.641	-0.300	1.728	160.5	74.6	59.4	55.3	0.264	23.8	42.98
22	0.333	0.017	-0.665	-0.315	1.780	160.5	74.5	59.3	55.5	0.265	23.8	43.15
23	0.346	0.017	-0.707	-0.343	1.866	161.3	74.4	58.9	55.7	0.264	23.7	43.39
24	0.387	0.002	-0.756	-0.366	1.936	161.3	74.3	58.5	55.9	0.266	23.7	43.74
25	0.402	0.002	-0.806	-0.402	2.037	161.9	74.1	58.5	56.1	0.263	23.7	43.82
26	0.451	-0.006	-0.924	-0.479	2.267	162.8	73.8	58.5	56.8	0.261	23.7	44.17
27	0.505	-0.019	-1.036	-0.550	2.468	163.1	73.5	57.8	57.1	0.262	23.7	44.66
28	0.530	-0.021	-1.116	-0.606	2.626	163.9	73.4	57.7	57.3	0.260	23.6	44.80
29	0.541	-0.021	-1.157	-0.637	2.714	163.9	73.3	57.8	57.3	0.260	23.6	44.82
30	0.563	-0.025	-1.224	-0.686	2.848	163.9	73.3	57.7	57.5	0.260	23.6	44.91
31	**0.656**	**-0.133**	**-1.356**	**-0.833**	**3.255**	**162.7**	**73.4**	**57.8**	**57.7**	**0.264**	**23.9**	**45.01**
32	0.727	-0.140	-1.567	-0.981	3.667	163.1	73.4	58.0	57.4	0.261	23.8	44.76

Torsion Shear Test on Fine Nevada Sand at a Target Void Ratio = 0.530 (D_r = 91.28 %) Test No. A03

Test Date: 12/03/2010

Test Data

Specimen Height = 39.96 cm

Initial Void Ratio = 0.524

Final Average Confining Pressure (savg) = 98.4 kPa

Maximum Friction Angle = 40.64°

Intermediate Principal Stress Ratio (b) at Failure = 0.26

Principal Stress Rotation Angle (a) = 23.4°

Shear Band Description

Average Inclination: 34°

Failure Method: (z-θ) mode

Point (No.)	εz (%)	εr (%)	εθ (%)	εv (%)	γθz (%)	σz (kPa)	σr (kPa)	σt (kPa)	τθz (kPa)	b	α (°)	φ (°)
1	0.001	0.000	0.000	0.001	0.001	92.9	100.0	99.1	3.7	0.917	65.0	2.88
2	0.001	0.001	0.000	0.002	0.002	95.3	99.3	98.2	5.6	0.722	52.3	3.41
3	0.003	0.003	0.003	0.008	0.023	106.3	95.1	90.9	13.7	0.386	30.3	9.16
4	0.004	0.004	0.004	0.012	0.048	112.0	92.9	87.8	18.0	0.340	28.0	12.55
5	0.008	0.004	0.003	0.015	0.094	117.9	90.8	84.4	23.6	0.322	27.3	16.65
6	0.020	0.002	-0.005	0.017	0.153	123.1	88.9	80.9	28.2	0.314	26.6	20.23
7	0.045	-0.005	-0.021	0.020	0.260	129.4	86.5	77.1	33.4	0.302	26.0	24.24
8	0.060	-0.008	-0.032	0.020	0.316	132.4	85.3	75.1	35.3	0.297	25.5	26.00
9	0.073	-0.010	-0.042	0.021	0.361	135.1	84.4	73.9	36.7	0.290	25.1	27.20
10	0.084	-0.012	-0.054	0.018	0.407	136.7	83.7	72.6	37.9	0.289	24.9	28.28
11	0.094	-0.013	-0.065	0.016	0.452	138.2	83.2	71.8	38.9	0.287	24.8	29.15
12	0.113	-0.015	-0.088	0.009	0.542	140.7	82.2	70.2	40.6	0.284	24.5	30.67
13	0.137	-0.019	-0.117	0.001	0.633	143.0	81.5	69.6	42.0	0.278	24.4	31.66
14	0.156	-0.022	-0.141	-0.008	0.702	144.1	81.0	68.2	42.9	0.280	24.3	32.64
15	0.181	-0.027	-0.177	-0.023	0.799	145.6	80.4	67.5	44.1	0.279	24.2	33.58
16	0.202	-0.032	-0.210	-0.039	0.886	146.7	80.0	67.0	44.9	0.277	24.2	34.21
17	0.232	-0.033	-0.262	-0.063	1.025	148.5	79.4	66.0	46.0	0.275	24.1	35.19
18	0.252	-0.032	-0.296	-0.077	1.108	149.1	79.1	65.4	46.5	0.275	24.0	35.69
19	0.320	-0.088	-0.371	-0.138	1.376	151.5	78.1	63.2	47.7	0.275	23.6	37.25
20	0.330	-0.089	-0.388	-0.147	1.412	151.6	78.0	63.0	47.8	0.275	23.6	37.42
21	0.331	-0.089	-0.390	-0.148	1.416	151.6	78.0	63.0	47.8	0.276	23.6	37.43
22	0.375	-0.098	-0.475	-0.198	1.602	153.2	77.5	62.6	48.8	0.271	23.6	38.11
23	0.407	-0.104	-0.539	-0.235	1.729	153.8	77.2	62.2	49.3	0.271	23.5	38.56
24	0.427	-0.104	-0.577	-0.254	1.806	154.2	77.1	62.0	49.6	0.271	23.6	38.76
25	0.458	-0.110	-0.640	-0.292	1.932	154.7	76.8	61.6	49.9	0.270	23.5	39.12
26	0.491	-0.121	-0.713	-0.342	2.082	155.5	76.6	61.5	50.4	0.268	23.5	39.39
27	0.526	-0.127	-0.790	-0.391	2.237	156.2	76.4	61.4	50.8	0.267	23.5	39.69
28	0.559	-0.119	-0.863	-0.423	2.384	156.7	76.2	61.2	51.1	0.266	23.5	39.93
29	0.692	-0.142	-1.186	-0.636	3.016	158.2	75.7	60.8	51.9	0.263	23.4	40.55
30	0.693	-0.142	-1.189	-0.637	3.022	158.2	75.7	60.7	51.9	0.263	23.4	40.56
31	0.694	-0.142	-1.192	-0.640	3.027	158.2	75.7	60.8	51.9	0.263	23.4	40.57
32	0.696	-0.142	-1.195	-0.642	3.033	158.2	75.7	60.7	51.9	0.263	23.4	40.59
33	0.734	-0.152	-1.295	-0.713	3.229	158.6	75.6	60.8	52.1	0.261	23.4	40.64
34	0.760	-0.148	-1.361	-0.750	3.358	158.8	75.5	60.9	52.2	0.260	23.4	40.64
35	**0.763**	**-0.150**	**-1.370**	**-0.757**	**3.376**	**158.9**	**75.5**	**61.0**	**52.2**	**0.260**	**23.4**	**40.64**
36	0.834	-0.155	-1.513	-0.834	3.605	157.5	75.7	60.9	51.2	0.262	23.3	40.13
37	0.871	-0.152	-1.586	-0.868	3.729	157.5	75.7	61.2	51.3	0.261	23.4	40.04
38	0.918	-0.160	-1.678	-0.921	3.882	158.0	75.7	61.6	51.5	0.258	23.4	39.97
39	0.969	-0.170	-1.773	-0.974	4.028	158.4	75.7	61.9	51.6	0.256	23.5	39.88
40	1.029	-0.175	-1.883	-1.029	4.191	158.7	75.6	62.0	51.7	0.254	23.5	39.87
41	1.091	-0.182	-1.997	-1.088	4.356	158.8	75.5	61.9	51.5	0.254	23.4	39.84

Torsion Shear Test on Fine Nevada Sand at a Target Void Ratio = 0.530 (D_r = 91.28 %) Test No. A04

Test Date: 08/31/2010

Test Data

Specimen Height = 40.13 cm

Initial Void Ratio = 0.552

Final Average Confining Pressure (savg) = 97.4 kPa

Maximum Friction Angle = 41.54°

Intermediate Principal Stress Ratio (b) at Failure = 0.89

Principal Stress Rotation Angle (a) = 24.4°

Shear Band Description

Average Inclination	Failure Method
64.4°	(r-θ) mode

Point (No.)	εz (%)	εr (%)	εθ (%)	εv (%)	γθz (%)	σz (kPa)	σr (kPa)	σt (kPa)	τθz (kPa)	b	α (°)	φ (°)
1	-0.003	0.032	-0.013	0.016	0.094	98.2	114.0	81.9	13.3	0.789	29.3	12.14
2	-0.003	0.034	-0.014	0.018	0.096	98.4	114.5	80.8	13.2	0.778	28.2	12.51
3	0.004	0.049	-0.027	0.026	0.150	99.8	117.8	75.5	18.3	0.843	28.2	16.52
4	0.008	0.056	-0.033	0.031	0.167	101.0	119.3	73.8	19.5	0.855	27.6	17.72
5	0.012	0.066	-0.043	0.036	0.196	102.1	121.4	70.6	21.1	0.859	26.6	19.80
6	0.014	0.085	-0.056	0.043	0.273	103.2	123.5	67.0	23.7	0.874	26.4	22.44
7	0.014	0.095	-0.063	0.046	0.299	103.5	124.4	65.6	24.4	0.873	26.1	23.39
8	0.013	0.118	-0.079	0.052	0.366	104.7	126.2	63.0	26.3	0.885	25.8	25.47
9	0.011	0.140	-0.094	0.057	0.428	105.4	127.6	61.2	27.8	0.890	25.8	27.08
10	0.011	0.151	-0.103	0.059	0.454	106.2	128.3	60.2	28.3	0.894	25.5	27.82
11	0.007	0.177	-0.121	0.063	0.518	106.1	129.4	58.6	29.5	0.892	25.6	29.21
12	0.002	0.212	-0.148	0.065	0.599	106.9	130.5	56.6	30.8	0.898	25.4	30.86
13	0.000	0.232	-0.166	0.065	0.641	107.2	131.2	55.4	30.6	0.891	24.9	31.43
14	0.001	0.245	-0.181	0.066	0.679	107.7	131.7	55.1	31.7	0.900	25.1	32.16
15	0.000	0.271	-0.208	0.064	0.739	107.9	132.3	53.7	32.3	0.900	25.0	33.21
16	-0.002	0.293	-0.228	0.062	0.791	108.2	132.9	53.5	33.0	0.904	25.2	33.69
17	-0.001	0.308	-0.246	0.061	0.829	108.0	132.6	53.0	33.4	0.908	25.3	34.14
18	-0.002	0.334	-0.275	0.057	0.895	108.8	133.8	52.0	34.1	0.908	25.1	35.13
19	-0.003	0.362	-0.308	0.051	0.954	109.1	134.4	51.0	34.3	0.905	24.9	35.85
20	-0.005	0.375	-0.322	0.048	0.985	109.3	134.5	50.8	34.5	0.907	24.9	36.05
21	-0.011	0.417	-0.369	0.037	1.079	109.4	135.1	49.8	34.9	0.905	24.7	36.90
22	-0.011	0.418	-0.369	0.038	1.082	109.4	135.1	49.7	34.8	0.904	24.7	36.95
23	-0.010	0.466	-0.435	0.022	1.203	109.9	135.7	49.1	35.5	0.908	24.7	37.68
24	-0.014	0.490	-0.463	0.013	1.258	109.8	135.8	48.7	35.7	0.907	24.7	38.06
25	-0.016	0.534	-0.521	-0.003	1.369	110.4	136.4	48.1	36.3	0.910	24.7	38.68
26	-0.020	0.565	-0.559	-0.015	1.437	110.4	136.7	47.8	36.4	0.909	24.7	39.02
27	-0.028	0.599	-0.601	-0.030	1.515	110.6	136.8	47.6	36.6	0.912	24.6	39.25
28	-0.022	0.651	-0.686	-0.056	1.655	110.6	137.0	47.4	37.3	0.914	24.9	39.73
29	-0.026	0.677	-0.719	-0.068	1.711	111.2	137.7	46.5	37.0	0.910	24.4	40.19
30	-0.030	0.707	-0.760	-0.084	1.778	111.2	137.8	46.2	37.3	0.912	24.5	40.52
31	-0.032	0.758	-0.839	-0.113	1.915	111.5	138.1	46.2	37.8	0.915	24.6	40.89
32	**-0.046**	**0.835**	**-0.953**	**-0.164**	**2.083**	**109.1**	**138.4**	**44.7**	**36.7**	**0.885**	**24.4**	**41.54**
33	-0.046	0.874	-1.011	-0.182	2.139	109.1	138.5	44.4	35.7	0.877	23.9	41.13
34	-0.044	0.913	-1.069	-0.200	2.200	109.0	138.6	43.9	34.4	0.865	23.3	40.79

Torsion Shear Test on Fine Nevada Sand at a Target Void Ratio = 0.530 (D_r = 91.28 %) Test No. A05

Test Date: 08/07/2010

Test Data

Specimen Height = 40.09 cm

Initial Void Ratio = 0.555

Final Average Confining Pressure (savg) = 98.6 kPa

Maximum Friction Angle = 37.79°

Intermediate Principal Stress Ratio (b) at Failure = 0.54

Principal Stress Rotation Angle (a) = 47.4°

Shear Band Description

Average Inclination: 15°

Failure Method: (z-θ) mode

Point (No.)	εz (%)	εr (%)	εθ (%)	εv (%)	γθz (%)	σz (kPa)	σr (kPa)	σt (kPa)	τθz (kPa)	b	α (°)	φ (°)
1	0.000	0.000	0.000	0.000	0.000	91.4	101.3	101.4	1.3	0.981	82.8	3.07
2	0.000	0.001	0.000	0.001	0.000	91.4	101.3	101.4	1.3	0.973	82.6	3.10
3	-0.005	0.001	0.005	0.002	0.036	91.2	101.4	101.3	9.1	0.745	59.5	6.18
4	-0.009	0.002	0.007	0.000	0.072	91.3	101.4	101.1	13.8	0.677	54.8	8.79
5	-0.014	0.002	0.012	0.001	0.111	91.7	101.3	101.4	18.0	0.629	52.6	11.13
6	-0.019	0.006	0.016	0.003	0.158	91.5	101.3	101.6	22.1	0.606	51.4	13.57
7	-0.019	0.006	0.017	0.004	0.199	91.4	101.3	101.1	25.1	0.600	50.5	15.38
8	-0.028	0.013	0.023	0.007	0.241	91.5	101.4	101.4	27.8	0.587	50.0	17.01
9	-0.036	0.017	0.027	0.008	0.297	91.4	101.3	101.4	30.8	0.579	49.6	18.89
10	-0.045	0.027	0.030	0.012	0.372	91.5	101.4	101.2	34.3	0.573	49.0	21.07
11	-0.053	0.036	0.032	0.015	0.460	91.4	101.3	101.3	37.8	0.566	48.7	23.28
12	-0.054	0.036	0.032	0.014	0.462	91.6	101.3	101.1	37.8	0.565	48.6	23.28
13	-0.061	0.041	0.035	0.015	0.503	91.2	101.4	101.1	39.1	0.566	48.6	24.18
14	-0.065	0.048	0.035	0.018	0.560	91.5	101.4	101.4	40.9	0.560	48.5	25.29
15	-0.073	0.055	0.036	0.018	0.618	91.5	101.4	101.4	42.5	0.558	48.3	26.36
16	-0.083	0.065	0.037	0.018	0.685	91.5	101.4	101.5	44.1	0.555	48.2	27.39
17	-0.092	0.073	0.036	0.017	0.750	91.4	101.4	101.3	45.4	0.555	48.1	28.28
18	-0.108	0.084	0.038	0.014	0.828	91.7	101.4	101.4	46.7	0.552	48.0	29.14
19	-0.122	0.096	0.038	0.011	0.903	91.4	101.3	101.4	47.8	0.551	48.0	29.91
20	-0.136	0.105	0.038	0.007	0.980	91.7	101.4	101.6	48.9	0.548	47.9	30.53
21	-0.156	0.118	0.039	0.001	1.065	91.7	101.4	101.6	49.9	0.547	47.8	31.24
22	-0.179	0.134	0.037	-0.008	1.178	91.5	101.4	101.0	51.0	0.550	47.7	32.14
23	-0.195	0.144	0.035	-0.017	1.262	91.6	101.4	101.4	51.9	0.547	47.7	32.70
24	-0.211	0.154	0.033	-0.024	1.338	91.8	101.4	101.4	52.6	0.546	47.6	33.15
25	-0.228	0.165	0.030	-0.033	1.425	91.6	101.4	101.1	53.2	0.547	47.5	33.66
26	-0.257	0.182	0.027	-0.048	1.551	91.5	101.4	101.1	54.2	0.546	47.5	34.37
27	-0.265	0.187	0.021	-0.057	1.622	91.7	101.4	101.4	54.7	0.544	47.5	34.66
28	-0.299	0.205	0.022	-0.071	1.730	92.0	101.4	101.6	55.4	0.542	47.5	35.10
29	-0.323	0.220	0.019	-0.084	1.825	91.7	101.4	101.5	56.0	0.543	47.5	35.55
30	-0.338	0.229	0.013	-0.096	1.915	91.9	101.4	101.6	56.5	0.541	47.4	35.91
31	-0.368	0.244	0.008	-0.116	2.043	91.9	101.3	101.5	57.2	0.540	47.4	36.37
32	-0.383	0.253	0.003	-0.127	2.121	92.1	101.4	101.9	57.6	0.538	47.4	36.61
33	-0.408	0.268	-0.004	-0.144	2.239	91.9	101.4	101.4	58.0	0.540	47.3	36.97
34	-0.432	0.280	-0.013	-0.165	2.365	92.1	101.3	101.9	58.4	0.537	47.4	37.20
35	-0.458	0.294	-0.019	-0.183	2.483	92.1	101.3	102.0	58.7	0.536	47.4	37.38
36	-0.493	0.313	-0.029	-0.209	2.646	92.2	101.3	101.6	59.1	0.537	47.3	37.70
37	**-0.522**	**0.327**	**-0.037**	**-0.231**	**2.788**	**92.3**	**101.4**	**102.1**	**59.3**	**0.535**	**47.4**	**37.79**
38	-0.539	0.335	-0.044	-0.248	2.897	92.1	101.3	101.9	58.6	0.537	47.4	37.31
39	-0.554	0.342	-0.045	-0.257	2.972	92.0	101.3	101.5	57.6	0.539	47.4	36.67

Torsion Shear Test on Fine Nevada Sand at a Target Void Ratio = 0.530 (D_r = 91.28 %) Test No. A06

Test Date: 08/28/2010

Test Data

Specimen Height = 40.09 cm

Initial Void Ratio = 0.559

Final Average Confining Pressure (savg) = 98.9 kPa

Maximum Friction Angle = 37.37°

Intermediate Principal Stress Ratio (b) at Failure = 0.80

Principal Stress Rotation Angle (a) = 47.8°

Shear Band Description

Average Inclination	Failure Method
30°	(r-θ) mode
21.3°	(z-θ) mode

Point (No.)	εz (%)	εr (%)	εθ (%)	εv (%)	γθz (%)	σz (kPa)	σr (kPa)	σt (kPa)	τθz (kPa)	b	α (°)	φ (°)
1	0.000	0.000	0.000	0.000	0.019	91.0	101.7	101.0	0.7	0.939	85.8	3.03
2	0.000	0.004	-0.001	0.003	0.020	91.0	101.7	101.2	0.7	0.951	85.9	3.05
3	0.000	0.009	0.001	0.010	0.050	89.3	104.7	99.5	9.8	0.969	58.7	6.70
4	0.000	0.017	0.005	0.022	0.079	88.4	106.6	98.9	15.3	0.902	54.4	9.91
5	0.000	0.027	0.006	0.032	0.109	87.7	108.3	97.9	19.7	0.880	52.3	12.67
6	0.009	0.032	0.002	0.043	0.150	86.8	109.6	97.1	24.3	0.855	51.0	15.67
7	0.015	0.039	-0.003	0.051	0.193	86.4	110.8	97.0	27.9	0.836	50.4	18.06
8	0.019	0.047	-0.007	0.059	0.238	85.8	111.8	96.1	30.8	0.835	49.8	20.06
9	0.023	0.057	-0.015	0.065	0.293	85.2	112.7	95.8	33.5	0.827	49.5	21.97
10	0.024	0.069	-0.024	0.069	0.351	85.0	113.4	95.3	35.7	0.823	49.1	23.58
11	0.025	0.084	-0.037	0.072	0.411	84.4	114.3	94.9	37.4	0.825	49.0	24.93
12	0.017	0.100	-0.047	0.070	0.511	84.3	115.0	94.9	39.9	0.815	48.8	26.72
13	0.012	0.112	-0.056	0.068	0.571	84.1	115.3	94.6	41.1	0.814	48.6	27.60
14	0.002	0.128	-0.067	0.062	0.652	83.4	115.8	94.4	42.2	0.816	48.7	28.62
15	-0.018	0.152	-0.081	0.052	0.775	83.4	116.4	94.3	44.0	0.811	48.5	29.91
16	-0.025	0.166	-0.099	0.043	0.858	83.4	116.7	94.2	44.9	0.809	48.4	30.64
17	-0.038	0.180	-0.108	0.035	0.941	83.2	117.0	94.1	45.7	0.807	48.4	31.29
18	-0.058	0.202	-0.128	0.016	1.085	83.0	117.4	93.7	46.8	0.808	48.3	32.26
19	-0.078	0.224	-0.147	-0.001	1.216	83.0	117.7	94.0	47.9	0.804	48.3	33.02
20	-0.097	0.244	-0.168	-0.022	1.339	82.9	118.0	93.8	48.6	0.804	48.2	33.63
21	-0.120	0.264	-0.182	-0.038	1.470	82.9	118.3	93.8	49.3	0.801	48.2	34.18
22	-0.147	0.288	-0.202	-0.061	1.615	82.5	118.5	93.4	49.8	0.805	48.1	34.72
23	-0.176	0.313	-0.223	-0.086	1.776	82.7	118.8	93.8	50.6	0.800	48.1	35.22
24	-0.231	0.356	-0.255	-0.130	2.023	82.1	119.0	92.9	51.0	0.808	48.0	35.86
25	-0.245	0.368	-0.266	-0.143	2.100	82.1	119.0	93.0	51.1	0.806	48.1	35.99
26	-0.296	0.408	-0.292	-0.181	2.311	82.8	119.2	93.8	51.9	0.797	48.0	36.21
27	-0.329	0.434	-0.313	-0.208	2.459	82.4	119.4	93.3	52.1	0.801	48.0	36.58
28	-0.369	0.468	-0.340	-0.241	2.639	82.7	119.6	93.5	52.4	0.799	47.9	36.77
29	-0.421	0.512	-0.371	-0.280	2.856	82.9	119.7	93.9	52.7	0.796	48.0	36.87
30	-0.457	0.543	-0.393	-0.307	3.003	82.9	119.8	93.9	52.9	0.795	48.0	37.03
31	-0.502	0.585	-0.426	-0.343	3.201	82.8	119.9	93.5	53.0	0.799	47.9	37.21
32	-0.524	0.604	-0.437	-0.357	3.277	82.7	120.0	93.4	53.0	0.800	47.9	37.23
33	**-0.574**	**0.653**	**-0.474**	**-0.394**	**3.484**	**83.0**	**120.1**	**93.5**	**53.3**	**0.798**	**47.8**	**37.37**
34	-0.596	0.676	-0.489	-0.410	3.578	83.2	120.2	93.8	53.4	0.795	47.9	37.30
35	-0.632	0.711	-0.514	-0.435	3.721	83.2	120.2	94.1	53.1	0.795	47.9	37.05
36	-0.661	0.738	-0.530	-0.453	3.821	83.2	120.1	93.9	52.9	0.796	47.9	36.93
37	-0.683	0.764	-0.550	-0.470	3.925	83.2	119.9	94.6	53.0	0.791	48.1	36.82
38	-0.720	0.805	-0.579	-0.493	4.085	83.3	119.9	94.2	52.4	0.795	48.0	36.38
39	-0.741	0.834	-0.599	-0.506	4.199	83.6	119.9	94.5	52.1	0.795	48.0	36.01
40	-0.758	0.859	-0.619	-0.518	4.303	83.4	119.8	94.2	51.8	0.797	48.0	35.90
41	-0.773	0.892	-0.644	-0.525	4.429	83.5	119.5	94.3	51.6	0.795	48.0	35.69

Torsion Shear Test on Fine Nevada Sand at a Target Void Ratio = 0.530 (D_r = 91.28 %) Test No. A07

Test Date: 08/31/2010

Test Data

Specimen Height = 40.03 cm

Initial Void Ratio = 0.533

Final Average Confining Pressure (savg) = 98.7 kPa

Maximum Friction Angle = 37.69°

Intermediate Principal Stress Ratio (b) at Failure = 0.95

Principal Stress Rotation Angle (a) = 48.1°

Shear Band Description

Average Inclination	Failure Method
No shear bands	top cap slip

Point (No.)	εz (%)	εr (%)	εθ (%)	εv (%)	γθz (%)	σz (kPa)	σr (kPa)	σt (kPa)	τθz (kPa)	b	α (°)	φ (°)
1	0.000	0.000	0.000	0.000	0.011	91.7	101.4	101.4	1.5	0.980	81.5	-0.06
2	-0.003	0.009	-0.001	0.005	0.027	88.5	106.7	98.6	9.9	0.916	58.5	7.38
3	-0.006	0.017	-0.002	0.009	0.035	87.1	109.7	97.1	13.1	0.884	55.5	9.70
4	-0.014	0.029	0.001	0.017	0.053	85.1	113.0	95.9	18.7	0.928	53.1	13.15
5	-0.027	0.045	0.004	0.021	0.096	83.5	116.0	93.9	23.7	0.941	51.2	16.61
6	-0.045	0.065	0.007	0.027	0.166	82.4	117.7	93.2	28.1	0.978	50.5	19.33
7	-0.070	0.093	0.009	0.032	0.267	80.8	120.7	91.9	31.7	0.968	50.0	22.38
8	-0.087	0.113	0.008	0.034	0.354	79.9	123.1	90.7	33.7	0.947	49.6	24.38
9	-0.113	0.139	0.008	0.034	0.434	78.5	123.9	90.8	35.4	0.956	49.9	25.80
10	-0.146	0.170	0.007	0.032	0.535	78.7	125.6	89.9	37.3	0.955	49.3	27.31
11	-0.216	0.233	0.002	0.019	0.739	78.2	126.9	89.5	40.0	0.969	49.0	29.34
12	-0.324	0.322	-0.006	-0.007	1.013	76.8	128.8	88.1	41.9	0.955	48.8	31.65
13	-0.420	0.403	-0.027	-0.045	1.295	76.6	130.2	88.1	43.9	0.961	48.7	33.17
14	-0.525	0.487	-0.052	-0.090	1.582	76.0	131.5	87.3	45.1	0.954	48.6	34.67
15	-0.609	0.552	-0.070	-0.127	1.794	75.3	132.4	86.4	45.5	0.941	48.5	35.54
16	-0.625	0.565	-0.065	-0.124	1.809	75.3	132.8	86.4	42.4	0.903	48.7	33.67
17	-0.623	0.565	-0.065	-0.122	1.809	76.1	130.7	87.1	41.2	0.917	48.8	32.04
18	-0.619	0.561	-0.058	-0.116	1.794	78.7	126.4	89.2	36.6	0.931	49.1	27.27
19	-0.614	0.561	-0.058	-0.112	1.775	78.3	127.0	89.4	34.1	0.888	49.6	26.15
20	-0.610	0.559	-0.056	-0.107	1.759	78.9	125.2	89.8	31.6	0.880	49.9	24.27
21	-0.602	0.556	-0.052	-0.097	1.730	80.2	123.6	90.9	27.5	0.848	50.5	21.40
22	-0.591	0.551	-0.045	-0.085	1.697	81.9	120.8	92.5	23.7	0.840	51.3	18.37
23	-0.584	0.548	-0.038	-0.074	1.679	83.7	118.3	93.5	20.9	0.839	51.6	16.02
24	-0.576	0.544	-0.033	-0.066	1.642	84.2	116.4	94.3	18.6	0.830	52.6	14.43
25	-0.565	0.538	-0.021	-0.049	1.594	87.1	112.6	96.0	14.9	0.848	53.3	11.18
26	-0.548	0.533	-0.015	-0.030	1.546	87.7	110.9	97.6	10.2	0.768	58.0	8.87
27	-0.530	0.523	-0.004	-0.011	1.479	89.3	106.7	99.3	7.3	0.831	62.3	6.36
28	-0.529	0.523	-0.003	-0.009	1.478	88.9	107.1	98.8	7.2	0.796	62.2	6.55
29	-0.527	0.522	-0.008	-0.012	1.529	88.9	107.9	98.6	20.3	0.838	51.7	11.17
30	-0.535	0.529	-0.013	-0.019	1.590	84.5	115.9	94.5	31.1	0.919	49.6	19.45
31	-0.557	0.548	-0.025	-0.034	1.683	78.8	125.7	90.2	40.1	0.992	49.0	28.78
32	-0.603	0.575	-0.041	-0.069	1.836	77.7	129.1	88.7	46.9	0.987	48.4	34.33
33	-0.756	0.683	-0.081	-0.154	2.204	75.3	133.9	86.1	46.8	0.939	48.3	36.81
34	-0.786	0.701	-0.082	-0.167	2.370	75.3	133.9	86.4	47.2	0.945	48.3	36.99
35	**-0.862**	**0.756**	**-0.110**	**-0.216**	**2.859**	**75.6**	**134.1**	**86.2**	**48.3**	**0.954**	**48.1**	**37.69**

Torsion Shear Test on Fine Nevada Sand at a Target Void Ratio = 0.530 (D_r = 91.28 %)

Test No. A08
Test Date: 09/07/2010

Test Data

Specimen Height = 40.13 cm
Initial Void Ratio = 0.536
Final Average Confining Pressure (savg) = 97.6 kPa
Maximum Friction Angle = 28.62°
Intermediate Principal Stress Ratio (b) at Failure = 0.97
Principal Stress Rotation Angle (a) = 71.2°

Shear Band Description

Average Inclination	Failure Method
0°	(θ-z) mode

Point (No.)	εz (%)	εr (%)	εθ (%)	εv (%)	γθz (%)	σz (kPa)	σr (kPa)	σt (kPa)	τθz (kPa)	b	α (°)	φ (°)
1	0.000	0.000	0.000	0.000	0.012	91.4	101.4	101.1	1.1	0.991	83.8	2.98
2	0.000	0.000	0.000	0.000	0.012	91.5	101.3	101.2	1.1	0.998	83.8	2.97
3	-0.006	0.006	0.001	0.001	0.031	83.7	105.9	103.6	5.7	0.965	75.0	7.02
4	-0.012	0.011	0.005	0.004	0.041	81.2	107.5	104.6	9.8	0.976	70.1	9.46
5	-0.021	0.021	0.010	0.011	0.051	77.0	110.5	106.6	9.9	0.977	73.2	11.20
6	-0.022	0.022	0.010	0.010	0.059	74.8	111.4	106.7	11.2	0.972	72.4	12.42
7	-0.030	0.028	0.013	0.012	0.072	72.7	112.6	107.1	12.5	0.966	72.0	13.69
8	-0.037	0.036	0.019	0.017	0.082	70.9	113.8	107.9	13.1	0.962	72.4	14.66
9	-0.043	0.040	0.022	0.019	0.091	70.1	114.3	108.5	13.7	0.971	72.2	15.32
10	-0.054	0.049	0.027	0.022	0.109	68.3	115.1	108.2	15.5	0.970	71.1	16.64
11	-0.068	0.061	0.034	0.026	0.133	66.3	116.7	109.8	16.9	0.980	71.1	18.23
12	-0.090	0.075	0.045	0.030	0.162	64.2	118.0	110.3	18.0	0.976	71.0	19.60
13	-0.114	0.095	0.054	0.035	0.193	62.4	119.0	110.9	18.8	0.973	71.1	20.72
14	-0.131	0.107	0.062	0.037	0.216	61.3	119.7	111.6	19.4	0.977	71.2	21.55
15	-0.151	0.120	0.069	0.038	0.239	60.2	120.4	111.4	19.6	0.964	71.3	22.06
16	-0.151	0.121	0.068	0.039	0.239	60.4	120.4	111.8	19.6	0.970	71.4	22.07
17	-0.152	0.122	0.069	0.039	0.241	60.3	120.4	111.7	19.5	0.968	71.4	22.06
18	-0.179	0.139	0.081	0.042	0.272	59.5	121.2	112.4	20.4	0.974	71.2	22.87
19	-0.201	0.153	0.089	0.041	0.302	58.9	121.7	113.0	21.3	0.981	70.9	23.60
20	-0.228	0.172	0.097	0.041	0.334	57.7	122.2	113.0	21.4	0.974	71.2	24.18
21	-0.289	0.210	0.119	0.040	0.405	56.6	123.1	113.5	22.4	0.976	70.9	25.23
22	-0.302	0.216	0.122	0.036	0.422	56.3	123.3	113.7	22.6	0.977	70.9	25.45
23	-0.324	0.231	0.129	0.036	0.453	55.8	123.6	114.0	22.8	0.977	71.0	25.83
24	-0.342	0.241	0.135	0.034	0.477	55.5	123.8	113.9	23.0	0.975	70.9	26.05
25	-0.368	0.257	0.142	0.032	0.507	55.1	124.0	114.1	23.3	0.977	70.8	26.38
26	-0.382	0.266	0.148	0.031	0.524	55.0	124.2	114.6	23.5	0.982	70.8	26.60
27	-0.403	0.276	0.153	0.026	0.546	54.5	124.4	114.6	23.4	0.977	71.0	26.78
28	-0.456	0.308	0.168	0.020	0.607	53.6	125.2	114.5	23.4	0.965	71.2	27.19
29	-0.473	0.317	0.174	0.017	0.635	54.3	124.8	114.4	24.6	0.980	70.3	27.42
30	-0.498	0.332	0.178	0.013	0.660	52.8	125.5	114.5	23.5	0.962	71.3	27.62
31	-0.563	0.365	0.198	0.000	0.735	51.9	126.0	115.0	23.3	0.958	71.8	28.01
32	-0.608	0.389	0.208	-0.011	0.801	52.2	126.1	115.3	23.9	0.967	71.4	28.20
33	**-0.670**	**0.421**	**0.221**	**-0.028**	**0.900**	**51.7**	**126.0**	**115.1**	**24.3**	**0.968**	**71.2**	**28.62**
34	-0.722	0.448	0.229	-0.045	1.014	51.4	126.5	115.2	23.9	0.960	71.6	28.57
35	-0.769	0.474	0.237	-0.058	1.157	52.7	125.8	115.3	24.6	0.975	70.9	28.30
36	-0.819	0.506	0.242	-0.071	1.295	53.7	125.6	115.3	24.9	0.981	70.5	27.95
37	-0.879	0.544	0.247	-0.087	1.454	55.7	124.6	114.8	24.8	0.989	70.0	26.91

Torsion Shear Test on Fine Nevada Sand at a Target Void Ratio = 0.530 (D_r = 91.28 %) Test No. A09

Test Date: 07/05/2010

Test Data

Specimen Height = 40.03 cm

Initial Void Ratio = 0.533

Final Average Confining Pressure (σavg) = 96.5 kPa

Maximum Friction Angle = 37.62°

Intermediate Principal Stress Ratio (b) at Failure = 0.06

Principal Stress Rotation Angle (α) = 90.0°

Shear Band Description

Average Inclination: 25°

Failure Method: (θ-r) mode & (θ-z) mode

Point (No.)	εz (%)	εr (%)	εθ (%)	εv (%)	γθz (%)	σz (kPa)	σr (kPa)	σt (kPa)	τθz (kPa)	b	α (°)	φ (°)
1	0.000	0.004	0.000	0.004	0.000	91.3	101.3	101.5	0.0	0.977	90.0	3.04
2	0.000	0.004	0.001	0.004	0.000	91.3	101.3	101.4	0.0	0.983	90.0	3.02
3	0.000	-0.002	0.010	0.008	0.000	86.2	96.4	110.8	0.0	0.414	90.0	7.17
4	0.000	-0.008	0.022	0.014	0.000	82.3	92.1	119.6	0.0	0.263	90.0	10.65
5	-0.005	-0.015	0.037	0.017	0.000	78.3	88.2	127.3	0.0	0.201	90.0	13.77
6	-0.013	-0.022	0.056	0.021	0.000	75.2	84.7	134.1	0.0	0.162	90.0	16.34
7	-0.023	-0.030	0.080	0.027	0.000	72.1	81.6	140.3	0.0	0.139	90.0	18.71
8	-0.037	-0.038	0.107	0.031	0.000	69.4	78.8	145.8	0.0	0.123	90.0	20.80
9	-0.056	-0.050	0.142	0.036	0.000	66.2	76.1	151.2	0.0	0.117	90.0	23.03
10	-0.075	-0.058	0.174	0.041	0.000	64.9	74.1	155.0	0.0	0.102	90.0	24.20
11	-0.100	-0.070	0.216	0.046	0.000	63.0	72.0	159.4	0.0	0.094	90.0	25.69
12	-0.130	-0.082	0.261	0.049	0.000	61.3	70.2	162.6	0.0	0.088	90.0	26.88
13	-0.166	-0.097	0.313	0.051	0.000	59.7	68.7	165.7	0.0	0.085	90.0	28.05
14	-0.206	-0.112	0.369	0.052	0.000	58.5	67.4	168.2	0.0	0.081	90.0	28.96
15	-0.248	-0.131	0.427	0.049	0.000	57.4	66.1	170.6	0.0	0.077	90.0	29.78
16	-0.292	-0.149	0.486	0.045	0.000	56.3	65.1	172.7	0.0	0.076	90.0	30.55
17	-0.336	-0.169	0.545	0.040	0.000	55.3	64.1	174.4	0.0	0.074	90.0	31.23
18	-0.380	-0.188	0.601	0.033	0.000	54.5	63.3	176.0	0.0	0.073	90.0	31.80
19	-0.427	-0.210	0.662	0.025	0.000	54.0	62.6	177.7	0.0	0.069	90.0	32.26
20	-0.475	-0.233	0.721	0.014	0.000	53.2	61.9	178.6	0.0	0.070	90.0	32.76
21	-0.523	-0.256	0.782	0.003	0.000	52.8	61.4	179.8	0.0	0.068	90.0	33.10
22	-0.649	-0.320	0.935	-0.033	0.000	51.5	60.3	182.3	0.0	0.067	90.0	34.00
23	-0.701	-0.340	0.994	-0.047	0.000	51.2	59.8	182.7	0.0	0.066	90.0	34.21
24	-0.763	-0.369	1.067	-0.065	0.000	50.8	59.2	183.8	0.0	0.063	90.0	34.52
25	-0.795	-0.386	1.106	-0.075	0.000	50.6	58.9	184.4	0.0	0.062	90.0	34.71
26	-0.848	-0.415	1.169	-0.094	0.000	50.0	58.5	185.2	0.0	0.062	90.0	35.07
27	-0.916	-0.450	1.247	-0.119	0.000	49.6	58.0	186.1	0.0	0.061	90.0	35.38
28	-0.965	-0.474	1.303	-0.136	0.000	49.4	57.7	186.4	0.0	0.060	90.0	35.53
29	-1.016	-0.503	1.362	-0.158	0.000	48.9	57.3	187.0	0.0	0.061	90.0	35.82
30	-1.083	-0.538	1.439	-0.182	0.000	48.9	57.1	187.8	0.0	0.059	90.0	35.95
31	-1.127	-0.560	1.487	-0.200	0.000	48.6	56.8	188.1	0.0	0.059	90.0	36.09
32	-1.208	-0.604	1.580	-0.232	0.000	48.2	56.4	188.6	0.0	0.059	90.0	36.37
33	-1.247	-0.624	1.623	-0.248	0.000	48.1	56.3	189.0	0.0	0.058	90.0	36.46
34	-1.337	-0.671	1.721	-0.287	0.000	47.8	55.9	189.4	0.0	0.058	90.0	36.67
35	-1.451	-0.722	1.841	-0.332	0.000	46.6	55.5	188.2	0.0	0.063	90.0	37.07
36	-1.500	-0.747	1.893	-0.354	0.000	46.4	55.5	188.1	0.0	0.064	90.0	37.20
37	-1.551	-0.773	1.947	-0.377	0.000	46.2	55.3	188.4	0.0	0.064	90.0	37.30
38	-1.624	-0.809	2.024	-0.409	0.000	46.1	55.1	188.5	0.0	0.064	90.0	37.38
39	-1.698	-0.843	2.101	-0.440	0.000	46.0	55.0	188.9	0.0	0.063	90.0	37.47
40	**-1.836**	**-0.890**	**2.248**	**-0.478**	**0.000**	**45.7**	**54.8**	**189.0**	**0.0**	**0.063**	**90.0**	**37.62**
41	-1.955	-0.920	2.382	-0.494	0.000	45.4	54.5	189.0	0.0	0.063	90.0	37.77
42	-2.113	-0.943	2.554	-0.502	0.000	45.5	54.3	189.7	0.0	0.061	90.0	37.82

Torsion Shear Test on Fine Nevada Sand at a Target Void Ratio = 0.530 (D_r = 91.28 %) Test No. A10

Test Date: 04/22/2010

Test Data

Specimen Height = 39.99 cm

Initial Void Ratio = 0.528

Final Average Confining Pressure (σavg) = 98.5 kPa

Maximum Friction Angle = 43.31°

Intermediate Principal Stress Ratio (b) at Failure = 0.53

Principal Stress Rotation Angle (α) = 90.0°

Shear Band Description

Average Inclination: 24°

Failure Method: (θ-z) mode

Point (No.)	εz (%)	εr (%)	εθ (%)	εv (%)	γθz (%)	σz (kPa)	σr (kPa)	σt (kPa)	τθz (kPa)	b	α (°)	φ (°)
1	-0.003	0.001	0.001	0.000	0.000	92.1	101.4	101.3	0.0	0.993	90.0	2.73
2	-0.003	0.001	0.001	0.000	0.000	91.9	101.4	100.8	0.0	0.935	90.0	2.64
3	-0.008	0.001	0.009	0.003	0.000	85.5	101.4	107.1	0.0	0.738	90.0	6.45
4	-0.012	0.002	0.015	0.005	0.000	79.7	101.3	111.9	0.0	0.672	90.0	9.67
5	-0.017	0.001	0.022	0.006	0.000	75.0	101.4	116.5	0.0	0.635	90.0	12.54
6	0.000	-0.010	0.019	0.009	0.000	71.1	101.4	121.3	0.0	0.603	90.0	15.14
7	-0.003	-0.012	0.027	0.011	0.000	67.2	101.3	124.5	0.0	0.596	90.0	17.39
8	-0.011	-0.010	0.038	0.017	0.000	63.9	101.3	127.6	0.0	0.588	90.0	19.45
9	-0.019	-0.011	0.050	0.020	0.000	61.0	101.4	130.9	0.0	0.578	90.0	21.34
10	-0.031	-0.011	0.065	0.023	0.000	58.2	101.4	133.4	0.0	0.574	90.0	23.12
11	-0.045	-0.007	0.079	0.026	0.000	55.7	101.4	135.7	0.0	0.571	90.0	24.70
12	-0.063	-0.003	0.097	0.031	0.000	53.6	101.3	137.8	0.0	0.567	90.0	26.11
13	-0.084	0.001	0.117	0.035	0.000	51.6	101.4	140.1	0.0	0.562	90.0	27.50
14	-0.110	0.007	0.140	0.037	0.000	49.4	101.4	141.8	0.0	0.563	90.0	28.91
15	-0.139	0.012	0.165	0.038	0.000	47.9	101.3	143.3	0.0	0.560	90.0	29.96
16	-0.176	0.019	0.197	0.040	0.000	46.5	101.4	145.1	0.0	0.557	90.0	30.98
17	-0.215	0.029	0.226	0.040	0.000	45.2	101.4	146.6	0.0	0.554	90.0	31.94
18	-0.259	0.039	0.259	0.039	0.000	43.9	101.4	147.6	0.0	0.554	90.0	32.78
19	-0.307	0.050	0.292	0.035	0.000	42.6	101.4	148.8	0.0	0.553	90.0	33.71
20	-0.359	0.060	0.328	0.030	0.000	41.5	101.4	149.8	0.0	0.553	90.0	34.49
21	-0.412	0.073	0.363	0.025	0.000	40.7	101.4	150.8	0.0	0.551	90.0	35.11
22	-0.481	0.089	0.409	0.018	0.000	39.8	101.4	152.0	0.0	0.549	90.0	35.79
23	-0.541	0.101	0.447	0.008	0.000	39.0	101.4	153.0	0.0	0.547	90.0	36.41
24	-0.605	0.116	0.486	-0.003	0.000	38.1	101.4	153.7	0.0	0.548	90.0	37.06
25	-0.725	0.141	0.559	-0.026	0.000	37.3	101.4	154.9	0.0	0.545	90.0	37.72
26	-0.886	0.176	0.648	-0.062	0.000	36.1	101.4	156.1	0.0	0.544	90.0	38.63
27	-0.897	0.177	0.656	-0.064	0.000	36.0	101.3	156.2	0.0	0.544	90.0	38.73
28	-0.918	0.182	0.668	-0.068	0.000	35.8	101.3	156.5	0.0	0.543	90.0	38.88
29	-1.005	0.200	0.714	-0.091	0.000	35.2	101.4	156.7	0.0	0.545	90.0	39.28
30	-1.097	0.221	0.764	-0.112	0.000	34.8	101.4	157.5	0.0	0.543	90.0	39.65
31	-1.172	0.236	0.806	-0.130	0.000	34.5	101.4	158.3	0.0	0.540	90.0	39.94
32	-1.263	0.253	0.852	-0.158	0.000	33.8	101.4	158.4	0.0	0.542	90.0	40.40
33	-1.336	0.267	0.891	-0.177	0.000	33.4	101.4	158.9	0.0	0.542	90.0	40.73
34	-1.466	0.292	0.956	-0.218	0.000	33.2	101.4	159.6	0.0	0.540	90.0	40.95
35	-1.552	0.309	0.999	-0.244	0.000	32.9	101.4	159.9	0.0	0.539	90.0	41.17
36	-1.670	0.330	1.058	-0.282	0.000	32.5	101.4	159.8	0.0	0.541	90.0	41.47
37	-1.778	0.355	1.114	-0.310	0.000	32.3	101.4	160.8	0.0	0.537	90.0	41.73
38	-1.814	0.361	1.131	-0.322	0.000	32.0	101.4	160.9	0.0	0.538	90.0	41.94
39	-1.922	0.379	1.183	-0.359	0.000	31.7	101.4	161.4	0.0	0.537	90.0	42.19
40	-2.048	0.402	1.244	-0.402	0.000	31.4	101.4	161.7	0.0	0.537	90.0	42.42
41	-2.157	0.419	1.296	-0.442	0.000	31.1	101.4	162.0	0.0	0.537	90.0	42.66
42	-2.268	0.439	1.348	-0.481	0.000	30.9	101.4	162.1	0.0	0.537	90.0	42.82
43	-2.381	0.459	1.401	-0.521	0.000	31.0	101.4	162.9	0.0	0.533	90.0	42.85
44	-2.530	0.484	1.470	-0.576	0.000	30.9	101.4	163.3	0.0	0.532	90.0	42.96
45	-2.630	0.500	1.514	-0.615	0.000	30.7	101.4	163.3	0.0	0.533	90.0	43.11
46	**-2.807**	**0.530**	**1.595**	**-0.682**	**0.000**	**30.5**	**101.4**	**163.7**	**0.0**	**0.533**	**90.0**	**43.31**
47	-2.913	0.545	1.643	-0.726	0.000	30.9	101.4	163.9	0.0	0.530	90.0	43.03
48	-3.027	0.546	1.697	-0.784	0.000	31.1	101.5	163.9	0.0	0.530	90.0	42.94

Torsion Shear Test on Fine Nevada Sand at a Target Void Ratio = 0.530 (D_r = 91.28 %) Test No. A11

Test Date: 06/26/2010

Test Data

Specimen Height = 39.96 cm

Initial Void Ratio = 0.524

Final Average Confining Pressure (σavg) = 97.9 kPa

Maximum Friction Angle = 38.14°

Intermediate Principal Stress Ratio (b) at Failure = 0.77

Principal Stress Rotation Angle (α) = 90.0°

Shear Band Description

Average Inclination: 24.4°

Failure Method: (θ-z) & (r-z) mode

Point (No.)	εz (%)	εr (%)	εθ (%)	εv (%)	γθz (%)	σz (kPa)	σr (kPa)	σt (kPa)	τθz (kPa)	b	α (°)	φ (°)
1	0.000	0.000	0.000	0.000	0.000	91.8	101.3	101.1	0.0	0.982	90.0	2.74
2	0.000	0.000	-0.001	-0.001	0.000	91.9	101.3	101.1	0.0	0.981	90.0	2.73
3	0.003	-0.004	0.002	0.001	0.000	84.3	103.2	106.0	0.0	0.870	90.0	6.55
4	0.003	-0.004	0.005	0.004	0.000	78.4	104.9	110.1	0.0	0.835	90.0	9.69
5	-0.001	-0.003	0.012	0.008	0.000	72.9	106.4	114.0	0.0	0.815	90.0	12.69
6	-0.007	-0.001	0.021	0.013	0.000	68.5	107.6	116.9	0.0	0.808	90.0	15.15
7	-0.019	0.006	0.031	0.018	0.000	64.9	108.7	119.7	0.0	0.799	90.0	17.27
8	-0.033	0.014	0.042	0.023	0.000	61.4	109.7	121.8	0.0	0.800	90.0	19.26
9	-0.050	0.023	0.056	0.029	0.000	58.7	110.5	124.6	0.0	0.786	90.0	21.05
10	-0.067	0.032	0.069	0.035	0.000	55.8	111.2	126.0	0.0	0.790	90.0	22.72
11	-0.086	0.042	0.082	0.039	0.000	53.6	111.9	127.7	0.0	0.787	90.0	24.12
12	-0.110	0.054	0.099	0.043	0.000	51.6	112.5	129.2	0.0	0.784	90.0	25.42
13	-0.137	0.068	0.115	0.046	0.000	50.0	113.0	130.4	0.0	0.783	90.0	26.48
14	-0.167	0.083	0.134	0.049	0.000	48.2	113.4	131.5	0.0	0.783	90.0	27.62
15	-0.199	0.098	0.152	0.051	0.000	46.9	113.8	132.5	0.0	0.782	90.0	28.51
16	-0.234	0.113	0.173	0.052	0.000	45.4	114.2	133.2	0.0	0.783	90.0	29.44
17	-0.264	0.127	0.191	0.054	0.000	44.4	114.5	134.0	0.0	0.782	90.0	30.14
18	-0.302	0.143	0.210	0.052	0.000	43.3	114.8	134.6	0.0	0.783	90.0	30.91
19	-0.335	0.158	0.229	0.052	0.000	42.7	115.1	135.5	0.0	0.780	90.0	31.38
20	-0.375	0.175	0.249	0.049	0.000	41.8	115.3	136.0	0.0	0.780	90.0	32.02
21	-0.414	0.191	0.269	0.047	0.000	41.0	115.5	136.8	0.0	0.778	90.0	32.63
22	-0.451	0.207	0.288	0.044	0.000	40.2	115.7	137.1	0.0	0.779	90.0	33.11
23	-0.493	0.224	0.308	0.039	0.000	39.4	115.9	137.1	0.0	0.784	90.0	33.62
24	-0.524	0.237	0.325	0.038	0.000	39.1	116.1	138.1	0.0	0.778	90.0	33.97
25	-0.565	0.253	0.343	0.031	0.000	38.5	116.2	138.6	0.0	0.776	90.0	34.44
26	-0.611	0.271	0.365	0.025	0.000	38.0	116.4	138.6	0.0	0.779	90.0	34.74
27	-0.653	0.287	0.385	0.018	0.000	37.5	116.5	139.2	0.0	0.777	90.0	35.10
28	-0.693	0.302	0.404	0.013	0.000	37.3	116.7	139.5	0.0	0.777	90.0	35.33
29	-0.731	0.317	0.421	0.007	0.000	36.7	116.8	139.5	0.0	0.779	90.0	35.72
30	-0.764	0.329	0.436	0.001	0.000	36.3	116.9	140.1	0.0	0.776	90.0	36.02
31	-0.820	0.350	0.462	-0.008	0.000	35.9	117.1	140.6	0.0	0.775	90.0	36.36
32	-0.844	0.358	0.473	-0.013	0.000	35.8	117.2	140.9	0.0	0.774	90.0	36.51
33	-0.878	0.370	0.488	-0.020	0.000	35.3	117.3	141.1	0.0	0.775	90.0	36.88
34	-0.922	0.386	0.506	-0.030	0.000	34.6	117.5	140.9	0.0	0.780	90.0	37.30
35	-0.970	0.402	0.526	-0.042	0.000	34.4	117.5	141.6	0.0	0.775	90.0	37.52
36	-1.002	0.412	0.540	-0.050	0.000	34.1	117.6	141.6	0.0	0.776	90.0	37.72
37	-1.058	0.433	0.564	-0.061	0.000	33.9	117.7	142.0	0.0	0.775	90.0	37.90
38	**-1.110**	**0.450**	**0.587**	**-0.073**	**0.000**	**33.6**	**117.8**	**142.3**	**0.0**	**0.775**	**90.0**	**38.14**

Torsion Shear Test on Fine Nevada Sand at a Target Void Ratio = 0.530 (D_r = 91.28 %) Test No. A12

Test Date: 06/29/2010

Test Data

Specimen Height = 39.96 cm

Initial Void Ratio = 0.517

Final Average Confining Pressure (savg) = 98.6 kPa

Maximum Friction Angle = 36.24°

Intermediate Principal Stress Ratio (b) at Failure = 0.99

Principal Stress Rotation Angle (a) = 90.0°

Shear Band Description

Average Inclination	Failure Method
0°	(r-z) mode
21.7°	(θ-z) mode

Point (No.)	εz (%)	εr (%)	εθ (%)	εv (%)	γθz (%)	σz (kPa)	σr (kPa)	σt (kPa)	τθz (kPa)	b	α (°)	φ (°)
1	-0.003	0.002	0.002	0.000	0.000	92.6	101.1	101.1	0.0	0.998	90.0	2.50
2	-0.003	0.002	0.000	-0.001	0.000	92.7	101.1	100.9	0.0	0.968	90.0	2.41
3	-0.006	0.003	0.004	0.001	0.000	88.2	103.4	103.5	0.0	0.990	90.0	4.57
4	-0.010	0.008	0.005	0.003	0.000	84.0	105.3	105.2	0.0	0.997	90.0	6.44
5	-0.014	0.013	0.010	0.008	0.000	80.3	107.0	106.9	0.0	0.995	90.0	8.18
6	-0.019	0.019	0.012	0.012	0.000	76.8	108.8	108.8	0.0	0.998	90.0	9.94
7	-0.024	0.023	0.016	0.015	0.000	73.8	110.2	110.3	0.0	0.999	90.0	11.45
8	-0.034	0.031	0.023	0.020	0.000	70.8	111.6	111.6	0.0	1.000	90.0	12.93
9	-0.043	0.040	0.029	0.026	0.000	68.3	112.9	112.9	0.0	0.999	90.0	14.25
10	-0.053	0.049	0.036	0.032	0.000	66.0	114.0	114.0	0.0	0.999	90.0	15.45
11	-0.063	0.057	0.043	0.036	0.000	63.8	115.1	114.9	0.0	0.996	90.0	16.62
12	-0.075	0.067	0.051	0.042	0.000	61.5	116.1	115.4	0.0	0.987	90.0	17.74
13	-0.088	0.077	0.059	0.048	0.000	59.8	117.1	117.1	0.0	0.999	90.0	18.90
14	-0.102	0.087	0.067	0.052	0.000	57.8	117.9	117.6	0.0	0.995	90.0	19.96
15	-0.116	0.096	0.076	0.056	0.000	56.2	118.8	118.6	0.0	0.997	90.0	20.89
16	-0.130	0.107	0.084	0.061	0.000	54.7	119.6	119.5	0.0	0.999	90.0	21.83
17	-0.146	0.119	0.094	0.066	0.000	53.3	120.3	120.5	0.0	0.996	90.0	22.74
18	-0.163	0.132	0.102	0.072	0.000	51.8	120.9	120.9	0.0	0.999	90.0	23.56
19	-0.182	0.146	0.111	0.075	0.000	50.5	121.6	121.5	0.0	0.999	90.0	24.40
20	-0.205	0.161	0.123	0.079	0.000	49.3	122.2	122.4	0.0	0.998	90.0	25.20
21	-0.228	0.176	0.134	0.082	0.000	48.1	122.8	122.6	0.0	0.997	90.0	25.89
22	-0.254	0.191	0.148	0.086	0.000	47.0	123.3	123.2	0.0	0.999	90.0	26.63
23	-0.268	0.200	0.155	0.087	0.000	46.4	123.7	123.6	0.0	0.998	90.0	27.01
24	-0.312	0.228	0.174	0.090	0.000	44.8	124.3	124.1	0.0	0.997	90.0	27.99
25	-0.340	0.244	0.188	0.092	0.000	44.1	124.8	124.9	0.0	0.999	90.0	28.53
26	-0.372	0.262	0.203	0.092	0.000	43.1	125.2	125.4	0.0	0.998	90.0	29.21
27	-0.405	0.281	0.215	0.092	0.000	42.3	125.7	125.4	0.0	0.996	90.0	29.72
28	-0.441	0.302	0.231	0.092	0.000	41.5	126.1	125.9	0.0	0.998	90.0	30.29
29	-0.479	0.323	0.247	0.091	0.000	40.5	126.5	126.2	0.0	0.996	90.0	30.90
30	-0.517	0.343	0.263	0.090	0.000	40.2	126.8	127.0	0.0	0.997	90.0	31.30
31	-0.561	0.368	0.280	0.087	0.000	39.4	127.2	127.1	0.0	0.999	90.0	31.77
32	-0.602	0.389	0.297	0.085	0.000	38.7	127.4	127.6	0.0	0.998	90.0	32.30
33	-0.659	0.420	0.318	0.079	0.000	38.0	127.9	127.9	0.0	1.000	90.0	32.80
34	-0.696	0.439	0.332	0.075	0.000	37.8	128.1	128.3	0.0	0.998	90.0	33.02
35	-0.751	0.467	0.352	0.068	0.000	37.0	128.4	128.5	0.0	0.999	90.0	33.54
36	-0.808	0.495	0.372	0.060	0.000	36.6	128.7	128.9	0.0	0.998	90.0	33.90
37	-0.844	0.514	0.386	0.055	0.000	36.3	128.9	129.2	0.0	0.997	90.0	34.16
38	-0.892	0.537	0.401	0.046	0.000	35.6	129.1	129.2	0.0	0.999	90.0	34.60
39	-0.950	0.567	0.421	0.037	0.000	35.3	129.4	129.8	0.0	0.996	90.0	34.94
40	-1.019	0.601	0.444	0.026	0.000	34.6	129.7	129.9	0.0	0.998	90.0	35.38
41	-1.093	0.640	0.463	0.010	0.000	34.4	129.9	130.2	0.0	0.997	90.0	35.60
42	-1.192	0.693	0.491	-0.009	0.000	34.2	130.1	130.7	0.0	0.994	90.0	35.81
43	-1.301	0.752	0.516	-0.034	0.000	33.8	130.3	130.7	0.0	0.995	90.0	36.07
44	-1.439	0.829	0.546	-0.064	0.000	33.8	130.4	131.2	0.0	0.992	90.0	36.19
45	**-1.565**	**0.912**	**0.556**	**-0.097**	**0.000**	**33.8**	**130.6**	**131.5**	**0.0**	**0.990**	**90.0**	**36.24**

Appendix I **Series B Test Data**

Torsion Shear Test on Fine Nevada Sand at a Target Void Ratio = 0.530 (D_r = 91.28 %) Test No. B01

Test Date: 10/10/2011

Test Data

Specimen Height = 39.96 cm

Initial Void Ratio = 0.529

Final Average Confining Pressure (savg) = 101.9 kPa

Maximum Friction Angle = 55.75°

Intermediate Principal Stress Ratio (b) at Failure = 0.75

Principal Stress Rotation Angle (a) = 0.0°

Shear Band Description

Average Inclination: 65.7°

Secondary = 90°

Failure Method: (z-θ) & (r-θ) mode

(r-θ) mode

Point (No.)	εz (%)	εr (%)	εθ (%)	εv (%)	γθz (%)	σz (kPa)	σr (kPa)	σt (kPa)	τθz (kPa)	b	α (°)	φ (°)
1	0.000	-0.001	0.000	-0.001	0.000	100.5	101.3	101.3	0.0	0.964	0.0	-0.25
2	0.000	-0.001	0.000	-0.001	0.000	100.8	101.3	101.4	0.0	0.888	0.0	-0.18
3	0.001	0.000	0.000	0.001	0.000	101.7	101.7	99.9	0.0	1.032	0.0	0.50
4	0.003	0.006	-0.003	0.006	0.000	106.4	103.6	93.6	0.0	0.781	0.0	3.68
5	0.012	0.018	-0.013	0.017	0.000	116.9	107.9	78.5	0.0	0.765	0.0	11.34
6	0.021	0.024	-0.024	0.022	0.000	124.8	110.9	68.1	0.0	0.754	0.0	17.11
7	0.030	0.027	-0.033	0.024	0.000	130.4	113.1	60.5	0.0	0.753	0.0	21.50
8	0.038	0.031	-0.043	0.026	0.000	134.8	115.0	53.7	0.0	0.756	0.0	25.48
9	0.046	0.033	-0.053	0.027	0.000	138.4	116.4	49.0	0.0	0.754	0.0	28.50
10	0.054	0.036	-0.063	0.027	0.000	141.2	117.6	44.9	0.0	0.755	0.0	31.19
11	0.063	0.038	-0.075	0.026	0.000	144.0	118.6	41.6	0.0	0.752	0.0	33.51
12	0.072	0.041	-0.090	0.023	0.000	146.1	119.5	38.3	0.0	0.753	0.0	35.75
13	0.082	0.044	-0.105	0.021	0.000	148.0	120.2	35.9	0.0	0.752	0.0	37.56
14	0.091	0.048	-0.119	0.019	0.000	149.4	120.8	34.0	0.0	0.752	0.0	39.03
15	0.100	0.051	-0.136	0.016	0.000	150.6	121.3	32.1	0.0	0.753	0.0	40.46
16	0.112	0.057	-0.157	0.012	0.000	152.0	121.8	30.2	0.0	0.752	0.0	41.94
17	0.123	0.062	-0.178	0.007	0.000	153.1	122.3	28.7	0.0	0.752	0.0	43.17
18	0.133	0.069	-0.200	0.002	0.000	154.0	122.6	27.5	0.0	0.752	0.0	44.21
19	0.143	0.075	-0.221	-0.003	0.000	154.6	122.9	26.4	0.0	0.753	0.0	45.13
20	0.153	0.080	-0.241	-0.008	0.000	155.4	123.2	25.5	0.0	0.752	0.0	45.90
21	0.163	0.085	-0.260	-0.012	0.000	156.2	123.5	24.5	0.0	0.752	0.0	46.77
22	0.178	0.094	-0.292	-0.021	0.000	157.2	123.9	23.3	0.0	0.751	0.0	47.90
23	0.187	0.100	-0.316	-0.028	0.000	157.6	124.1	22.7	0.0	0.752	0.0	48.46
24	0.198	0.106	-0.339	-0.035	0.000	158.0	124.2	22.1	0.0	0.751	0.0	49.00
25	0.210	0.114	-0.368	-0.044	0.000	158.4	124.5	21.3	0.0	0.752	0.0	49.70
26	0.221	0.121	-0.393	-0.052	0.000	158.9	124.5	20.9	0.0	0.751	0.0	50.10
27	0.237	0.130	-0.430	-0.063	0.000	159.6	124.8	20.3	0.0	0.750	0.0	50.75
28	0.255	0.142	-0.474	-0.077	0.000	160.3	125.2	19.5	0.0	0.750	0.0	51.54
29	0.263	0.148	-0.493	-0.083	0.000	160.7	125.2	19.3	0.0	0.749	0.0	51.78
30	0.283	0.160	-0.542	-0.100	0.000	160.8	125.3	18.7	0.0	0.750	0.0	52.36
31	0.292	0.165	-0.566	-0.108	0.000	160.9	125.4	18.3	0.0	0.751	0.0	52.71
32	0.300	0.170	-0.584	-0.115	0.000	161.1	125.5	18.1	0.0	0.751	0.0	52.89
33	0.317	0.180	-0.627	-0.130	0.000	161.6	125.6	17.8	0.0	0.750	0.0	53.29
34	0.329	0.187	-0.657	-0.141	0.000	161.8	125.7	17.5	0.0	0.750	0.0	53.59
35	0.353	0.202	-0.719	-0.165	0.000	162.2	125.9	16.9	0.0	0.750	0.0	54.23
36	0.362	0.208	-0.744	-0.174	0.000	162.6	126.0	16.8	0.0	0.749	0.0	54.39
37	0.375	0.216	-0.778	-0.187	0.000	162.8	126.1	16.5	0.0	0.749	0.0	54.72
38	0.389	0.225	-0.816	-0.202	0.000	163.0	126.2	16.3	0.0	0.749	0.0	54.94
39	0.408	0.238	-0.866	-0.221	0.000	163.3	126.3	16.0	0.0	0.749	0.0	55.24
40	0.424	0.248	-0.911	-0.239	0.000	163.5	126.4	15.8	0.0	0.749	0.0	55.49
41	**0.441**	**0.258**	**-0.956**	**-0.256**	**0.000**	**163.7**	**126.4**	**15.5**	**0.0**	**0.748**	**0.0**	**55.75**

Torsion Shear Test on Fine Nevada Sand at a Target Void Ratio = 0.530 (D_r = 91.28 %) Test No. B02

Test Date: 07/29/2011

Test Data

Specimen Height = 39.99 cm

Initial Void Ratio = 0.524

Final Average Confining Pressure (savg) = 101.2 kPa

Maximum Friction Angle = 38.21°

Intermediate Principal Stress Ratio (b) at Failure = -0.01

Principal Stress Rotation Angle (a) = 22.3°

Shear Band Description

Average Inclination: 20.7°

Failure Method: (z-r) & (z-θ) mode

Point (No.)	εz (%)	εr (%)	εθ (%)	εv (%)	γθz (%)	σz (kPa)	σr (kPa)	σt (kPa)	τθz (kPa)	b	α (°)	φ (°)
1	0.000	0.000	0.000	0.000	0.014	102.5	100.1	101.0	2.5	0.169	36.5	1.47
2	0.001	-0.001	0.000	0.000	0.018	105.3	98.3	99.5	4.3	0.107	28.0	2.91
3	0.001	-0.001	-0.001	-0.001	0.032	127.8	83.8	91.4	20.5	0.030	24.2	14.51
4	0.001	-0.002	-0.003	-0.003	0.056	135.6	79.0	88.8	25.7	0.022	23.8	18.05
5	0.005	-0.005	-0.008	-0.007	0.116	143.6	73.6	85.5	32.8	0.033	24.2	22.51
6	0.012	-0.010	-0.015	-0.013	0.174	150.1	69.7	83.5	36.7	0.025	23.9	25.11
7	0.024	-0.018	-0.026	-0.020	0.245	155.8	66.0	81.3	40.0	0.019	23.5	27.42
8	0.044	-0.032	-0.045	-0.033	0.327	160.6	62.9	79.8	43.0	0.014	23.4	29.42
9	0.076	-0.053	-0.074	-0.050	0.421	165.0	59.9	77.8	44.8	0.008	22.9	30.99
10	0.106	-0.073	-0.099	-0.066	0.499	167.6	58.3	76.9	46.1	0.006	22.7	31.94
11	0.111	-0.080	-0.114	-0.083	0.526	169.6	57.0	76.8	47.2	0.000	22.7	32.52
12	0.161	-0.115	-0.161	-0.115	0.651	172.4	55.2	75.5	48.7	-0.001	22.6	33.62
13	0.186	-0.132	-0.185	-0.131	0.710	173.7	54.5	75.3	49.3	-0.002	22.5	34.01
14	0.250	-0.178	-0.250	-0.178	0.863	175.4	53.2	74.2	50.6	-0.001	22.5	34.97
15	0.303	-0.216	-0.304	-0.217	0.981	177.0	52.2	74.0	51.4	-0.004	22.5	35.44
16	0.411	-0.297	-0.419	-0.304	1.227	179.6	50.7	73.3	52.5	-0.007	22.3	36.25
17	0.491	-0.357	-0.507	-0.373	1.400	180.5	49.9	72.9	53.3	-0.007	22.4	36.71
18	0.577	-0.424	-0.605	-0.451	1.597	181.6	49.2	72.7	54.0	-0.008	22.4	37.09
19	0.654	-0.482	-0.690	-0.519	1.757	182.3	48.7	72.4	54.5	-0.009	22.4	37.41
20	0.740	-0.551	-0.791	-0.601	1.951	183.1	48.1	72.3	55.0	-0.010	22.4	37.66
21	0.797	-0.596	-0.860	-0.660	2.086	183.5	47.8	72.1	55.2	-0.010	22.4	37.84
22	0.868	-0.652	-0.942	-0.727	2.237	184.1	47.5	72.2	55.4	-0.012	22.4	37.93
23	0.937	-0.707	-1.025	-0.796	2.395	184.4	47.2	72.1	55.6	-0.013	22.4	38.04
24	1.004	-0.761	-1.105	-0.862	2.542	184.7	47.0	71.9	55.7	-0.013	22.3	38.18
25	**1.050**	**-0.797**	**-1.159**	**-0.907**	**2.643**	**185.0**	**46.8**	**71.9**	**55.8**	**-0.014**	**22.3**	**38.21**

Torsion Shear Test on Fine Nevada Sand at a Target Void Ratio = 0.530 (D_r = 91.28 %) Test No. B03

Test Date: 08/31/2011

Test Data

Specimen Height = 40.53 cm

Initial Void Ratio = 0.548

Final Average Confining Pressure (savg) = 101.8 kPa

Maximum Friction Angle = 44.71°

Intermediate Principal Stress Ratio (b) at Failure = 0.50

Principal Stress Rotation Angle (a) = 22.4°

Shear Band Description

Average Inclination: 47.6°

Failure Method: (z-θ) mode

Point (No.)	εz (%)	εr (%)	εθ (%)	εv (%)	γθz (%)	σz (kPa)	σr (kPa)	σt (kPa)	τθz (kPa)	b	α (°)	φ (°)
1	0.000	0.000	0.000	0.000	0.001	101.4	101.3	100.2	0.4	0.871	16.4	0.42
2	0.001	-0.001	0.000	0.000	0.004	102.4	101.4	98.8	3.7	0.592	31.9	2.36
3	0.004	0.000	-0.002	0.002	0.013	110.1	101.4	92.6	8.4	0.501	21.9	6.86
4	0.006	0.001	-0.004	0.003	0.023	115.1	101.3	88.0	14.0	0.494	22.9	11.06
5	0.008	0.002	-0.006	0.004	0.033	118.7	101.3	83.8	18.3	0.502	23.2	14.48
6	0.010	0.004	-0.009	0.006	0.043	122.6	101.4	80.3	20.9	0.499	22.3	17.07
7	0.014	0.006	-0.013	0.007	0.058	126.7	101.3	76.2	25.3	0.498	22.5	20.61
8	0.016	0.007	-0.015	0.008	0.068	128.5	101.4	73.6	27.5	0.504	22.5	22.62
9	0.019	0.009	-0.020	0.008	0.082	131.5	101.4	71.1	30.2	0.501	22.5	24.92
10	0.024	0.011	-0.028	0.008	0.107	134.0	101.4	68.6	32.6	0.501	22.4	27.11
11	0.040	0.012	-0.048	0.004	0.172	136.0	101.3	64.6	36.9	0.509	23.0	30.79
12	0.043	0.013	-0.052	0.004	0.185	138.3	101.3	64.3	37.6	0.500	22.7	31.39
13	0.052	0.015	-0.066	0.002	0.221	140.0	101.3	63.0	39.3	0.499	22.8	32.82
14	0.063	0.015	-0.081	-0.003	0.263	141.7	101.4	61.2	40.5	0.499	22.6	34.25
15	0.066	0.019	-0.090	-0.005	0.280	142.1	101.4	60.8	41.2	0.500	22.7	34.77
16	0.078	0.026	-0.120	-0.016	0.345	143.5	101.3	58.6	42.6	0.502	22.5	36.51
17	0.083	0.031	-0.140	-0.026	0.384	144.6	101.3	57.8	43.5	0.501	22.5	37.39
18	0.087	0.037	-0.155	-0.032	0.411	147.1	101.4	57.4	44.1	0.493	22.3	37.97
19	0.098	0.039	-0.179	-0.042	0.459	145.7	101.3	55.9	44.4	0.504	22.3	38.81
20	0.116	0.045	-0.222	-0.061	0.546	147.1	101.4	55.5	45.7	0.500	22.5	39.66
21	0.133	0.052	-0.268	-0.083	0.630	148.0	101.4	54.7	46.5	0.501	22.5	40.54
22	0.160	0.064	-0.343	-0.119	0.766	148.9	101.3	53.9	47.5	0.499	22.5	41.53
23	0.180	0.070	-0.394	-0.144	0.850	149.4	101.3	53.3	48.0	0.500	22.5	42.10
24	0.193	0.076	-0.430	-0.161	0.909	149.8	101.3	53.1	48.4	0.499	22.5	42.41
25	0.215	0.084	-0.488	-0.189	1.003	150.6	101.4	52.5	48.9	0.498	22.5	43.00
27	0.278	0.112	-0.668	-0.279	1.294	151.6	101.3	51.6	49.7	0.498	22.4	43.93
28	0.315	0.132	-0.786	-0.339	1.479	152.3	101.4	51.4	50.2	0.497	22.4	44.32
29	0.351	0.161	-0.916	-0.403	1.676	152.3	101.4	51.1	50.0	0.498	22.3	44.41
30	0.396	0.186	-1.049	-0.467	1.885	153.0	101.3	51.1	50.3	0.495	22.3	44.55
31	**0.413**	**0.193**	**-1.095**	**-0.489**	**1.954**	**152.9**	**101.3**	**51.1**	**50.6**	**0.495**	**22.4**	**44.71**
32	0.421	0.206	-1.140	-0.513	2.030	152.6	101.3	51.4	50.7	0.495	22.5	44.61
33	0.423	0.208	-1.148	-0.517	2.041	152.6	101.3	51.3	50.1	0.496	22.3	44.31
34	0.429	0.219	-1.182	-0.534	2.091	152.7	101.4	51.5	49.4	0.495	22.2	43.85
35	0.433	0.224	-1.202	-0.544	2.120	152.8	101.4	51.8	49.3	0.493	22.2	43.61
36	0.447	0.244	-1.265	-0.573	2.222	153.5	101.4	52.7	49.4	0.488	22.2	43.20

Torsion Shear Test on Fine Nevada Sand at a Target Void Ratio = 0.530 (D_r = 91.28 %) Test No. B04

Test Date: 01/01/1904

Test Data

Specimen Height = 39.99 cm

Initial Void Ratio = 0.541

Final Average Confining Pressure (savg) = 102.8 kPa

Maximum Friction Angle = 41.11°

Intermediate Principal Stress Ratio (b) at Failure = 0.99

Principal Stress Rotation Angle (a) = 22.4°

Shear Band Description

Average Inclination: 67.0°

Failure Method: (r-θ) mode

Point (No.)	εz (%)	εr (%)	εθ (%)	εv (%)	γθz (%)	σz (kPa)	σr (kPa)	σt (kPa)	τθz (kPa)	b	α (°)	φ (°)
1	0.000	0.000	0.000	0.000	0.000	102.1	102.5	99.8	1.2	0.978	22.6	0.94
2	-0.006	0.012	-0.001	0.005	0.021	105.2	108.3	91.0	9.7	0.923	26.9	7.03
3	-0.006	0.015	-0.003	0.006	0.028	107.0	110.6	88.0	12.2	0.921	26.0	9.16
4	-0.006	0.020	-0.006	0.009	0.036	108.4	113.0	83.9	14.5	0.945	24.9	11.39
5	-0.006	0.025	-0.008	0.011	0.043	109.5	115.1	80.4	15.9	0.967	23.8	13.12
6	-0.006	0.032	-0.013	0.013	0.056	111.0	117.9	76.2	18.7	0.976	23.6	15.83
7	-0.005	0.036	-0.016	0.015	0.063	111.6	119.2	74.0	20.5	0.976	23.7	17.40
8	-0.006	0.042	-0.019	0.016	0.071	112.5	120.8	71.8	21.9	0.978	23.6	18.94
9	-0.006	0.047	-0.023	0.018	0.077	113.3	122.2	69.5	22.9	0.986	23.1	20.28
10	-0.006	0.051	-0.026	0.019	0.084	113.9	123.2	68.2	24.4	0.980	23.4	21.53
11	-0.006	0.058	-0.032	0.020	0.096	114.6	124.5	65.9	25.6	0.985	23.2	23.04
12	-0.004	0.064	-0.039	0.021	0.112	115.5	125.7	64.5	27.6	0.976	23.6	24.66
13	-0.001	0.078	-0.055	0.021	0.146	116.6	127.6	61.4	29.6	0.977	23.5	27.04
14	0.003	0.096	-0.081	0.018	0.192	117.3	129.5	57.9	31.0	0.988	23.1	29.33
15	0.010	0.114	-0.110	0.014	0.248	118.5	130.9	56.6	33.4	0.976	23.6	31.37
16	0.011	0.155	-0.170	-0.003	0.343	119.7	133.2	52.8	34.5	0.988	22.9	33.86
17	0.010	0.188	-0.219	-0.020	0.417	120.5	134.3	51.7	35.9	0.984	23.1	35.31
18	0.003	0.244	-0.300	-0.054	0.528	121.1	135.7	49.2	36.5	0.993	22.7	37.04
19	0.006	0.278	-0.363	-0.079	0.629	121.7	136.4	48.5	37.4	0.990	22.8	37.96
20	0.004	0.321	-0.438	-0.113	0.736	122.2	137.2	47.4	37.8	0.993	22.6	38.84
21	0.001	0.357	-0.499	-0.140	0.820	122.5	137.6	46.7	38.1	0.993	22.6	39.41
22	-0.001	0.392	-0.559	-0.168	0.907	122.7	137.9	46.5	38.6	0.991	22.7	39.92
23	-0.005	0.435	-0.632	-0.203	1.004	123.3	138.5	46.0	39.0	0.990	22.6	40.41
24	-0.008	0.482	-0.717	-0.243	1.114	123.5	138.8	45.5	39.1	0.992	22.5	40.84
25	**-0.012**	**0.514**	**-0.771**	**-0.270**	**1.183**	**124.3**	**138.9**	**45.3**	**39.3**	**0.985**	**22.4**	**41.11**

Torsion Shear Test on Fine Nevada Sand at a Target Void Ratio = 0.530 (D_r = 91.28 %) Test No. B05

Test Date: 09/09/2011

Test Data

Specimen Height = 39.96 cm

Initial Void Ratio = 0.530

Final Average Confining Pressure (savg) = 102.0 kPa

Maximum Friction Angle = 37.45°

Intermediate Principal Stress Ratio (b) at Failure = 0.23

Principal Stress Rotation Angle (a) = 45.1°

Shear Band Description

Average Inclination	Failure Method
19.3°	(z-θ) mode

Point (No.)	εz (%)	εr (%)	εθ (%)	εv (%)	γθz (%)	σz (kPa)	σr (kPa)	σt (kPa)	τθz (kPa)	b	α (°)	φ (°)
1	0.000	0.000	0.000	0.000	0.000	101.8	100.9	102.4	1.3	0.066	51.1	0.76
2	0.000	-0.001	0.001	0.000	0.009	102.5	100.4	102.9	4.7	0.254	46.3	2.60
3	0.000	-0.003	0.006	0.003	0.048	104.0	97.1	104.4	15.3	0.268	45.3	8.47
4	-0.001	-0.005	0.009	0.003	0.076	105.1	95.2	105.2	20.7	0.261	45.1	11.37
5	-0.002	-0.007	0.016	0.007	0.119	106.2	92.8	106.4	27.0	0.250	45.1	14.74
6	-0.004	-0.008	0.023	0.011	0.183	107.4	90.5	107.6	34.0	0.250	45.1	18.43
7	-0.006	-0.009	0.029	0.013	0.228	108.1	89.2	108.2	37.8	0.249	45.0	20.45
8	-0.009	-0.011	0.036	0.016	0.302	108.7	87.8	108.9	42.1	0.251	45.1	22.79
9	-0.014	-0.013	0.045	0.019	0.414	109.4	86.1	110.0	46.7	0.247	45.2	25.19
10	-0.015	-0.015	0.049	0.019	0.460	109.9	85.5	110.4	48.2	0.245	45.1	25.98
11	-0.019	-0.018	0.056	0.019	0.564	110.7	84.4	110.8	51.2	0.243	45.0	27.51
12	-0.022	-0.022	0.060	0.016	0.658	111.1	83.6	111.4	53.3	0.241	45.1	28.65
13	-0.025	-0.026	0.065	0.014	0.739	111.5	82.9	111.8	54.9	0.239	45.1	29.46
14	-0.028	-0.031	0.069	0.009	0.846	111.6	82.2	112.0	56.7	0.239	45.1	30.46
15	-0.033	-0.038	0.072	0.001	0.981	112.0	81.5	112.4	58.6	0.239	45.1	31.49
16	-0.040	-0.044	0.075	-0.009	1.103	112.3	81.0	112.7	60.3	0.239	45.1	32.42
17	-0.045	-0.049	0.076	-0.018	1.212	112.5	80.5	112.9	61.4	0.238	45.1	33.00
18	-0.049	-0.056	0.078	-0.027	1.312	112.6	80.2	113.4	62.2	0.236	45.2	33.36
19	-0.061	-0.066	0.078	-0.049	1.502	113.0	79.7	113.5	63.9	0.238	45.1	34.36
20	-0.069	-0.074	0.075	-0.068	1.664	113.0	79.4	113.4	64.7	0.238	45.1	34.86
21	-0.077	-0.082	0.073	-0.087	1.825	113.3	79.0	113.8	65.6	0.237	45.1	35.30
22	-0.082	-0.089	0.069	-0.101	1.941	113.5	78.8	114.0	66.1	0.236	45.1	35.55
23	-0.093	-0.099	0.064	-0.128	2.143	113.6	78.4	114.1	67.1	0.236	45.1	36.10
24	-0.099	-0.103	0.061	-0.140	2.235	113.6	78.3	114.0	67.3	0.237	45.1	36.26
25	-0.107	-0.108	0.058	-0.157	2.359	113.8	78.2	114.2	67.7	0.236	45.1	36.46
26	-0.120	-0.118	0.048	-0.191	2.582	113.9	78.0	114.3	68.2	0.235	45.1	36.72
27	-0.124	-0.123	0.039	-0.207	2.700	113.9	77.9	114.4	68.3	0.235	45.1	36.78
28	-0.132	-0.130	0.030	-0.232	2.869	113.9	77.7	114.7	68.7	0.234	45.2	36.92
29	-0.144	-0.137	0.021	-0.260	3.057	114.1	77.7	114.8	69.0	0.234	45.2	37.10
30	-0.174	-0.131	0.022	-0.283	3.204	114.1	77.6	114.6	69.2	0.234	45.1	37.24
31	-0.202	-0.127	0.023	-0.306	3.365	114.2	77.5	114.5	69.4	0.234	45.1	37.37
32	**-0.205**	**-0.130**	**0.019**	**-0.316**	**3.436**	**114.2**	**77.4**	**114.5**	**69.5**	**0.235**	**45.1**	**37.45**
33	-0.212	-0.131	0.019	-0.324	3.493	114.4	77.4	114.9	69.6	0.232	45.1	37.42
34	-0.220	-0.138	0.016	-0.342	3.650	114.4	77.4	114.8	69.6	0.233	45.1	37.37
35	-0.223	-0.145	0.014	-0.354	3.771	114.2	77.4	114.5	69.3	0.233	45.0	37.28
36	-0.229	-0.148	0.014	-0.364	3.881	114.3	77.4	114.5	69.1	0.232	45.0	37.16
37	-0.235	-0.152	0.013	-0.374	4.006	114.3	77.4	114.5	68.9	0.231	45.0	37.02
38	-0.239	-0.156	0.014	-0.381	4.121	114.3	77.4	114.3	68.7	0.232	45.0	36.95
39	-0.240	-0.163	0.013	-0.391	4.283	114.2	77.6	114.9	68.5	0.230	45.1	36.72
40	-0.244	-0.164	0.013	-0.394	4.344	114.3	77.6	114.8	68.5	0.230	45.1	36.72
41	-0.246	-0.168	0.013	-0.401	4.460	114.3	77.6	114.8	68.3	0.229	45.1	36.59

Torsion Shear Test on Fine Nevada Sand at a Target Void Ratio = 0.530 (D_r = 91.28 %) Test No. B06

Test Date: 09/23/2011

Test Data

Specimen Height = 39.99 cm

Initial Void Ratio = 0.540

Final Average Confining Pressure (savg) = 102.2 kPa

Maximum Friction Angle = 38.36°

Intermediate Principal Stress Ratio (b) at Failure = 0.74

Principal Stress Rotation Angle (a) = 44.9°

Shear Band Description

Average Inclination	Failure Method
22.5°	(z-θ) mode
Secondary 3.5°	(z-θ) mode

Point (No.)	εz (%)	εr (%)	εθ (%)	εv (%)	γθz (%)	σz (kPa)	σr (kPa)	σt (kPa)	τθz (kPa)	b	α (°)	φ (°)
1	0.000	0.002	0.001	0.002	0.003	100.8	101.6	101.4	1.7	0.659	50.0	0.98
2	0.000	0.001	0.001	0.002	0.005	100.8	101.9	100.9	2.6	0.702	45.8	1.46
3	-0.003	0.009	0.003	0.009	0.038	100.1	104.7	99.9	10.8	0.719	44.8	6.21
4	-0.012	0.027	0.008	0.023	0.134	98.0	109.3	97.8	25.1	0.728	44.9	14.88
5	-0.016	0.035	0.010	0.028	0.170	97.2	110.7	97.0	28.6	0.737	44.9	17.15
6	-0.022	0.046	0.011	0.035	0.226	96.8	111.9	96.7	33.1	0.729	45.0	20.02
7	-0.031	0.061	0.011	0.041	0.289	95.1	114.5	95.0	39.9	0.743	45.0	24.80
8	-0.044	0.079	0.010	0.045	0.378	95.1	114.5	95.0	39.9	0.743	45.0	24.80
9	-0.056	0.095	0.009	0.048	0.452	94.8	115.2	94.8	41.9	0.743	45.0	26.20
10	-0.070	0.112	0.006	0.048	0.530	94.6	115.8	94.4	43.6	0.745	44.9	27.49
11	-0.087	0.132	0.003	0.049	0.633	94.3	116.6	94.3	45.7	0.744	45.0	29.00
12	-0.104	0.151	-0.001	0.047	0.723	93.9	117.1	93.6	46.9	0.749	44.9	30.02
13	-0.137	0.185	-0.010	0.038	0.888	93.6	117.8	93.5	49.0	0.747	44.9	31.56
14	-0.159	0.206	-0.017	0.029	0.999	93.6	118.1	93.4	50.0	0.747	44.9	32.32
15	-0.216	0.256	-0.036	0.004	1.265	93.3	119.0	93.2	52.1	0.747	45.0	33.98
16	-0.257	0.291	-0.053	-0.018	1.440	93.2	119.2	92.9	53.0	0.746	44.9	34.72
17	-0.295	0.323	-0.068	-0.040	1.606	93.2	119.5	93.0	53.9	0.745	44.9	35.38
18	-0.345	0.364	-0.089	-0.070	1.819	92.9	119.9	92.8	54.7	0.747	44.9	36.10
19	-0.380	0.393	-0.106	-0.092	1.971	92.9	120.1	92.8	55.3	0.746	45.0	36.56
20	-0.421	0.428	-0.127	-0.121	2.159	93.0	120.3	92.6	56.0	0.745	44.9	37.11
21	-0.466	0.466	-0.152	-0.152	2.362	93.1	120.6	92.7	56.7	0.745	44.9	37.64
22	-0.501	0.496	-0.174	-0.178	2.533	93.1	120.8	92.6	57.2	0.745	44.9	38.00
23	-0.544	0.533	-0.202	-0.213	2.743	92.9	121.0	92.6	57.5	0.745	44.9	38.29
24	**-0.556**	**0.542**	**-0.210**	**-0.224**	**2.813**	**92.9**	**120.9**	**92.6**	**57.6**	**0.745**	**44.9**	**38.36**
25	-0.569	0.551	-0.215	-0.234	2.880	92.8	121.0	92.4	57.0	0.749	44.9	37.96
26	-0.580	0.557	-0.216	-0.239	2.929	93.0	120.8	92.6	56.2	0.749	44.9	37.27
27	-0.595	0.565	-0.216	-0.246	3.000	93.1	120.5	92.4	55.4	0.750	44.8	36.70
28	-0.599	0.567	-0.217	-0.249	3.052	93.3	120.3	92.7	55.1	0.748	44.8	36.32
29	-0.604	0.570	-0.216	-0.251	3.090	93.4	120.3	92.9	54.9	0.747	44.9	36.10
30	-0.612	0.576	-0.216	-0.252	3.174	93.3	120.1	92.9	54.1	0.750	44.9	35.52
31	-0.623	0.579	-0.214	-0.259	3.262	93.5	120.0	92.8	54.1	0.748	44.8	35.51

Torsion Shear Test on Fine Nevada Sand at a Target Void Ratio = 0.530 (D_r = 91.28 %) Test No. B07

Test Date: 01/01/1904

Test Data

Specimen Height = 39.99 cm

Initial Void Ratio = 0.538

Final Average Confining Pressure (savg) = 100.2 kPa

Maximum Friction Angle = 33.94°

Intermediate Principal Stress Ratio (b) at Failure = 0.00

Principal Stress Rotation Angle (a) = 67.3°

Shear Band Description

Average Inclination: 0°

Failure Method: (θ-z) mode

Point (No.)	εz (%)	εr (%)	εθ (%)	εv (%)	γθz (%)	σz (kPa)	σr (kPa)	σt (kPa)	τθz (kPa)	b	α (°)	φ (°)
1	0.000	0.000	0.000	0.000	0.000	100.6	100.2	102.4	1.2	0.062	62.7	0.86
2	0.000	0.000	0.000	-0.001	0.000	100.6	100.2	102.4	1.2	0.069	62.5	0.86
3	-0.019	-0.004	0.024	0.001	0.030	96.2	92.4	114.9	11.0	0.043	65.1	7.86
4	-0.033	-0.010	0.050	0.006	0.079	93.1	86.8	123.3	16.8	0.025	66.0	12.04
5	-0.052	-0.020	0.085	0.013	0.147	90.0	81.5	131.3	21.7	0.013	66.8	15.68
6	-0.061	-0.037	0.117	0.019	0.222	88.0	77.9	136.9	25.5	0.012	66.9	18.33
7	-0.080	-0.053	0.158	0.025	0.317	86.2	74.6	142.1	29.3	0.011	66.8	20.78
8	-0.105	-0.076	0.210	0.029	0.420	84.6	71.4	147.5	31.9	0.002	67.3	22.72
9	-0.124	-0.095	0.247	0.029	0.501	83.6	69.8	149.5	34.2	0.008	67.0	24.05
10	-0.149	-0.120	0.295	0.027	0.590	82.3	68.0	152.0	35.9	0.009	67.1	25.28
11	-0.180	-0.152	0.354	0.022	0.695	81.3	66.3	154.6	37.4	0.007	67.2	26.39
12	-0.214	-0.182	0.411	0.015	0.792	80.6	65.0	156.5	38.8	0.006	67.2	27.24
13	-0.250	-0.217	0.472	0.004	0.898	80.0	63.7	158.5	39.8	0.004	67.3	27.96
14	-0.297	-0.262	0.546	-0.014	1.027	79.4	62.6	160.5	41.2	0.003	67.3	28.79
15	-0.330	-0.290	0.595	-0.025	1.107	79.3	61.8	162.0	41.7	0.000	67.4	29.13
16	-0.377	-0.331	0.664	-0.044	1.223	78.6	61.0	162.8	42.6	0.001	67.3	29.74
17	-0.448	-0.396	0.770	-0.073	1.407	78.8	60.3	165.0	44.1	0.000	67.2	30.38
18	-0.491	-0.437	0.834	-0.095	1.515	77.9	59.4	165.4	44.5	0.001	67.3	30.84
19	-0.522	-0.466	0.877	-0.111	1.586	77.2	58.7	165.7	44.5	0.000	67.4	31.12
20	-0.576	-0.516	0.955	-0.137	1.719	77.1	58.2	167.0	45.1	-0.002	67.4	31.45
21	-0.618	-0.556	1.014	-0.161	1.822	76.6	57.6	167.1	45.6	0.000	67.4	31.83
22	-0.649	-0.584	1.057	-0.176	1.895	76.6	57.4	167.9	45.9	-0.001	67.4	31.96
23	-0.702	-0.634	1.130	-0.206	2.018	76.5	57.0	168.5	46.3	-0.002	67.4	32.22
24	-0.755	-0.684	1.203	-0.236	2.143	76.3	56.6	169.2	46.7	-0.002	67.4	32.45
25	-0.783	-0.709	1.240	-0.252	2.210	76.0	56.3	169.2	46.9	-0.001	67.4	32.62
26	-0.829	-0.750	1.301	-0.279	2.315	75.8	56.2	169.3	47.2	0.000	67.4	32.81
27	-0.892	-0.811	1.386	-0.317	2.459	75.7	55.7	170.2	47.4	-0.002	67.4	32.98
28	-0.941	-0.854	1.449	-0.345	2.568	75.7	55.5	170.4	47.7	-0.002	67.4	33.13
29	-0.973	-0.885	1.493	-0.366	2.641	75.5	55.3	170.6	47.8	-0.003	67.4	33.20
30	-1.036	-0.947	1.577	-0.405	2.788	75.4	55.0	171.0	48.0	-0.003	67.4	33.38
31	-1.078	-0.992	1.636	-0.433	2.888	75.3	54.8	171.2	48.2	-0.003	67.4	33.48
32	-1.106	-1.018	1.673	-0.451	2.956	75.2	54.8	171.0	48.3	-0.002	67.4	33.55
33	-1.150	-1.064	1.734	-0.481	3.062	75.1	54.5	171.5	48.4	-0.003	67.4	33.64
34	-1.198	-1.114	1.799	-0.513	3.178	74.9	54.2	171.8	48.4	-0.005	67.5	33.71
35	-1.247	-1.161	1.865	-0.543	3.294	75.1	54.2	172.1	48.5	-0.006	67.5	33.71
36	-1.291	-1.200	1.921	-0.569	3.395	75.0	54.1	172.1	48.6	-0.005	67.5	33.76
37	-1.353	-1.253	2.000	-0.606	3.539	75.0	54.1	172.1	48.8	-0.005	67.4	33.84
38	-1.390	-1.291	2.051	-0.631	3.629	75.0	54.0	172.0	48.8	-0.004	67.4	33.88
39	-1.430	-1.325	2.101	-0.655	3.720	74.9	54.1	171.6	48.9	-0.003	67.3	33.92
40	**-1.414**	**-1.336**	**2.094**	**-0.656**	**3.726**	**74.8**	**54.1**	**171.6**	**48.9**	**-0.003**	**67.3**	**33.94**
41	-1.447	-1.390	2.153	-0.684	3.827	75.4	54.0	172.4	48.9	-0.008	67.4	33.77
42	-1.489	-1.454	2.223	-0.720	3.951	75.2	53.9	172.2	48.7	-0.007	67.4	33.77

Torsion Shear Test on Fine Nevada Sand at a Target Void Ratio = 0.530 (D_r = 91.28 %) Test No. B08

Test Date: 10/06/2011

Test Data

Specimen Height = 39.96 cm

Initial Void Ratio = 0.525

Final Average Confining Pressure (savg) = 101.8 kPa

Maximum Friction Angle = 38.38°

Intermediate Principal Stress Ratio (b) at Failure = 0.50

Principal Stress Rotation Angle (a) = 67.5°

Shear Band Description

Average Inclination	Failure Method
8°	(θ-z) mode

Point (No.)	εz (%)	εr (%)	εθ (%)	εv (%)	γθz (%)	σz (kPa)	σr (kPa)	σt (kPa)	τθz (kPa)	b	α (°)	φ (°)
1	0.000	0.000	0.000	0.000	0.000	100.7	101.3	102.7	1.3	0.382	64.5	0.91
2	0.000	0.000	0.001	0.000	0.000	99.7	101.4	102.8	2.0	0.527	63.9	1.42
3	-0.002	-0.001	0.004	0.001	0.005	95.3	101.4	107.4	6.6	0.500	66.2	5.08
4	-0.007	0.000	0.010	0.004	0.018	90.8	101.3	111.6	11.1	0.503	66.6	8.64
5	-0.015	0.004	0.020	0.009	0.043	87.2	101.4	115.5	15.0	0.501	66.6	11.73
6	-0.026	0.008	0.030	0.012	0.073	83.6	101.3	118.3	18.4	0.507	66.6	14.52
7	-0.039	0.014	0.041	0.016	0.109	81.2	101.3	121.4	21.1	0.501	66.8	16.72
8	-0.057	0.021	0.057	0.021	0.161	78.2	101.4	124.4	24.0	0.501	66.9	19.17
9	-0.070	0.025	0.069	0.024	0.197	76.4	101.4	125.9	25.4	0.503	67.1	20.53
10	-0.081	0.026	0.082	0.028	0.232	74.9	101.3	127.8	26.6	0.500	67.4	21.73
11	-0.100	0.031	0.104	0.035	0.293	72.9	101.4	129.8	29.0	0.501	67.2	23.64
12	-0.121	0.040	0.119	0.037	0.344	71.3	101.4	131.1	30.4	0.502	67.2	24.93
13	-0.143	0.047	0.135	0.040	0.399	70.0	101.3	132.5	31.8	0.501	67.3	26.14
14	-0.194	0.065	0.171	0.043	0.512	67.7	101.4	134.2	33.8	0.504	67.3	28.00
15	-0.241	0.078	0.206	0.043	0.612	66.5	101.4	136.5	35.3	0.499	67.4	29.30
16	-0.282	0.089	0.233	0.040	0.692	65.5	101.4	137.3	36.2	0.500	67.4	30.21
17	-0.325	0.100	0.261	0.036	0.775	64.7	101.3	138.3	37.2	0.498	67.4	31.02
18	-0.341	0.105	0.270	0.034	0.804	64.1	101.4	138.2	37.4	0.502	67.4	31.33
19	-0.387	0.117	0.297	0.027	0.890	63.6	101.4	139.1	38.2	0.501	67.4	31.99
20	-0.441	0.131	0.328	0.018	0.989	62.5	101.4	140.0	38.9	0.501	67.5	32.82
21	-0.486	0.141	0.353	0.008	1.072	62.1	101.4	141.0	39.6	0.498	67.5	33.38
22	-0.526	0.152	0.374	0.000	1.141	61.7	101.4	141.2	40.0	0.499	67.4	33.75
23	-0.589	0.167	0.405	-0.017	1.253	61.0	101.4	141.8	40.6	0.500	67.4	34.35
24	-0.631	0.178	0.426	-0.026	1.327	60.6	101.4	142.1	40.8	0.500	67.5	34.68
25	-0.693	0.195	0.456	-0.042	1.436	60.3	101.4	142.5	41.3	0.500	67.4	35.07
26	-0.741	0.212	0.477	-0.052	1.519	59.7	101.4	142.9	41.6	0.501	67.5	35.51
27	-0.808	0.232	0.508	-0.068	1.637	59.4	101.4	144.1	42.5	0.497	67.5	36.13
28	-0.856	0.246	0.529	-0.080	1.719	59.0	101.4	143.9	42.7	0.500	67.4	36.41
29	-0.911	0.254	0.554	-0.103	1.817	58.7	101.4	144.6	43.1	0.498	67.4	36.76
30	-0.965	0.270	0.579	-0.117	1.911	58.5	101.4	144.9	43.6	0.498	67.4	37.11
31	-1.029	0.289	0.608	-0.132	2.022	58.1	101.4	145.2	43.6	0.498	67.5	37.35
32	-1.081	0.304	0.631	-0.145	2.112	57.4	101.4	145.6	43.3	0.499	67.7	37.52
33	-1.170	0.330	0.671	-0.168	2.268	57.7	101.4	146.4	44.1	0.495	67.6	37.83
34	-1.228	0.347	0.698	-0.183	2.370	57.7	101.3	146.1	44.1	0.495	67.5	37.81
35	-1.295	0.367	0.728	-0.200	2.489	57.7	101.3	146.0	44.4	0.496	67.4	37.96
36	-1.354	0.385	0.754	-0.215	2.593	57.2	101.4	146.6	44.5	0.496	67.6	38.24
37	-1.427	0.408	0.785	-0.234	2.719	57.1	101.4	146.4	44.6	0.497	67.5	38.32
38	**-1.491**	**0.430**	**0.812**	**-0.249**	**2.821**	**57.2**	**101.4**	**146.7**	**44.7**	**0.496**	**67.5**	**38.38**
39	-1.514	0.434	0.821	-0.259	2.893	57.4	101.4	146.8	44.8	0.495	67.5	38.30

Torsion Shear Test on Fine Nevada Sand at a Target Void Ratio = 0.530 (D_r = 91.28 %) Test No. B09

Test Date: 10/04/2011

Test Data

Specimen Height = 39.96 cm

Initial Void Ratio = 0.532

Final Average Confining Pressure (savg) = 102.7 kPa

Maximum Friction Angle = 36.38°

Intermediate Principal Stress Ratio (b) at Failure = 1.01

Principal Stress Rotation Angle (a) = 68.3°

Shear Band Description

Average Inclination	Failure Method
5.8°	(θ-z)&(r-z)mode
Secondary 12°	(θ-z)

Point (No.)	εz (%)	εr (%)	εθ (%)	εv (%)	γθz (%)	σz (kPa)	σr (kPa)	σt (kPa)	τθz (kPa)	b	α (°)	φ (°)
1	-0.011	0.013	0.006	0.007	0.000	99.8	102.8	102.2	1.4	0.973	65.7	1.06
2	0.000	0.004	0.000	0.004	0.000	99.2	103.0	102.3	2.4	0.896	61.1	1.64
3	0.000	0.004	0.000	0.004	0.056	80.3	115.0	109.1	15.3	0.983	66.6	12.83
4	-0.003	0.006	0.002	0.005	0.082	77.5	116.9	110.6	17.7	0.971	66.5	14.93
5	-0.006	0.009	0.003	0.006	0.102	75.9	118.2	111.6	19.2	0.966	66.5	16.21
6	-0.017	0.017	0.009	0.009	0.160	70.9	120.9	112.7	21.7	0.983	66.9	19.15
7	-0.022	0.021	0.011	0.010	0.188	69.9	122.0	113.8	23.0	0.974	66.8	20.23
8	-0.032	0.029	0.016	0.013	0.235	67.4	123.3	113.9	24.4	0.983	66.8	21.83
9	-0.043	0.038	0.021	0.015	0.277	65.7	124.5	114.4	25.5	0.989	66.9	23.06
10	-0.062	0.052	0.029	0.019	0.327	64.2	125.6	115.4	26.6	0.984	66.9	24.31
11	-0.080	0.065	0.037	0.023	0.369	62.7	126.7	116.3	27.1	0.988	67.4	25.22
12	-0.095	0.077	0.044	0.026	0.400	61.6	127.1	116.1	27.5	0.994	67.4	25.85
13	-0.107	0.085	0.049	0.028	0.424	60.9	127.6	116.4	27.9	0.995	67.4	26.32
14	-0.117	0.093	0.053	0.030	0.445	60.3	127.8	116.3	28.1	0.999	67.4	26.68
15	-0.130	0.102	0.059	0.032	0.470	59.9	128.3	116.8	28.5	0.996	67.5	27.12
16	-0.146	0.114	0.066	0.034	0.498	59.2	128.7	116.8	28.8	0.999	67.5	27.59
17	-0.168	0.130	0.075	0.036	0.538	58.5	129.1	117.4	29.4	0.995	67.5	28.20
19	-0.245	0.182	0.104	0.041	0.674	56.8	130.5	117.7	31.5	0.994	67.0	30.10
20	-0.277	0.203	0.116	0.042	0.731	56.1	131.1	118.0	31.6	0.999	67.2	30.54
21	-0.306	0.221	0.126	0.041	0.781	54.5	131.8	118.9	31.6	1.000	67.8	31.34
22	-0.356	0.252	0.142	0.038	0.867	54.9	132.0	118.3	32.8	0.997	67.0	31.75
23	-0.386	0.270	0.151	0.035	0.917	53.3	132.8	119.1	32.0	1.008	67.9	32.15
24	-0.479	0.322	0.177	0.019	1.063	52.5	133.5	119.3	32.5	1.011	67.9	32.85
25	-0.511	0.338	0.185	0.012	1.109	53.8	132.6	117.8	33.9	1.001	66.7	32.93
26	-0.608	0.389	0.206	-0.013	1.242	52.9	133.2	119.1	34.4	0.995	66.9	33.67
27	-0.648	0.410	0.214	-0.024	1.296	51.4	134.4	119.9	33.5	1.008	67.8	34.05
28	-0.716	0.448	0.226	-0.043	1.388	51.9	134.0	119.6	34.9	0.996	67.1	34.55
29	-0.782	0.486	0.235	-0.061	1.472	50.8	135.0	120.6	34.7	1.002	67.6	35.05
30	-0.910	0.565	0.249	-0.096	1.633	51.7	134.4	120.7	36.1	0.983	66.9	35.38
31	-0.975	0.607	0.254	-0.114	1.710	48.9	136.3	120.9	33.5	1.022	68.5	35.42
32	-1.205	0.769	0.258	-0.178	1.971	50.6	135.8	121.6	35.8	0.993	67.4	35.81
33	-1.356	0.886	0.250	-0.220	2.135	50.8	136.0	121.2	36.6	0.992	66.9	36.20
34	**-1.447**	**0.961**	**0.241**	**-0.245**	**2.228**	**48.6**	**137.2**	**122.3**	**34.8**	**1.011**	**68.3**	**36.38**
35	-1.537	1.037	0.229	-0.270	2.316	48.7	136.9	121.1	34.4	1.021	68.2	36.04
36	-1.589	1.084	0.221	-0.285	2.367	52.3	135.1	121.5	37.0	0.976	66.5	35.67
37	-1.681	1.167	0.204	-0.310	2.450	49.1	137.7	123.3	31.1	1.031	70.0	34.19

Torsion Shear Test on Fine Nevada Sand at a Target Void Ratio = 0.530 (D_r = 91.28 %)

Test No. B10
Test Date: 10/13/2011

Test Data

Specimen Height = 39.96 cm
Initial Void Ratio = 0.538
Final Average Confining Pressure (savg) = 98.6 kPa
Maximum Friction Angle = 33.56°
Intermediate Principal Stress Ratio (b) at Failure = 0.05
Principal Stress Rotation Angle (a) = 90.0°

Shear Band Description

Average Inclination	Failure Method
22.5°	(θ-z) mode

Point (No.)	εz (%)	εr (%)	εθ (%)	εv (%)	γθz (%)	σz (kPa)	σr (kPa)	σt (kPa)	τθz (kPa)	b	α (°)	φ (°)
1	0.000	0.000	0.000	0.000	0.000	94.8	101.3	101.5	0.0	0.965	90.0	1.96
2	0.000	0.000	0.000	0.000	0.000	94.7	101.2	101.4	0.0	0.973	90.0	1.98
3	0.000	0.000	0.000	0.000	0.000	94.6	101.2	101.6	0.0	0.945	90.0	2.04
4	0.000	-0.001	0.000	0.000	0.000	94.5	101.1	101.7	0.0	0.919	90.0	2.11
5	0.000	-0.001	0.001	0.000	0.000	94.5	101.0	102.0	0.0	0.875	90.0	2.18
6	0.000	-0.001	0.000	-0.001	0.000	94.3	101.0	101.8	0.0	0.889	90.0	2.19
7	0.000	-0.001	0.000	0.000	0.000	94.4	100.9	102.3	0.0	0.831	90.0	2.29
8	0.000	-0.002	0.001	-0.001	0.000	94.3	100.8	102.4	0.0	0.804	90.0	2.36
9	0.000	-0.002	0.001	-0.001	0.000	94.2	100.7	102.7	0.0	0.766	90.0	2.49
10	0.000	-0.002	0.001	-0.001	0.000	93.9	100.6	102.8	0.0	0.753	90.0	2.59
11	-0.002	-0.010	0.008	-0.003	0.000	91.5	98.1	107.7	0.0	0.410	90.0	4.66
12	-0.006	-0.021	0.019	-0.008	0.000	88.2	94.9	114.2	0.0	0.255	90.0	7.37
13	-0.012	-0.030	0.033	-0.009	0.000	85.3	91.8	120.4	0.0	0.187	90.0	9.83
14	-0.020	-0.039	0.051	-0.008	0.000	82.3	88.9	125.9	0.0	0.151	90.0	12.10
15	-0.030	-0.047	0.072	-0.005	0.000	79.4	86.4	131.1	0.0	0.136	90.0	14.23
16	-0.040	-0.056	0.094	-0.002	0.000	77.3	83.8	136.2	0.0	0.111	90.0	16.02
17	-0.053	-0.064	0.119	0.002	0.000	75.0	81.6	140.6	0.0	0.101	90.0	17.73
18	-0.066	-0.076	0.148	0.006	0.000	72.6	79.2	145.2	0.0	0.091	90.0	19.46
19	-0.083	-0.087	0.179	0.009	0.000	70.7	77.5	148.6	0.0	0.087	90.0	20.80
20	-0.108	-0.101	0.225	0.015	0.000	68.7	75.6	152.3	0.0	0.082	90.0	22.22
21	-0.138	-0.116	0.275	0.021	0.000	66.9	73.8	155.8	0.0	0.077	90.0	23.53
22	-0.166	-0.131	0.321	0.024	0.000	65.5	72.5	158.2	0.0	0.075	90.0	24.49
23	-0.207	-0.153	0.387	0.027	0.000	64.2	70.9	161.6	0.0	0.069	90.0	25.57
24	-0.250	-0.173	0.453	0.030	0.000	62.9	69.7	163.8	0.0	0.068	90.0	26.44
25	-0.303	-0.199	0.532	0.031	0.000	61.6	68.5	166.1	0.0	0.066	90.0	27.31
26	-0.349	-0.224	0.603	0.029	0.000	60.7	67.4	168.3	0.0	0.062	90.0	28.02
27	-0.406	-0.254	0.684	0.024	0.000	59.3	66.4	169.8	0.0	0.065	90.0	28.85
28	-0.480	-0.291	0.790	0.019	0.000	58.7	65.5	171.7	0.0	0.061	90.0	29.39
29	-0.520	-0.311	0.846	0.014	0.000	58.2	65.0	172.7	0.0	0.060	90.0	29.73
30	-0.594	-0.350	0.947	0.003	0.000	57.3	64.2	174.2	0.0	0.059	90.0	30.33
31	-0.664	-0.388	1.042	-0.010	0.000	56.6	63.5	175.5	0.0	0.058	90.0	30.80
32	-0.713	-0.414	1.109	-0.019	0.000	56.3	63.1	176.4	0.0	0.056	90.0	31.07
33	-0.765	-0.444	1.179	-0.030	0.000	55.8	62.6	177.1	0.0	0.056	90.0	31.39
34	-0.818	-0.472	1.249	-0.041	0.000	55.5	62.2	178.0	0.0	0.055	90.0	31.63
35	-0.887	-0.514	1.339	-0.061	0.000	54.5	61.6	178.1	0.0	0.058	90.0	32.11
36	-0.844	-0.488	1.282	-0.050	0.000	54.9	61.9	177.9	0.0	0.057	90.0	31.90
37	-0.886	-0.579	1.391	-0.074	0.000	54.6	61.4	179.5	0.0	0.054	90.0	32.22
38	-0.921	-0.626	1.458	-0.089	0.000	54.2	61.1	180.3	0.0	0.054	90.0	32.51
39	-0.969	-0.655	1.522	-0.103	0.000	54.0	60.6	180.8	0.0	0.052	90.0	32.70
40	-1.009	-0.676	1.572	-0.112	0.000	53.9	60.4	181.2	0.0	0.051	90.0	32.80
41	-1.079	-0.716	1.662	-0.133	0.000	53.3	60.0	181.6	0.0	0.052	90.0	33.11
42	-1.178	-0.774	1.789	-0.163	0.000	52.9	59.6	182.2	0.0	0.052	90.0	33.37
43	-1.245	-0.812	1.873	-0.184	0.000	52.8	59.4	183.0	0.0	0.051	90.0	33.51
44	**-1.305**	**-0.852**	**1.965**	**-0.192**	**0.000**	**52.9**	**59.1**	**183.8**	**0.0**	**0.047**	**90.0**	**33.56**

Appendix J **Derivation**

Traditional Definitions

$$\sigma_1 = \frac{\sigma_z + \sigma_\theta}{2} + \sqrt{\left(\frac{\sigma_z - \sigma_\theta}{2}\right)^2 + {\tau_{z\theta}}^2}$$

$$\sigma_2 = \sigma_r$$

$$\sigma_1 \geq \sigma_2$$

However, if the Major Principal Stress is Radial

$$\sigma_1 = \sigma_r$$

$$\sigma_2 = \frac{\sigma_z + \sigma_\theta}{2} + \sqrt{\left(\frac{\sigma_z - \sigma_\theta}{2}\right)^2 + {\tau_{z\theta}}^2}$$

$$\sigma_r \geq \frac{\sigma_z + \sigma_\theta}{2} + \sqrt{\left(\frac{\sigma_z - \sigma_\theta}{2}\right)^2 + {\tau_{z\theta}}^2}$$

Define Stresses

$$\sigma_r = \frac{P_o R_o + P_i R_i}{(R_o + R_i)}$$

$$\sigma_\theta = \frac{P_o R_o - P_i R_i}{(R_o - R_i)}$$

$$\sigma_z = \frac{F_v}{\pi(R_o^2 - R_i^2)} + \frac{P_o R_o^2 - P_i R_i^2}{(R_o^2 - R_i^2)}$$

$$\tau_{z\theta} = \frac{3M}{2\pi(R_o^3 - R_i^3)}$$

Simplify the term $\left(\frac{\sigma_z - \sigma_\theta}{2}\right)$

$$\left(\frac{\sigma_z - \sigma_\theta}{2}\right) = \frac{F_v}{2\pi(R_o - R_i)(R_o + R_i)} + \frac{P_o R_o^2 - P_i R_i^2}{2(R_o - R_i)(R_o + R_i)} - \frac{(P_o R_o - P_i R_i)(R_o + R_i)}{2(R_o - R_i)(R_o + R_i)}$$

$$= \frac{F_v}{2\pi(R_o - R_i)(R_o + R_i)} + \frac{P_i R_i R_o - P_o R_o R_i}{2(R_o - R_i)(R_o + R_i)}$$

$$= \frac{F_v}{2\pi(R_o - R_i)(R_o + R_i)} + \frac{(P_i - P_o)R_i R_o}{2(R_o - R_i)(R_o + R_i)}$$

$$= \frac{F_v + \pi R_i R_o (P_i - P_o)}{2\pi(R_o - R_i)(R_o + R_i)}$$

Simplify the Term $\left(\frac{\boldsymbol{3M(R_o - R_i)(R_o + R_i)}}{\boldsymbol{(R_o^3 - R_i^3)}}\right)^{\boldsymbol{2}}$

$$\tan(2\alpha) = \frac{\frac{3M}{(R_o^3 - R_i^3)}}{\frac{F_v + \pi R_i R_o (P_i - P_o)}{(R_o - R_i)(R_o + R_i)}}$$

$$\tan(2\alpha) = \frac{3M(R_o - R_i)(R_o + R_i)}{(R_o^3 - R_i^3)[F_v + \pi R_i R_o (P_i - P_o)]}$$

$$\tan^2(2\alpha)[F_v + \pi R_i R_o (P_i - P_o)]^2 = \left[\frac{3M(R_o - R_i)(R_o + R_i)}{(R_o^3 - R_i^3)}\right]^2$$

Simplify Radical $\sqrt{\left(\frac{\boldsymbol{\sigma_z - \sigma_\theta}}{\boldsymbol{2}}\right)^{\boldsymbol{2}} + \boldsymbol{\tau_{z\theta}}^{\boldsymbol{2}}}$

$$\sqrt{\left(\frac{\sigma_z - \sigma_\theta}{2}\right)^2 + \tau_{z\theta}{}^2} = \sqrt{\left(\frac{F_v + \pi R_i R_o (P_i - P_o)}{2\pi(R_o - R_i)(R_o + R_i)}\right)^2 + \left(\frac{3M}{2\pi(R_o^3 - R_i^3)}\right)^2}$$

$$= \frac{1}{2\pi}\sqrt{\left(\frac{F_v + \pi R_i R_o (P_i - P_o)}{(R_o - R_i)(R_o + R_i)}\right)^2 + \left(\frac{3M(R_o - R_i)(R_o + R_i)}{(R_o^3 - R_i^3)}\right)^2 \left(\frac{1}{(R_o - R_i)(R_o + R_i)}\right)^2}$$

$$= \frac{1}{2\pi}\sqrt{\left(\frac{F_v + \pi R_i R_o (P_i - P_o)}{(R_o - R_i)(R_o + R_i)}\right)^2 + \tan^2(2\alpha)[F_v + \pi R_i R_o (P_i - P_o)]^2 \left(\frac{1}{(R_o - R_i)(R_o + R_i)}\right)^2}$$

$$= \frac{1}{2\pi}\sqrt{\left(\frac{[F_v + \pi R_i R_o (P_i - P_o)]^2}{[(R_o - R_i)(R_o + R_i)]^2}\right)(1 + \tan^2 2\alpha)}$$

$$= \frac{1}{2\pi(R_o - R_i)(R_o + R_i)}\sqrt{\left(\frac{[F_v + \pi R_i R_o (P_i - P_o)]^2}{\cos^2 2\alpha}\right)}$$

$$= \frac{1}{2\pi(R_o - R_i)(R_o + R_i)\cos 2\alpha}[F_v + \pi R_i R_o (P_i - P_o)]$$

$$\sqrt{\left(\frac{\sigma_z - \sigma_\theta}{2}\right)^2 + {\tau_{z\theta}}^2} = \frac{\frac{F_v}{\pi} + R_i R_o (P_i - P_o)}{2(R_o - R_i)(R_o + R_i)\cos 2\alpha}$$

Simplify $\left(\frac{\sigma_z + \sigma_\theta}{2}\right)$

$$\left(\frac{\sigma_z + \sigma_\theta}{2}\right) = \frac{F_v}{2\pi(R_o - R_i)(R_o + R_i)} + \left\{\frac{P_o R_o^2 - P_i R_i^2}{2\pi(R_o - R_i)(R_o + R_i)} + \frac{(P_o R_o - P_i R_i)(R_o + R_i)}{2(R_o - R_i)(R_o + R_i)}\right\}_a$$

$$\{\quad\}_a = \frac{P_o R_o^2 - P_i R_i^2 + (P_o R_o - P_i R_i)(R_o + R_i)}{2(R_o - R_i)(R_o + R_i)}$$

$$\{\quad\}_a = \frac{2P_o R_o^2 - 2P_i R_i^2 + R_o R_i (P_o - P_i)}{2(R_o - R_i)(R_o + R_i)}$$

$$\left(\frac{\sigma_z + \sigma_\theta}{2}\right) = \frac{F_v}{2\pi(R_o - R_i)(R_o + R_i)} + \frac{2P_o R_o^2 - 2P_i R_i^2 + R_o R_i (P_o - P_i)}{2(R_o - R_i)(R_o + R_i)}$$

For the Major Principal Stress to be in the Radial Direction

$\sigma_1 \geq \sigma_2$

$$\sigma_2 = \frac{\sigma_z + \sigma_\theta}{2} + \sqrt{\left(\frac{\sigma_z - \sigma_\theta}{2}\right)^2 + {\tau_{z\theta}}^2}$$

$$= \frac{F_v}{2\pi(R_o - R_i)(R_o + R_i)} + \frac{2P_o R_o^2 - 2P_i R_i^2 + R_o R_i (P_o - P_i)}{2(R_o - R_i)(R_o + R_i)} + \frac{\frac{F_v}{\pi} + R_i R_o (P_i - P_o)}{2(R_o - R_i)(R_o + R_i)\cos 2\alpha}$$

$$\sigma_1 = \frac{P_o R_o + P_i R_i}{(R_o + R_i)}$$

$$\frac{P_o R_o + P_i R_i}{(R_o + R_i)} \geq \frac{F_v}{2\pi(R_o - R_i)(R_o + R_i)} + \frac{2P_o R_o^2 - 2P_i R_i^2 + R_o R_i (P_o - P_i)}{2(R_o - R_i)(R_o + R_i)} + \frac{\frac{F_v}{\pi} + R_i R_o (P_i - P_o)}{2(R_o - R_i)(R_o + R_i)\cos 2\alpha}$$

$$\frac{P_o R_o + P_i R_i}{\cancel{(R_o + R_i)}} 2 \geq \frac{F_v}{2\pi(R_o - R_i)\cancel{(R_o + R_i)}} + \frac{2P_o R_o^2 - 2P_i R_i^2 + R_o R_i (P_o - P_i)}{2(R_o - R_i)\cancel{(R_o + R_i)}} + \frac{\frac{F_v}{\pi} + R_i R_o (P_i - P_o)}{2(R_o - R_i)\cancel{(R_o + R_i)}\cos 2\alpha}$$

$$2(R_o - R_i)\cos 2\alpha\,(P_o R_o + P_i R_i) \geq$$

$$\frac{F_v}{\pi}\cos 2\alpha + \cos 2\alpha\,[2P_o R_o^2 - 2P_i R_i^2 + R_o R_i (P_o - P_i)] + \frac{F_v}{\pi} - R_o R_i (P_o - P_i)$$

$$\text{Cos}(2\alpha)\left[2P_oR_o^2 - 2P_iR_i^2 - 2R_oR_i(P_o - P_i)\right] \geq \frac{F_v}{\pi}\cos(2\alpha) + 2\cos(2\alpha)P_oR_o^2 - 2\cos(2\alpha)P_iR_i^2 + \cos(2\alpha)\,R_oR_i(P_o - P_i) + \frac{F_v}{\pi} + R_iR_o(P_i - P_o)$$

$$\cancel{P_oR_o^2 2\cos(2\alpha) + 2\cos(2\alpha)P_iR_i^2} \geq \frac{F_v}{\pi}\cos(2\alpha) + \cancel{2\cos(2\Psi)P_oR_o^2} - \cancel{2\cos(2\alpha)P_iR_i^2} + 2\cos(2\alpha)\,R_oR_i(P_o - P_i) + \cos(2\alpha)\,R_oR_i(P_o - P_i) + \frac{F_v}{\pi} + R_iR_o(P_i - P_o)$$

$$0 \geq \frac{F_v}{\pi}\cos(2\alpha) + 3\cos(2\alpha)\,R_oR_i(P_o - P_i) + \frac{F_v}{\pi} - R_oR_i(P_o - P_i)$$

$$0 \geq \frac{F_v}{\pi}[\cos(2\alpha) + 1] + R_oR_i(P_o - P_i)[3\cos(2\alpha) - 1]$$

$$\frac{F_v}{\pi}[\cos(2\alpha) + 1] < R_oR_i(P_o - P_i)[3\cos(2\alpha) - 1]$$

$$\boxed{F_v < \pi R_oR_i(P_o - P_i)\frac{[3\cos(2\alpha) - 1]}{[\cos(2\alpha) + 1]}}$$

Appendix K **Skempton Values**

Skempton's B values

Test No.	B Value
A01	99.00%
A02	74.00%
A03	99.00%
A04	not measured
A05	79.49%
A06	98.00%
A07	not measured
A08	not measured
A09	90.08%
A10	87.00%
A11	89.00%
A12	95.00%
B01	93.30%
B02	99.00%
B03	98.00%
B04	1.00%
B05	98.00%
B06	1.01%
B07	98.00%
B08	96.80%
B09	99.00%
B10	94.50%

Appendix L **Pictures**

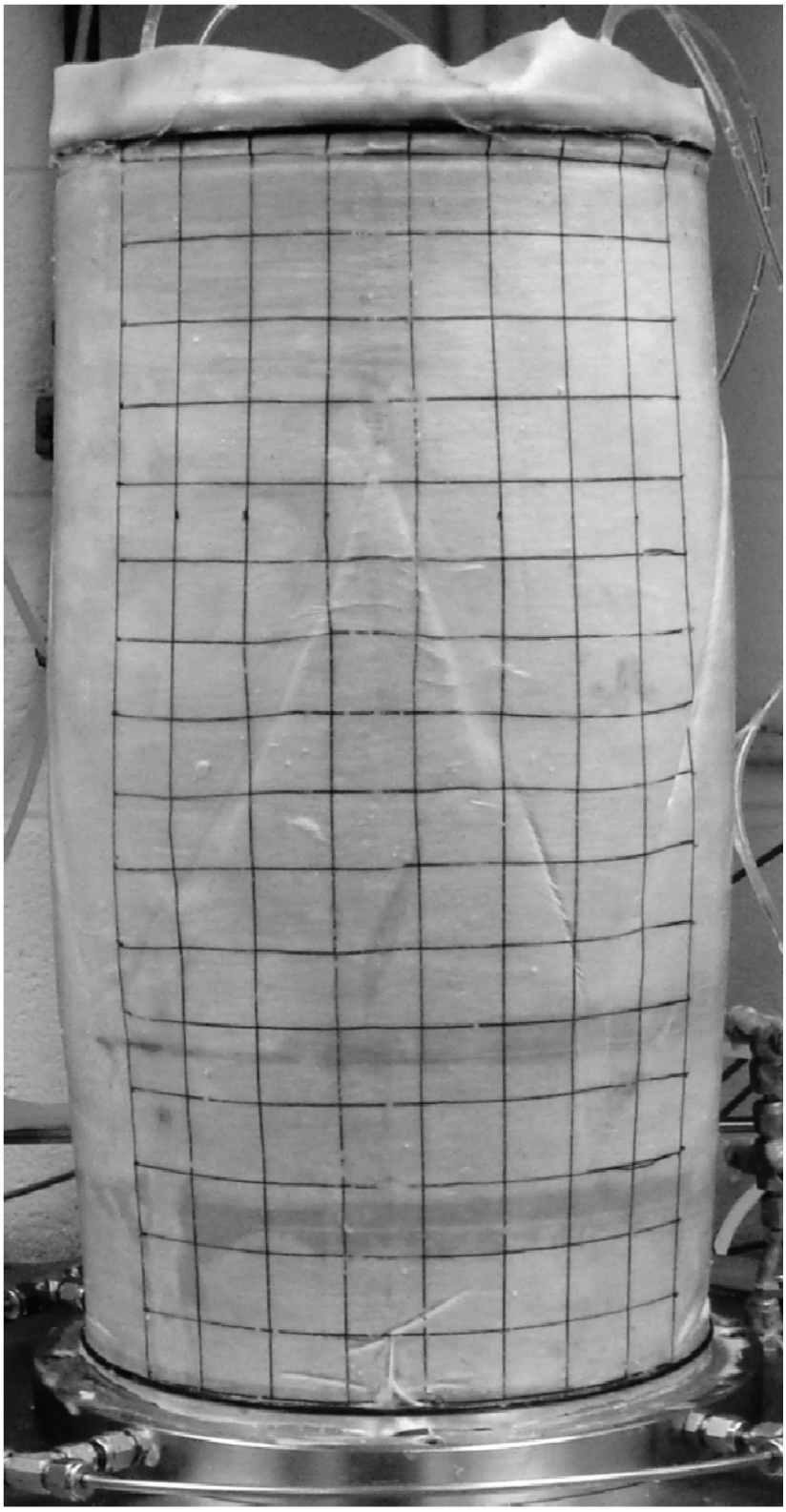

Figure L-1: Test B01 (α = 0°, b = 0.75)

Figure L-2: Test B02 (α = 22.3°, b = -0.01)

Figure L-3: Test B03 (α = 22.4°, b = 0.50)

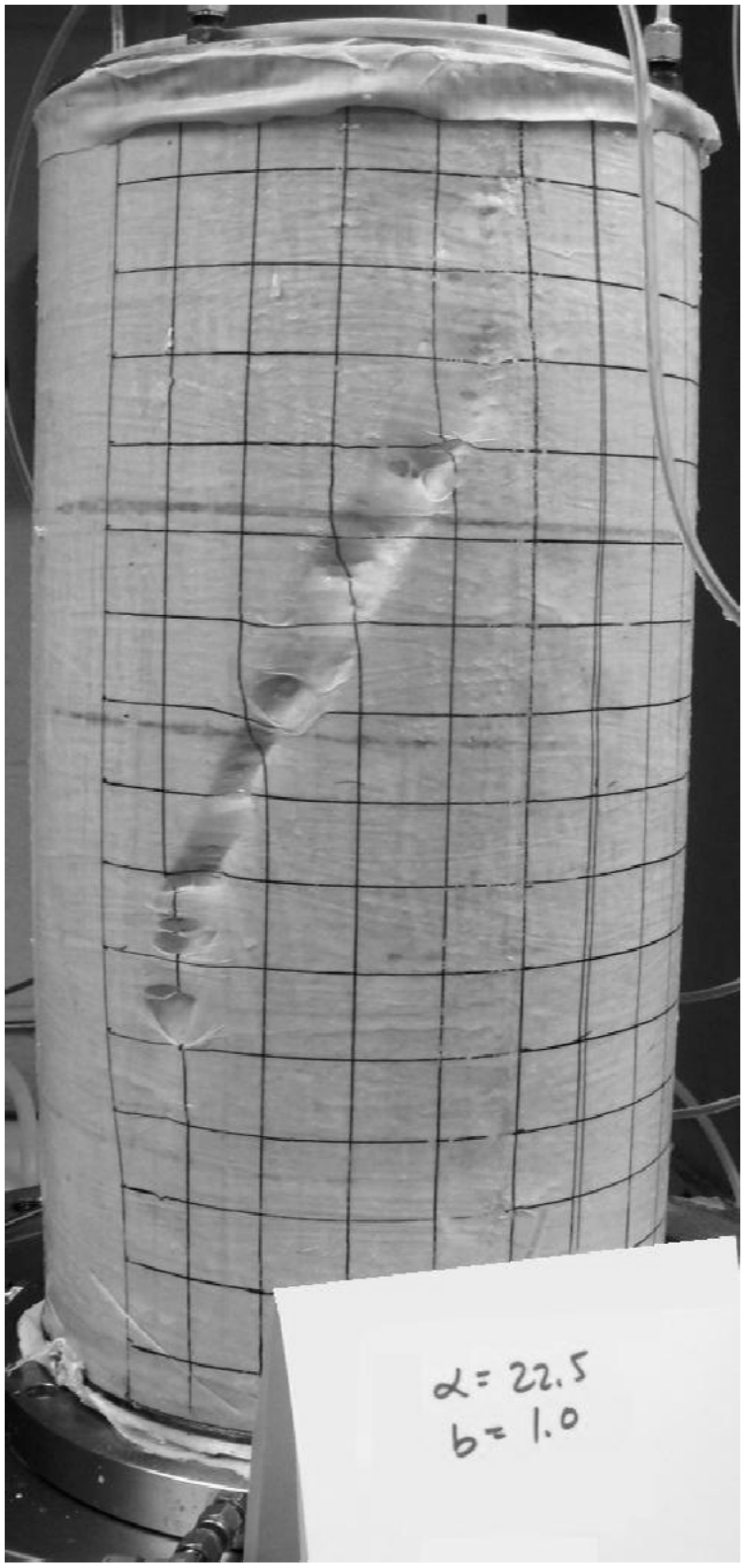

Figure L-4: Test B04 (α = 22.4°, b = 0.99)

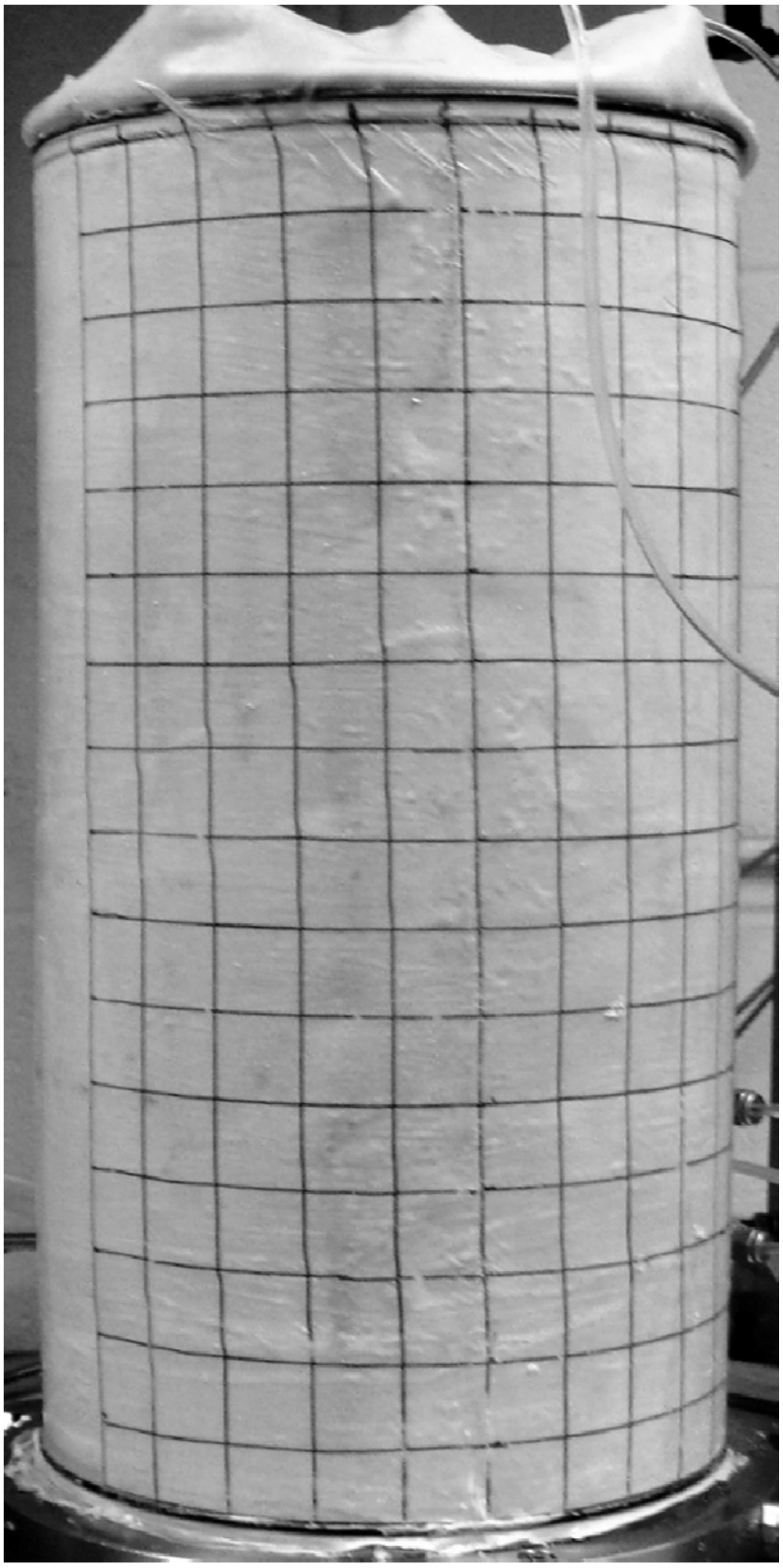

Figure L-5: Test B05 (α = 45.1°, b = 0.23)

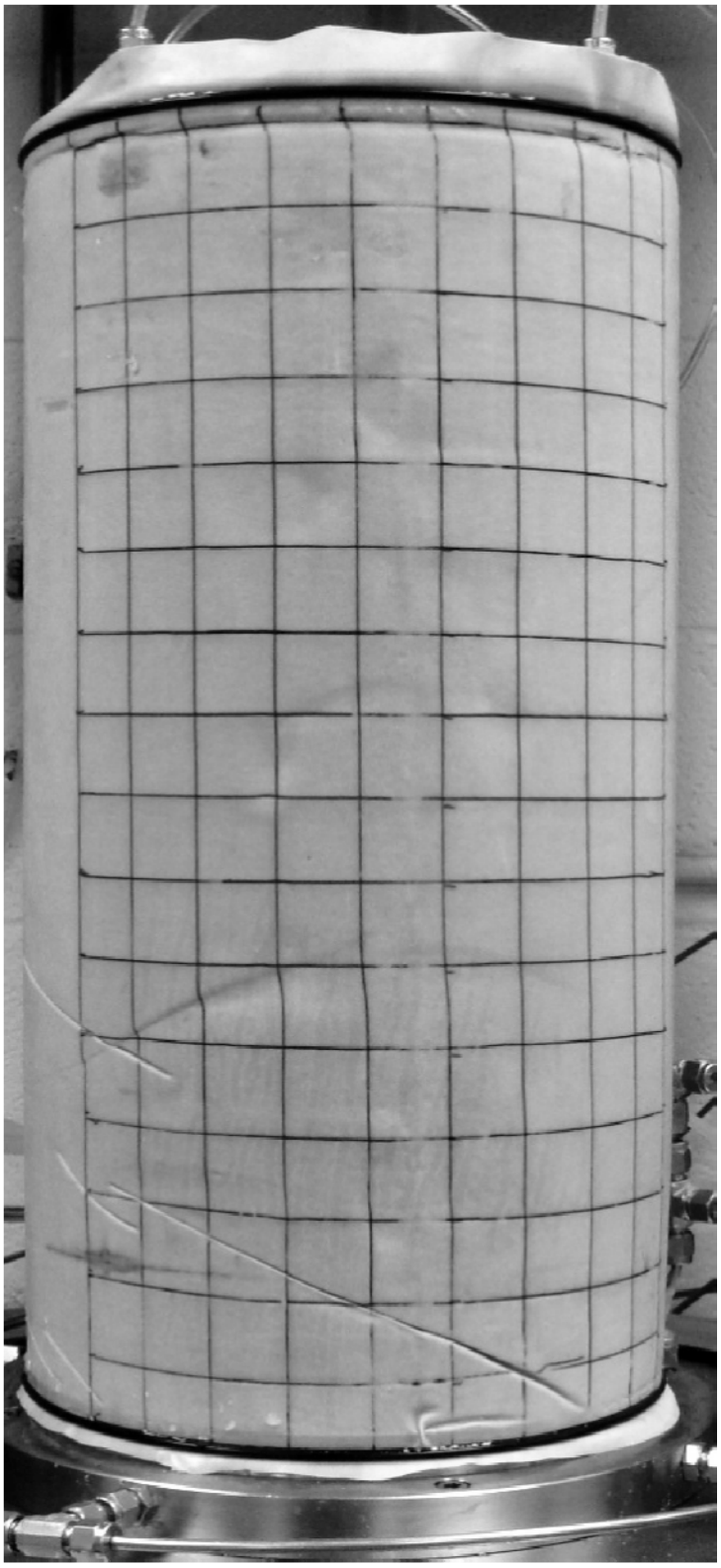

Figure L-6: Test B06 (α = 44.9°, b = 0.74)

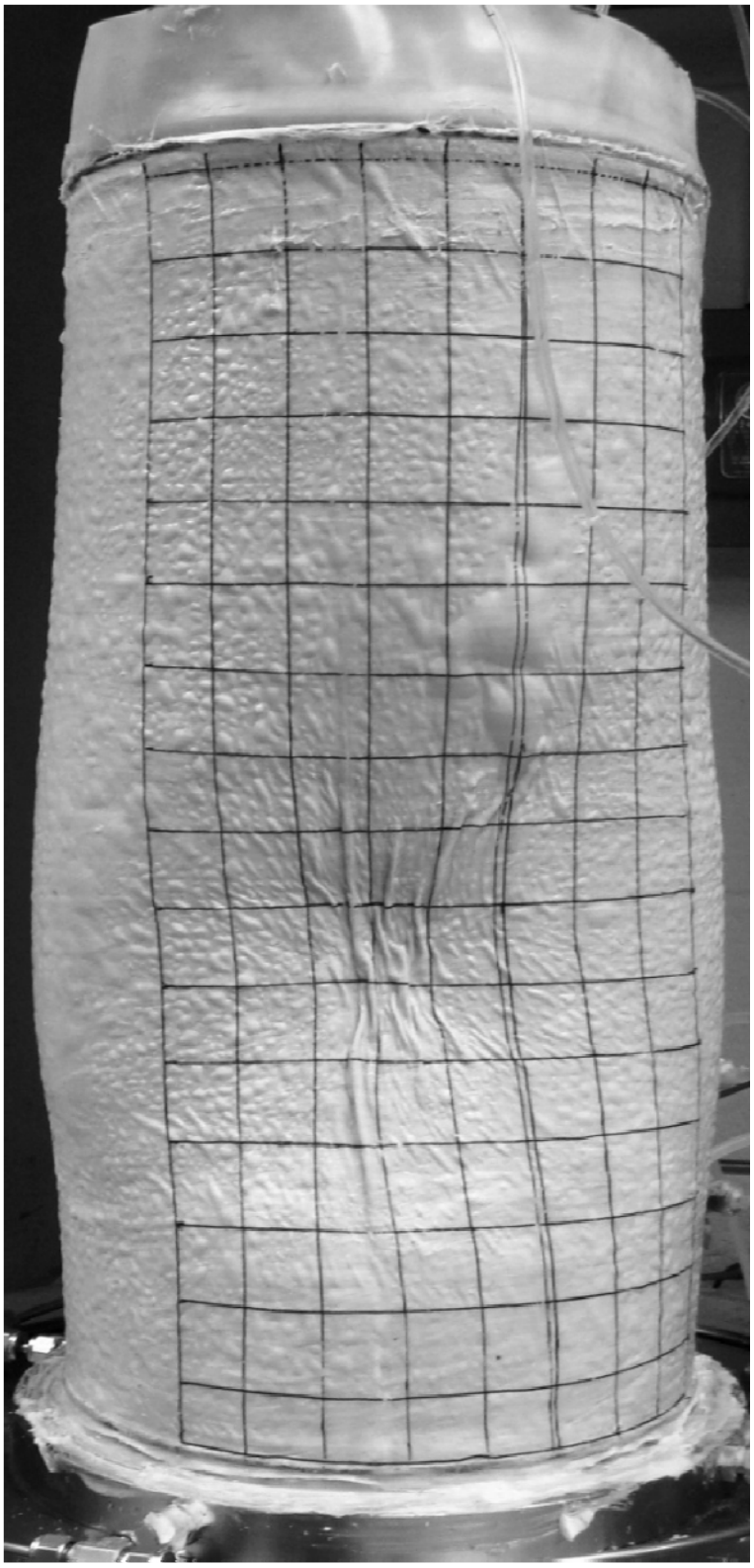

Figure L-7: Test B07 (α = 67.3°, b = 0.00)

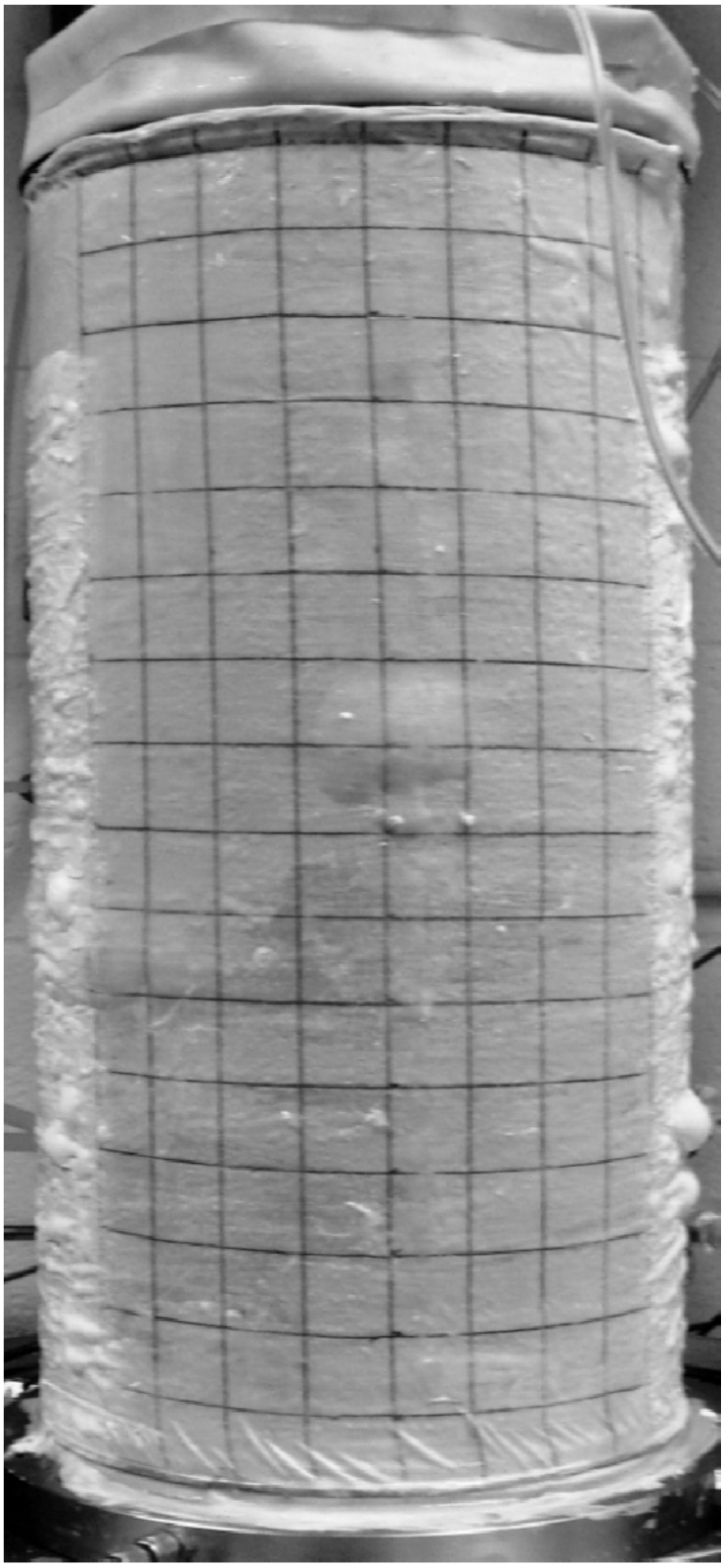

Figure L-8: Test B08 (α = 67.5°, b = 0.50)

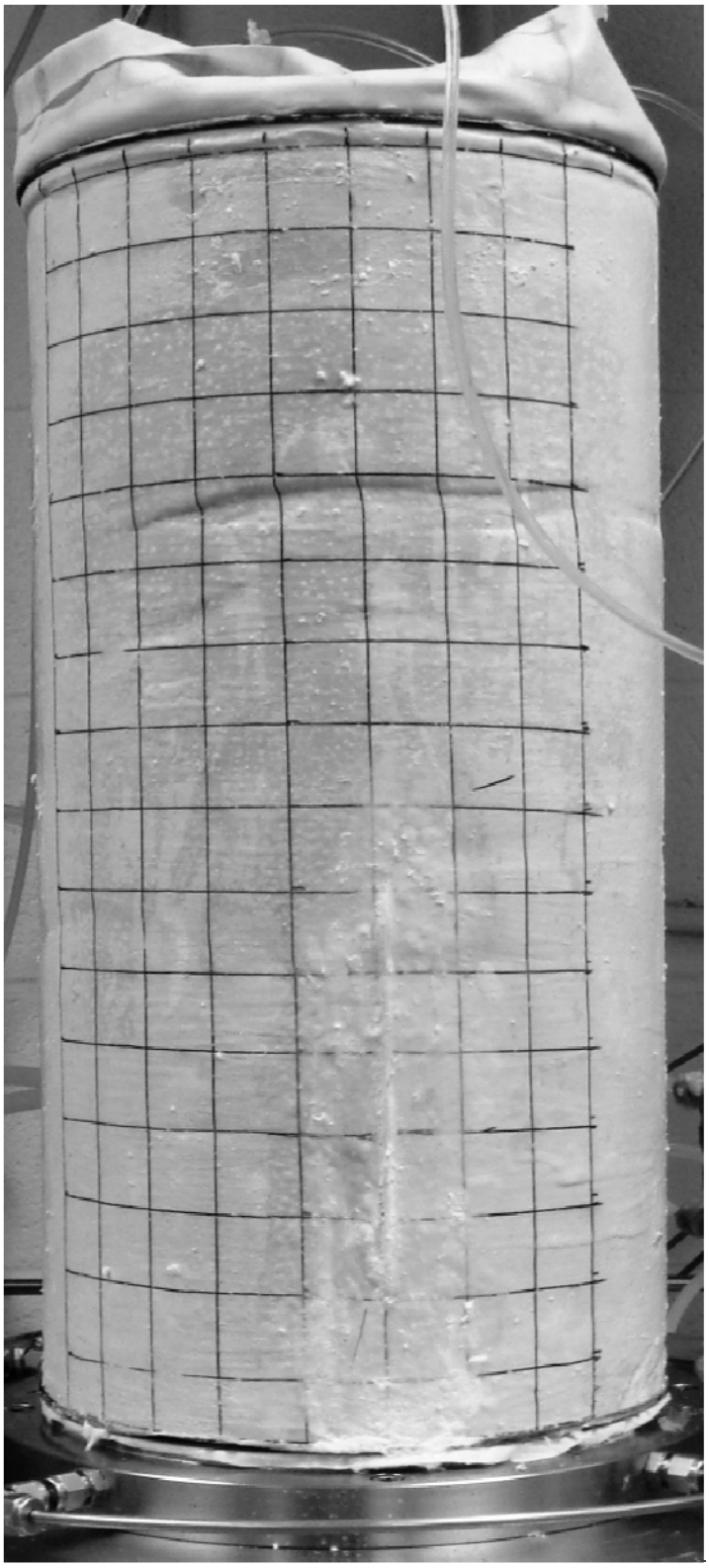

Figure L-9: Test B09 (α = 68.3°, b = 1.01)

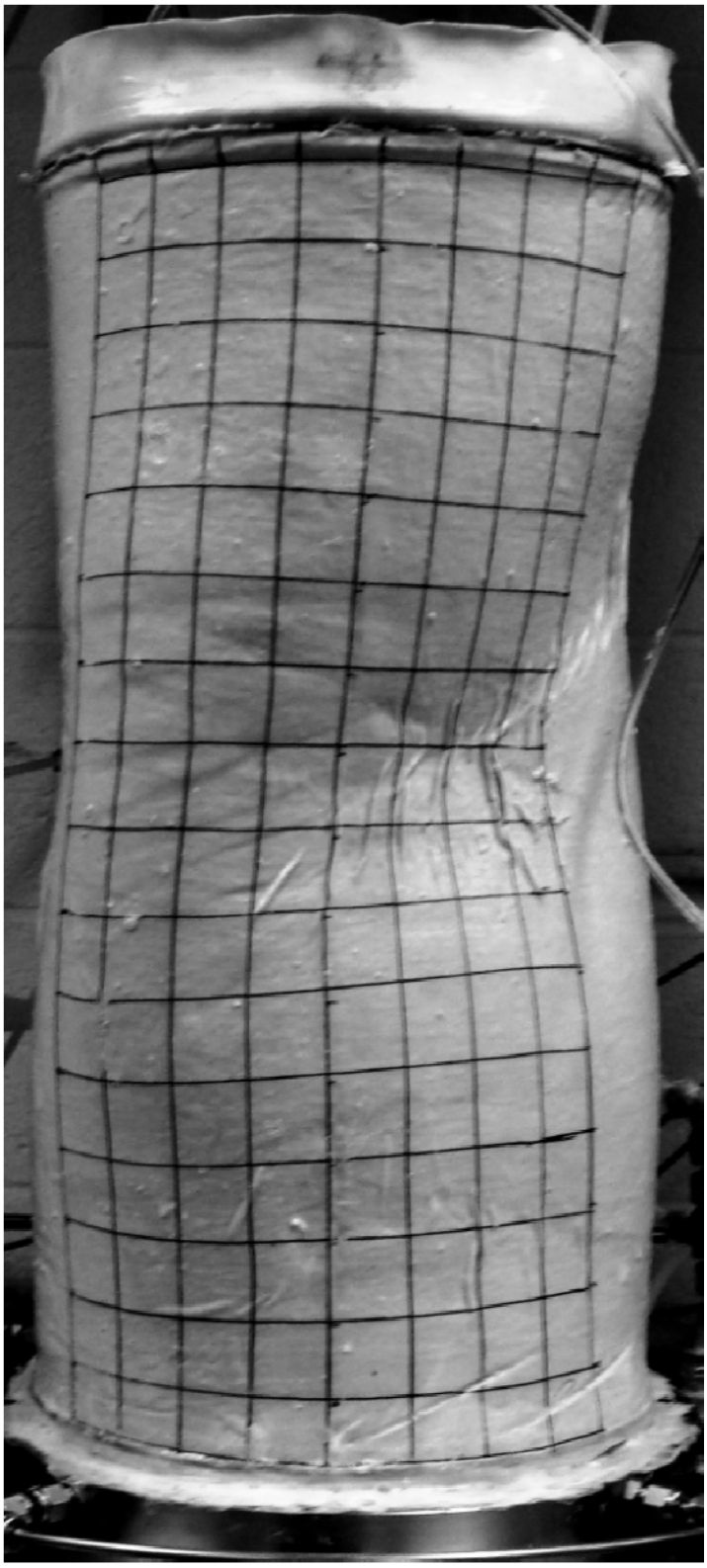

Figure L-10: Test B10 (α = 90°, b = 0.05)

Appendix M **Shear Band Sketches**

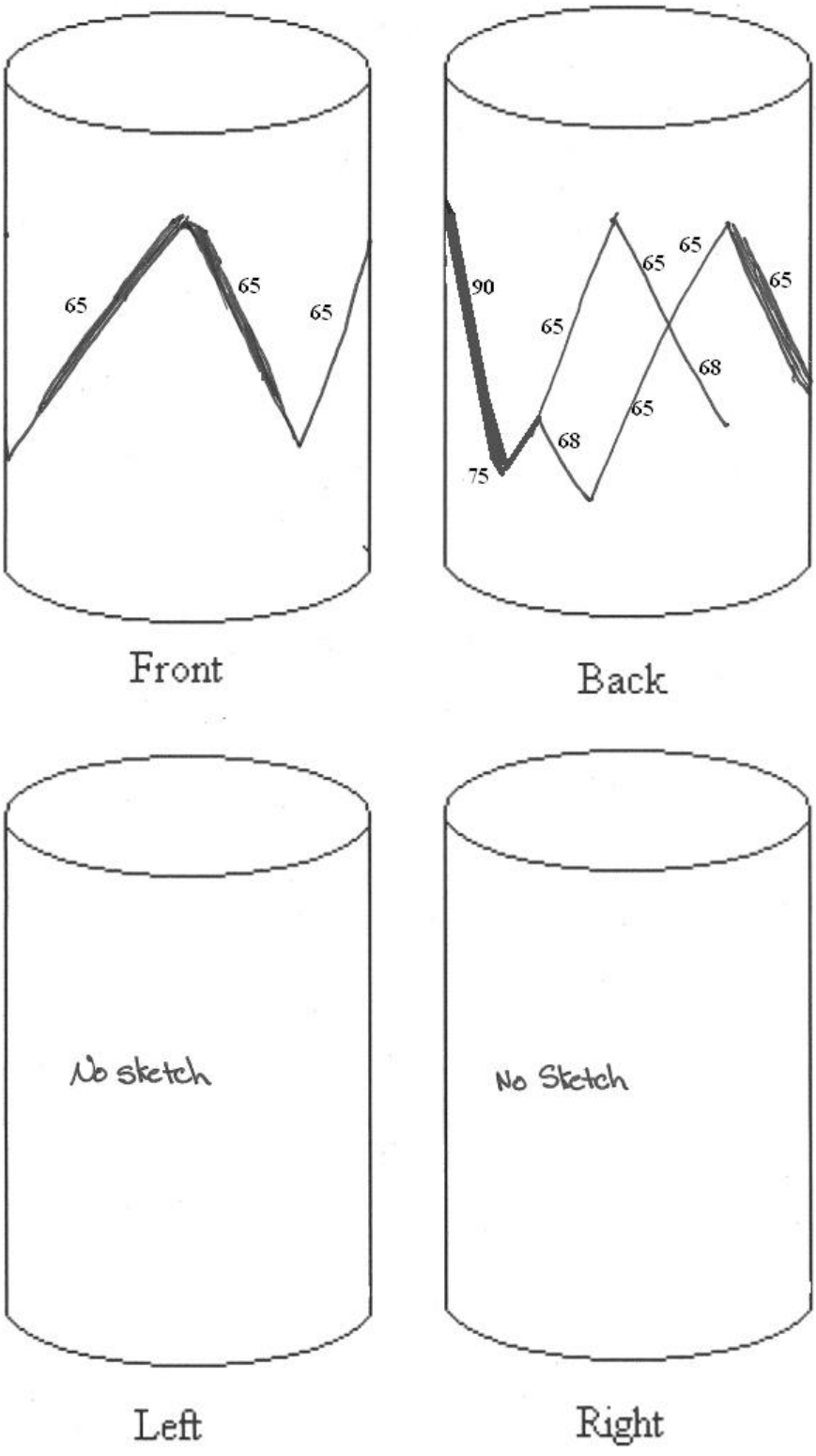

Figure M-1: Test B01 (α = 0°, b = 0.75)

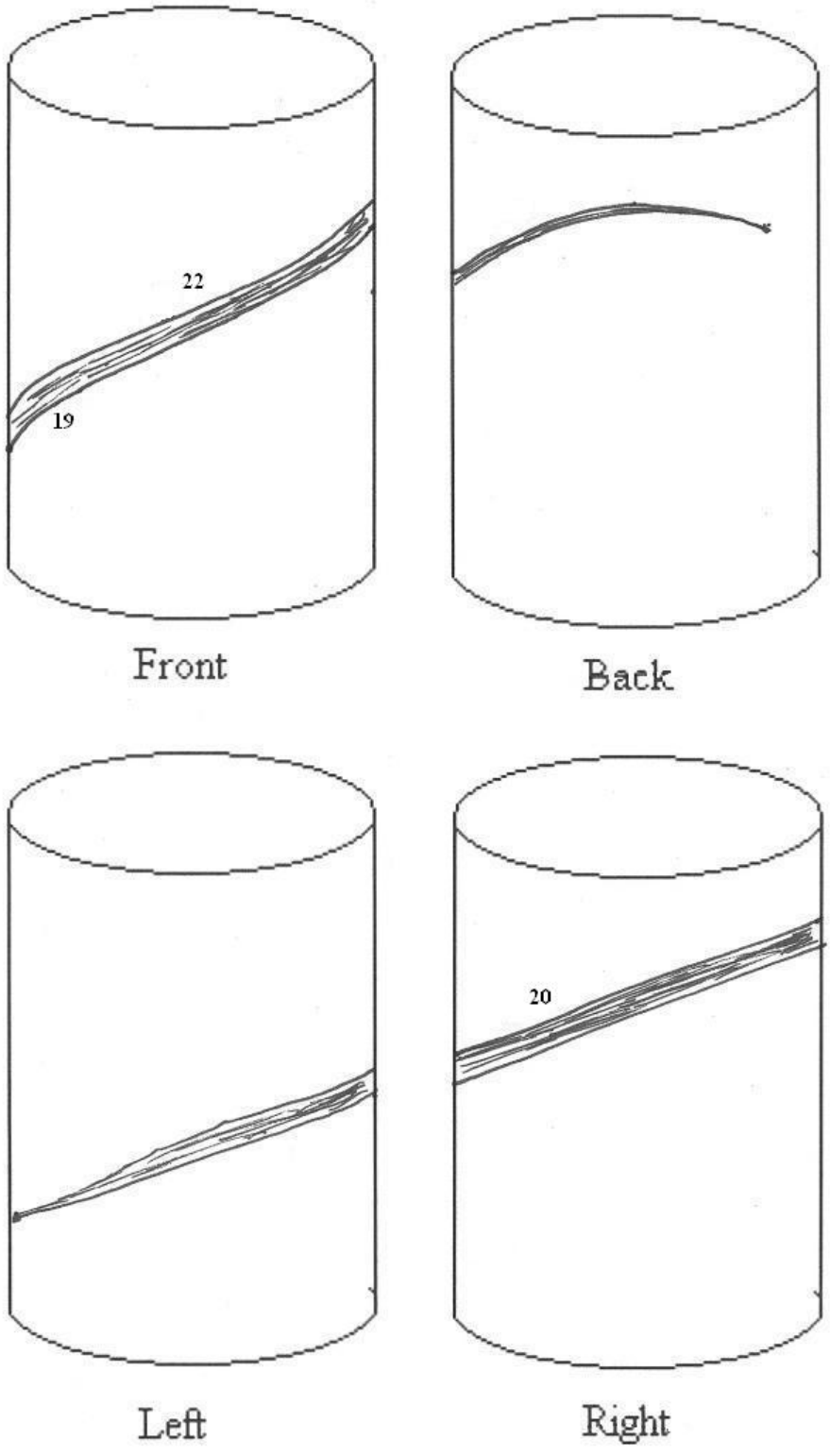

Figure M-2: Test B02 (α = 22.3°, b = -0.01)

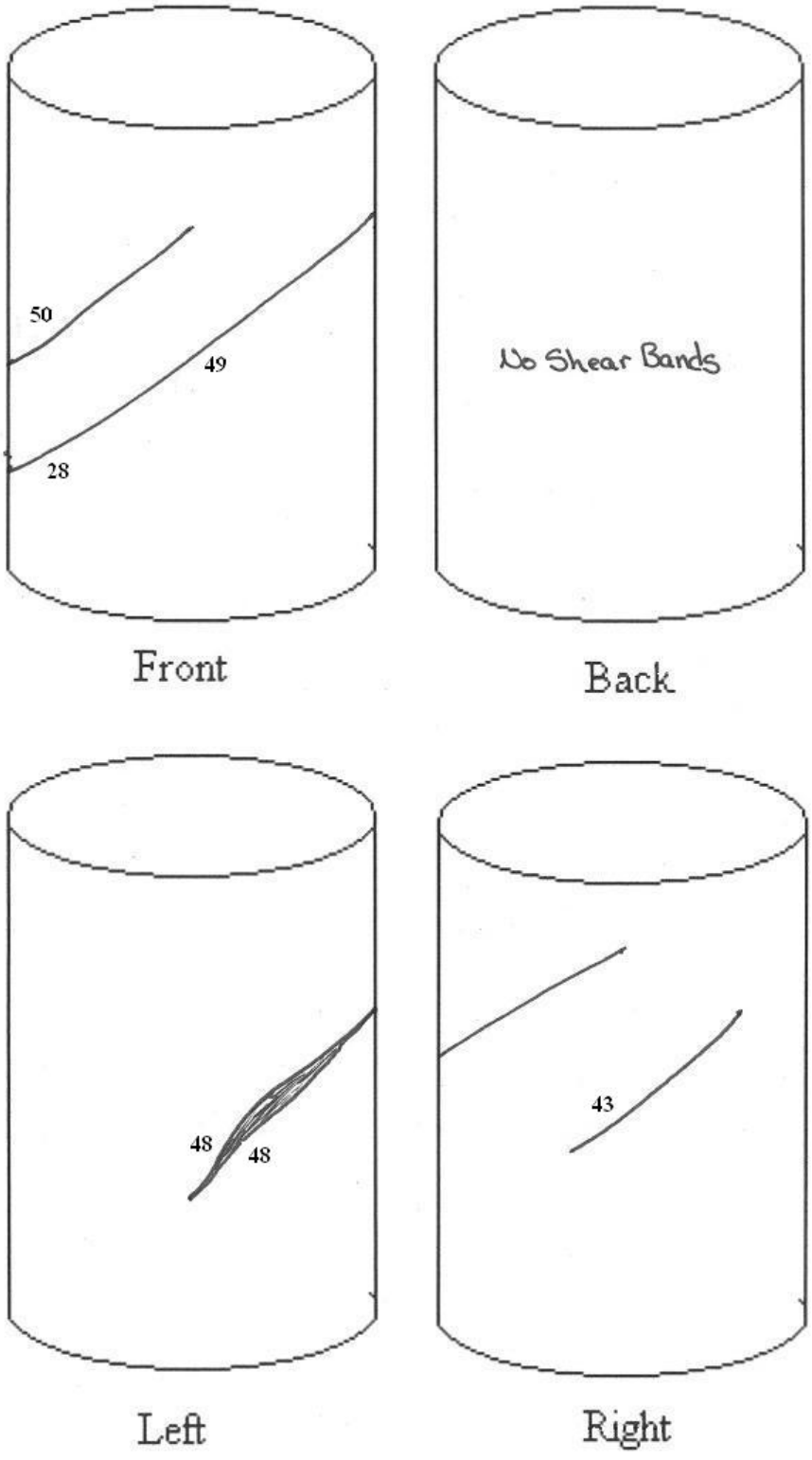

Figure M-3: Test B03 (α = 22.4°, b = 0.50)

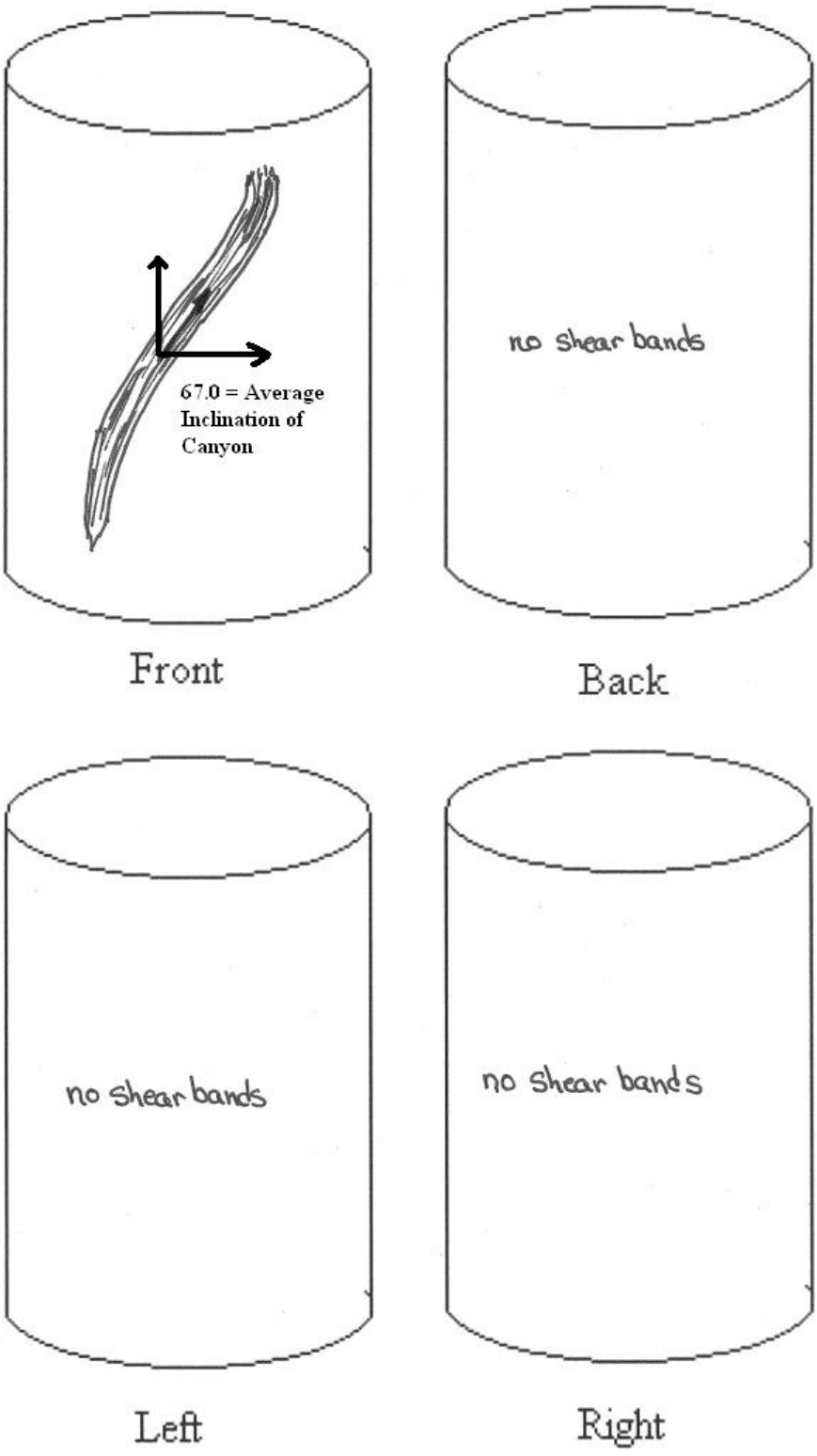

Figure M-4: Test B04 (α = 22.4° , b = 0.99)

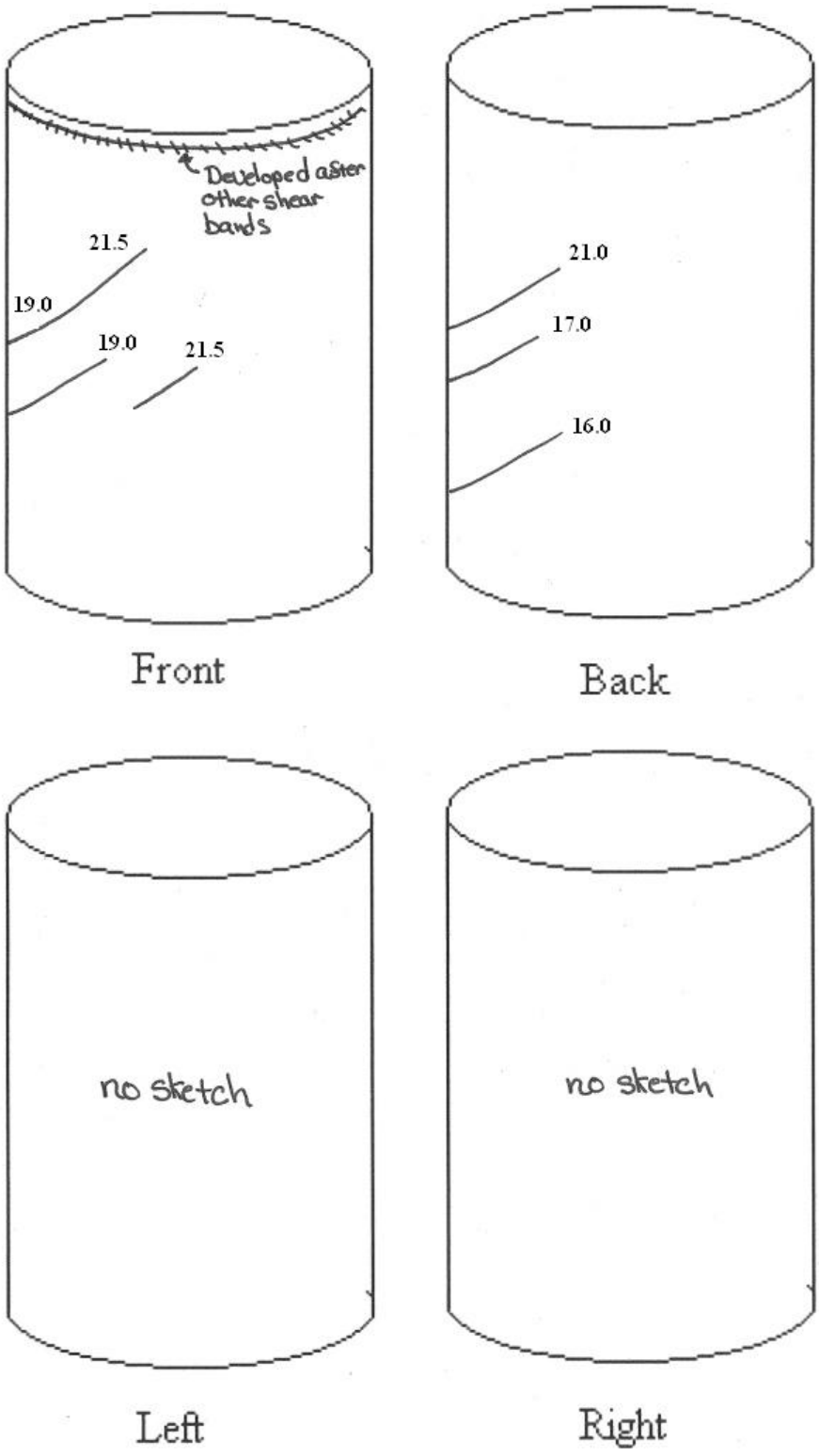

Figure M-5: Test B05 (α = 45.1°, b = 0.23)

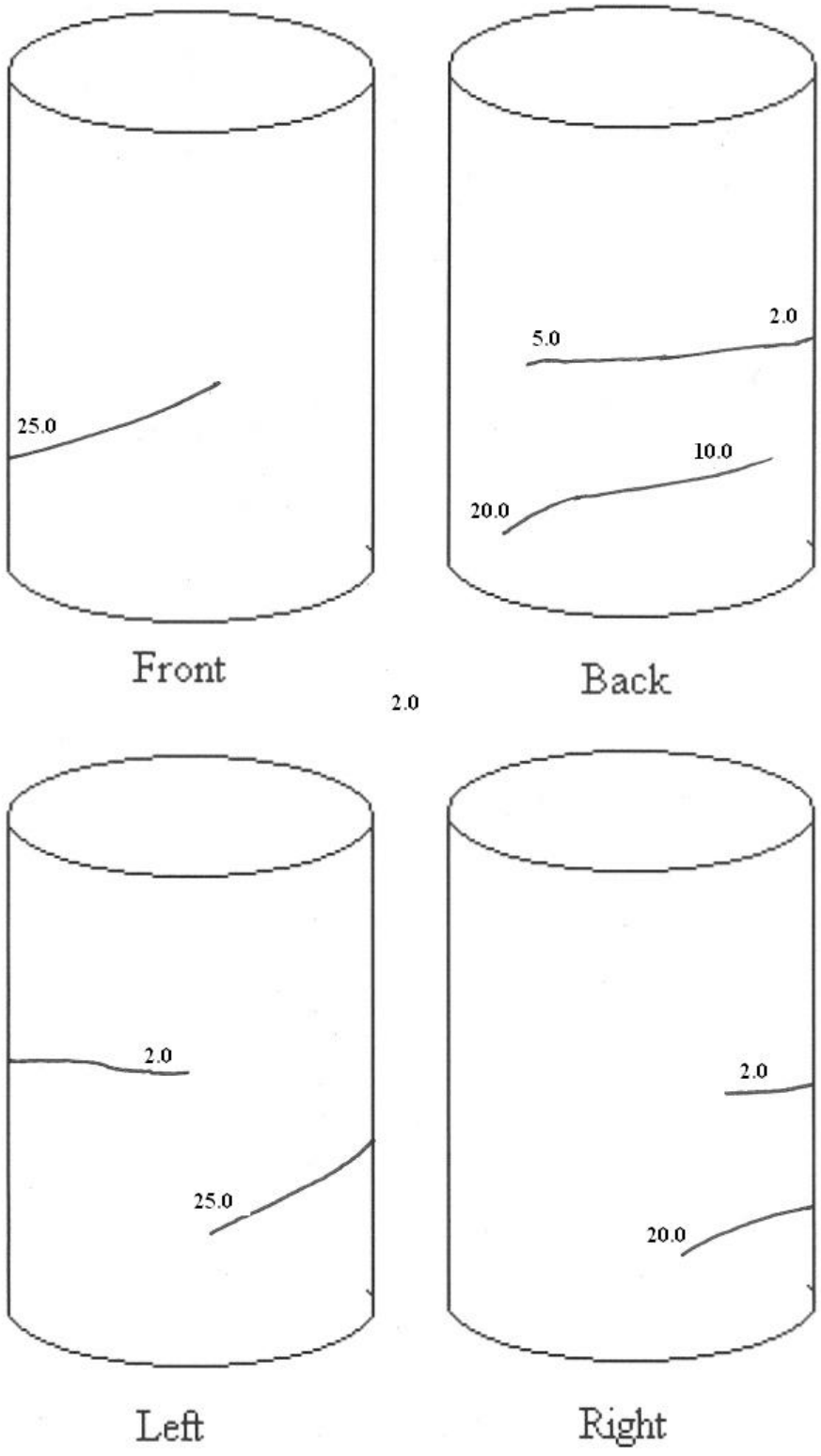

Figure M-6: Test B06 (α = 44.9°, b = 0.74)

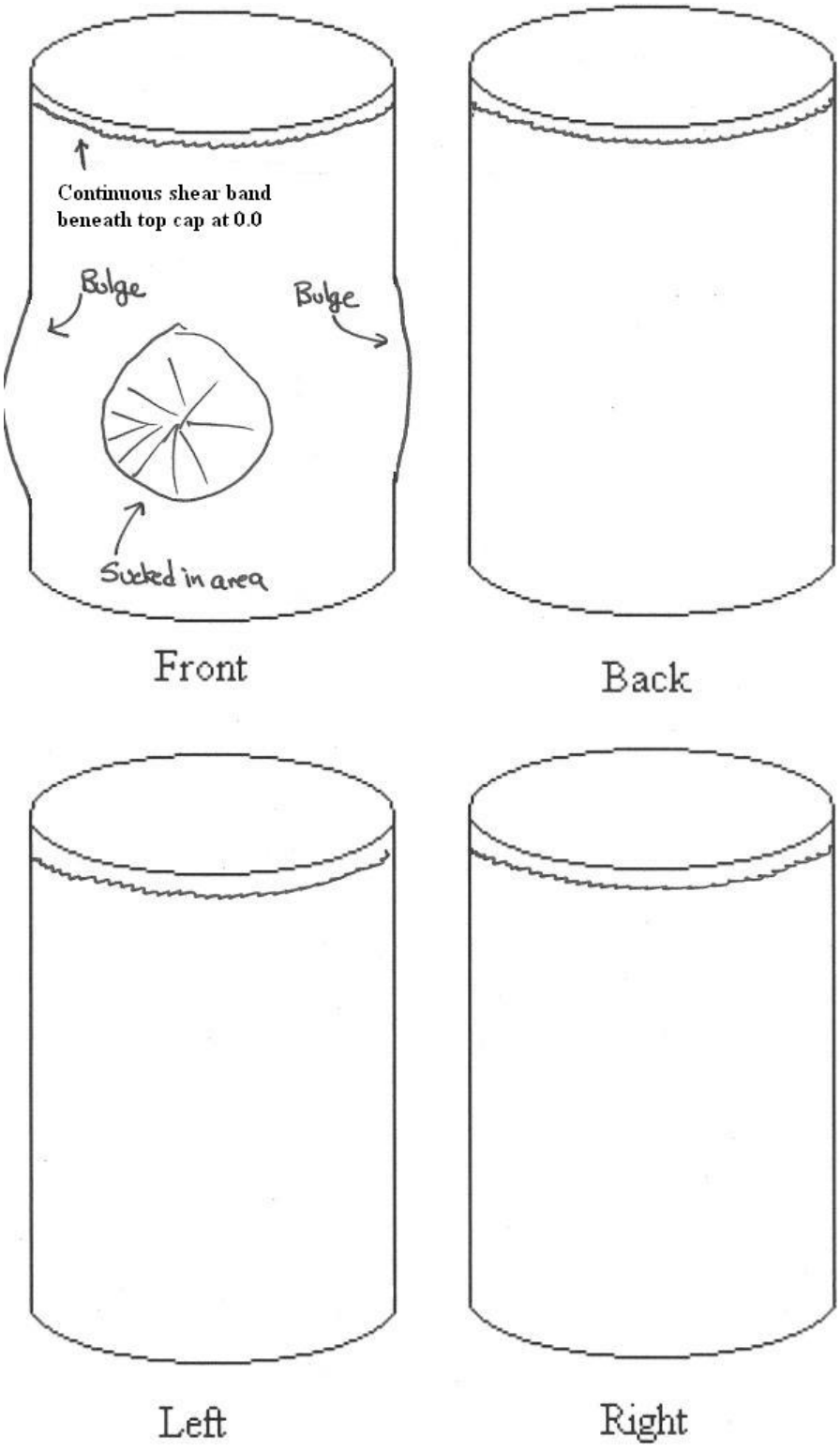

Figure M-7: Test B07 (α = 67.3°, b = 0.00)

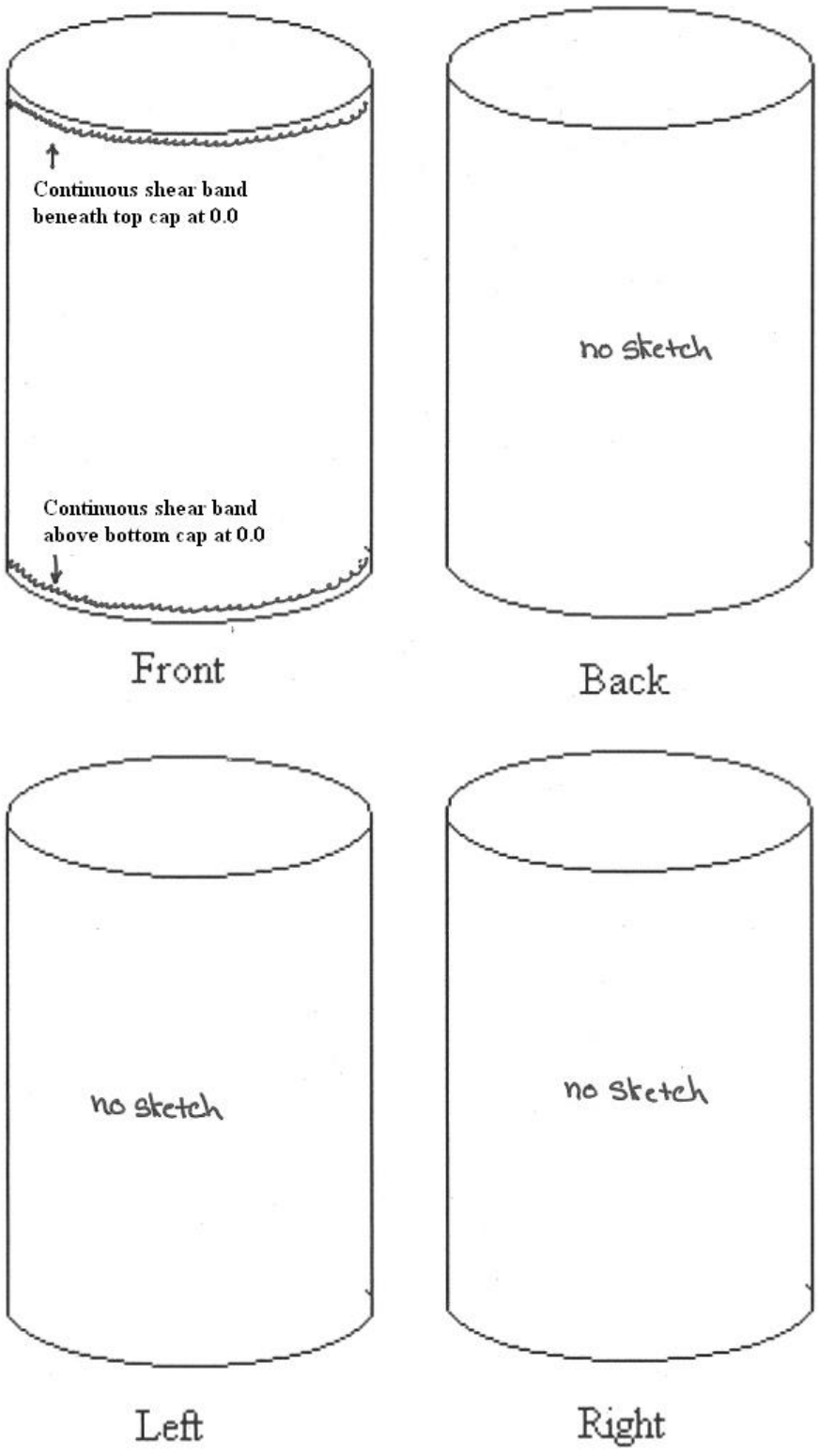

Figure M-8: Test B08 (α = 67.5°, b = 0.50)

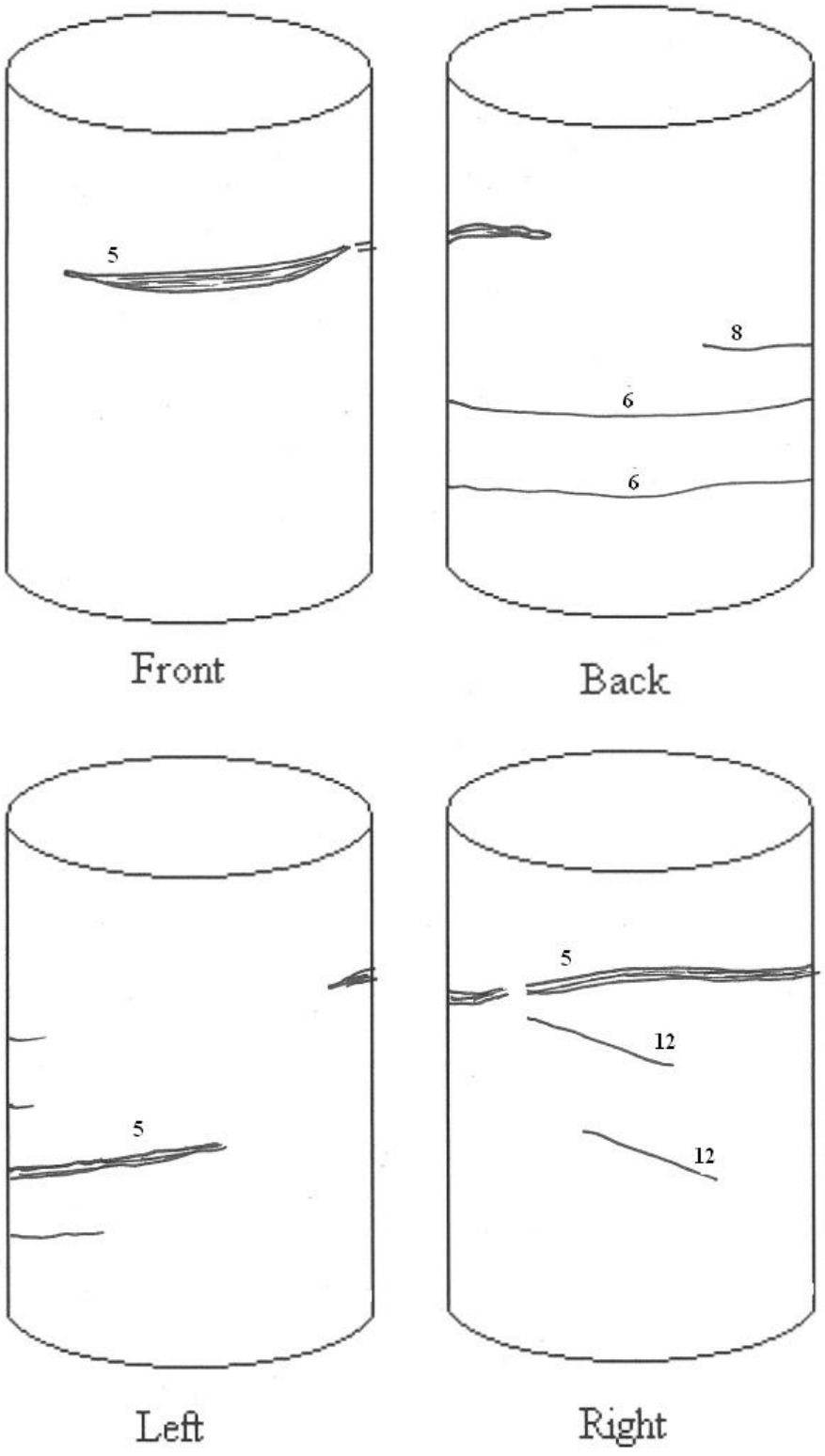

Figure M-9: Test B09 (α = 68.3°, b = 1.01)

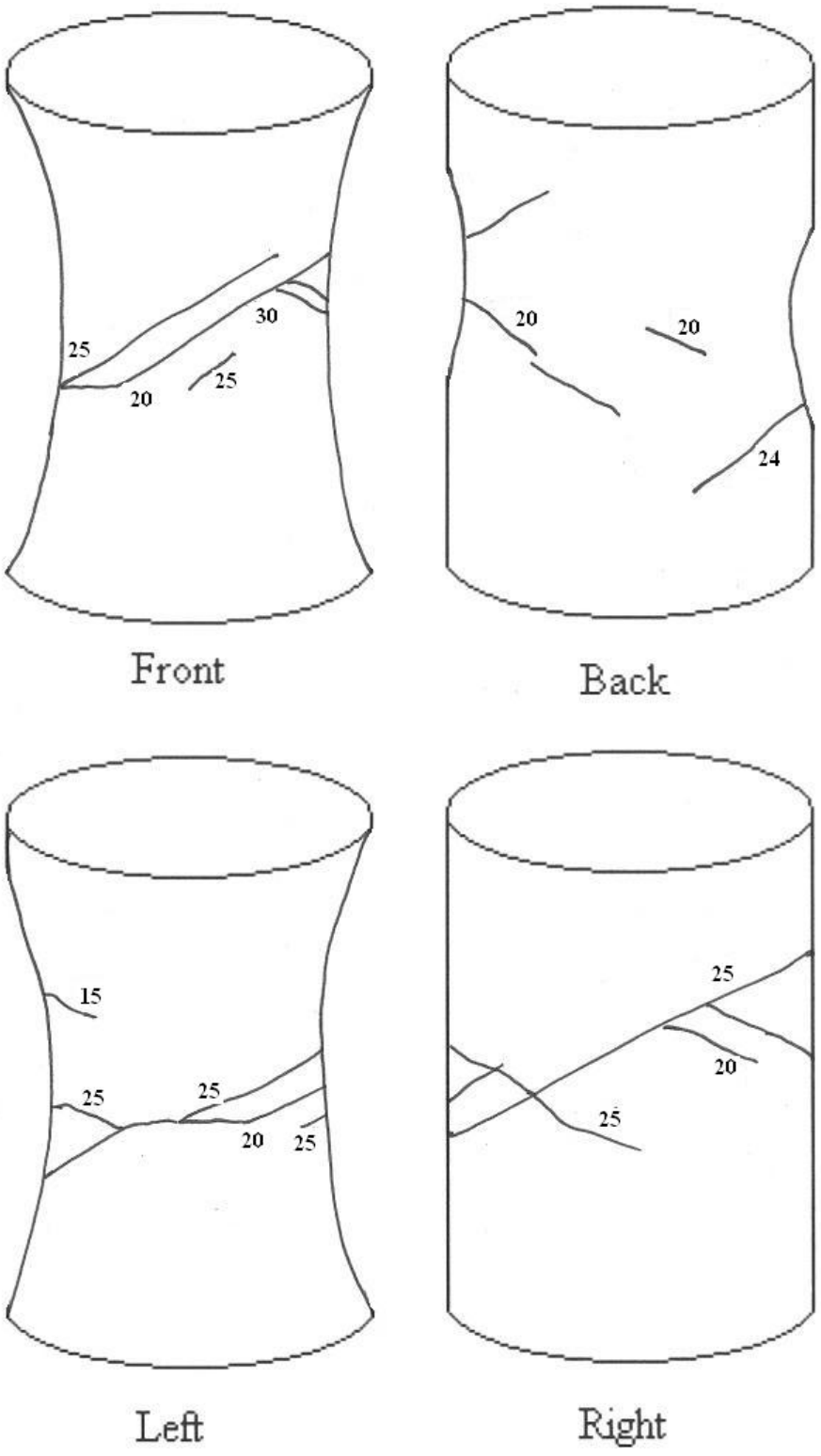

Figure M-10: Test B10 (α = 90°, b = 0.05)

Bibliography

Abelev, A. and Lade, P. (2004), "Characterization of Failure in Cross-Anisotropic Soils", *ASCE: Journal of Engineering Mechanics*, 130(5), 599 - 606

Alarcon, A., Chameau, J.L. and Leonards, G.A. (1986), "A New Apparatus for Investigating the Stress Strain Characteristics of Sand", *Geotechnical Testing Journal*, 9(4), 204 - 212

Allen, J.C. and Stokoe, K.H. (1982), *Development of a Resonant Column Apparatus with Anisotropic Loading*, Report GR82-28, Austin, Texas: Civil Engineering Department, University of Texas at Austin.

Ampadu, A.K. and Tatsuoka, F. (1993), "A Hollow Cylinder Torsional Simple Shear Apparatus Capable of a Wide Range of Shear Strain Measurement", *Geotechnical Testing Journal*, 15(1), 3 - 17

Arthur, J.R. (1988), "State of the Art Paper: Cubical Devices: Versatility and Constraints" *Advanced Triaxial Testing of Soil and Rock, STM STP 977,* Philadelphia: American Society for Testing and Materials, 743 - 765

Arthur, J.R., Chua, K.S. and Dunstan, T. (1977a), "Induced Anisotropy in Sand", *Geotechnique*, 27(1), 13 - 30

Arthur, J.R., Dunstan, T., Al-Ani, Q.A. and Assadi, A. (1977b), "Plastic Deformation and Failure in Granular Media", *Geotechnique*, 27, 53 - 74

Arthur, J. and Menzies, B. (1972), "Inherent Anisotropy in Sand", *Geotechnique*, 22(1), 115 – 128

Arulanandan, K., and R. Scott. (1993), "Experimental Results and Numerical Predictions 9Class A & B), " *Proceedings of the International Conference on the Verificiaton of Numerical Procedures for the Analysis of Soil Liquefaction Problem,* Davis: A.A. Balkema

ASTM D6913 (2009), Standard Test Methods for Particle-Size Distribution (Gradation) of Soils Using Sieve Analysis, West Conshohocken, PA: ASTM International, www.astm.org

ASTM Standard D854 (2010), 10.1520/D0854-10 Standard Test Methods for Specific Gravity of Soil Solids by Water Pycnometer. West Conshohocken, USA: ASTM International, www.astm.org

Baldi, G. and Nova, R. (1984), "Membrane Penetration Effects in Triaxial Testing", *ASCE: Journal of Geotechnical Engineering*, 110(3), 403 - 420

Bishop, A.W. (1966), "The 10th Rankine Lecture: The Strength of Soils as Engineering Materials", *Geotechnique*, 16(2), 91 - 128

Bjerrum, L., Kringstad, S. and Kummeneje, O. (1961), "The Shear Strength of Fine Sand", *In Proceedings of the 5th International Conference on Soil Mechanics and Foundation Engineering*, Paris, 29 - 37

Brewer, R. (1964), Fabric and Mineral Analysis of Soils, London: John Wiley and Sons

Broms, B.B. and Casbarian, A.O. (1965), "Effects of Rotation of the Principal Stress Axes and of the Intermediate Principal Stress on the Shear Strength", In *Proceedings: Sixth International Conference on Soil Mechanics and Foundation Engineering,* Montreal, 179 - 183

Casagrande, A. and Carrillo, N. (1944), "Discussion on Study of Failure Envelope of Soils", *ASCE: Journal of Soil Mechanics and Foundations Divisions*, 89(SM4), 243

Chaudhary, S.K. and Kuwano, J. (2003), "Anisotropic Multiple Yielding of Dense Toyoura Sand in P'- Constant Shear Plane", *Soils and Foundations*, 43(4), 59 - 69

Chen, Y.R. (1995), *Behavior of a Fine Sand in Triaxial, Torsional and Rotational Shear Tests*, Ph.D. Thesis, University of California at Davis

Cooling, L.F. and Smith, D.B. (1936), "The Shearing Resistance of Soils", *Journal of the Institution of Civil Engineers*, 3, 333 - 343

Cornforth, D.M. (1964), "Some Experiments on the Influence of Strain Conditions on the Strength of Sand", *Geotechnique*, 14(2), 143 - 167

d'Onofrio, A., Silvestri, F. and Vinale, F. (1999), "A New Torsional Shear Device", *Geotechnical Testing Journal*, 22(2), 101 - 111

El-Sohby, M.A. and Andrawes, K.Z. (1973), "Experimental Examination of Sand Anisotropy", *In Proceedings: Eighth International Conference on Soil Mechanics and Foundation Engineering,* Moscow, 103 - 109

Ergun, M.U. (1981), "Evaluation of Three-Dimensional Shear Testing", *In Proceedings of the 10th International Conference on Soil Mechanics and Foundation Engineering,* Stockholm, 593 - 596

Frydman, S., Zeitlen, J.G. and Alpan, I. (1973), "The Yielding Behavior of Particulate Media", *Canadian Geotechnical Journal*, 10, 341 - 362

Fukushima, S. and Tatsuoka, F. 1982, "Deformation and Strength of Sand in Torsional Simple Shear", *In Proceedings: International Union of Theoretical and Applied Mechanics Conference on Deformation and Failure of Granular Materials,* Delft, 371 - 379

Gens, A. and Potts, D.M. (1984), "Formulation of Quasi-Axisymmetric Boundary Value Problems for Finite Element Analysis", *Engineering Computations*, 1(2), 144 - 150

Georgiannou, V.N. and Tsomokos, A. (2008), "Comparison of Two Fine Sands Under Torsional Loading", Canadian Geotechnical Journal, 45, 1659 - 1672

Georgiannou, V.N., Tsomokos, A. and Stavrou, K. (2008), "Monotonic and Cyclic Behavior of Sand Under Torsional Loading", *Geotechnique*, 58(2), 113 - 124

Goldscheider, M. and Gudehus, G. (1973), "Rectilinear Extension of Dry Sand", *In Proceedings: Eighth International Conference on Soil Mechanics and Foundation Engineering*, Moscow, 143 - 150

Goode, C.D. and Helmy, M.A. (1967), "The strength of Concrete Under Combined Shear and Direct Stress", *Magazine of Concrete Research*, 19(59), 105 - 112

Graton, L.C. and Fraser, H.J. (1935), "Systematic Packing of Spheres with Particular Relation to Porosity and Permeability", *The Journal of Geology*, 35(8), 785 - 909

Green, G.E. (1967), "Discussion: A New Soil Testing Apparatus", *Geotechnique*, 17(3), 295

Green, G.E. and Bishop, A.W. (1969), "A Note on the Drained Strength of Sand Under Generalized Strain Conditions", *Geotechnique*, 19(1), 144 - 149

Habib, P. (1953), "Influence of the Variation of the Average Principal Stress Upon the Shearing Strength of Soils", *In Proceedings of the Third International Conference on Soil Mechanics and Foundation Engineering*, Zurich, 131- 136

Hambly, E.C. (1969), "A New Triaxial Apparatus", *Geotechnique*, 19(2), 307 - 309

Haruyama, M. (1981), "Anisotropic Deformation-Strength Characteristics of an Assembly of Spherical Particles under Three Dimensional Stresses", *Soils and Foundations*, 21(4), 41 - 55

Haythornthwaite, R.M. (1960), "Stress and Strain in Soils", In Plasticity, Edited by Lee, E.H. and Symonds P.S., London: Pergamon Press, 185 - 193

Hight, D.W., Gens, A. and Symes, M.J. (1983), "The Development of a New Hollow Cylinder Apparatus for Investigating the Effects of Principal Stress Rotation in Soils", *Geotechnique*, 33(4), 355 - 383

Hong, W.P. and Lade, P.V. (1989), "Strain Increment and Stress Directions in Torsion Shear Tests", *ASCE Journal of Geotechnical Engineering*, 115(10), 1388 - 1401

Ishibashi, I. and Sherif, M.A. (1974), "Soil Liquefaction by Torsional Simple Shear Device", *ASCE: Journal of Geotechnical Engineering*, 100(GT-8), 871 - 888

Ishihara, K. and Towhata, I. (1983), "Sand Response to Cyclic Rotation of Principal Stress Direction as Induced by Wave Loads", *Soils and Foundations*, 33(4), 11 - 26

Kammerrer, A.M. et al. (2000), Cyclic Simple Shear Testing of Nevada Sand for PEER Center Project 2051999, Geotechnical Engineering Report No. UCB/GT/00-01, University of California at Berkeley

Ko and Scott (1967), "A New Soil Testing Apparatus", *Geotechnique*, 17(1), 40 - 57

Kuerbis, R. and Vaid, Y.P. (1988), "Sand Sample Preparation - The Slurry Deposition Method", *Soils and Foundations*, 4, 107 - 118

Kumruzzaman, M. and Yin, J.H. (2010), "Influences of Principal Stress Direction and Intermediate Principal Stress on the Stress-Strain-Strength Behavior of Completely Decomposed Granite", *Canadian Geotechnical Journal*, 47, 164 - 179

Kutter, B.L., Chen, Y.R. and Shen, C.K. (1994), Triaxial and Torsional Shear Test Results for Sand, Rep. No. CR94.003-SHR, Port Hueneme, California: US Navel Civil Engineering Laboratory

Kuwano, R. (1999), The Stiffness and Yielding Anisotropy of Sand, Ph.D. Thesis, London: Imperial College, University of London

Lade, P.V. (1975), "Torsion Shear Tests on Cohesionless Soil", *In 5th Pan-American Conference on Soil Mechanics and Foundation Engineering,* Buenos Aires, 117 - 127

Lade, P.V. (1976), "Interpretation of Torsion Shear Tests on Sand ", In *Proceedings of the 2nd International Conference on Numerical Methods in Geomechanics*, Blacksburg, 381 - 389

Lade, P.V. (1977), "Elasto-plastic Stress-Strain Theory for Cohesionless Soil with Curved Yield Surfaces", *International Journal of Solids and Structures*, 13, 1019 - 1035

Lade, P.V. (1978), "Cubical Triaxial Apparatus for Soil Testing", *Geotechnical Testing Journal*, 1, 93 - 101

Lade, P.V. (1981), "Torsion Shear Apparatus for Soil Testing", American Society for Testing Materials (STP Publication No. 740), 145 - 163

Lade, P.V. (1984), "Failure Criterion for Frictional Materials", In *Mechanics of Engineering Materials*, by Desai, C.S. and Gallagher, R.H., New York: John Wiley & Sons, Ltd., 385 - 401

Lade, P.V. (2006), "Assessment of Test Data for Selection of 3-D Failure Criterion for Sand", *International Journal for Numerical and Analytical Methods in Geomechanics*, 30, 307 - 333

Lade, P.V. (2007), CE 504 Stress Strain Behavior of Soils Notes, Department of Civil Engineering: Catholic University of America, Washington, D.C.

Lade, P.V. (2008), "Failure Criterion for Cross-Anisotropic Soils", *ASCE: Journal of Geotechnical and Geoenviornmental Engineering*, 134(1), 117 - 124

Lade, P.V. and Duncan, M. (1973), "Cubical Triaxial Tests on Cohesionless Soil", *ASCE: Journal of the Soil Mechanics and Foundations Division*, 99(SM10), 793 – 812

Lade, P.V. and Kirkgard, M. (2000), "Effects of Stress Rotation and Changes of b-Values on Cross-Anisotropic Behavior of Natural Ko Consolidated Soft Clay", *Soils and Foundations*, 40(6), 93 - 105

Lade, P.V., Nam, J. and Hong, W.P. (2008), "Shear Banding and Cross-Anisotropic Behavior Observed in Laboratory Sand Tests with Stress Rotation", *Canadian Geotechnical Journal*, 45, 74 - 84

Lade, P.V., Nam, J. and Hong, W.P. (2009), "Interpretation of Strains in Torsion Shear Tests", *Computers and Geotechnics*, 36, 211 - 225

Lade, P.V. and Wang, Q. (2001), "Analysis of Shear Banding in True Triaxial Tests on Sand", *Journal of Engineering Mechanics*, 127(8), 762 - 768

Lade, P.V. and Wang, Q. (2002), "Effects of Slenderness Ratio on Shear Banding in True-Triaxial Tests", In *Proceedings of the 8th International Symposium NUMOG VIII*, Edited by G. N. Pande and S. Pietruszczak, Rome: Taylor & Francis, 148 - 154

Lade, P.V. and Yamamuro, J. (1997), "Effects of Nonplastic Fines on Static Liquefaction of Sands", *Canadian Geotechnical Journal*, 34(6), 918 - 928

Lee, K.L. (1970), "Comparison of Plane Strain and Triaxial Tests on Sand", *ASCE: Journal of Soil Mechanics and Foundations Division*, 96(3), 901 - 923

Leroueil, S. and Hight, D.W. (2002), "Behavior and Properties of Natural Soils and Rocks", In *Proceedings of the International Workshop in Characterization and Engineering Properties of Natural Soils and Rocks*, Singapore, 29 - 254

Leussnik, H. and Wittke, W. (1963), “Difference in Triaxial and Plane strain Shear Strength”, American Society of Testing Materials: Report No. 361, Ottoway, 77-89

Lode, W., (1925), "The Influence of the Intermediate Principal Stress on Yielding on Iron, Copper, and Nickel", Zeits. Eng. Math. Mech., 5, 142

Lomize, G.M., Kryzhanovsk, A.L., Vorontsov, E.I. and Goldin, A.L. (1969), "Study on Deformation and Strength of Soils under 3 Dimensional State of Stress", In *Proceedings of the 7th International Conference on Soil Mechanics and Foundation Engineering*, Mexico City, 257 - 265

Matsuoka, H. and Ishizaki, H. (1981), "Deformation and Strength of Anisotropic Soil", In *Proceedings of the International Conference on Soil Mechanics and Foundation Engineering,* Stockholm, 699 - 702

Matsuoka, H. and Nakai, T. (1974), "Stress-Deformation and Strength Characteristics of Soil Under Different Principal Stresses", In *Proceedings of the Japanese Society of Civil Engineers*, 232, 59 - 70

Menkiti, C.O. (1995), "Behavior of Clay and Clayey-Sand, with Particular Reference to Principal Stress Rotation", Ph.D. Thesis, Imperial College of Science, Technology and Medicine, University of London

Miura, K., Miura, S. and Toki, S. (1986), "Deformation Behavior of Anisotropic Densse Sand Under Principal Stress Axes Rotation", *Soils and Foundations*, 26(1), 36 - 52

Miura, S. and Toki, S. (1982), "A Sample Preparation Method and its Effect on Static and Cyclic Deformation - Strength Properties of Sand", *Soils and Foundations*, 22(1), 61 - 77

Murthy, K., Nagaraj, T.S. and Sridharan, A. (1980), "Strength Anisotropy of Layered Soil System", *ASCE: Journal of Geotechnical Engineering,* 106(GT10), 1143 - 1142

National Instruments (2011), Accuracy Calculator. [Online] Available at: http://www.ni.com/advisor/accuracy/ [Accessed 5 May 2011]

Ochiai, H. and Lade, P.V. (1983), "Three Dimensional Behavior of Sand with Anisotropic Fabric", *ASCE: Journal of Geotechnical Engineering*, 109, 1313 – 1328

Oda, M. (1972a), "Initial Fabrics and Their Relations to Mechanical Properties of Granular Material", *Soils and Foundations*, 12(1), 17 - 36

Oda, M. (1972b), "The Mechanism of Fabric Changes During Compressional Deformation of Sand", *Soils and Foundations*, 12(2), 1 - 18

Oda, M. and Iwashita, K. (1999), *Mechanics of Granular Materials: An Introduction*, Rotterdam: A.A. Balkema

Oda, M., Koishikawa, I. and Higuchi, T. (1978), "Experimental Study of Anisotropic Shear Strength of Sand by Plane Strain Test", *Soils and Foundations*, 18(1), 25 - 38

O'Kelly, B. and Naughton, P. (2009), "Study of the Yielding of Sand Under Generalized Stress Conditions Using a Versatile Hollow Cylinder Torsional Apparatus", *Mechanics of Materials*, 41, 187 - 198

Parkin, A.K., Gerrard, C.M. and Willoughby, D.R. (1968), "Discussion on Deformation of Sand in Shear", *ASCE: Journal of Soil Mechanics and Foundation Division*, 94(1), 336 - 340

Potts, D.M. and Gens, A. (1984), "Effect of the Plastic Potential in Boundary Value Problems Involving Plane Strain Deformations", *International Journal for Numerical and Analytical Methods in Geomechanics*, 8(3), 259 - 286

Pradhan, B.S., Tatsuoka, F. and Horii, N. (1988), "Simple Shear Testing on Sand in a Torsional Shear Apparatus", *Soils and Foundations*, 28(2), 95 – 112

Procter, D.C. and Barden, L. (1969), "Correspondence on Green and Bishop: A Note on the Drained Strength of Sand Under Generalized Strain Conditions", *Geotechnique*, 19(3), 424 - 426

Ramamurthy, T. and Rawat, P.C. (1973), "Shear Strength of Sand Under General Stress System”", In *The 8th International Conference on Soil Mechanics and Foundation Engineering*, Moscow, 339 - 342

Roscoe, K.H. (1970), "The 10th Rankine Lecture: The Influence of Strains in Soil Mechanics", *Geotechnique*, 20, 129 – 170

Rudnicki, J.W. and Rice, J.R. (1975), "Conditions for the Localization of Deformation in Pressure-Sensitive Dilatant Materials", *Journal of Mechanics and Physics of Solids*, 23, 374 - 391

Saada, A.S. (1988), "Hollow Cylinder Torsional Devices: Their Advantages and Limitations", In *Advanced Triaxial Testing of Soil and Rock - ASTM STP 977*, 767 - 789

Saada, A.S. and Baah, A.K. 1967, "Deformation and Failure of a Cross Anisotropic Clay Under Combined Stresses", In *Proceedings: Third Pan-American Conference on Soil Mechanics and Foundation Engineering,* Caracas, 67 - 88

Saada, A.S., Liang, L., Figueroa, J.L. and Cope, C.T. (1999), "Bifurcation and Shear Banding Propagation in Sands", *Geotechnique*, 49(3), 367 – 385

Saada, A.S. and Puccini, P. (1985), "Discussion of Undrained Anisotropy and Principal Stress Rotation in Saturated Sand", *Geotechnique*, 35(1), 78 - 85

Saada, A.S. and Townsend, F.C. (1981), "State of the Art: Laboratory Strength Testing of Soils", *Special Technical Publication (STP) 740*, Philadelphia: ASTM, 7 - 77

Saada, A.S. and Zamani, K.K. (1969), "The Mechanical Behavior of Cross Anisotropic Clays", In *Proceedings: Seventh International Conference on Soil Mechanics and Foundation Engineering,* Mexico City, 351 - 359

Sayao, A.S. (1989), *Behavior of Sand Under General Stress Paths in the Hollow Cylinder Torsional Device,* Ph.D. Thesis, Vancouver: University of British Columbia

Sayao, A. and Vaid, Y.P. (1991), "A Critical Assessment of Stress Non-Uniformity in the Hollow Cylinder Torsional Test Specimens", *Soils and Foundations*, 31(1), 60 - 72

Sayao, A. and Vaid, Y.P. (1996), "Effect of Intermediate Principal Stress on the Deformation Response of Sand", *Canadian Geotechnical Journal*, 33, 822 - 828

Serra, J.P. and Hooker, P. (2003), "New computer controlled hollow cylinder torsional shear apparatus", In *The Proceedings of the 13th European Conference on Soil Mechanics and Geotechnical Engineering,* Volume II: Geotechnical Problems with Man-made and Man Influenced Grounds, Prague, 471- 478

Shibuya, S. (1988), "A Servo System for Hollow Cylinder Testing of Soils", *Geotechnical Testing Journal*, 11(2), 109 - 118

Sivathayalan, S. and Vaid, Y.P. (2002), "Influence of Generalized Initial State and Principal Stress Rotation on the Undrained Response of Sands", *Canadian Geotechnical Journal*, 39, 63 - 76

Skempton, A.W. (1954), "The Pore Pressure Coefficients A and B", *Geotechnique*, 4, 143 - 147

Sutherland, H.B. and Mesdary, M.S. (1969), "The Influence of the Intermediate Principal Stress on the Strength of Sand", In *Proceedings of the Seventh International Conference on Soil Mechanics and Foundation Engineering*, Mexico City, 391 - 399

Symes, M.J., Gens, A. and Hight, D.W. (1984), "Undrained Anisotropy and Principal Stress Rotation in Saturated Sand", *Geotechnique*, 34(1), 11 - 27

Symes, M.J., Gens, A. and Hight, D.W. (1988), "Drained Principal Stress Rotation in Saturated Sand", *Geotechnique*, 28(1), 59 - 81

Symes, M.J., Hight, D.W. and Gens, A. (1982), "Investigating Anisotropy and the Effects of Principal Stress Rotation and of the Intermediate Principal Stress Using a Hollow Cylinder Apparatus", In *Symposium on Deformation and Failure of Granular Materials,* Delft, 441- 449

Tatsuoka, F., Nakamura, S., Huang, C. and Tani, K. (1990), "Strength Anisotropy and Shear Band Direction in Plane Strain Tests on Sand", *Soils and Foundations*, 30(1), 35 - 54

Tatsuoka, F. et al. (1986), "Failure and Deformation of Sand in Torsional Shear", *Soils and Foundations*, 26(4), 79 - 97

Taylor, G.I. and Quinney, H. (1931), "The Plastic Distortion of Metal", In *Philosophical Transactions of the Royal Society of London*, A230, 323 - 362

Tong, P. (1970), *Plane Strain Deformation of Sands*, Ph.D. Thesis, Manchester University

Vaid, Y.P. and Sayao, A. (1995), "Proportional Loading Behavior of Sand Under Multiaxial Stresses", *Soils and Foundations*, 35(3), 23 - 29

Vaid, Y.P., Sayo, A., Hou, E. and Negussey, D. (1990), "Generalized Stress-Path-Dependent Soil Behavior with a New Hollow Cylinder Torsional Apparatus", *Canadian Geotechnical Journal*, 27, 601 - 616

Wang, Q. and Lade, P.V. (2001), "Shear Banding in True Triaxial Tests and its Effect on Failure in Sand", *Journal of Engineering Mechanics*, 127(8), 754 - 761

Weindieck, K.W. (1963), "Discussion on: Soil Stresses and Deformations beneath Rigid Wheels", *Journal of Terramechanics*, 5(1), No. 1, 5

Wijewickreme, D. and Vaid, Y.P. (1991), "Stress Non-Uniformities in Hollow Cylinder Torsional Specimens", *ASTM: Geotechnical Testing Journal*, 14, 349 - 362

Wijewickreme, D. and Vaid, Y.P. (1993), "Behavior of Loose Sand Under Simultaneous Increase in Stress Ratio and Principal Stress Rotation", *Canadian Geotechnical Journal*, 30, 953 - 964

Wijewickreme, D. and Vaid, Y.P. (2008), "Experimental Observations on the Response of Loose Sand under Simultaneous Increase in Stress Ratio and Rotation of Principal Stresses", *Canadian Geotechnical Journal*, 45(5), 1 - 14

Yamada, Y. and Ishihara, K. (1979), "Anisotropic Deformation Characteristics of Sand under Three-Dimensional Stress Conditions", *Soils and Foundations*, 19(2), 79 - 93

Yamada, Y. and Ishihara, K. (1981), "Undrained Deformation Characteristics of Loose Sand under Three-Dimensional Stress Conditions", *Soils and Foundations*, 21(1), 97 - 107

Yamamuro, J. and Lade, P.V. (1997), "Static Liquefaction of Very Loose Sands", *Canadian Geotechnical Journal*, 34(6), 905 - 917

Yang, Z.X., Li, X.S. and Yang, J. (2007), "Undrained Anisotropy and Rotational Shear in Granular Soil", *Geotechnique*, 57(4), 371 - 384

Yoshimine, Y., Ishihara, K. and Vargas, W. (1998), "Effects of Principal Stress Direction and Intermediate Principal Stress on Undrained Shear Behavior of Sand", *Soils and Foundations*, 38(3), 179 - 188

Yoshimine, M., Ozay, R., Sezen, A. and Ansal, A. (1999), "Undrained Plane Strain Shear Tests on Saturated Sand Using a Hollow Cylinder Torsional Shear Apparatus", *Soils and Foundations*, 39(2), 131 - 136

Zdravkovic, L. and Jardine, J. (2001), "Effect of Anisotropy of Rotating the Principal Stress Axes During Consolidation", *Geotechnique*, 51(1), 69 - 83